Advances in the functionalisation of polyphosphorus ligands

Dissertation

zur Erlangung des
DOKTORGRADES DER NATURWISSENSCHAFTEN
(DR. RER. NAT.)
an der Naturwissenschaftlichen Fakultät IV
- Chemie und Pharmazie -
der Universität Regensburg



vorgelegt von:

Martin Weber
aus Karlsfeld

Regensburg, 2023

Diese Arbeit wurde angeleitet von Prof. Dr. Manfred Scheer.

Promotionsgesuch eingereicht am:	16.5.2023
Tag der mündlichen Prüfung:	30.6.2023

Prüfungsvorsitz:	Prof. Dr. Alkwin Slenczka
Prüfungsausschuss:	Prof. Dr. Manfred Scheer
	Prof. Dr. Nikolaus Korber
	Prof. Dr. Frank-Michael Matysik

Eidesstattliche Erklärung:

Ich erkläre hiermit des Eides statt, dass ich die vorliegende Arbeit ohne unzulässige Hilfe Dritter und ohne Benutzung anderer als der angegebenen Hilfsmittel angefertigt habe; die aus anderen Quellen direkt oder indirekt übernommenen Daten und Konzepte sind unter Angabe des Literaturzitats gekennzeichnet.

Martin Weber, Regensburg, 16.5.2023

This thesis was elaborated within the period from September 2018 till May 2023 in the Institute of Inorganic Chemistry at the University of Regensburg under the supervision of Prof. Dr. Manfred Scheer.

Parts of this work were already published and presented to a scientific audience on international conferences:

M. Weber, G. Balázs, A. V. Virovets, E. Peresypkina, M. Scheer, *Molecules* **2021**, *26*, 3920.
Results presented as poster presentation: European Workshop on Phosphorus Chemistry (EWPC) 2022 (Rostock, 15.9.2023)

R. Yadav, M. Weber, A. K. Singh, L. Münzfeld, J. Gramüller, R. M. Gschwind, M. Scheer, P. W. Roesky, *Chem. Eur. J.* **2021**, *27*, 14128.
Results presented as poster presentation: Online Workshop on Phosphorus Chemistry (OWPC) 2021 (online, 29-31.3.2021) and 44th International Conference on Coordination Chemistry (ICCC) 2022 (Rimini, 30.8.2022)

Each chapter includes a list of authors including their contribution to the presented results. The uniform design of the thesis may vary in chapters which were already published, but any numberings (compounds, references and otherwise) were fitted. A general "Introduction" and "Research Objectives" are given at the beginning of this thesis. In addition, a comprehensive "Conclusion" of this work is presented at the end of this thesis.

For Andrea

"Aut quid non miraculo est, cum primum in notitiam venit? Quam multa fieri non posse prius quam sunt facta iudicantur?"

freely translated: But what is not regarded a miracle, when noticed for the first time? How much is regarded impossible to do, until it is done for the first time?

Gaius Plinius Secundus Maior, *Naturalis Historia*

Contents

1 Introduction **12**

1.1 Phosphorus and organophosphorus compounds 12
1.2 Polyphosphorus ligand complexes 15
1.3 The complex $[\{Cp'''Fe(CO)_2\}_2(\mu,\eta^{1:1}\text{-}P_4)]$ 18
1.4 The complex $[Cp^*Fe(\eta^5\text{-}P_5)]$ 22
1.5 Reactivity of phosphenium ions 26
1.6 Organometallic chemistry of group 2 metals 30

2 Research objectives **33**

3 Insertion of Phosphenium Ions into a Bicyclo[1.1.0]Tetraphosphabutane Iron Complex **35**

3.1 Introduction 36
3.2 Results 38
3.2.1 Reactions of **VIIIa** with $[(C_6H_5)_2P]^+[A]^-$ at room temperature 38
3.2.2 Reactions of **VIIIa** with $[(C_6H_5)_2As]^+[OTf]^-$ 41
3.3 Discussion 43
3.4 Conclusions 46
3.5 Supporting Information 47
3.5.1 General techniques and materials 47
3.5.2 Experimental details and analytical data 47
3.5.3 NMR spectra and spectroscopic data 50
3.5.4 Crystallographic data and solid state structures 69
3.5.5 Details on DFT calculations and Cartesian coordinates 75

4 Structural Diversity of Molecular Alkaline-Earth-Metal Polyphosphides **80**

4.1 Introduction 81
4.2 Results and Discussion 83

4.2.1 Magnesium polyphosphides 83
4.2.2 Calcium polyphosphides 90
4.2.3 Molecular modelling 93
4.2.4 Conclusions 96
4.3 Supporting information 97
4.3.1 General remarks 97
4.3.2 Experimental procedure and analytical data 97
4.3.3 NMR spectra 102
4.3.4 Simulation of NMR spectra 114
4.3.5 Details of the DOSY-measurements 117
4.3.6 Crystallographic details 119
4.3.7 Quantum chemical calculations 124

5 From P_5 to P_7 : The way to highly substituted 1,3-bis(phosphanyl)-pentaphospholanide iron complexes from pentaphosphaferrocene 131
5.1 Introduction 132
5.2 Results and Discussion 134
5.2.1 Quenching $[Cp^*Fe(\eta^4\text{-}P_5R)]^-$ with chlorophosphines 134
5.2.2 Reactivity of $[Cp^*Fe(\eta^{3:1}\text{-}(1\text{-}R\text{-}2\text{-}PPh_2\text{-}P_5))]$ $(R = Me, {}^tBu)$ towards charged nucleophiles and quenching with chlorophosphines 141
5.2.3 Further reactions of $[Cp^*Fe(\eta^4\text{-}P_5R)]^-$ with chlorophosphines and arsines (treasury) 147
5.3 Conclusion 154
5.4 Supporting information 156
5.4.1 General remarks 156
5.4.2 Experimental procedure and analytical data 157
5.4.3 NMR spectra and simulations of spin systems 171
5.4.4 Crystallographic details 225
5.4.5 Details on quantum chemical calculations 248

6 Synthons for group 2 metals - An updated synthesis of group 2 anthracenides and their use as reducing agents for polypnictogenide ligand complexes. 258
6.1 Introduction 259
6.2 Results on the synthesis of alkaline earth metal anthracenides 261
6.3 Reactivity of alkaline earth metal anthracenides towards pentaphosphaferrocene 262

6.4 Investigations on the redox chemistry of $[Cp^*Fe(\eta^{3:1}\text{-}(1\text{-}CH_3\text{-}2\text{-}PPh_2\text{-}P_5))]$ 266
6.5 Conclusion . . . 270
6.6 Supporting information . . . 272
6.6.1 General techniques and materials . . . 272
6.6.2 Experimental details . . . 273
6.6.3 NMR spectra . . . 280
6.6.4 Crystallographic details . . . 292

7 Supramolecular aggregates of $[\mathbf{Cp^*Fe(\eta^{3:1}\text{-}(1\text{-}CH_3\text{-}2\text{-}PPh_2\text{-}P_5))}]$ 305
7.1 Introduction . . . 305
7.2 Results . . . 307
7.3 Conclusion . . . 312
7.4 Supporting information . . . 313
7.4.1 General techniques and materials . . . 313
7.4.2 Experimental Details . . . 313
7.4.3 NMR spectra . . . 315
7.4.4 Crystallographic details . . . 316

8 Conclusion 325
8.1 Reactivity of $[\{Cp'''Fe(CO)_2\}_2(\mu,\eta^{1:1}\text{-}P_4)]$ towards phosphenium ions . 326
8.2 Consecutive functionalisation of $[Cp^*Fe(\eta^5\text{-}P_5)]$ with carbon nucleophiles and phosphorus electrophiles. . . . 328
8.2.1 Reactivity of the complex $[Cp^*Fe(\eta^{3:1}\text{-}(1\text{-}Me\text{-}2\text{-}PPh_2\text{-}P_5))]$ . . 330
8.2.2 Supramolecular aggregates of the complex $[Cp^*Fe(\eta^{3:1}\text{-}(1\text{-}Me\text{-}2\text{-}PPh_2\text{-}P_5))]$ . . . 331
8.3 Reactivity of group 2 metal compounds towards P_n-ligand complexes . 333
8.3.1 Reactivity of bis-ketiminate stabilized Mg and Ca compounds towards $[Cp^*Fe(\eta^5\text{-}P_5)]$ . . . 333
8.3.2 Reactivity of group 2 anthracene compounds towards polyphosphorus ligand complexes . . . 335

Appendix 338
List of compounds . . . 338
List of abbreviations . . . 342
List of figures . . . 352
List of schemes . . . 354
List of tables . . . 356
References . . . 357

Chapter 1

Introduction

1.1 Phosphorus and organophosphorus compounds

The discovery of phosphorus (from Greek $\varphi\omega\sigma$: light $\varphi o\rho o\zeta$: bearer) in the year 1669 is attributed to the alchemist *Hennig Brandt* from Hamburg. By the pyrolysis of urine residues, small amounts of phosphorus were produced. This represents the first discovery of an element in modern times and was received and documented by some of the most renowned scientists in Europe of the time with great interest, including *Boyle* and *Leibnitz*. The latter even wrote a poem (in Latin) on the discovery of white phosphorus.[1–6] The elaborate and expensive synthesis from urine is based on the pyrolytic reduction of $NaNH_4HPO_4$ by carbon, the latter being generated by the carbonization of other components in urine.[5] This method persisted until *Gahn* and *Scheele* discovered that bones and the horns of animals consist mainly of calcium and phosphate. A new, much more effective and cheaper synthetic pathway to white phosphorus was devised by *Scheele* by heating bone ash with powdered coal and sand (Figure 1.1).[8–12] This method was refined (e.g. by the extraction and purification of Calcium phosphate from bone material) and used as the main synthesis route to white phosphorus for a long time and still is the basis for the industrial phosphorus synthesis used today: Large quantities of fluorine rich apatite (usually from mineral deposits)

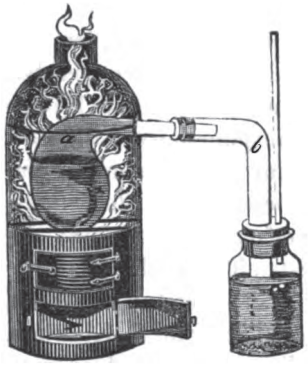
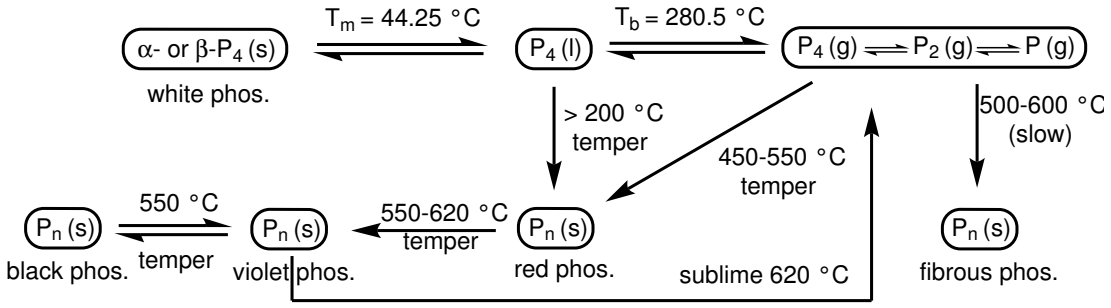


Figure 1.1: Historic apparatus for the synthesis of white phosphorus. Phosphorus vapour from a is condensed in the copper tubing b and collected in a bottle filled with water.[7]

are reduced on carbon electrodes of an electric arc furnace at temperatures of 1400-1500 °C.[5,7] At these temperatures, phosphorus vapour is consisting of both tetrahedral P_4 and linear P_2 molecules while at temperatures below 800 °C exclusively P_4 is present in the vapour which condenses at 280.5 °C (Scheme 1.1). The highly refractive, colourless liquid solidifies at 44.25 °C to form cubic white phosphorus in form of a waxy, off-white substance.[5] Due to its toxicity and pyrophoric character, white phosphorus is either stored under water or under inert conditions by the exclusion of light. There are other allotropes of phosphorus, that are metastable at room temperature. These are synthesized by treatment of white phosphorus with heat and/or pressure (scheme 1.1).



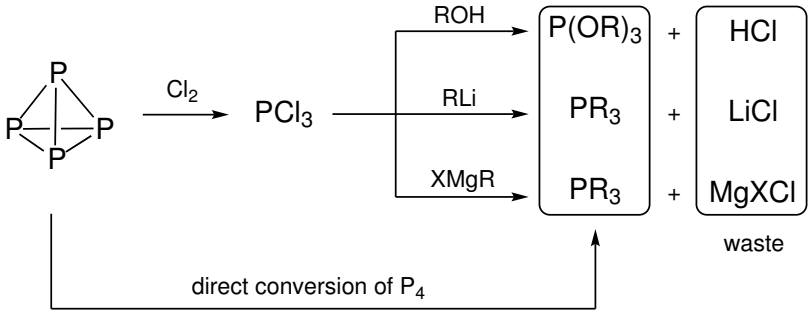
Scheme 1.1: Overview of the conditions for phase transitions of the allotropes of phosphorus.[5]

In industry or in the laboratory phosphorus is seldom used in its elemental form. The most important use of elemental phosphorus is as a strong reducing agent.[13,14] If pure white phosphorus without any impurities of polymerized phosphorus is needed for a reaction, it can be sublimed and stored under the exclusion of light in a glovebox with under dry nitrogen or argon atmosphere.

The preferred oxidation states of phosphorus are III and V. While there are a lot of air stable compounds of phosphorus in oxidation state V, such as phosphoric acid and its derivatives, compounds of phosphorus in oxidation state III are usually sensitive towards oxidation and sometimes hydrolysis. While P(V) compounds are found all over in every day life in the form of fertilizers, herbicides, food- and cleaning-agent additives as well as fire retardants, compounds of P(III) are usually only found in the laboratory or in industrial applications due to their sensitivity and toxicity. The latter can also be true for some P(V) compounds, especially for esters of the phosphoric acid such as the well known nerve agents and chemical weapons sarin, tabun and other inhibitors of cholinesterase.[15–22]

Most synthetic routes to organophosphorus compounds in oxidation state III start from the synthesis of phosphine gas or phosphorus trichloride, which are obtained from white

phosphorus (Scheme 1.2). Both highly toxic and hazardous compounds are then reacted with alcohols or organometallic compounds such as alkyl lithium or grignard reagents to form phosphines (PR_3) or phosphites ($P(OR)_3$, scheme 1.2). Due to the stoichiometric amount of waste products like HCl or metal salts, more atom economic and environmentally friendly routes towards these compounds are required. For the synthesis of asymmetrically substituted organophosphines ($PRR'R''$) this means multiple salt metathesis reactions and fractionated distillations under reduced pressure in an inert gas atmosphere of highly toxic and hazardous liquids, which lowers the overall yield drastically. Therefore a major research objective in phosphorus chemistry has been the synthesis of organophosphorus compounds from white phosphorus as directly as possible.[23–28]



Scheme 1.2: Industrial pathway of the synthesis of organophosphorus compounds.

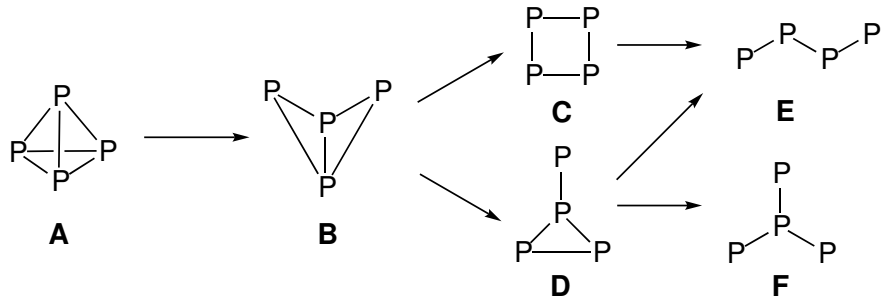
Modern synthetic pathways include stannylation, photocatalytic conversion, oxidative "onioation", reaction of fluorinated alkyl iodides with SmI_2, titanium mediated radical synthesis or electrochemical transformation.[29–40] Most of these methods yield symmetrically substituted organophosphines PR_3 and/or arylphosphines. Although the ecological and economical benefit of using fluorinated alkyls or the trifluoromethanesulfonate ion $[CF_3OSO_2]^-$ instead of chloride can be questioned, all these synthetic methods represent alternative routes from the classical pathway over PCl_3 and use P_4 as a starting material. Also, e.g., in the case of organotin compounds, the reagents for the conversion of P_4 can be recycled in some cases, so that only small amounts of hazardous by-products are produced.

The organophosphines or halogenated phosphines are important building blocks in inorganic and organic chemistry alike, but represent just the end result in the conversion of the P_4 tetrahedron by main group reactants. Research therefore also includes the synthesis and characterisation of polyphosphorus compounds from either P_4 or organophosphines.[41–44] White phosphorus also undergoes similar reactions with reactive transition metal complexes and complex fragments to form polypnictogen (P_n) ligand complexes. For the analysis of polyphosphorus compounds ^{31}P NMR spectroscopy is one

of the most valuable tools available, since not only is the ^{31}P nucleus relatively NMR active, but couplings among the different phosphorus atoms are usually well resolved and can be analysed thoroughly by iterative fitting and simulation. This allows prediction of the connectivity of polyphosphorus compounds, making NMR spectroscopy a powerful tool for structure elucidation.[45–49]

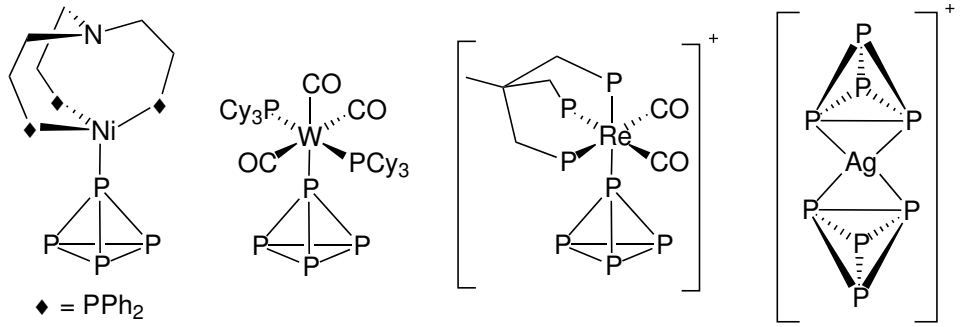
1.2 Polyphosphorus ligand complexes

The conversion of the P_4 tetrahedron in a controlled manner, by opening one P-P bond at the time, is achieved by attack of an electrophile, nucleophile or radical.[24] For this purpose reactive main group reactants or transition metal complexes and their fragments are used. Such transition metal complexes dissociate into radicals in solution or form radical species upon photolysis or thermolysis.[50] By reaction of white phosphorus with this electron deficient metal fragments, these can be stabilized through the formation of polyphosphorus ligand complexes. Depending on the reactivity of the metal fragment and the reaction conditions, P-P bond breakage and rearrangements may occur. From the results of many years of research, since the first synthesis of



Scheme 1.3: Stepwise activation of the P_4 tetrahedron, neglecting the charge.

a P_n ligand complex by *Ginsberg et al.* in 1971 to the present day, the stepwise opening of the P_4 tetrahedron can be comprehended (Scheme 1.3).[51] If only end-on coordination of the transition metal fragment at P_4 occurs, the tetrahedral structure is preserved (Scheme 1.3 - **A**). This was first observed in 1979 by *Sacconi et al.* in the complex $[(np_3)Ni(\eta^1\text{-}P_4)]$ (**I**, np = tris(2-diphenylphosphinoethyl)amine, Fig. 1.2).[52] Other examples of complexes in which intact P_4 tetrahedra, coordinated end-on to a transition metal include the neutral complex $[W(CO)_3(PCy_3)_2(\eta^1\text{-}P_4)]$ (**II**, Cy = cyclohexyl), reported in 1998 by *Scheer et al.* and the cationic complex $[(triphos)Re(CO)_2(\eta^1\text{-}P_4)][OTf]$ (**III**, triphos = 1,1,1-tris(diphenyl-phosphinomethyl)-ethane, $OTf = OSO_2CF_3$), reported in 1999 by *Peruzzini et al.* (Figure 1.2).[53,54]



I **II** **III** **IV**

Figure 1.2: Structures of complexes **I**, **II**, **III** and **IV** with the structural motif **A**.

Besides end-on coordination by the free electron pairs of the P_4 tetrahedron, the σ-orbitals of the P-P bonds can also coordinate side-on to the transition metal fragment, as exemplified by the complex $[Ag(\eta^2\text{-}P_4)_2][TEF]$ (**IV**, $TEF = Al\{OC(CF_3)_3\}_4$).[55] If this P-P bond is broken, a tetraphosphabicyclo[1.1.0]butane structural motif (Scheme 1.3 - **B**), which is also called butterfly structure motif due to its geometry, is formed. As already mentioned, the complexes $[L_2RhCl(\eta^{1:1}\text{-}P_4)]$ (**Va**, $L = PPh_3$; **Vb**, $L = P(m\text{-}tol)_3$; **Vc**, $L = P(p\text{-}tol)_3$; **Vd**, $L = AsPh_3$) described by *Ginsberg et al.* 1971 can be considered the first P_n-ligand complexes and exhibit the structural motif **B** (Fig. 1.3).[51] The first compound in which this structural motif was observed bridging two metal fragments is $sMes_2P_4$ (**VI**, sMes = 1,3,5-tritertbutylbenzene, Fig. 1.3) and was reported in 1985 by *Fluck et al.* by the reaction of P_4 with sMesLi and sMesBr.[56] A more recent example for the structural motif **B** is $[cis,\ trans\text{-}DmpP_4Dmp]$ (**VII**; Dmp = 2,6-dimesitylpheyl), observed in 2010 by *Cummins et al.* . Compound **VII** is formed by reacting DmpI with $[Ti(N[^tBu]Ar)_3]$ $(Ar = 3,5\text{-}C_6H_3Me_2)$ in the presence of P_4.[57] The complex $[\{Cp'''Fe(CO)_2\}_2(\mu,\eta^{1:1}\text{-}P_4)]$ (**VIIIa**, Fig. 1.3) was first reported by *Scherer et al.* in 1998, the isostructural derivative with Cp'' (**VIIIb**) in 1995.[58,59] By opening a second bond of the P_4 ligand, the butterfly motif (**B**) is converted into a *cyclo*-P_4 (**C**) or tetraphospha-methylcyclopropane motif (**D**). The first complex with a *cyclo*-P_4 structural motif **C** was observed by *Scherer et al.* in 1989 by photolysis of $[Cp^*Nb(CO)_4]$ $(Cp^* = C_5(CH_3)_5)$ in the presence of P_4 (**IX**, Fig. 1.4).[60] However, NMR spectroscopic studies show that the *cyclo*-P_4 ligand in **IX** is highly distorted and is kite-shaped rather than square. Another example of a *cyclo*-P_4 ligand can be observed in the complex $[\{Zr(L_{PN})\}_2(\mu,\eta^{4:4}\text{-}P_4)]$ (**X**, $L_{PN} = PhP(CH_2SiMe_2NSiMe_2CH_2)_2PPh$), reported in 2008 by *Fryzuk et al.* (Fig. 1.4).[61] In contrast to **IX**, the *cyclo*-P_4-ligand in **X** has a square planar geometry, being formally a P_4^{4-}-ligand. By photolysis of the complex **VIIIb**, the compound $[\{Cp''Fe\}(\mu,\eta^{4:1}\text{-}P_4)\{Fe(CO)_2Cp''\}]$ (**XI**, Fig. 1.4) with a

cyclo-P_4-ligand, as well as the complex $[\{Cp''Fe\}_2(\mu,\eta^{4:4}\text{-}P_4)]$ (**XII**), with a *catena*-P_4 unit, are synthesized (Chapter 1.3).[59]

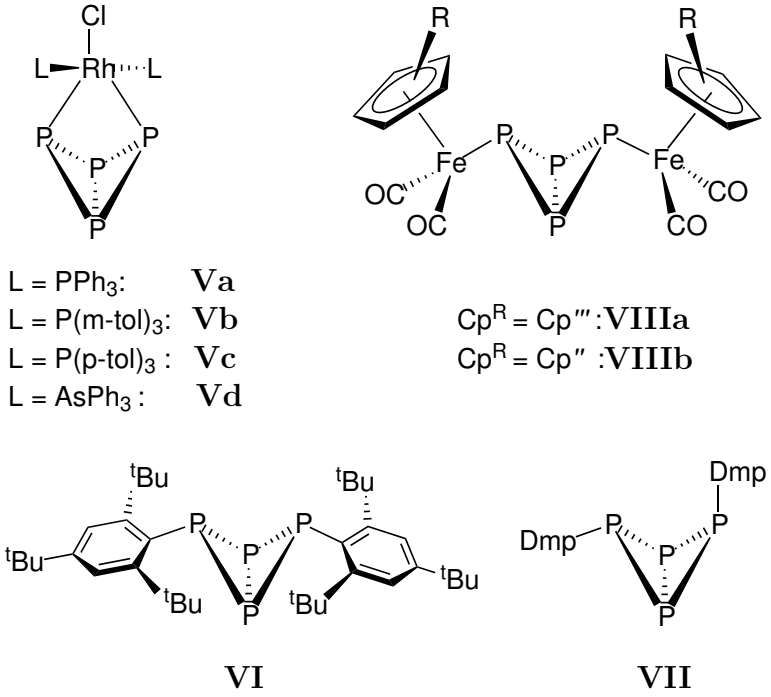


Figure 1.3: Structures of the complexes **V**, **VI**, **VII** and **VIII** which show the butterfly structural motif **B**.

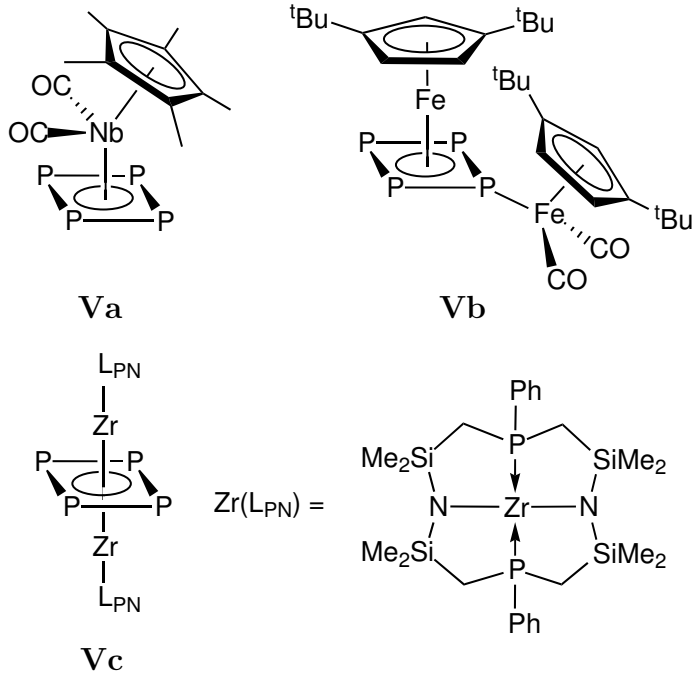
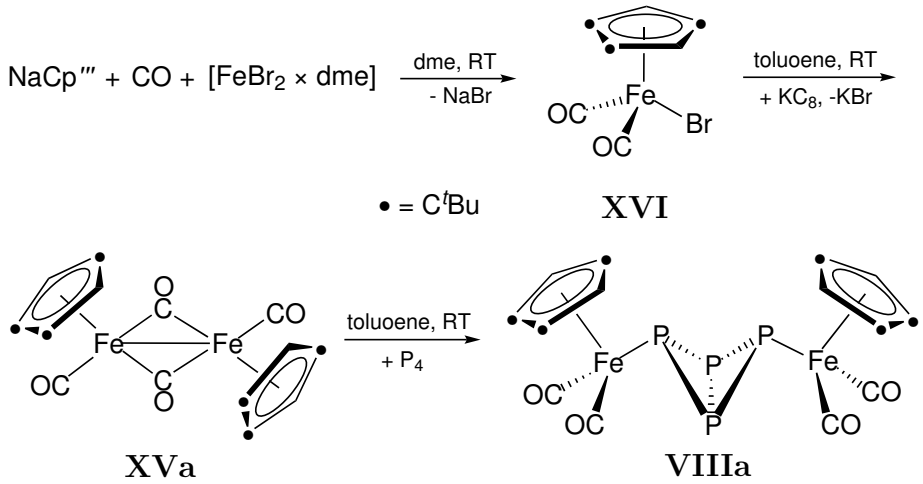


Figure 1.4: Structures of selected complexes bearing a *cyclo*-P_4 unit (structural motif **C**).

Catena P_4 motifs (type **E**) were obtained by *Bertrand et al.* in 2007 by reacting a sterically demanding menthyl-substituted cyclic alkylaminocarbene (CAAC) with white phosphorus.[62] By using the sterically less demanding, cyclohexyl-substituted CAAC, a mixture of two products is obtained: the tetraphospha-isobutane derivative $[(^{Cy}CAAC)_3P_4]$ (**XIII**, type **F**) and $[(^{Cy}CAAC)_2P_2]$.[63] If the acyclic alkylaminocarbene $^{t}BuCN(Cy)_2$ is used, the compound $[(^{t}BuCN(Cy)_2)_2P_4]$ (**XIV**) is obtained, which shows a *cyclo*-P_3 ligand with exocyclic P atom as structural motif (type **D**).[63]

1.3 The complex $[\{Cp'''Fe(CO)_2\}_2(\mu,\eta^{1:1}\text{-}P_4)]$

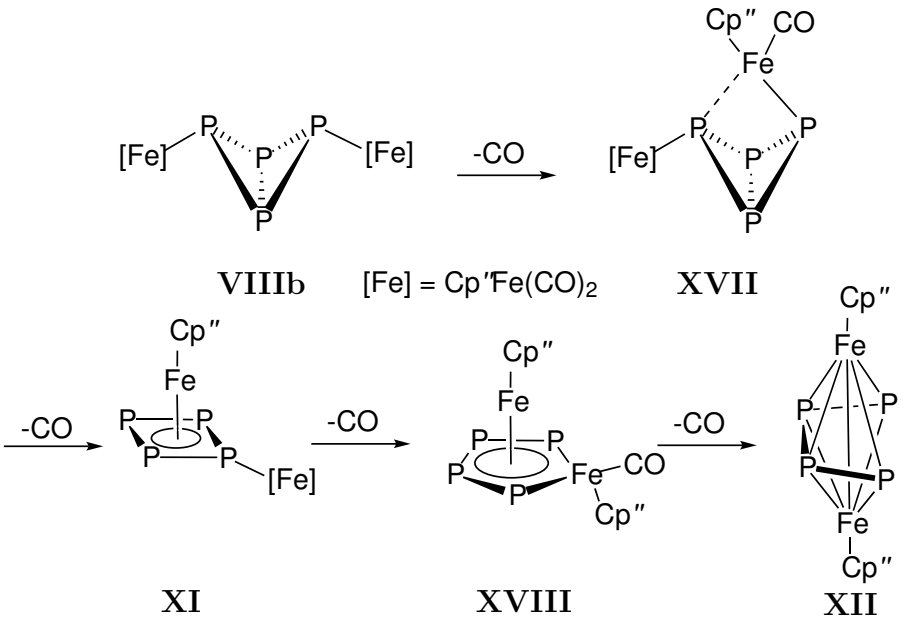
The preparation and reactivity of the P_4-butterfly complex $[\{Cp'''Fe(CO)_2\}_2(\mu,\eta^{1:1}\text{-}P_4)]$ (**VIIIa**) serves as an example for the first step in the conversion of white phosphorus with transition metal complex fragments. The synthesis of **VIIIa** is carried out by reacting $[Cp'''Fe(CO)_2]_2$ (**XVa**, $Cp''' = C_5H_2(C(CH_3)_3)_3$) with P_4 in boiling toluene as reported by *Scherer et al.* in 1998.[58] However, in 2014 our group was able to show that **XVa** partially dissociates into two reactive 17 valence electron fragments at room temperature.[64] Therefore also the preparation of **VIIIa** can be performed at room temperature (Scheme 1.4). To obtain **XVa**, the complex $[Cp'''Fe(CO)_2Br]$ (**XVI**) is reduced with a suitable reducing agent (formerly cobaltocene, now KC_8). A twofold reduction to $K[Cp'''Fe(CO)_2]$ is observed when more than one equivalent of the reducing agent is used.[65,66] Upon photolysis of the analogous complex with a Cp''



Scheme 1.4: Synthesis of **VIIIa** over **XVa** (dme = dimethoxyethane).

ligand (**VIIIb**), decarbonylation occurs. All resulting complexes of the stepwise decarbonylation are known in literature (Scheme 1.5).[59] After cleavage of one of the carbonyl groups on one of the two iron fragments in **VIIIb**, this fragment coordinates

to the opposite wing tip of the butterfly backbone, forming complex **XVII** (Scheme 1.5). After cleavage of the last carbonyl group on the same fragment, compound **XI** with a *cyclo*-P_4 ligand is formed. Decarbonylation of the remaining $[Cp''Fe(CO)_2]$ fragment gives the tetraphosphaferrol derivative **XVIII** and, after complete CO cleavage, the complex **XII** (Scheme 1.5). Thermolysis of **VIIIa** in boiling decalin gives the



Scheme 1.5: Follow-up complexes of the decarbonylation of **VIIIb** to **XI**, **XII**, **XVII** and **XVIII**.

complex $[\{Cp'''Fe\}_2(\mu,\eta^{4:4}\text{-}P_4)]$ (isostructural to **XII** and the pentaphosphaferrocene derivative $[Cp'''Fe(\eta^5\text{-}P_5)]$.[58] DFT calculations show that the electron density of the HOMO (highest occupied molecular orbital) and the HOMO-1 in complex **VIIIa** are mainly located at the wing tip atoms of the butterfly structural motif (Figure 1.5).[67] This allows for coordination of the ligand to Lewis acids, with the LUMO (lowest unoccupied molecular orbital) with its location between the wing tips being available for backbonding. Since the electron density in the HOMO is also slightly located at the two bridgehead atoms, coordination should also be possible at these atoms.

Thus, the reaction of **VIIIa** with a half equivalent of the salt $[Cu(MeCN)_4]$ $[BF_4]$ gives the *spiro* compound $[\{\{Cp'''Fe(CO)_2\}_2(\mu_3,\eta^{1:1:1:1}\text{-}P_4)\}_2Cu][BF_4]$ (**XIX**) and the mono-adduct $[\{Cp'''Fe(CO)_2\}_2(\mu_3,\eta^{1:1:2}\text{-}P_4)\{Cu(MeCN)\}][BF_4]$ (**XX**, fig. 1.6) with one equivalent.[67] The reaction of **VIIIa** with $Ag[PF_6]$ gives a *spiro* compound similar to **XIX**: $[\{\{Cp'''Fe(CO)_2\}_2(\mu_3,\eta^{1:1:1:1}\text{-}P_4)\}_2Ag][PF_6]$ (**XXI**). The reaction of **VIIIa** with $[(PPh_3)Au(tht)][PF_6]$ (tht = tetrahydrothiophene) yields a compound isostructural to **XX**: $[\{Cp'''Fe(CO)_2\}_2(\mu_3,\eta^{1:1:2}\text{-}P_4)\{Au(PPh_3)\}][PF_6]$ (**XXII**, Figure 1.6).[66]

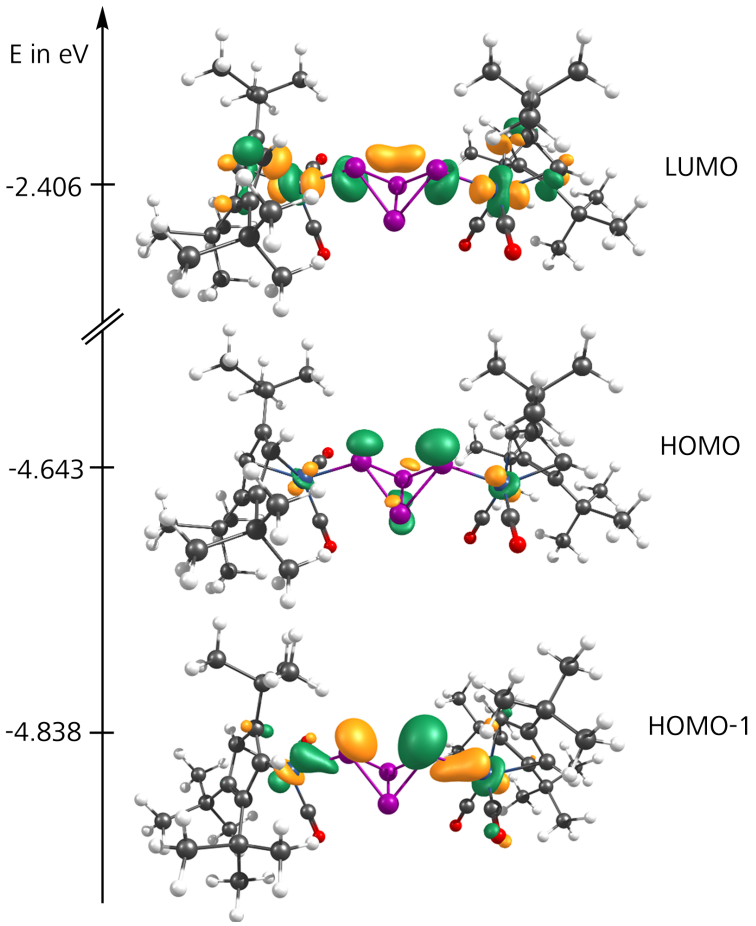
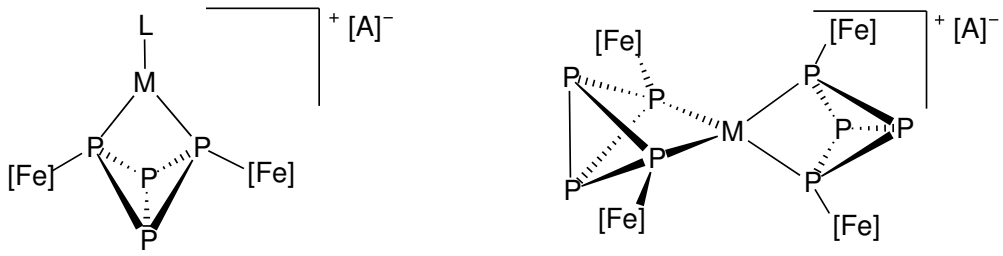


Figure 1.5: Electron density of the HOMO, HOMO-1 and the LUMO calculated at the BP86/def-SVP level in **VIIIa**.

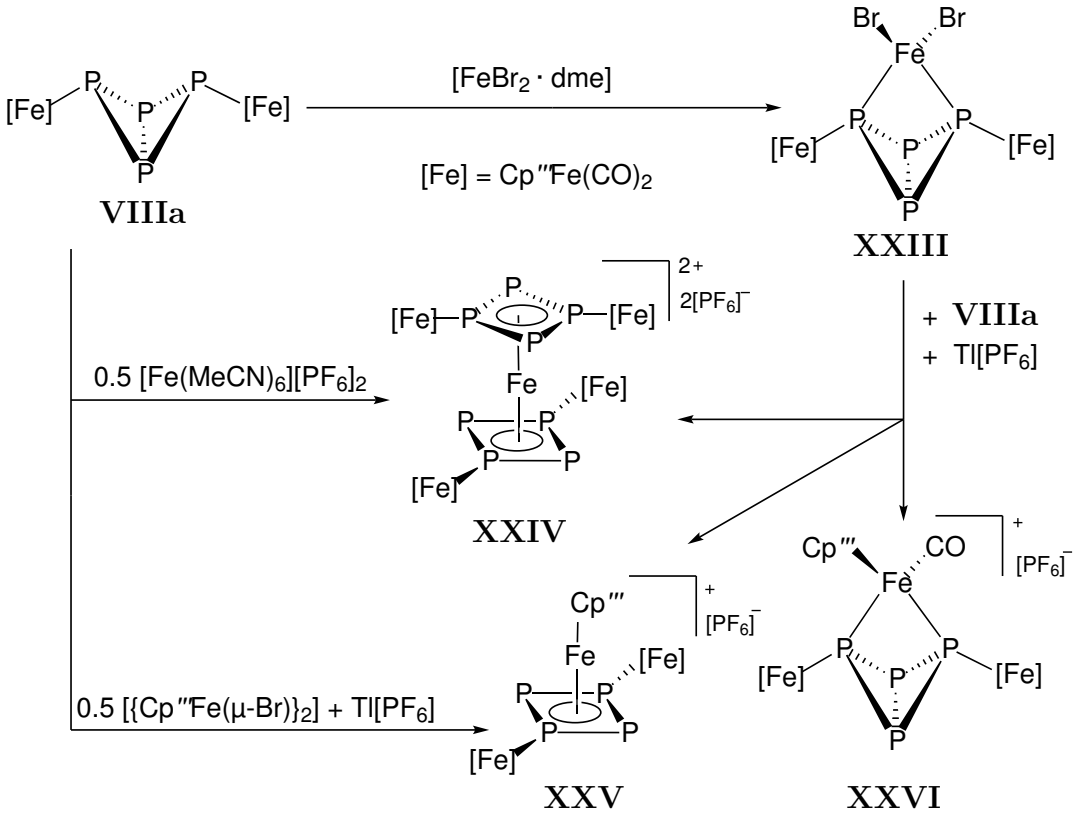


M = Cu, L = MeCN, A = BF_4^- : **XIX**
M = Au, L = PPh_3, A = PF_6^- : **XXI**

M = Cu, A = BF_4^- : **XX**
M = Ag, A = PF_6^- : **XXII**

Figure 1.6: Coordination compounds of **VIIIa** with Lewis acidic coinage metal salts.

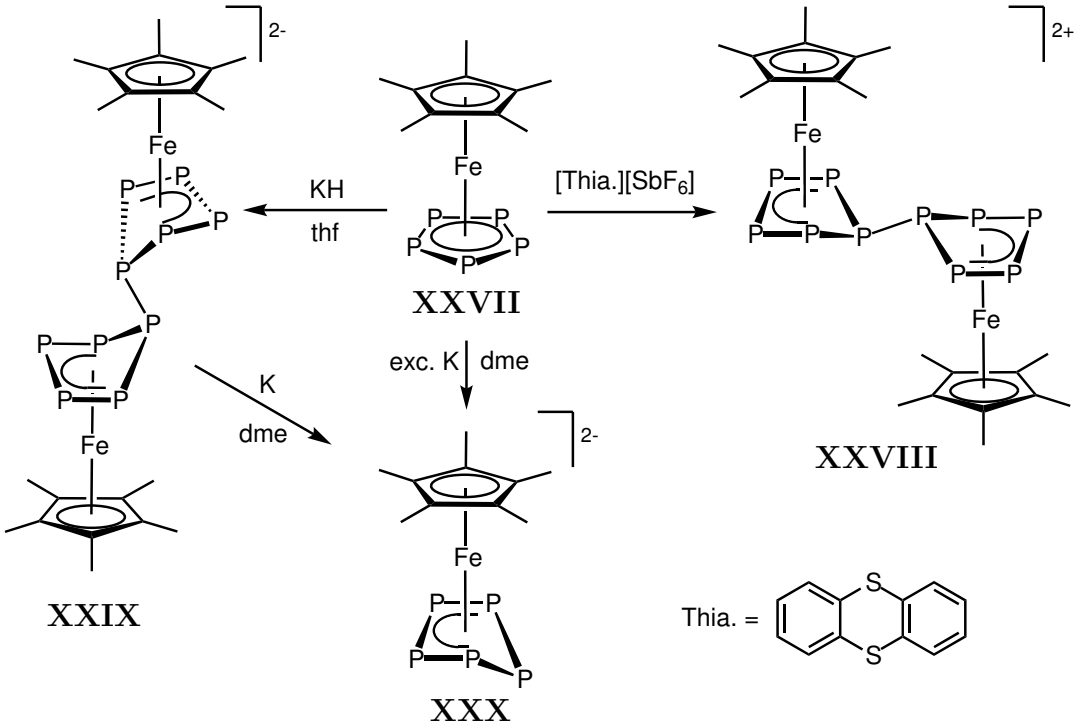
Reacting **VIIIa** with $[FeBr_2 \cdot dme]$ (dme = dimethoxyethane) gives the complex $[\{Cp'''Fe(CO)_2\}_2(\mu_3,\eta^{1:1:2}\text{-}P_4)\{FeBr_2\}]$ (**XXIII**), which reacts with another equivalent of **VIIIa** and $Tl[PF_6]$ to the complex $[\{(Cp'''Fe(CO)_2)_2(\mu_3,\eta^{1:1:4}\text{-}P_4)\}_2 Fe][PF_6]_2$ (**XXIV**) under isomerisation of the butterfly structural motif to *cyclo*-P_4 units.[68] By-products of this reaction are $[\{Cp'''Fe(CO)_2\}_2(\mu_3,\eta^{1:1:4}\text{-}P_4)\{Cp'''Fe\}][PF_6]$ (**XXV**) and the complex $[\{Cp'''Fe(CO)_2\}_2(\mu_3,\eta^{1:1:2}\text{-}P_4)\{Cp'''Fe(CO)\}][PF_6]$ (**XXVI**, Scheme 1.6). Compound **XXV** can also be prepared selectively by reacting **VIIIa** with half an equivalent of $[\{Cp'''Fe(\mu\text{-}Br)\}_2]$ and $Tl[PF_6]$. The sandwich complex **XXIV** can also be selectively prepared by reacting **VIIIa** with half an equivalent of $[Fe(MeCN)_6][PF_6]_2$.



Scheme 1.6: Reaction of **VIIIa** with Fe(II)-based Lewis acids.

1.4 The complex $[Cp^*Fe(\eta^5\text{-}P_5)]$

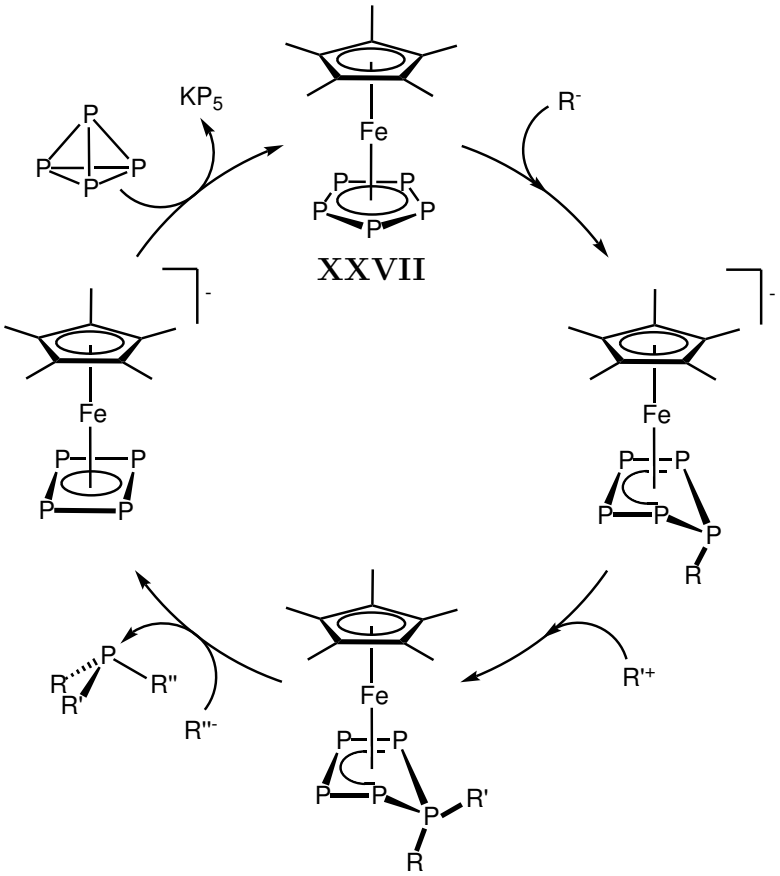
As mentioned before, the thermal conversion of white phosphorus with reactive transition metal complex fragments involves fragmentation of the P_4 unit and rearrangement to e.g., planar aromatic *cyclo*-P_n moieties. Due to its isolobality to the cyclopentadienide anion the *cyclo*-P_5 in the pentaphosphaferrocene $[Cp^*Fe(\eta^5\text{-}P_5)]$ (**XXVII**) is easily formed during thermolysis and can be regarded as one of the most stable P_n ligands. The complex **XXVII** was first synthesised by *Scheer et al.* by cothermolysis of $[Cp^*Fe(CO)_2]_2$ and P_4.[69] Pentaphosphaferrocenes with other derivatives of the Cp ligand e.g., Cp", Cp"' or Cp are known[70–73] but the Cp^* derivative is yet most commonly used due to high yields in updated synthesis methods, good solubility in common solvents and well explored chemistry. In the following, the chemistry of **XXVII** is explained in more detail:



Scheme 1.7: Reduction and oxidation products of **XXVII**.[74,75]

First of all **XXVII** shows a unique stability for a polyphosphorus ligand complex. The dark green crystalline needles are air-stable and solutions of the compound are also relatively stable towards hydrolysis or oxidation.[69] The redox chemistry of **XXVII** was first explored in more detail in 1998 by *Geiger and Winter*, who performed cyclic voltammetry studies on the compound.[74] In contrast to ferrocene, reduction and oxidation processes in **XXVII** are centred on the *cyclo*-P_5 ligand and not on the central

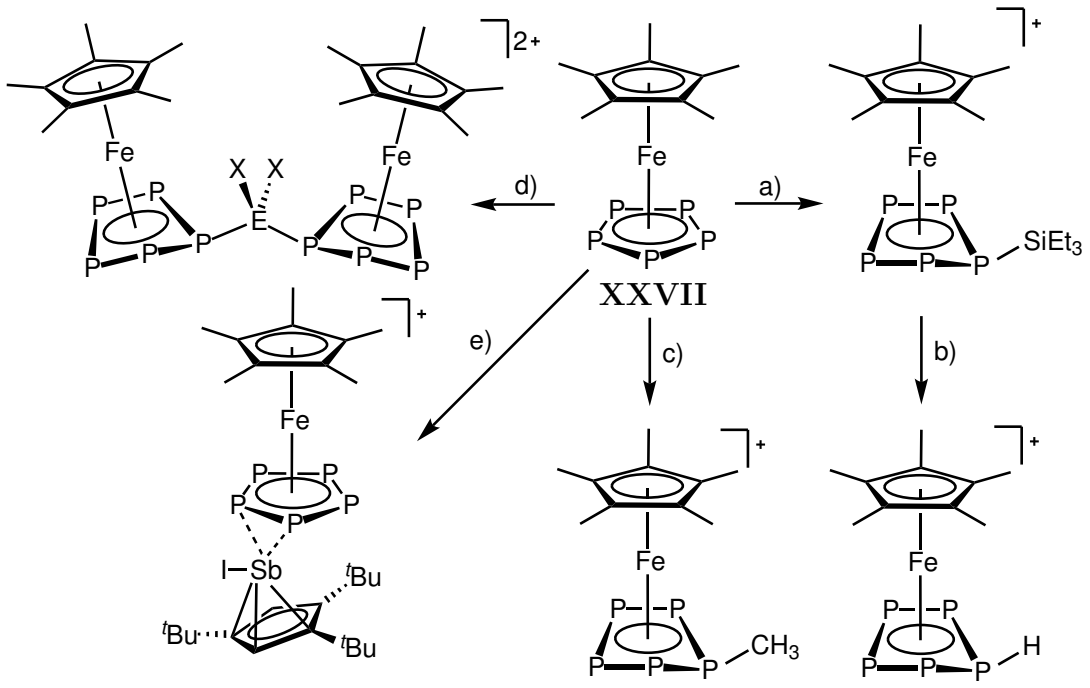
iron atom. According to the cyclic voltammogram both the one electron oxidation to [**XXVII**]$^+$ and the one electron reduction to [**XXVII**]$^-$ are not coulomb reversible and the respective products undergo dimerisation processes, visible as ECEC signals (conversion cascade: **E**lectrochemical reaction, **C**hemical reaction, **E**lectrochemical reaction, **C**hemical reaction) in the cyclic voltammogram. The proposed structures of the dimeric dianion and dication of **XXVII** were confirmed by full scale chemical oxidation and reduction (Scheme 1.7).[75] Using potassium hydride, the postulated P_{10}^{2-} moiety in $[K(dme)_2K(dme)][Cp^*Fe(\mu,\eta^{4:4}\text{-}P_{10})]$ (**XXIX**) was observed. Upon reduction with potassium metal the dianionic product $[K(dme)K(dibenzo\text{-}[18]\ crown\text{-}6)][Cp^*Fe(\eta^4\text{-}P_5)]$ (**XXX**) of the twofold reduction of **XXVII** was observed. Upon oxidation with thianthrenium hexafluoroantimonate the oxidation product $[Cp^*Fe(\mu,\eta^{5:5}\text{-}P_{10})][SbF_6]$ **XXVIII** is formed, showing the P_{10}^{2+} moiety proposed by *Geiger* and *Winter* (Scheme 1.7).



Scheme 1.8: Cyclic reaction pathway to asymmetrically substituted phosphines by consecutive functionalisation of **XXVII**.[76]

The versatile chemistry of **XXVII** is also shown in the reactivity towards nucleophiles and electrophiles of main group elements. Upon attack of a main group nucleophile,

the latter is bound to the phosphorus atom bent out of plane in the formed envelope η^4-P_5 ligand.[77] While carbon nucleophiles such as MeLi or ^{t}BuLi give functionalized anionic complexes of the type $[Cp^*Fe(\eta^4\text{-}P_5R)]^-$ in high yields, phosphorus nucleophiles such as $NaPH_2$ only give low yields of the respective anionic P_6 ligand complexes.[77] The carbon functionalized anionic complexes $[Cp^*Fe(\eta^4\text{-}P_5R)]^-$ also were quenched with alkyl- and aryl-halogenides to yield 1,1-functionalized neutral complexes $[Cp^*Fe(\eta^4\text{-}P_5\text{-}1,1R,R')]$.[76,77] By a second attack of a carbon nucleophile, the functionalized phosphorus atom is cleaved from the complex to yield an asymmetrically substituted phosphine and the *cyclo*-P_4 ligand in $[K(18\text{-cr-}6)(thf)][Cp^*Fe(\eta^4\text{-}P_4)]$ (Scheme 1.8)



Scheme 1.9: Reactivity of **XXVII** towards main group electrophiles: a) $(Et_3Si)_2(\mu\text{-H})][B(C_6F_5)_4]$ in o-DFB (ortho-difluorobenzene), b) 0.5 equivalents of H_2O in o-DFB, c) $[Me_3O][BF_4]$ in o-DFB and two equivalents of $B(C_6F_5)_3$ or MeOTf in o-DFB and two equivalents of $[Li(OEt_2)_2][B(C_6F_5)_4]$ in o-DFB, d) BBr_3 or GaI_3 with Tl[TEF] in o-DFB, e) [Cp‴SbI][TEF] in o-DFB.[78,79]

When reacting **XXVII** with main group electrophiles, the functionalized *cyclo*-P_5 ligand is more similar to the *cyclo*-P_5 monomers of the oxidation product **XXVIII** (*vide supra*). Therefore the ligand is still η^5 coordinating and the functionalized phosphorus atom is only slightly shifted from the plane of the ligand.[78,79] Along with C, Si, B, As and Sb based electrophiles, the respective complex of the parent phosphole of

the pentaphospha cyclopentadienyl ligand was isolated in [Cp*Fe(η^5-P_5H)][$B(C_6F_5)_4$] (Scheme 1.9).[78]

Furthermore **XXVII** can coordinate to Lewis acidic transition metals due to the readily available lone pairs on the phosphorus atoms of the *cyclo*-P_5 ligand. In contrast to the functionalisation of **XXVII**, coordination to Lewis acidic transition metal compounds does not change the geometry of the *cyclo*-P_5 moiety. Coinage metal salts such as CuX (X = Cl, Br, I)[80–88] or AgX (X = O_3SCF_3, PF_6, SbF_6)[89,90] form spherical supramolecular aggregates with **XXVII** (e.g., the sphere in Figure 1.7) through self assembly processes. Other examples of such supramolecular structures include host-guest chemistry and linkage with organic nitriles) as well as 1-, 2- or 3- dimensional polymers. In some cases redox reactions were observed during the formation of the above mentioned supramolecular aggregates, giving products with the η^4 coordination mode of the *cyclo*-P_5 ligand , of different geometries in comparison to the undistorted *cyclo*-P_5 moiety.[82]

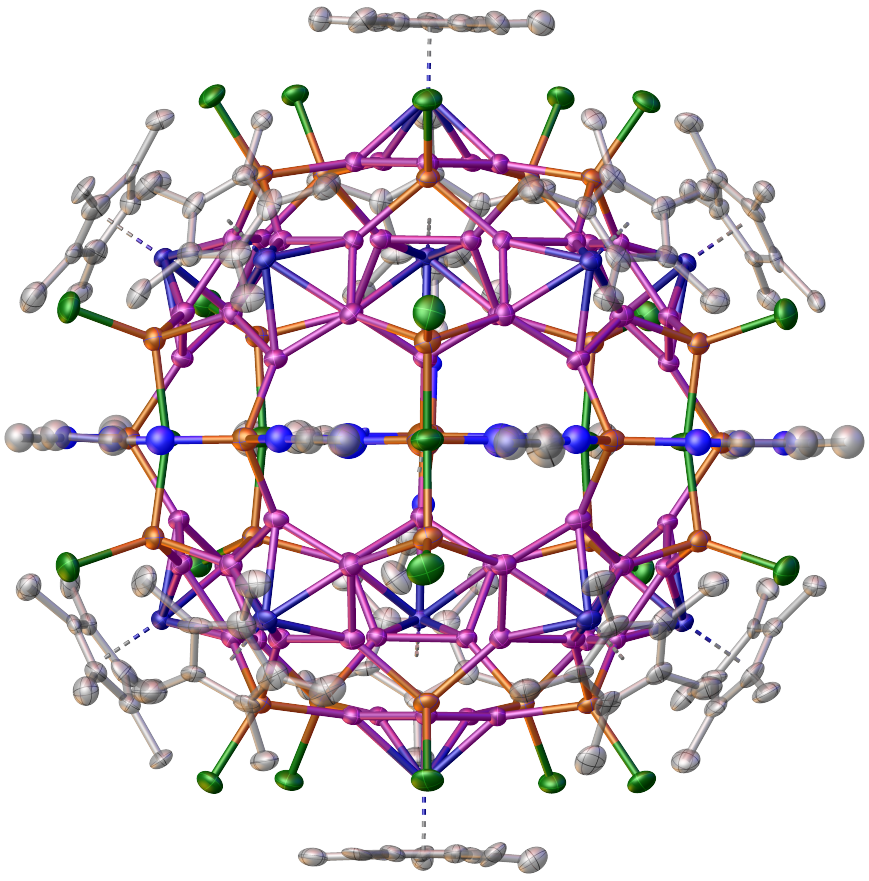
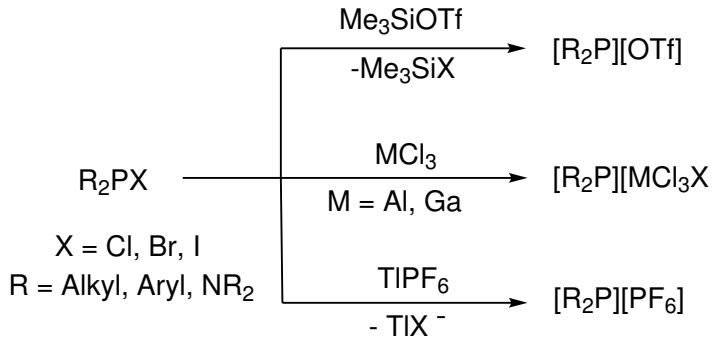


Figure 1.7: Example for a supramolecular aggregate of **XXVII**.[83]

1.5 Reactivity of phosphenium ions



Scheme 1.10: Preparation of phosphenium ions by halogen abstraction.

By abstraction of the halogen atom from a disubstituted halogenated phosphine, short lived phosphenium ions $[R_2P]^+$, which are isolobal to carbenes, are generated. Lewis acids such as $AlCl_3$ or $GaCl_3$, thallium salts or trimethylsilyltrifluoromethanesulfonate (Scheme 1.10) may serve as halogen abstractors.[91] Phosphenium ions are highly reactive but can, for example, be stabilized with amino substituents through the interaction of the free electron pairs of the nitrogen atoms with the unoccupied p-orbital on the phosphorus atom (Fig. 1.8).[91] These stabilised phosphenium ions, in contrast to the dialkyl- or diaryl-substituted ions, can be isolated and their structure determined by X-ray diffraction experiments.[92] For amino-substituted phosphenium ions, two other synthesis pathways exist: Protolysis of P-N single bonds by Brønstedt acids and coordination of strong Lewis acids at P-N double bonds.[93] The isolation of unstabilised phosphenium ions is usually not possible, as they immediately react further with halogen abstractors and halogenated phosphines (the respective starting materials for the generation of the phosphenium ions) to form phosphanylphosphonium ions.[94] For example, the reaction of two equivalents of diphenylchlorophosphine with $GaCl_3$ yields the phosphanylphosphonium salt $[Ph_2P-PPh_2Cl][GaCl_4]$ (**XXXI**),[95] whereby two reaction mechanisms are conceivable (Scheme 1.11): One is the generation of the phosphenium ion by abstraction of the chlorine atom by $GaCl_3$ and subsequent reaction of the $[Ph_2P]^+$ ion with one equivalent of Ph_2PCl (reaction path a in Scheme 1.11). The other possible reaction pathway proceeds via the zwitterionic species **XXXII** (Scheme 1.11), in which the free electron pair donates to the σ^*(P-Cl) orbital.

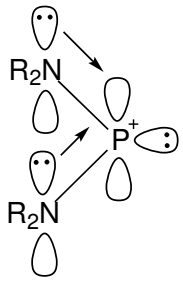
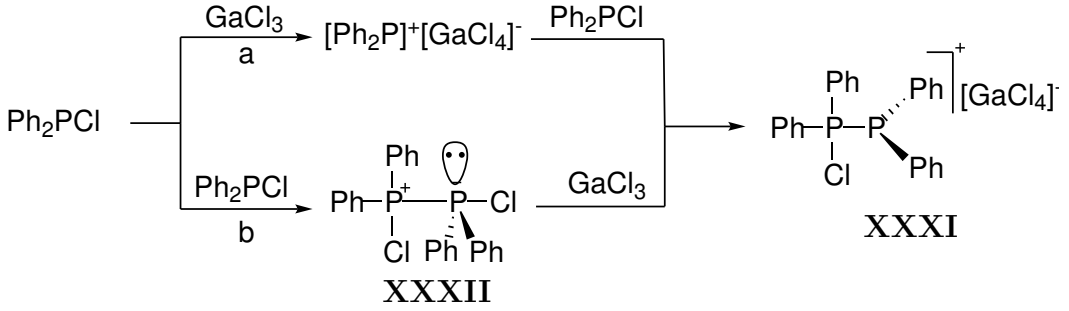


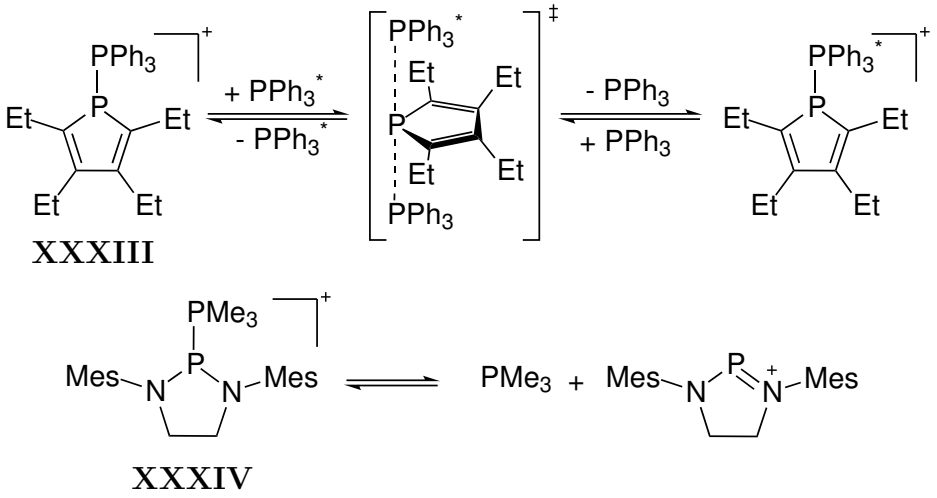
Figure 1.8: Stabilisation of diaminosubstituted phosphenium ions.



Scheme 1.11: Possible reaction mechanisms for the formation of the phosphanylphosphonium salt **XXXI**.[96]

Then, without generating a free phosphenium ion, the chlorine atom is abstracted by $GaCl_3$ (reaction path b in Scheme 1.11).[96]

If phosphanylphosphonium salts such as **XXXI** are reacted with phosphines of higher basicity, such as PPh_3, the corresponding chlorophosphine is displaced.[97] Studies of the exchange behaviour of PPh_3 on the phosphanylphosphonium salt **XXXIII** show second-order kinetics, suggesting a S_N2 mechanism (Scheme 1.12). This is also supported by quantum chemical calculations predicting a phosphoranide-like transition state.[98]

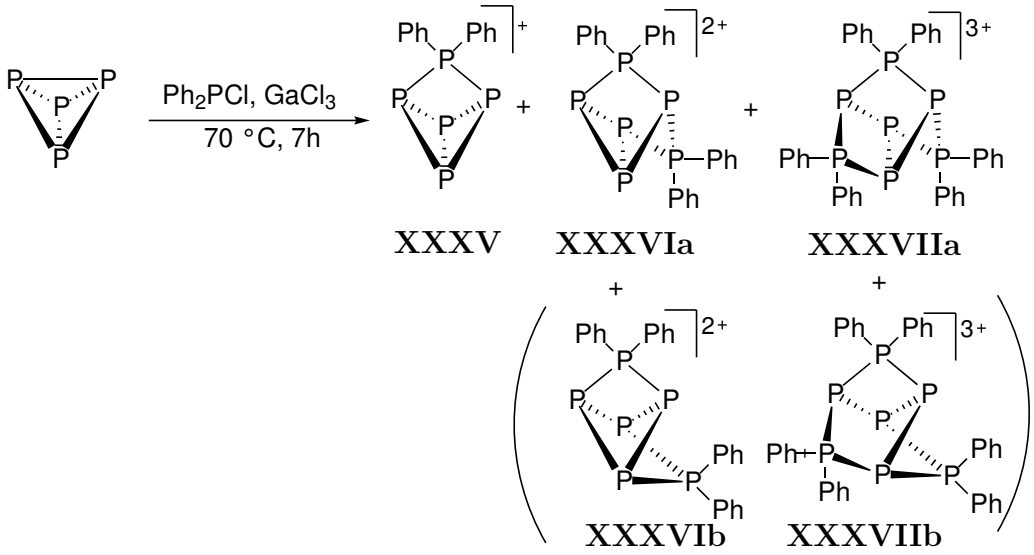


Scheme 1.12: S_N2-like exchange of PPh_3 at **XXXIII** (top, marking with $*$ at PPh_3 only for clarity) and S_N1-like exchange of PMe_3 at **XXXIV** (bottom).

In contrast, a more S_N1-like exchange of trimethylphosphine is reported for the phosphanylphosphonium salt of the NHC-like (NHC = N-heterocyclic carbene) diamino-substituted phosphenium ion $[P(NMesCH_2CH_2NMes)]^+$ with PMe_3 (**XXXIV**, Scheme 1.12).[99]

The abstraction of the halogen atom can be conducted both in solution and, in the case of $GaCl_3$, in a salt melt. For example, the phosphenium ion $[Ph_2P]^+$, described

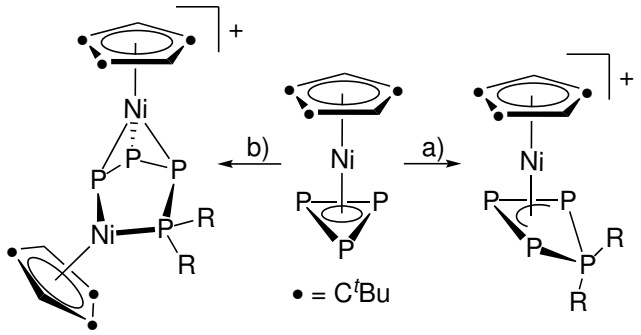
by *Weigand et al.* in 2008, generated by the reaction of diphenyl chlorophosphine with white phosphorus in a $GaCl_3$ melt, gradually inserts into the P_4 tetrahedron.[100] However, the reaction is not selective for the multiple insertion and a mixture of the cationic clusters $[Ph_2P_5]^+$ (**XXXV**), $[Ph_4P_6]^{2+}$ (**XXXVI**) and $[Ph_6P_7]^{3+}$ (**XXXVII**) is formed. While for the clusters **XXXVI** and **XXXVII** two isomers each are conceivable, only the isomers **XXXVIa** and **XXXVIIa** are observed (Scheme 1.13). The cluster **XXXV** represents another example of an activated P_4-tetrahedron with the structural motif **B** (section 1.2, page 15, Figure 1.3). Phosphenium ions were also used rather recently to synthesise novel catena-phosphines.[101,102]



Scheme 1.13: Insertion of the phosphenium ion $[Ph_2P]^+$ into the P_4 tetrahedron. Counterions of the type $[Ga_nCl_{3n+1}]^-$ (n = 1, 2, 3) are not shown for reasons of clarity.[100]

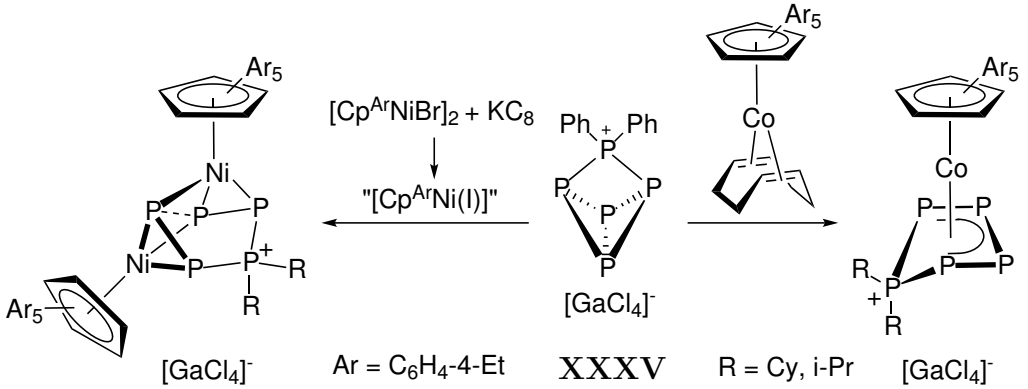
The analogues of the phosphenium ions and the phosphanylphosphonium salts also exist for the heavier homologues of phosphorus. The first compounds of the type $[R_2As-PR'_3]X$ (R = alkyl, aryl = R', X = halogen) are known since the late 1950s and are obtained by reacting the corresponding dialkylated halogen arsine with a tertiary phosphine. The arsinophosphonium salt $[Me_2As-PMe_3]I$ is stable towards hydrolysis and the salts $[R_2As-PR'_3][PF_6]$ are prepared in a two-phase system of dichloromethane and water.[103,104] Recent examples include the stibine-stabilised stibenium salt $[Me_2Sb-SbMe_3][(MeSbBr_3)_2]$ and the triphenylphosphine-stabilised diphenylpentelenium salts $[Ph_2E-PPh_3][PF_6]$ (E = As, Sb, Bi).[105,106] Some examples for the reactivity of arsenium and stibenium ions towards the pentaphosphaferrocene **XXVII** are given in section 1.4 of this chapter (*vide supra*) and the according literature.[79] The reactivity of phosphenium ions towards P_n ligand complexes was also explored in the re-

cent past. A ring expansion of the *cyclo*-P_3 ligand in $[Cp'''Ni(\eta^3\text{-}P_3)]$ is observed upon the insertion of *in situ* generated phosphenium ions.[107] The products of the insertion $[Cp'''Ni(\eta^3\text{-}P_4R_2)][X]$ ($R = Ph, Mes, Cy, Me$; $[X]^- = TEF, GaCl_4$; $TEF = [Al\text{-}(OC_4F_9)_4]^-$) show an envelope configuration for the resulting *cyclo*-P_4 ligands. For phosphenium ions generated from PBr_3 or 5-chloro-5H-dibenzophosphole, the resulting products undergo fragmentation to yield $[\{Cp'''Ni\}_2(\mu, \eta^{3:1:1}\text{-}RP_4R'_2)][X]$ ($R = R' = Br$ or $R = Cl$ and $R' = C_{12}H_8$) (Scheme 1.14).[107] The P_4 tetrahedron may as well first be



Scheme 1.14: Insertion of phosphenium ion $[R_2P]^+$ (R,R' = Ph, Mes, Cy, Me, $C_{12}H_8$; R = Ph, ^{t}Bu and R' = Cl) into $[Cp'''Ni(\eta^3\text{-}P_3)]$ (reaction a)). For phosphenium ions generated from PBr_3 and 5-chloro-5H-dibenzophosphole the fragmentation b) is observed.[107]

converted with phosphenium ions and then attacked by reactive transition metal fragments. This was shown by *Wolf et al.* by reaction of derivatives of **XXXV** (*vide supra*, Scheme 1.13) with $[Cp^{Ar}Co(cod)]$ (cod = 1,5-cyclooctadiene, $CpAr = C_5(C_6H_4\text{-}4\text{-}Et)_5$) or the transient "$Cp^{Ar}Ni(I)$" (generated from $[Cp^{Ar}Ni(\mu\text{-}Br)]_2$ and KC_8).[108] This results in *cyclo*-P_5 ligands with an envelope conformation in both cases, as depicted in Scheme 1.15.



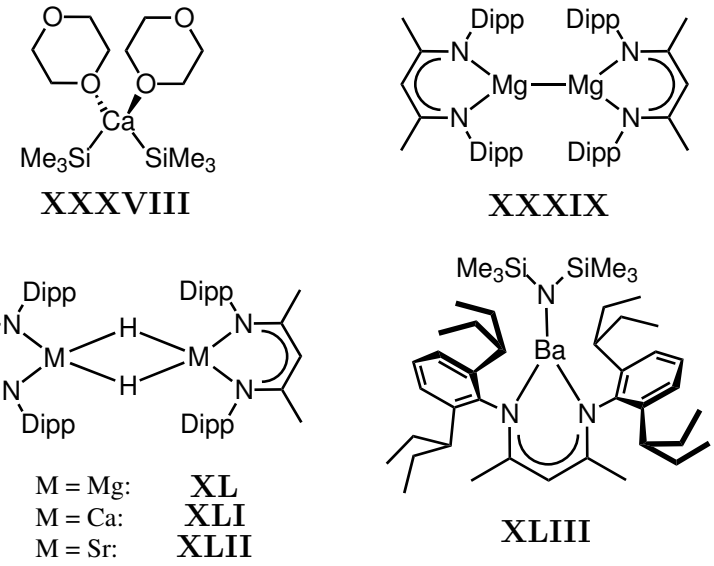
Scheme 1.15: Reaction of reactive transition metal complex fragments with **XXXV** to the cationic *cyclo*-P_5 ligand complexes $[(Cp^{Ar}Co)(\eta^4\text{-}P_5R_2)]$ and $[(Cp^{Ar}Ni)_2(\eta^{3:3}\text{-}P_5R_2)]$ ($Ar = C_6H_4\text{-}4\text{-}Et$, $R = Cy$, ^{i}Pr).[108]

1.6 Organometallic chemistry of group 2 metals

For a long time the chemistry of the heavy alkaline earth metals Ca, Sr and Ba was not as well explored as the chemistry of organo magnesium compounds. Due the diagonal relationship of Li and Mg in the periodic table of elements, organo magnesium compounds are similar to organo lithium compounds in their reactivity, solubility and stability in solution. The most important class of organometallic compounds of magnesium are grignard reagents, named after *Victor Grignard*. Although *Wanklyn* first reported the synthesis of diethyl magnesium in 1866, the synthesis of compounds of the general form of RMgX ($\mathrm{R} = \mathrm{alkyl\ or\ aryl}, \mathrm{X} = \mathrm{Cl, Br, I}$) is generally attributed to *Grignard*, who published the synthesis pathway to these reagents in 1901 and was honoured with the Nobel prize in chemistry for his discovery in 1912.[109,110] These reagents are easily prepared by reacting alkyl or aryl halogenides with magnesium turnings in diethyl ether, thf or other aprotic donor solvents. In some cases the reaction has to be activated by the addition of small amounts of methyliodide or by using a ultrasonic bath. In 1929 *Wilhelm Schlenk* first described the behaviour of grignard reagents in solution: The grignard reagents only exist in an equilibrium between $2\,\mathrm{RMgX}$ and $\mathrm{MgR_2} + \mathrm{MgX_2}$ in solution.[111] Addition of dioxane to the solutions shifts the equilibrium to the side of the respective dialkylmagnesium compounds, since insoluble coordination polymers of magnesiumdihalogenides and dioxane are formed.[112] Shortly after the first report of the grignard reagents, *Beckmann* reported the respective organometallic compounds for calcium to be formed at low temperatures.[113] The identity of the formed products could not be proven and only reactivity studies, which gave the same products as classic grignard reagents, were used as indirect proof that the organocalcium compounds in question were formed during the reaction. In the following 90 years after *Beckmann's* report in 1905, numerous research groups tried to synthesize the so called heavy-grignard reagents and fully characterize them, yet the results of these studies remain controversial.[114–119] In contrast to magnesium the grignard type reagents of Ca where challenging to synthesize due to the relatively low reactivity of Ca metal and the high reactivity of the respective organometallic compounds, leading to Wurz-type coupling reactions and cleavage of the ethers used as solvents. This was also the case for the dialkyl compounds such as calcium-, strontium- and barium-dimethyl. *Sanderson et al.* reported the synthesis of these compounds from MeI and powders of the respective alkaline earth metals in anhydrous pyridine in 1958, but the results could not be confirmed or reproduced by other research groups.[120–123] Only in 1991 *Lappert et al.* could isolate and fully characterize the first dialkyl calcium derivative $[(\mathrm{diox})_2\mathrm{Ca}\{\mathrm{CH}(\mathrm{SiMe_3})_2\}_2]$ (**XXXVIII**, Figure 1.9, *vide infra*).[124] This shows that bulky ligands are required in or-

der to stabilize the formed products and prevent the decomposition due to ether cleavage (of the solvent) or coupling reactions. In 2018 *Anwander et al.* could isolate dimethyl calcium aggregates such as $[(\mathrm{thf})_{10}\mathrm{Ca}_7(\mu_2\text{-}\mathrm{Me})_{10}(\mu_3\text{-}\mathrm{Me})_4]$ as well as the heavy group 2 metal grignard reagent $[(\mathrm{thf})_3\mathrm{Ca}(_2\text{-}\mathrm{Me})(\mathrm{I})]_2$ and fully characterize the compounds, including X-ray structure determinations.[125]

Another rather recent breakthrough in the chemistry of group 2 metals was the discovery of Mg(I) compounds, bearing a Mg-Mg bond by *Jones et al.* in 2007.[126] The compounds $[^{\mathrm{R}}\mathrm{BDIMg}]_2$ ($\mathrm{R} = \mathrm{Dipp}$ (**XXXIX**), Mes) require stabilisation and steric shielding by the bulky 1,3-bisketiminate ligand $^{\mathrm{Dipp}}\mathrm{BDI} = \{[2,6\text{-}^{\mathrm{i}}\mathrm{Pr}_2\mathrm{C}_6\mathrm{H}_3\mathrm{NCMe}]_2\mathrm{CH}\}^-$ (Figure 1.9). These Mg(I) compounds have proven to be powerful reducing agents.[127,128] Additionally the alkyl substituted derivatives $[^{\mathrm{Dipp}}\mathrm{BDIMgR}]_\mathrm{n}$ ($\mathrm{R} = {}^t\mathrm{Bu}(\mathrm{n}=1), \mathrm{Me}$ $(\mathrm{n}=2), n\text{-}\mathrm{Bu}(\mathrm{n}=1), {}^i\mathrm{Pr}(\mathrm{n}=1)$) and the hydride $[^{\mathrm{Dipp}}\mathrm{BDIMgH}]_2$ (**XL**) are known. For the heavier group two metals Ca and Sr, only the respective organo-substituted-



XXXVIII **XXXIX**

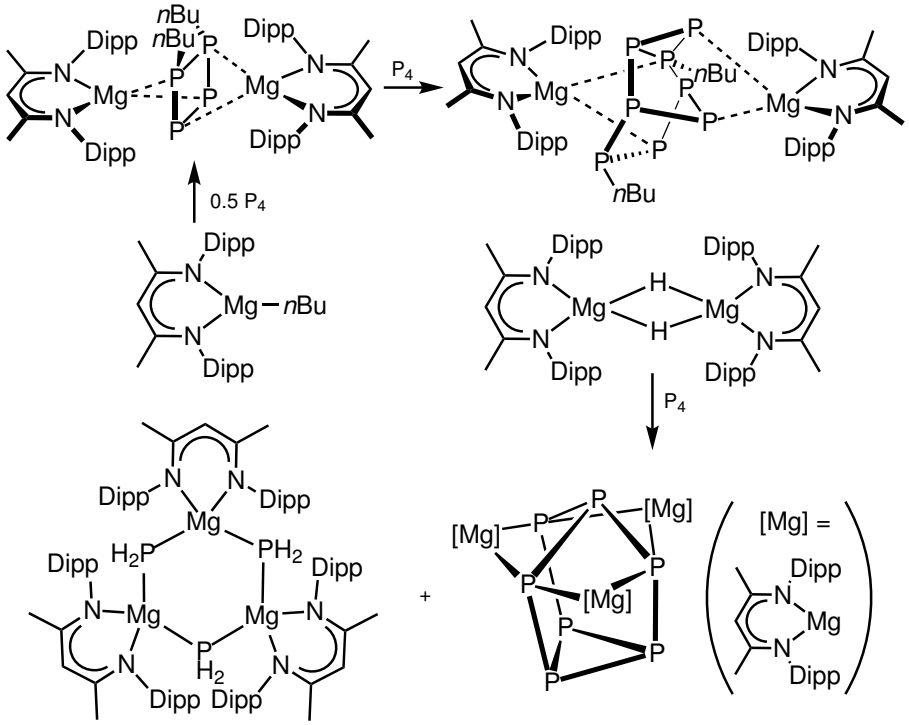
M = Mg: **XL**
M = Ca: **XLI**
M = Sr: **XLII**

XLIII

Figure 1.9: Some examples of earth alkaline metal compounds, stabilized by bulky and electron donating ligands.

or hydride- compounds (Figure 1.9) were isolated so far and no attempts to synthesize the according Ca(I) or Sr(I) dimeric compounds were successful so far. More over, $[^{\mathrm{Dipp}}\mathrm{BDICaH}]_2$ (**XLI**) and $[^{\mathrm{DNPP}}\mathrm{BDISrH}]_2$ (**XLII**, DNPP = 1,3-di(pentan-3-yl)-benzene) can also act as extremely powerful reducing agents.[129,130] The increased steric bulk of the DNPP substituents on the bisketiminate ligand is required for additional steric shielding due to the high reactivity and accompanying instability of Sr compounds. As the reactivity of group 2 metal compounds increases with the heavier metals, the according Ba compounds are not stable at temperatures above 0 °C , so more sterically demanding ligands such as $^{\mathrm{DNPP}}\mathrm{BDI}$ as well as more electron donating

substituents such as $-\mathrm{N(SiMe_3)_2}$ are required to yield stable compounds as exemplified in $[^{\mathrm{DNPP}}\mathrm{BDIBaN(SiMe_3)_2}]$ (**XLIII**, Figure 1.9).[131] It should also be mentioned, that the hydride complexes **XLI** and **XLII** are suitable for catalytic hydrogenation of benzene or hydrophosphinations.[129,130]



Scheme 1.16: Synthesis of the first molecular polyphosphides of a group 2 element observed in solution by *Hill et al.*.[132]

The chemistry of polypnictogenides of the group 2 metals is still relatively unexplored. Most examples of phosphides of Mg, Ca, Sr or Ba are following the same principles of steric shielding mentioned above.[133–136] Most examples of polyphosphides of these metals are only known in the solid state, since compounds of earth alkaline metals and phosphides in oxidation state III tend to be barely soluble in most organic solvents (only Zintl ions, soluble in liquid ammonia are known).[137–148] Using the highly soluble Mg(I) compound **XXXIX** and its organo substituted derivatives, it was recently possible to observe the first polyphosphides of magnesium in solution: By reaction of white phosphorus with two equivalents of $[^{\mathrm{Dipp}}\mathrm{BDIMg}\text{-}^{n}\mathrm{Bu}]$ the nonplanar $[^{n}\mathrm{Bu_2P_4}]^{2-}$ dianion in $[\{^{\mathrm{Dipp}}\mathrm{BDIMg}\}_2(\mu,\eta^{1:1:1:1}\text{-}^{n}\mathrm{Bu_2P_4})]$ is formed (Scheme 1.16).[132] This compound forms $[\{^{\mathrm{Dipp}}\mathrm{BDIMg}\}_2(\mu,\eta^{1:1:1:1}\text{-}^{n}\mathrm{Bu_2P_8})]$ by reaction with an additional equivalent of white phosphorus. If the magnesium hydride dimer **XL** is used as a reducing agent the formation of the trimeric primary magnesium phosphide $[(^{\mathrm{Dipp}}\mathrm{BDIMg})(\mu\text{-}\mathrm{PH_2})]_3$ and $[\{^{\mathrm{Dipp}}\mathrm{BDIMg}\}_3(\mu_3,\eta^{1:1:1:1:1:1}\text{-}\mathrm{P_7}]$, a polyphosphide with the typical nortricyclane motif of a $[\mathrm{P_7}]^{3-}$ Zintl ion cage, are formed (Scheme 1.16).

Chapter 2

Research objectives

Reacting $\mathrm{P_n}$ ligand complexes with phosphorus nucleophiles or electrophiles gave novel functionalized *cyclo*-$\mathrm{P_4}$ and *cyclo*-$\mathrm{P_5}$ ligands in the past. The $\mathrm{P_n}$ ligand iron complexes $[\{\mathrm{Cp'''Fe(CO)_2}\}_2(\mu,\eta^{1:1}\text{-}\mathrm{P_4})]$ and $[\mathrm{Cp^*Fe}(\eta^5\text{-}\mathrm{P_5})]$ were reacted so far with electrophilic transition metal fragments or main group electrophiles to yield novel coordination compounds. Except for $[\mathrm{Cp'''Ni}(\eta^3\text{-}\mathrm{P_3})]$ no $\mathrm{P_n}$ ligand complex was functionalized by the attack of *in situ* generated phosphenium ions so far. The attack of carbon nucleophiles on pentaphosphaferrocene $[\mathrm{Cp^*Fe}(\eta^5\text{-}\mathrm{P_5})]$ and the quenching of the resulting products with carbon electrophiles was investigated and produced an improved synthetic pathway to asymmetrically substituted phosphines. During these investigations first observations of a possible 1,2 functionalization of the *cyclo*-$\mathrm{P_5}$ ligand were made. Thus, the following objectives arise for this work :

- Investigation of the reactivity of *in situ* generated phosphenium- and arsenium ions towards $[\{\mathrm{Cp'''Fe(CO)_2}\}_2(\mu,\eta^{1:1}\text{-}\mathrm{P_4})]$.
- *In situ* generation of the anionic complexes $[\mathrm{Cp^*Fe}(\eta^4\text{-}\mathrm{P_5R})]^-$ from $[\mathrm{Cp^*Fe}(\eta^5\text{-}\mathrm{P_5})]$ and organo lithium compounds and investigation of their reactivity towards chloro-phosphines in order to synthesize highly functionalized phosphorus ligands with novel structural motifs. The characteristics of the resulting products and the possibility of further functionalisation of these complexes are to be explored in more detail.
- Targeted synthesis of 1,2 functionalized *cyclo*-$\mathrm{P_5}$ moieties by functionalisation of $[\mathrm{Cp^*Fe}(\eta^5\text{-}\mathrm{P_5})]$ and exploring the limit of the maximum number of functionalized phosphorus atoms in this ligand.

The reactivity of group 2 metal reagents towards poly pnictogen compounds in classic, carbon based solvents is, with the exception of one report, still unexplored. The Mg(I) dimer $[^{\mathrm{Dipp}}\mathrm{BDIMg}]_2$ has proven to be a powerful reducing agent. The synthesis of the organometallic compounds of the higher homologues of Mg is challenging due to their sensitivity and reactivity as well as activation and handling of the metals in the first place. This results in the following synthetic challenges for this work:

- Studies on the reactivity of $[^{\mathrm{Dipp}}\mathrm{BDIMg}]_2$ and $[^{\mathrm{Dipp}}\mathrm{BDIMgCH_3}]_2$ towards the complex $[\mathrm{Cp^*Fe}(\eta^5\text{-}\mathrm{P_5})]$
- Synthesis of first group 2 element polypnictogenides in carbon based solvents without the use of any stabilizing, sterically demanding ligands on the metal by utilizing the anthracenides of the heavy group two metals. For these investigations a new synthetic pathway to the anthracene compounds of the respective metals has to be found.

Chapter 3

Insertion of Phosphenium Ions into a Bicyclo[1.1.0]Tetraphosphabutane Iron Complex

Results of this chapter have already been published in: Insertion of Phosphenium Ions into a Bicyclo[1.1.0]Tetraphosphabutane Iron Complex by Martin Weber, Gábor Balázs, Alexander V. Virovets, Eugenia Peresypkina and Manfred Scheer in *Molecules* **2021**, *26*, 3920 and belongs to the special issue "Recent Advances in Phosphorus Chemistry".[149] The open access article was published under the creative commons license and the work was supported by the Deutsche Forschungsgemeinschaft within the project Sche 384/36-1.
Contributions: Conceptualization: M.W., G.B. and M.S.; methodology, M.W.; software, M.W. and G.B.; validation, M.W. and G.B.; formal analysis, M.W., A.V.V. and E.P.; investigation, M.W.; resources, M.S.; data curation, M.W.; writing-original draft preparation, M.W.; writing-review and editing, M.W., G.B., A.V.V., E.P. and M.S.; visualization, M.W.; supervision, M.S. and G.B.; project administration, M.S.; funding acquisition, M.S. All authors have read and agreed to the published version of the manuscript. The numbering of figures, schemes, tables, references and compounds have been changed respective to the original publication for a uniform appearance of this thesis.

Abstract

By reacting $[\{Cp'''Fe(CO)_2\}_2(\mu,\eta^{1:1}\text{-}P_4)]$ (**VIIIa**) with *in situ* generated phosphenium ions $[Ph_2P][A]$ ($[A]^- = [OTf]^- = [O_3SCF_3]^-, [PF_6]^-$), a mixture of two main products of the composition $[Cp'''Fe(CO)_2{}_2(\mu,\eta^{1:1}\text{-}P_5(C_6H_5)_2)][PF_6]$ (**2a** and **3a**) could

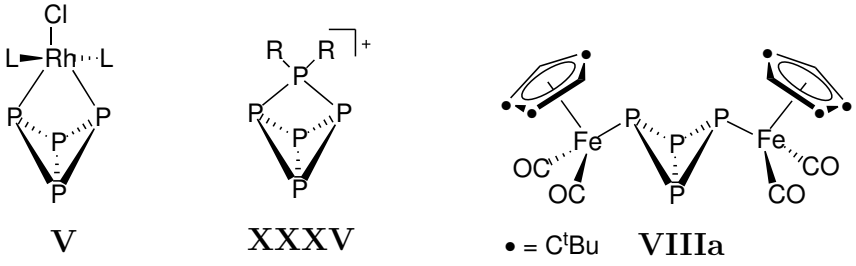
be identified by extensive ^{31}P NMR spectroscopic studies at 193 K. Compound **3a** was also characterized by X-ray diffraction analysis, showing the rarely observed bicyclo[2.1.0]pentaphosphapentane unit. At room temperature, the novel compound $[Cp'''Fe(\mu,\eta^{4:1}\text{-}P_5Ph_2)Cp'''(CO)_2Fe][PF_6]$ (**1**) is formed by decarbonylation. Reacting **VIIIa** with *in situ* generated diphenyl arsenium ions gives short-lived intermediates at 193 K which disproportionate at room temperature into tetraphenyldiarsine and $[Cp'''Fe(CO)_{2_4}(\mu_4,\eta^{1:1:1:1}\text{-}P_8)][OTf]_2$ (**4**) containing a tetracyclo[$3.3.0.0^{2,7}.0^{3,6}$]octaphosphaoctane ligand.

3.1 Introduction

The activation of small molecules like N_2 or P_4 with reactive transition metal fragments or main group reactants is one of the most important aspects of modern chemistry. More energy-efficient reaction pathways leading, by higher atom economy, to compounds containing nitrogen or phosphorus seem more tangible with every new insight gained into the activation pathways.[23–27]

The opening of one P-P bond of the P_4 tetrahedron leading to the tetraphosphabicyclo[1.1.0] unit (also called the butterfly unit) is one of the first activation steps for P_4 and is well-studied for reactive transition metal compounds. The activation leads to a cage-like compound by insertion of a metal fragment as observed for example in $[L_2RhCl(\eta^{1:1}\text{-}P_4)]$ ($L = PPh_3$, $P(m\text{-tol})_3$, $P(p\text{-tol})_3$, $AsPh_3$) (**V**), the first reported polyphosphorus ligand complex (Scheme 3.1).[51] Also, a $\mu,\eta^{1:1}$-coordination mode can be observed, e.g., in the complex $[\{Cp'''Fe(CO)_2\}_2(\mu,\eta^{1:1}\text{-}P_4)]$ ($Cp''' = C_5H_2(C(CH_3)_3)$) (**VIIIa**), synthesized by the reaction of $[Cp'''Fe(CO)_2]_2$ with white phosphorus.[58,150] Since the highest occupied molecular orbital (HOMO) in **VIIIa** is localized on the "wing tip" phosphorus atoms of the butterfly unit, we have investigated the reactivity towards Lewis-acidic transition metal fragments[68,151–153] or the coinage metal salts such as Cu(I), Ag(I) and Au(I)[153–155]. In most of the cases, the coordination of the "wing tip" phosphorus atoms of the intact butterfly to the electron-poor metal centre is observed, but also a rearrangement to a *cyclo*-P_4 unit. The complex $[\{Cp^*Cr(CO)_3\}_2(\mu,\eta^{1:1}\text{-}P_4)](Cp^* = C_5(CH_3)_5)$, which is similar to **VIIIa**, isomerizes in reactions with $M(CO)_5$ ($M = Cr, Mo$) entities, while fragmentation occurs in reactions with N-heterocyclic carbenes.[156,157]

A prominent example for main group electrophiles which have been used in the activation of P_4 are phosphenium cations $[R_2P]^+$ (R = alkyl or aryl) which, in general, are too reactive to be isolated, but can be generated *in situ* by halogen abstraction



V **XXXV** **VIIIa**

Scheme 3.1: Selected compounds with a tetraphosphabicyclo[1.1.0] motif.[51,58,100]

from halogenophosphines with abstractors, such as, for instance $GaCl_3$, silver or thallium salts in the presence of a suitable substrate to react with. This way new cationic polyphosphorus compounds with catena[94–97,101,102], ring[96,158,159] or cage[96,100,160] units could be synthesized, in particular by *Burford* and *Weigand*, who observed the stepwise opening of the P-P bonds of the P_4 tetrahedron by insertion of $[R_2P]^+$ in a solvent-free reaction set up to the cationic cage compounds [$[Ph_2P_5]^+$ (**XXXV**), $[Ph_4P_6]^{2+}$ and $[Ph_6P_7]^{3+}$.[100]

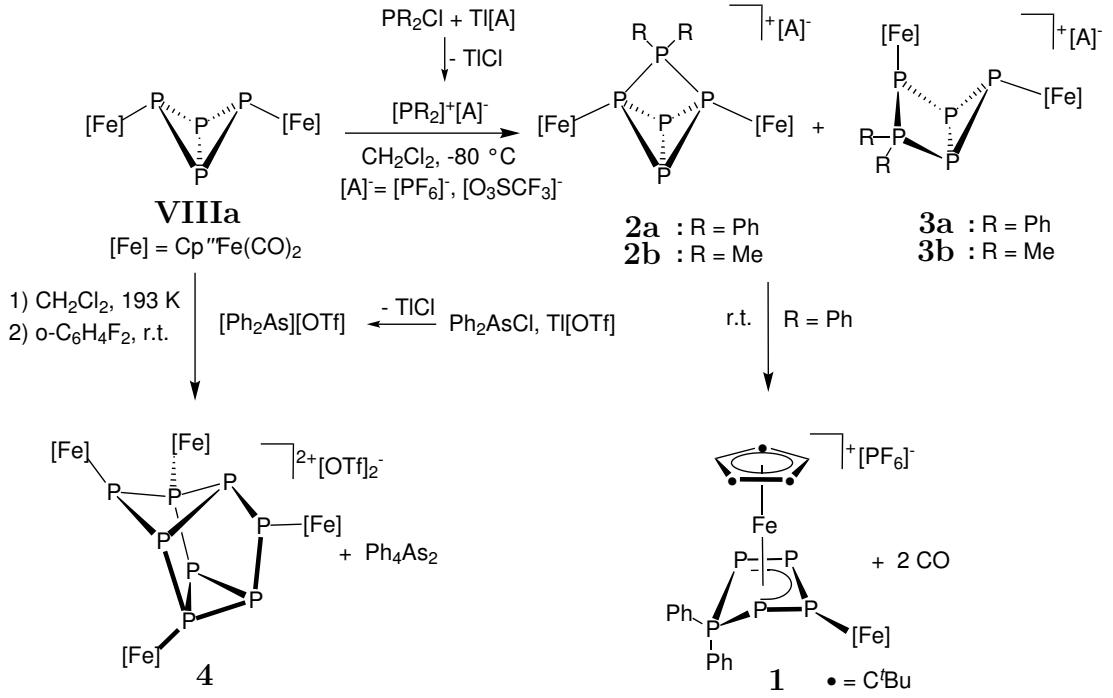
Besides P_4, the tetrahedral complex $[Cp'''Ni(\eta^3\text{-}P_3)]$ also reacts with phosphenium cations by insertion into one P-P bond.[78] In contrast, $[Cp^*Fe(\eta^5\text{-}P_5)]$ (**XXVII**) reacts with main group electrophiles, such as, for instance, H^+ or CH_3^+ with the formation of a P-E bond.[107] Our preliminary studies have shown that **VIIIa** reacts with HBF_4, leading to the protonation of one of the wing tip phosphorus atoms.[154] Therefore, the question arises as to whether the reaction of **VIIIa** with phosphenium cations leads to a simple coordination as observed for some transition metal fragments leading to type **V** complexes or to the insertion into one of the P-P bonds as reported for white phosphorus or $[Cp'''Ni(\eta^3\text{-}P_3)]$, respectively. Furthermore, cations of the type $[R_2E]^+$ are not only known for phosphorus but also for the heavier homologue arsenic[103,104,161], yet no studies on the reactivity towards polyphosphorus compounds or white phosphorus are known. Herein, we report on the reactivity of **VIIIa** towards in situ generated phosphenium and arsenium cations $[R_2E]^+$ (E = P, As) leading to short-lived insertion and coordination products at low temperatures, which react further at room temperature to a *cyclo*-P5 unit in the case of E = P and to a compound featuring the rarely observed tetracyclo[3.3.0.0^{2,7}.0^{3,6}]octaphosphaoctane entity in the case of E = As.

3.2 Results

3.2.1 Reactions of VIIIa with $[(C_6H_5)_2P]^+[A]^-$ at room temperature

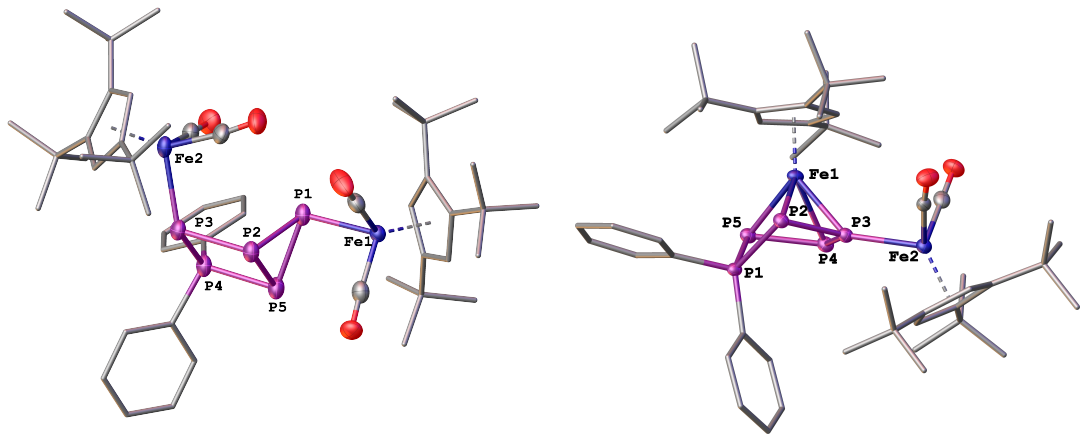
The complex $[\{Cp'''Fe(CO)_2\}_2(\mu,\eta^{1:1}\text{-}P_4)]$ (**VIIIa**) readily reacts with *in situ* generated diphenyl phosphenium salts generated from Ph_2PCl and $Tl[A]$ ($[A]^- = [OTf]^-$, $[PF_6]^-$ ($OTf = O_3SCF_3$)) in ortho-difluorobenzene (o-DFB) at room temperature. In the $^{31}P\{^1H\}$ NMR spectrum of the reaction solution of $[\{Cp'''Fe(CO)_2\}_2(\mu,\eta^{1:1}\text{-}P_4)]$ (**VIIIa**) with Ph_2PCl and Tl[PF6], two sets of signals are visible for two main products - a well-resolved ADEMX spin system[162] corresponding to the *cyclo*-P5 unit of the novel compound $[Cp'''Fe(\mu,\eta^{4:1}\text{-}P_5Ph_2)Cp'''(CO)_2Fe][PF_6]$ (**1**, Scheme 3.2) and a set of broad signals with one resolved multiplet. This set of signals cannot be definitely attributed to a specific compound, but very probably contains a phosphorus core similar to that of **2a**. After removal of the solvent from the reaction mixture and extraction of the residue with a mixture of toluene and diethylether, some tiny needles of **1** could be obtained, very weakly scattering in the routine single crystal X-ray diffraction experiment but suitable for the diffraction study using high-flux synchrotron radiation (see Figure 3.1b, crystallographic details in the supporting information). The remaining red oil was dissolved in a mixture of o-DFB and pentane. By storing the saturated solution at -30°C, a few red crystals of $[\{Cp'''Fe(CO)_2\}_2(\mu,\eta^{1:1}\text{-}P_5(C_6H_5)_2)][PF_6]$ (**3a**), suitable for X-ray diffraction analysis, could be obtained (Figure 3.25a). All attempts to isolate **2a** failed, due to its high instability and presumably to its rearrangement to **3a**. The presumed rearrangement of **2a** to **3a** is also supported by DFT calculations (*vide infra*).

In order to identify the intermediates which are formed in the reaction of **VIIIa** with $[R_2P]^+$ and to further investigate the nature of the dynamic behaviour in solution, $^{31}P\{^1H\}$ NMR spectroscopic studies were performed at low temperatures. For this purpose, corresponding reaction samples were prepared in dichloromethane at 193 K and kept at this temperature, without allowing them to warm up. The reaction solutions of **VIIIa** with $[Ph_2P][OTf]$ showed two independent spin systems, ADMVX and ADMQX, with one multiplet of each spin system overlying. The connectivity of the phosphorus cores of the two spin systems could be determined by ^{31}P-^{31}P COSY NMR (homonuclear correlation spectroscopy) experiments and iterative simulations (Figure 3.2 and supplementary materials). The ADMVX spin system can be attributed to **3a**, while the ADMQX spin system can very likely be attributed to **2a**. The ratio of **2a**:**3a** at 193 K was determined to be 5:2. Upon warming the sample, the signals



Scheme 3.2: Reaction of **VIIIa** with in situ generated pnictogenium ions yielding the compounds mentioned in this paper.

of both spin systems broaden and collapse into each other at 253 K to give only one set of broad signals (four broad ones and one relatively sharp one, Figure 3.3). A further increase of the temperature only leads to a further broadening of the signals. Finally, at 300 K, four broad signals and one well-resolved one are detected in the $^{31}P\{^{1}H\}$ NMR spectrum. These findings show that **2a** and **3a** are formed in the first step of the reaction of **VIIIa** with $[Ph_2P]^+$, at temperatures above 253 K, however, they are in an equilibrium. The fact that one of the signals remains unaffected by the broadening within the whole temperature range, which we tentatively attribute to the Ph_2P unit in **2a**, indicates that, at room temperature, **2a** might be the major component and that the Ph_2P unit is interchanged between the two wing-tip phosphorus atoms in a fast process on the NMR time scale. A similar behaviour was observed for $[(Cp^{Ar}Ni)_2(\eta^{3:3}\text{-}P_5R_2)][GaCl_4](Cp^{Ar} = C_5(C_6H_4\text{-}4\text{-}Et)_5, R = {}^{i}Pr$ and 2,4,6-$Me_3C_6H_2)$[108] as well as for $[Cp'''Fe(CO)_2{}_2(\mu, \eta^{1:1}\text{-}P_4H)]^+$ - the protonated complex of **VIIIa**[154]. According to DFT calculations in **2a**, the Ph_2P unit binds only to one wing-tip phosphorus atom (*vide infra*). Increasing the temperature above 300 K leads to a rapid decomposition in dichloromethane. Unfortunately, o-DFB is not suitable for performing the experiments at 193 K due to its relatively high point of solidification (239 K).



a b

Figure 3.1: Cationic parts of the molecular structures of **3a** (a) and **1** (b), respectively, in the solid state. Hydrogen atoms, solvent molecules and counter ions are omitted for more clarity. Selected bond lengths in **3a** (for complete geometric data see the ESI): Fe1-P1 2.3162(12), Fe2-P3 2.3004(15), P1-P5 2.2010(18), P2-P1 2.1971(15), P2-P5 2.2546(17), P3-P2 2.2305(15), P3-P4 2.2128(17), P4-P5 2.1974(16). Selected bond lengths in **1** (for complete geometric data see the ESI): Fe1-P3 2.2925(7), Fe1-P5 2.3422(7), Fe1-P4 2.3517(8), Fe1-P2 2.3610(8), Fe2-P3 2.2567(7), P1-P5 2.1590(9), P1-P2 2.1761(9), P2-P3 2.1293(9), P3-P4 2.1337(9), P4-P5 2.1322(10)

By the reaction of $[Me_2P][OTf]$, generated *in situ* from Me_2PCl and Tl[OTF], with **VIIIa** at 193 K in dichloromethane, the two products **2b** and **3b** could be identified in the $^{31}P\{^1H\}$ NMR spectrum at 193 K. Compound **2b** reveals an ADMQX and **3b** an ABMWX spin system. The phosphorus cores of both these compounds could be determined by iterative simulation as well as by ^{31}P-^{31}P COSY NMR experiments, showing the same connectivity as **2a** and **3a**. By warming the NMR sample to room temperature for the time of one measurement and subsequent cooling to 193 K, besides signs of decomposition, the relative ratio of the two products in solution changes in favour of the insertion product **3b** (**3b**:**2b** = 4:1 before r.t., 10:1 after). This suggests that either **2b** is less stable than **3b** and decomposes faster or that both compounds exist in a dynamic equilibrium at room temperature and the formation of **3b** is favoured as being the thermodynamically more stable product. For the structurally similar products **2a** and **3a**, we assume a similar behaviour (*vide supra*; cf. Supplementary Materials).

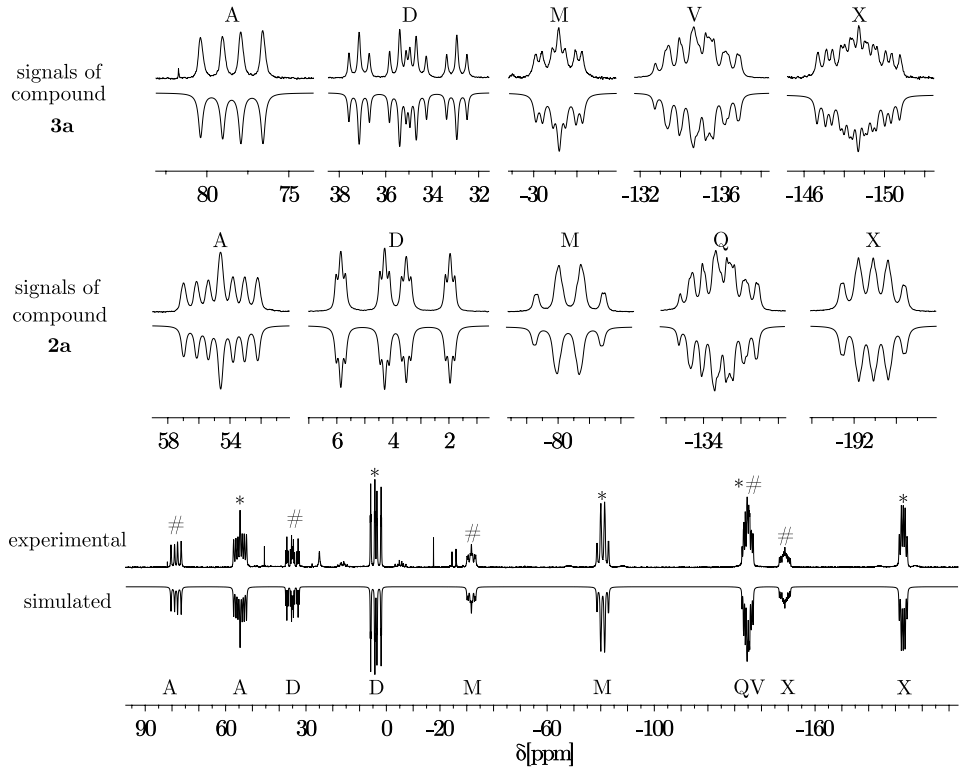


Figure 3.2: Experimental and simulated $^{31}P\{^1H\}$-NMR-spectrum at 193 K of compounds **2a** and **3a** ($* =$**2a**, $\# =$**3a**). The multiplet Q/V is the result of two overlapping multiplets from the two different spin systems.

3.2.2 Reactions of VIIIa with $[(C_6H_5)_2As]^+[OTf]^-$

If **VIIIa** is reacted with $[Ph_2As][OTf]$ at 193 K, generated *in situ* from Ph_2AsCl and $Tl[OTf]$ in dichloromethane, two compounds showing ABX_2 spin systems at room temperature and an ABWX for one of the compounds at 193 K are observed in the $^{31}P\{^1H\}$ NMR spectrum of the reaction solution. Iterative simulation enabled the determination of the connectivity of the phosphorus cores. However, the structural motifs of these compounds could not be undoubtedly determined, since the connectivity of the Ph_2As fragment could not be ascertained from the NMR data. Due to their instability as well as their high solubility, these compounds could not be isolated despite several attempts. The reaction solutions in dichloromethane are only stable for a few hours at room temperature. If the reaction is performed at 193 K, the dichloromethane removed at -60 °C and the resulting dark red oil is redissolved in a mixture of o-DFB and *n*-pentane (1:1), single crystals of the complex $[\{Cp'''Fe(CO)_2\}_4(\mu_4\eta^{1:1:1:1}\text{-}P_8)][OTf]_2$ (**4**) can be obtained (Scheme 3.2 and Figure 3.26). Compound **4** contains a tetracyclo $[3.3.0.0^{2,7}.0^{3,6}]$-octaphosphaoctane unit which is rarely observed and represents an unexpected isomer for a P_8 core. The only other compound reported so far contain-

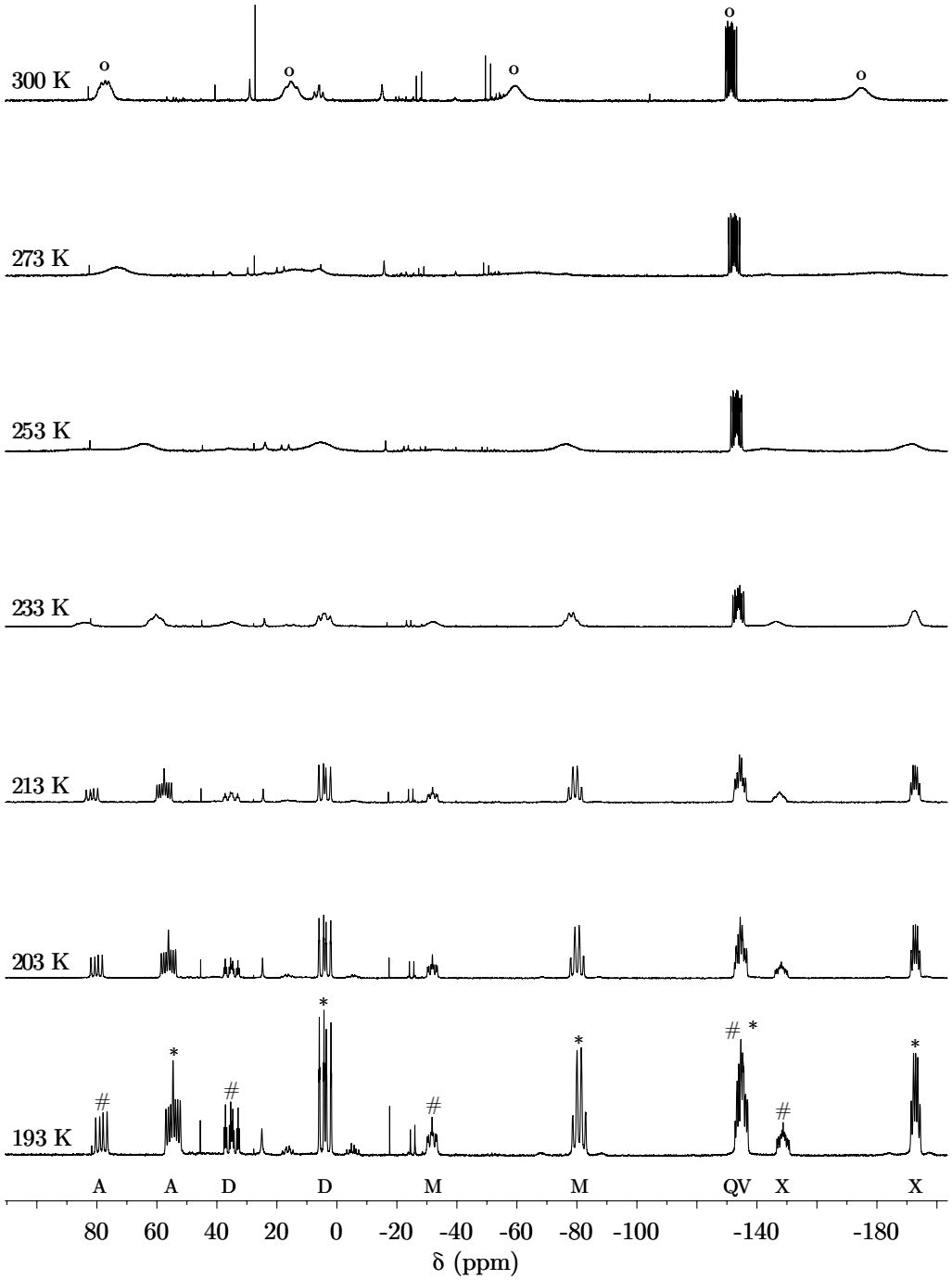


Figure 3.3: $^{31}P\{^{1}H\}$-VT-NMR-spectrum in CD_2Cl_2 from the reaction of **VIII** with $[Ph_2P][OTf]$ at 193 K ($*$ =**2a**,#=**3** o = broad signals at r.t.).

ing a similar P_8 core is $[(DDP)GaBr_2P_8]$ (DDP = (2,6-diisopropylphenyl)(4-((2,6-diisopropylphenyl)imino)pent-2-en-2-yl)amide).[163] The most common P_8 motif is the

realgar-type motif which can also be viewed as a subunit of Hittorf's phosphorus and considered as an important building block of hierarchical structures of elemental phosphorus.[164–171]

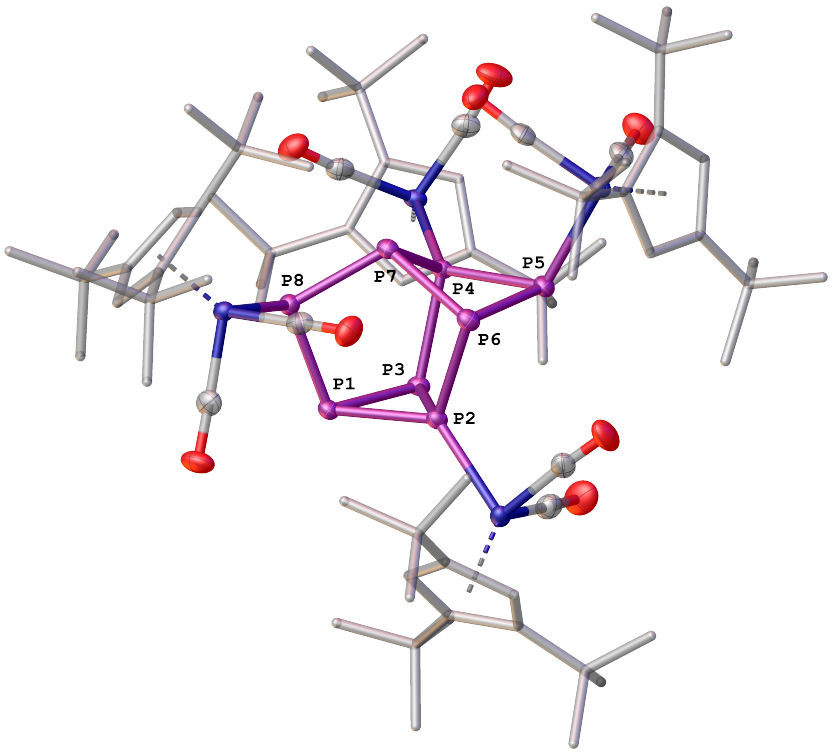
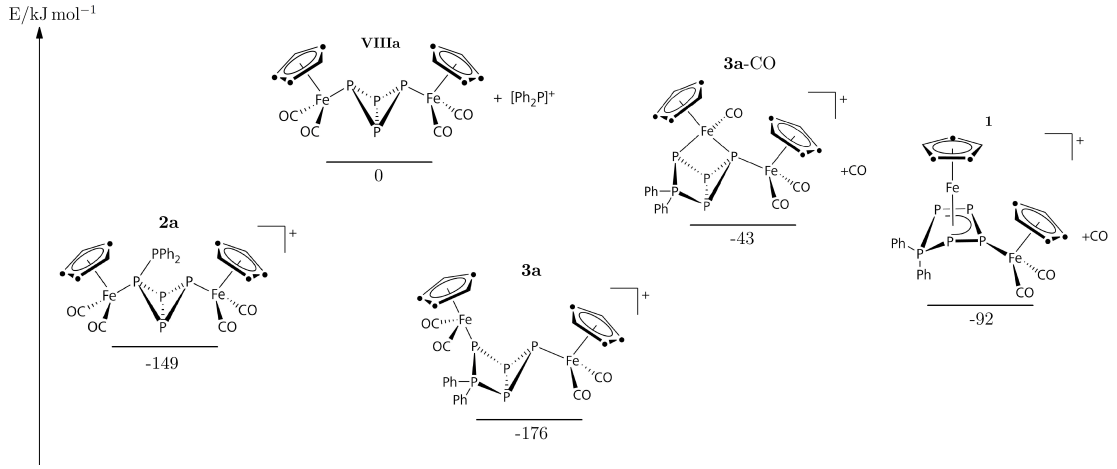


Figure 3.4: Cationic part of the molecular structure of **4** in the solid state. Hydrogen atoms, solvent molecules and counter ions are omitted for more clarity. Selected bond lengths and angles (for complete geometric data see the ESI): Fe1-P8 2.2753(5), Fe2-P2 2.2470(5), Fe3-P4 2.2585(5), Fe4-P5 2.3044(6), P2-P3 2.2115(7), P2-P1 2.1916(7), P2-P6 2.2133(7), P4-P7 2.1890(7), P4-P3 2.2715(6), P4-P5 2.2756(7), P7-P8 2.1612(7), P7-P6 2.2062(7), P3-P1 2.2070(7), P8-P1 2.1926(7), P6-P5 2.2400(7).

3.3 Discussion

The structural motif in the crystal structure of **3a** is identical with the postulated bicyclo[2.1.0]pentaphosphapentane framework from the low temperature NMR experiments. This structural motif is the result of the insertion of $[Ph_2P]^+$ into one of the edge-P-P bonds in **VIIIa**. The P-P bond lengths in **3a** lie in the expected range of P-P single bonds (average P-P distance in **3a**: 2.215 Å) and compare well with the P-P bond lengths in **VIIIa**.[58] The three-membered ring built up by P1, P2 and P5 (Figure

3.25a) and the P2P3P4P5 four-membered ring are slightly distorted. The dihedral angle between the two rings is 99° and therefore **VIIIa** is considerably more folded than **3a** (fold angle 80°). The endo-$[Cp'''(CO)_2Fe]$ fragment of Fe2 as well as the fragment of Fe1, remaining in an exo-position as in **VIIIa**, show a slightly shorter Fe-P bond distance (Fe1-P1 = 2.3162(12) Å and Fe2-P3 = 2.3004(15) Å) compared with the Fe-P distances in **VIIIa** (Fe1-P1 is 2.355(3) Å and Fe2-P3 is 2.346(2) Å). To the best of our knowledge, the only other compound containing a bicyclo[2.1.0]pentaphosphapentane core crystallographically characterized is the supersilylphosphine$(^tBu_3Si)_3P_5$.[172]



Scheme 3.3: Relative energies of starting material **VIIIa** and $[PPh_2]^+$, **3a** and its decarbonylation to **1** on the BP86/def2(SV(P) level.

The formation of the *cyclo*-P_5 unit in **1** (Figure 3.25b) is the result of the twofold decarbonylation of one iron center (probably Fe2) in **3a** (Figure 3.25a) with a consequent opening of the P2-P6 bond. As an η^4-coordinating *cyclo*-P_5 ligand with one phosphorus atom bent out of the plane, the *cyclo*-P_5 unit in **1** can be compared to the known P_5 ligand in $[K(dme)K(dibenzo\text{-}[18]crown\text{-}6)][Cp^*Fe(\eta^4\text{-}P_5)]$[173], the functionalized P_5-ligands in $[Cp^*Fe(\eta^5\text{-}P_5)]$ (R = NMe_2, PH_2, CH_2SiMe_3)[174] or the cationic complex $[Cp^{Ar}Co(\eta^4\text{-}P_5R_2)][CaCl_4]$ ($Ar = C_5(C_6H_4\text{-}4\text{-}Et)_5$, R = ^{i}Pr and Cy)[108], but differs in bond lengths and angles due to its cationic character and its coordination of a second iron fragment. This is also the reason why **1** shows a complex ADEMX spin system for an asymmetric P_5 moiety of magnetically inequivalent phosphorus atoms instead of an AMM'XX' spin system as expected for the aforementioned compounds. In **1**, the bond distances of the Ph_2P fragment P1-P2 (2.1761(9) Å) and P1-P5 (2.1590(9) Å) to the rest of the P_5 moiety are noticeably different. The other bond distances are significantly shorter, with P2-P3 being the shortest one (2.1293(9) Å). Apart from the lack of symmetry, the bond lengths are also in agreement with the known *cyclo*-P_5

moieties mentioned above. According to the variable temperature NMR experiments, the reaction mixtures of **VIIIa** with phosphenium ions turned out to be stable only up to -60 °C in dichloromethane. By changing the solvent and the anion in order to find a reaction set up stable enough to obtain the single crystals of **3a** and **1**, respectively, the cationic parts of **2a** and **3a** were found to be more stable in o-DFB, using stronger coordinating counter ions such as $[\mathrm{OTf}]^-$. Using weakly coordinating anions such as $[\mathrm{TEF}]^-$ ($[\mathrm{TEF}]^- = [\mathrm{Al(OC(CF_3)_3)_4}]^-$)[175] leads to less stable reaction mixtures or to the formation of larger quantities of **1** in dichloromethane. Using o-DFB and the $[\mathrm{PF_6}]^-$ anion, the products were stable enough for crystallization, and small amounts of single crystals of **3a** and **1** suitable for X-ray diffraction studies could be obtained. This leads to the presumption that the cationic parts of **2a** and **3a** are not stable enough without being stabilized by a coordinating anion so that at least **3a** undergoes two consecutive decarbonylations to form **1** (Scheme 3.3). The decarbonylation of $[\mathrm{Cp''Fe(CO)_2}_2(\mu,\eta^{1:1}\text{-}\mathrm{P_4})]$ leading to $[\mathrm{Cp''Fe(CO)_2}(\mu,\eta^{1:2}\text{-}\mathrm{P_4})\mathrm{Cp''Fe(CO)}]$ was reported.[59] To clarify if **1** was formed via the decarbonylation of **3a**, DFT calculations at the BP86/def2-SVP level were performed. The results show that the attack of the phosphenium ion is exergonic, while the first decarbonylation of **3a** is noticeably endergonic. The fact that the second decarbonylation is exergonic would explain why the product from the first decarbonylation of **3a** could not be detected, except in the ESI-MS spectra of freshly prepared reaction solutions. At room temperature, the reaction energy released from the formation of **3a** was large enough to trigger the first decarbonylation to some degree, which would explain the formation of **1** at room temperature as well as the absence of **1** when reaction solutions are prepared at low temperatures and with stabilizing anions. It is uncertain so far whether **2a** undergoes a twofold decarbonylation at room temperature as well. Since $^{31}\mathrm{P}$ NMR experiments showed that **2b** and **3b** are not equally stable upon varying the temperature and because **2a** and **3a** exhibited a similar behaviour, DFT calculations were performed on **2a**. Their results also show that the cationic part in **3a** is 27 kJ/mol lower in energy than 2a.
The variation of chlorophosphine to dimethyl-, dicyclohexyl-, ditertbutyl- or bis-diethylamino-chlorophosphine or bisbenzochlorophosphole only leads to satisfactory results in the case of dimethylchlorophosphine giving similar structural motifs in the low-temperature $^{31}\mathrm{P}$ NMR experiments as the phenyl-substituted derivatives **2a** and **3a**. Compounds **2b** and **3a** show an even higher sensitivity than the phenyl-substituted compounds. The products formed by the coordination of $[\mathrm{Ph_2As}]^+$ to **VIIIa** are even less stable and convert to compound **4** and $\mathrm{Ph_4As_2}$. Compound **4** can formally be described as the dimer of the radical cation of **VIIIa**. As already mentioned, the $\mathrm{P_8}$ unit in **4** is a very rare example of a tetracyclo$[3.3.0.0^{2,7}.0^{3,6}]$octaphosphaoctane core, which had

only been observed in $[(\mathrm{DDP})\mathrm{GaBr_2P_8}]$.[163] The P-P bond lengths in the solid-state structure of **4** are very similar and vary from 2.1612(7) Å (P3-P8) to 2.2758(7) Å (P2-P1). The $^{31}\mathrm{P}$ NMR spectrum of **4** shows six broadened and two sharp multiplets of an AEGHMQTX spin system of eight chemically inequivalent phosphorus atoms. In order to assign the signals properly to the corresponding phosphorus atoms in the solid-state structure, we conducted variable temperature NMR experiments (193 to 300 K, Supplementary Information). These experiments did not result in freezing any dynamic process in solution to the extent that the spin system is resolved well enough on the NMR time scale for iterative simulation. However, the couplings were resolved well enough for $^{31}\mathrm{P}$-$^{31}\mathrm{P}$ COSY NMR measurements from which the connectivity of the $\mathrm{P_8}$ moiety in **4** could be determined. The general principle of formally oxidizing compounds by attacking the diphenylarsenium cations and consequently forming tetraphenyldiarsine as a thermodynamic driving force should be applicable to electron-rich starting materials other than **VIIIa** and prove to be a good starting point for future studies.

3.4 Conclusions

It could be shown that the insertion of phosphenium ions into the bicylo-[1.1.0]-tetraphosphabutane unit of $[\{\mathrm{Cp'''Fe(CO)_2}\}_2(\mu,\eta^{1:1}\text{-}\mathrm{P_4})]$ (**VIIIa**) is possible. Due to the sensitivity of the reaction solutions, extensive low-temperature NMR studies involving $^{31}\mathrm{P}$-$^{31}\mathrm{P}$ COSY NMR and iterative simulation of the complex spin systems were performed to ascertain the connectivity of the phosphorus cores of the compounds formed at 193 K. These resulted in the characterization of a 2-diphenylphosphabicyclo[1.1.0]-tetraphosphabutane unit in **2a** as well as a rarely observed bicyclo[2.1.0]pentaphosphapentane unit in $[\{\mathrm{Cp'''Fe(CO)_2}\}_2(\mu,\eta^{1:1}\text{-}\mathrm{P_5(C_6H_5)_2})][\mathrm{PF_6}]$ (**3a**), which could be confirmed by single crystal X-ray diffraction. Regardless of the low isolated yield of crystalline **2a** and **1**, the $^{31}\mathrm{P}$ NMR spectra of freshly prepared reaction solutions show full conversion of **VIIIa** to the corresponding products. Additionally, DFT computations were used to gain more insight into the decarbonylation process of **3a** to the cationic compound $[\{\mathrm{Cp'''Fe}\}(\mu,\eta^{4:1}\text{-}\mathrm{P_5(C_6H_5)_2})\{\mathrm{Cp'''(CO)_2Fe}\}][\mathrm{PF_6}]$ (**1**). Furthermore, the reactivity of diphenylarsenium ions towards **VIIIa** was investigated, showing two temperature-sensitive coordination products by applying low-temperature NMR studies. By exposing solutions of these product mixtures to room temperature, the formation of $\mathrm{Ph_4As_2}$ and the disproportionation product $[\{\mathrm{Cp'''Fe(CO)_2}\}_4(\mu_4\eta^{1:1:1:1}\text{-}\mathrm{P_8})][\mathrm{OTf}]_2$ (**4**) with a rarely found tetracyclo[$3.3.0.0^{2,7}.0^{3,6}$]octaphosphaoctane unit could be observed.

3.5 Supporting Information

3.5.1 General techniques and materials

All manipulations were performed using standard schlenk techniques on a dual manifold schlenk line or a glove box under an atmosphere of dry argon. Traces of oxygen in the inert gas were removed by passing it over a BASF R 3-11 (CuO/$MgSiO_3$) catalyst. Residual moisture in the inert gas was removed, by passing it through concentrated H_2SO_4, orange gel and sicapent on dried pumice stone. All glassware was vigorously heated in dynamic vacuum before use and any teflon tubing was stored in an oven at 170 °C.

Toluene, hexane and pentane were purified and dried by the solvent purification system SPS-800 from mbraun. Deuterated solvents were dried and distilled over CaH_2. All solvents were stored over molecular sieve, which was dried in dynamic vacuum at 350 °C.

Ph_2PCl was obtained from Sigma Aldrich and distilled before use. $TlPF_6$ and TlOTf were obtained from Sigma Aldrich and used without further purification. Ph_2PCl and its standard solutions were stored and handled at temperatures below 4 °C at all times. $[\{Cp'''Fe(CO)_2\}_2(\mu,\eta^{1:1}\text{-}P_4)]$[58] and Ph_2AsCl[176] were synthesized according to literature procedures.

NMR spectra were measured with a Bruker Avance 400 (^{1}H: 400.132 MHz; ^{13}C: 100.613 MHz; ^{31}P: 161.97 MHz) using special NMR tubes with a screw cap or a J. Young valve. Any working steps preparing samples for measurement at -80 °C were performed at this temperature and the samples stored at -80 °C until measured. The spin systems of the ^{31}P-NMR spectra were simulated with the DAISY package in TopSpin 3.2 from Bruker using the data from 2D-NMR spectra to assign the multiplets to the corresponding compounds and get more information about the connectivity of the phosphorus framework.

3.5.2 Experimental details and analytical data

Low temperature NMR experiments

To a solution of $[\{Cp'''Fe(CO)_2\}_2(\mu,\eta^{1:1}\text{-}P_4)]$ (**VIIIa**) (100 mg, 0.122 mmol) and TlOTf (65 mg, 0.183 mmol)) in 5 ml dichloromethane, a standard solution of a chlorophosphine R_2PCl (R = Ph, Me, 0.122 M) in toluene was added at -80 °C. While stirring for 5 hours a colourless precipitate of TlCl was formed, from which the dark red solution was quickly but meticulously decanted at -80 °C into a cooled schlenk flask

after sedimentation. The solvent was carefully removed, the dark red oil redissolved in pre cooled CD_2Cl_2 and transferred into a pre cooled NMR tube with a J. Young valve, maintaining -80 °C at all times. For mass spectrometry, the amount of time in between removing the sample (before removing the solvent) from the cooled schlenk and injection was minimized (ca. 2 minutes)

Yield in NMR: full conversion

Analytical data for R = Ph:

ESI-MS: $\frac{m}{z}$ = 1001 ($[\{[Cp'''Fe(CO)_2\}_2(\mu,\eta^{1:1}\text{-}P_4)] + [PPh_2]^+$); 971 ($[M]^+ - CO$); 941 ($[M]^+ - 2CO$)

^{1}H-NMR: (CD_2Cl_2; 300 K): δ[ppm] = 1.39 to 1.57 (m, 54H), 5.18 (m, 2H), 7.68 to 8.15 (m, 10H)

^{31}P{^{1}H}-NMR Data of compounds 2a and **3a**: (CD_2Cl_2; 193 K): see section 3.5.3

Analytical data for R = Me:

IR (DCM): $\tilde{\nu}$ $[cm^{-1}]$ = 1966 (s); 2015 (s); 2046 (s)

ESI-MS : $\frac{m}{z}$ = 875 ($[\{[Cp'''Fe(CO)_2\}_2(\mu,\eta^{1:1}\text{-}P_4)] + [PMe_2]^+$); 847 ($[M]^+ - CO$); 819 ($[M]^+ - 2CO$)

^{1}H-NMR: (CD_2Cl_2; 300 K): δ[ppm] = 1,39 bis 1,57 (m; 54H); 5,18 (m; 2H); 7,68 bis 8,15 (m; 10H)

^{31}P{^{1}H}-NMR Data of compounds 2b and **3b**: (CD_2Cl_2; 193 K): see section 3.5.3

Reaction of VIIIa with in situ generated $[Ph_2P][PF_6]$ at room temperature

To a solution of $[\{Cp'''Fe(CO)_2\}_2(\mu,\eta^{1:1}\text{-}P_4)]$ (**VIIIa**) (82 mg, 0.1 mmol) and $TlPF_6$ (36 mg, 0.103 mmol)) in 5 ml o-difluorobenzene, a standard solution of diphenylchlorophosphine Ph_2PCl in toluene (c = 0.2 mmol ml^{-1}) was added at room

temperature. While stirring for 12 hours a colourless precipitate of TlCl was formed, from which the dark red solution was decanted. The solvent is carefully removed and the resulting red oil extracted with a mixture of diethylether and toluene (10:1, Et_2O:C_6H_8) (three times with 5 ml). The pale red diethylether/toluene solution was stored at 4 °C for 2 months. A large amount of crystalline $[Cp'''Fe(CO)_3][PF_6]$ as well as some extremely fine needles of **1** suitable for diffraction with synchrotron radiation were retrieved from the flask. The residual oil was redissolved in o-difluorobenzene at room temperature and upon addition of pentane at -30 °C formation of a dark red oil could be observed. After storage at room temperature until the oil redissolved, the flask was stored at -30 °C for crystallisation. After one month a few crystals of **3a** suitable for x-ray diffraction could be received.

Yield in NMR: full conversion

$^{31}P\{^1H\}$-NMR Data of compound 3a: (CD_2Cl_2; 300 K): see section 3.5.3

Reaction of VIIIa with in situ generated $[Ph_2As][OTf]$ at -80 °C.

To a mixture of $[\{Cp'''Fe(CO)_2\}_2(\mu,\eta^{1:1}\text{-}P_4)]$ (**VIIIa**) (100 mg, 0.122 mmol), TlOTf (65 mg, 0.183 mmol)) and Ph_2AsCl (32 mg, 0.122 mmol) 10 ml of pre cooled dichloromethane was added at -80 °C under stirring. After one hour of stirring and storing the mixture for two days at -80 °C to let the colourless solid settle, the vibrant red solution is decanted via short teflon tubing into a pre cooled schlenk flask. After removing the solvent at this temperature, a viscous, dark red oil is formed.

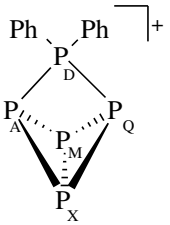
Yield in NMR: full conversion

$^{31}P\{^1H\}$-NMR-Data: CD_2Cl_2 at -80 °C: see section see section 3.5.3

3.5.3 NMR spectra and spectroscopic data

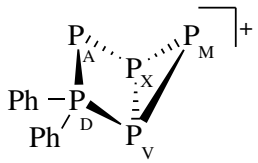
NMR spectroscopic data

Table 3.1: $^{31}P\{^1H\}$ NMR data of **2a**: (CD_2Cl_2; 193 K) with assignment of the individual phosphorus atoms:



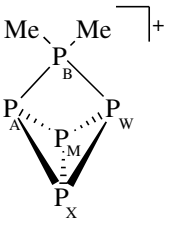
	δ (ppm)		J (Hz)		
P_A	54.5	$^1J_{P_AP_D}$	379	$^1J_{P_MP_X}$	228
P_D	3.9	$^1J_{P_AP_M}$	256	$^1J_{P_QP_X}$	122
P_M	-80.7	$^1J_{P_AP_X}$	134	$^2J_{P_AP_Q}$	19
P_Q	-135.0	$^1J_{P_DP_Q}$	254	$^2J_{P_DP_M}$	29
P_X	-192.8	$^1J_{P_MP_Q}$	211	$^2J_{P_DP_X}$	24

Table 3.2: $^{31}P\{^1H\}$ NMR data of **3a**: (CD_2Cl_2; 193 K) with assignment of the individual phosphorus atoms:



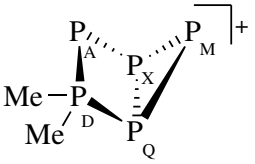
	δ (ppm)		J (Hz)		
P_A	78.4	$^1J_{P_AP_D}$	390	$^1J_{P_VP_X}$	119
P_D	35.0	$^1J_{P_AP_X}$	218	$^2J_{P_DP_M}$	76
P_M	-31.7	$^1J_{P_DP_V}$	283	$^2J_{P_DP_X}$	68
P_V	-134.5	$^1J_{P_MP_V}$	190		
P_X	-148.7	$^1J_{P_MP_X}$	260		

Table 3.3: $^{31}P\{^1H\}$ NMR data of **2b**: (CD_2Cl_2; 193 K) with assignment of the individual phosphorus atoms:



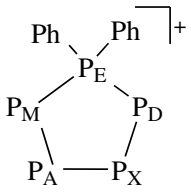
	δ (ppm)		J (Hz)		
P_A	45.6	$^1J_{P_AP_B}$	352	$^1J_{P_WP_X}$	261
P_B	37.4	$^1J_{P_AP_W}$	223	$^2J_{P_BP_W}$	60
P_M	-48.6	$^1J_{P_BP_M}$	265	$^2J_{P_MP_W}$	99
P_W	-146.0	$^1J_{P_BP_X}$	106		
P_X	-150.7	$^1J_{P_MP_X}$	192		

Table 3.4: $^{31}P\{^1H\}$ NMR data of **3b**: (CD_2Cl_2; 193 K) with assignment of the individual phosphorus atoms:



δ (ppm)		J (Hz)			
P_A	39.6	$^1J_{P_AP_D}$	353	$^1J_{P_MP_X}$	237
P_D	2.1	$^1J_{P_AP_M}$	243	$^1J_{P_QP_X}$	114
P_M	-82.6	$^1J_{P_AP_X}$	130	$^2J_{P_AP_Q}$	25
P_Q	-140.2	$^1J_{P_DP_Q}$	244	$^2J_{P_DP_M}$	32
P_X	-182.3	$^1J_{P_MP_Q}$	206	$^2J_{P_DP_X}$	26

Table 3.5: $^{31}P\{^1H\}$ NMR data of **1**: (CD_2Cl_2; 300 K) with assignment of the individual phosphorus atoms:



δ (ppm)		J (Hz)			
P_A	210.8	$^1J_{P_AP_M}$	365	$^2J_{P_AP_D}$	26
P_D	150.6	$^1J_{P_AP_X}$	390	$^2J_{P_DP_M}$	14
P_E	125.4	$^1J_{P_DP_E}$	415	$^2J_{P_EP_X}$	11
P_M	53.9	$^1J_{P_DP_X}$	370	$^2J_{P_MP_X}$	16
P_X	-25.6	$^1J_{P_EP_M}$	516		

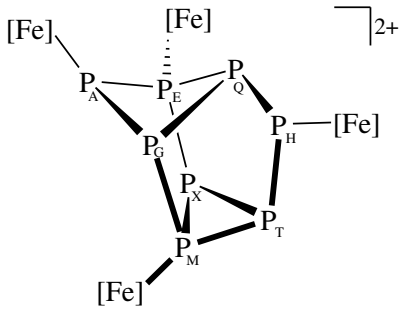
Table 3.6: $^{31}P\{^1H\}$ NMR data of coordination mode 1 of [Ph_2As][OTf] on **VIIIa** from the simulation (in CD_2Cl_2 at -80 °C).

δ (ppm)		J (Hz)			
P_A	57.7	$^1J_{P_AP_W}$	259	$^1J_{P_BP_X}$	218
P_B	43.8	$^1J_{P_AP_X}$	244	$J_{P_WP_X}$	109
P_W	-237.0	$^1J_{P_BP_W}$	214	$^2J_{P_AP_B}$	24
P_X	-250.6				

Table 3.7: $^{31}P\{^{1}H\}$ NMR data of coordination mode 2 of $[Ph_2As][OTf]$ on **VIII** from the simulation (in CD_2Cl_2 at -80 °C).

δ (ppm)		J (Hz)	
P_A	-10.9	$^{1}J_{P_AP_B}$	125
P_B	-12.1	$^{1}J_{P_AP_{X_2}}$	203
P_{X_2}	-274.9	$^{1}J_{P_BP_{X_2}}$	256

Table 3.8: ^{31}P NMR data of **4**: (CD_2Cl_2; 273 K) with assignment of the individual phosphorus atoms:



δ (ppm)		Coupling with
P_A	244.3	P_E
P_E	183.3	P_A P_Q P_X
P_G	136.3	P_Q P_M
P_H	128.4	P_T P_Q
P_M	69.5	P_T P_G P_X
P_Q	40.3	P_E P_G P_H
P_T	2.5	P_H P_M P_X
P_X	-165.4	P_E P_M P_T

NMR spectra of reactions of VIIIa with [Ph_2P][OTf] at 193 K

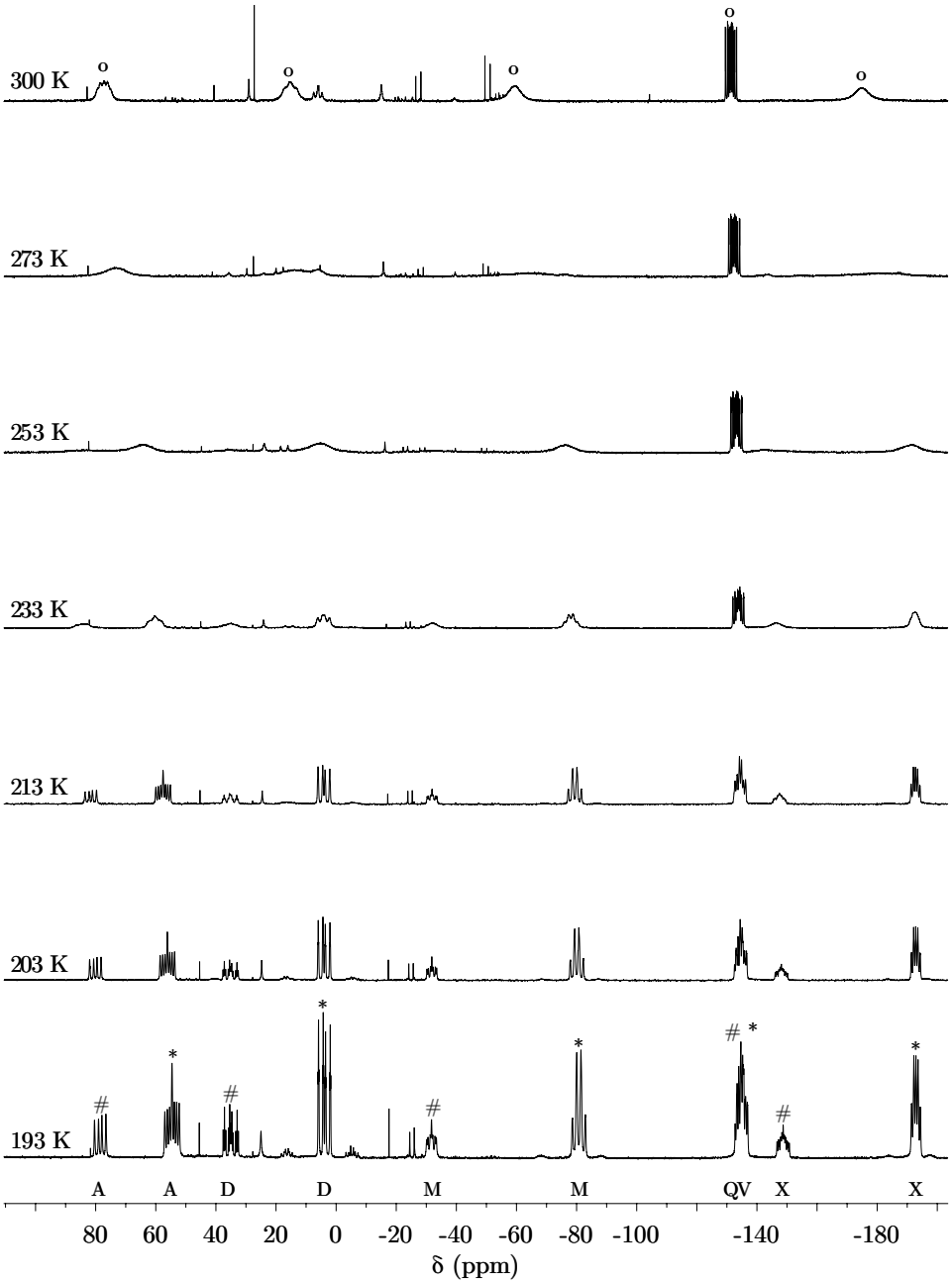


Figure 3.5: $^{31}P\{^1H\}$ VT NMR spectrum in CD_2Cl_2 from the reaction of **VIIIa** with [Ph_2P][OTf]. The signals of compound **2a** are marked with $*$, of compound **3a** with # and signals showing dynamic behaviour at room temperature with o.

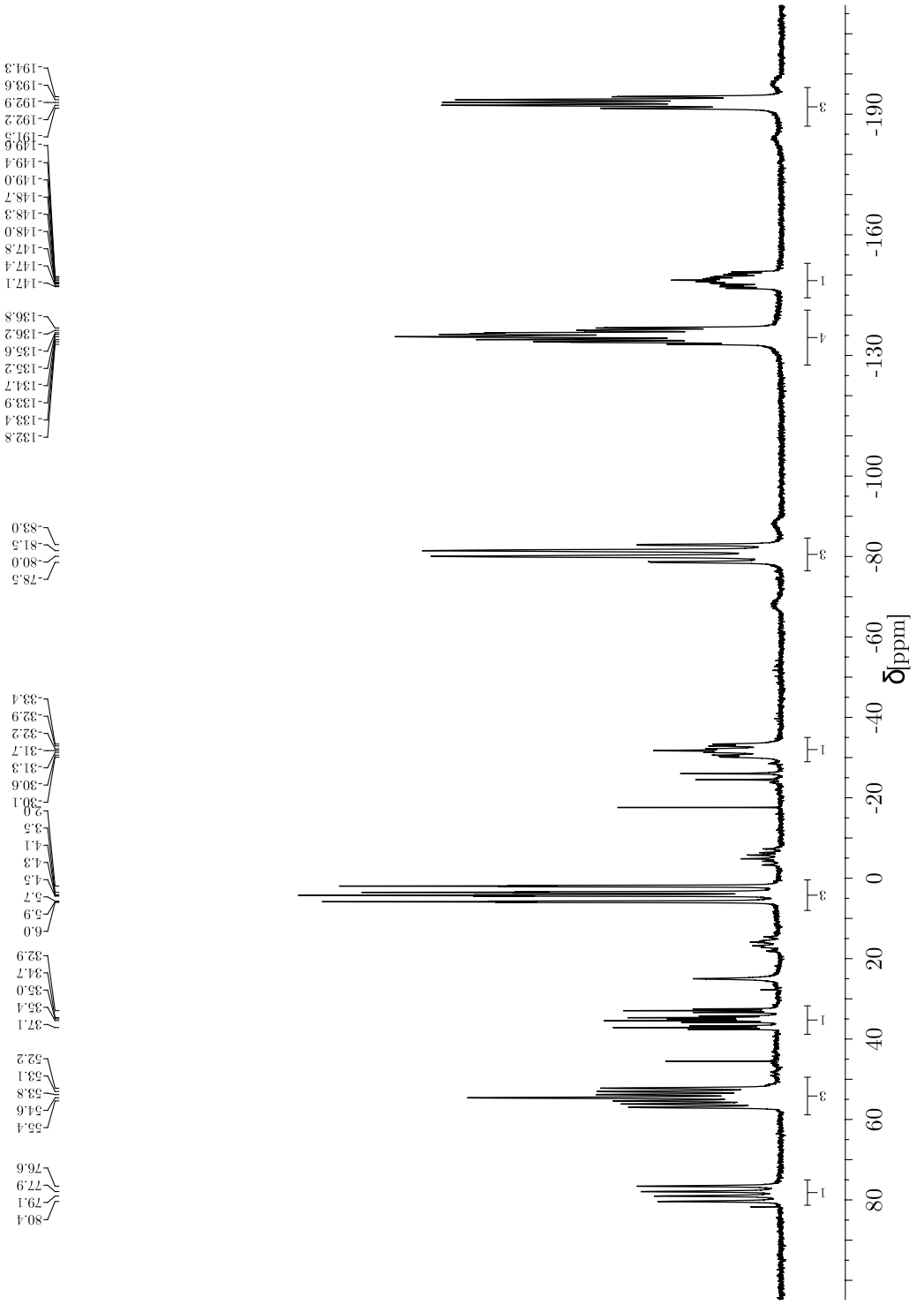


Figure 3.6: $^{31}P\{^{1}H\}$ NMR spectrum at 193 K in CD_2Cl_2 from the reaction of **VIIIa** with $[Ph_2P][OTf]$ at 193 K with chemical shifts and integrals depicted in the spectrum.

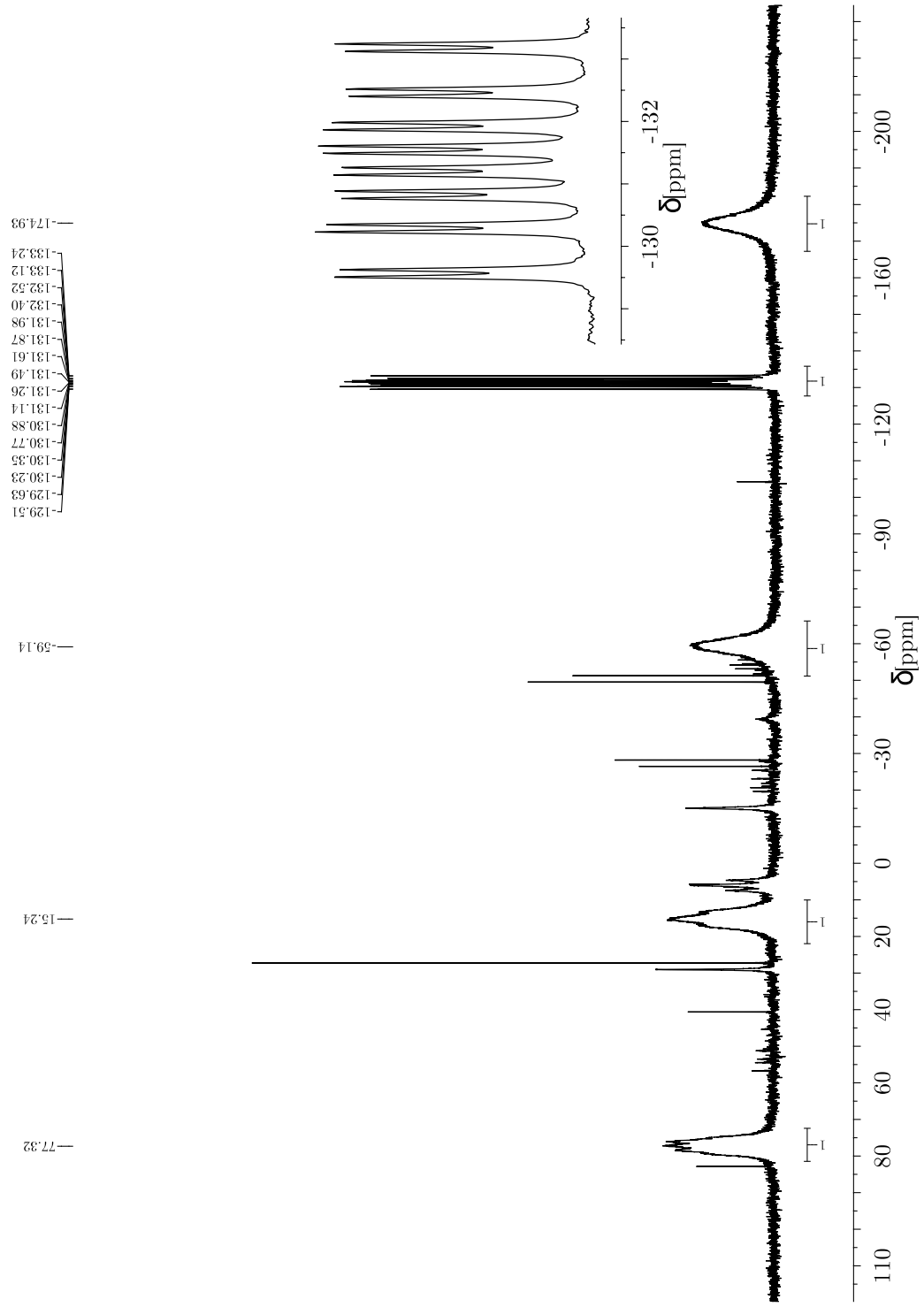


Figure 3.7: $^{31}P\{^{1}H\}$ NMR spectrum at room temperature in CD_2Cl_2 from the reaction of **VIIIa** with $[Ph_2P][OTf]$ at 193 K with chemical shifts and integrals depicted in the spectrum.

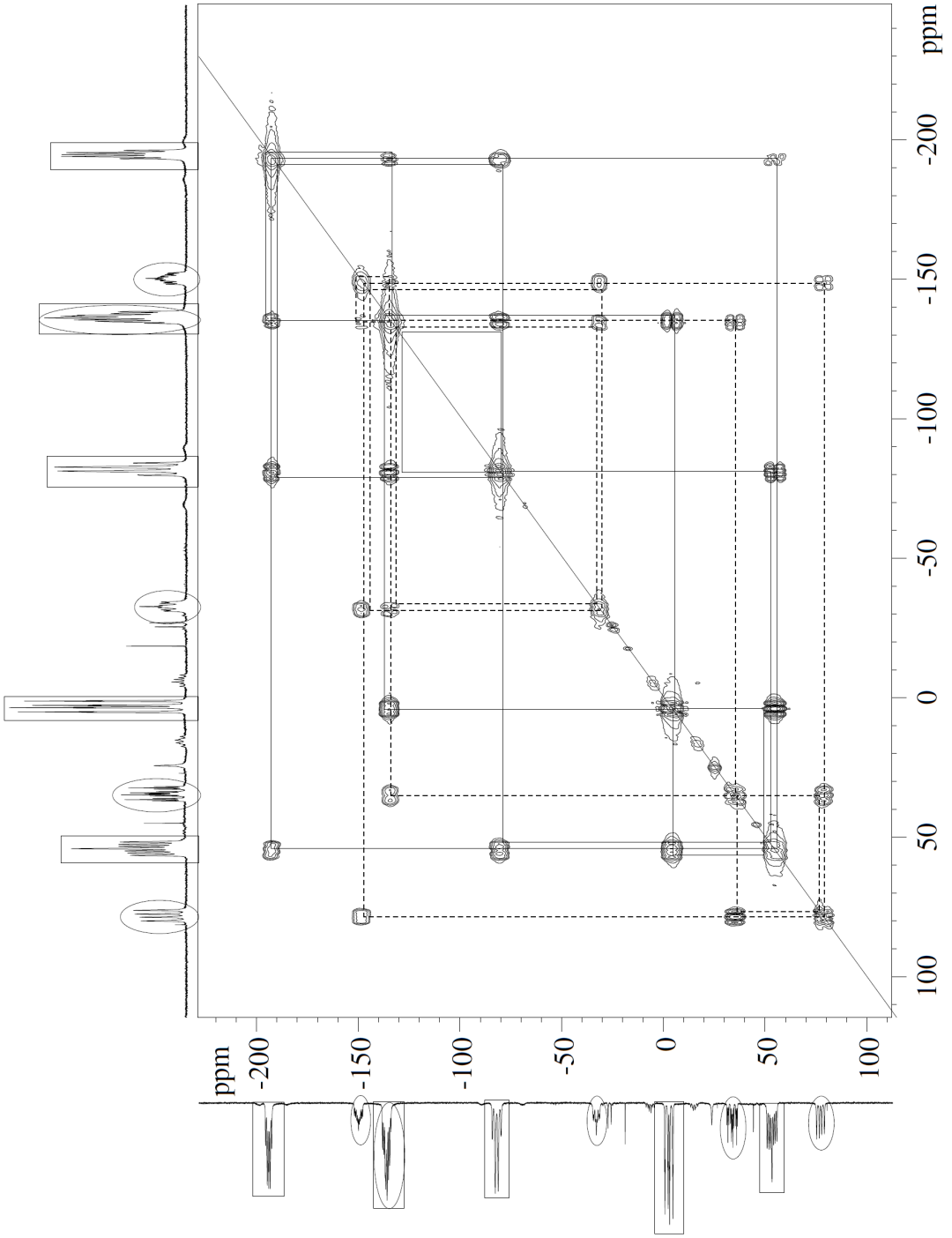


Figure 3.8: ^{31}P-^{31}P COSY NMR spectrum in CD_2Cl_2 at -80 °C of the product mixture from the reaction of $[Ph_2P][OTf]$ with **VIIIa** at -80 °C. Signals of **2a** are marked with rectangles, of **3a** with ellipses. Couplings in compound **2a** are drawn as rectangles with solid lines, couplings in **3a** with dashed lines. For easier understanding, the diagonal signals are connected via a solid line.

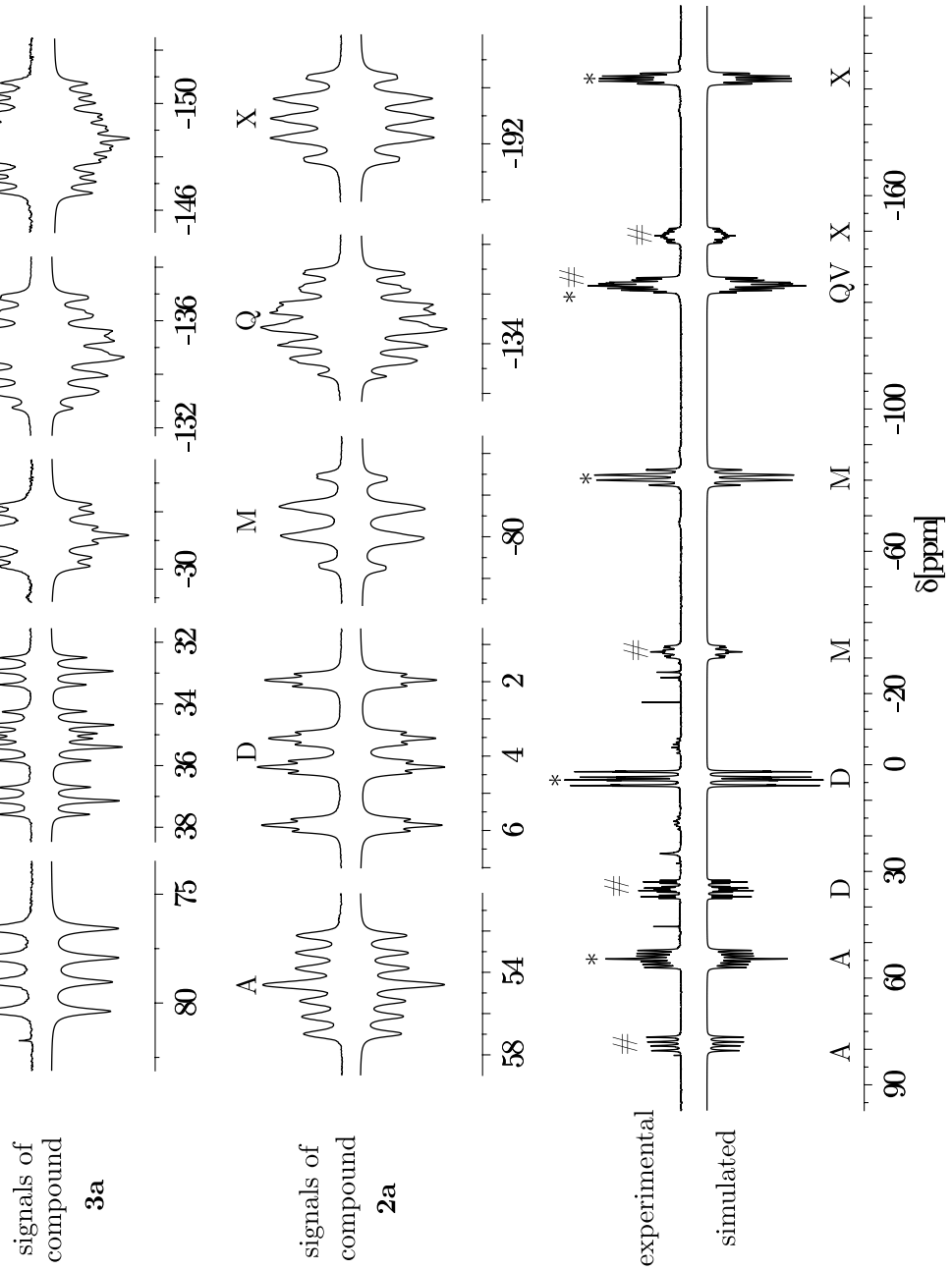


Figure 3.9: Simulation of the spinsystems in the $^{31}P\{^{1}H\}$ NMR spectrum of compounds **2a** and **3a**. The multiplets of compound **2a** are marked with $*$, the multiplets of compound **3a** with # . The multiplet Q/V is the result of two overlapping multiplets from the two different spin systems. The simulation of the spin system is shown inverted.

NMR spectra of reactions of VIIIa with [Me_2P][OTf] at 193 K

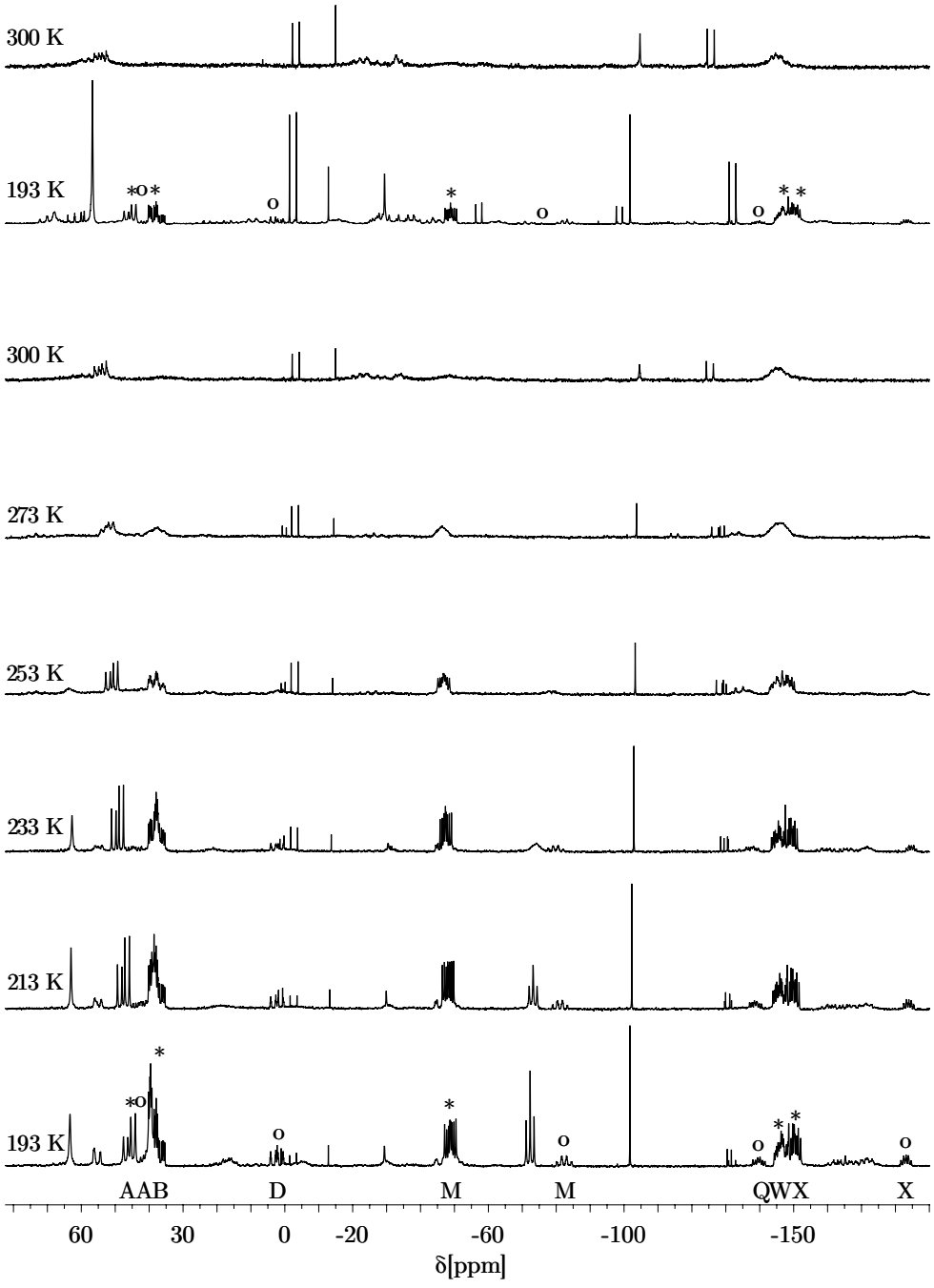


Figure 3.10: $^{31}P\{^1H\}$ VT NMR spectrum in CD_2Cl_2 of the reaction of **VIIIa** with in situ generated [Me_2P][OTf]. The signals of **2b** are marked with ∗, the signals of **3b** with o.

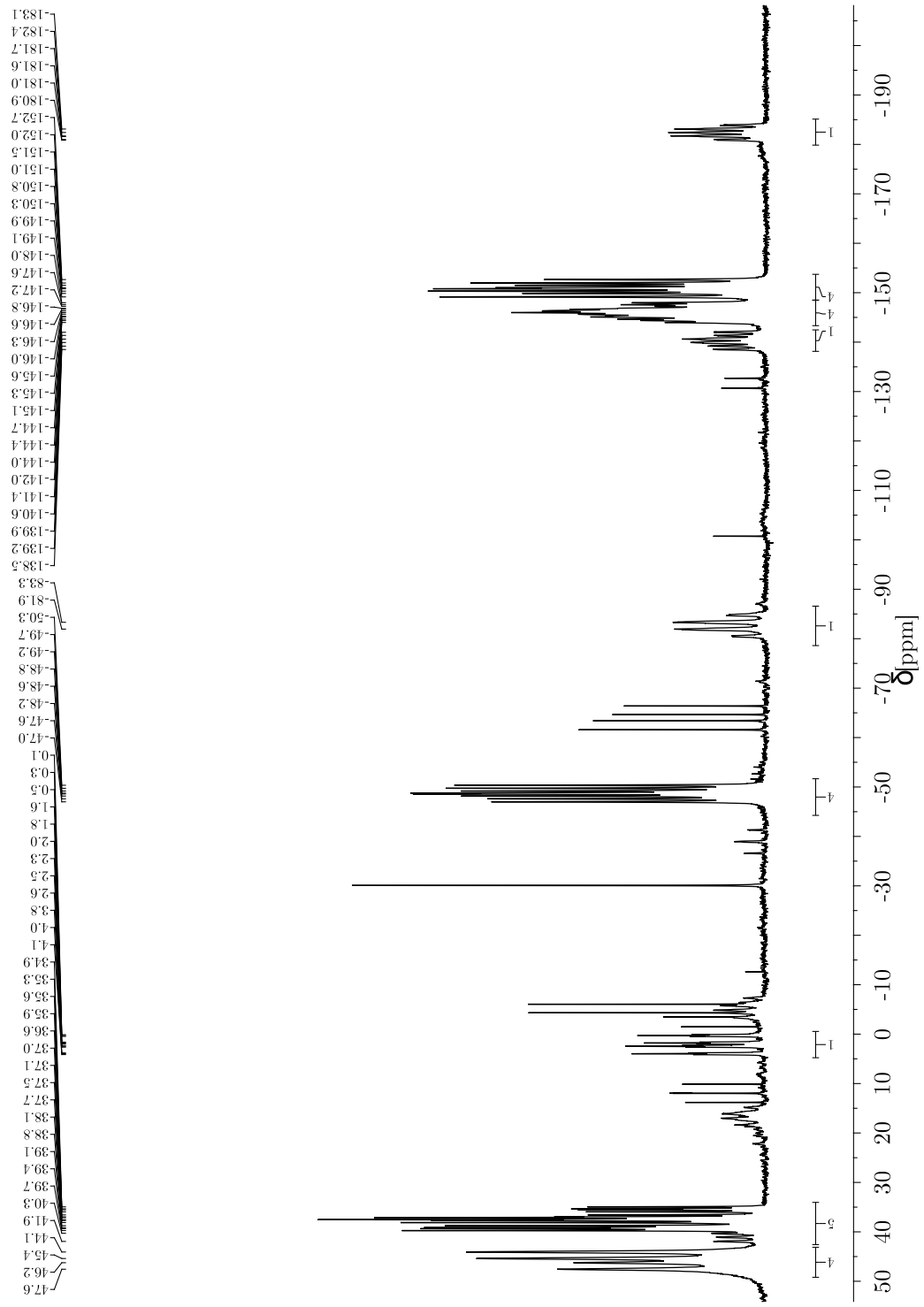


Figure 3.11: $^{31}P\{^{1}H\}$ NMR spectrum in CD_2Cl_2 from the reaction of **VIIIa** with $[Me_2P][OTf]$ at 193 K with chemical shifts and integrals depicted in the spectrum.

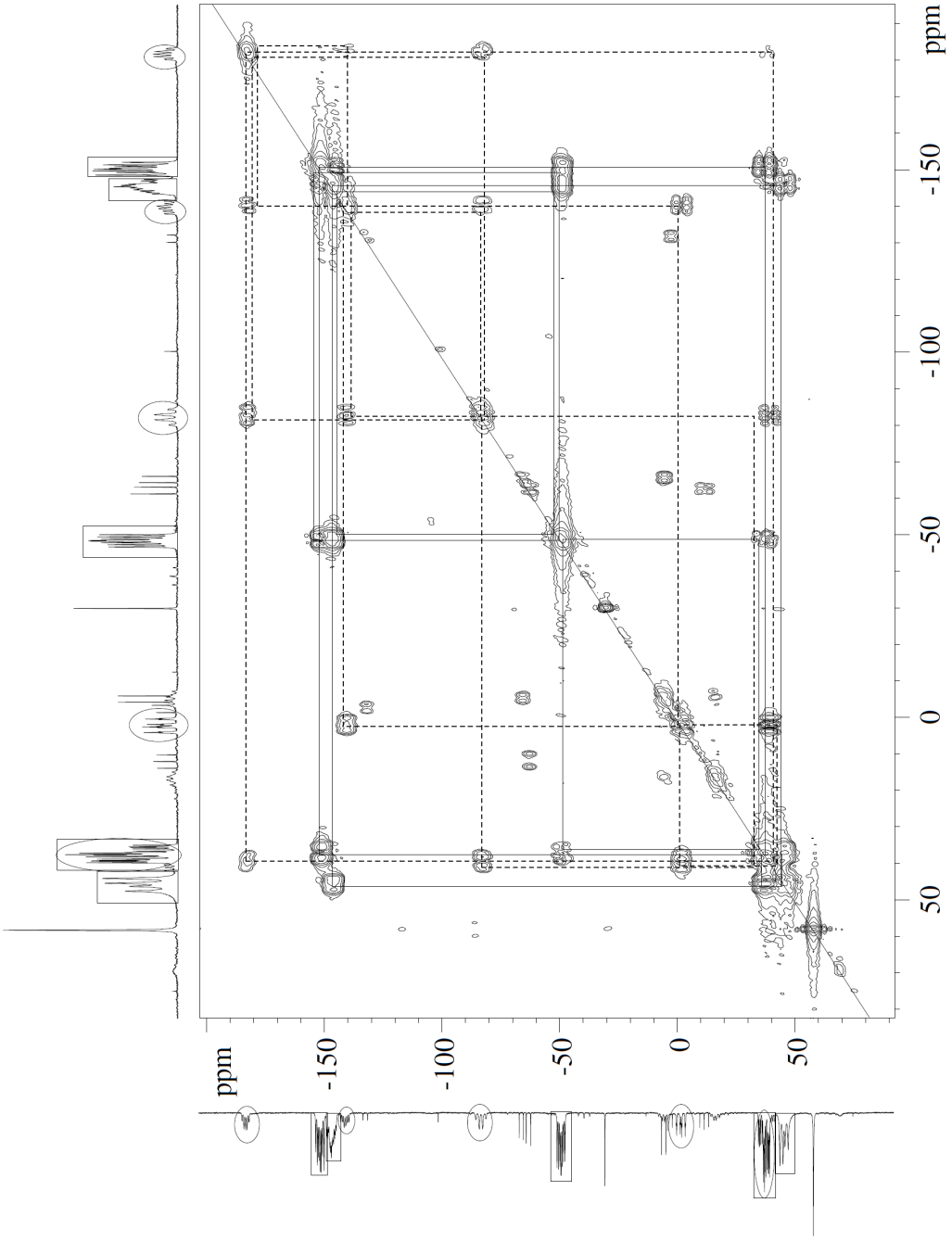


Figure 3.12: ^{31}P-^{31}P COSY NMR spectrum in CD_2Cl_2 at -80 °C of the product mix from the reaction of [Me_2P][OTf] with **VIIIa** at -80 °C. Signals of **2b** are marked with rectangles, signals of **3b** with ellipses. Couplings in compound **2b** are drawn as rectangles with solid lines, couplings in compound **3b** with dashed lines. For easier understanding, the diagonal signals are connected via a solid line. The couplings between multiplets A and B as well as between W and X of compound **3b** are not resolved in this figure since they appear in close proximity to each other.

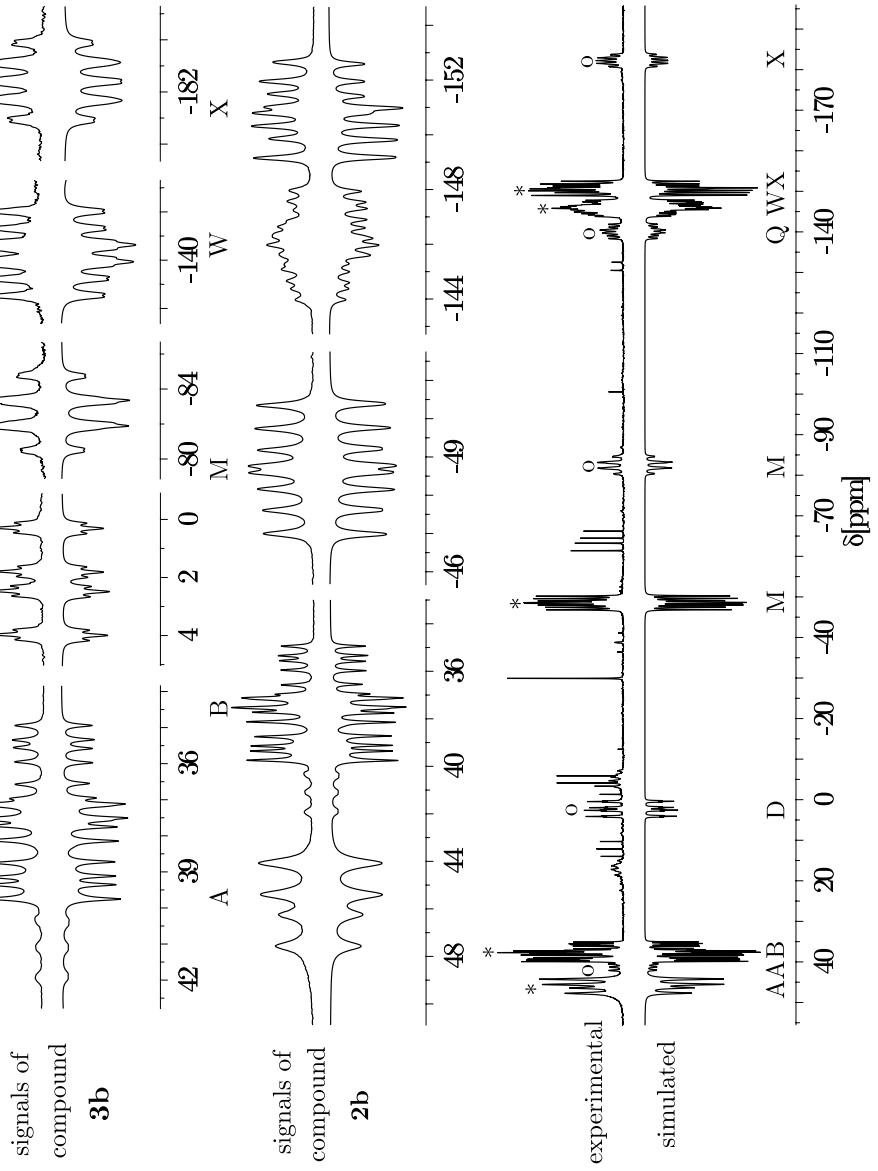


Figure 3.13: Simulation of the spin systems in the $^{31}P\{^{1}H\}$ NMR spectrum of compounds **2b** and **3b**. The multiplets of compound **2b** are marked with $*$, the multiplets of **3b** with o. The signal at 40 ppm is the result of overlapping multiplets B of compound **2b** and A of compound **3b**. The simulation of the spin system is shown inverted. The simulated multiplets W and X of **2b** differ from the signals in the real spectrum in intensity, which can be explained by overlaps with signals from minor products not accounted for in the iterative fit. The coupling pattern of the simulated multiplet does not differ from the real one.

NMR spectra of the reaction of VIIIa with in situ generated [Ph_2P][PF_6] at room temperature

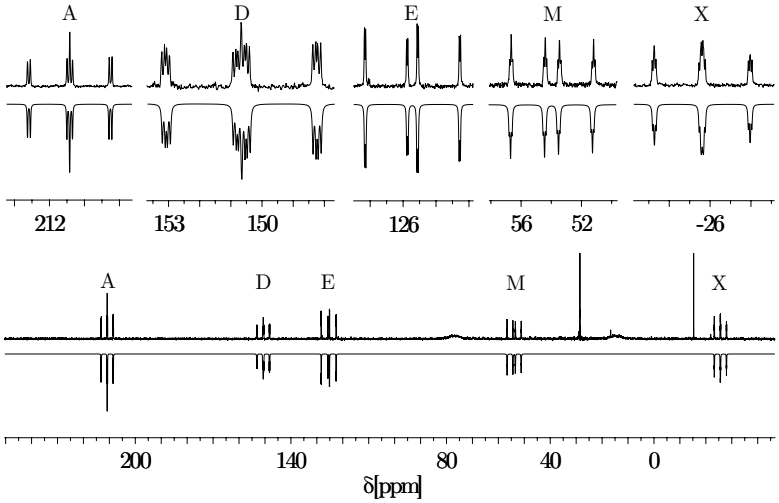


Figure 3.14: Simulation (inverted) of the $^{31}\{^{1}H\}$ NMR spectrum of **1**.

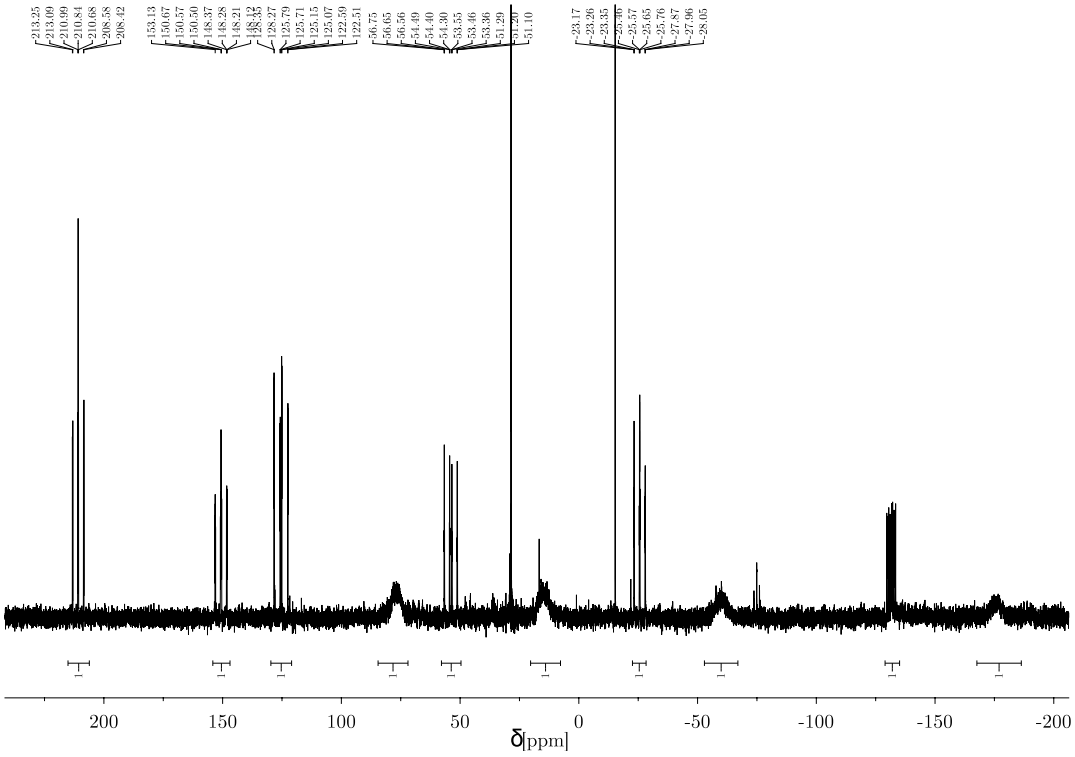


Figure 3.15: $^{31}P\{^{1}H\}$ NMR spectrum in CD_2Cl_2 from the reaction of **VIIIa** with [Ph_2P][PF_6] at room temperature with chemical shifts and integrals depicted in the spectrum.

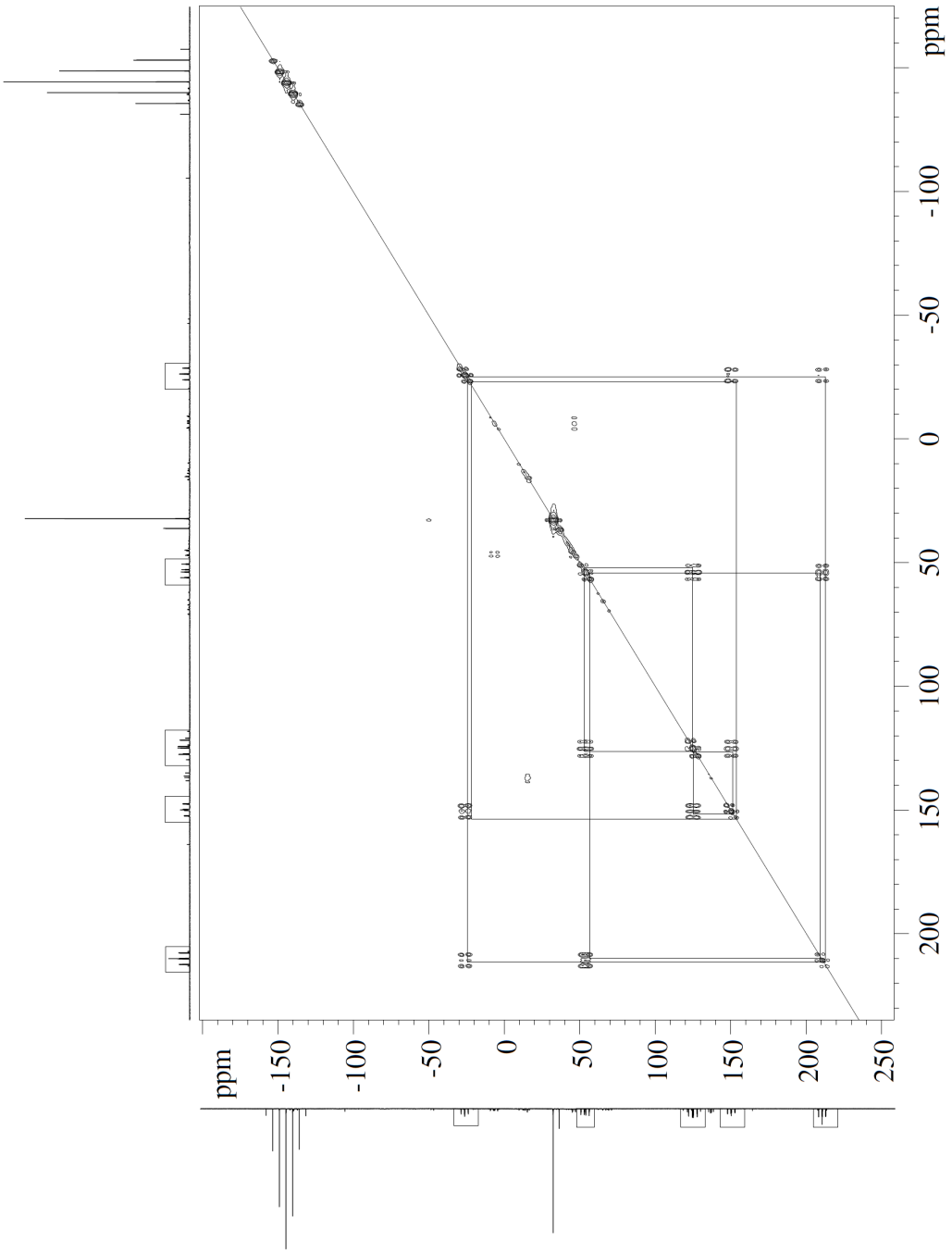


Figure 3.16: ^{31}P-^{31}P-COSY NMR spectrum of **1** at room temperature. Couplings are marked with rectangles for easier understanding.

NMR spectra of the reaction of VIIIa with in situ generated [Ph_2As][OTf].

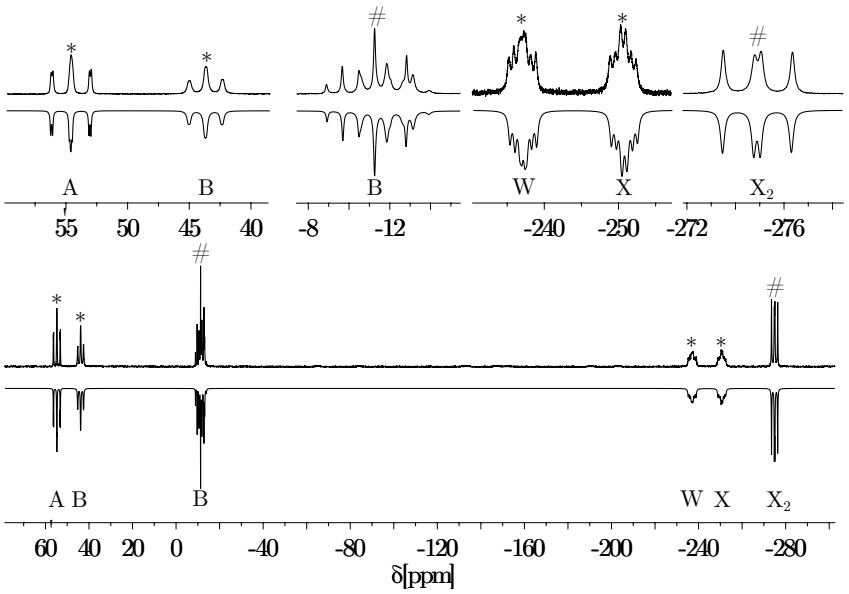


Figure 3.17: Simulation of the $^{31}P\{^1H\}$ NMR spectrum of coordination mode 1 and 2 of [Ph_2As][OTf] on **VIIIa**. Signals of coordination mode 1 are marked with $*$, signals of coordination mode 2 with # . The simulated spectrum is shown inverted.

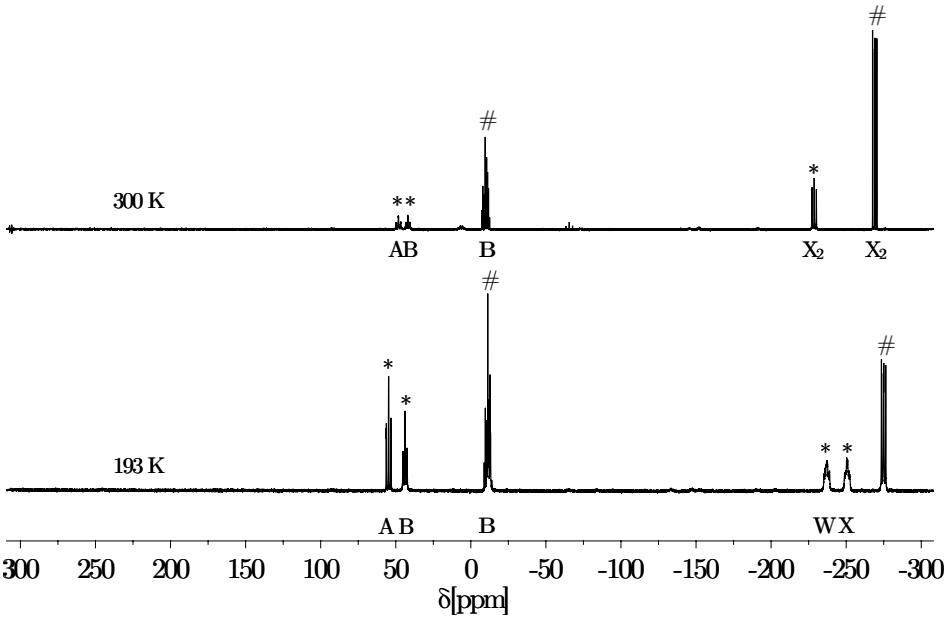


Figure 3.18: Comparison of the $^{31}P\{^1H\}$ NMR spectrum of coordination mode 1 and 2 of [Ph_2As][OTf] on **VIIIa** at 193 K and room temperature. Signals of coordination mode 1 are marked with $*$, signals of coordination mode 2 with # .

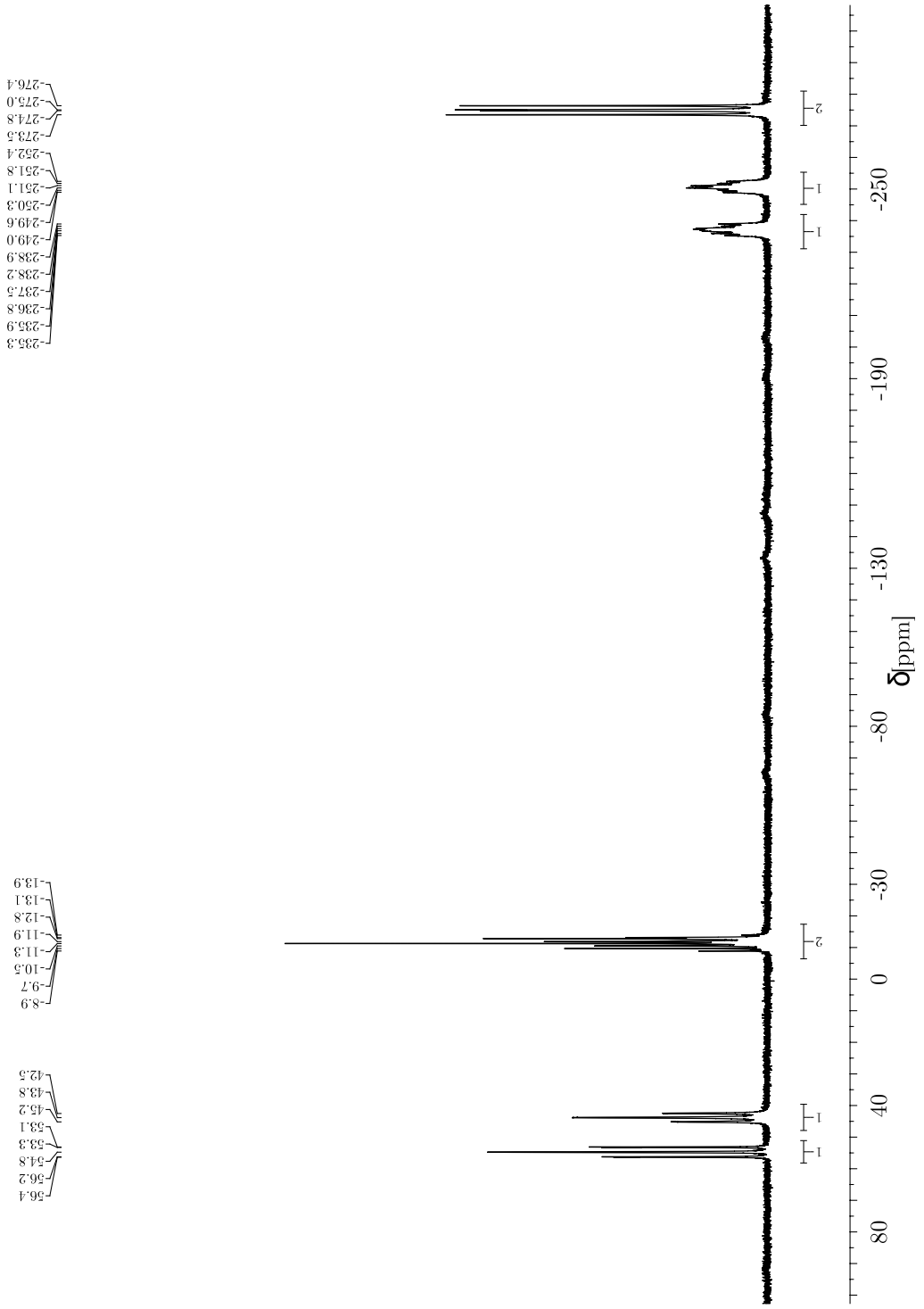


Figure 3.19: $^{31}P\{^{1}H\}$ NMR spectrum in CD_2Cl_2 right after warming to room temperature from the reaction of **VIIIa** with $[Ph_2As][OTf]$ at 193 K with chemical shifts and integrals depicted in the spectrum.

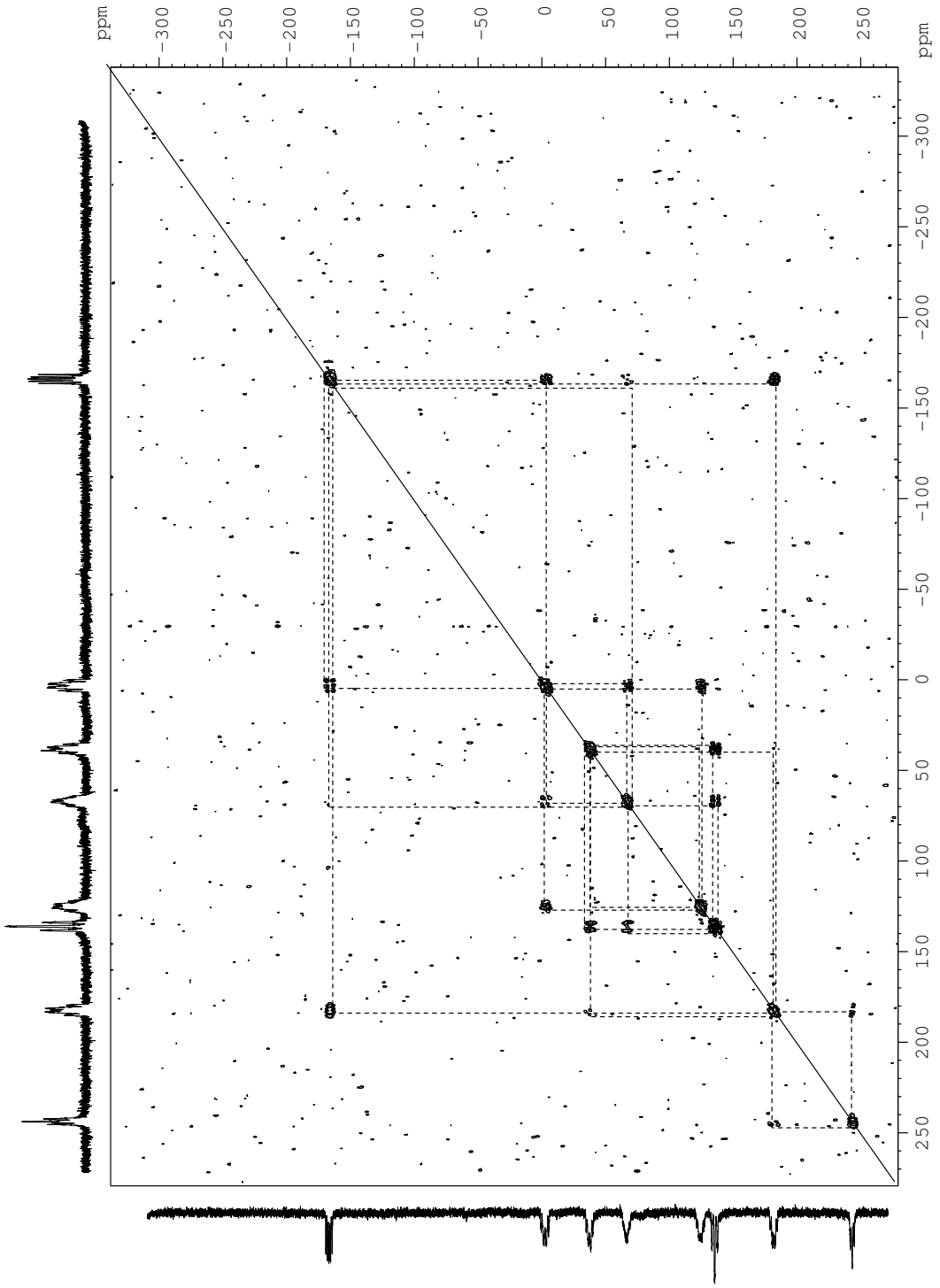


Figure 3.20: ^{31}P-^{31}P COSY NMR spectrum in CD_2Cl_2 at 273 K of **4**. For easier understanding, the diagonal signals are connected via a solid line and the couplings between multiplets marked with dotted rectangles. Due to the dynamic behaviour some couplings are not or badly resolved.

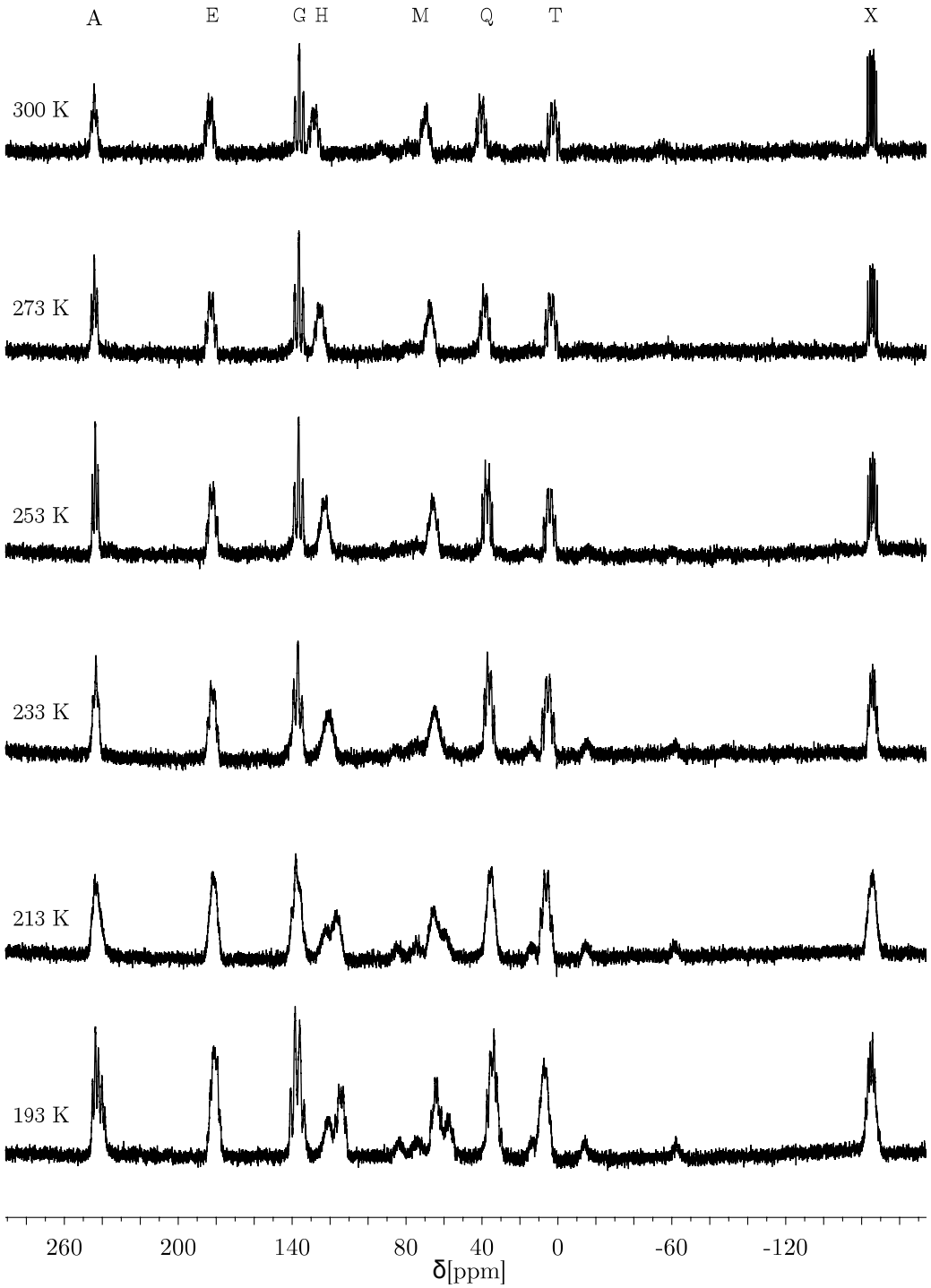


Figure 3.21: ^{31}P VT NMR spectrum in CD_2Cl_2 of crystals of **4**. The Splitting of H and M as well as the beginning splitting in the other multiplets of the spin system can be explained that freezing dynamic processes, inhibiting free rotation of the [Cp‴Fe(CO)$_2$] fragments.

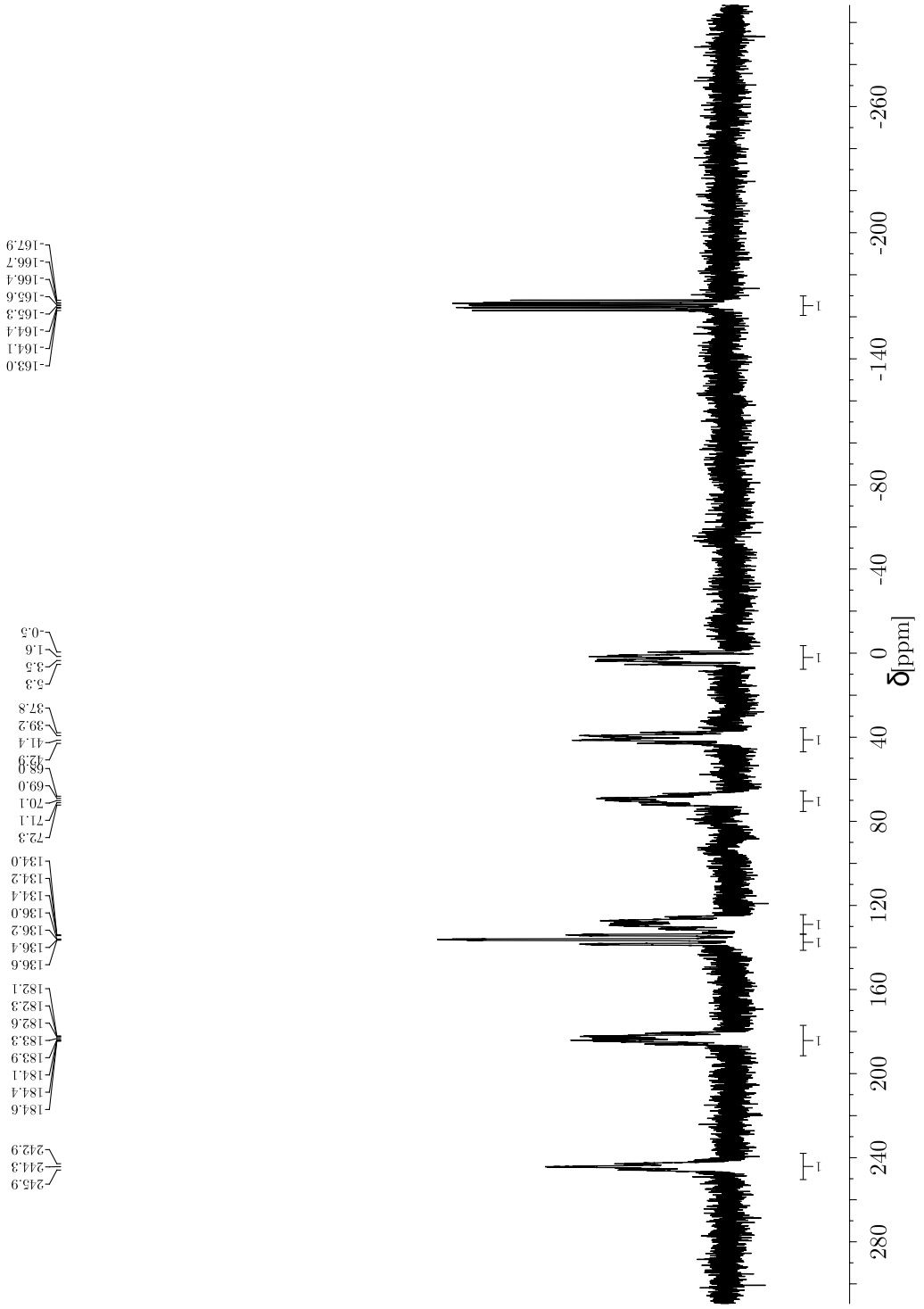


Figure 3.22: ^{31}P NMR spectrum of **4** in CD_2Cl_2 at room temperature with chemical shifts and integrals depicted in the spectrum.

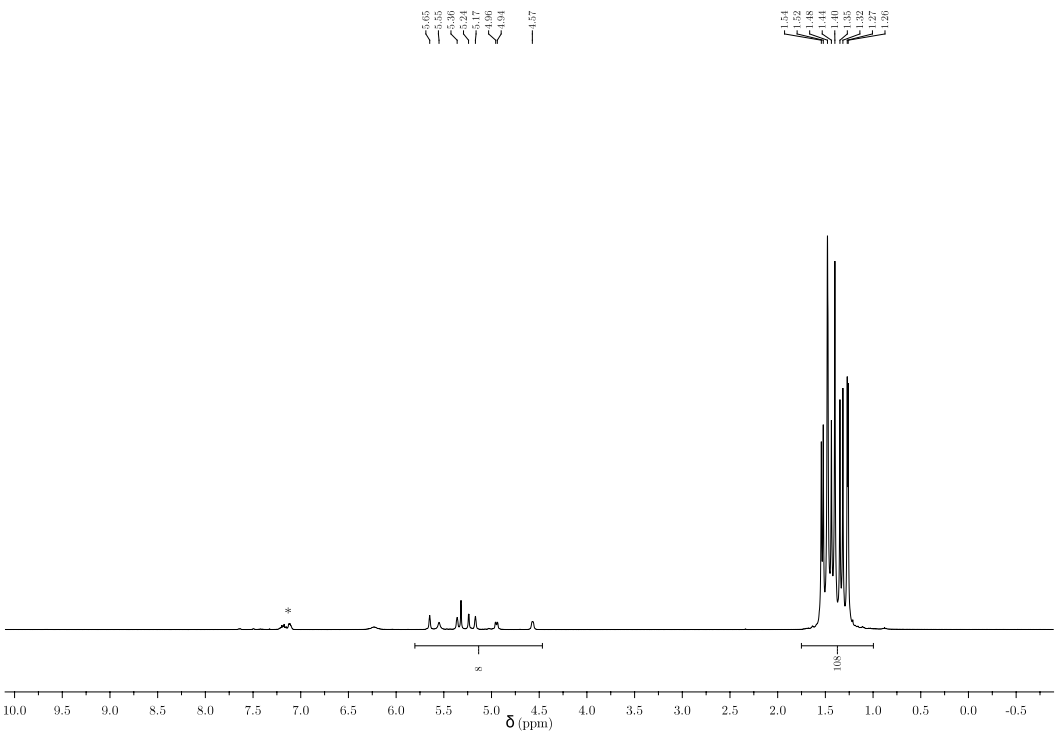


Figure 3.23: ^{1}H NMR spectrum of **4** in CD_2Cl_2 at room temperature with chemical shifts and integrals depicted in the spectrum. Signals from residual ortho difluoro benzene are marked with $*$.

3.5.4 Crystallographic data and solid state structures

Crystallographic details on 3a

Compound **3a** was crystallized in very small amounts from an ortho-difluorobenzene pentane mixture by storing at -30 °C for one month. A suitable clear red block-shaped crystal of **3a** with dimensions $0.07 \times 0.05 \times 0.04\ \mathrm{mm}^3$ was selected and mounted on a GV1000, TitanS2 diffractometer. The crystal was kept at a steady T = 123.00(10) K during data collection. The structure was solved with the ShelXT 2018/2[177] solution program using iterative methods and by using Olex2 1.3-alpha[178] as the graphical interface. The model was refined with ShelXL 2018/3[179] using full matrix least squares minimisation on F^2. Two of the tert butyl groups on the Cp''' on Fe1 were disordered due to rotation.

Crystallographic details on 1

Compound **1** was crystallized in very small amounts from a 1:1 toluene-diethylether mixture at 4 °C. The needle-shaped crystals of **1** were significantly undergrown, showing no scattering on the laboratory diffractometer. Therefore, we decided to perform the diffraction study using synchrotron radiation. The diffraction data for **1** were collected on the P11 beamline at PETRAIII accelerator at DESY, Hamburg, Germany[180]. The microscopic needle crystal was mounted on the 100 μm MiTeGen® loop in the drop of the mineral oil. The X-ray beam (E = 18 keV, λ = 0.6888 $\mathrm{\AA}$) was preliminary focused to 200×200 $\mu\mathrm{m}$ with the focusing bendable KB mirror system[180] and then additionally collimated to 50 μm. As a result, the background was significantly reduced resulting in quite appropriate $\mathrm{I_{hkl}}/\sigma$ values (average 5 before merging, 14 after the merging for the data up to 0.834 $\mathrm{\AA}$). Total 1800 frames were collected using 0.2° frames in the shutterless mode using Pilatus 6M detector. The CrysAlisPro software was used to extract the reflection intensities from the set of the frames. After the data finalization, the reflections up to $\mathrm{d_{min.}}$ = 0.83 $\mathrm{\AA}$ were used for the refinement. The structure was solved using SHELXT program and refined in the anisotropic approximation using SHELX2018/3 program. Both solvent molecules are disordered and therefore some restraints were applied in the refinement.

Crystallographic details on 4

Compound **4** was crystallized from an ortho-difluorobenzene pentane mixture at room temperature. A suitable clear orange plate-shaped crystal of **4** with dimensions $0.26 \times 0.17 \times 0.13\ \mathrm{mm^3}$ was selected and mounted on a GV1000, TitanS2 diffractometer. The crystal was kept at a steady T = 133.00(10) K during data collection, since we noticed loss of crystalinity at lower temperatures. The structure was solved with the ShelXT[177] solution program using dual methods and by using Olex2 1.5-alpha[178] as the graphical interface. The model was refined with ShelXL 2018/3[179] using full matrix least squares minimisation on F^2. A solvent mask was calculated and 121 electrons were found in a volume of 493 $\mathrm{\AA^3}$ in 1 void per unit cell. This is consistent with the presence of 1[$\mathrm{C_6H_4F_2}$] per asymmetric unit which account for 116 electrons per unit cell. One triflate counter ion was disordered.

Crystallographic data

Table 3.9: Crystallographic data for **1**, **3a** and **4**:

Compound	**1**	**3a**	**4**
Formula	$C_{53.5}H_{77}F_6Fe_2O_{2.5}P_6$	$C_{50}H_{68}F_6Fe_2O_4P_6$	$C_{96}H_{128}F_{12}Fe_4O_{14}P_8S_2$
$\rho_{calc.}/gcm^{-3}$	1.378	1.409	1.403
μ/mm^{-1}	0.700	6.525	6.400
Formula Weight	1171.67	1144.56	2269.26
Colour	black	clear red	orange
Shape	needle	block-shaped	plate-shaped
Size/mm^3	$0.05 \times 0.01 \times 0.00$	$0.07 \times 0.05 \times 0.04$	$0.26 \times 0.17 \times 0.13$
T/K	100.00(10)	123.00(10)	133.00(10)
Crystal System	monoclinic	triclinic	triclinic
Space Group	C2/c	P-1	P-1
a/Å	45.1781(12)	10.4574(5)	14.36190(10)
b/Å	9.86897(17)	13.7684(4)	15.92590(10)
c/Å	27.6331(5)	20.0423(11)	26.1504(2)
$\alpha/^\circ$	90	99.992(3)	93.8200(10)
$\beta/^\circ$	113.564(2)	102.592(4)	104.6430(10)
$\gamma/^\circ$	90	100.656(3)	109.6900(10)
V/Å^3	11293.1(5)	2698.1(2)	5372.45(8)
Z	8	2	2
Z'	1	1	1
Wavelength/Å	0.6888	1.54184	1.54184
Radiation type	synchrotron	Cu Kα	Cu Kα
$\theta_{min}/^\circ$	1.558	3.351	3.543
$\theta_{max}/^\circ$	25.499	65.089	66.734
Measured Refl's.	43651	14949	105406
Indep't Refl's	11357	8833	18923
Refl's I $\geq 2\sigma$(I)	6508	6565	18211
R_{int}	0.0773	0.0649	0.0433
Parameters	703	691	1234
Restraints	94	0	48
Largest Peak	0.521	0.724	0.599
Deepest Hole	-0.468	-0.895	-0.552
GooF	0.797	1.006	1.057
wR2 (all data)	0.0691	0.1469	0.0936
wR2	0.0665	0.1332	0.0924
R1 (all data)	0.0629	0.0783	0.0368
R1	0.0339	0.0562	0.0356

Solid state structures

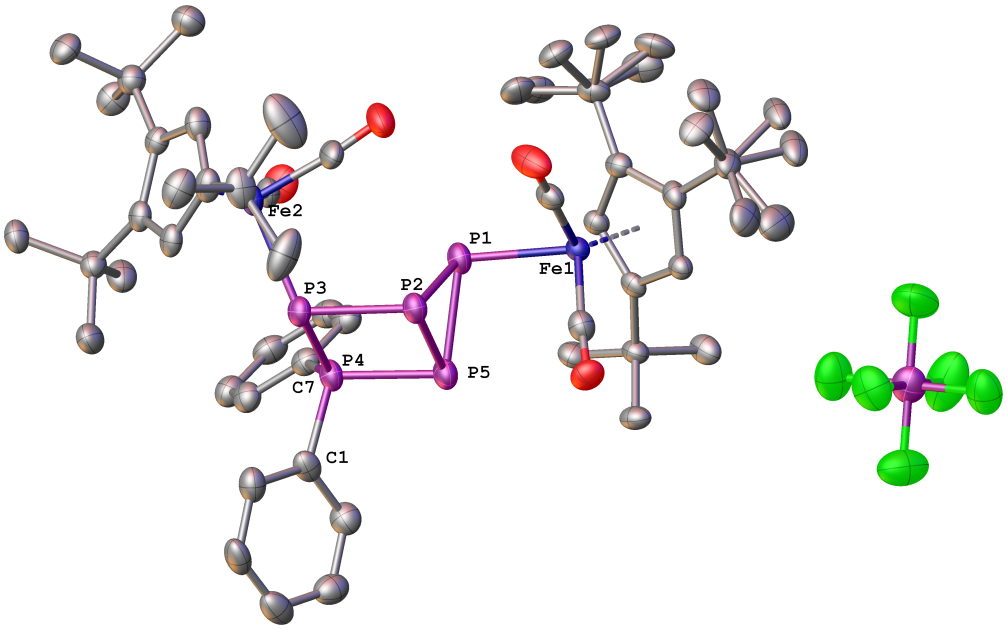


Figure 3.24: Molecular structure of **3a** in the solid state. Hydrogen atoms are omitted for clarity. Selected bond lengths and angles: Fe1-P1 2.3162(12), Fe2-P3 2.3004(15), P1-P5 2.2010(18), P2-P1 2.1971(15), P2-P5 2.2546(17), P3-P2 2.2305(15), P3-P4 2.2128(17), P4-P5 2.1974(16), P4-C1 1.813(5), P4-C7 1.819(4), P2-P3-Fe2 111.52(6), P4-P3-Fe2 124.22(6), P4-P3-P2 84.67(6), P3-P2-P5 94.38(6), P1-P2-P3 103.02(6), P1-P2-P5 59.24(5), P5-P4-P3 96.52(6), C1-P4-P3 107.66(16), C1-P4-P5 103.03(15), C1-P4-C7 104.1(2), C7-P4-P3 127.21(16), C7-P4-P5 115.93(15), P2-P1-Fe1 101.85(5), P2-P1-P5 61.71(5), P5-P1-Fe1 101.19(6), P4-P5-P2 84.43(6), P4-P5-P1 97.58(7), P1-P5-P2 59.05(5).

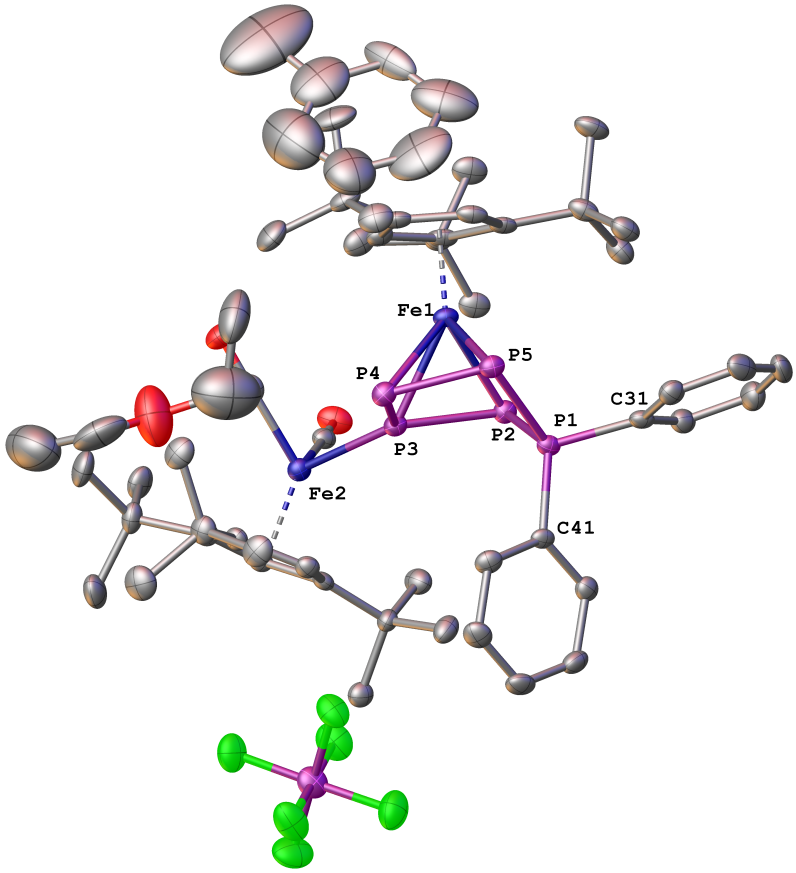


Figure 3.25: Molecular structure of **1** in the solid state. Hydrogen atoms are omitted for clarity. Selected bond lengths and angles: Fe1-P3 2.2925(7), Fe1-P5 2.3422(7), Fe1-P4 2.3517(8), Fe1-P2 2.3610(8), Fe2-P3 2.2567(7), P1-P5 2.1590(9), P1-P2 2.1761(9), P2-P3 2.1293(9), P3-P4 2.1337(9), P4-P5 2.1322(10), P3-Fe1-P2 54.44(2), P3-Fe1-P4 54.68(2), P3-Fe1-P5 90.91(3), P4-Fe1-P2 94.13(3), P5-Fe1-P2 86.41(3), P5-Fe1-P4 54.03(2), P5-P1-P2 95.93(4), C31-P1-P2 107.51(9), C31-P1-P5 106.08(9), C41-P1-P2 118.24(8), C41-P1-P5 119.46(9), C41-P1-C31 108.34(11), P1-P2-Fe1 88.26(3), P3-P2-Fe1 61.14(3), P3-P2-P1 95.50(4), Fe2-P3-Fe1 140.08(3), P2-P3-Fe1 64.42(3), P2-P3-Fe2 132.67(4), P2-P3-P4 108.06(4), P4-P3-Fe1 64.07(3), P4-P3-Fe2 119.16(4), P3-P4-Fe1 61.25(3), P5-P4-Fe1 62.76(3), P5-P4-P3 101.50(4), P1-P5-Fe1 89.16(3), P4-P5-Fe1 63.21(3), P4-P5-P1 99.70(4).

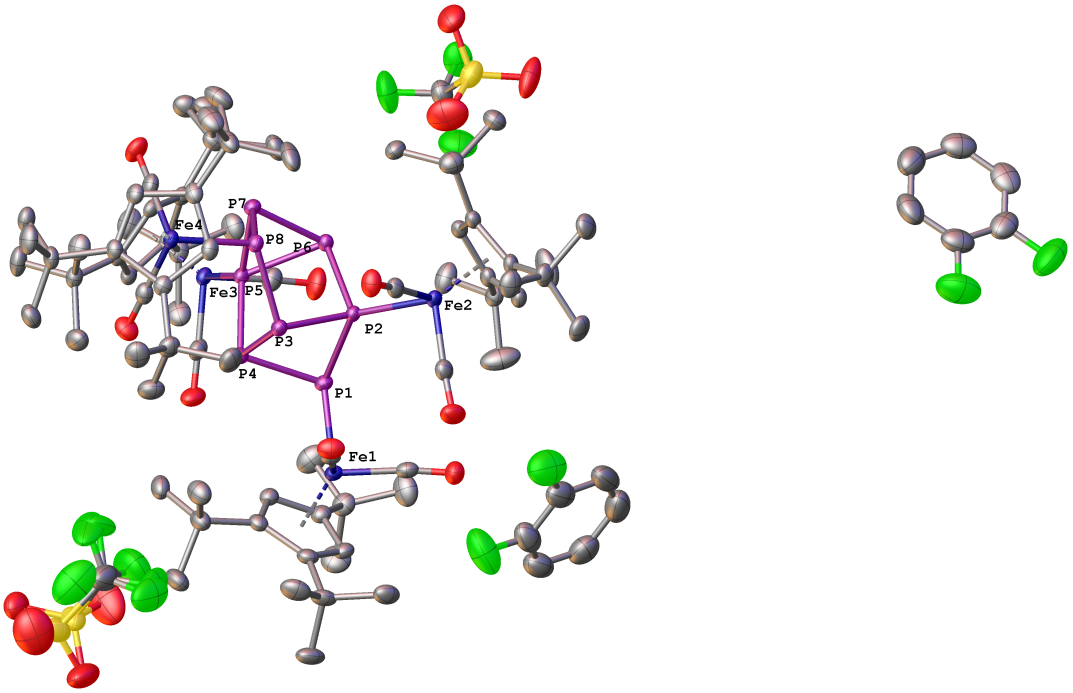


Figure 3.26: Molecular structure of **4** in the solid state. Hydrogen atoms are omitted for clarity. Selected bond lengths and angles: Fe4-P8 2.2756(5), Fe3-P5 2.2468(5), Fe2-P2 2.2587(5), Fe1-P1 2.3040(5), P5-P6 2.2115(7), P5-P7 2.1916(7), P5-P4 2.2134(7), P2-P3 2.1890(7), P2-P6 2.2713(6), P2-P1 2.2758(7), P3-P8 2.1612(7), P3-P4 2.2062(7), P6-P7 2.2071(6), P8-P7 2.1925(7), P4-P1 2.2402(7), P6-P5-Fe3 122.66(3), P6-P5-P4 103.66(2), P7-P5-Fe3 130.27(3), P7-P5-P6 60.17(2), P7-P5-P4 109.69(3), P4-P5-Fe3 116.00(2), Fe2-P2-P6 114.17(2), Fe2-P2-P1 132.07(2), P3-P2-Fe2 117.79(2), P3-P2-P6 102.17(2), P3-P2-P1 88.64(2), P6-P2-P1 96.02(2), P2-P3-P4 85.04(2), P8-P3-P2 100.83(3), P8-P3-P4 110.76(3), P5-P6-P2 95.91(2), P7-P6-P5 59.47(2), P7-P6-P2 104.70(3), P3-P8-Fe4 111.77(2), P3-P8-P7 100.87(3), P7-P8-Fe4 110.90(2), P5-P7-P6 60.36(2), P5-P7-P8 107.42(3), P8-P7-P6 103.88(2), P5-P4-P1 94.68(2), P3-P4-P5 98.62(3), P3-P4-P1 89.12(2), P2-P1-Fe1 117.51(2), P4-P1-Fe1 105.49(2), P4-P1-P2 82.26(2).

3.5.5 Details on DFT calculations and Cartesian coordinates

General remarks

DFT Calculations were performed using the ORCA program package[181]. All calculations were performed in the gas phase and optimized and frequency calculations were performed on geometry optimisations to check for imaginary frequencies indicating local minima. Frequency calculation after geometry optimisation of **3a** gave one very small negative frequency at 5.9 cm^{-1} assigned to the rotation of one Cp''' fragment after multiple optimisation attempts and therefore was ignored. The relative energies of **VIII**, **2a**, **3a**, the decarbonlyated form of **3a** and **1** along with all reagents involved were calculated on the BP86/def2-SV(P)[182,183] level. Input files were generated from solid state structures if possible. Avogadro was used as the graphical user interface[184]. The relative energy of the isomers shown in Figure 5 in the main text has been calculated at the RI-B3LYP/def2-TZVP[182,183,185–193] level of theory using the TURBOMOLE[194–196] program package. The Multipole Accelerated Resolution of Identity (MARI-J)[197] approach has been used in the geometry optimization steps to speed up the calculations. The final energy has been determined by single point calculations on the optimized geometries without the RI approximation. The SCF energies has been used without corrections for zero-point vibration energies.

Thermodynamic data from frequency calculations

Table 3.10: VIIIa, **2a**, **3a**, the decarbonlyated form of **3a**, **1**, CO and $[Ph_2P]^+$ (T=298,15 K; Energies are given in Hartree):

Compound	H	S	G
VIII	$-5.6745817079 \cdot 10^3$	$4.81382458494 \cdot 10^{-4}$	$-5.67472523208 \cdot 10^3$
2a	$-6.47844652692 \cdot 10^3$	$5.594013080664 \cdot 10^{-4}$	$-6.47861331242 \cdot 10^3$
3a	$-6.47845889017 \cdot 10^3$	$5.522705014255 \cdot 10^{-4}$	$-6.47862354962 \cdot 10^3$
3a−CO	$-6.36517179163 \cdot 10^3$	$5.402108334731 \cdot 10^{-4}$	$-6.36533285549 \cdot 10^3$
1	$-6.25195515914 \cdot 10^3$	$5.244931745766 \cdot 10^{-4}$	$-6.25211153678 \cdot 10^3$
CO	$-1.1321765259 \cdot 10^2$	$7.530273352339 \cdot 10^{-5}$	$-1.132401041 \cdot 10^2$
$[Ph_2P]^+$	$-8.0378271557 \cdot 10^2$	$1.629339929566 \cdot 10^{-4}$	$-8.0383129434 \cdot 10^2$

Cartesian coordinates for VIII

Fe	3.46707827004776	5.83255580306058	4.76552523561312	H	-0.37998967444559	5.26536196863209	7.72713444971145
Fe	9.33205094794833	9.95471874186724	3.65058297647087	H	-0.26329269477831	3.51094526250431	8.07757961137690
P	4.82821982199349	7.56432261214437	3.92636772528074	H	1.99585545161762	3.69990388273630	9.08977026485194
P	6.98304365452824	6.89857327931471	3.74085139956528	H	1.96971157740024	5.46940029097200	8.90569298682104
P	6.41713451293886	8.23198822404679	5.41704754611118	H	3.35355193812042	4.52189061973758	8.26433477010797
P	7.13405175462827	9.15505490285786	3.48034492883929	H	1.31237437033780	2.56759933608668	5.69659923711691
O	5.43686405330763	5.09768179620043	6.78389482639981	H	1.80423058726294	2.17017159124495	7.35887694698044
O	4.64739429040817	3.97760303240448	2.85208539983040	H	2.99221422113581	2.90447138898197	6.23069334907500
O	8.59463360093019	11.55604418182907	5.97177403638688	H	0.74708872701137	6.92839957836682	8.56034891621296
O	10.08312534190273	7.68141357154358	5.31344590990229	H	-0.08080185378215	7.97883961894429	7.37024249224677
C	1.75972621241572	5.38462354505798	5.96616679330905	H	0.86408480864385	8.70242301410079	8.71222022491248
C	1.97731044978123	6.85247411672182	5.96415873272510	H	3.39288556027809	8.48863890332653	8.76963444294316
C	1.88518614956429	7.26469727251698	4.58537973110867	H	4.28758733210304	7.89981903902760	7.33266097686595
C	1.60830383368218	6.16008496819697	3.72509267634951	H	3.46603355957740	6.73967056277335	8.41247163106923
C	1.54427064943468	5.01204944557006	4.59292582757097	H	2.28230497582482	10.07063007444876	7.30616793710545
C	10.69172395233700	9.47761630485248	2.04628381888130	H	1.26367205347426	9.59466457218142	5.91749857688390
C	11.22630091101673	10.59151212541045	2.85799281386399	H	3.05826572655074	9.45570947859599	5.82003381425070
C	10.23651535793696	11.63692564629830	2.78147293939379	H	-0.51096531720805	6.93913219085956	1.10763786321080
C	9.13266799721689	11.26286524476249	1.93932197068116	H	-0.13956353722689	7.92888813094469	2.55666324576181
C	9.42389624871807	9.92879708190272	1.51775369800801	H	-0.91875696071912	6.32469196501465	2.74498469433026
C	1.51290488401715	4.31859614702052	7.06305480494812	H	3.24448294808247	6.57715399644605	1.41877454361333
C	-0.01781836005398	4.29633984467156	7.33213441666073	H	2.38409763491514	8.07682198156960	1.85911057862105
C	2.25466793395623	4.52913418481932	8.39942300627070	H	1.90053831970810	7.17632887927104	0.38856308649558
C	1.93056945649511	2.91550574119002	6.54745778548596	H	0.88643287175268	4.87461984791629	0.55725184245512
C	4.19107318427659	4.74365209598225	3.60649899385280	H	0.35830949323681	4.19738453898974	2.12495879659444
C	4.65619515867948	5.43203791067793	5.98249480833576	H	2.10808022459696	4.26740826082314	1.71671965457037
C	8.85375213100492	10.90152776297255	5.04078938099886	H	12.87113373210825	9.16483598914802	0.34428718538648
C	9.76364368780446	8.57520900126706	4.63371340047387	H	11.32618259677543	8.97328418885304	-0.53910790778846
C	2.10894029978755	7.90617700334577	7.09270464182215	H	12.39573500123542	7.55467873718596	-0.28605926571768
C	0.83860905996682	7.86699466487775	7.98185301090749	H	13.17170204061032	7.99231375974435	2.66799021523124
C	3.38309937256180	7.73757500719080	7.95222875222434	H	12.58331806384829	6.46896852191910	1.96398058718662
C	2.17986530260463	9.33157205079824	6.48561066363732	H	11.78066827605907	7.13571047538196	3.41134319505434
C	1.23306708742998	6.22313811896751	2.24346441555480	H	10.57308337635641	6.17748735140047	0.88370910739141
C	-0.16583133159493	6.89341333045907	2.16164313394887	H	9.49450327789576	7.48879726453334	0.35384118128655
C	2.24806012894747	7.06127229284180	1.43626946920056	H	9.48749801762101	6.97359477287645	2.06999075928021
C	1.14406714705048	4.80726320541628	1.63389737959565	H	14.69218311839327	11.02001712397613	3.03328649010750
C	11.28069057514398	8.14830756794409	1.51186831947524	H	13.56670014737877	11.42592214450076	1.69826653948901
C	12.01248588991017	8.48498912358574	0.18247167191640	H	13.85414348090408	9.71773632885737	2.14629179400305
C	12.25805515275884	7.41043803951217	2.45111854567352	H	13.58970478134708	12.42339841610084	4.67676451016195
C	10.13768401768110	7.14962634692831	1.18977344553939	H	11.82165828865059	12.43712487354585	4.91348958450124
C	12.57602810144450	10.83320402901804	3.57930593742151	H	12.53369917498405	13.04604285625540	3.37598910739340
C	13.73278812043468	10.73768611152832	2.55238649361690	H	12.75976713438804	8.81163173480157	4.48977132873082
C	12.61962527479949	12.26888080614346	4.16251504767968	H	12.07297574462517	10.05462224297802	5.56732533605726
C	12.82014252764407	9.87617695761061	4.76917527540661	H	13.82824651749585	10.05761865587989	5.19889159948996
C	8.02119527218459	12.19114332818658	1.44472154739870	H	9.23264451227385	12.81553695406731	-0.29752281100224
C	8.69191394063063	13.27326747512046	0.55643495433757	H	9.41887425209552	13.88377966290610	1.13098365139148
C	7.29766864088352	12.87763490779248	2.62522592190753	H	7.92372498837783	13.96042055338324	0.14395100825146
C	6.99129295296075	11.41506145260804	0.59733360458798	H	6.55614796001459	13.61328984104542	2.24897308532580
H	2.02035538278442	8.29503725182757	4.24107782547994	H	8.00377372578613	13.42438449632983	3.28370837328723
H	1.34651765585157	3.99100651122922	4.25297219156670	H	6.75786998311212	12.13341218305217	3.24504977315318
H	10.32308489975553	12.60725724843680	3.28057402267174	H	7.45740102757104	10.96581766937958	-0.30389569101747
H	8.77601710304090	9.32496483674490	0.87518095611553	H	6.19300012386769	12.10168469219501	0.24789193408914
H	-0.58598345645635	4.07960010533362	6.40461961954534	H	6.51560310762961	10.60482717659705	1.18722196454130

Cartesian coordinates for 2a

Fe	3.43103480027236	6.27653491873993	4.22122356596875	C	1.57723242751476	7.29841861056179	4.52333203960959
Fe	9.44125697807932	10.11913957509240	3.62384711103469	C	1.30853806302225	6.13728658936456	3.73363698056255
P	4.56087226051688	8.13131354006404	3.40573316732215	C	1.77472213631231	5.03033155253414	4.52532272843292
P	6.74004640390710	7.62402880155145	3.07528422440876	C	11.01114543072608	9.45501496158686	2.29695381915431
P	6.14748099088583	8.95463961996078	4.77991099813488	C	11.54636808942367	10.43213188267729	3.27001093968568
P	7.23396797725428	9.84353187723092	2.99407759436126	C	10.78214103973571	11.63845912889292	3.06610604667307
O	5.74629999994932	5.48041179990348	5.81901997811696	C	9.83117007485840	11.49447432086660	1.99911274659786
O	4.41179947206707	4.65992619126567	1.99078688582499	C	9.97128630971882	10.13969873710549	1.56038589644288
O	8.63875675751899	11.76411700521482	5.89884826063651	C	2.43850323256122	4.37517422732114	6.90658895447245
O	9.52843561592740	7.68450122855279	5.23250049086745	C	1.00555296191329	4.02716682966231	7.41220932094519
C	2.22602548546462	5.46476839724110	5.82263884668119	C	3.31382334906211	4.73759855042628	8.12399682982595
C	2.12116906791885	6.94266407368171	5.81832533322243	C	3.04732350693861	3.08969375048084	6.28424692078662

C	4.00074244622587	5.32967353310077	2.84703981843808	H	1.23155233817468	4.01783745257609	1.92154335577730
C	4.84680430161142	5.85029419488300	5.18406121840497	H	1.92384804758680	5.39427459616162	0.99631433827555
C	8.93048980388848	11.10408357536747	4.98469619465009	H	13.37035939052943	8.90518423172002	0.97576452511862
C	9.48776027376164	8.64329254081378	4.57102929916533	H	12.00076300847407	8.94586384154482	-0.17616324650344
C	2.27700799851183	7.99978840797371	6.93570477048651	H	12.82079751771098	7.39291949514392	0.18790515539744
C	1.21294622189551	7.71479540991639	8.03080636198386	H	13.09107925898501	7.58261206553142	3.24009450285238
C	3.69291408533477	8.05055945196674	7.55273310403552	H	12.44021642819557	6.19961354351041	2.33402154382194
C	1.97906465533086	9.41382576903332	6.38165600704456	H	11.48538875844271	6.90161611244284	3.66763501734475
C	0.42810722772883	6.00558593518067	2.49144879604764	H	10.63964765948275	6.27250394038968	0.87820480699960
C	-0.93721564834960	5.47180115519720	3.01606082647130	H	9.82735823241388	7.75312929447331	0.32552675924200
C	0.19772972322138	7.36374479479193	1.80703010645984	H	9.49245454885784	7.10853499133043	1.96842214914230
C	1.00183060429177	5.00311721184299	1.46791947640632	H	14.92819482344987	10.30259827613476	4.12793796942167
C	11.47981643717554	8.06920345068049	1.79060899801108	H	14.16217517605191	10.94366004862021	2.64146975418267
C	12.47691921436214	8.35091245095660	0.62934465716600	H	14.11348358358132	9.18880051976041	2.99788685264438
C	12.16122648885010	7.15239186685429	2.82759765856610	H	13.73481003006717	11.76695412266050	5.65228568859861
C	10.28551648113706	7.26883787486498	1.21006851878079	H	11.97951167118477	12.05702595079877	5.54254650776653
C	12.74430217789690	10.41794150859940	4.25383872810959	H	13.07819063049477	12.61678316636676	4.22836167591524
C	14.05481629788708	10.19497762980991	3.45288859233754	H	12.46444109411515	8.34463985013433	5.01969291701068
C	12.87929267374302	11.79764620335348	4.94863592108316	H	11.75947953736619	9.62256145617508	6.05014566394634
C	12.61173645208715	9.37328868434279	5.38735828950073	H	13.53163268027935	9.37973149965043	6.00736315949867
C	9.03912564712142	12.62735274715373	1.34434412644372	H	10.67563465701716	12.98797985566118	-0.10075303325216
C	10.07723975731132	13.54869392964141	0.64596717213403	H	10.77921412001335	14.00276348178456	1.37465087530728
C	8.25792546335351	13.44713897866547	2.39545477283552	H	9.55863139305021	14.37424858242818	0.11632460619565
C	8.06114245017773	12.08476381987266	0.28090822528167	H	7.75825342142272	14.31112366173096	1.91158008063861
H	1.37487087919809	8.32583167492497	4.20342028511442	H	8.92062261616328	13.84975508605015	3.18821638157268
H	1.72279364500403	3.98204297544477	4.21283751123087	H	7.47680493378325	12.82882780728919	2.88276319757959
H	10.93201432354375	12.56285587767455	3.63301399841508	H	8.59302713782558	11.54959514770107	-0.53223310883845
H	9.38977334801091	9.68427446352273	0.75246466790113	H	7.50792551450303	12.92473997152439	-0.18595041362974
H	0.35645094212247	3.67334417545788	6.58596007803908	H	7.31446668931123	11.39385925454224	0.72423746364264
H	0.50904970931466	4.89581326807390	7.88641284439197	P	4.14170673665717	9.83731953860904	1.96267039218050
H	1.06597402985737	3.21689555562110	8.16710844741066	C	2.89335615325153	10.87275303510507	2.84386413890554
H	3.36074900364963	3.85811997090997	8.79697930004868	C	3.44115711869234	11.88163707429697	3.67489266953831
H	2.90240289557686	5.57096091503135	8.72045826233907	C	2.60398645011460	12.77548746111229	4.36104526440232
H	4.35380980924249	4.98271531429173	7.83826156199103	H	3.04495457773025	13.55479276713573	5.00128600024333
H	2.39852009157699	2.62785738698390	5.51518576951245	C	1.20885011804230	12.68653333853819	4.21506067838764
H	3.17640799359774	2.33115845241338	7.08131891617290	H	0.55190040536160	13.39586785358161	4.74128277739651
H	4.04409612216832	3.27371834125675	5.83771991514564	C	0.65484989263055	11.69448343026586	3.38579241833535
H	1.39167946216915	6.76202812061228	8.56241173858276	H	-0.43727760415453	11.62643485022103	3.26263672394948
H	0.19149394620960	7.68112629086620	7.59954358457888	H	4.53531152179849	11.96831778942984	3.77390109979093
H	1.23241940908356	8.52527310154457	8.78753808360903	C	1.48793008056452	10.78934366707325	2.70802151886432
H	3.71514021573731	8.79481340674042	8.37459065485336	H	1.04232478459846	10.02280844628166	2.05907730205358
H	4.43845357669952	8.36747667825052	6.79640690393689	C	3.30758784327981	9.06271597068704	0.51849242661061
H	4.02460740942974	7.08541454007375	7.96724551285326	C	2.44275504121830	9.83492645570127	-0.29749984810060
H	2.12452973824047	10.15748898914586	7.18982420076111	H	2.14417665064110	10.84826337823548	0.01094656905430
H	0.93440174726062	9.51857132979711	6.02693167220172	C	1.97258760346017	9.32441355199917	-1.51832061189396
H	2.65998628838832	9.69403480428249	5.55320138787248	H	1.29884199820329	9.93743927033893	-2.13669274285747
H	-1.65495390565630	5.38993210339649	2.17443748540670	C	2.36347755983834	8.04705941702553	-1.95490106992737
H	-1.37581674343576	6.15300161021888	3.77340710094123	C	3.24203367999152	7.28423445956157	-1.16583093961863
H	-0.83782287601389	4.46719525349044	3.47481171582343	H	3.56832550317920	6.28884447976334	-1.50465634412033
H	1.14918904432056	7.80655943269299	1.45373527110776	H	1.99426163265661	7.65195683021970	-2.91340929070970
H	-0.30484853608628	8.08195175079295	2.48633122043678	C	3.71515564024440	7.78762389302061	0.05607578111698
H	-0.45829023141258	7.23477074010024	0.92315307073336	H	4.41845075891517	7.18269828231720	0.64861725710564
H	0.26239595064603	4.82714363718351	0.66084020259713				

Cartesian coordinates for 3a

Fe	-4.28432384517194	-1.08635026421967	14.49345434516177	C	-3.54433914977195	-2.80769787722160	15.56712937306604
Fe	0.38110441495623	3.37136145016491	15.27134811087277	C	-1.30859706366093	3.31572893505732	10.22322462691571
P	-1.13355655726442	3.45452891538698	13.52660563874998	C	0.86043185777133	4.27237742791809	17.09663473127102
P	-3.05768887263011	2.27039888607939	13.88994855536273	H	0.82934695598464	3.75221809673559	18.05859490374191
P	-0.95829653179676	2.20066717604805	11.64461124835378	C	0.46394538686825	1.17225448483395	11.11067755995518
P	-2.36918391933369	0.13730449711481	13.94839020816314	C	0.24431378251242	5.51057592081118	15.29151364003471
P	-2.87975820179563	1.05999448059073	11.94867595167144	H	-0.35633303753508	6.09871149580465	14.59203289929357
O	-6.27399752683393	0.40835093726180	12.95957249644302	C	3.36848728659290	3.81126300974156	16.80450884575129
O	-0.99781271285914	1.27760176440884	16.75844564450651	C	1.62086960839630	5.14916928377919	15.06983973148482
O	2.06173263515945	1.33976589395275	14.01767481733544	C	-5.15922971685563	-2.35606065429385	10.98686215686806
O	-4.67283459117002	0.69395263594883	16.77667570397388	H	-6.18825070198836	-2.46560589717837	11.38360017285219
C	-4.18177097474932	-2.87553634228374	13.27790713855908	H	-5.18194235243724	-2.69234512203073	9.93040705602872
C	-3.08996392117691	-2.82874866382621	14.19910866801904	H	-4.90271646004744	-1.27840562343823	10.99192508643703
H	-2.03774584843683	-2.82615590930430	13.90324339716268	C	-5.36051322449343	-2.83853738626779	14.10226446099879
C	-4.13021573957701	-3.18603330464482	11.78305475353670	H	-6.38504099434870	-2.86158010425530	13.71633388778511
C	2.02255793369649	4.33819596293472	16.24558968966759	C	-0.24506210829508	5.00615136728649	16.53452624094781

C	-5.02699965391393	-2.80956898348829	15.50457337417935	C	-1.68804739678141	3.54370840219907	7.82437774627766
C	2.40577046111582	5.73944358679540	13.87349273054795	H	-1.73817327076851	3.09226964582122	6.82240284137163
C	-2.53261106943822	-2.96778415785412	16.73163965445164	C	-1.93610423080970	4.91796786373506	7.99412957376906
C	-5.44104056881643	-0.16133314783903	13.53923532268880	H	-2.18339276707158	5.54332018591288	7.12340125685244
C	1.43218854026837	1.70350507668751	10.22603794548602	C	-1.88252041988417	5.48696695985515	9.27661231612985
H	1.31712294167105	2.71865919578743	9.81913894789621	H	-2.09003807923038	6.55833096023456	9.41530218213261
C	-2.72098151694810	-2.94001837297040	11.20998645936072	C	-1.56077062410225	5.38026237299359	17.21504079605489
H	-2.40907671200388	-1.88489823508430	11.34402268114765	C	-1.39769315739872	6.84882409956995	17.69651660054159
H	-2.70864805196560	-3.15775758063176	10.12312238862765	H	-0.54275390819908	6.95498355977341	18.39442523278737
H	-1.95845249141404	-3.59275268583833	11.68126957728109	H	-2.31257741160858	7.17844164767431	18.22944862822595
C	4.45908638776180	3.46368643182441	15.77100369179582	H	-1.23208913196109	7.54223315970254	16.84756395362416
H	4.13617656841163	2.66829719626300	15.07297578806444	C	-0.48993335573157	2.11140536134737	16.12463336320094
H	5.35022874586805	3.08141732040828	16.30803445129287	C	1.48759735295817	6.66503201159138	13.03826494857312
H	4.79611542363540	4.33490847855530	15.18237214914751	H	0.61587669250874	6.12078930441512	12.62204315468960
C	1.72045930760550	-0.91221990999457	11.22593546402446	H	2.06083949861827	7.06810155902522	12.18022125093042
H	1.83751405856225	-1.93203605510205	11.62136837827411	H	1.11740351927402	7.53344133640575	13.61881266211213
C	1.39456036388918	2.17934139679477	14.47081251485488	C	-2.74673538138279	5.29551751754009	16.23142549209401
C	0.62173293647050	-0.13481290916619	11.62225327666467	H	-2.59396371716008	5.91943999498399	15.32791448007250
H	-0.11054685878318	-0.53097434401524	12.34307592255851	H	-3.67552981834100	5.65155938293559	16.72085471526922
C	-4.49187864473015	-0.02070226765552	15.87569509316664	H	-2.92591542938196	4.25221377283484	15.89929754071711
C	3.55778496927620	6.62685775413403	14.41339767428180	C	-1.84154153073634	4.48171826454922	18.43680949975048
H	3.17647426321698	7.39907518906846	15.11175669587889	H	-1.93380873571883	3.41392051213543	18.15853379225103
H	4.05108945699246	7.15260857687259	13.57090832438602	H	-2.79687347151602	4.78130655188271	18.91213653991218
H	4.33815246176344	6.04874659996578	14.94060101904093	H	-1.05405472003849	4.57294430297805	19.21207779289810
C	3.13853868889570	2.52990453128964	17.64734814542216	C	-6.46969366827795	-4.53073652233897	16.56558196047142
H	2.50973409484967	2.70095390122969	18.54225212280535	H	-6.74363512293890	-4.90977603163459	15.56064149057548
H	4.11363931894377	2.15767489734551	18.01888757843645	H	-7.32168762513735	-4.73298045559899	17.24638958728093
H	2.67708133066863	1.72006610958274	17.04835078615872	H	-5.60379531132705	-5.12034680466513	16.92367044041973
C	2.94853336627422	4.66667520968902	12.90201138644809	C	-1.08453755592253	-3.00811992898669	16.18091837437208
H	3.59231111843788	3.91797947985272	13.39044667197397	H	-0.90687842817235	-3.87375990754388	15.51174229997505
H	3.54574786105125	5.15104102239227	12.10256475748594	H	-0.37749224466553	-3.10506022614956	17.02867103891087
H	2.11371037834853	4.12432376412923	12.41492116184816	H	-0.81918182602333	-2.07753597270808	15.63899903454442
C	2.67555975430061	-0.38762016079618	10.33818562684948	C	-2.79125666715952	-4.33688330052161	17.41500179998911
H	3.53796181413491	-0.99884256114320	10.03312200652596	H	-3.76842979125112	-4.38166930640628	17.92989188453145
C	-6.16535664252833	-3.00655976235871	16.53583839067441	H	-2.00849550692229	-4.52977758928258	18.17669303364558
C	-1.57742979756871	4.68863882360059	10.39238750917242	H	-2.75643537991244	-5.16632547198252	16.67994648110616
H	-1.56644069692265	5.12231261920019	11.40420795148386	C	-2.56990692180060	-1.82304864165864	17.76789297508499
C	-1.37543048263854	2.74127828311424	8.93106285543512	H	-2.23809932337913	-0.86878908317225	17.31454467576807
H	-1.18523825534704	1.66642444884602	8.78707251417854	H	-1.87291178836409	-2.05396864513687	18.59939354535644
C	-4.47485580150624	-4.69447055192677	11.64477780543668	H	-3.56613573064386	-1.66000827521313	18.20821981681405
H	-3.77184113085546	-5.32663508155447	12.22389116080596	C	-5.88099721007206	-2.52561881716565	17.97297537231664
H	-4.41328277577888	-5.00385573792441	10.58134722198741	H	-5.04856055227088	-3.06735921135310	18.45640997782057
H	-5.50150922476166	-4.91428351890760	12.00060883634232	H	-6.78041361409629	-2.70719017412157	18.59463816438281
C	3.90498552407290	4.92001439879648	17.75377314146854	H	-5.66993880131754	-1.44028277637191	18.01648749875545
H	4.11323020912858	5.86487381853761	17.21631537042123	C	-7.44684556664476	-2.26618524498277	16.07135481438912
H	4.85004634711436	4.58548054034794	18.22791285029179	H	-7.27616547534453	-1.17581244994261	15.97339855449829
H	3.18207709684721	5.14557134445537	18.56329829377528	H	-8.24711550060002	-2.41416046920333	16.82299514171477
C	2.53199434142094	0.91997758702134	9.84392397600968	H	-7.84795970291251	-2.64092205982401	15.10993355254547
H	3.27836524483485	1.33379160463648	9.14966273698435				

Cartesian coordinates for 3a−CO

Fe	-3.79274893401707	-0.43117540822468	14.69834596898268	C	-0.26193997808202	4.28401711240403	16.04369428311523
Fe	-0.16455514756921	2.47425853107216	14.89366228948742	C	-4.46513672706116	-1.89493390331271	16.11798191555630
P	-0.96542257714830	3.78192660908364	13.20257730288496	C	-4.80352807698086	0.06612082185305	13.33503221559349
P	-3.12257926449535	2.82785801719101	13.14670551826543	C	1.54691924527975	2.98180361112802	9.94592836435172
P	-0.87931978048603	2.61232248399241	11.29839357117721	H	1.32244640877816	4.05842583241473	10.00692929045469
P	-2.05239036926348	1.20438391724470	14.23955610715702	C	2.10441758997176	0.22720775798698	9.74401753516963
P	-2.28191883678942	1.00628962439929	11.98740613479659	H	2.32061810237286	-0.84879563016811	9.66065115688307
O	-5.63284041201494	0.35637800382934	12.57169963888122	C	0.90265331050501	1.48001784357785	13.96657425025658
O	1.67086463668876	0.81877080682433	13.37577892303305	C	0.94168557164806	0.65505766702732	10.40454024815515
O	-5.23933415717160	1.58853112335828	16.21170732553819	H	0.25524970959564	-0.08505623201186	10.84542095888627
C	-3.57056809101099	-2.53671063888149	14.00843027225371	C	-4.59709176835826	0.79708787950273	15.64767147721786
C	-2.45273861146942	-2.22137205537041	14.89507378642024	C	2.99142326707553	1.17000844069731	9.19769507500065
C	0.21909088640953	2.25315971203630	16.96135153919878	H	3.90550833497280	0.83114184159938	8.68673341774186
C	-3.03283929015984	-1.77623547876756	16.14900908840967	C	-2.30168688841297	4.83505033936373	10.25331558532064
C	-1.76683375683805	3.55450919432219	9.99696573086388	H	-2.16273626263765	5.30451064143123	11.24087673497659
C	-0.80745417193434	3.25271832458963	16.85504662748795	C	-1.92680115034937	2.96383578995411	8.72209421372581
C	0.65908138889822	2.03252467024500	10.50279712900297	H	-1.50514101711237	1.96899372088574	8.51061621024881
C	1.11617609949291	4.00417201083299	15.68992557714011	C	2.71406311040656	2.54545712828857	9.30145838103545
C	1.42942049605003	2.69998121263024	16.30967212395317	H	3.40752578727893	3.28347334278537	8.87084727753810
C	-4.77848274192223	-2.27910778701995	14.77997454144299	C	-2.62267583091782	3.65248849450882	7.71764293108936

H	-2.74827737594602	3.18961156497411	6.72700452959975	C	-0.73998874205827	-4.04589104758989	14.83977776823799
C	-3.15502785693372	4.92879416478582	7.97376578917213	H	0.34236577900258	-4.28172335193825	14.90246350174265
H	-3.69627237978532	5.46712161263052	7.18086334570149	H	-1.23611764685925	-4.50291197102140	15.72029226527273
C	-2.99120198158756	5.51873221939898	9.23805619164085	H	-1.13336667879232	-4.53660018899378	13.93025401390074
H	-3.39817194377432	6.52105462428302	9.43841673191512	C	1.98972829275856	5.08245427592940	14.99554081513650
H	0.13324337664713	1.32670010778166	17.53659265064532	C	3.11083624819714	5.55387174517046	15.96045693112976
H	-0.79598263617078	5.19907143242913	15.76857356155015	H	2.68819172700955	5.88895506839561	16.92966698931976
H	-2.45881878074236	-1.47833268920434	17.02983767575366	H	3.64304516080822	6.41839969672773	15.51309255486704
H	-5.79396133586183	-2.44935613423727	14.40754664817624	H	3.86631805912720	4.77541730336186	16.16936553689704
C	-5.42902995478625	-1.91167120197980	17.30414862822415	C	1.14387610598092	6.34466438060886	14.68318032577837
C	-5.49310377209706	-3.40658656948586	17.73768846048051	H	0.75022318984578	6.82276283627818	15.60288176848022
H	-5.87644646107529	-4.05138024410736	16.92118435061351	H	1.78499998390645	7.09309207163459	14.17542575453169
H	-6.17353854688440	-3.51444879618793	18.60701308844901	H	0.29408264411178	6.12249378352266	14.00751714525605
H	-4.49519130124577	-3.78714755654752	18.03516117215141	C	2.59038866800226	4.60186314976150	13.65304516397056
C	-6.84888921565381	-1.45002800429743	16.90698249823079	H	3.25702804720448	5.38390081222246	13.23365283484870
H	-7.27244223423443	-2.06412335265014	16.08682673580662	H	3.17433031203279	3.67133696178964	13.74987027630929
H	-7.53105070803927	-1.55544452796952	17.77433691284298	H	1.78411141756165	4.41182662989516	12.91541482320754
H	-6.86774366867830	-0.38860105608842	16.59369409206458	C	2.75593455237989	1.95841352760666	16.62113197267238
C	-4.91519091242102	-1.07749002090686	18.49502564692337	C	2.51538606469149	0.44130081728962	16.82034512946971
H	-5.61729456864227	-1.17257246285150	19.34803941509978	H	1.82114716722978	0.21848897648801	17.65428271262075
H	-3.92576612335808	-1.43006230684773	18.85062594990987	H	3.47790335761163	-0.04822158551255	17.07069922468538
H	-4.83562346848133	-0.00171700977011	18.24951158902283	H	2.12763489698683	-0.03580976404868	15.90105509218789
C	-3.73290612639183	-3.32213094593134	12.68014456392559	C	3.23965795903209	2.53377626532860	17.98585693798961
C	-4.01990515632537	-4.79190837443552	13.11148163286516	H	2.48032533965027	2.37354192182585	18.77793446857617
H	-3.18802495210261	-5.21982894291296	13.70391029928859	H	4.17267838283447	2.02157020735630	18.29800068719972
H	-4.15950858023284	-5.42478148301176	12.21146413024788	H	3.44707635005361	3.61886084698327	17.93177514670373
H	-4.94225626697614	-4.86325929241185	13.72260878871443	C	3.89492176470733	2.08637012171174	15.58758726714621
C	-2.53668233178256	-3.31263115905206	11.71212140775382	H	4.77400024151341	1.52257810260204	15.95963067893735
H	-1.65059533607957	-3.83076281515055	12.12016244062459	H	3.61862036623567	1.65433821429396	14.60747762425740
H	-2.82183626476124	-3.85080103205428	10.78589509196604	H	4.22670769354692	3.12668726365280	15.43286338025723
H	-2.25478951977403	-2.28144362724667	11.42214042967373	C	-2.08526857005474	3.35373288368588	17.67751075570891
C	-4.94766195438659	-2.82107296440243	11.85745728242455	C	-1.73448261055044	4.21875910017361	18.92300194868951
H	-5.10806103558575	-3.51039481318067	11.00497196184321	H	-0.91205106121377	3.76198008723811	19.51032197043137
H	-5.89699476565693	-2.79646327555904	12.42630817092031	H	-2.62145332248529	4.30876502473551	19.58412688990003
H	-4.76708743298938	-1.81351064291502	11.43836079372020	H	-1.42111243795459	5.24164926004560	18.63197781358327
C	-0.93366038807072	-2.50594849111312	14.81261661860111	C	-2.53482984763037	1.96347960145948	18.16828827438465
C	-0.21900501822698	-1.93248754071057	16.06035836311983	H	-1.79103933044759	1.51990244014614	18.86162552166951
H	-0.34630003359766	-0.83262242963649	16.12796722570407	H	-3.49261057090050	2.04301125659659	18.71944769956563
H	0.86614369796847	-2.14043836421768	15.98324824361138	H	-2.67841594117193	1.25733817432605	17.32627515054448
H	-0.56930286284660	-2.39432418798939	17.00453492631174	C	-3.20739334667797	4.05865988849017	16.88758921489974
C	-0.21866562440198	-1.90132189710108	13.58682567240050	H	-4.13245733245737	4.11682272655561	17.49512155905033
H	-0.37294621112859	-0.80769611716316	13.54614569069479	H	-2.92438257816234	5.09588479834239	16.61881674162069
H	0.87224851474041	-2.08200554043651	13.66631580911454	H	-3.45493659104368	3.52156012147193	15.95036576310923
H	-0.55753376842338	-2.32870766442255	12.63192597905620				

Cartesian coordinates for $[Ph_2P]^+$

H	-2.81029505290288	6.18397711900421	9.73143037677821	C	2.67353777695092	-0.75773397638718	10.91838497280118
C	-2.24702713037520	5.27392744734249	9.47754953187262	H	-0.14587056829463	-0.24034308566063	12.79655356104819
C	-1.90202971837021	4.36151777232332	10.47640779071743	C	1.66428772162779	-0.99835467523601	11.87317508848743
H	-2.20281528533194	4.54836769972163	11.52029975337520	H	1.69999374350247	-1.90093365438379	12.50112644638162
C	-1.13713761431867	3.18937994572326	10.15672250278754	H	-2.18521851750466	5.71609500237519	7.34797467426603
C	-0.80527590809520	2.92891836861653	8.78789233436006	C	-1.88969314153858	5.00991548890581	8.13945318165062
P	-0.81735175870561	2.14943739386979	11.56292238883900	C	-1.18553003501509	3.83235768468136	7.79603181936613
H	1.62219666368201	2.25248355329552	9.65428430310182	H	-0.95144011831427	3.62165862347850	6.74170058125130
C	1.60851311628775	1.32501557616092	10.24426236489007	H	-0.30081549306715	1.99334005582346	8.50744766779533
C	0.56035497790163	1.08868204700339	11.19123147693557	H	3.47242565119205	0.60217735761383	9.41088051151404
C	2.65309650238373	0.40938938836373	10.11992226993722	H	3.50320316552303	-1.47409748051324	10.81018711197529
C	0.63139102278270	-0.07217765212211	12.03285928986797				

Chapter 4

Structural Diversity of Molecular Alkaline-Earth-Metal Polyphosphides

Results of this chapter have already been published in: A Structural Diversity of Molecular Alkaline-Earth-Metal Polyphosphides: From Supramolecular Wheel to Zintl Ion by Martin Weber, Ravi Yadav, Akhil K. Singh, Luca Münzfeld, Johannes Gramüller, Ruth Gschwind, Manfred Scheer and Peter W. Roesky in *Chem. Eur. J.* **2021**, *27*, 14128-14137.[198] The open access article was published under the creative commons license and the work was supported by the Deutsche Forschungsgemeinschaft within the projects Ro 2008/21-1 and Sche 384/45-1.
Contributions: Conceptualization: M.W., R.Y., M.S and H.R; methodology, M.W., A.S., L.M. and R.Y.; software, M.W., R.Y., J.G. and A.S.; validation, M.W., R.Y.; formal analysis, M.W., R.Y, L.M. and J.G.; investigation, M.W. and R.Y.; resources, M.S., P.R.; data curation, M.W. and R.Y.; writing-original draft preparation, M.W. and R.Y.; writing-review and editing, M.W., R.Y., J.G., M.S. and P.R.; visualization, R.Y.; supervision, M.S. and P.R..; project administration, M.S. and P.R.; funding acquisition, M.S. and P.R. All authors have read and agreed to the published version of the manuscript.
Details to contribution: Synthesis and characterization of all compounds with $^{\mathrm{Dipp}}$BDI-Mg was performed by Martin Weber, while all $^{\mathrm{Mes}}$BDI-Mg containing products where synthesized and characterized by Ravi Yadav. The numbering of figures, schemes, tables, references and compounds have been changed respective to the original publication for a uniform appearance of this thesis.

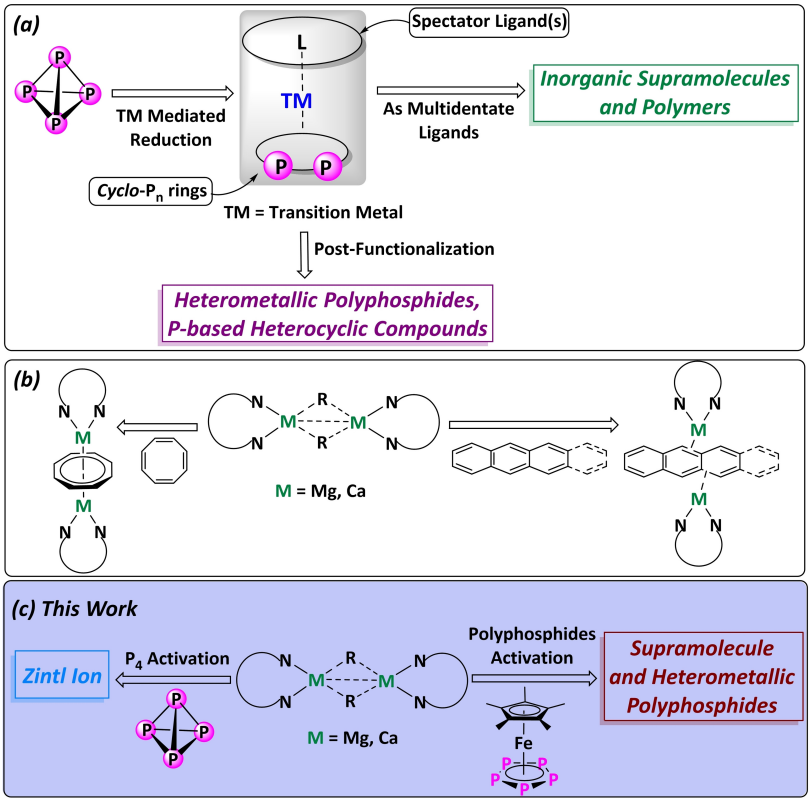
Abstract

A series of molecular group 2 polyphosphides has been synthesized by using air-stable $[Cp^*Fe(\eta^5\text{-}P_5)]$ ($Cp^* = C_5Me_5$) or white phosphorus as polyphosphorus precursors. Different types of group 2 reagents such as organo-magnesium, mono-valent magnesium, and molecular calcium hydride complexes have been investigated to activate these polyphosphorus sources. The organomagnesium complex $[(^{Dipp}BDI\text{-}Mg(CH_3))_2]$ ($^{Dipp}BDI = \{[2,6\text{-}^iPr_2C_6H_3NCMe]_2CH\}^-$) reacts with $[Cp^*Fe(\eta^5\text{-}P_5)]$ to give an unprecedented Mg/Fe-supramolecular wheel. Kinetically controlled activation of $[Cp^*Fe(\eta^5\text{-}P_5)]$ by different mono-valent magnesium complexes allowed the isolation of Mg-coordinated formally mono- and di-reduced products of $[Cp^*Fe(\eta^5\text{-}P_5)]$. To obtain the first examples of molecular calcium-polyphosphides, a molecular calcium hydride complex was used to reduce the aromatic *cyclo*-P_5 ring of $[Cp^*Fe(\eta^5\text{-}P_5)]$. The Ca-Fe-polyphosphide is also characterized by quantum chemical calculations and compared with the corresponding Mg complex. Moreover, a calcium coordinated Zintl ion $(P_7)^{3-}$ was obtained by molecular calcium hydride mediated P_4 reduction.

4.1 Introduction

The recent years have witnessed a surge in the development of new methodologies for the transformation of white phosphorus (P_4) to valuable compounds.[199–206] The conventional methods for P_4 utilization involve toxic (Cl_2), corrosive (PCl_3), and pyrophoric (Na) reagents.[207] To circumvent such routes, the reductive functionalization of P_4 at ambient conditions by low-valent compounds offers an attractive alternative.[23–25,208–212] As a result, a variety of metal/non-metal coordinated P_n (n = 2 to 7) structural motifs have been obtained by a reductive approach. Despite a plethora of such polyphosphides, their further functionalization and utilization has been scarcely investigated.[213] The utilization of such stable polyphosphide-based systems instead of the highly strained P_4 cage as a polyphosphorus source is an elegant approach (Scheme 4.1).

In a breakthrough report in 1987, *Scherer and Brück* successfully synthesized the air-stable pentaphosphaferrocene, $[Cp^*Fe(\eta^5\text{-}P_5)]$ (**XXVII**), via co-thermolysis of $[Cp^*Fe(CO)_2]_2$ and P_4.[69] The *cyclo*-P_5 ring in **XXVII** has five lone pairs in C_5 symmetry and the Scheer group has advantageously utilized this property to pioneer a new area of inorganic supramolecular and coordination polymer chemistry.[80,83,85,86,90,214,215] Interestingly, the frontier molecular orbitals of **XXVII** show significant contribution of the phosphorus atoms indicating the involvement of the *cyclo*-P_5 ring in redox



Scheme 4.1: (a) TM mediated P_4 functionalization and its further use as ligands and as phosphorus source, (b) group 2 complexes as reductant for organic substrates, (c) overview of this work.

events,[173,216] which has been confirmed by cyclic voltammetry[74,173] and synthetically[173,216,217] as well. The air-stability and redox non-innocent nature of the *cyclo*-P_5 ring towards low-valent species makes **XXVII** a suitable candidate as a polyphosphorus source. Very recently, we have used **XXVII** to obtain E-phosphorus (E = Si, Ge, Al species) heterocyclic rings.[218–220]

Also, **XXVII** shows nucleophilic-addition type reactivity towards various main group nucleophiles.[77] The reported examples of s-block polyphosphides, synthesised in solution or by solid-state routes, are dominated by group 1 elements.[221] Only a few structurally characterised group 2 polyphosphides are known.[222,223] This scarcity could be attributed to the instability of group 2 polyphosphides due to hard-soft mismatch and Schlenk equilibria. In 2016, *Hill* and co-workers reported molecular magnesium polyphosphides by the reaction of P_4 with organo-magnesium reagents.[224] To date this is the only report of group 2 element molecular polyphosphides.

In 2007, *Jones and Stasch et al.* reported a series of stable molecular mono-valent magnesium complexes.[126] Apart from being a fundamental breakthrough, Mg(I) complexes featuring a Mg-Mg bond have shown a wide range of potential applications due

to their strong reducing nature. The selectivity of Mg(I) compounds in reduction reactions has rendered them a promising class of reductants, and they have been promoted as "quasi-universal" reducing agents.[127,128] Recently, *Schulz* and co-workers used β-diketiminate coordinated Mg(I) with $\mathrm{Pn_2R_4}$ (Pn = Sb, R = Me, Et; Pn = Bi, R = Ph) to isolate Mg-coordinated realgar type $[\mathrm{Pn_8}]^{4-}$ polypnictides.[225,226] However, the reactivity of Mg compounds towards metal-coordinated polyphosphides has not been studied till date. Unlike Mg, monovalent-Ca species with a Ca-Ca bond are not yet known.[227] In 2006, *Harder* and co-workers reported the hydrocarbon-soluble molecular calcium hydride complex, $[\{(^{\mathrm{Dipp}}\mathrm{BDI\text{-}Ca\text{-}H(thf)_2}\}_2]$ ($^{\mathrm{Dipp}}\mathrm{BDI} = \{[2,6\text{-}^{i}\mathrm{Pr_2C_6H_3NCMe}]_2\mathrm{CH}\}^{-}$),[228] to reduce organic substrates.[229–232] Very recently, *Hill* and co-workers have isolated trifold-coordinated $[(^{\mathrm{Dipp}}\mathrm{BDI\text{-}Ca\text{-}H})_2]$[233] and used it to reduce alkenes,[234] cyclooctadiene,[235] and polyaromatic compounds.[236] Recently, the chemistry of molecular calcium compounds has witnessed a renaissance and a variety of neutral and cationic molecular calcium hydride complexes have been reported and used in small molecule activation and catalysis.[237]

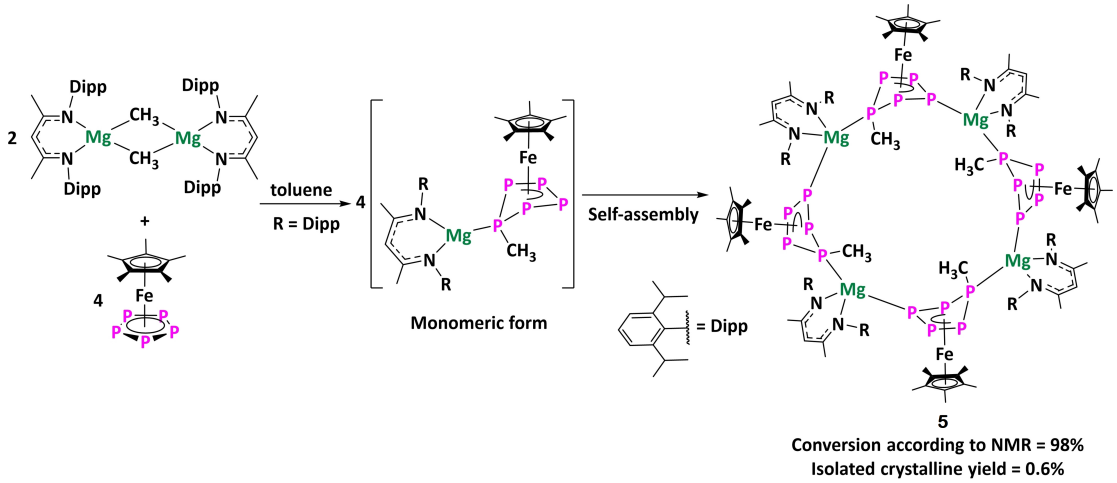
Herein, we report on the reactivity of $[\mathrm{Cp^*Fe}(\eta^5\text{-}\mathrm{P_5})]$ (**XXVII**) with β-diketiminate coordinated mono-valent magnesium compounds, resulting in the first examples of heterometallic Mg-polyphosphides. Also, the reactivity of β-diketiminate coordinated organo-magnesium compounds with **XXVII** has been investigated to isolate an unprecendented Fe-supramolecular wheel assembled by Mg cations. Furthermore, the first ever example of a molecular calcium polyphosphide[238] has been obtained by reducing **XXVII** with molecular calcium hydride complex. The generality of the calcium hydride complex as a suitable reductant for polypnictogens has been established by accessing hydrocarbon soluble Ca-coordinated $[\mathrm{P_7}]^{3-}$ Zintl ions by the controlled activation of $\mathrm{P_4}$.

4.2 Results and Discussion

4.2.1 Magnesium polyphosphides

The addition of toluene to a mixture of one equivalent of $[(^{\mathrm{Dipp}}\mathrm{BDI\text{-}Mg(CH_3)})_2]$[239] and two equivalents of $[\mathrm{Cp^*Fe}(\eta^5\text{-}\mathrm{P_5})]$ (**XXVII**) at room temperature immediately resulted in a brown-coloured reaction mixture (Scheme 4.2). Monitoring the reaction by $^{31}\mathrm{P}\ \{^1\mathrm{H}\}$ NMR shows an AMM'XX' spin system and a singlet corresponding to some residual **XXVII** (Figure 4.33). This spin system shows similarities to the NMR spectrum of the products isolated upon attack of alkali metal based nucleophiles on **XXVII**.[174] Therefore, it is likely that the reaction product in solution is

$[Cp^*Fe(\eta^4\text{-}P_5(CH_3))]^-$ with a $[^{Dipp}BDI\text{-}Mg]^+$ fragment attached to it. After removing the solvent and dissolving the brown residue in n-hexane and storing the resulting solution at -30 °C, crystals of a tetrameric Mg-Fe-polyphosphide species $[(^{Dipp}BDI\text{-}Mg)_4(\mu,\eta^{4:1:1}\text{-}P_5(CH_3))_4(FeCp^*)_4]$ (**5**) were obtained (Figure 4.1). The tetrameric structure is built up from the self-assembly of the monomeric form by coordination of the $[^{Dipp}BDI\text{-}Mg]^+$ fragment to the envelope-shaped *cyclo*-P_5 ring at 1,4 position. Complex **5** represents the largest supramolecular self-assembly of a s- and d-block heterometallic polyphosphide system. The tetrameric form could be arising from the combination of a coordinatively unsaturated Mg centre, the 1,4-coordination mode of the *cyclo*-P_5 ring and the sterically demanding ^{Dipp}BDI-ligand on the Mg atom. Also, complex **5** is the first example of a discrete cyclic tetrameric assembly based on pentaphosphaferrocene system.



Scheme 4.2: Synthesis of the Mg-Fe organo-polyphosphide supramolecular complex **5**.

The P-Mg-P angles deviate by 7° and twist angles between the planes of the unshifted phosphorus atoms of the *cyclo*-P_5-ligand (e.g. the plane [P3-P2-P5-P4] in Figure 4.1), deviates by more than 25°. Therefore, the tetramer itself is highly asymmetric. The monomeric units, as shown in Figure 4.1 have within the error range comparable bond lengths, but angles within the *cyclo*-P_5 moieties differ slightly (up to more than 1°). The Mg-P bond distances in complex **5** are ranging from 2.5757(11) to 2.7676(11) Å and are in line with previous reports (2.5592(7)-2.831(3) Å).[224] The bond of the $[^{Dipp}BDI\text{-}Mg]^+$ fragment to the unshifted 4-position of the *cyclo*-P_5-ring (average Mg-P 2.6004(11) Å) is shorter than the one with the methylated phosphorus atom (average Mg-P(CH_3) 2.7260(11) Å). This is in line with the assumption that the negative charge on the $[(\eta^4\text{-}P_5(CH_3))]$ moiety is located primarily on the P_4 plane,

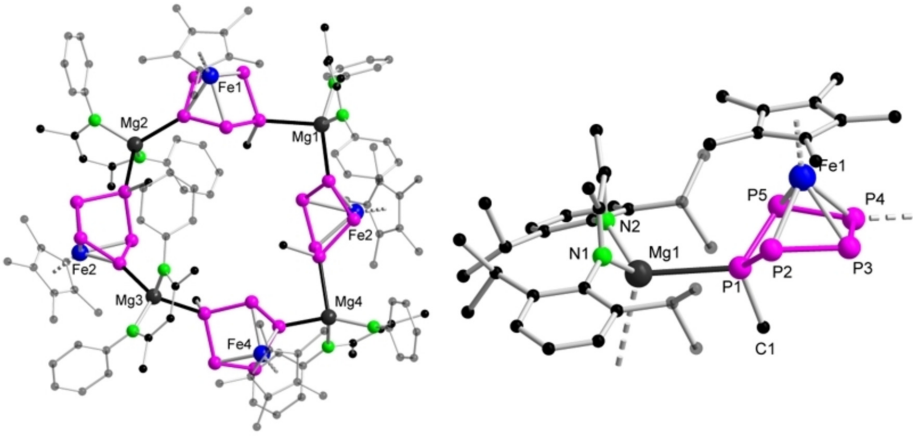
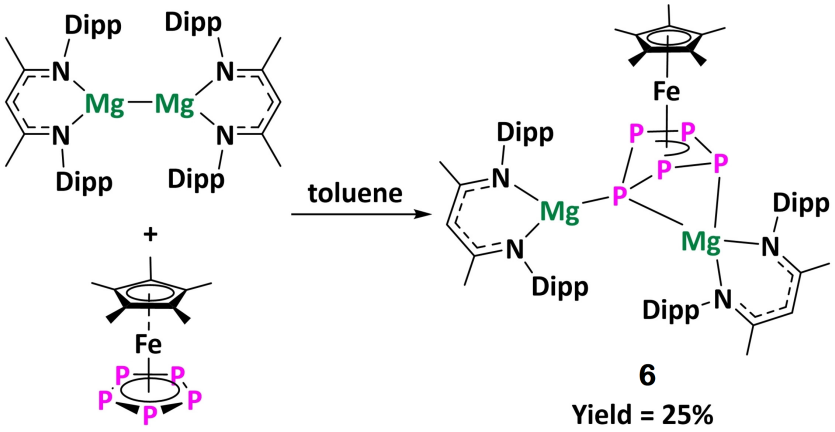


Figure 4.1: Molecular structure of complex **5** (left) in the solid state (the isopropyl groups are omitted for clarity) and a view of the monomeric section of complex **5** (right). Hydrogen atoms are omitted for clarity. Selected bond lengths and angles are given in the Supporting Information.

as described for the known products of the reaction of main group nucleophiles on **XXVII**.[174]

Since the $^{31}\mathrm{P}\ \{^{1}\mathrm{H}\}$ NMR spectrum of the reaction solution does not show a complex spin system but an AMM'XX' system with resonances $\delta = 142.6$ (m), 46.5 (m) and -114.9 (m) ppm, we suggest that the tetramer **5** is not formed in solution. This was validated by Diffusion Ordered Spectroscopy (DOSY) NMR experiments, since the derived hydrodynamic volume of **5** (1748$\pm$74 Å^3) is too small for a tetrameric or dimeric species and can rather be compared with the hydrodynamic volume of compound **6** (1339$\pm$75 Å^3) (*vide infa*, for experimental details and diffusion coefficients see section 4.3.5, Supporting Information). Despite complete conversion of the reactants the crystalline yield of **5** is very low, which can be attributed to its high solubility in n-hexane and the dynamic process of self-assembly in solution.[240]

A different reaction was observed by treating **XXVII** with the mono-valent magnesium compound $[^{\mathrm{Dipp}}\mathrm{BDI\text{-}Mg}]_2$ (**XXXIXa**).[126] Combining both precursors at room temperature led to an immediate colour change from green to dark brown (Scheme 4.3). Dark brown crystals of $[(^{\mathrm{Dipp}}\mathrm{BDI\text{-}Mg})_2(\mu,\eta^{4:2:1}\text{-}\mathrm{P}_5)(\mathrm{FeCp}^*))]$ (**6**) were isolated (Figure 4.2) by cooling a saturated pentane solution of the reaction mixture.



Scheme 4.3: Synthesis of complex **6**.

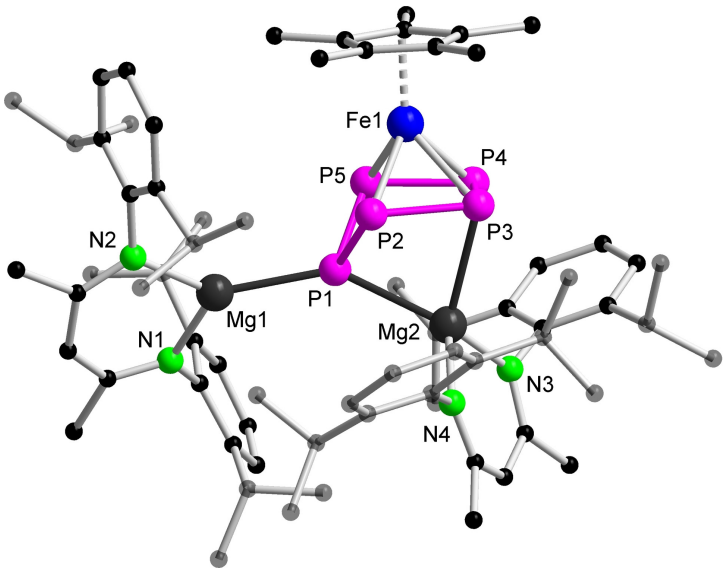


Figure 4.2: Molecular structure of complex **6** in the solid state. Hydrogen atoms are removed for clarity. Selected bond lengths and angles are given in the Supporting Information.

Complex **6** is formed by a two electron transfer from the Mg-Mg bond to one molecule of **XXVII**, resulting in a formally twofold-reduced $[Cp^*Fe(\eta^4\text{-}P_5)]^{2-}$ unit coordinated by two $[^{Dipp}BDI\text{-}Mg]^+$ moieties. When compared to other already reported $[Cp^*Fe(\eta^4\text{-}P_5)]^{2-}$ motifs, such as $[K(dme)K(dibenzo\text{-}[18]crown\text{-}6)][Cp^*Fe(\eta_4\text{-}P_5)]$,[173] the *cyclo*-$P_5$ ring in **6** is highly asymmetric due to the coordination of Mg2 to the P3 atom. Compared to the sum of the covalent radii for Mg-P single (2.50 Å) and double (2.34 Å) bonds,[241] the bond lengths Mg1-P1 (2.4627(6) Å) and Mg2-P1 (2.5452(6) Å) lie in the range of a single bond and are similar to known Mg-P bonds for example $[Mg(PSi^tBu_3)]_6$ (2.474(2) Å)[145] and $[Mg(P(H)Si^iPr_2)_2O(thf)]_3$ (2.557(2) Å).[242] However, electrostatic interactions and packing effects play a significant role. The long Mg2-P3 (2.6764(6) Å) bond distance indicates a relatively weaker interaction also observed in $[(PNNP)Mg]_2$ (2.6737(12) Å; PNHNHP=N,N-bis(2-(diphenyl-phosphino)phenyl)-ethane-1,2-diaine).[243]

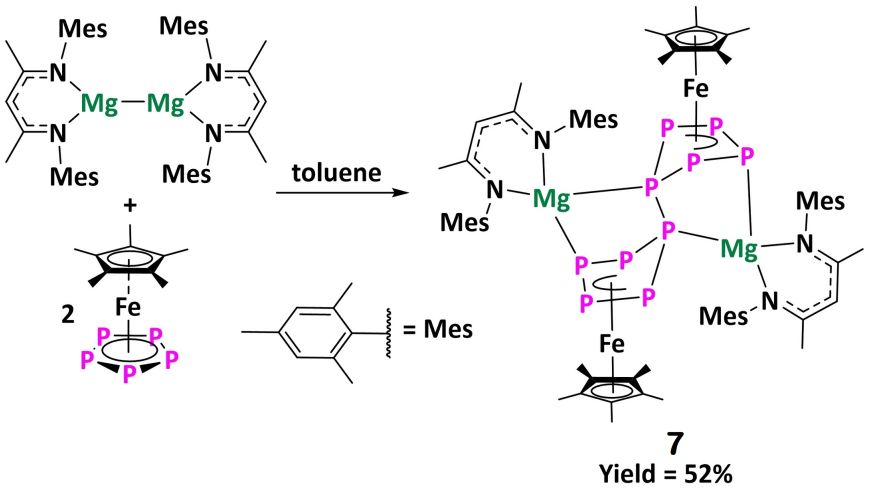
The $^{31}P\ \{^1H\}$ NMR spectrum of complex **6** shows four broad signals and one well-resolved triplet at room temperature. Upon cooling the solution, the broad signals start splitting up (coalescence temperature at about 0 °C) until an ADMOX spin system is best resolved at -40 °C (Figure 4.33).

The ^1H NMR spectrum also shows a dynamic behaviour, since for the isopropyl groups of the ^{Dipp}BDI ligands only an extremely broad signal is observed at room temperature, which splits up into a septet at -40 °C (Figure 4.15). In order to identify all coupling constants in the $^{31}P\ \{^1H\}$ NMR spectrum, the ADMOX spin system resonances at $\delta =$ 66.5, 59.3, -8.4, -22.8, and -54.6 ppm at -40 °C were simulated (see Table 4.3 and Figure 4.33). Due to the line broadening at these temperatures, only one ^2J-coupling was resolved (linewidth for all signals larger than 25 Hz). The dynamic behaviour, which is seen in the $^{31}P\ \{^1H\}$ NMR spectrum is a result of electrostatic interaction between Mg and P. The multiplets in the low temperature $^{31}P\ \{^1H\}$ NMR can be assigned to the corresponding phosphorus atoms in the solid state structure (Table 4.3) by simulation of the ADMOX spin system.

Interestingly, VT NMR-experiments showed no difference when the reaction between **XXXIXa** and **XXVII** was started at either -80 °C or room temperature and there was no hint for the formation of a formally mono-reduced $[P_{10}]^{4-}$ moiety. Also, when the reaction between **XXXIXa** and **XXVII** in 1:2 molar ratio was carried out at either -80 °C or room temperature only complex **6** is observed. We assume that the radical intermediate, $[(^{Dipp}BDI\text{-}Mg)(\mu,\eta^4\text{-}P_5)(FeCp^*)]$, is too bulky to dimerize via a P-P bond formation (see below). Instead, the intermediate is reduced a second time.

To support this hypothesis, we employed the less bulky Mg reagent $(^{\mathrm{Mes}}\mathrm{BDI\text{-}Mg})_2]$ (**XXXIXb**)[244] ($^{\mathrm{Mes}}\mathrm{BDI} = \{[2,4,6\text{-}\mathrm{Me_3C_6H_3NCMe}]_2\mathrm{CH}\}^-$) to reduce **XXVII**. In fact, the reaction between **XXXIXb** with **XXVII** in a 1:2 molar ratio leads to the formation of $[(^{\mathrm{Mes}}\mathrm{BDI\text{-}Mg})_2(\mu,\eta^{4:4:2:2}\text{-}\mathrm{P_{10}})(\mathrm{FeCp^*})_2]$ **7** (Scheme 4.4). The molecular structure showed the formation of a $[\mathrm{P_{10}}]^{4-}$ fragment, η^4-coordinated to two $[\mathrm{Cp^*Fe}]^+$ and η^2-coordinated to two $[^{\mathrm{Mes}}\mathrm{BDI\text{-}Mg}]^+$ moieties (Figure 4.3). Similar $[(\eta^4\text{-}\mathrm{P_{10}})(\mathrm{Fe\ Cp^*})_2]^{2-}$ moieties have been obtained coordinated to potassium or samarium ions upon reduction of **XXVII** by potassium hydride and divalent samarocene, respectively.[173,217] A similar $\mathrm{P_{10}}$ moiety has also been reported in anorgano-cobalt compound.[245] The Mg1-P7 (2.5879(14) Å), Mg1-P3 (2.639(2) Å), Mg2-P1 (2.577(2) Å), and Mg2-P9 (2.613(2) Å) bond lengths are similar to those observed in previously reported magnesium polyphosphide complexes (2.5592(7)-2.831(3) Å).[224] The Mg1$\cdots$P2 (3.142(2) Å) and Mg2$\cdots$P8 (3.192(2) Å) separations are however significantly longer than the Mg-P bonds reported in the literature (2.45-2.99 Å), precluding a bonding interaction between P10 and Mg1 on the one hand, and P3 and Mg2 on the other hand.[246] The P-P bond lengths (2.154(2)-2.172(2) Å) within the *cyclo*-$\mathrm{P_5}$ ring are intermediate between single and double bonds, indicating a partial double-bond character.[247] The distance of the newly formed P5-P6 bond (2.1992(13) Å) in **XXXIXb** is also slightly shorter than the analogous P-P bond in $[(\mathrm{Cp^*_2Sm})_2(\mu\text{-}\eta^{4:4}\text{-}\mathrm{P_{10}})(\mathrm{FeCp^*})_2]$ (2.2089(13) Å).[217] The formation of complex **7** can be explained by the transfer of two electrons from the Mg-Mg dimer to two molecules of **XXVII**. As a result, two radical iron species with the unpaired electron localized on one P atom of the *cyclo*-$\mathrm{P_5}$ ring are generated *in situ* and subsequently dimerize through the coupling of the radicals resulting in the formation of a P-P bond, which is now sterically not hindered like in the case of **6**. Moreover, this transformation is accompanied by a conformational change of the *cyclo*-$\mathrm{P_5}$ rings, from planar to envelope-shaped. The ^{1}H NMR spectrum of complex **7** shows a downfield shift for the protons of the $\mathrm{Cp^*}$ group, from $\delta = 1.08$ to 1.21 ppm, compared to **XXVII** (Figure 4.19). The protons of the ($^{\mathrm{Mes}}$BDI) ligands coordinated to the magnesium centres are also shifted downfield. For example, the o-$\mathrm{CH_3}$ of the mesityl group are shifted from $\delta = 1.91$ ppm in $[(^{\mathrm{Mes}}\mathrm{BDI\text{-}Mg})_2]$ to $\delta = 2.53$ ppm in complex **7**.[248] The $^{31}\mathrm{P}\ \{^1\mathrm{H}\}$ NMR spectrum confirms the formation of a $[\mathrm{P_{10}}]^{4-}$ moiety by the presence of four resonances at $\delta =$ -30.6 (br, $\Delta\nu_{\frac{1}{2}} \approx 60$ Hz), 24.5 (br, $\Delta\nu_{\frac{1}{2}} \approx 550$ Hz)), 126.5 (br, $\Delta\nu_{\frac{1}{2}} \approx 500$ Hz)), and 152.1 (br, $\Delta\nu_{\frac{1}{2}} \approx 500$ Hz)) ppm. Unfortunately, the P-P coupling constants could not be determined as finely resolved $^{31}\mathrm{P}\ \{^1\mathrm{H}\}$ NMR spectra could not be obtained even at low temperature (-80 °C) due to the low solubility of **7** at low temperatures and the fluxional behaviour of the $[\mathrm{P_{10}}]^{4-}$ fragment (Figure 4.20-4.21). Complex **7** slowly decomposes to unidentified products at room temperature,

both in solution and in the solid-state. However, no decomposition was observed when stored at -40 °C for at least 4-5 weeks.



Scheme 4.4: Synthesis of complex **7**.

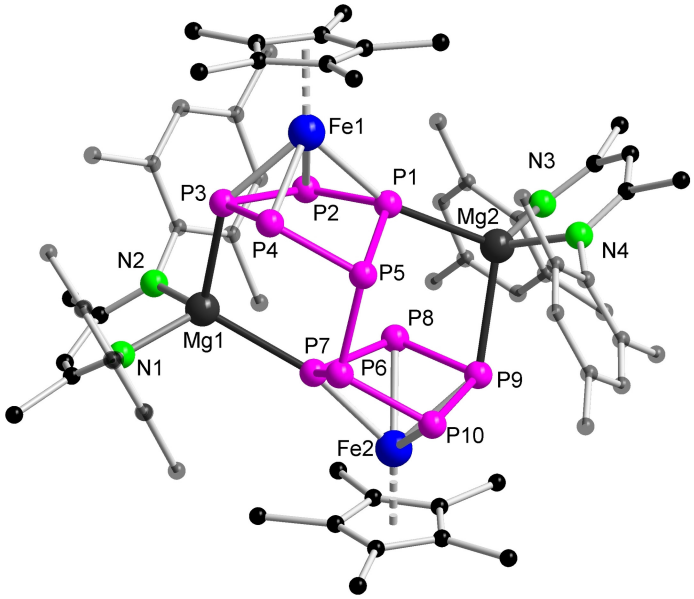
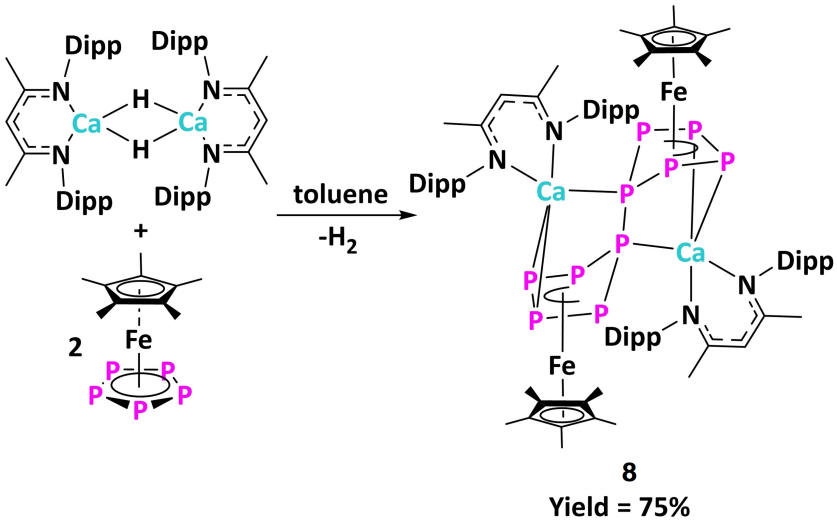


Figure 4.3: Molecular structure of complex **7** in the solid state. Hydrogen atoms and the non-coordinating solvent molecules are removed for clarity. Selected bond distances and angles are given in the Supporting Information.

4.2.2 Calcium polyphosphides

After the investigation of **XXVII** with organo-magnesium and monovalent-magnesium reducing agents, we were intrigued to study the next heavier alkaline earth metal calcium for comparison. Surprisingly, to the best of our knowledge, there is no structurally characterized example known of calcium polyphosphides.[222] The Mg-polyphosphide complexes (**5**, **6** and **7**) are stabilized by efficient kinetic- and thermodynamic stabilization by bulky β-diketiminate ligands. We envisaged to use $[(^{Dipp}BDI\text{-}Ca\text{-}H)_2]$ to reduce **XXVII**, where the [Ca-H] unit reduces the aromatic polyphosphide ring and the bulky β-diketiminate ligand stabilizes the resulting Ca-polyphosphide species.
Upon addition of toluene to a mixture of $[(^{Dipp}BDI\text{-}Ca\text{-}H)_2]$ and **XXVII** in a 1:2 molar ratio immediate change from green to dark brown along with the liberation of gaseous H_2 occurred (Scheme 4.5). After workup, dark coloured crystals of $[(^{Dipp}BDI\text{-}Ca)_2(\mu, \eta^{4:4:3:3}\text{-}P_{10})(FeCp^*)_2]$ (**8**) were isolated in 75 % yield. Complex **8** is formed by a formal mono-reduction of **XXVII** accompanied by dihydrogen liberation. Notably, complex **8** is the first example of a structurally characterized calcium-coordinated polyphosphide. A similar reaction was observed when KH was reacted with **XXVII** to give $[\{K(dme)_2\}\{K(dme)\}(\mu, \eta^4\text{-}P_{10})(FeCp^*)_2]$ as a polymer, however.[173]



Scheme 4.5: Synthesis of complex **8**.

Apart from a remarkable extension of polyphosphides to calcium, the better solubility of complex **8** compared to that of $[\{K(dme)_2\}\{K(dme)\}(\mu, \eta^4\text{-}P_{10})(FeCp^*)_2]$ in hydrocarbon solvents with low-polarity, such as toluene or benzene, could be an advantage for its further utility as polyphosphide transfer agent. In contrast to complex **7**, the two *cyclo*-P_5 units in complex **8** are completely in a trans arrangement (Figure4.4).
In complex **8** each $(^{Dipp}BDI\text{-}Ca)]^+$ moiety is -η^3-coordinated to the $[(\mu, \eta^4\text{-}P_{10})(Fe$

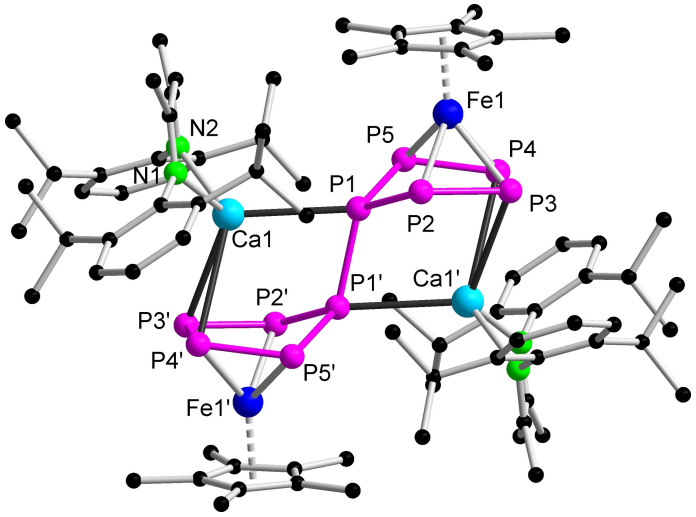


Figure 4.4: Molecular structure of complex **8** in the solid state. Hydrogen atoms and the non-coordinating solvent molecules are removed for clarity. Selected bond distances and angles are given in the Supporting Information.

$Cp^*)_2]$ fragment. The Ca-P1 (2.9605(8) Å) and Ca-P3 (2.9748(8) Å) bond lengths are comparable to $[(Me_3Si)_2NCa[P(H)(Si^iPr_3)]_3Ca(thp)_3]$ (thp = tetrahydropyran) (2.882(2)-2.978(4) Å).[249] The Ca-P4 bond distance (3.1430(8) Å) indicates a weak interaction. The P-P bond distances (2.1488(11)-2.1767(10) Å) within *cyclo*-P_5 rings are similar to complex **7**. The P1-P1' (2.3455(12) Å) bond connecting two halves is significantly longer than in complex **7** (2.1992(13) Å). The ^1H NMR spectrum of com-

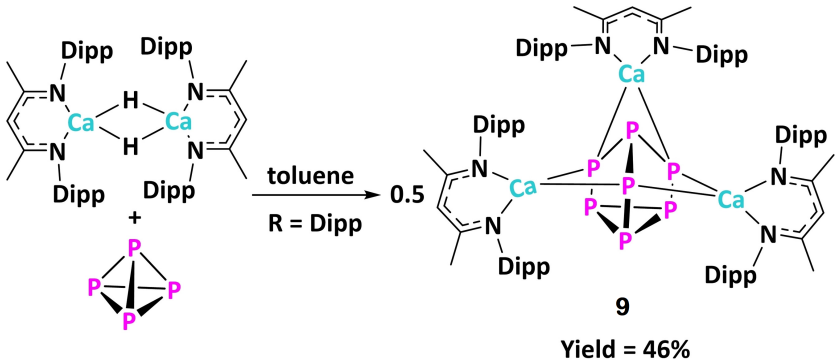


Figure 4.5: Synthesis of complex **9**

plex **8** confirmed the C_2 symmetric nature as per the solid-state structure (Figure 4.23). Similarly to complex **7**, the $^{31}P\{^1H\}$ NMR spectrum of **8** at room temperature also showed broad resonances at δ= -21.0 (br), -18.7 (br), 152.4 (br), 182.3 (br) ppm due to the fluxional coordination of the $[(^{Dipp}BDI\text{-}Ca)]^+$ moiety within the (P_{10}) framework. Unfortunately, recording the $^{31}P\{^1H\}$ NMR at low temperature did not give any better

resolution due to low solubility at low temperatures and strong dynamic behaviour (cf. Figure 4.24-4.25).

After the reduction of the transition metal polyphosphide **XXVII** with a molecular calcium hydride, we were challenged to establish the generality of $[(^{\mathrm{Dipp}}\mathrm{BDI\text{-}Ca\text{-}H})_2]$ as a suitable reductant for the synthesis polypnictogen complexes. In this context, we employed $[(^{\mathrm{Dipp}}\mathrm{BDI\text{-}Ca\text{-}H})_2]$ for the reduction of P_4 (Scheme 4.5). The reaction of $[(^{\mathrm{Dipp}}\mathrm{BDI\text{-}Ca\text{-}H})_2]$ with P_4 resulted in two major products as evidenced by the $^{31}\mathrm{P}\{^1\mathrm{H}\}$ NMR spectrum of the crude reaction mixture (Figure 4.28). After work-up, $[(^{\mathrm{Dipp}}\mathrm{BDI\text{-}Ca})_3(\mu,\eta^{2:2:2}\text{-}\mathrm{P}_7)]$ (**9**) was isolated in pure form as pale-yellow coloured crystals in 46 % yield. Unfortunately, the second product formed along with complex **9** with a resonance at -241.3 ppm in the $^{31}\mathrm{P}\{^1\mathrm{H}\}$ NMR spectrum could not be isolated, and its identity remains elusive. The molecular structure of complex **9** showed the formation of a $(\mathrm{P}_7)^{3-}$ Zintl ion encapsulated by three $[(^{\mathrm{Dipp}}\mathrm{BDI\text{-}Ca})]^+$ moieties (Figure 4.6). The Ca-P bond lengths in complex **9** are in the range of 2.8667(9)-2.9346(9) Å which are similar to those in previously reported examples, such as $[^{\mathrm{Dipp}}\mathrm{BDI\text{-}Ca\text{-}PPh_2(thf)}]$ (2.872(4) Å),[129] $[(\mathrm{Me_3Si})_2\mathrm{NCa[P(H)(Si}^i\mathrm{Pr_3)]_3Ca(thp)_3}]$ (2.882(2)-2.978(4) Å)[249]. The P-P bond distances (2.1748(10)-2.2586(11) Å) in the (P_7)-cage are in the expected range for such a nortricyclane-like cage.[221] Complex **9** is the first structurally characterized molecular calcium-coordinated pnictogen Zintl ion. Molecular group 2 based Zintl ions are very challenging to obtain in a pure form and reasonable yield. Previously, *Hill et. al.* reported the reaction between $[(^{\mathrm{Mes}}\mathrm{BDI\text{-}Mg\text{-}}n\text{-butyl}]$ and P_4 to give $[(^{\mathrm{Mes}}\mathrm{BDI\text{-}Mg})_3(\mu,\eta^{2:2:2}\text{-}\mathrm{P}_7)]$ in 5 % yield along with other unidentified products.[132]

The $^1\mathrm{H}$ NMR spectrum of complex **9** showed a single set of resonances for the different chemical groups indicating a symmetric arrangement of the $[(^{\mathrm{Dipp}}\mathrm{BDI\text{-}Ca})]^+$ moieties around the $(\mathrm{P}_7)^{3-}$ ion in solution (Figure 4.27). The room temperature $^{31}\mathrm{P}\{^1\mathrm{H}\}$ NMR spectrum of complex **9** showed a very broad resonance at δ=-87.7 ppm. Upon measuring VT $^{31}\mathrm{P}\{^1\mathrm{H}\}$ NMR spectra, the broad resonance transformed to three new signals at δ=-137.8 (br, $\delta\nu_{1/2}$ ≈430 Hz, 3P), -60.5 (br, $\delta\nu_{1/2}$ ≈570 Hz, 3P), and -40.9 (br, m, 1P) ppm at -90 °C (Figure 4.30), which are in line with previous reports of $(\mathrm{P}_7)^{3-}$ species showing three sets of resonances δ=-162 (3P), -103 (3P), and -57 (1P) ppm at -60 °C.[221] However,$^{\mathrm{n}}J_{\mathrm{PP}}$ coupling constants were not observed as the strong dynamics could not be suppressed even at -90 °C, which is due to the rapid rearrangement (similar to bullvalene) within $(\mathrm{P}_7)^{3-}$ in solution.[221] An NMR scale reaction between $[(^{\mathrm{Dipp}}\mathrm{BDI\text{-}Ca\text{-}H})_2]$ and P_4 showed a very broad resonance at δ=-87.7 ppm corresponding to complex **9** and an unidentified by-product at δ=-241.3 ppm (Figure 4.28). In contrast, the reaction of $[(^{\mathrm{Dipp}}\mathrm{BDI\text{-}Mg\text{-}H})_2]$ with P_4 led to the formation

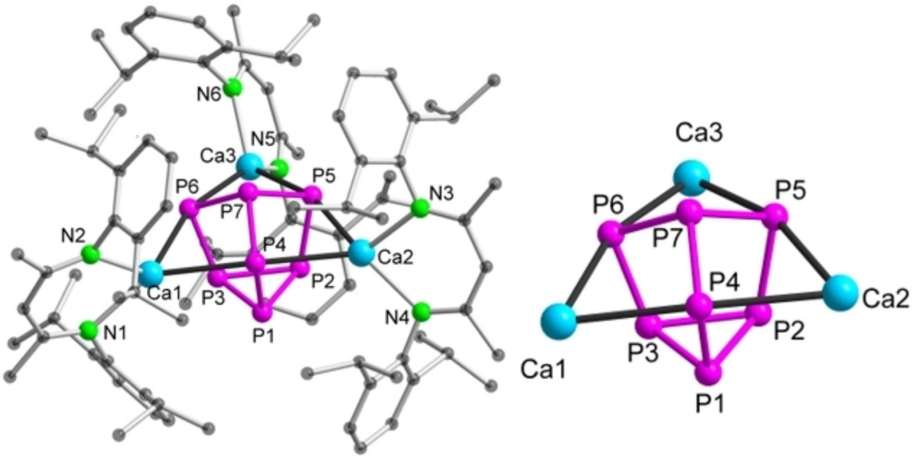


Figure 4.6: Molecular structure of complex **9** (left) in the solid state and a view of **9** (right) without β-diketiminate moieties of the core structure. Hydrogen atoms and the non-coordinating solvent molecules are removed for clarity. Selected bond distances and angles are given in the Supporting Information.

of a primary magnesium phosphide, $[(^{Dipp}BDI\text{-}Mg\text{-}\mu\text{-}PH_2)_3]$, PH_3, and several other unidentified species.[224] *Mézailles et al.* have reacted $LiB(Et)_3H$ with P_4 to obtain $[(TMEDA\text{-}Li)_3(P_7)]$ (TMEDA=tetramethylethylenediamine) along with $[LiPH_2\{B(Et)_3\}]$.[250] Complex **9** is stable at room temperature in the solid state and in solution (benzene, toluene) under inert conditions for at least two weeks. However, storing for longer periods shows the formation of $(^{Dipp}BDI\text{-}H)$ and an insoluble precipitate.

4.2.3 Molecular modelling

The geometries of the P_{10} moieties in the solid-state structures of complexes **7** (eclipsed) and **8** (trans) are different. There can be three possible factors; 1) crystal packing 2) ligand bulkiness i.e. mesityl vs. di-isopropyl groups on the BDI ligands, and 3) effect of different ion Mg vs. Ca. A series of density functional theory (DFT) calculations have been carried out by using the Gaussian 16 package[251] to get more insights at the UB97D/LANL2DZ/6-31G** level[252–254]. The geometries of complexes **7** and **8** were optimized (Figure 4.7). The calculated frontier molecular orbitals are given in the Supporting Information. The calculations revealed that the solid-state geometries are also retained in gas phase. Two different types of geometries of the P_{10} are also found in optimized structures as we have observed in the corresponding crystal structures of **7** and **8**. Owing to this, the role of crystal packing to stabilize different geometries can be excluded. We have also calculated the ground state energy for the two different geometries of $[Cp^*_2Fe_2P_{10}]^{2-}$ moiety after removing the corresponding $[^{R}BDI\text{-}M]$ (R =

Mes, M = Mg; R = Dipp, M = Ca) ions and the fully trans geometry was found to be 6 kcal/mol more stable than the eclipsed conformation. This is also reflected in the relatively more thermal stability of complex **8** (trans conformation) than that of **7** (eclipsed conformation). We have also optimized complex **7Ca** and **8Mg** by replacing the metal

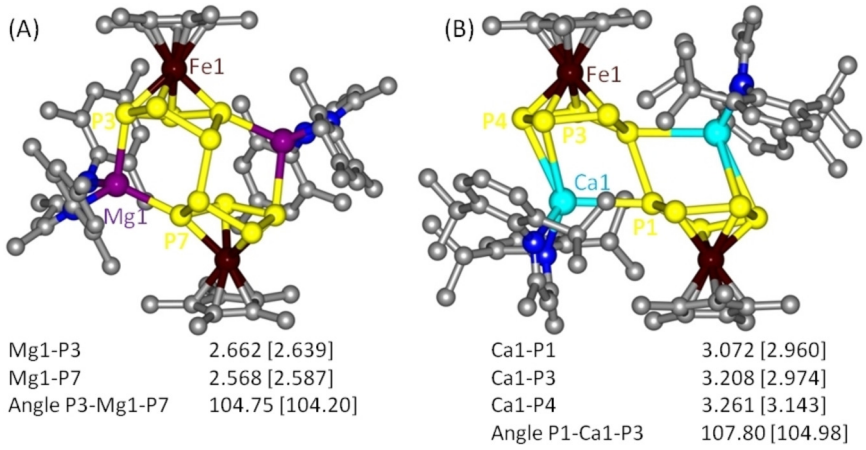


Figure 4.7: UB97D optimized geometries of complex **7** (A) and complex **8** (B) with bond lengths in Å and angles in degree as calculated using LANL2DZ basis set for iron, magnesium and calcium atom and 6-31G** for all other atoms. Parentheses contain the experimental value obtained from the respective X-ray structures.

ions in complex **7** and **8** with Ca and Mg, respectively. The enthalpies and free energies have been compared for all four possible complexes (Table 4.4). The free energies of complexes **7** and **7Ca** are nearly equal however, complex **8** display 6 kcal/mol less free energy than complex **8Mg**. This further support the feasible formation of trans isomer by calcium ion. To examine the role of ligand bulkiness, ($^{\text{Mes}}$BDI (**7**) vs. $^{\text{Dipp}}$BDI (**8**)), to stabilize such different geometries we have also optimized complex **8** without side chain isopropyl groups of the phenyl ring while keeping other things intact, at the same level of theory. The calculation showed no conformational change which further clarifies that there is no role of the ligand bulkiness in stabilization of different geometries (Figure 4.40). The topological analysis of the electron density within the framework of *Bader's* theory (QTAIM)[255,256] analysis of complex **7** and **8** were also performed. The value of electron density ρ and the sign of Laplacian distribution $\nabla^2\rho(r)$ at bond critical point (BCP) are closely related to bonding strength and nature of interaction respectively in any pair of interacting atoms.[257–259] The values of several relevant parameters for selected bond pairs are summarized in Table 4.1. The strength of such interactions were also determined according to the method proposed by *Espinosa et al.*[260] and *Vener et al.*[261]. Based on the crystal structure data and the aforementioned guideline of QTAIM analysis, we found that in complex **7**, each Mg atom binds with

only two P atoms, whereas each Ca atom binds with three P atoms in complex **8** (Figure 4.8). Hence, the different topologies of the P_{10} moieties in **7** and **8** can be attributed to the more coordination of Ca to P atoms as compared to Mg due to the larger ion size.

Table 4.1: Topological parameters of electron density: electron density $[\rho(r)]$, its Laplacian distribution $[\nabla^2\rho(r)]$, potential energy density $[V(r)]$, and kinetic energy density $[G(r)]$ at the selected bond critical points (3,-1). All parameters are in atomic units (a.u).

Atom Pairs	Electron Density $\rho(r)$	Laplacian Distribution $\nabla^2\rho(r)$	Potential Energy Density $V(r)$	Kinetic Energy Density $G(r)$	Interaction Energy [kcal/mol] $E_{\text{int}}{}^a$	$E_{\text{int}}{}^b$
Mg1-P3	0.026	0.111	-0.010	0.006	3.38	1.67
Mg1-P7	0.021	0.092	-0.008	0.005	2.80	1.53
Ca1-P1	0.017	0.063	-0.013	0.014	4.37	4.01
Ca1-P3	0.018	0.068	-0.015	0.016	4.80	4.36
Ca1-P4	0.004	0.017	-0.004	0.004	1.32	1.16

$E_{\text{int}}{}^a = -V(r)/2$.[260] $E_{\text{int}}{}^b = 0.429\,G(r)$.[261]

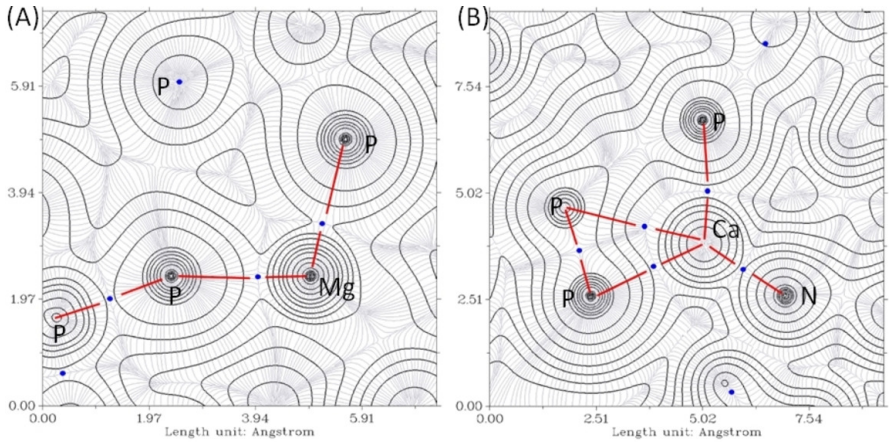


Figure 4.8: QTAIM analysis of (A) complex complex **7** and complex **8**. Contour line plots of the electron density showing bond critical points between selected atom pairs.

4.2.4 Conclusions

We have synthesized a series of molecular group 2 polyphosphides by using $[\mathrm{Cp^*Fe}(\eta^5\text{-}P_5)]$ as an air-stable polyphosphorus source. The organo-magnesium reagent, $[(^{\mathrm{Dipp}}\mathrm{BDI\text{-}Mg(CH_3)})_2]$, reacts with $[\mathrm{Cp^*Fe}(\eta^5\text{-}\mathrm{P_5})]$ in a nucleophilic-addition-type reaction resulting in $[(^{\mathrm{Dipp}}\mathrm{BDI\text{-}Mg})(\mu,\eta^4\text{-}\mathrm{P_5(CH_3)(FeCp^*)}]$ (in situ) which, upon crystallization, undergoes self-assembly to give an unprecedented Mg/Fe-polyphosphide supramolecular wheel (**5**). Complex **5** is the first example of a discrete cyclic-tetrameric assembly based on a pentaphosphaferrocene system. The different reactivity of monovalent magnesium complexes demonstrates the role of ancillary ligand bound to the Mg centre on the outcome of the resulting polyphosphide. In case of $[(^{\mathrm{Dipp}}\mathrm{BDI\text{-}Mg})_2]$, the formally twofold-reduced product **XXXIXa** was obtained exclusively, whereas, upon employing $[(^{\mathrm{Mes}}\mathrm{BDI\text{-}Mg})_2]$, featuring a slightly lower steric demand, the formally mono-reduced species $(\mathrm{P_{10}})^{2-}$ species **XXXIXb** could be isolated. The polyphosphide chemistry is remarkably extended to previously unknown calcium-polyphosphide. The sterically encumbered molecular calcium hydride $[(^{\mathrm{Dipp}}\mathrm{BDI\text{-}Ca\text{-}H})_2]$ proved to be a suitable reductant for diverse polyphosphorus systems. The aromatic *cyclo*-$\mathrm{P_5}$ ring in $[\mathrm{Cp^*Fe}(\eta^5\text{-}\mathrm{P_5})]$ was readily reduced by $[(^{\mathrm{Dipp}}\mathrm{BDI\text{-}Ca\text{-}H})_2]$ to selectively give the formally mono-reduced product **8**. The subtle changes in the polyphosphide topology upon changing the alkaline-earth-metal ion (Mg (**XXXIXa**) vs. Ca (**8**)) were also analysed by theoretical calculations. The activation of $\mathrm{P_4}$ by $[(^{\mathrm{Dipp}}\mathrm{BDI\text{-}Ca\text{-}H})_2]$ resulted in complex **9** in which a phosphorus Zintl ion is coordinated by calcium atoms for the first time in a molecular species. The use of $[(^{\mathrm{Dipp}}\mathrm{BDI\text{-}Ca\text{-}H})_2]$ as an efficient reductant for polyphosphide systems opens new avenues for heavy alkaline earth metal polypnictogenides.

4.3 Supporting information

4.3.1 General remarks

All the manipulations of air- and water-sensitive reactions were performed with rigorous exclusion of oxygen and moisture in flame-dried Schlenk-type glassware either on a dual manifold Schlenk line, interfaced to a high vacuum (10-3 torr) line or in an argon-filled MBraun glove box. Solvents were dried by using an MBraun solvent purification system (SPS 800), degassed and stored in vacuo over $LiAlH_4$. Elemental analyses were carried out with an Elementar vario Micro cube. Toluene-d_8 and C_6D_6 were stored over Na/K alloy and were degassed by freeze-pump-thaw cycles. IR spectra were obtained on a Bruker Tensor 37 spectrometer equipped with a room temperature DLaTGS detector and a diamond ATR (attenuated total reflection) unit. NMR spectra were recorded on Bruker spectrometers (Avance III 400 MHz). Chemical shifts are referenced using signals of the residual protio solvent (^1H) or the solvent ($^{13}C\{^1H\}$) and are reported relative to tetramethylsilane. The chemical shifts in the $^{31}P\{^1H\}$ spectra are reported relative to H_3PO_4 (85 %). All NMR spectra were measured at 298 K, unless otherwise specified. The multiplicity of the signals is indicated as s = singlet, d = doublet, t = triplet, sept = septet, m = multiplet and br = broad. $[Cp^*Fe(\eta^5\text{-}P_5)]$,[69] $[(^{Dipp}BDI\text{-}Mg(CH_3))_2]$,[239] $[(^{Dipp}BDI\text{-}Mg)_2]$,[262] $[(^{Mes}BDI\text{-}Mg)_2]$,[248] and $[(^{Dipp}BDI\text{-}Ca\text{-}H)_2]$[233] were prepared according to the literature procedure.

4.3.2 Experimental procedure and analytical data

Synthesis of $[(^{Dipp}\mathbf{BDI\text{-}Mg})_4(\mu,\eta^{4:1:1}\text{-}\mathbf{P_5(CH_3)})_4(\mathbf{FeCp^*})_4)]$

To a mixture of $[Cp^*Fe(\eta^5\text{-}P_5)]$ (104 mg; 0.3 mmol) and $[(^{Dipp}BDI\text{-}Mg(CH_3))_2]$ (137 mg; 0.15 mmol) 5 mL of toluene were added. After stirring the dark brown solution for 24 h, the solvent was removed. The solid residue was dissolved in 10 mL of hexane and the solution was allowed to stand at room temperature. After 1 week, some crystals of $[(^{Dipp}BDI\text{-}Mg)_4(\mu,\eta^{4:1:1}\text{-}P_5(CH_3))_4(FeCp^*)_4)]$ were isolated by decanting off the mother liquor.
Conversion according to NMR of reaction solution (toluene): 98 %.
Crystalline yield of **5**: 6 mg (0.002 mmol, 0.6 %).

Elemental analysis of **5** did not give satisfactory results after multiple attempts, probably due to the high sensitivity of the compound towards hydrolysis and oxidation.

The NMR data is given for an *in situ* sample, since NMR data of the crystals shows the same signals as a freshly prepared reaction solution, but free of any signals from decomposition.

^{1}H NMR (*in situ*): (400 MHz, 298 K, C_6D_6): δ[ppm] = 1.15 (d, 12 H,$CH(CH_3)_2$), $^{3}J_{HH}$ = 6.8 Hz), 1.36 (s, 15 H, $Cp(CH_3)_5$), 1.62 (d, 12 H, $CH(CH_3)_2$), $^{3}J_{HH}$ = 6.8 Hz), 1.69 (s, 6 H, $NC(CH_3$)), 1.71-1.76 (m, br, 3 H, $(CH_3)P$), 3.29 (sept, 4 H, $CH(CH_3)_2$, $^{3}J_{HH}$ = 6.8 Hz), 4.89 (s, 1 H, NC(C*H*)CN)), 7.19-7.27 (m, 6 H, Ar*H*).

^{31}P NMR (*in situ*): (toluene with D_2O-capillary; 300 K): δ[ppm] = 142.6 (m; P_A; 1 P; $^{1}J_{P_AP_X} = 189$ Hz $^{1}J_{P_AP_{X'}} = 185$ Hz; $^{2}J_{P_AP_{M'}} = 13$ Hz; $^{2}J_{P_AH_{CH_3}} = 10$ Hz); 46.5 (m; $P_{MM'}$; 2 P; $^{1}J_{P_MP_{M'}} = 255$ Hz; $^{1}J_{P_MP_X} = 317$ Hz; $^{1}J_{P_{M'}P_{X'}} = 379$ Hz; $^{2}J_{P_MP_{X'}} = -38$ Hz; $^{2}J_{P_{M'}P_X} = 10$ Hz; $^{2}J_{P_{M'}P_A} = 13$ Hz); -114.9 (m; $P_{XX'}$; 2 P; $^{1}J_{P_{X'}P_A} = 185$ Hz; $^{1}J_{P_XP_A} = 189$ Hz; $^{1}J_{P_XP_M} = 317$ Hz; $^{1}J_{P_{X'}P_{M'}} = 379$ Hz; $^{2}J_{P_{X'}P_M} = -38$ Hz; $^{2}J_{P_XP_{M'}} = 10$ Hz; $^{2}J_{P_XP_{X'}} = -15$ Hz)

^{13}C NMR (*in situ*) (100 MHz, 298 K, C_6D_6): δ[ppm] = 10.6 ($Cp(CH_3)$), 13.0 (br, CH_3) 24.6 ($NC(CH_3)$), 24.7 ($CH(CH_3)_2$), 24.9 ($CH(CH_3)_2$), 29.2 ($CH(CH_3)_2$), 91.8 ($Cp(CH_3)$), 95.2 (NC(*C*H)CN), 124.4 (Ar-*C*), 126.2 (Ar-*C*), 142.6 (Ar-*C*), 144.9 (Ar-*C*), 169.9 (CH*C*N).

Synthesis of $[(^{Dipp}BDI\text{-}Mg)_2(\mu,\eta^{4:2:1}\text{-}P_5)(FeCp^*))]$

To 10 mL of a solution of $[Cp^*Fe(\eta^5\text{-}P_5)]$ (104 mg; 0.3 mmol) in toluene 10 mL of a solution of $(^{Dipp}BDIMg)_2$ (265 mg; 0.3 mmol) in toluene were added under vigorous stirring at room temperature, whereupon the colour changed immediately to dark brown. After removing the solvent the solid residue was dissolved in 20 mL of pentane and the resulting mixture filtered through a P4 glass frit. The filtrate was reduced in volume and stored at 4 °C. Decanting off the mother liquor and drying in vacuo gave compound **6** as dark brown crystals.

Yield: 123 mg (0.1 mmol; 25 %)

Elemental analysis: calculated for $C_{68}H_{97}FeMg_2N_4P_5$: C, 66.40 %; H, 7.94%; N, 4.55 %. found: C, 65.53 %; H, 7.44 %; N, 4.37 %. Note: The elemental analysis of 2 gives a bit lower values than expected, probably due to a small amount of $[Cp^*Fe(\eta^5\text{-}P_5)]$. This problem could not be resolved by attempts to wash the product further or change the work up or crystallization method.

^{1}H-NMR: (tol-d8; 300 K): δ[ppm] = 1.04 (s; 15H; $Cp(CH_3)_5$); 1.23 (br; 24 H; $CH(CH_3)_2$); 1.55 (br; 24 H; $CH(CH_3)_2$); 1.7 (br; 12H; ^{Dipp}BDI$(CH_3)_2$); 2.4 bis 4.2 (br; 8H; $CH(CH_3)_2$); 4.74 (br; 2H; ^{Dipp}BDIH); 7.17 (br; 12H; Dipp)

^{1}H-NMR: (tol-d8; 233 K): δ[ppm] = 0.86 (d; CH_3; $^3J_{HH} = 6.7$ Hz); 1.04 (s; 15H; $Cp(CH_3)_5$); 1.10 bis 1.75 (m; 51H; $CH(CH_3)_2$ und ^{Dipp}BDI$(CH_3)_2$); 1.97 (d; CH_3; $^3J_{HH} = 6.7$ Hz); 2.15 (d; CH_3; $^3J_{HH} = 6.7$ Hz); 2.35 (sep.; 1H; $CH(CH_3)_2$; 2.86 (sep.; 1H; $CH(CH_3)_2$); 3.08 (sep.; 1H; $CH(CH_3)_2$); 3.18 (m; 2H; $CH(CH_3)_2$); 3.30 (sep.; 1H; $CH(CH_3)_2$); 3.60 (sep.; 1H; $CH(CH_3)_2$); 4.09 (sep.; 1H; $CH(CH_3)_2$); 4.60 (s; 1H; ^{Dipp}BDIH); 4.75 (s; 1H; ^{Dipp}BDIH); 6.92 bis 7.48 (m; 12H; Dipp)

^{31}P$\{^1$H$\}$ NMR: (tol-d8; 300 K): δ[ppm] = 69.2 (br; 1P); 60.0 (pt; 1P; $^1J_{PP} = 199$ Hz); -9.1 (br; 1P); -17.5 (br; 1P); -52.8 (br; 1P)

^{31}P$\{^1$H$\}$ NMR: (tol-d8; 233 K): δ[ppm] = 66.5 (t; P_A; $^1J_{P_AP_O} = 331$ Hz; $^1J_{P_AP_X} = 332$ Hz); 59.3 (dd; P_D; $^1J_{P_DP_M} = 172$ Hz; $^1J_{P_DP_X} = 219$ Hz); -8.4 (ddd; P_M; $^1J_{P_MP_D} = 172$ Hz; $^1J_{P_MP_O} = 271$ Hz; $^2J_{P_MP_X} = 43$ Hz); -22.8 (dd; P_O; $^1J_{P_OP_A} = 331$ Hz; $^1J_{P_OP_M} = 271$ Hz); -8.4 (ddd; P_X; $^1J_{P_XP_A} = 332$ Hz; $^1J_{P_XP_D} = 219$ Hz; $^2J_{P_XP_M} = 43$ Hz)

^{13}C NMR (*in situ*) (100 MHz, 298 K, C_6D_6): Owing to the dynamic behavior of the compound in solution at room temperature, the signals are extremely broadened and could not be assigned.

Synthesis of $[(^{\mathbf{Mes}}\mathbf{BDI\text{-}Mg})_{\mathbf{2}}(\mu,\eta^{\mathbf{4:4:2:2}}\text{-}\mathbf{P_{10}})(\mathbf{FeCp^*})_{\mathbf{2}}]$

To a mixture of $(^{\mathrm{Mes}}\mathrm{BDIMg})_2$ (100 mg, 0.139 mmol) and $[\mathrm{Cp^*Fe}(\eta^5\text{-}\mathrm{P_5})]$ (96 mg, 0.279 mmol) was condensed toluene (ca. 10 mL) at -78 °C and slowly warmed to room temperature while stirring. The reaction mixture was further stirred for 3 hours and filtered. The filtrate was concentrated to ca. 5 mL under vacuum and stored at -30 °C. Red colored crystals were obtained after few days. The crystals were separated from the mother liquor by decantation and dried in vacuo.
Yield of **7** = 105 mg (0.072 mmol; 52 %).

Elemental analysis: calculated for $\mathrm{C_{66}H_{88}N_4P_{10}Mg_2Fe_2}\cdot 0.5(\mathrm{C_7H_8})$: C, 57.43 %; H, 6.38 %; N, 3.85 %. Found: C, 57.66 %; H, 5.96 %; N, 3.80 %.

^{1}H-NMR: (400 MHz, 298 K, $\mathrm{C_6D_6}$): δ[ppm] = 1.21 (s, 30 H, $\mathrm{C(C}H_3)$), 1.77 (s, 12 H, $\mathrm{NCC}H3$), 2.39 (s, 12 H, p-$\mathrm{C}H_3$), 2.53 (s, 24 H, o-$\mathrm{C}H_3$), 4.97 (s, 2 H, NCC*H*CN), 7.12 (s, 8 H, Ar-*H*).

^{31}P$\{^1$H$\}$ NMR: (162 MHz, 298 K, toluene-$\mathrm{d_8}$): δ[ppm] = -30.2 (br, $\Delta\nu_{1/2}\approx 600$ Hz), 25.2 (br, $\Delta\nu_{1/2}\approx 550$ Hz), 126.6 (br, $\Delta\nu_{1/2}\approx 500$ Hz), 151.5 (br, $\Delta\nu_{1/2}\approx 500$ Hz).

^{13}C NMR: (100 MHz, 298 K, toluene-$\mathrm{d_8}$): δ[ppm] = 11.2 ($\mathrm{Cp}(C\mathrm{H_3})$), 21.4 (p-$C\mathrm{H_3}$), 21.6 (o-$C\mathrm{H_3}$), 24.1 ($\mathrm{NC}C\mathrm{H_3}$), 91.2 ($Cp(\mathrm{CH_3})$), 95.3 (NC*C*HCN), 130.3 (*C*-Ar), 132.7 (*C*-Ar), 133.9 (*C*-Ar), 145.5 (C-Ar), 169.3 ($\mathrm{N}C\mathrm{CH_3}$).

Synthesis of $[(^{\mathbf{Dipp}}\mathbf{BDI\text{-}Ca})_{\mathbf{2}}(\mu,\eta^{\mathbf{4:4:3:3}}\text{-}\mathbf{P_{10}})(\mathbf{FeCp^*})_{\mathbf{2}}]$

To a mixture of $[^{\mathrm{Dipp}}\mathrm{BDICaH}]_2$ (100 mg, 0.108 mmol) and $[\mathrm{Cp^*Fe}(\eta^5\text{-}\mathrm{P_5})]$ (75 mg, 0.217 mmol) was condensed toluene (ca. 10 mL) at -78 °C and slowly warmed to room temperature while stirring. The reaction mixture was further stirred for 1 hours and transferred to a double ampoule and sealed under vacuum. Dark green colored crystals of compound **8** were obtained upon slow evaporation of toluene. The crystals were carefully washed with cold toluene within the double ampoule and then dried.

Yield of **8** = 130 mg (0.081 mmol; 75 %).

Elemental analysis: calculated for: $C_{78}H_{112}Fe_2Ca_2N_4P_{10}$: C, 58.29 %; H, 7.02 %; N, 3.49 %. Found: C, 58.85 %; H, 6.64 %; N, 3.46 %.

^{1}H-NMR: (400 MHz, 298 K, C_6D_6): δ[ppm] = 1.11 (br, $\Delta\nu_{1/2} \approx 13$ Hz, 30 H, $Cp(CH_3)_5$), 1.30 (d, $^3J_{HH}$ = 6.5 Hz, 24 H, $CH(CH_3)_2$), 1.62 (d, $^3J_{HH}$ = 6.7 Hz, 24 H, $CH(CH_3)_2$), 1.75 (s, 12 H, $NC(CH_3)$, 3.40 (br, $\Delta\nu_{1/2} \approx 25$ Hz, 8 H, $CH(CH3)_2$), 4.83 (s, 2 H, NC(C*H*)CN), 7.23-7.31 (m, 12 H, Ar-*H*).

^{31}P$\{^1$H$\}$ NMR: (162 MHz, 298 K, C_6D_6): δ[ppm] = -21.0 (br), -18.7 (br), 152.4 (br), 182.3 (br).

^{13}C NMR: (100 MHz, 298 K, C_6D_6): δ[ppm] = 10.7 ($Cp(CH3)$), 24.9 ($NC(CH3)$), 25.2 ($CH(CH3)2$), 26.1 ($CH(CH3)2$), 90.1 ($Cp(CH3)$), 124.6 (Ar-*C*), 125.4 (Ar-*C*), 142.1 (Ar-*C*), 166.6 (CH*C*N). Due to low solubility and dynamic coordination in solution NC(*C*H)CN and Ar-C_{ipso} could not be observed.

Synthesis of $[(^{Dipp}BDI\text{-}Ca)_3(\mu,\eta^{2:2:2}\text{-}P_7)]$

To a mixture of $[^{Dipp}BDICaH]_2$ (100 mg, 0.108 mmol) and P_4 (14 mg, 0.108 mmol) was condensed toluene (ca. 10 mL) at -78 °C and slowly warmed to room temperature over a period of 3 hours while stirring. The reaction mixture was further stirred for 1 hours and transferred to a double ampoule and sealed under vacuum. Pale yellow colored crystals of compound **9** were obtained upon slow evaporation of toluene. The crystals were carefully washed with cold toluene within the double ampoule and then dried.
Yield of **9** = 40 mg (0.025 mmol; 46 %), yield is calculated according to $[^{Dipp}BDICaH]_2$ (1 equivalent of $[^{Dipp}BDICaH]_2$ gives 0.5 equivalents of **9**).

Elemental analysis: calculated for: $C_{87}H_{123}Ca_3N_6P_7$: C, 65.72 %; H, 7.80 %; N, 5.29 %. Found: C, 65.12 %; H, 7.57 %; N, 5.22 %.

^{1}H-NMR: (400 MHz, 298 K, C_6D_6): δ[ppm] = 1.19 (d, $^3J_{HH}$ = 6.4 Hz, 36 H, $CH(CH_3)_2$), 1.41 (d, $^3J_{HH}$ = 6.7 Hz, 36 H, $CH(CH_3)_2$), 1.63 (s, 18 H, $NC(CH_3)$), 2.87 (sept, $^3J_{HH}$ = 6.7 Hz, 12 H, $CH(CH_3)_2$), 4.78 (s, 3 H, NC(C*H*)CN), 7.25-7.30 (m, 18 H, Ar-*H*).

^{31}P{^{1}H} NMR: (162 MHz, 298 K, toluene-d_8): δ[ppm] = -87.7 (br, $\Delta\nu_{1/2} \approx 2000$ Hz).

^{31}P{^{1}H} NMR: (162 MHz, 183 K, toluene-d_8): δ[ppm] = -137.8 (br, $\Delta\nu_{1/2} \approx 430$ Hz), -60.5 (br, $\Delta\nu_{1/2} \approx 570$ Hz), -40.9 (br, m).

^{13}C NMR: (100 MHz, 298 K, C_6D_6): δ[ppm] = 23.8 (NC(CH3)), 24.3 (CH(CH3)2), 26.4 (CH(CH3)2), 29.2 (CH(CH3)2), 95.3 (NC(*C*H)CN), 124.8 (Ar-*C*), 125.7 (Ar-*C*), 141.6 (Ar-*C*), 143.7 (Ar-*C*), 165.5 (CH*C*N)

4.3.3 NMR spectra

Spectra of [((^{Dipp}BDI-Mg)$_4$(μ,$\eta^{4:1:1}$-P$_5$(CH$_3$))$_4$(FeCp*)$_4$)]

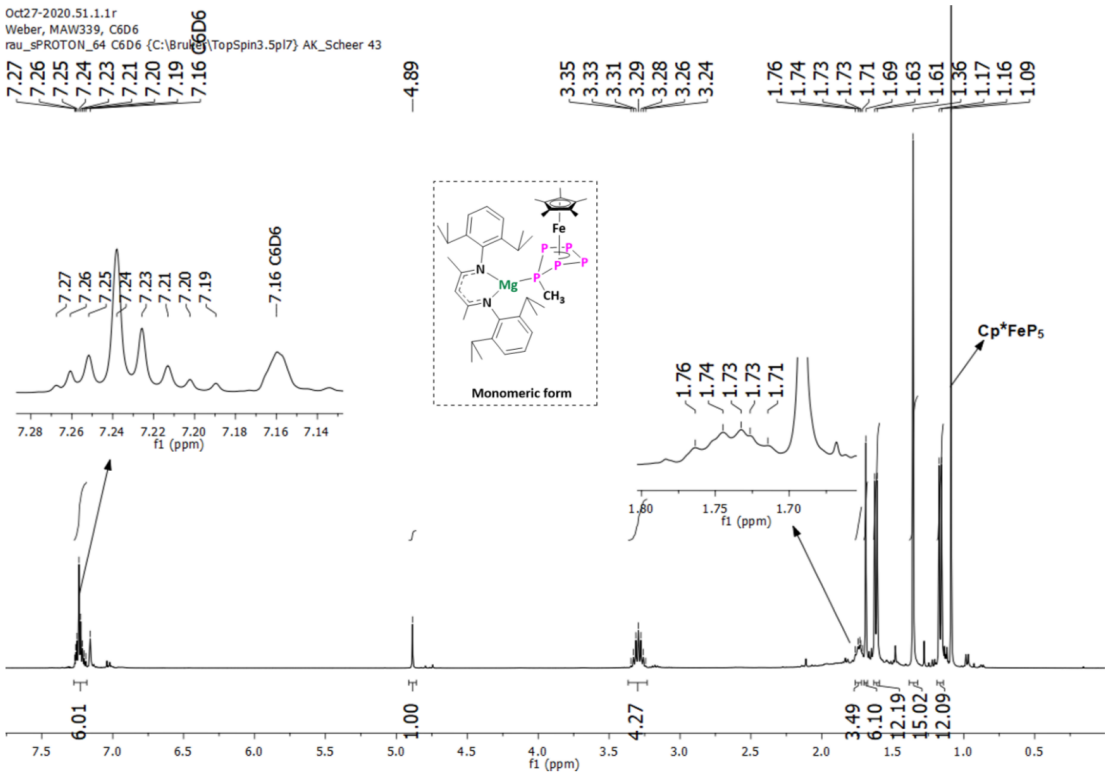


Figure 4.9: ^{1}H NMR (400 MHz, 300 K, C_6D_6) spectrum of complex **5** taken from an *in situ* experiment.

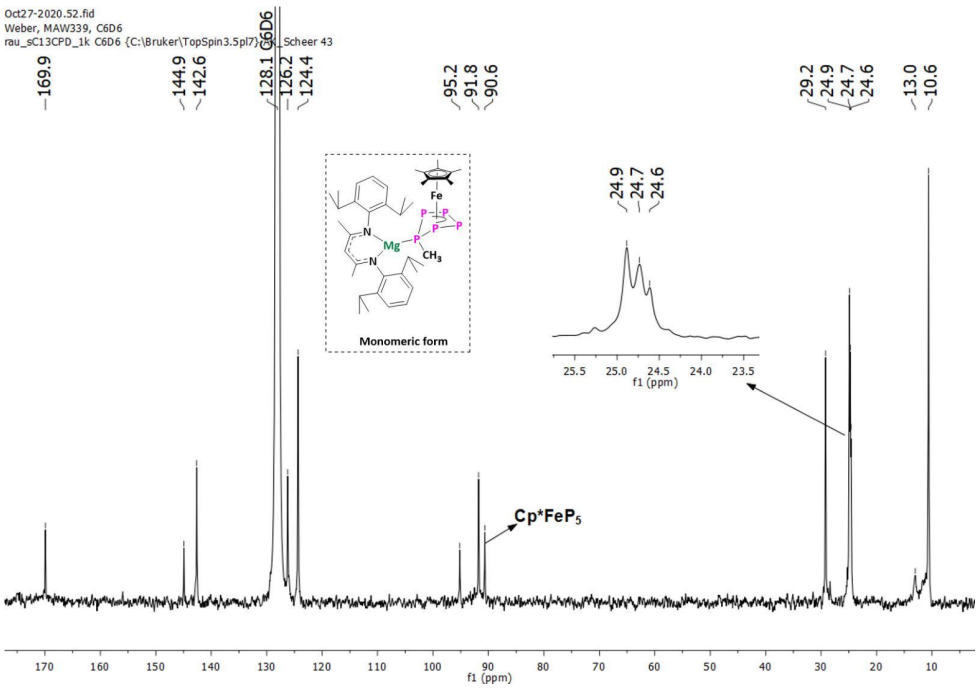


Figure 4.10: $^{13}C\{^{1}H\}$ NMR spectrum (100 MHz, 298 K, C_6D_6) of complex **5** taken from an in situ experiment. The resonance for $Cp(CH_3)$ of both complex **5** and excess $[Cp^*Fe(\eta^5\text{-}P_5)]$ is at the same position at 10.6 ppm. Also, the peak at 10.6 ppm is slightly broad indicating presence of more than one peak.

Spectra of $[(^{\mathbf{Dipp}}\mathbf{BDI\text{-}Mg})_2(\mu,\eta^{\mathbf{4:2:1}}\text{-}\mathbf{P_5})(\mathbf{FeCp^*})]$

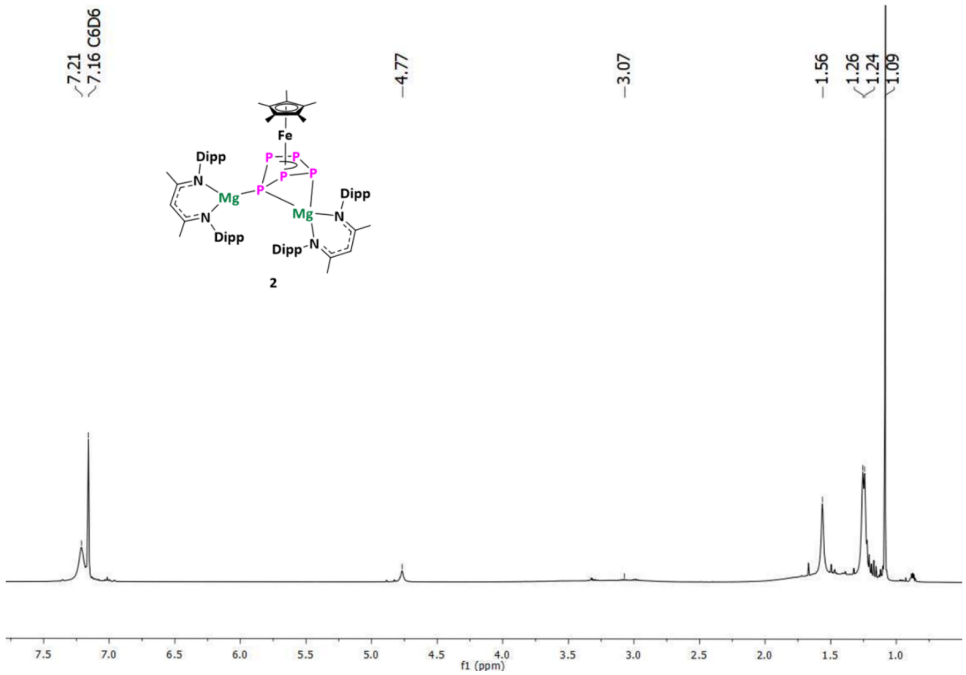


Figure 4.11: ^{1}H NMR (400 MHz, 300 K, C_6D_6) spectrum of complex **6**.

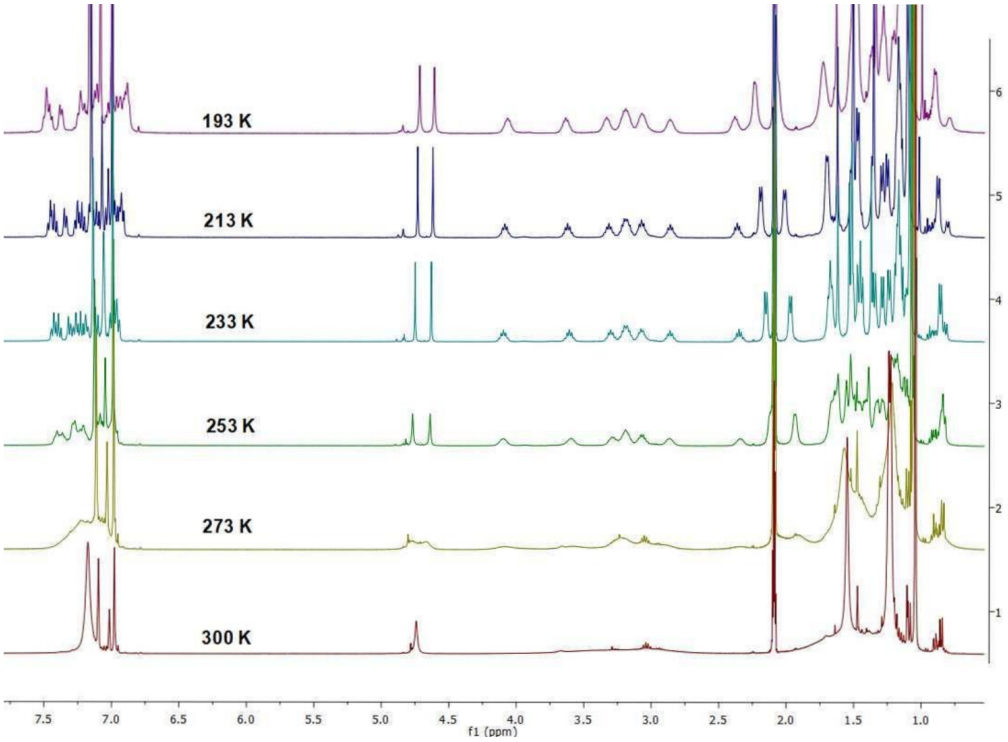


Figure 4.12: Variable temperature ^{1}H NMR (400 MHz, toluene-d_8) spectrum of complex **6**.

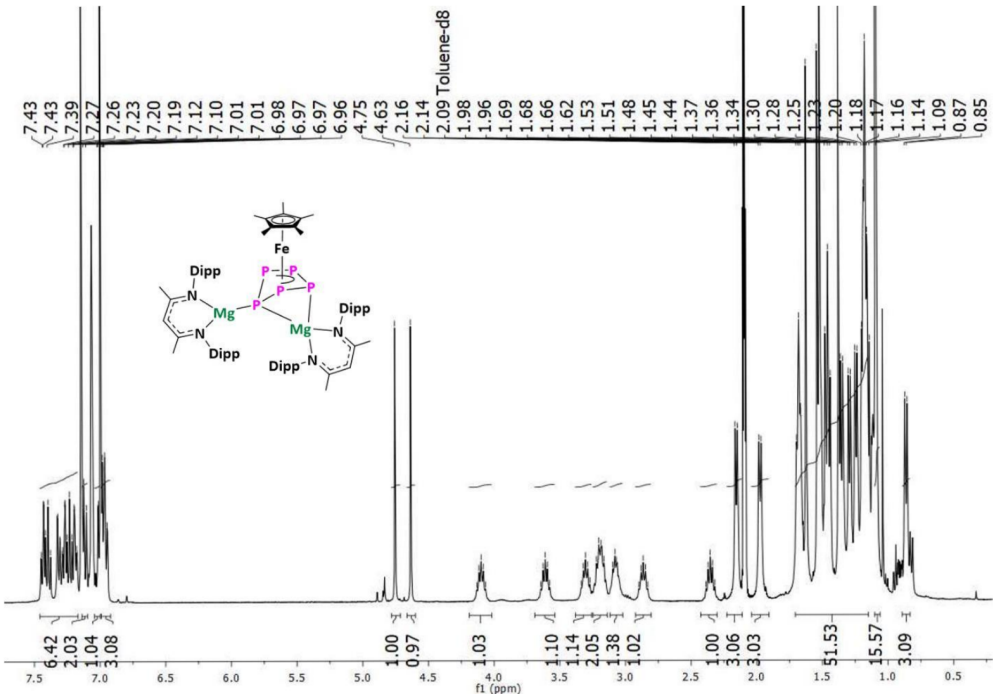


Figure 4.13: ^{1}H NMR (400 MHz, 233 K, toluene-d_8) spectrum of complex **6**.

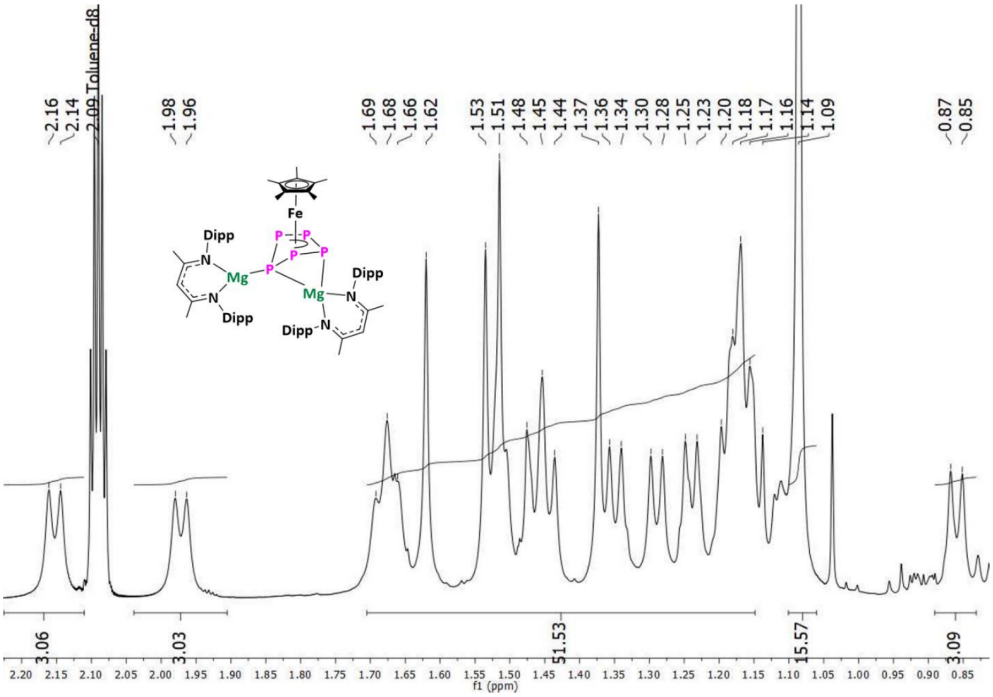


Figure 4.14: Cutout of aliphatic section of ^{1}H NMR (400 MHz, 233 K, toluene-d_8) spectrum of complex **6**.

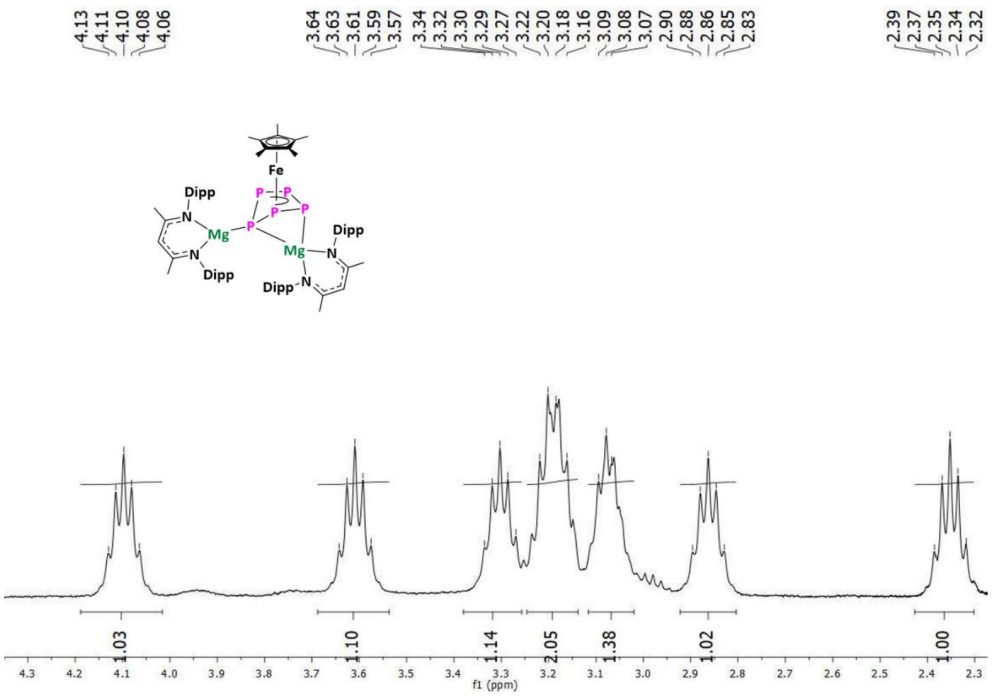


Figure 4.15: Cutout of aliphatic section of ^{1}H NMR (400 MHz, 233 K, toluene-d_8) spectrum of complex **6**.

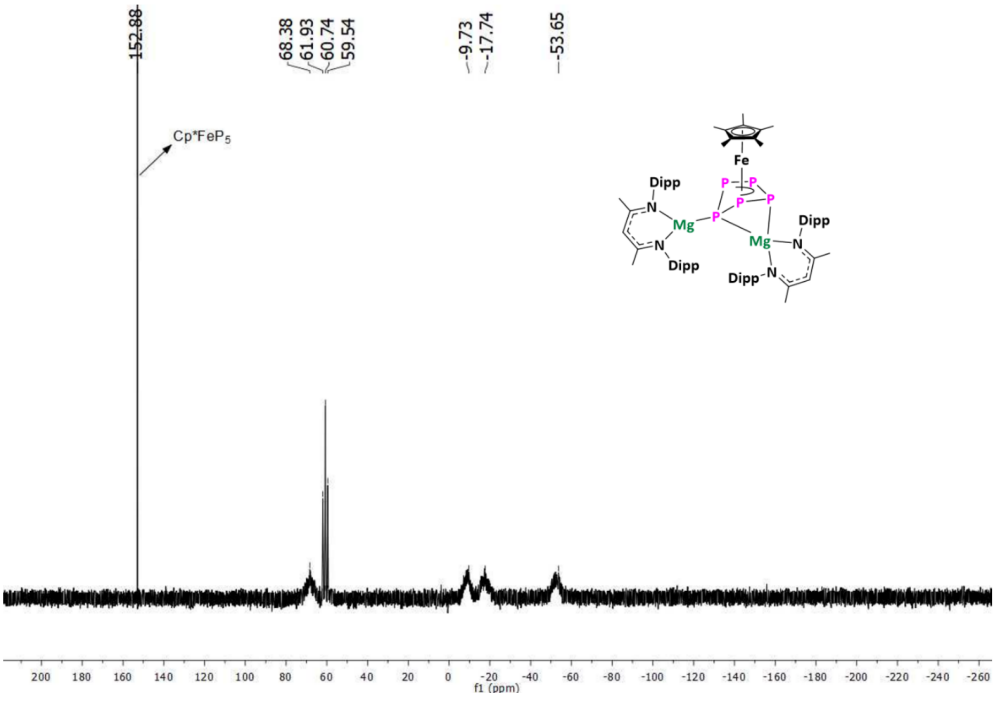


Figure 4.16: $^{31}P\{^{1}H\}$ NMR (400 MHz, 300 K, toluene-d_8) spectrum of complex **6**.

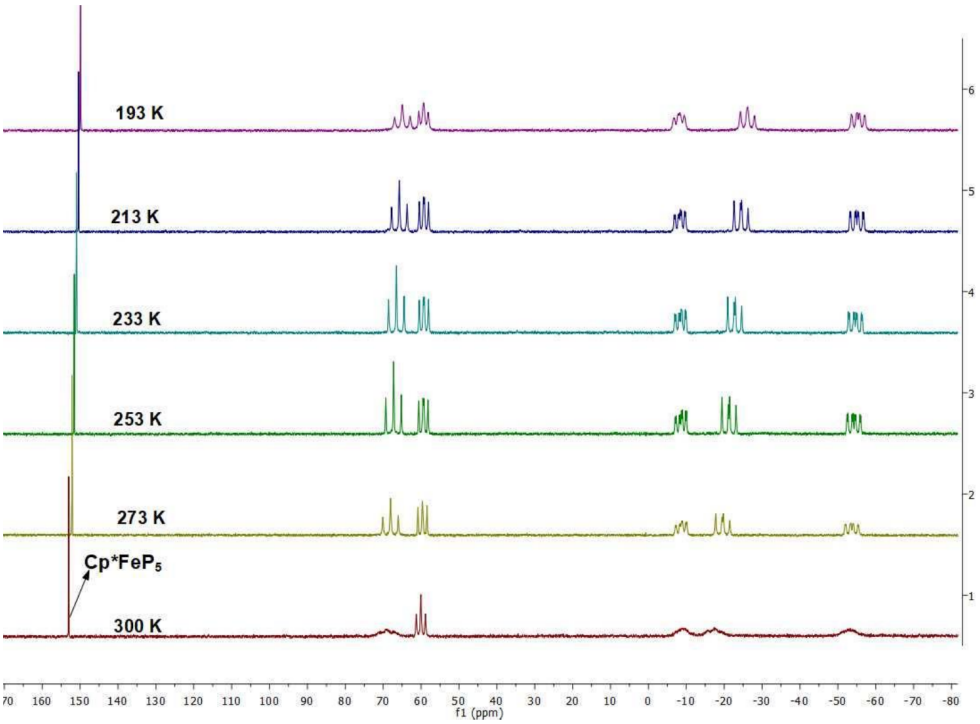


Figure 4.17: Variable temperature $^{31}P\{^{1}H\}$ NMR (400 MHz, toluene-d_8) spectrum of complex **6**.

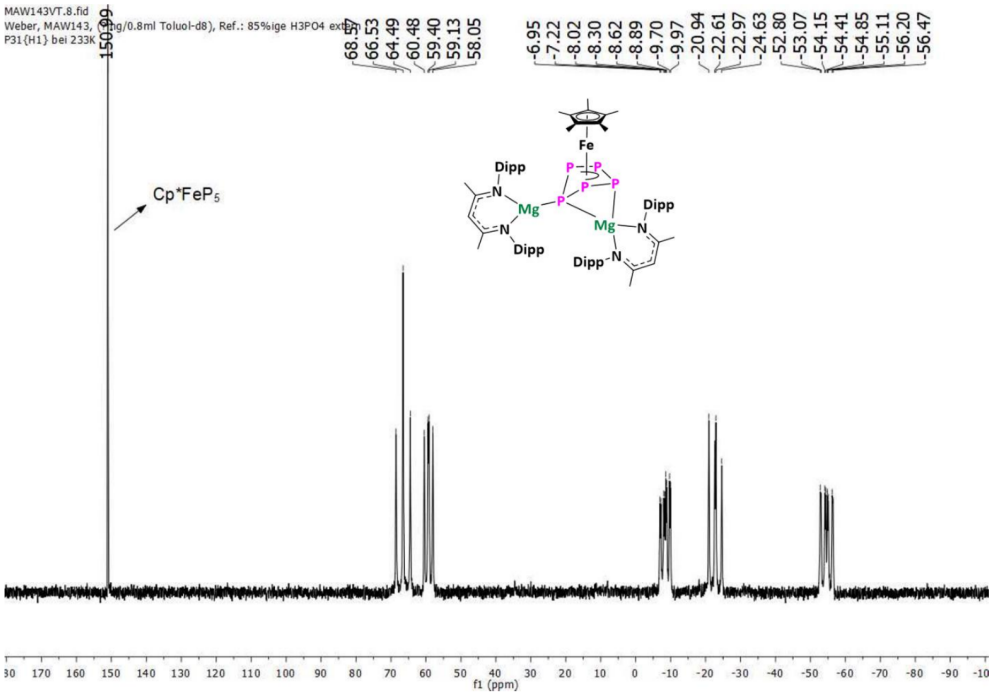


Figure 4.18: $^{31}P\{^{1}H\}$ NMR (400 MHz, 233 K, toluene-d_8) spectrum of complex **6**.

Spectra of $[(^{\mathbf{Mes}}\mathbf{BDI\text{-}Mg})_{\mathbf{2}}(\mu,\eta^{\mathbf{4:4:2:2}}\text{-}\mathbf{P_{10}})(\mathbf{FeCp^{*}})_{\mathbf{2}}]$

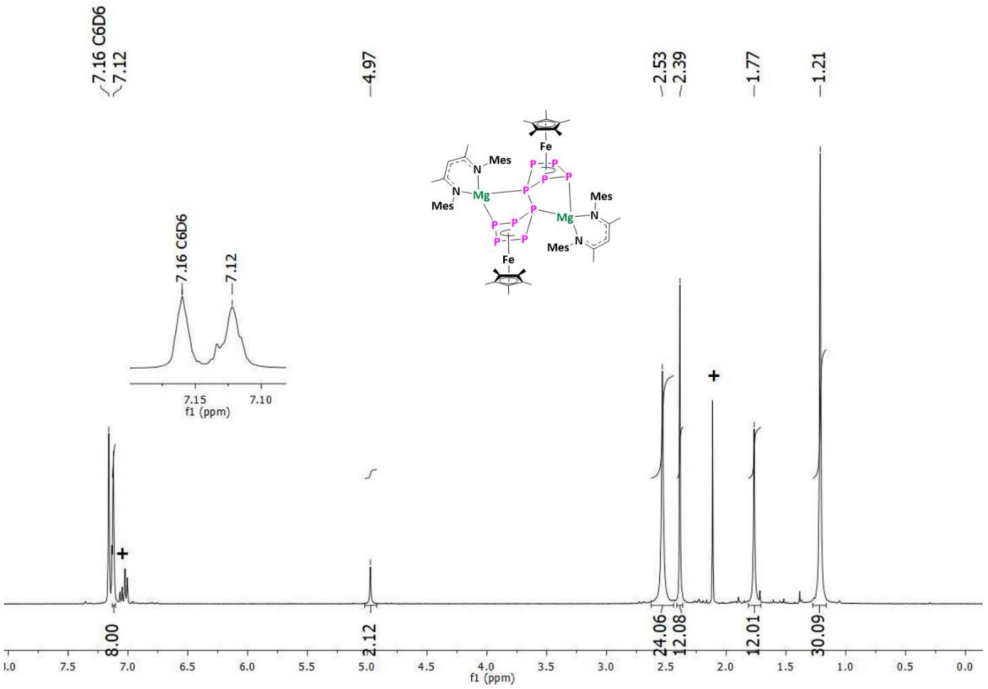


Figure 4.19: ^{1}H NMR (400 MHz, 233 K, C_6D_6) spectrum of complex **7**. + = residual toluene

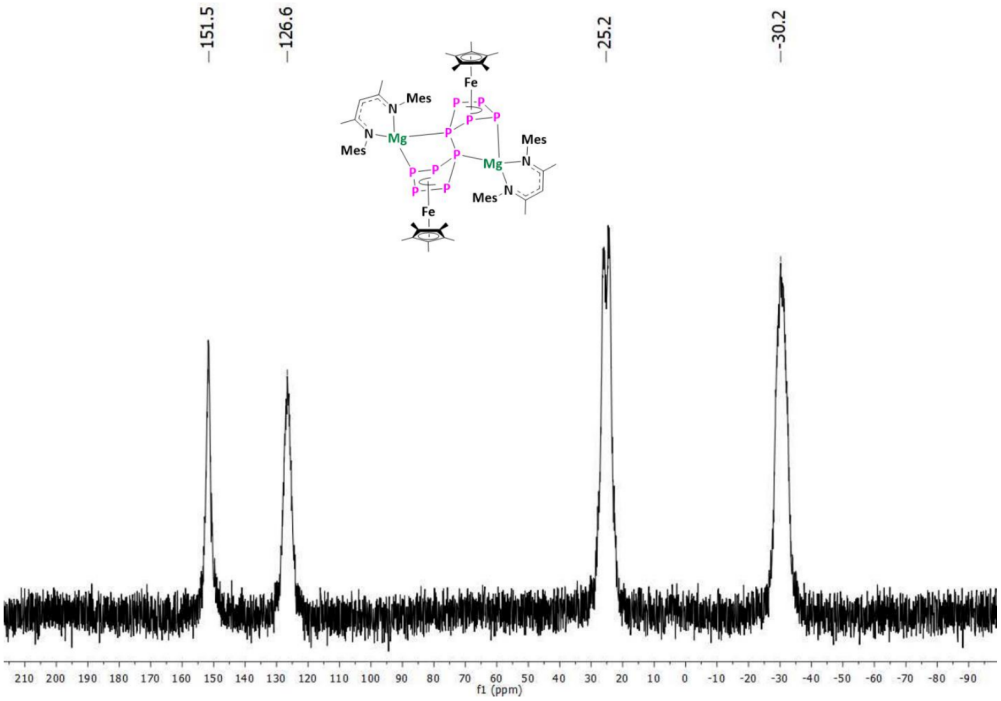


Figure 4.20: $^{31}P\{^{1}H\}$ NMR (162 MHz, 298 K, toluene-d_8) spectrum of complex **7**.

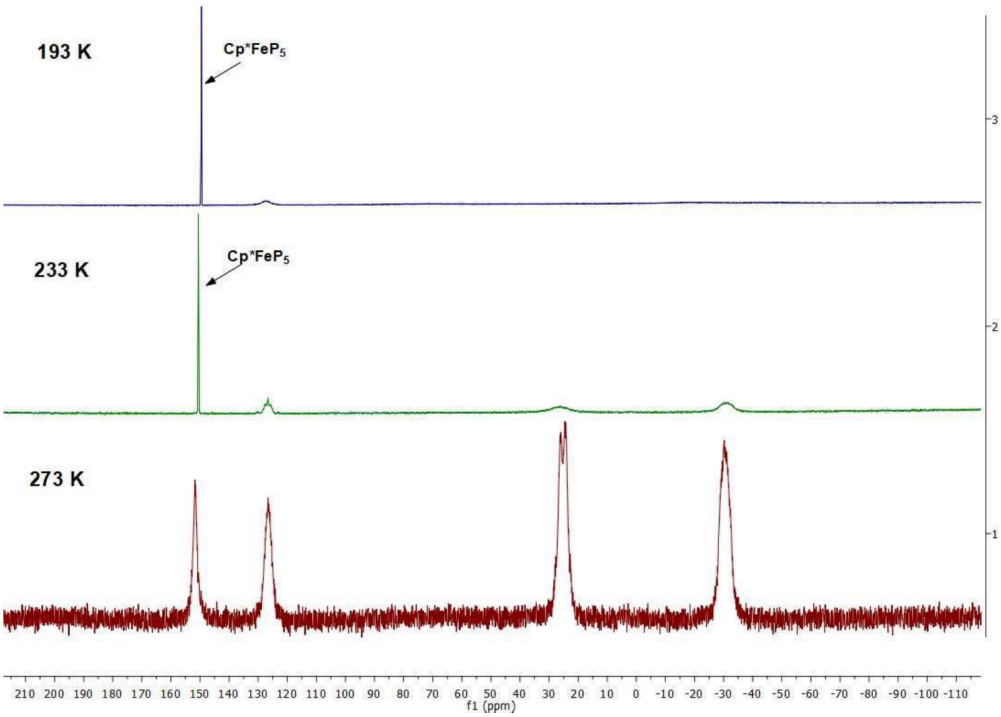


Figure 4.21: Variable temperature $^{31}P\{^{1}H\}$ NMR (162 MHz, toluene-d_8) spectrum of complex **7**.

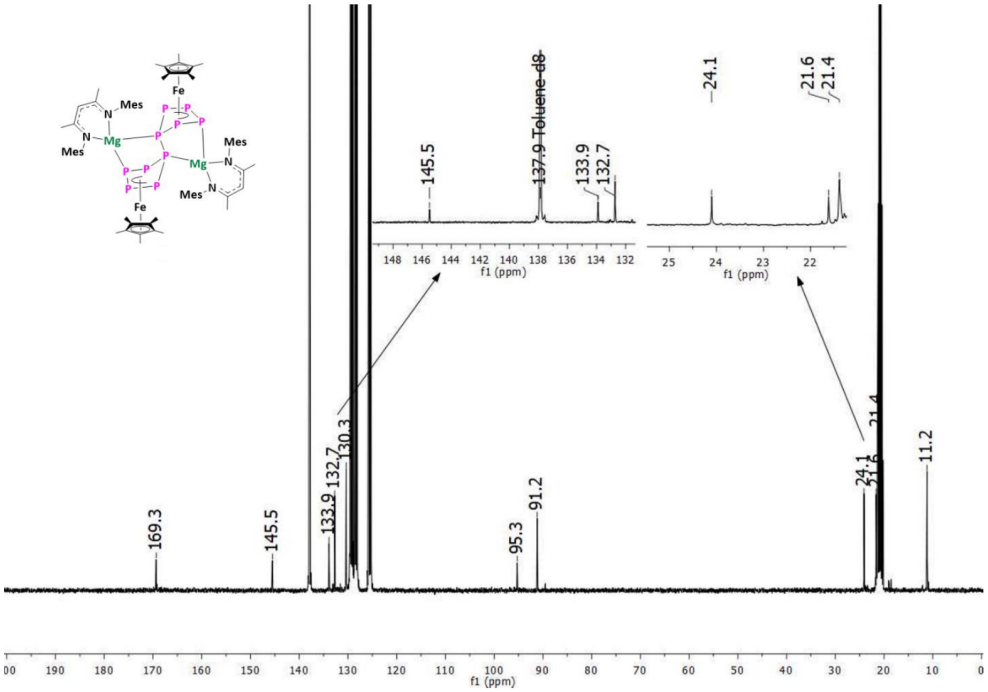


Figure 4.22: $^{13}C\{^{1}H\}$ NMR spectrum (100 MHz, 298 K, toluene-d_8) of complex **7**.

Spectra of $[(^{Dipp}\mathbf{BDI\text{-}Ca})_2(\mu,\eta^{4:4:3:3}\text{-}\mathbf{P_{10}})(\mathbf{FeCp^*})_2]$

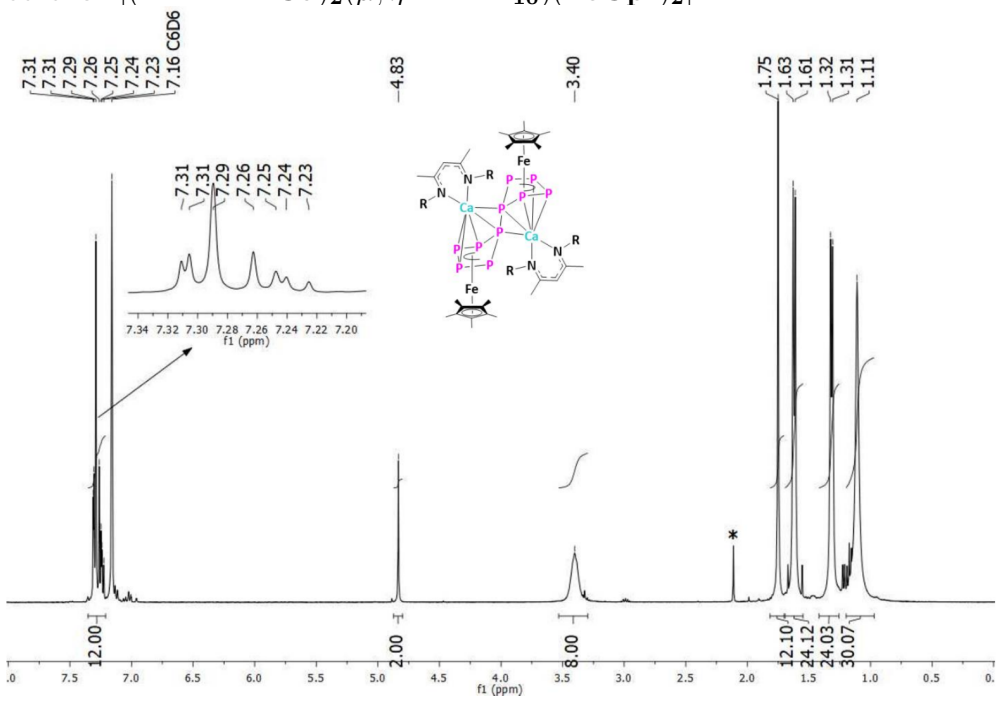


Figure 4.23: ^{1}H NMR (400 MHz, 300 K, C_6D_6) spectrum of complex **8**. $*$ = residual toluene

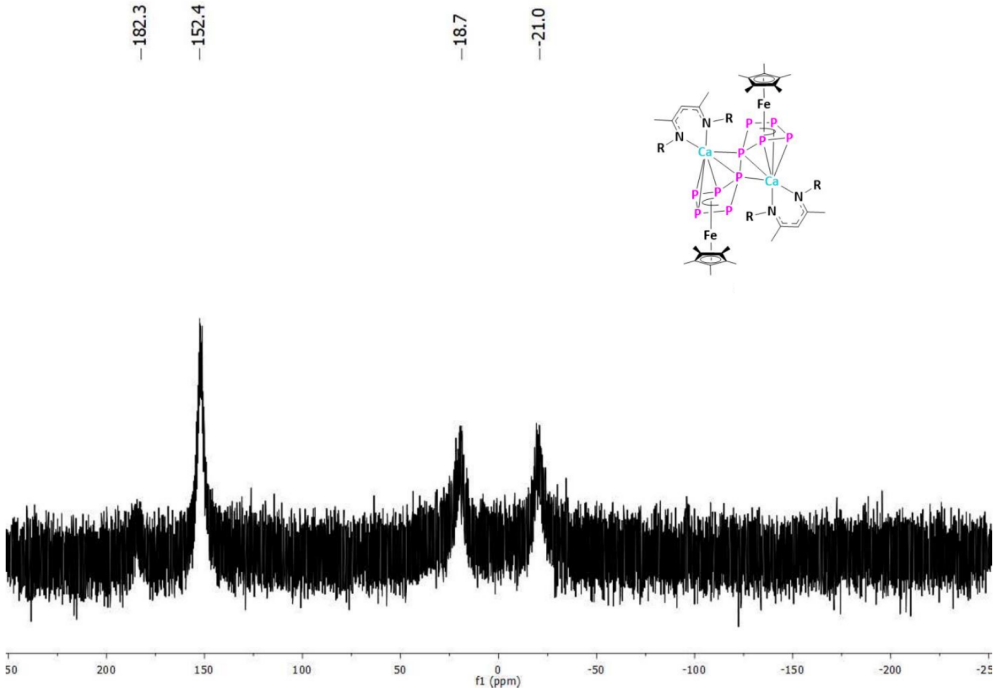


Figure 4.24: $^{31}P\{^{1}H\}$ NMR (162 MHz, 298 K, toluene-d_8) spectrum of complex **8**.

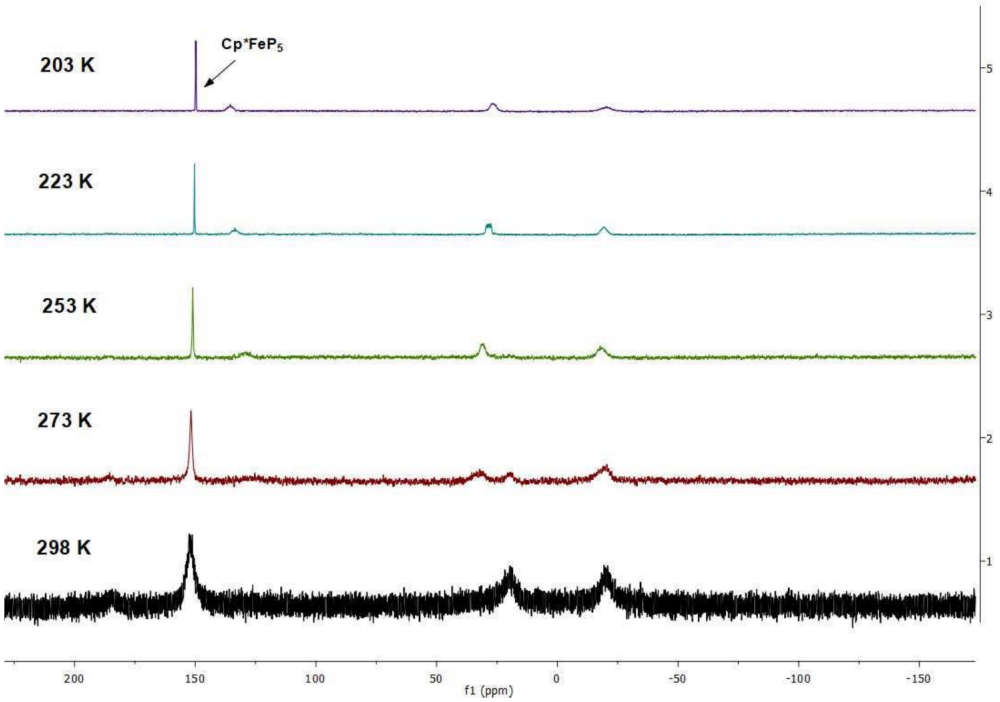


Figure 4.25: Variable temperature $^{31}P\{^{1}H\}$ NMR (162 MHz, toluene-d_8) spectrum of complex **8**.

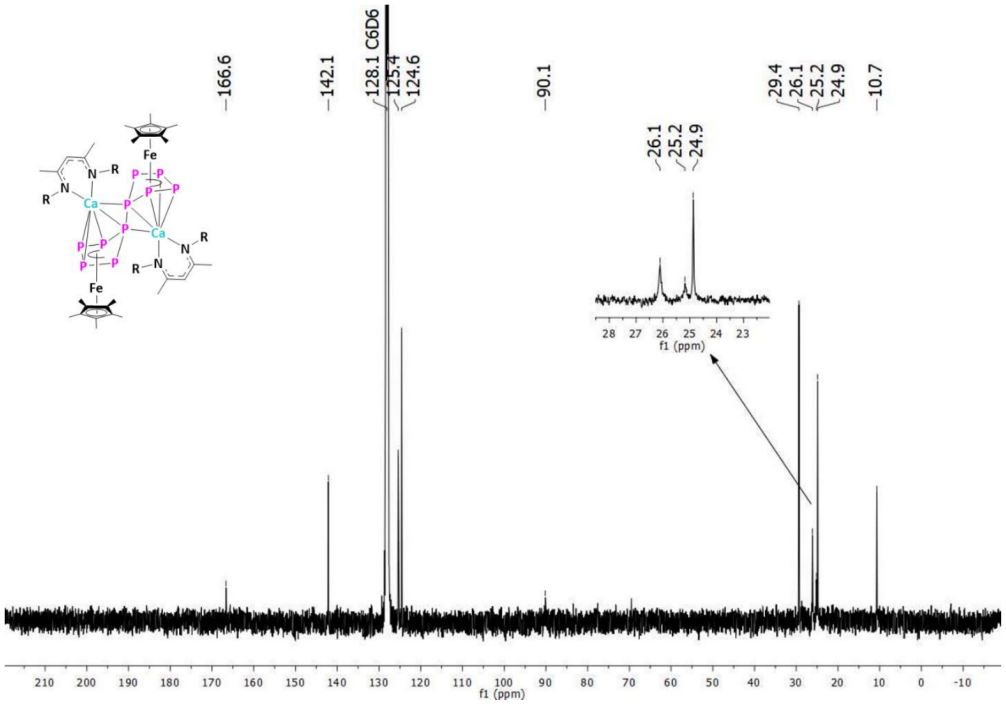


Figure 4.26: $^{13}C\{^{1}H\}$ NMR spectrum (100 MHz, 298 K, C_6D_6) of complex **8**.

Spectra of $[(^{Dipp}BDI\text{-}Ca)_3(\mu,\eta^{2:2:2}\text{-}P_7)]$

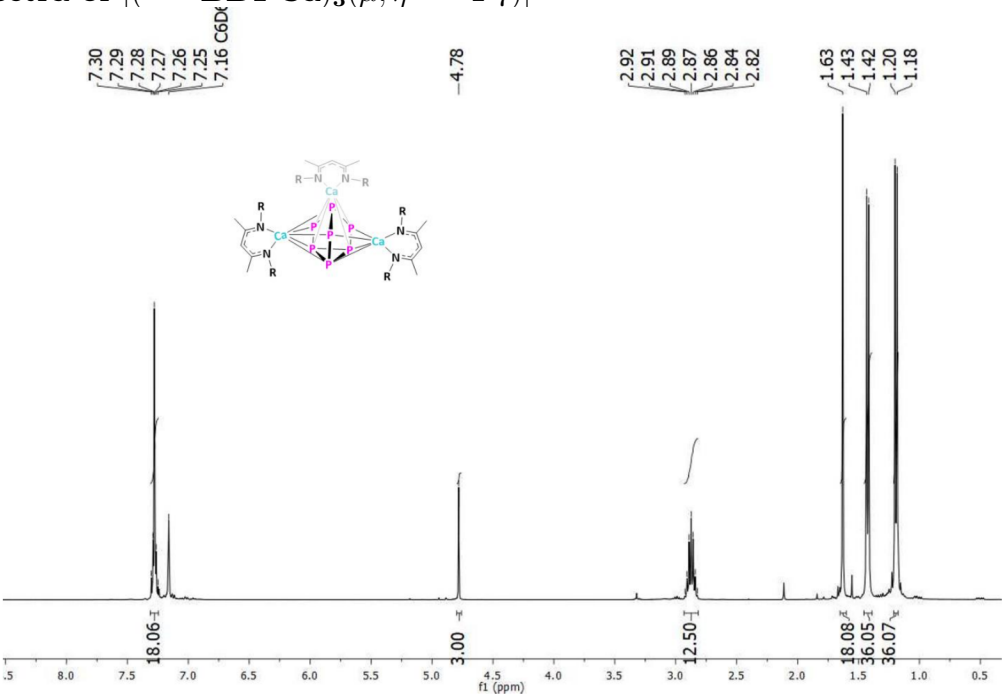


Figure 4.27: ^{1}H NMR (400 MHz, 300 K, C_6D_6) spectrum of complex **9**.

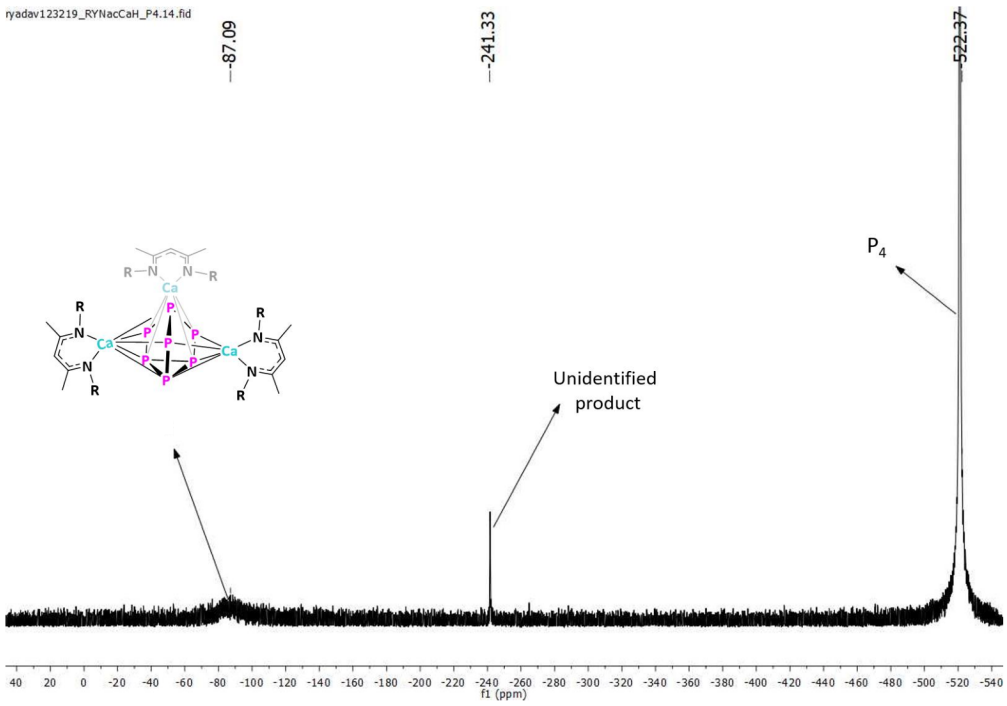


Figure 4.28: $^{31}P\{^{1}H\}$ NMR (162 MHz, 298 K, toluene-d_8) spectrum of NMR scale reaction between [(^{Dipp}BDI-Ca-H)$_2$] and P_4.

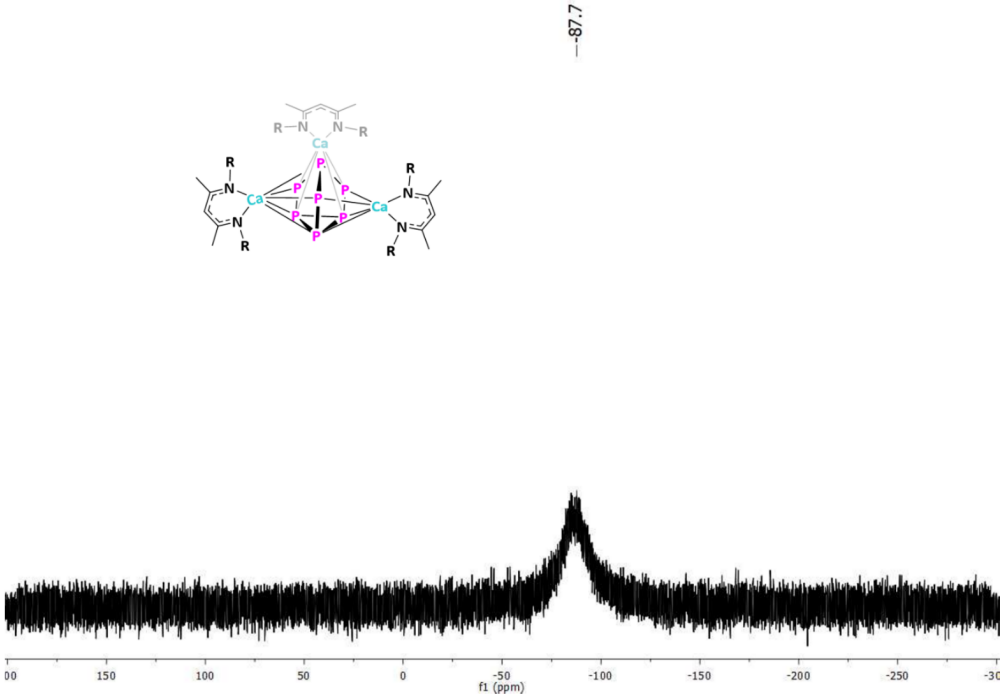


Figure 4.29: $^{31}P\{^{1}H\}$ NMR (162 MHz, 298 K, toluene-d_8) spectrum of complex **9**.

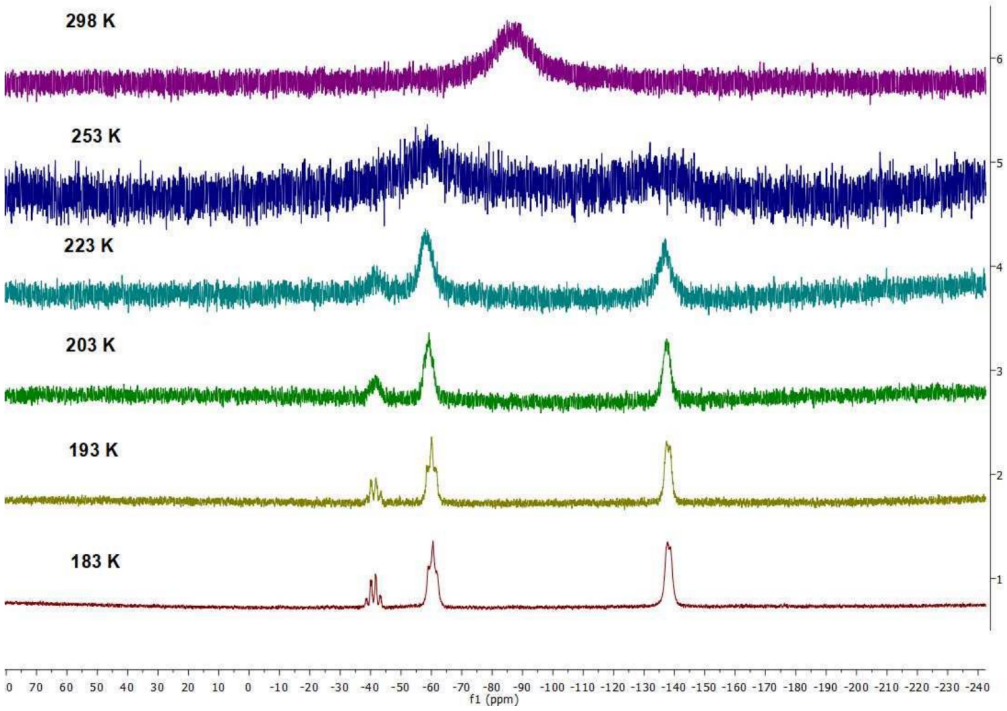


Figure 4.30: Variable temperature $^{31}P\{^{1}H\}$ NMR (162 MHz, toluene-d_8) spectrum of complex **9**.

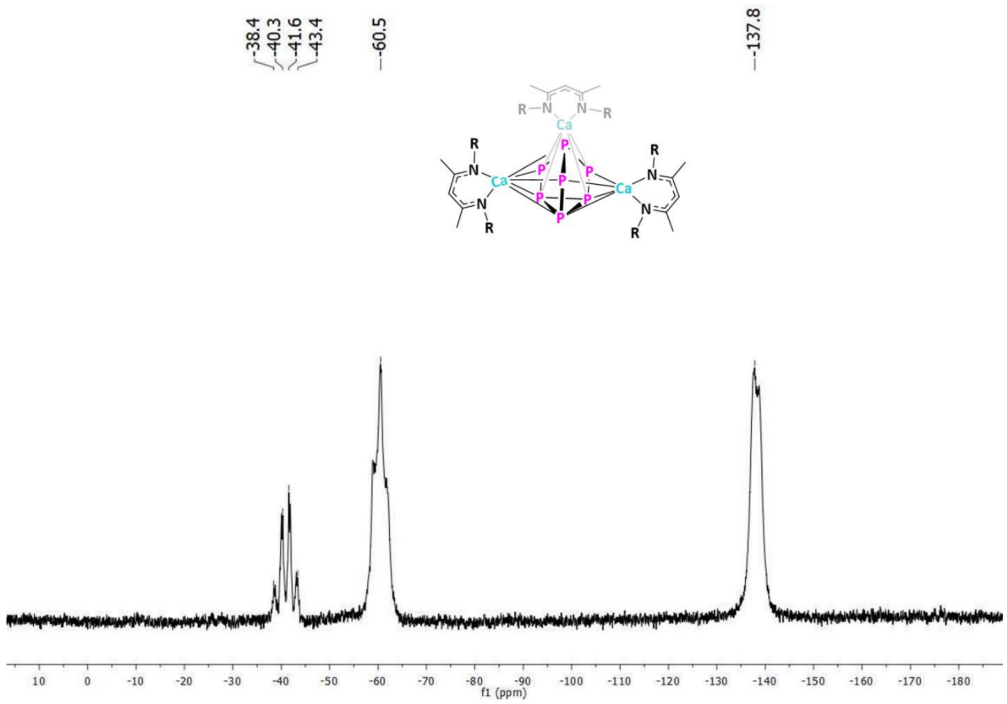


Figure 4.31: $^{31}P\{^{1}H\}$ NMR (162 MHz, toluene-d_8) spectrum of complex **9**.

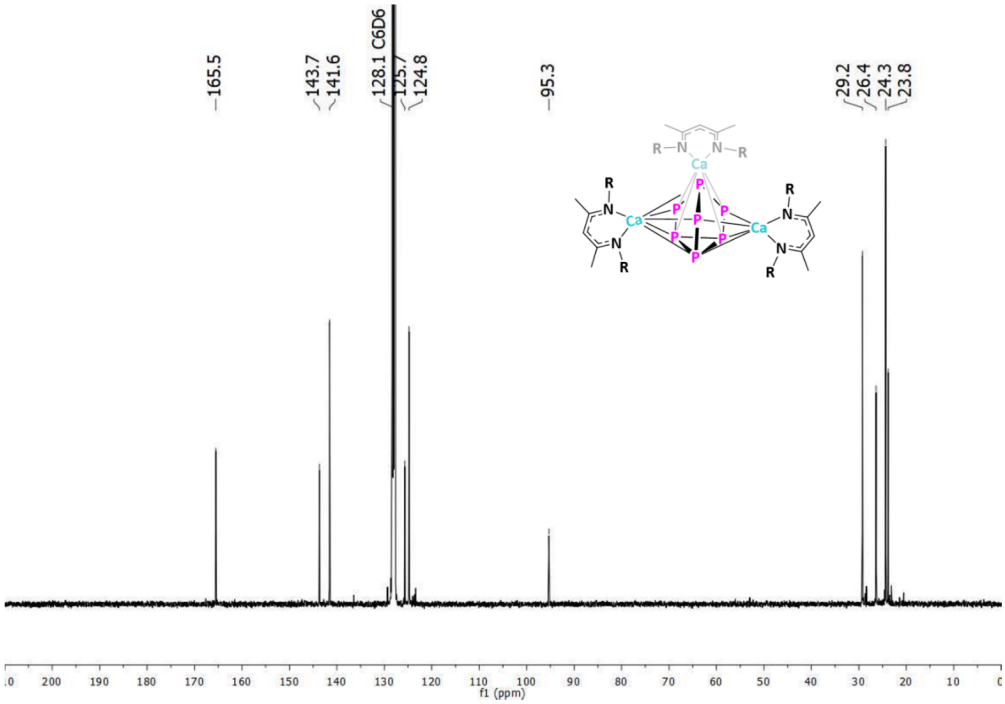


Figure 4.32: $^{13}C\{^1H\}$ NMR spectrum (100 MHz, 298 K, C_6D_6) of complex **9**.

4.3.4 Simulation of NMR spectra

Data from NMR simulations

Simulation and iterative fitting of the $^{31}P\{^1H\}$ NMR spectra were performed using the daisy plug-in of TopSpin 3.2 from Bruker. The parameters chemical shift (δ) and coupling constants (J) for the simulation of the spectra are compiled in the tables provided.

Data for 5

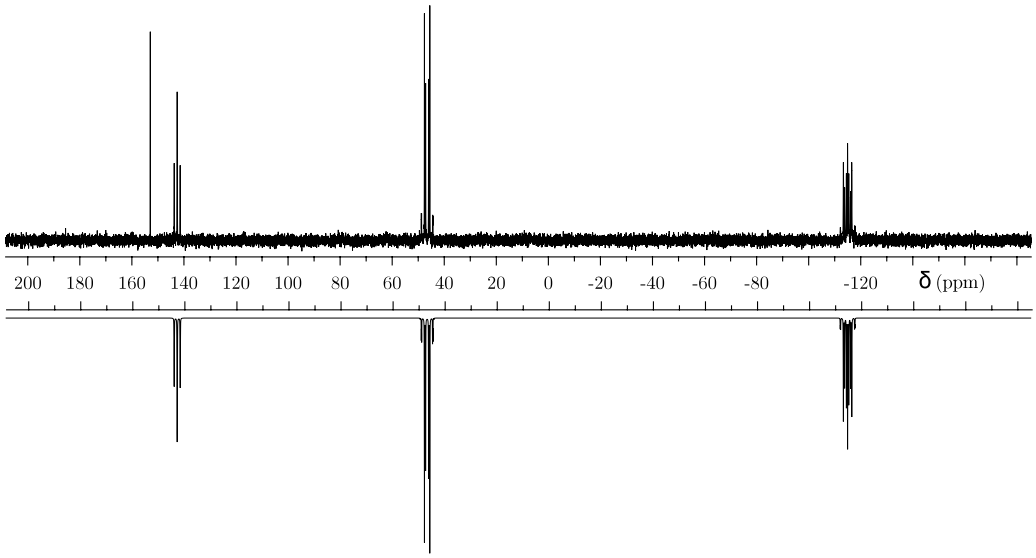


Figure 4.33: ^{31}P NMR of the reaction solution (toluene with D_2O capillary) with simulation (inverted) of the spin system. The singlet at 152 ppm is attributed to residual pentaphosphaferrocene, while the monomeric form of **5** shows up as an AMM'XX' spin system.

Table 4.2: Chemical shifts and coupling constants of the AMM'XX' spin system in the ^{31}P-NMR spectrum of **5** shown in figure 4.33. The multiplets are assigned to the phosphorus atoms in the simplified excerpt of the tetrameric structure in the solid phase shown in figure 4.35.

δ (ppm)		J (Hz)			
		$^1J_{P_AP_X}$	189	$^1J_{P_AP_{X'}}$	185
$P_A = P1$	142.6	$^2J_{P_AP_{M'}}$	13	$^2J_{P_AH_{CH_3}}$	10
$P_{MM'} = P3, P4$	46.5	$^1J_{P_MP_{M'}}$	255	$^1J_{P_MP_X}$	317
$P_{XX'} = P2, P5$	-114.9	$^2J_{P_MP_{X'}}$	-38	$^1J_{P_{M'}P_{X'}}$	379
		$^2J_{P_{M'}P_X}$	10	$^2J_{P_XP_{X'}}$	-15

Data for 6

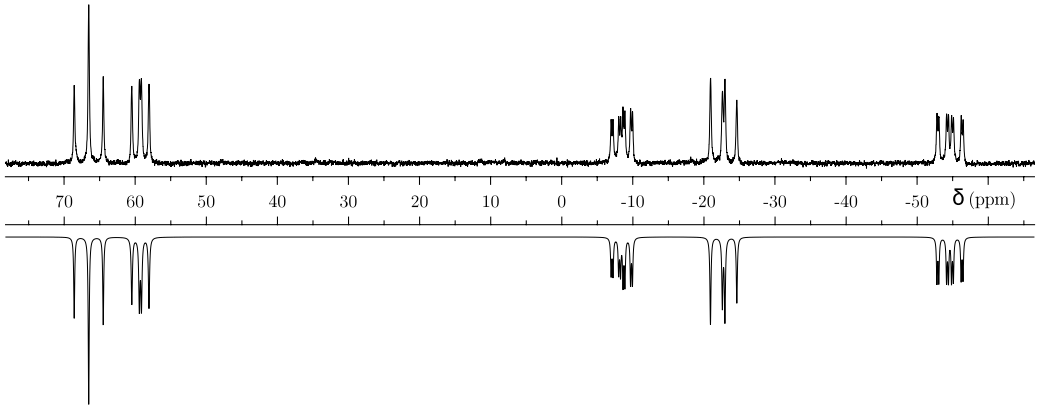


Figure 4.34: ^{31}P NMR spectra (experiment top, simulation bottom) of compound **6** in toluene-d_8 at 233 K, showing the ADMOX spin system of **6**.

Table 4.3: Chemical shifts and coupling constants of the ADMOX spin system in the $^{31}P\{^1H\}$-NMR spectrum of **6** at -40 ℃ (in toluene-d8) and assignment of the P atoms from the solid state structure to the spin system.

δ (ppm)		J (Hz)			
$P_A = P4$	66.5				
$P_D = P1$	59.2	$^1J_{P_AP_O}$	330	$^1J_{P_AP_X}$	331
$P_M = P2$	-8,5	$^1J_{P_DP_X}$	219	$^1J_{P_MP_O}$	271
$P_O = P3$	-22.72	$^1J_{P_DP_M}$	172	$^2J_{P_MP_X}$	43
$P_X = P5$	-54.61				

4.3.5 Details of the DOSY-measurements

General Information

Diffusion ordered NMR spectroscopy experiments were performed on Bruker Avance III HD 600 MHz spectrometer, equipped with a 5 mm CPPBBO BB-1H/19F. All measurements were performed at 298 K and temperature was controlled by BVTE 3900. NMR Data were processed, evaluated and plotted with TopSpin 3.2 software. Further analysis of the measurements was performed with Microsoft Excel (Version 16.0.10359.20023 64 Bit). All traces of oxygen in the TMS were removed by repeatedly freezing in liquid nitrogen and evacuating the flask. For adding TMS to a sample, 1 mL of the atmosphere right above the liquid TMS at room temperature was added to the atmosphere of the NMR tube with the already prepared sample.

Diffusion ordered spectroscopy (DOSY)

The DOSY measurements were performed with the convection suppressing DSTE (double stimulated echo) pulse sequence developed by Jerschow and Müller in a pseudo 2D mode.[263] Smoothed square (SMSQ10.100) gradient shapes and a linear gradient ramp with 20 increments between 5 % and 95 % of the maximum gradient strength (5.35 G/mm) were used. The diffusion time delay was set to 45 ms. For the homospoil gradient strengths, values of 100, -13.17, 20 and -17.13 % were used. Gradient pulse lengths (p16) were first optimized to obtain a sigmoidal signal decay for increasing gradient strength (0.9 ms for TMS, 1.6 ms for the investigated molecules). NMR spectra were processed with Bruker TopSpin 3.2 (T1/T2 relaxation package) and diffusion coefficients were derived according to Jerschow and Müller.[263] tetramethylsilane was added to the samples to reference chemical shifts and the viscosity of each sample.
The molecular radii were derived by the Stokes-Einstein equation[264] using Chens correction.[265]

$$D_i = \frac{k_b T}{6\pi\eta r_H} \cdot \left(1 + 0.695 \cdot \left(\frac{r_{solv}}{r_H}\right)^{2.234}\right)$$

D_i is the self-diffusion coefficient derived by the measurement, η is the viscosity of the solvent, r_H is the hydrodynamic radius of the observed molecule and r_{solv} the radius of the solvent. No form factor correction was applied. The viscosity was determined by measuring the diffusion coefficient of the reference tetramethylsilane (TMS) and solving the equation for η with the literature value[266] of the radius of 2.96 Å. The

solvent radius of C_6D_6 (2.655 Å) was calculated according to the increment system by Bondi.[267]

To estimate the error, diffusion coefficients for different signals of the same molecule were averaged and the standard deviation was determined. The molecular radii were calculated based on the averaged diffusion coefficient, the averaged diffusion coefficient plus the standard deviation and the averaged diffusion coefficient minus the standard deviation. The resulting radii are given as the radius derived from the averaged diffusion coefficient and the error range is given by:

$$\text{Error range} = \frac{1}{2} \cdot \left[\left(r_i^{\text{aver.}} - r_i^{\text{aver.+St.dev.}} \right) + \left(r_i^{\text{aver.-St.dev.}} - r_i^{\text{aver.}} \right) \right]$$

Where $r_i^{\text{aver.}}$ is the radius derived from the averaged diffusion coefficient, $r_i^{\text{aver.+St.dev.}}$ is the minimum radius derived from the averaged diffusion coefficient plus the standard deviation and $r_i^{\text{aver.-St.dev.}}$ is the maximum radius derived from the averaged diffusion coefficient minus the standard deviation. The error of the volume was estimated analogously.

Table 4.4: Results of the DOSY measurements at 298 K and 600 MHz in C_6D_6

Sample	Chem.Shift [ppm]	p16 [ms]	D_i [m^2/s]	$r_i^{\text{aver.}}$ Å	$V^{\text{aver.}}$ Å^3
5	0.00	0.9	$1.97 \cdot 10^{-9}$	7.47±0.11	1748±74
	1.69	1.6	$5.33 \cdot 10^{-10}$		
	1.65	1.6	$5.34 \cdot 10^{-10}$		
	1.61	1.6	$5.52 \cdot 10^{-10}$		
6	0.00	0.9	$2.15 \cdot 10^{-9}$	6.84±0.13	1339±75
	4.77	1.6	$6.66 \cdot 10^{-10}$		
	1.56	1.6	$6.34 \cdot 10^{-10}$		
	1.24	1.6	$6.63 \cdot 10^{-10}$		

4.3.6 Crystallographic details

A suitable crystal was covered in mineral oil (Aldrich) and mounted on a glass fibre. The crystal was transferred directly to the cold stream of a STOE IPDS 2 or a STOE StadiVari diffractometer or Rigaku GV50, TitanS2 diffractometer. All structures were solved by using the program SHELXS/T[177] and Olex2.[178] The remaining non-hydrogen atoms were located from successive difference Fourier map calculations. The refinements were carried out by using full-matrix least-squares techniques on F^2 by using the program SHELXL.[179] In each case, the locations of the largest peaks in the final difference Fourier map calculations, as well as the magnitude of the residual electron densities, were of no chemical significance. Crystallographic data for the structures reported in this paper have been deposited with the Cambridge Crystallographic Data Centre as a supplementary publication no. 2050401-2050405 Copies of the data can be obtained free of charge on application to CCDC, 12 Union Road, Cambridge CB21EZ, UK (fax: (+(44)1223-336-033; email: deposit@ccdc.cam.ac.uk).

Refinement details

For complex **7** and **8**, the Cp^* moiety appears to be freely rotating around the ct-Fe axis. To address this problem, various split positions were modelled and refined. Due to the low electron density, correlated to each of these parts, strong SIMU restraints were applied during the refinement process. For complex **9**, one diispropylphenyl moiety (C76-C87) shows signs of slight slipping. Most likely caused by two possible interaction modes, between the isopropyl groups and the neighbouring calcium atom. This results in unusually elongated ellipsoids of the corresponding carbon atoms. To address this problem, two split positions were modelled and refined. In order to appropriately model the split structure, strong SIMU restraints were applied during the refinement process.

Table 4.5: Crystallographic data for **5**, **6** and **7**:

Compound	**5**	**6**	**7**
Formula	$C_{189}H_{304}Fe_4Mg_4N_8P_{20}$	$C_{68}H_{97}FeMgN_4P_5$	$C_{73}H_{96}Fe_2Mg_2N_4P_{10}$
$\rho_{calc.}$/gcm^{-3}	1.210	1.173	1.275
μ/mm^{-1}	4.312	3.299	0.634
Formula Weight	3628.42	1229.81	1499.55
Colour	metallic dark green	dark brown	clear green
Shape	irregular	irregular	fragment
Size/mm^3	0.22 × 0.14 × 0.10	0.32 × 0.25 × 0.20	0.25 × 0.18 × 0.10
T/K	122.99(15)	123.00(10)	150
Crystal System	monoclinic	monoclinic	orthorhombic
Space Group	$P2_1/n$	$P2_1/c$	Pbcn
a/Å	20.3548(3)	23.4260(2)	22.3753(5)
b/Å	24.7873(4)	12.58444(10)	28.9852(7)
c/Å	39.7011(5)	25.1951(2)	24.0922(7)
α/°	90	96.2970(10)	90
β/°	90	110.1968(10)	90
γ/°	90	90	90
V/Å^3	19910.0(5)	6970.90(11)	15625.1(7)
Z	4	4	8
Z'	1	1	1
Wavelength/Å	1.54184	1.54184	0.71073
Radiation type	Cu K_α	Cu K_α	Mo K_α
θ_{min}/°	2.105	3.582	1.150
θ_{max}/°	68.299	74.174	25.623
Measured Refl's.	85009	41946	49509
Indep't Refl's	35475	13977	14578
Refl's I ≥ 2σ(I)	29553	13151	9532
R_{int}	0.0451	0.0323	0.0455
Parameters	1862	775	1021
Restraints	7	1	300
Largest Peak	0.384	0.505	0.450
Deepest Hole	-0.421	-0.320	-0.372
GooF	1.032	1.030	1.021
wR2 (all data)	0.1250	0.0992	0.1218
wR2	0.1187	0.0969	0.1034
R1 (all data)	0.0604	0.0392	0.0953
R1	0.0503	0.0370	0.0497

Table 4.6: Crystallographic data for **8** and **9**:

Compound	**8**	**9**
Formula	$C_{78}H_{112}Fe_2Ca_2N_4P_{10}$	$C_{111.5}H_{151}Ca_3N_6FeP_7$
$\rho_{calc.}/gcm^{-3}$	1.281	1.168
μ/mm^{-1}	0.706	0.303
Formula Weight	1607.27	1912.40
Colour	clear green	clear yellow
Shape	irregular	rod
$Size/mm^3$	$0.23 \times 0.15 \times 0.08$	$0.42 \times 0.18 \times 0.18$
T/K	100	100
Crystal System	triclinic	triclinic
Space Group	$P-1$	$P-1$
a/Å	13.1706(5)	12.1797(3)
b/Å	13.3112(6)	16.9575(4)
c/Å	14.2308(6)	27.3063(8)
$\alpha/^\circ$	116.232(3)	86.719(2)
$\beta/^\circ$	97.200(3)	89.662(2)
$\gamma/^\circ$	104.596(3)	75.016(2)
$V/Å^3$	2083.64(16)	5438.8(2)
Z	1	2
Z'	0.5	1
Wavelength/Å	0.71073	0.71073
Radiation type	Mo K_α	Mo K_α
$\theta_{min}/^\circ$	2.001	1.879
$\theta_{max}/^\circ$	30.141	30.414
Measured Refl's.	22713	60500
Indep't Refl's	10471	27388
Refl's $I \geq 2\sigma(I)$	7954	19233
R_{int}	0.0291	0.0401
Parameters	637	1354
Restraints	240	177
Largest Peak	0.764	0.836
Deepest Hole	-0.599	-0.663
GooF	1.069	1.014
wR2 (all data)	0.1270	0.1703
wR2	0.1175	0.1471
R1 (all data)	0.0664	0.0953
R1	0.0465	0.0612

Crystal structures

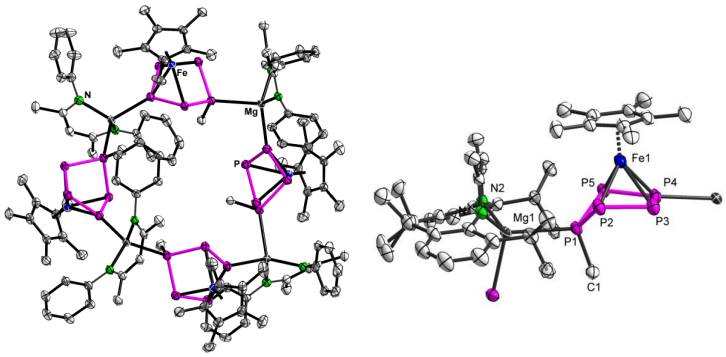


Figure 4.35: Molecular structure of complex **5** (left) in the solid state and a view of the monomeric moiety (right). The thermal ellipsoids are displayed at 40 % probability. The hydrogen atoms are omitted for clarity. Selected bond distances in the monomeric part: Fe1-P5 2.3250(8), Fe1-P2 2.3228(8), Fe1-P4 2.2883(8), Fe1-P3 2.3346(9), Fe1-C3 2.091(3), Fe1-C4 2.062(3), Fe1-C2 2.112(3), Fe1- C5 2.065(3), Fe1-C6 2.091(3), P1-Mg1 2.6983(11), P1-P5 2.1923(9), P1-P2 2.1920(10), P1-C1 1.823(3), P5- P4 2.1479(11), P2-P3 2.1423(11), P4-P3 2.1436(11), Mg1-N2 2.044(2), Mg1-N1 2.034(3); P5-P1-Mg1 131.33(4), P2-P1-P5 90.75(4), P2-P1-Mg1 111.76(4), P4 P5-P1-99.46(4), P3-P2-P1 103.28(4), P2-P3-P4 100.53(4), P3-P4-P5 105.78(4), P4-P5-P1 99.46(4).

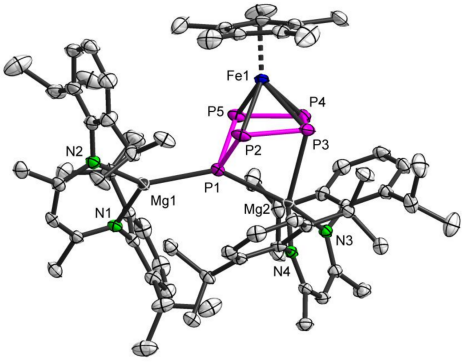


Figure 4.36: Molecular structure of complex **6** solid state. The thermal ellipsoids are displayed at 40 % probability. The hydrogen atoms are omitted for clarity. Selected bond distances: Fe1- P2 2.2635(4), Fe1-P3 2.2976(4), Fe1-P4 2.3148(4), Fe1-P5 2.2712(4), Fe1-C4 2.113(2), Fe1 C5 2.0731(14), Fe1-C1 2.067(2), Fe1-C3 2.135(2), Fe1-C2 2.100(2), P1-P2 2.2158(6), P2-P3 2.2089(6), P4-P3 2.1814(7), P5-P4 2.1691(6), P1-P5 2.1968(5), P1-Mg2 2.5452(6), P1-Mg1 2.4627(6), P2-Mg2 3.0865(6), P4-Mg2 3.1050(6), P3-Mg2 2.6764(6), Mg2-N3 2.0411(13), Mg2-N4 2.0516(12), Mg1-N1 2.0186(13), Mg1-N2 2.0162(13); P5-P1-P2 85.93(2), P5-P1-Mg2 98.64(2), P5-P1-Mg1 118.02(2), P2-P1-Mg2 80.50(2), P2-P1- Mg1 110.88(2), Mg1-P1-Mg2 141.76(2), P4-P5-P1 101.56(2), P3-P2-P1 100.90(2), P5-P4-P3 101.25(2), P4- P3-P2 100.50(2).

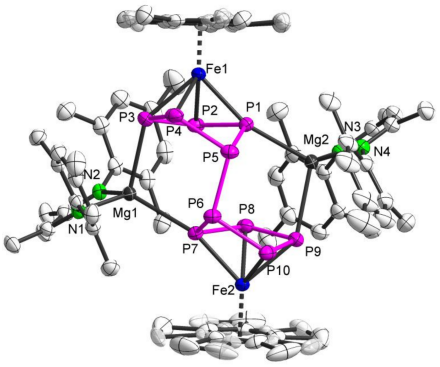


Figure 4.37: Molecular structure of complex **7** in the solid state. The thermal ellipsoids are displayed at 40 % probability. The hydrogen atoms and coordinating solvent molecules are omitted for clarity. Selected bond distances: Fe1-P1 2.2782(10), Fe1-P2 2.3283(11), Fe1-P3 2.3020(11), Fe1-P4 2.3284(12), Fe2-P7 2.2851(10), Fe2-P8 2.3279(11), Fe2-P9 2.2948(11), Fe2-P10 2.3274(12), P1-P2 2.1571(14), P2-P3 2.172(2), P4-P3 2.161(2), P5-P4 2.1718(14), P1-P5 2.1614(14), P5-P6 2.1992(13), P7-P6 2.1668(14), P7-P8 2.154(2), P8-P9 2.167(2), P10-P9 2.162(2), P6-P10 2.171(2), P2-Mg1 3.142(2), P7-Mg1 2.5879(14), P3-Mg1 2.639(2), P1-Mg2 2.577(2), P8-Mg2 3.192(2), P9-Mg2 2.613(2), Mg1-N1 2.031(3), Mg1-N2 2.029(3), Mg2-N3 2.025(3), Mg2-N4 2.034(3); P2-P1-P5 111.91(6), P8-P7-P6 111.48(6), P1-P5-P6 112.60(6), P1-P5-P4 90.28(5), P4-P5-P6 108.61(6), P1-P2-P3 99.59(6), P7-P6-P5 113.14(6), P7-P6-P10 90.25(5), P10-P6-P5 108.21(6), P7-P8-P9 99.96(6), P3-P4-P5 108.35(6), P9-P10-P6 108.39(6), P4-P3-P2 104.47(6), P10-P9-P8 104.31(6).

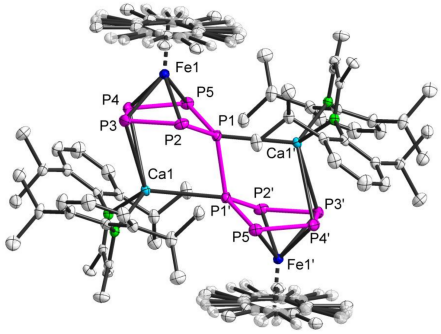


Figure 4.38: Molecular structure of complex **8** solid state. The thermal ellipsoids are displayed at 40 % probability. The hydrogen atoms and non-coordinating solvent molecules are omitted for clarity. Selected bond distances: Fe1-P2 2.2958(7), Fe1-P3 2.3053(8), Fe1-P4 2.3330(7), Fe1-P5 2.2895(7), Ca1-P1 2.9605(8), Ca1-P4 3.1430(8), Ca1-P3 2.9748(8), Ca1-N1 2.317(2), Ca1-N2 2.329(2), P1-P1' 2.3455(12), P1-P2 2.1634(9), P2-P3 2.1767(10), P4-P3 2.1488(11), P5-P4 2.1640(10), P1-P5 2.1495(9); P5-P1-P1' 116.37(4), P5-P1-P2 96.19(3), P1-P2- P3 110.12(4), P1-P5-P4 109.84(4), P3-P4-P5 104.40(4), P4-P3-P2 103.87(4).

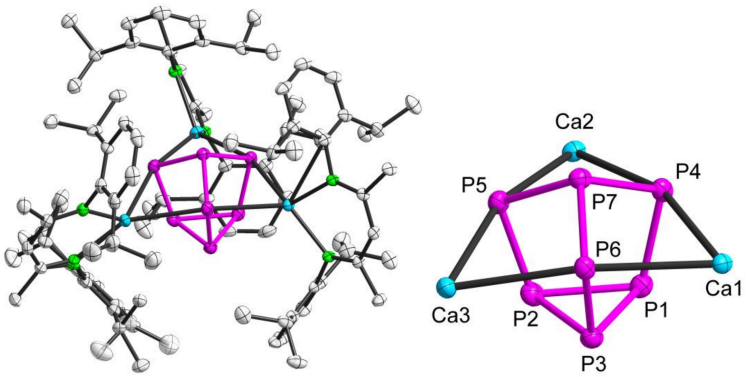


Figure 4.39: Molecular structure of complex **9** (left) in the solid state and a view of complex **9** (right) without β-diketiminate moieties for a clearer view of the core structure. The thermal ellipsoids are displayed at 40 % probability. The hydrogen atoms and non-coordinating solvent molecules are omitted for clarity. Selected bond distances: Ca1-P6 2.8667(9), Ca1-P4 2.9305(8), Ca2-P4 2.9256(8), Ca2-P5 2.8814(9), Ca3-P6 2.9346(9), Ca3-P5 2.9079(9), P6- P7 2.1944(10), P6-P3 2.1828(10), P4-P7 2.1988(10), P4-P1 2.1748(10), P5-P7 2.2009(9), P5-P2 2.1752(10), P3-P1 2.2511(11), P3-P2 2.2575(10), P1-P2 2.2586(11); P3-P6-P7 99.47(4), P1-P4-P7 99.61(4), P2-P5-P7 99.73(4), P6-P7-P4 101.90(4), P6-P7-P4 101.90(4), P4-P7-P5 101.05(4), P6- P3-P1 105.88(4), P6-P3-P2 104.32(4), P1-P3-P2 60.13(3), P4-P1-P3 105.00(4), P4-P1-P2 105.32(4), P3-P-P2 60.08(3), P5-P2-P3 104.95(4), P5-P2-P1 105.0(4), P3-P2-P1 59.80(3).

4.3.7 Quantum chemical calculations

The geometry optimizations were initiated from the coordinates taken from the crystal structure coordinates of complex **7** and complex **8** and labeled as **7Mg** and **8Ca** in Gibbs free energy comparison to make easier to follow. The geometry optimization of **7Ca** and **8Mg** was done by replacement of metal ions with Ca and Mg in crystal coordinates of **7Mg** and **8Ca**, respectively. All structure optimizations were carried out using the Gaussian 16, revision C.01, package.[251] The geometry optimizations have been done without any constraints and frequency calculations were also performed on all the optimized geometries to ensure that the optimized geometries did not have any imaginary frequencies. Geometry optimizations have been carried out using the unrestricted density functional method B97D[268] functional. The basis set was LANL2DZ for the calcium, magnesium and iron atom and 6-31G** for C, N, P and H atoms. The complexes were optimized as a charge neutral species with a spin multiplicity of singlet. The QTAIM analysis were performed with the Multiwfn[269] software on wave functions generated with the Gaussian 16 program. Visualization of the molecular orbitals and the corresponding diagrams were done employing the Chemcraft software (www.chemcraftprog.com).

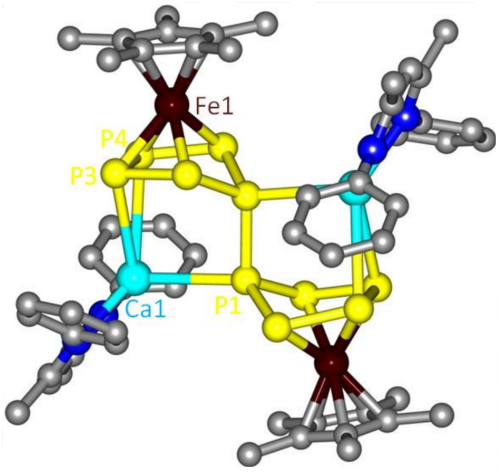


Figure 4.40: UB97D optimized geometries of complex **8** after removing the isopropyl groups on phenyl ring substitution using LANL2DZ basis set for iron, magnesium and calcium atom and 6-31G** for all other atoms.

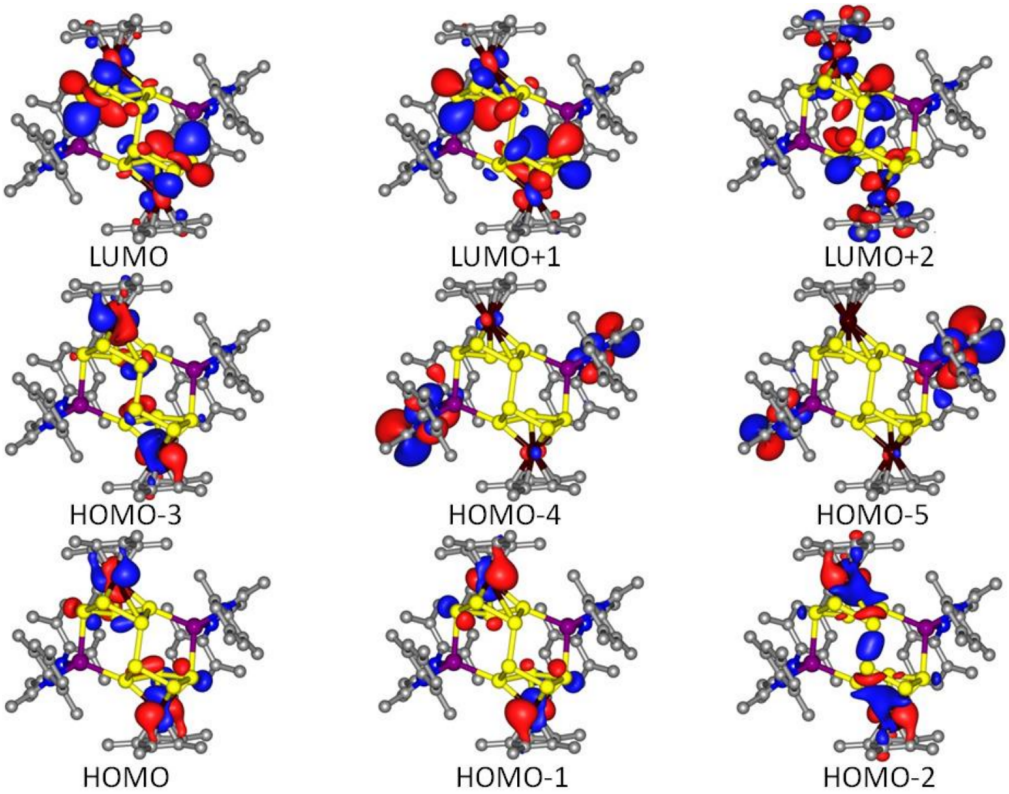


Figure 4.41: Selected Kohn-Sham orbitals (top view) of UB97D/6-31G**/LANL2DZ optimized geometry of complex **7**.

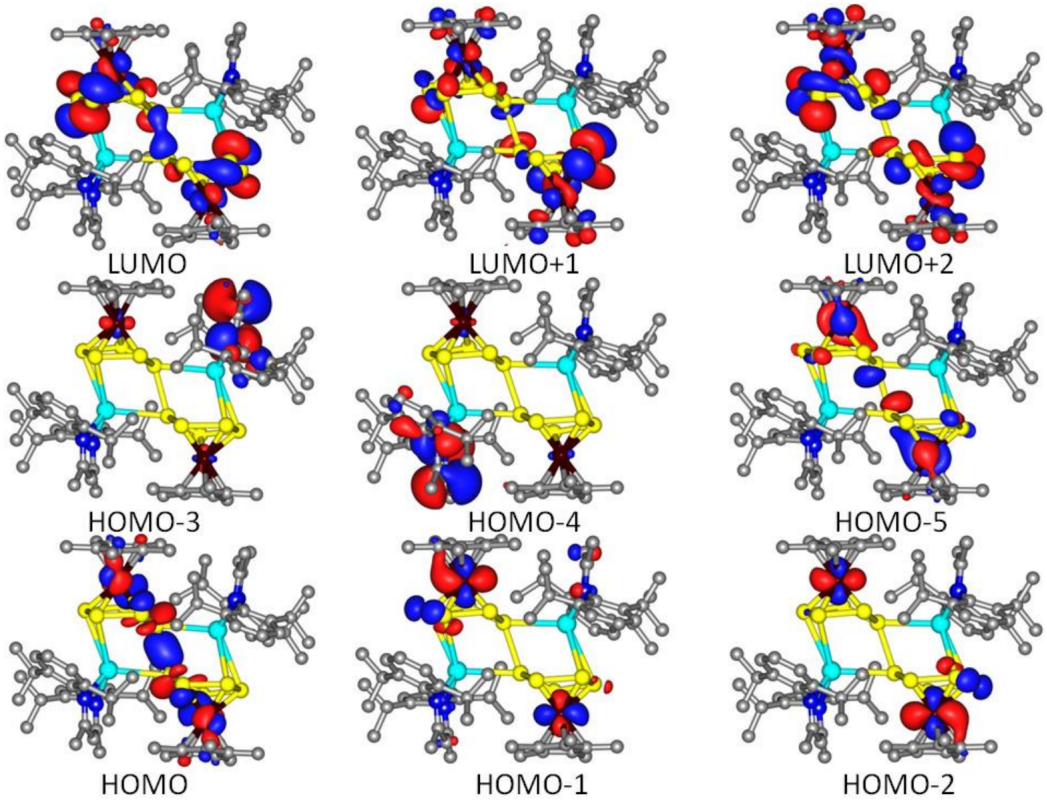


Figure 4.42: Selected Kohn-Sham orbitals (top view) of UB97D/6-31G**/LANL2DZ optimized geometry of complex **8**.

Table 4.7: Free energies and enthalpies of Complexes **7Mg**, **8Ca**,**7Ca** and **8Mg**:

Complex	**7Mg**	**7Ca**	**8Ca**	**8Mg**
Enthalpy (kcal/mol)	922.94	922.12	1144.39	1146.46
Free energy (kcal/mol)	766.88	766.06	974.27	980.23

Cartesian coordinates for complex 7Mg

26 1.005944000 3.398272000 -0.379605000
26 -1.002249000 -3.390128000 -0.429134000
15 -0.185562000 1.124891000 -2.382718000
15 -0.675452000 1.838785000 -0.362373000
15 0.984595000 1.561104000 1.038418000
15 2.688008000 1.790701000 -0.360652000
15 1.734935000 2.232739000 -2.299303000
15 0.195635000 -1.089576000 -2.397602000
15 0.678696000 -1.830313000 -0.385535000
15 -1.724438000 -2.199546000 -2.336174000
15 -2.684797000 -1.783357000 -0.395581000
15 -0.986673000 -1.572218000 1.012827000
12 -2.956341000 0.798174000 0.192342000
12 2.958283000 -0.799075000 0.190342000
7 4.536851000 -1.590886000 -0.823197000
7 3.871521000 -0.929046000 2.001358000
7 -4.528962000 1.606331000 -0.817812000
7 -3.880598000 0.897483000 1.999844000
6 4.644421000 -1.295871000 -2.222254000
6 3.988199000 -2.107574000 -3.175190000
6 4.005324000 -1.715549000 -4.524689000
1 3.488656000 -2.339087000 -5.258275000
6 4.662375000 -0.549682000 -4.949698000
6 5.347143000 0.213037000 -3.988071000
1 5.886845000 1.110600000 -4.300395000
6 5.354788000 -0.140024000 -2.628991000
6 6.110277000 0.694869000 -1.617349000
1 5.423843000 1.146207000 -0.884754000
1 6.661346000 1.503930000 -2.117389000
1 6.826723000 0.086502000 -1.043432000
6 3.297604000 -3.384258000 -2.753709000
1 3.958085000 -4.015797000 -2.139346000
1 2.978171000 -3.959705000 -3.633818000
1 2.403386000 -3.171974000 -2.148727000
6 4.613836000 -0.111673000 -6.398787000
1 4.486065000 -0.971982000 -7.072696000
1 5.532013000 0.422492000 -6.686549000
1 3.766571000 0.572892000 -6.572627000
6 3.420878000 -0.061185000 3.044501000
6 2.307585000 -0.423814000 3.836341000
6 1.821906000 0.496735000 4.779124000
1 0.976644000 0.209025000 5.404680000
6 2.392821000 1.769175000 4.941679000
6 3.514527000 2.094560000 4.159562000
1 3.995132000 3.067665000 4.289140000
6 4.048083000 1.197731000 3.218257000
6 5.264173000 1.570608000 2.399430000
1 6.062109000 0.818117000 2.492286000
1 5.661819000 2.544786000 2.716793000
1 5.008669000 1.632447000 1.330952000
6 1.796671000 2.769216000 5.910595000
1 0.995815000 3.354973000 5.428077000
1 2.554631000 3.481672000 6.268862000
1 1.353363000 2.265792000 6.783048000
6 1.665092000 -1.782970000 3.674424000
1 0.719697000 -1.842111000 4.228753000
1 2.334251000 -2.588019000 4.022468000
1 1.447699000 -1.990781000 2.616171000
6 6.597254000 -2.922345000 -1.061203000
1 7.248804000 -3.567041000 -0.458232000
1 7.210730000 -2.137400000 -1.529470000
1 6.159535000 -3.507462000 -1.882827000
6 5.504459000 -2.286901000 -0.212729000
6 5.606132000 -2.436910000 1.193709000
1 6.411362000 -3.085343000 1.534222000
6 4.924653000 -1.734505000 2.214707000
6 5.458430000 -1.875518000 3.633887000
1 5.895979000 -0.922904000 3.969644000
1 6.225843000 -2.657046000 3.697217000
1 4.640369000 -2.107458000 4.331639000
6 -3.438582000 0.011841000 3.031788000
6 -4.068547000 -1.248800000 3.180742000
6 -3.543357000 -2.161077000 4.111987000
1 -4.026042000 -3.135503000 4.222396000
6 -2.428058000 -1.849246000 4.908529000
6 -1.854677000 -0.574887000 4.770858000
1 -1.015262000 -0.297701000 5.409028000
6 -2.331390000 0.360704000 3.838366000
6 -5.278802000 -1.607508000 2.347051000
1 -5.683284000 -2.583388000 2.650275000
1 -5.013855000 -1.659147000 1.280301000
1 -6.074326000 -0.852655000 2.440912000
6 -1.841318000 -2.864603000 5.867204000
1 -1.030523000 -3.437380000 5.385748000
1 -2.601028000 -3.587083000 6.200752000
1 -1.413351000 -2.375660000 6.755438000
6 -1.685894000 1.721274000 3.702113000
1 -1.447719000 1.939037000 2.650271000
1 -0.751403000 1.774721000 4.275201000
1 -2.361660000 2.523053000 4.044629000
6 -4.630563000 1.330577000 -2.221284000
6 -5.339445000 0.180369000 -2.646340000
6 -5.325773000 -0.154978000 -4.009831000
1 -5.864126000 -1.048339000 -4.336211000
6 -4.636700000 0.620178000 -4.958346000
6 -3.981753000 1.780468000 -4.515242000
1 -3.462144000 2.413679000 -5.238394000
6 -3.970444000 2.154828000 -3.160651000
6 -6.099846000 -0.667215000 -1.649087000
1 -5.417323000 -1.125762000 -0.917388000
1 -6.646579000 -1.471291000 -2.161753000
1 -6.820798000 -0.066500000 -1.072721000
6 -4.581584000 0.201044000 -6.412766000
1 -4.451146000 1.070058000 -7.074890000
1 -5.498269000 -0.329647000 -6.711504000
1 -3.733292000 -0.480935000 -6.591685000
6 -3.281779000 3.426008000 -2.719754000
1 -3.942573000 4.046068000 -2.094254000
1 -2.964977000 4.016211000 -3.591035000
1 -2.386081000 3.205850000 -2.119780000
6 -5.477482000 1.818241000 3.637571000
1 -5.919904000 0.861103000 3.953509000
1 -6.243311000 2.600607000 3.709208000
1 -4.663769000 2.035650000 4.344992000
6 -4.934364000 1.700557000 2.219790000
6 -5.608894000 2.420503000 1.206410000
1 -6.415529000 3.064082000 1.552768000
6 -5.499767000 2.292756000 -0.201705000
6 -6.588281000 2.941228000 -1.045805000
1 -6.146487000 3.538237000 -1.856617000
1 -7.242440000 3.577184000 -0.436405000
1 -7.199852000 2.163545000 -1.528475000
6 -0.499927000 -5.230225000 -1.186949000
6 0.186352000 -5.044683000 0.071335000
6 -0.796878000 -4.864184000 1.102548000
6 -2.095531000 -4.924373000 0.494184000
6 -1.919703000 -5.163750000 -0.919974000
6 0.141200000 -5.525352000 -2.511650000
1 0.281382000 -6.612312000 -2.650967000
1 1.123211000 -5.042891000 -2.585419000
1 -0.481737000 -5.151110000 -3.334607000
6 1.671961000 -5.086992000 0.286590000
1 2.211434000 -4.830669000 -0.632276000
1 1.986314000 -6.097513000 0.600699000
1 1.981160000 -4.379467000 1.068445000
6 -0.524060000 -4.654958000 2.565011000
1 0.468050000 -4.212086000 2.720817000
1 -0.556920000 -5.616231000 3.107210000
1 -1.268679000 -3.981427000 3.009108000
6 -3.399213000 -4.785408000 1.225930000
1 -4.196949000 -4.461463000 0.545636000
1 -3.315095000 -4.038335000 2.026625000
1 -3.697007000 -5.746782000 1.679905000
6 -3.022430000 -5.361761000 -1.918180000
1 -2.693144000 -5.069718000 -2.923954000
1 -3.896461000 -4.747294000 -1.660100000
1 -3.341840000 -6.417877000 -1.949423000
6 0.512364000 5.249199000 -1.118231000
6 -0.185858000 5.048616000 0.130910000
6 0.787245000 4.852217000 1.168710000
6 2.091781000 4.918062000 0.573382000
1 1.929529000 5.176794000 -0.839119000
1 -1.096462000 5.078690000 -2.535498000
6 -0.116086000 5.561753000 -2.445048000
1 0.515768000 5.199963000 -3.266750000
1 -0.256776000 6.650308000 -2.570681000
1 -1.991862000 4.369893000 1.098573000
6 -1.673222000 5.091272000 0.333322000
1 -2.204987000 4.854488000 -0.595139000
1 -1.987245000 6.096621000 0.663917000
6 0.499430000 4.622572000 2.625162000
1 0.521699000 5.576500000 3.180697000
1 1.242115000 3.946245000 3.068204000
6 3.388372000 4.766648000 1.315168000
1 3.295058000 4.009762000 2.105545000
1 3.684634000 5.721405000 1.783842000
1 4.191304000 4.448757000 0.638159000
1 2.721995000 5.104343000 -2.836587000
1 3.360306000 6.442688000 -1.841942000
6 3.041518000 5.386064000 -1.824692000
1 3.913599000 4.769613000 -1.564837000

Cartesian coordinates for complex 8Ca

26 1.001688000 3.914155000 -0.135139000
20 -2.879493000 0.104083000 0.253656000
15 -0.053781000 1.267289000 0.574786000
15 1.279096000 2.585110000 1.732603000
15 0.332593000 2.090267000 -1.405806000
15 2.449281000 2.728339000 -1.566967000
15 3.082825000 3.068985000 0.502981000
7 -4.191051000 1.199914000 1.939476000
7 -4.326247000 1.318975000 -1.233329000
6 -4.150564000 0.573697000 3.220912000
6 -4.657865000 0.704352000 -2.483161000
6 -3.342778000 1.064138000 4.286593000
6 -4.869385000 -0.651938000 3.386119000
6 -4.958516000 2.985144000 0.450048000
1 -5.419688000 3.971931000 0.507227000
6 -5.832544000 -1.130749000 2.300136000
1 -5.341664000 -0.997851000 1.320581000
6 -3.872810000 0.895171000 -3.652548000
6 -2.529096000 2.351170000 4.194728000
1 -2.682911000 2.796623000 3.204304000
6 -4.898177000 2.473735000 -0.873927000

```
6 -5.780286000 -0.175792000 -2.515777000
6 -4.790000000 2.374250000 1.724983000
6 -6.669088000 -0.366786000 -1.289364000
1 -6.099625000 -0.052881000 -0.403783000
6 -2.674584000 1.837941000 -3.692397000
1 -2.430301000 2.126625000 -2.659395000
6 -1.024456000 2.050939000 4.347540000
1 -0.812037000 1.620350000 5.337747000
1 -0.429497000 2.969360000 4.240365000
1 -0.686052000 1.335211000 3.589567000
6 -2.955352000 3.379976000 5.267972000
1 -4.031043000 3.595422000 5.226845000
1 -2.401626000 4.322200000 5.130747000
1 -2.725629000 2.998333000 6.274623000
6 -5.408476000 3.163220000 2.879893000
1 -5.573413000 2.529878000 3.759299000
1 -6.363237000 3.609345000 2.570401000
1 -4.736920000 3.982702000 3.176298000
6 -7.097650000 -0.240006000 2.293182000
1 -7.603132000 -0.310360000 3.268734000
1 -7.799276000 -0.570138000 1.513686000
1 -6.843452000 0.809901000 2.104252000
6 -4.746224000 -1.361342000 4.592560000
1 -5.291186000 -2.294973000 4.722529000
6 -3.259896000 0.319188000 5.478674000
1 -2.637121000 0.700234000 6.289591000
6 -5.342766000 -0.634228000 -4.876347000
1 -5.610307000 -1.143925000 -5.803411000
6 -4.237490000 0.219419000 -4.832757000
1 -3.643432000 0.376903000 -5.733862000
6 -5.559085000 3.372742000 -1.922853000
1 -6.481714000 3.823034000 -1.532333000
1 -5.785773000 2.826041000 -2.844956000
1 -4.869280000 4.194272000 -2.172890000
6 -6.227743000 -2.614176000 2.416067000
1 -5.341477000 -3.260310000 2.483977000
1 -6.805878000 -2.914441000 1.533045000
1 -6.856541000 -2.784798000 3.303995000
6 -7.904136000 0.558798000 -1.377791000
1 -7.600102000 1.610583000 -1.465371000
1 -8.532362000 0.451118000 -0.479896000
1 -8.509762000 0.300893000 -2.261011000
6 -1.431251000 1.166491000 -4.310481000
1 -1.170781000 0.242203000 -3.779696000
1 -0.568159000 1.844250000 -4.254092000
1 -1.601062000 0.920768000 -5.369936000
6 -6.104760000 -0.825689000 -3.718681000
1 -6.971758000 -1.485789000 -3.751459000
6 -3.944212000 -0.886722000 5.638216000
1 -3.860445000 -1.451835000 6.567736000
6 -7.103479000 -1.831148000 -1.081091000
1 -7.725846000 -2.192744000 -1.913023000
1 -7.705091000 -1.914954000 -0.165515000
1 -6.231959000 -2.495856000 -0.989477000
6 -3.010394000 3.123018000 -4.484705000
1 -3.251608000 2.868099000 -5.528396000
1 -2.145215000 3.805549000 -4.493550000
1 -3.870366000 3.653484000 -4.056179000
6 0.946795000 5.743284000 0.838911000
6 1.499683000 5.894938000 -0.487353000
6 0.492021000 5.489458000 -1.432952000
6 -0.677925000 5.087754000 -0.693500000
6 -0.399114000 5.237309000 0.705213000
6 1.634335000 6.069041000 2.131850000
1 1.271040000 5.415260000 2.937082000
1 1.446771000 7.115106000 2.428770000
1 2.719727000 5.924124000 2.043759000
6 2.865382000 6.416600000 -0.827790000
1 3.570608000 6.229402000 -0.006980000
1 2.837266000 7.503207000 -1.017725000
1 3.255481000 5.921627000 -1.728045000
6 0.621065000 5.473510000 -2.927551000
1 1.673713000 5.380872000 -3.225923000
1 0.212050000 6.397310000 -3.371429000
1 0.072102000 4.621441000 -3.353956000
6 -1.990415000 4.661687000 -1.280723000
1 -1.854133000 4.222135000 -2.274090000
1 -2.656675000 5.536222000 -1.385489000
1 -2.507386000 3.930827000 -0.644296000
6 -1.372480000 4.968004000 1.815770000
1 -2.094276000 4.194335000 1.521742000
1 -1.941193000 5.881520000 2.063364000
1 -0.856861000 4.629529000 2.723265000
15 0.093383000 -1.297304000 0.303022000
15 -0.550023000 -1.842536000 -1.710618000
15 -1.073755000 -2.762219000 1.435610000
15 -3.021245000 -3.097799000 0.409040000
15 -2.665880000 -2.516675000 -1.676292000
26 -1.049267000 -3.831705000 -0.611042000
20 2.902489000 -0.072712000 0.170380000
7 4.325168000 -0.984414000 -1.528609000
7 4.169939000 -1.548922000 1.558102000
6 4.602744000 -0.134308000 -2.640343000
6 4.399465000 -1.291485000 2.945536000
6 3.900357000 -0.234497000 -3.871793000
6 5.547718000 0.917932000 -2.442376000
6 4.646811000 -3.071832000 -0.305150000
1 4.913527000 -4.112012000 -0.489602000
6 6.334234000 1.009689000 -1.137312000
1 5.664660000 0.707540000 -0.313979000
6 3.381853000 -1.494922000 3.915342000
6 2.820226000 -1.280410000 -4.123960000
1 2.712609000 -1.892390000 -3.218912000
6 4.508527000 -2.752506000 1.070515000
6 5.669984000 -0.784458000 3.344215000
6 4.737305000 -2.249760000 -1.467442000
6 6.779046000 -0.521230000 2.327284000
1 6.338092000 -0.578395000 1.323944000
6 1.982324000 -1.969646000 3.540432000
1 1.969763000 -2.202295000 2.465631000
6 1.464548000 -0.596607000 -4.400082000
1 1.519164000 0.011800000 -5.315591000
1 0.671313000 -1.346440000 -4.530656000
1 1.174078000 0.062345000 -3.572637000
6 3.178920000 -2.208774000 -5.306681000
1 4.157214000 -2.688480000 -5.171080000
1 2.414615000 -2.993903000 -5.420706000
1 3.212079000 -1.633458000 -6.244615000
6 5.357663000 -2.934326000 -2.683140000
1 5.758585000 -2.202363000 -3.394190000
1 6.155042000 -3.625108000 -2.378512000
1 4.585323000 -3.519522000 -3.205209000
6 7.496139000 -0.011419000 -1.154547000
1 8.182142000 0.221085000 -1.983787000
1 8.060716000 0.026690000 -0.211796000
1 7.117929000 -1.033322000 -1.289322000
6 5.787532000 1.824708000 -3.487755000
1 6.508842000 2.628616000 -3.345751000
6 4.177671000 0.697456000 -4.889974000
1 3.637971000 0.615878000 -5.834900000
6 4.916451000 -0.754835000 5.671522000
1 5.118686000 -0.557156000 6.725434000
6 3.660907000 -1.217337000 5.266499000
1 2.875606000 -1.374539000 6.007802000
6 4.791227000 -3.888735000 2.051910000
1 5.074192000 -4.814617000 1.536045000
1 5.593031000 -3.606553000 2.748628000
1 3.898091000 -4.077955000 2.664856000
6 6.854510000 2.423027000 -0.815987000
1 6.044695000 3.165341000 -0.866200000
1 7.280742000 2.439796000 0.195229000
1 7.647447000 2.724540000 -1.517895000
6 7.880828000 -1.601335000 2.407720000
1 7.470757000 -2.600611000 2.204723000
1 8.672685000 -1.398777000 1.669294000
1 8.337524000 -1.612731000 3.409987000
6 0.959836000 -0.843491000 3.812005000
1 1.201786000 0.066391000 3.241433000
1 -0.059419000 -1.163699000 3.552570000
1 0.968538000 -0.567368000 4.876927000
6 5.907942000 -0.536941000 4.707457000
1 6.887027000 -0.166558000 5.015301000
6 5.113416000 1.718290000 -4.710847000
1 5.313056000 2.431570000 -5.512044000
6 7.391349000 0.885244000 2.499656000
1 7.881065000 0.992897000 3.479127000
1 8.154117000 1.063986000 1.727512000
1 6.620301000 1.665602000 2.416429000
6 1.567436000 -3.251316000 4.294745000
1 1.507454000 -3.065825000 5.378148000
1 0.576261000 -3.581239000 3.948434000
1 2.289521000 -4.065260000 4.131333000
6 -0.730296000 -5.235635000 -2.146339000
6 -1.588637000 -5.770177000 -1.121478000
6 -0.850112000 -5.761554000 0.119402000
6 0.462015000 -5.214950000 -0.143909000
6 0.533083000 -4.898855000 -1.541363000
6 -1.065371000 -5.062787000 -3.598620000
1 -0.611138000 -4.143557000 -3.995640000
1 -0.685710000 -5.911441000 -4.193315000
1 -2.150919000 -4.995823000 -3.747209000
6 -2.988571000 -6.273140000 -1.322390000
1 -3.499862000 -5.692594000 -2.102717000
1 -2.988466000 -7.333639000 -1.626780000
1 -3.573103000 -6.179584000 -0.397543000
6 -1.332729000 -6.258249000 1.450274000
1 -2.428530000 -6.218966000 1.511389000
1 -1.014877000 -7.301059000 1.620829000
1 -0.925121000 -5.640767000 2.263420000
6 1.572251000 -5.040679000 0.851066000
1 1.174084000 -4.853457000 1.856123000
1 2.201735000 -5.946739000 0.895021000
1 2.221213000 -4.199741000 0.573730000
6 1.731694000 -4.361932000 -2.265956000
1 2.393147000 -3.799208000 -1.592979000
1 2.319779000 -5.191880000 -2.695903000
1 1.424995000 -3.701951000 -3.086601000
```

Cartesian coordinates for complex 7Ca

```
26 -1.549875000 -3.654269000 -0.534615000
26 1.550095000 3.654674000 -0.534526000
15 -0.176815000 -1.173362000 -1.527783000
15 -0.210972000 -2.077494000 0.465148000
15 -2.269168000 -2.345752000 1.256932000
15 -3.488475000 -2.347068000 -0.574243000
15 -2.021444000 -2.155466000 -2.240431000
15 0.177499000 1.173421000 -1.527442000
15 0.211810000 2.077513000 0.465492000
15 2.021609000 2.156044000 -2.240535000
15 3.488958000 2.347806000 -0.574665000
15 2.270032000 2.346535000 1.256826000
7 -4.270710000 2.042013000 -0.933112000
7 -3.555399000 1.800898000 2.007810000
7 4.270102000 -2.042699000 -0.933075000
7 3.555292000 -1.801128000 2.007950000
6 -4.633961000 1.477095000 -2.189821000
6 -3.905370000 1.786487000 -3.364795000
```

6 -4.182865000 1.079326000 -4.547370000
1 -3.615638000 1.322481000 -5.449593000
6 -5.166230000 0.077490000 -4.600741000
6 -5.901931000 -0.188917000 -3.433139000
1 -6.685189000 -0.951152000 -3.454845000
6 -5.656456000 0.492689000 -2.230368000
6 -6.459915000 0.181946000 -0.985727000
1 -5.815864000 -0.195094000 -0.175416000
1 -7.222756000 -0.580998000 -1.194454000
1 -6.957034000 1.080960000 -0.589210000
6 -2.849886000 2.868677000 -3.342896000
1 -3.245269000 3.807329000 -2.925224000
1 -2.472236000 3.067108000 -4.356205000
1 -1.989178000 2.576648000 -2.718709000
6 -5.407380000 -0.711680000 -5.871116000
1 -5.195968000 -0.105497000 -6.764960000
1 -6.447703000 -1.065473000 -5.930282000
1 -4.753889000 -1.599650000 -5.914220000
6 -3.177909000 1.119871000 3.200458000
6 -2.037189000 1.489240000 3.957948000
6 -1.628572000 0.665559000 5.022728000
1 -0.744642000 0.954114000 5.593375000
6 -2.318028000 -0.505305000 5.369864000
6 -3.469261000 -0.834961000 4.632674000
1 -4.040856000 -1.727764000 4.898951000
6 -3.910422000 -0.047124000 3.559456000
6 -5.158012000 -0.428238000 2.790167000
1 -5.813059000 0.439567000 2.627102000
1 -5.719178000 -1.209227000 3.322868000
1 -4.913629000 -0.832026000 1.791691000
6 -1.828929000 -1.400882000 6.489786000
1 -1.211999000 -2.227941000 6.098192000
1 -2.669856000 -1.854018000 7.036744000
1 -1.211564000 -0.841487000 7.208491000
6 -1.261883000 2.758044000 3.672294000
1 -0.181888000 2.556012000 3.612948000
1 -1.415764000 3.499409000 4.475172000
1 -1.580409000 3.209862000 2.725822000
6 -5.905851000 3.834947000 -1.353365000
1 -6.278929000 4.755711000 -0.887059000
1 -6.765371000 3.188933000 -1.591424000
1 -5.425539000 4.079538000 -2.312439000
6 -4.935722000 3.090409000 -0.439781000
6 -4.844795000 3.547562000 0.900033000
1 -5.405365000 4.457370000 1.110057000
6 -4.294941000 2.911653000 2.044805000
6 -4.630007000 3.528976000 3.399688000
1 -5.111583000 2.776740000 4.043404000
1 -5.296896000 4.394659000 3.300427000
1 -3.712047000 3.842677000 3.918185000
6 3.177800000 -1.120083000 3.200579000
6 3.910304000 0.046956000 3.559480000
6 3.469109000 0.834912000 4.632600000
1 4.040707000 1.727731000 4.898822000
6 2.317873000 0.505319000 5.369806000
6 1.628434000 -0.665592000 5.022780000
1 0.744495000 -0.954081000 5.593446000
6 2.037059000 -1.489378000 3.958090000
6 5.157971000 0.427974000 2.790247000
1 5.719608000 1.208299000 3.323429000
1 4.913664000 0.832680000 1.792110000
1 5.812521000 -0.440056000 2.626470000
6 1.828732000 1.400996000 6.489630000
1 1.211830000 2.228025000 6.097936000
1 2.669635000 1.854169000 7.036594000
1 1.211323000 0.841665000 7.208348000
6 1.261660000 -2.758123000 3.672454000
1 1.580096000 -3.209930000 2.725953000
1 0.181674000 -2.556018000 3.613172000
1 1.415531000 -3.499522000 4.475308000
6 4.633709000 -1.477791000 -2.189702000
6 5.656413000 -0.493575000 -2.229928000
6 5.902242000 0.188151000 -3.432552000
1 6.685677000 0.950210000 -3.454030000
6 5.166656000 -0.077927000 -4.600311000
6 4.183102000 -1.079589000 -4.547261000
1 3.615969000 -1.322477000 -5.449613000
6 3.905285000 -1.786898000 -3.364842000
6 6.459537000 -0.183027000 -0.985016000
1 5.815799000 0.197561000 -0.176069000
1 7.224817000 0.577324000 -1.194318000
1 6.953517000 -1.082787000 -0.586367000
6 5.408165000 0.711411000 -5.870512000
1 5.196141000 0.105635000 -6.764484000
1 6.448739000 1.064456000 -5.929770000
1 4.755330000 1.599882000 -5.913238000
6 2.849615000 -2.868903000 -3.343259000
1 3.244985000 -3.807919000 -2.926370000
1 2.471532000 -3.066600000 -4.356550000
1 1.989266000 -2.577115000 -2.718497000
6 4.628748000 -3.530075000 3.399711000
1 5.109112000 -2.777783000 4.044251000
1 5.296455000 -4.395132000 3.300476000
1 3.710659000 -3.844963000 3.917280000
6 4.294153000 -2.912341000 2.044896000
6 4.843652000 -3.548464000 0.900076000
1 5.403812000 -4.458539000 1.110045000
6 4.934707000 -3.091353000 -0.439745000
6 5.904715000 -3.836167000 -1.353247000
1 5.424811000 -4.079736000 -2.312774000
1 6.276718000 -4.757534000 -0.887265000
1 6.764983000 -3.190769000 -1.590324000
6 0.789124000 5.168149000 -1.781592000
6 0.066798000 5.161236000 -0.541798000
6 1.009411000 5.387943000 0.526441000
6 2.320657000 5.521310000 -0.052933000
6 2.185039000 5.387913000 -1.484191000
6 0.189380000 5.021877000 -3.148772000
1 -0.166478000 5.997695000 -3.523049000
1 -0.663043000 4.333557000 -3.128440000
1 0.927395000 4.629699000 -3.860409000
6 -1.419537000 5.001753000 -0.392723000
1 -1.833683000 4.360863000 -1.180805000
1 -1.920613000 5.983068000 -0.459718000
1 -1.682966000 4.556253000 0.574714000
6 0.669228000 5.472518000 1.984652000
1 -0.146968000 4.782920000 2.231886000
1 0.346866000 6.492762000 2.255072000
1 1.535595000 5.209094000 2.605708000
6 3.592385000 5.776047000 0.702136000
1 4.458649000 5.395897000 0.144536000
1 3.570571000 5.267343000 1.675967000
1 3.740723000 6.854856000 0.879179000
6 3.284480000 5.491140000 -2.499459000
1 3.109335000 4.793349000 -3.330557000
1 4.255992000 5.246266000 -2.050454000
1 3.342495000 6.511371000 -2.915896000
6 -0.789360000 -5.167966000 -1.781624000
6 -0.066938000 -5.161252000 -0.541863000
6 -1.009542000 -5.387608000 0.526429000
6 -2.320872000 -5.520616000 -0.052854000
6 -2.185320000 -5.387305000 -1.484134000
1 0.662850000 -4.333501000 -3.128466000
6 -0.189687000 -5.021672000 -3.148835000
1 -0.927686000 -4.629243000 -3.860352000
1 0.165957000 -5.997502000 -3.523283000
1 1.683151000 -4.556425000 0.574287000
6 1.419465000 -5.002258000 -0.392925000
1 1.833830000 -4.361885000 -1.181310000
1 1.920135000 -5.983811000 -0.459490000
6 -0.669323000 -5.472261000 1.984626000
1 0.147545000 -4.783392000 2.231664000
1 -0.347895000 -6.492763000 2.255181000
1 -1.535396000 -5.207909000 2.605700000
6 -3.592576000 -5.774951000 0.702402000
1 -3.570623000 -5.265863000 1.676028000
1 -3.740997000 -6.853675000 0.879881000
1 -4.458850000 -5.394922000 0.144740000
1 -3.109657000 -4.792586000 -3.330441000
1 -3.343050000 -6.510574000 -2.915761000
6 -3.284848000 -5.490352000 -2.499330000
1 -4.256287000 -5.245314000 -2.050254000
20 2.611302000 -0.666706000 0.114943000
20 -2.610589000 0.667431000 0.114632000

Cartesian coordinates for complex 8Mg

26 1.742500000 3.405606000 -1.019225000
15 -0.143504000 0.973238000 -0.828122000
15 0.993946000 2.061054000 0.705009000
15 0.892351000 1.876899000 -2.535937000
15 3.033692000 1.756368000 -2.091868000
15 3.155864000 1.910097000 0.102184000
7 -3.115073000 2.139825000 1.616413000
7 -3.824074000 1.587491000 -1.392899000
6 -3.070437000 1.802926000 3.019611000
6 -4.411635000 0.829699000 -2.466045000
6 -2.203486000 2.444825000 3.953267000
6 -3.935522000 0.761126000 3.470092000
6 -3.829769000 3.686833000 -0.152231000
1 -4.102774000 4.734788000 -0.271454000
6 -5.021062000 0.208001000 2.555295000
1 -4.619555000 0.142868000 1.534494000
6 -3.775803000 0.686931000 -3.725818000
6 -1.267684000 3.601809000 3.609604000
1 -1.341163000 3.788379000 2.532837000
6 -4.047674000 2.909106000 -1.316455000
6 -5.666987000 0.201432000 -2.223426000
6 -3.618131000 3.315627000 1.205295000
6 -6.403286000 0.395611000 -0.901469000
1 -5.656303000 0.634436000 -0.135479000
6 -2.423398000 1.305775000 -4.061923000
1 -2.048263000 1.831880000 -3.172290000
6 0.208571000 3.290947000 3.953033000
1 0.327119000 3.143799000 5.037338000
1 0.842706000 4.144145000 3.664412000
1 0.578407000 2.400265000 3.440967000
6 -1.647593000 4.892721000 4.382299000
1 -2.709788000 5.149085000 4.301708000
1 -1.051913000 5.740975000 4.009684000
1 -1.416080000 4.767380000 5.451099000
6 -4.072960000 4.381947000 2.196281000
1 -4.196402000 3.979823000 3.206449000
1 -5.024947000 4.815074000 1.861815000
1 -3.333013000 5.193857000 2.236459000
6 -6.199373000 1.209177000 2.521451000
1 -6.598374000 1.348643000 3.538043000
1 -7.007167000 0.838892000 1.876176000
1 -5.874558000 2.185281000 2.137972000
6 -3.885012000 0.349503000 4.812455000
1 -4.543767000 -0.449239000 5.150481000
6 -2.218241000 2.016421000 5.295098000
1 -1.557557000 2.516603000 6.004257000
6 -5.652626000 -0.681251000 -4.502430000
1 -6.132889000 -1.261218000 -5.292102000
6 -4.419483000 -0.067762000 -4.726268000
1 -3.933007000 -0.170496000 -5.697015000
6 -4.585853000 3.668834000 -2.523367000

```
1 -5.085603000 4.597359000 -2.219948000
1 -5.282386000 3.054958000 -3.107198000
1 -3.744840000 3.930465000 -3.182445000
6 -5.510511000 -1.204494000 2.919094000
1 -4.664329000 -1.895640000 3.035532000
1 -6.159590000 -1.582870000 2.118826000
1 -6.091712000 -1.200547000 3.854478000
6 -7.353342000 1.611738000 -0.996553000
1 -6.794035000 2.528627000 -1.228218000
1 -7.884351000 1.763105000 -0.043894000
1 -8.099795000 1.450961000 -1.790276000
6 -1.410437000 0.205877000 -4.447434000
1 -1.237152000 -0.485864000 -3.614374000
1 -0.449613000 0.650845000 -4.736289000
1 -1.787037000 -0.382663000 -5.297611000
6 -6.266145000 -0.544964000 -3.252358000
1 -7.231050000 -1.019504000 -3.075800000
6 -3.030270000 0.969815000 5.729404000
1 -3.007706000 0.645873000 6.771039000
6 -7.167827000 -0.861567000 -0.442025000
1 -8.004171000 -1.097728000 -1.117225000
1 -7.596601000 -0.698650000 0.557060000
1 -6.496420000 -1.731249000 -0.397536000
6 -2.525917000 2.322977000 -5.222693000
1 -2.794772000 1.809070000 -6.158623000
1 -1.552189000 2.814251000 -5.374973000
1 -3.286171000 3.093905000 -5.036697000
6 2.272132000 5.199717000 -0.052977000
6 2.949262000 5.057339000 -1.320528000
6 1.942589000 4.979897000 -2.353671000
6 0.647746000 5.039135000 -1.717592000
6 0.858750000 5.191946000 -0.304279000
6 2.918010000 5.318442000 1.296940000
1 2.328275000 4.786813000 2.056854000
1 3.001733000 6.374066000 1.607757000
1 3.924862000 4.880933000 1.287186000
6 4.435761000 5.040325000 -1.530348000
1 4.944340000 4.591839000 -0.666057000
1 4.829397000 6.061742000 -1.670355000
1 4.693841000 4.446102000 -2.417292000
6 2.188096000 4.861781000 -3.828889000
1 3.149101000 4.367536000 -4.026362000
1 2.203463000 5.855473000 -4.308656000
1 1.397317000 4.265896000 -4.306544000
6 -0.691919000 5.017606000 -2.397867000
1 -0.646859000 4.450264000 -3.336524000
1 -1.025933000 6.044216000 -2.632300000
1 -1.451003000 4.553294000 -1.752251000
6 -0.223322000 5.373229000 0.717009000
1 -1.104308000 4.762456000 0.476026000
1 -0.541498000 6.430251000 0.751232000
1 0.133208000 5.093702000 1.714359000
15 0.140212000 -1.262240000 -0.420384000
15 -0.589236000 -2.752974000 -1.863354000
15 -1.370122000 -1.720196000 1.115932000
15 -3.330259000 -1.847583000 -0.013174000
15 -2.755594000 -2.518093000 -1.993625000
26 -1.816850000 -3.622225000 -0.103894000
7 3.834136000 -1.871664000 -1.008463000
7 3.147092000 -1.564246000 1.999241000
6 4.415104000 -1.464641000 -2.262395000
6 3.288643000 -0.914153000 3.277787000
6 3.843800000 -1.823509000 -3.512686000
6 5.586315000 -0.653809000 -2.227628000
6 3.615264000 -3.593575000 0.718653000
1 3.734379000 -4.667385000 0.851963000
6 6.220414000 -0.243552000 -0.904197000
1 5.409982000 -0.102561000 -0.173065000
6 2.203980000 -0.795042000 4.185694000
6 2.521987000 -2.566599000 -3.654178000
1 2.157939000 -2.838167000 -2.654175000
6 3.380758000 -2.887172000 1.925050000
6 4.565729000 -0.389864000 3.628709000
6 3.974677000 -3.136281000 -0.582362000
6 5.792929000 -0.576385000 2.741401000
1 5.459005000 -0.930388000 1.759181000
6 0.810788000 -1.353075000 3.917057000
1 0.825288000 -1.889610000 2.957778000
6 1.484168000 -1.630782000 -4.313971000
1 1.840569000 -1.308657000 -5.304421000
1 0.522265000 -2.144845000 -4.440024000
1 1.320108000 -0.730753000 -3.707892000
6 2.643336000 -3.858701000 -4.493952000
1 3.440116000 -4.521718000 -4.129244000
1 1.688115000 -4.405560000 -4.469777000
1 2.865802000 -3.617770000 -5.544921000
6 4.564760000 -4.207333000 -1.492115000
1 5.274598000 -3.781193000 -2.210868000
1 5.064542000 -4.986170000 -0.902313000
1 3.755390000 -4.681039000 -2.066446000
6 7.124795000 -1.384155000 -0.384631000
1 7.908220000 -1.607124000 -1.125649000
1 7.610190000 -1.100408000 0.559481000
1 6.540300000 -2.297964000 -0.209492000
6 6.192877000 -0.275192000 -3.437398000
1 7.095598000 0.333126000 -3.415292000
6 4.489347000 -1.419008000 -4.696877000
1 4.048167000 -1.703275000 -5.652996000
6 3.655037000 0.401933000 5.755529000
1 3.794115000 0.910313000 6.711078000
6 2.410049000 -0.123366000 5.406716000
1 1.570105000 -0.024500000 6.095528000
6 3.428266000 -3.704870000 3.208656000
1 3.698404000 -4.749404000 3.012009000
1 4.150252000 -3.271841000 3.914671000
1 2.447422000 -3.675895000 3.700766000
6 6.993300000 1.088098000 -0.989726000
1 6.376617000 1.866200000 -1.462652000
1 7.271688000 1.427210000 0.014631000
1 7.920950000 0.977928000 -1.572430000
6 6.720078000 -1.663558000 3.332831000
1 6.198703000 -2.627952000 3.412908000
1 7.605563000 -1.804209000 2.694073000
1 7.060815000 -1.372629000 4.338737000
6 -0.206489000 -0.198561000 3.837736000
1 -0.019651000 0.428943000 2.957192000
1 -1.236578000 -0.570693000 3.780802000
1 -0.129047000 0.435982000 4.728408000
6 4.724373000 0.256813000 4.867147000
1 5.706961000 0.641249000 5.142282000
6 5.660264000 -0.661455000 -4.671306000
1 6.147935000 -0.363046000 -5.600728000
6 6.567357000 0.741743000 2.538363000
1 6.907304000 1.162268000 3.496044000
1 7.462178000 0.561182000 1.927058000
1 5.939142000 1.490423000 2.034512000
6 0.359351000 -2.338133000 5.021163000
1 0.252986000 -1.815594000 5.983773000
1 -0.624494000 -2.759696000 4.763520000
1 1.068747000 -3.165781000 5.166405000
6 -2.061552000 -5.606230000 -0.726926000
6 -3.064698000 -5.228338000 0.241074000
6 -2.384422000 -4.859647000 1.461357000
6 -0.965816000 -4.985411000 1.230815000
6 -0.769339000 -5.452035000 -0.113505000
6 -2.307806000 -6.073912000 -2.131290000
1 -1.510796000 -5.721877000 -2.801650000
1 -2.332838000 -7.176297000 -2.182335000
1 -3.263053000 -5.687471000 -2.509895000
6 -4.549865000 -5.255796000 0.021188000
1 -4.789046000 -5.000742000 -1.020410000
1 -4.966879000 -6.254584000 0.236903000
1 -5.051668000 -4.524223000 0.668541000
6 -3.022583000 -4.416339000 2.745143000
1 -4.033353000 -4.028303000 2.563382000
1 -3.097257000 -5.248971000 3.465557000
1 -2.431464000 -3.615410000 3.213500000
6 0.131781000 -4.727992000 2.221143000
1 -0.197382000 -4.030680000 2.998869000
1 0.442951000 -5.667514000 2.711520000
1 1.011446000 -4.298555000 1.723689000
6 0.562042000 -5.758418000 -0.737505000
1 1.338544000 -5.080504000 -0.355629000
1 0.865520000 -6.794808000 -0.505836000
1 0.520311000 -5.649877000 -1.829130000
12 2.684587000 -0.680014000 0.207397000
12 -2.642910000 0.806312000 0.079603000
```

Chapter 5

From P_5 to P_7 : The way to highly substituted 1,3-bis(phosphanyl)-pentaphospholanide iron complexes from pentaphosphaferrocene

This chapter was written as a manuscript ready for submission (introduction and the two first sections). Additional results are appended in the form of a treasury as a additional section of this chapter. Conceptualisation, writing of the manuscript, preparation of compounds and analytic samples as well as evaluation of all analytic data was done by Martin Weber. DFT calculations were performed by Gábor Balázs. X-Ray diffraction measurements were performed and evaluated by Martin Weber and checked by Michael Seidl. Supervision, writing review, project administration and funding acquisition: Manfred Scheer

Abstract

Nucleophilic attack of carbon nucleophiles such as CH_3Li or ^tBuLi on pentaphosphaferrocene $[Cp^*Fe(\eta^5\text{-}P_5)]$ (**XXVII**) and consecutive quenching with R_2PCl in a one pot reaction yields new phosphorus rich compounds: for R = Cy = C_6H_{11} the 1,1-functionalized complex $[Cp^*Fe(\eta^4\text{-}(1\text{-}Me\text{-}1\text{-}PCy_2\text{-}P_5))]$ (**12**) and for R = Ph = C_6H_5 the 1,2-functionalized complex $[Cp^*Fe(\eta^{3:1}\text{-}(1\text{-}Me\text{-}2\text{-}PPh_2\text{-}P_5))]$ (**11**) are formed selectively. The formation of endo and exo isomers of **12** by thermal control of the reaction, as well as the reaction pathway to **11** are investigated more closely. A reactivity study on further functionalisation of complex **11** with ^tBuLi and Cy_2PCl is performed

in which the formation of the highly functionalized P_7 ligands in $[Cp^*Fe(\eta^{1:1:1}\text{-}(1\text{-}^t Bu\text{-}2\text{-}PPh_2\text{-}3\text{-}Me\text{-}4\text{-}PCy_2\text{-}P_5))]$ (**13**) and $[Cp^*Fe(\eta^{1:2}\text{-}(1\text{-}^t Bu\text{-}2\text{-}PCy_2\text{-}3\text{-}Me\text{-}4\text{-}PPh_2\text{-}P_5))]$ (**14**) is observed. Optimized reaction conditions and the use of $^t Bu_2PCl$ provide a pathway to the 1,3-bis(phosphanyl)pentaphospholanide iron complex $[Cp^*Fe(\eta^{1:2}\text{-}(1\text{-}^t Bu\text{-}2\text{-}P^t Bu_2\text{-}3\text{-}Me\text{-}4\text{-}PPh_2\text{-}P_5))]$ (**15**).

5.1 Introduction

The industrial processes to convert white phosphorus to desirable organophosphines and phosphites so far includes large amounts of hazardous chemicals such as chlorine gas and yield stoichiometric amounts of waste products. Therefore more sustainable and environmentally friendly synthetic methods are in the focus of research in modern inorganic chemistry.[23–28] In the recent past, this was achieved by using either main group element reactants such as the tin compounds $(Bu_3Sn)_2$ and Bu_3SnH, diarsonium compounds such as $[Ph_3As-AsPh_3][OTf]_2$ or reactive transition metal complexes and their fragments such as $Ti(N[^t Bu]Ar)_3$ $(Ar = 3,5\text{-}C_6H_3Me_2)$.[29,32,33,37] While these approaches have proven to yield symmetrically substituted phosphines, these reactions still partially involve highly reactive and toxic chemicals and produce aforementioned waste products.[29–32,34–40] Decades of research show that by activating the P_4 tetrahedron with reactive transition metal complex fragments and functionalizing the resulting P_n ligand complexes by nucleophilic or electrophilic attack, complex functionalized phosphorus frameworks are formed.[51,58,59,69,77,167,173,198,216] Utilizing the rather well explored and versatile chemistry of this class of compounds, P_n ligand complex mediated conversion of white phosphorus can be a promising alternative to the direct conversion.

Recently our group investigated the functionalisation of the *cyclo*-P_5 ligand in $[Cp^*Fe(\eta^5\text{-}P_5)]$ (**XXVII**, $Cp^* = C_5(CH_3)_5$) to form asymmetrically substituted organophosphines in a cyclic reaction pathway.[76] After attack of a charged carbon nucleophile, the *in situ* generated anionic complex $[Cp^*Fe(\eta^4\text{-}P_5R)]^-$ is quenched with alkyl halogenides $R'X$ to form $[Cp^*Fe(\eta^4\text{-}P_5RR')]$. In some cases 1,2-functionalization of the *cyclo*-P_5 ligand is observed as a side reaction in the NMR spectra of the respective reaction solutions. The 1,1-functionalized P-atom in the complexes $[Cp^*Fe(\eta^4\text{-}P_5RR')]$ can be displaced by attack of a strong nucleophile like benzyl potassium to yield the phosphine (Figure 5.1). The envelope conformation of a *cyclo*-P_n ligand with a disubstituted phosphorus atom bent out of plane as in $[Cp^*Fe(\eta^4\text{-}P_5RR')]$, is also formed by ring expansion as observed for the attack and insertion of *in situ* generated phosphe-

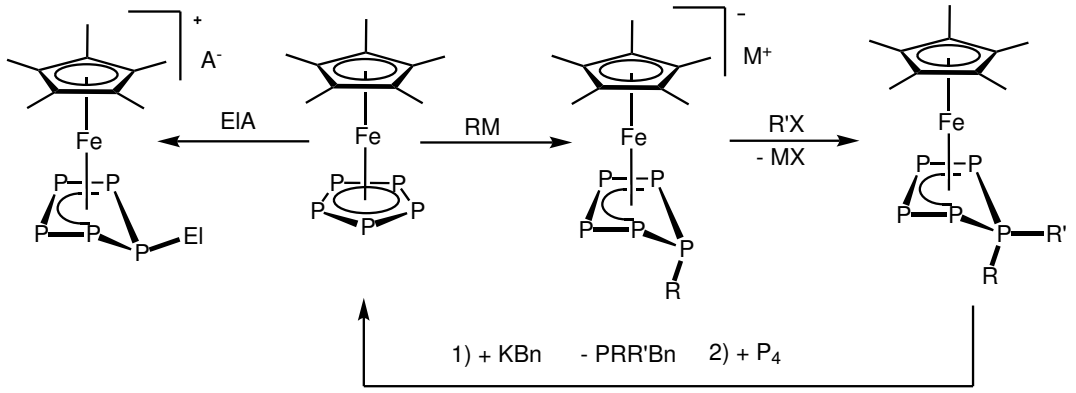


Figure 5.1: General depiction of a nucleophilic attack on **XXVII** with consecutive quenching by an electrophile (right) and attack of an electrophile (left). The 1,1 functionalized compound is utilized to synthesize asymmetrically substituted phosphines, while **XXVII** is regenerated from the reaction mixture by reaction with more white phosphorus (Bn = CH_2Ph = CH_2-C_6H_5).

nium ions in P_n ligand complexes with a tetraphospha[1.1.0]-bicyclobutane- or *cyclo*-P_3 moiety (in the latter case forming a *cyclo*-P_4 envelope).[107,149]

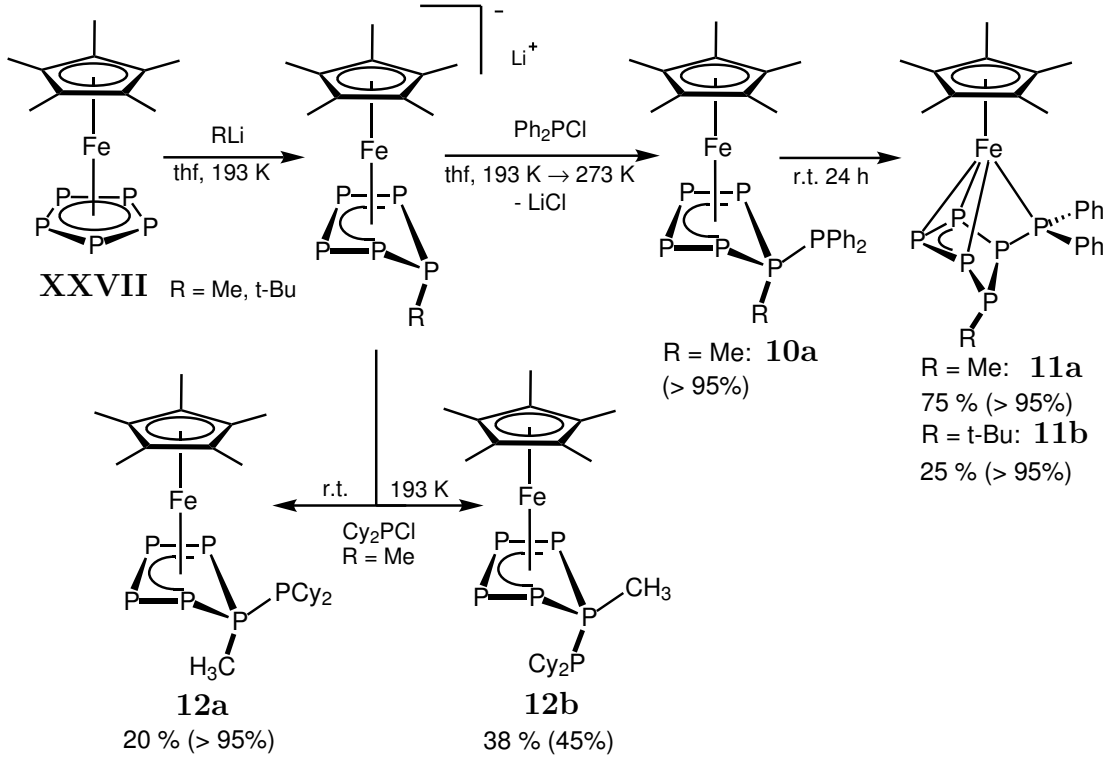
Along with the success of this synthetic pathway to asymmetrically substituted phosphines, new challenges arose. For one, the functionalisation of **XXVII** with dihydrogenphosphides such as $NaPH_2$ as nucleophlies or *in situ* generated phosphenium ions $[R_2P]^+$ as electrophiles has proven to be challenging or not synthetically feasible.[77,78] Furthermore the question arises if more than one of the phosphorus atoms in **XXVII** can be funtionalized in a controlled manner. The number of different P-atoms that can be functionalized in **XXVII** and the characteristics of the resulting, highly functionalized products have not yet been determined.

In order to overcome these challenges and expand our knowledge on the reaction behaviour of functionalized derivatives of **XXVII**, quenching the known anionic complexes $[Cp^*Fe(\eta^4\text{-}P_5R)]^-$ with chlorophosphines R_2PCl is tested as a feasible way for the functionalisation and expansion of the *cyclo*-P_5 ligand. Herein the synthesis of the novel phosphorus-rich compounds $[Cp^*Fe(\eta^{3:1}\text{-}(1\text{-R-}2\text{-}PR'_2\text{-}P_5))]$ as well as endo- and exo- substituted products $[Cp^*Fe(\eta^4\text{-}1,1\text{-R},PR'_2\text{-}P_5)]$ is reported. Furthermore it is shown that the same kind of one pot reaction on two selected complexes of the type $[Cp^*Fe(\eta^{3:1}\text{-}(1\text{-R-}2\text{-}PR'_2\text{-}P_5))]$ is forming the highly functionalized P_7 moieties in $[Cp^*Fe(\eta^{1:1:1}\text{-}(1\text{-R-}2\text{-}PR'_2\text{-}3\text{-R}''\text{-}4\text{-}PR''_2\text{-}P_5))]$ and $[Cp^*Fe(\eta^{2:1}\text{-}(1\text{-R-}2\text{-}PR'_2\text{-}3\text{-R}''\text{-}4\text{-}PR'''_2\text{-}P_5))]$.

5.2 Results and Discussion

5.2.1 Quenching $[Cp^*Fe(\eta^4\text{-}P_5R)]^-$ with chlorophosphines

Upon addition of the organolithium compounds CH_3Li or ^tBuLi to a solution of $[Cp^*Fe(\eta^5\text{-}P_5)]$ (**XXVII**) in thf (tetrahydrofurane) at - 80 °C the exclusive formation of exo-$Li[Cp^*Fe(\eta^4\text{-}P_5R)]$ ($R = CH_3,\ ^tBu$; exo relative to the Cp^*Fe fragment) is observed in the $^{31}P\{^1H\}$ NMR spectra of the reaction solutions at - 80 °C, as formerly reported.[77] To these anionic complexes $Li[Cp^*Fe(\eta^4\text{-}P_5R)]$ ($R = Me,^t Bu$) the chlorophosphines Ph_2PCl and Cy_2PCl are added (at -80 °C or at room temperature, depending on the desired product, *vide infra* scheme 5.1).



Scheme 5.1: *In situ* generation of $Li[Cp^*Fe(\eta^4\text{-}P_5R)]$ ($R = Me,\ ^tBu$) and quenching with R'_2PCl ($R' = Ph,\ Cy$). The displayed yield corresponds to the isolated crystalline yield referred to **XXVII**. The yields according to ^{31}P NMR spectroscopy of the reaction mixtures are displayed in brackets.

The ^{31}P NMR spectra of the reaction solution of $[Cp^*Fe(\eta^4\text{-}P_5Me)]^-$ with Ph_2PCl show a clean reaction to $[Cp^*Fe(\eta^{3:1}\text{-}(1\text{-}CH_3\text{-}2\text{-}PPh_2\text{-}P_5))]$ (**11a**) with six chemically inequivalent phosphorus atoms, visible as a complex ALMQXY spin system (*vide infra* Figure 5.2). When using ^tBuLi instead of MeLi in the same reaction set-up, the isostructural tert-butyl substituted complex $[Cp^*Fe(\eta^{3:1}\text{-}(1\text{-}^tBu\text{-}2\text{-}PPh_2\text{-}P_5))]$ (**11b**) is obtained and characterized in the same way as **11a** (Scheme 5.1).

A slight colour change is observed upon warming reaction solutions of $Li[Cp^*Fe(\eta^4\text{-}P_5Me)]$ and Ph_2PCl to room temperature, indicating the formation of a different product at low temperatures. In order to isolate the product, the reaction work-up is performed at -30 °C. The complex endo-$[Cp^*Fe(\eta^4\text{-}1,1\text{-}CH_3,PPh_2\text{-}P_5)]$ (**10a**; endo-PPh_2 relative to Cp^*Fe) is isolated in the form of dark green crystals by removing dichloromethane from a concentrated solution of the raw reaction product in hexane and dichloromethane at -30 °C. X-ray diffraction analysis shows a 1,1-substitution pattern in **10a** (Figure 5.5, *vide infra*).

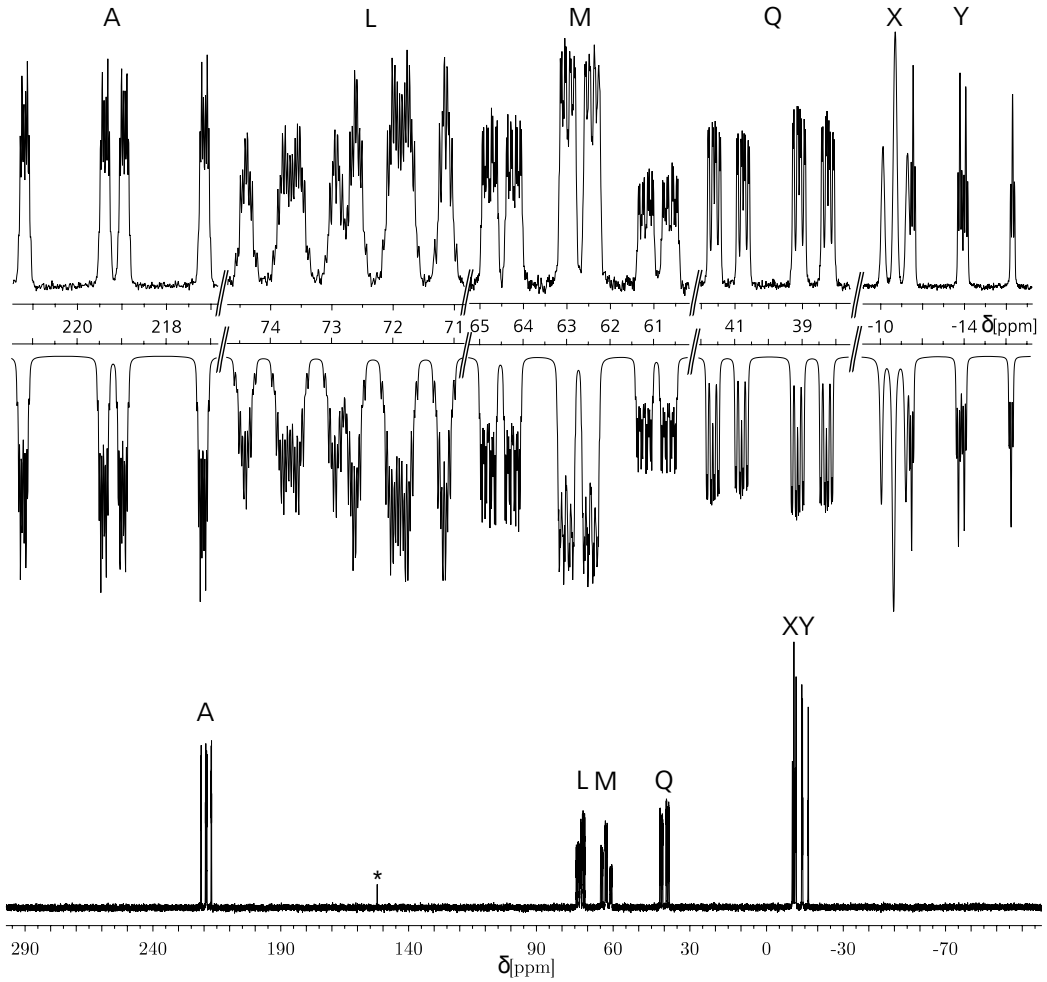


Figure 5.2: ^{31}P NMR spectrum (bottom) of **11a** in CD_2Cl_2 at room temperature and enlarged depiction of the spin system (top) with a simulation of the iteratively fitted ALMQXY spin system (inverted). Traces of residual **XXVII** are marked with an asterisk. The complex coupling pattern of spin L is explained by a well resolved coupling to the methyl group ($^2J_{P_LH} = 6$ Hz).

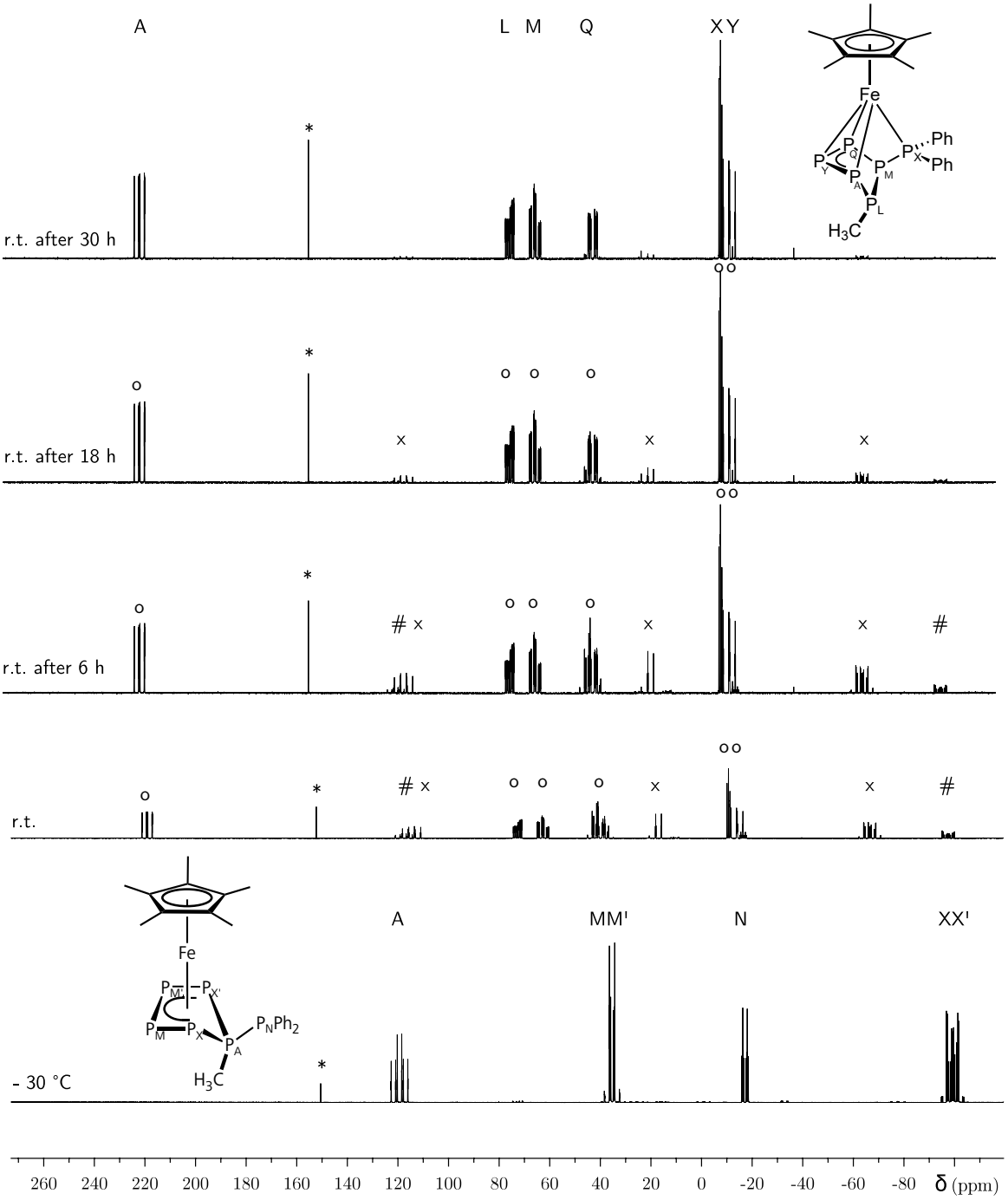


Figure 5.3: ^{31}P $\{^1H\}$ NMR spectra of **10a** in CD_2Cl_2 at different temperatures and times. Traces of **XXVII** are marked with an asterisk. Distinguishable signals of endo-**10a** are marked with #, of the exo isomer with x, while signals of **11a** are marked with o in the spectra at room temperature. The other signals of these isomers are superimposed with the signals of **11a**, which after 30 hours remains the only product in solution with the exception of minute traces of exo-**10a**.

By changing the substituents on the chlorophosphine R'_2PCl (R' = Cy, ^tBu, Me, NEt_2, Mes), 1,2-migration alongside 1,1-substituted products in complex mixtures in the $^{31}P\{^1H\}$ NMR spectra of the reaction solutions are observed (*vide infra*, Section 5.2.3). The products of these reactions are not stable enough for chromatographic work-up and fractional crystallisation is only an option in the case of **12a** and **12b** (R' = Cy), since co crystallisation makes isolation of one specific product impossible for the other cases. Interestingly, the 1,2-migration is not visible in the $^{31}P\{^1H\}$ NMR spectra of the reaction solution of $Li[Cp^*Fe(\eta^4\text{-}P_5Me)]$ and Cy_2PCl. Instead, two AMM'NXX' spin systems are assigned to the endo and exo isomer of the C_S symmetric polyphosphorus ligands in the products **12a** and **12b** as shown in scheme 5.1. If Cy_2PCl is added to a freshly prepared solution of $Li[Cp^*Fe(\eta^4\text{-}P_5CH_3)]$ in thf at - 80 °C the exo isomer **12b** is observed in a 9:11 mixture with the endo isomer (**12b**:**12a**). If on the other hand Cy_2PCl is added at room temperature, the endo isomer **12a** is observed as the exclusive product in $^{31}P\{^1H\}$ NMR spectra of the reaction solution. Both isomers are isolated as pure compounds from the respective reaction solution by fractionated crystallisation from either pure *n*-hexane (**12a**) or a *n*-hexane/CH_2Cl_2 mixture (**12b**). Heating solutions of **12a** to 60 °C for more than one hour does not result in conversion to the exo isomer, but $^{31}P\{^1H\}$ NMR spectra only show decomposition of **12a**. Only when storing a NMR sample of **12a** in CD_2Cl_2 for 15 days at room temperature, conversion of **12a** into the exo isomer **12b** is observed (Supporting information, Figure 5.42, approximately 1:1 ratio endo:exo, but signals of **12b** are strongly broadened).

Due to the characteristic difference in the spin systems of **11a** and **11b** or **10a** and **12**, migration of the phosphine fragment is easily identified by $^{31}P\{^1H\}$ NMR spectroscopy. Variable temperature NMR studies on crystals of **10a** dissolved in CD_2Cl_2 at -30 °C show, that **10a** quantitatively converts via a 1,2-migration to **11a** over the period of 30 hours (Figure 5.3). The AMM'NXX' spin system of the C_S symmetric ligand in **10a** slowly disappears, while the signals of the ALMQXY system of **11a** are appearing. There are also traces of another AMM'NXX' system visible, which are assigned to the exo isomer of **10a** since similar results were observed for the quenching products of Cy_2PCl (*vide supra*). After 18 hours at room temperature the endo product is no longer detected by ^{31}P NMR spectroscopy, while the exo isomer has only fully converted after 30 hours. To examine the impact of the steric demand of the used Cp^R ligand in derivatives of **XXVII** on the 1,2-migration of the diphenylphosphine fragment, a NMR study using *in situ* prepared $Li[Cp''Fe(\eta^4\text{-}P_5CH_3)]$ $(Cp'' = C_5H_3\text{-}1,3\text{-}(C(CH_3)_3)_2)$ and $Li[Cp^{BIG}Fe(\eta^4\text{-}P_5CH_3)](Cp^{BIG} = C_5(C_6H_4(C_4H_9))_5)$ as starting materials was performed (cf. Supporting Information, Figure 5.43). In the case of the Cp'' ligand derivative, an ALMQXY spin system is observed in the $^{31}P\{^1H\}$ NMR spectrum of the reac-

tion solution. This indicates a 1,2-migration and the formation of the same asymmetric P_6 moiety as observed in **11a**. For the Cp^{BIG} substituted pentaphosphaferrocene, no 1,2-migration, but two AMM'NXX' spin systems for the respective endo- and exo-1,1-substituted products are observed. This is analogue to reaction solutions of **12**, if the chlorophosphine is added at - 80 °C and shows that the 1,2-migration is hindered by extremely sterically demanding Cp^R ligands like Cp^{BIG}.

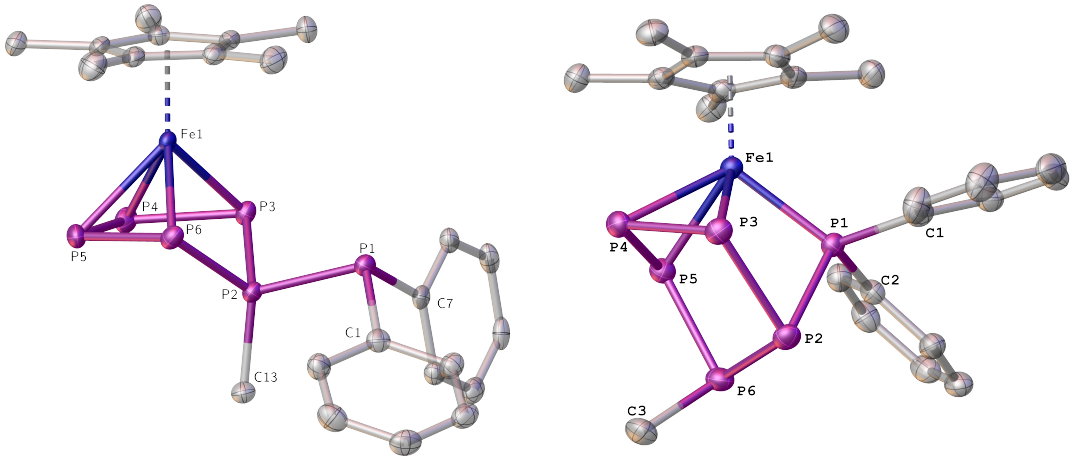


Figure 5.4: Molecular structures of **10a** (left) and **11a** (right) in the solid state. Hydrogen atoms are omitted for clarity. Selected bond lengths of **10a**: Fe1-P3 2.3178(7), Fe1-P6 2.3080(7), Fe1-P4 2.3318(7), Fe1-P5 2.3390(7), P2-P3 2.1433(8), P2-P1 2.2093(9), P2-P6 2.1535(8), P2-C13 1.821(3), P3-P4 2.1484(8), P1-C7 1.835(2), P1-C1 1.833(2), P6-P5 2.1540(9), P4-P5 2.1519(10). Selected bond lengths of **11a**: Fe1-P1 2.1988(7), Fe1-P4 2.3544(7), Fe1-P5 2.3382(7), Fe1-P3 2.3724(7), P1-P2 2.1965(9), P1-C1 1.841(3), P1-C2 1.833(3), P4-P5 2.1359(9), P4-P3 2.1207(9), P2-P6 2.1868(10), P2-P3 2.2828(9), P5-P6 2.2090(9), P6-C3 1.845(3).

Crystals of products **10**, **11** and **12** are obtained by storing a saturated solutions of the respective complex at -30 °C for 24 hours (for details see the Supporting Information). X-ray diffraction analysis confirms the asymmetric nature of the phosphorus ligand in $[Cp^*Fe(\eta^{3:1}\text{-}(1\text{-}CH_3\text{-}2\text{-}PPh_2\text{-}P_5))]$ (**11a**; *vide infra* Figure 5.4). The structural motif in **11** has not been reported yet. Due to the migration of the diphenylphosphine fragment from P6 to P2 (numbering according to the solid state structure of **11a**, figure 5.4), the latter atom is shifted significantly further away from the iron atom, which is instead coordinated by the diphenylphosphine fragment of P1. By comparison the Fe-P6 distance in **11a** (3.66446(5) Å) is 0.6 Å longer than the Fe-P2 distance in **10a** (3.06572(18) Å). Also the Fe-P2 distance in **11a** (3.36656(5) Å) is marginally larger than in **10a**. In the solid state structure of **11a** P3, P4 and P5 remain in a η^3 coordination mode. The tilt angle towards the mean plane of the Cp^* ligand is larger for the mean plane of P3, P4 and

P5 in **11a** (17.8 °) than it is for the mean plane of P3, P4, P5 and P6 in **10a** (4.3 °) The normals of the mean planes of the functionalized *cyclo*-P_5 ring P2, P3, P4, P5 and Cp^* ring in **11a** are tilted to each other by 46.6 °. Compared to **11a** no significant change of bond lengths or angles occur in the tert-butyl derivative **11b**. With increasing number of functionalized phosphorus atoms, the distance of the centroid of the *cyclo*-P_5 ring to the central iron atom increases (1.75 Å for **10a** and 2.23 Å for **11a**). Additionally one of the phenyl groups in **11a** and **11b** is in such close proximity to one of the methyl groups of the Cp^* ligand, that a CH-π interaction is feasible. The distances of the interaction for **11a** (atom-centroid 3.856 Å and atom-bond 3.458 Å) are slightly larger in comparison to the ones in **11b** (atom-centroid 3.651 Å and atom-bond 3.415 Å). The distances for both compounds are in the range of literature known CH-π interactions and are the first examples of this interaction being observed in a P_n ligand complex.[270–273] The structural motifs in **10a** and **12** are essentially similar to the known 1,1-substituted pentaphosphaferrocenes with two organic substituents and both solid state structures show similar bond lengths and angles.[76,77]

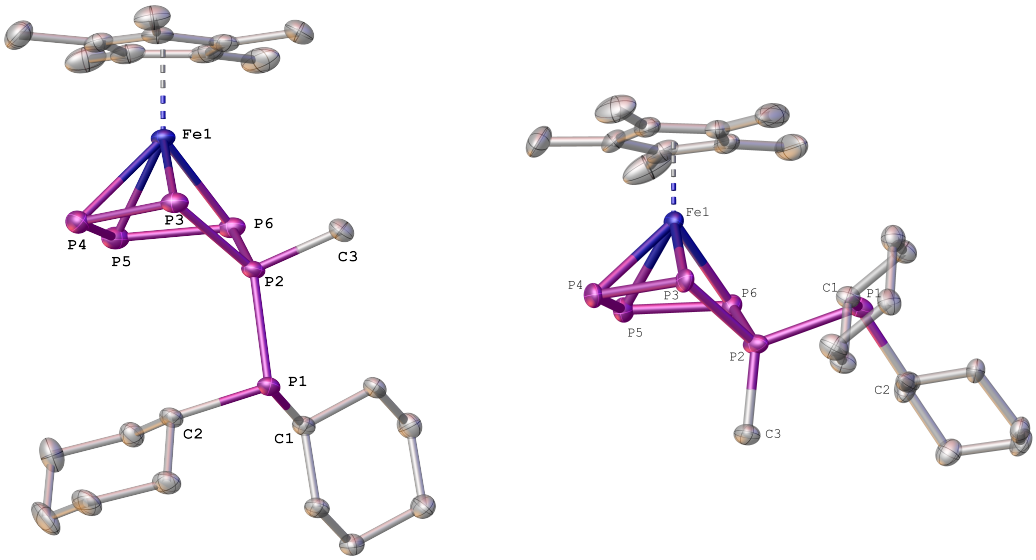
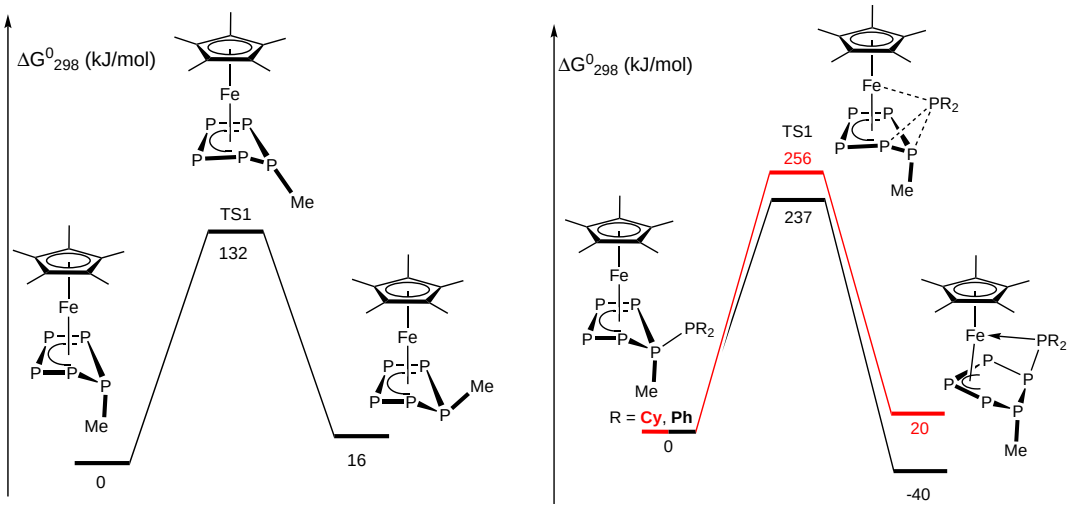


Figure 5.5: Molecular structures of **12b** (left) and **12a** (right) in the solid state. Hydrogen atoms are omitted for clarity. Selected bond lengths of **12a**: Fe1-P6 2.3175(5), Fe1-P3 2.257(4), Fe1-P5 2.369(4), Fe1-P4 2.330(3), P2-P1 2.2076(6), P2-P6 2.1466(6), P2-P3 2.186(4), P2-C3 1.8278(18), P1-C2 1.8649(19), P1-C1 1.883(3), P6-P5 2.157(4), P3-P4 2.136(3), P5-P4 2.141(4). Selected bond lengths of **12b**: Fe1-P6 2.3171(6), Fe1-P3 2.3177(7), Fe1-P4 2.3502(6), Fe1-P5 2.3379(6), P2-P1 2.2271(7), P2-P6 2.1610(8), P2-P3 2.1619(7), P2-C3 1.833(2), P1-C2 1.871(2), P1-C1 1.869(2), P6-P5 2.1389(8), P3-P4 2.1383(9), P4-P5 2.1495(9).

The formation of **12b** and the exo isomers in reactions starting from $Li[Cp^{BIG}Fe(\eta^4\text{-}P_5CH_3)]$ are unexpected and represent a first example of a functionalized derivative of **XXVII** with the nucleophile in endo position relative to Cp^RFe. Also neither a shift nor a second spin system is observed in the VT NMR studies of freshly prepared $Li[Cp^*Fe(\eta^4\text{-}P_5CH_3)]$ upon warming from -80 °C to room temperature. Nevertheless the dynamic process can be too fast to be resolved on the NMR time scale and inversion of phosphines is known to occur upon P-C bond formation.[274]



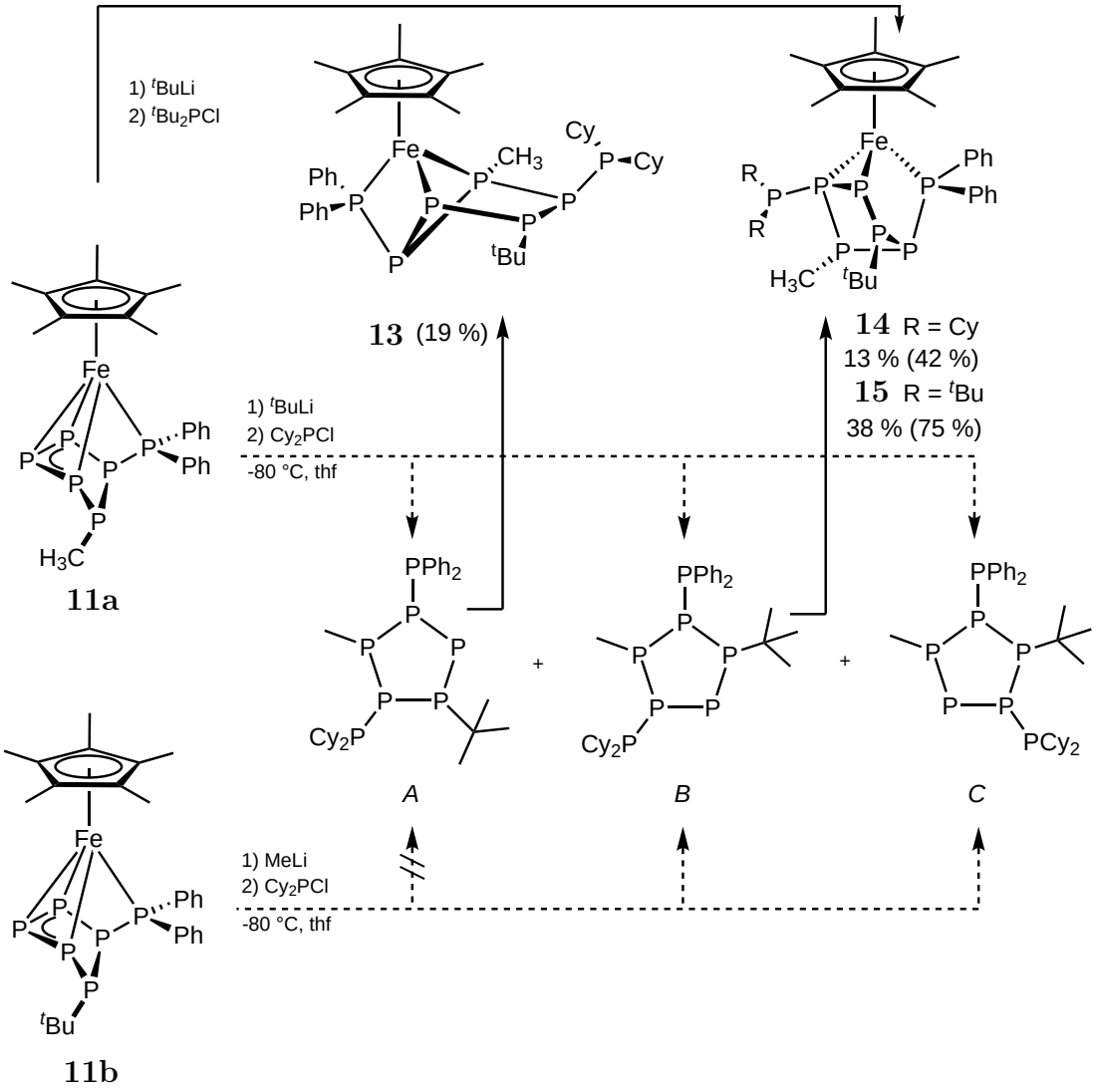
Scheme 5.2: Calculated energy profiles for the transition of the exo into the endo isomer of $Li[Cp^*Fe(\eta^4\text{-}P_5CH_3)]$ and the 1,2-migration of the phosphine fragments in **10a** (black) and **12a** (red, ωB97-XD4/def2-TZVPPD CPM(THF) level of theory, ΔG^0_{298} is the change of the Gibb's free energy relative to the respective starting material).

DFT calculations on $[Cp^*Fe(\eta^4\text{-}P_5CH_3)]^-$ show an energy barrier of 132 $kJ\,mol^{-1}$ for the transition state necessary to convert the exo into the endo isomer (scheme 5.2), which is thermodynamically slightly less favourable. According to NMR studies only tiny traces of exo-CH_3 substituted product are observed for reactions utilizing Ph_2PCl as an electrophile. Also the exo-isomer **12b** can only slowly be converted to the endo-isomer **12a** by storing solutions of the isolated products over a prolonged period of time (Supporting Information, Figure 5.42). This and the fact that no 1,2-migration is observed for **12** is explained by the energies of the transition state and product of the 1,2-migration as calculated on the ωB97-XD4/def2-TZVPPD CPM(THF) level of theory (Figure 5.2): Both the transition state as well as the 1,2-migration product are higher in energy for the cyclohexyl derivative **12** than for the phenyl substituted **10a**. While the 1,2-shift in **10a** to **11a** is thermodynamically favourable, the formation of the 1,2-shift product is endergonic for the cyclohexyl derivative. The relative energies of

the exo and endo isomers only differ by 6 or 10 $\mathrm{kJ\,mol^{-1}}$, depending on the orientation of the cyclohexyl groups in the exo isomer (Supporting Information, Section 5.4.5).
The initial goal of finding a synthetic pathway towards complexes with a higher phosphorus content by the functionalisation of the *cyclo*-$\mathrm{P_5}$ ligand in **XXVII** is achieved. Due to the new, asymmetric substituted structural motif in **11a** and **11b** and the comparatively good yields (75 %) paired with an easy synthetic pathway, the subsequent reactivity of these compounds is further explored in more detail .

5.2.2 Reactivity of $[\mathbf{Cp^*Fe(\eta^{3:1}\text{-}(1\text{-}R\text{-}2\text{-}PPh_2\text{-}P_5))}]$ ($\mathbf{R = Me}$, $^t\mathbf{Bu}$) towards charged nucleophiles and quenching with chlorophosphines

For the further exploration of the reactivity of **11a** a second nucleophilic attack and quenching with chlorophosphines, analogue to the first performed one pot reaction is investigated. When to a solution of **11a** in thf at - 80 °C, $^t\mathrm{BuLi}$ is slowly added, a dark brown reaction mixture is formed. $^{31}\mathrm{P}\{^1\mathrm{H}\}$ NMR spectra of the reaction solution at room temperature show two complex spin systems of which one can be assigned to the anionic complex $\mathrm{Li[Cp^*Fe(1\text{-}CH_3\text{-}PPh_2\text{-}4\text{-}}{}^t\mathrm{Bu})]$ (*vide infra*). These anionic reaction products cannot be isolated due to their high sensitivity and bad crystallisation behaviour.[275] Changing reaction conditions like solvent (thf mixtures with diethylether), temperature and the nucleophile (MeLi, PhLi, $^t\mathrm{BuLi}$, $^t\mathrm{BuMgCl}$, MeMgBr, $(\mathrm{CH_3})_3\mathrm{SiCH_2Li}$) do not improve the selectivity of the nucleophilic attack on **11a**. Therefore quenching experiments are proceeded after $^t\mathrm{BuLi}$ was added at - 80 °C, since this nucleophile shows the highest selectivity. Upon quenching with $\mathrm{Cy_2PCl}$ (standard solution in toluene) at -80 °C, an intense red solution is obtained. $^{31}\mathrm{P}$ NMR spectra of the reaction solution show the formation of one minor and two major products. The two major products $[\mathrm{Cp^*Fe}(\eta^{1:1:1}\text{-}(1\text{-}{}^t\mathrm{Bu}\text{-}2\text{-}\mathrm{PPh_2}\text{-}3\text{-}\mathrm{Me}\text{-}4\text{-}\mathrm{PCy_2}\text{-}\mathrm{P_5}))]$ (**13**) and $[\mathrm{Cp^*Fe}(\eta^{1:2}\text{-}(1\text{-}{}^t\mathrm{Bu}\text{-}2\text{-}\mathrm{PCy_2}\text{-}3\text{-}\mathrm{Me}\text{-}4\text{-}\mathrm{PPh_2}\text{-}\mathrm{P_5}))]$ (**14**) are crystallized from a saturated *n*-pentane solution at - 30 °C (Figure 5.6). Unfortunately both products co crystallize and cannot be separated chromatographically due to their high sensitivity. Thus, the only way to analyse at least **13** as a pure compound is by manual separation of the crystals under a microscope in a glove box (**13** crystallizes as intense red prisms, while **14** crystallizes as fine needles).
Under the assumption, that steric effects could lead to a more selective nucleophilic attack in the first reaction step, the starting material **11a** is changed for the tert-butyl substituted derivative **11b** (Scheme 5.3). The goal of a higher selectivity is yet not



Scheme 5.3: Nucleophilic attack on **11a** (with MeLi) and **11b** (with ^{t}BuLi). The connectivity of the resulting phosphorus ligands are drawn in a simplified way for easier understanding, with the dotted line indicating the reaction to the three substitution patterns observed in ^{31}P NMR spectra of the reaction solutions and the proper representation of the reaction products **13** and **14** with full lines. The displayed yield corresponds to the isolated crystalline yield referred to **11a**. Yields according to ^{31}P NMR spectra are displayed in brackets.

achieved by this method, but surprisingly by using MeLi as a nucleophile in the reaction with **11b** and then quenching with Cy_2PCl, the obtained reaction solutions show the same $^{31}P\{^{1}H\}$ NMR spectra as the reaction of **11a**, except for the signals attributed to **13**, being absent. Compound **13** cannot be synthesized directly by this reaction pathway, since the ^{t}Bu and PPh_2 groups have to be bound in 1,2-position to the *cyclo*-P_5 ligand in the starting material **11b** (substitution pattern *A* in Scheme 5.3). This is not the case for the connectivity of the phosphorus framework in **13** (1,3 for ^{t}Bu and

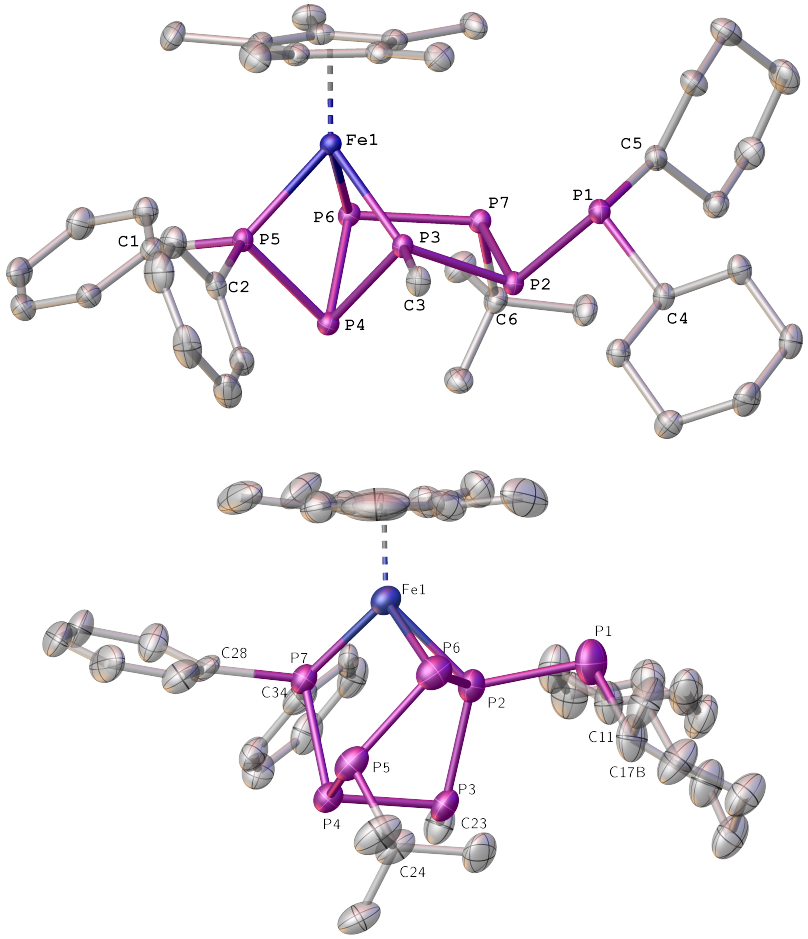


Figure 5.6: Molecular structures of **13** (top) and **14** (bottom) in the solid state. Hydrogen atoms are omitted for clarity. Selected bond lengths of **13**: Fe1-P5 2.2116(4), Fe1-P3 2.1943(4), Fe1-P6 2.3141(4), P5-P4 2.2113(5), P5-C1 1.8390(16), P5-C2 1.8421(16), P2-P3 2.2217(5), P2-P7 2.1984(5), P2-P1 2.2337(5), P3-P4 2.2222(5), P3-C3 1.8393(16), P7-P6 2.2418(5), P7-C6 1.9008(16), P4-P6 2.2689(5), P1-C4 1.8719(16), P1-C5 1.8689(16). Selected bond lengths of **14**: Fe1-P7 2.166(4), Fe1-P2 2.203(4), Fe1-P6 2.307(4), P7-P4 2.262(5), P7-C34 1.857(12), P7-C28 1.836(13), P3-P4 2.193(5), P3-P2 2.232(5), P3-C23 1.873(12), P4-P5 2.193(4), P5-P6 2.221(6), P5-C24 1.908(14), P2-P6 2.163(5), P2-P1 2.208(6), P1-C11 1.881(14), P1-C17A 1.87(2), P1-C17B 1.88(3).

PPh_2, substitution pattern *B*, Scheme 5.3). Under the assumption, that there is no shift of a substituent occurring during the reaction, this leaves only one possibility for the connectivity of the so far uncharacterised reaction product observed in the ^{31}P NMR spectra of the reaction solution: with the PCy_2 fragment next to the ^{t}Bu group instead of the methyl group, as depicted in substitution pattern *C* on the right side in scheme 5.3 (*vide supra*).

Although for **13** and **14** it is not possible to get larger quantities of a clean product, it was possible to isolate the ditertbutylphosphine substituted derivative of **14**, $[Cp^*Fe(\eta^{1:1:1}\text{-}(1\text{-t-Bu-2-P}^t\text{Bu}_2\text{-3-Me-4-PPh}_2\text{-P}_5))]$ (**15**). The $^{31}P\{^1H\}$ NMR spectra of the reaction solution are comparable to the ones obtained from quenching with Cy_2PCl in their complexity and the presence of more than one product. Yet, **15** is the main product of the reaction and is isolated as dark red crystals by slowly removing the diethylehter from a concentrated solution of **15** in a mixture of acetonitrile and diethylether without co crystallisation of any side products. X-ray diffraction experiments show the same structural motif as in **14** (cf. Supporting Information, Figure 5.75 on page 240). The minor reaction product visible in the $^{31}P\{^1H\}$ NMR spectra of the reaction solution bearing an unknown substitution pattern could not be isolated so far.
The multiplets in the $^{31}P\{^1H\}$ NMR spectra of **15** are well separated compared to the the signals of **13** and **14**. Therefore iterative fitting and simulation of the ADHMQVX spin system resulting from the seven chemically inequivalent phosphorus atoms is possible (Figure 5.7). For **13** and **14** only two to four isolated multiplets of each compound can be observed. The other signals (of one compound) superimpose each other and the strongly superimposed spin systems cannot be interpreted in an analytically doubtless way. Therefore iterative fitting and simulation of the spin system is not sufficiently powerful in order to predict the connectivity of the formed phosphorus moieties by $^{31}P\{^1H\}$ NMR spectroscopy. Due to the mentioned difficulties in separation of the product mixture (*vide supra*) the only way to measure a $^{31}P\{^1H\}$ NMR spectrum of one of the products (**13**) is manual crystal picking. Even with a pure sample, the spin system of **13** cannot be properly analysed due to the superimposed and complex multiplets. Regarding the $^{31}P\{^1H\}$ NMR spectra of reaction solutions of the nucleophilic attack of ^{t}BuLi on **11a**, only the ADMQVX spin system of the major product $Li[Cp^*Fe(1\text{-}CH_3\text{-2-}PPh_2\text{-4-}^t\text{Bu})]$ is resolved well enough for iterative fitting of the spin system and simulation thereof. From this simulation the connectivity of the ^{t}Bu group is determined by the characteristic $^3J_{PH}$ coupling in the ^{31}P NMR spectrum. Another similar spin system of a minor product is visible as well, but due to the low intensity of the signals, no further analysis of the spin system and thus the nature of the product is possible. Yet from the substitution patterns B and C (both $1\text{-}CH_3\text{-2-}PPh_2\text{-3-}^t\text{Bu}$, Scheme 5.3, *vide supra*) this product is likely $Li[Cp^*Fe(1\text{-}CH_3\text{-2-}PPh_2\text{-3-}^t\text{Bu})]$.
The central structural motifs (in proximity to the central atom) of **14** and **15** are best described as metallo-nortricyclan moieties - a structural motif e.g., observed for the iodination product of **XXVII**: $[Cp^*Fe(\eta^{1:1:1}\text{-}(P_6I_6))]$.[276] The *cyclo*-$P_5$ ligand in $[Cp^*Fe(\eta^5\text{-}P_5)]$ (**XXVII**) did not undergo a ring opening or rearrangement and is still intact in the highly substituted P_7 ligands of the functiolazied products (e.g., P2-P3-P4-P5-P6,

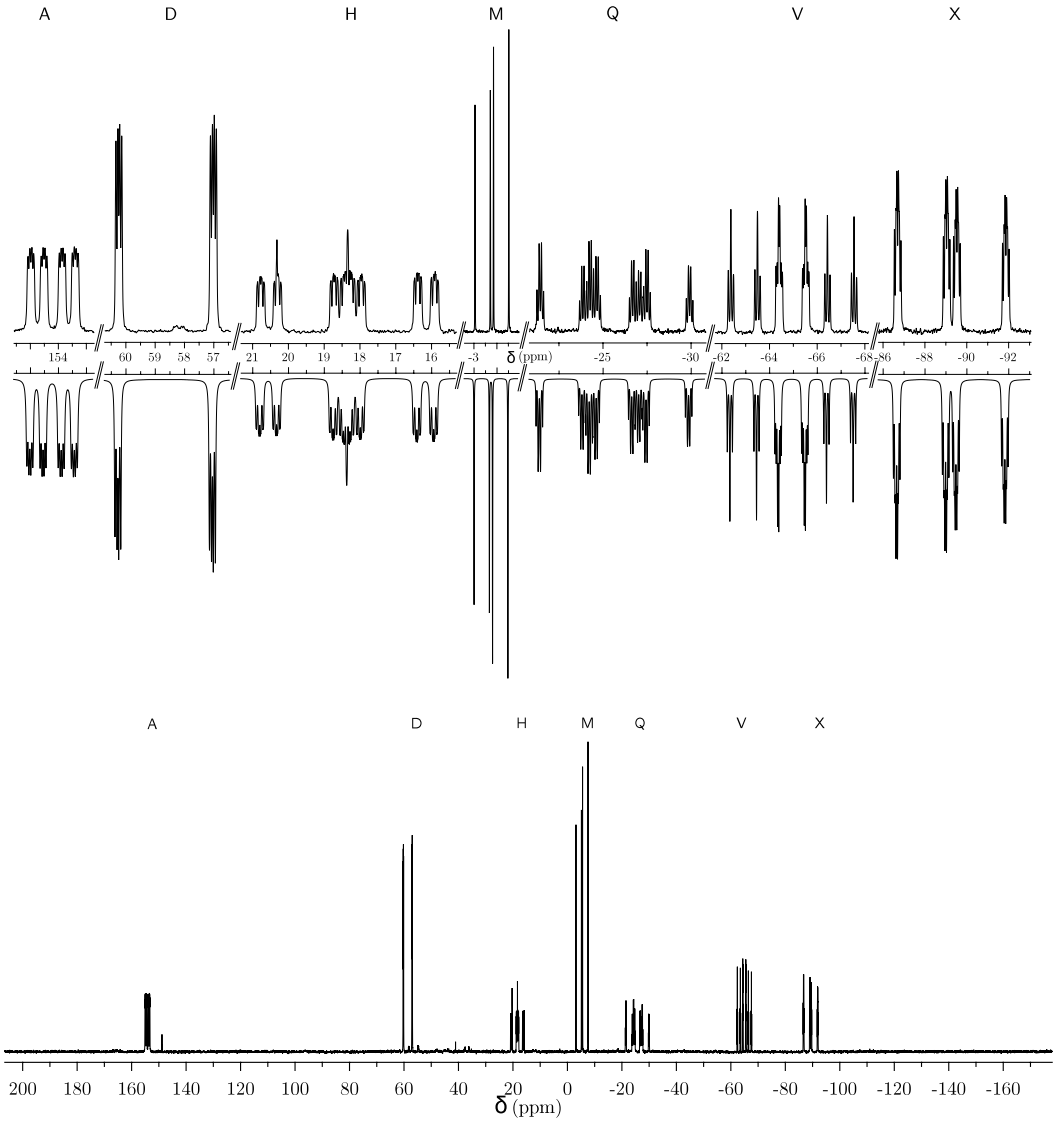
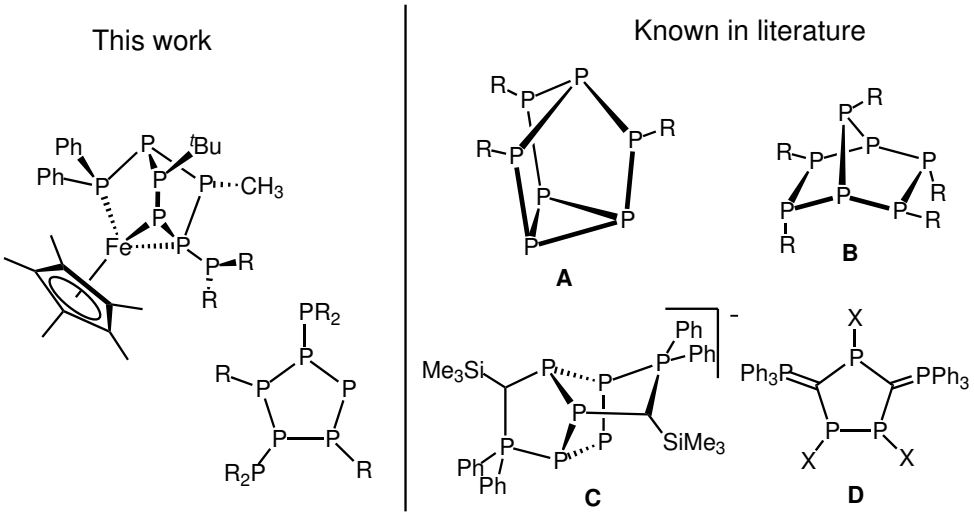


Figure 5.7: $^{31}P\{^{1}H\}$ NMR spectrum (bottom) of **15** in C_6D_6 at room temperature and enlarged depiction of the spin system (top) with a simulation of the iteratively fitted ADHMQVX spin system (inverted).

numbering according to solid state structure of **14** in figure 5.6). In contrast to the cage-like nature of **14** and **15**, the central structural motif of **13** is better described as a metallo-bicyclo[1.1.1]heteropentane-like trigonal bipyramid. In both cases the highly substituted, 1,3 diphosphanyl functionalized *cyclo*-P_5 ligand is only coordinating to the central iron atom by two phosphorus atoms, with the difference that the P-atoms coordinating to the Cp^*Fe moiety are in 1,3-position in **13** and in 1,2-position in **14** and **15**, respectively. In all three compounds, the functionalized P_n ligand is coordinating to the iron atom by two R_2P fragments and one phosphorus atom without any

functional groups. The effect of the organic substituents on the accessibility of the lone pairs of the phosphorus atoms is also reflected in the Fe-P distances in all three compounds: While the functionalized phosphorus atoms have an average Fe-P bond distance of 2.20061(4) Å, the remaining unfunctionalized phosphorus atom shows an average Fe-P bond distance of 2.30021(4) Å. As mentioned before, increased functionalisation of the former *cyclo*-P_5 ligand on different phosphorus atoms reduces hapticity of the ligand and increases the distance between the central iron atom and the centroid of the *cyclo*-P_5 unit (1.56031(1) Å and η^4 for **10**, 2.23178(3) Å and $\eta^{3:1}$ for **11a**, 2.57567(11) Å and $\eta^{1:1:1}$ for **13**, 2.66964(7) Å and $\eta^{1:2}$ for **14**).



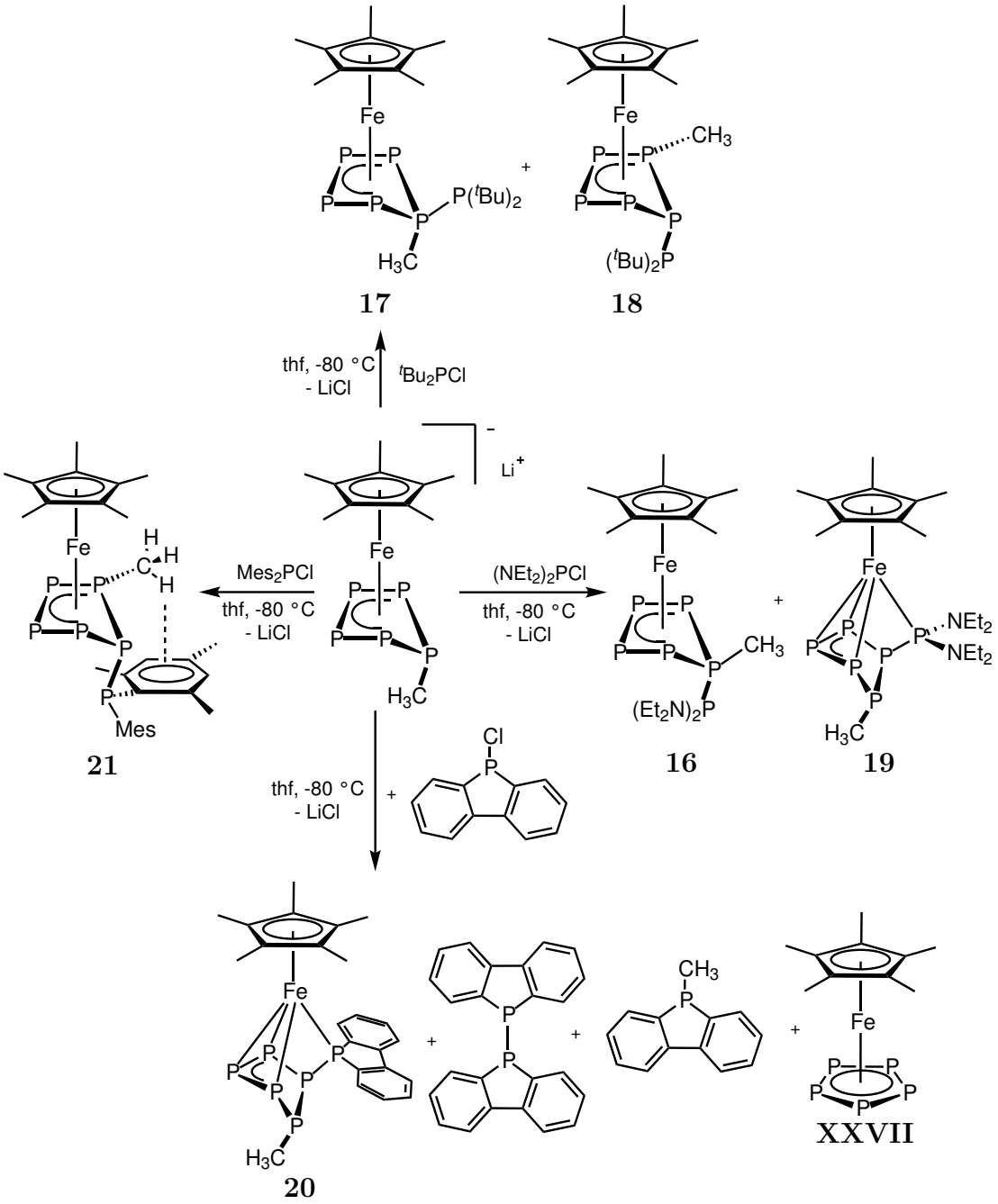
Scheme 5.4: Structures of polycyclic P_7 moieties known in literature in comparison with the results from this work.

The phosphorus ligands in **13**, **14** and **15** themselves are described best as highly substituted 1,3-bis(phosphanyl)pentaphospholanides. Due to the tendency of phosphorus to form polycyclic compounds the most common structural motifs for P_7 moieties are phospha-nortricyclanes (**A**, Scheme 5.4) and phospha-norbornadienes (**B**).[277–281] The only other example for a 1,3-bis(phosphanyl)pentaphospholanide as a substructure is found in $[P_5\{C(SiMe_3)(PPh_2)\}_2]^-$ (**C**, Scheme 5.4), which is a polycyclic compound in contrast to the aforementioned ligands in the transition metal complexes **13**, **14** and **15**.[282] A 1,3-bis(phosphanyl) substituted five membered ring with less than seven phosphorus atoms is observed in tetrachloro- and tetrabromodiphosphanyltriphenylphosphonium ylides, in which the phosphanyl substituents are bound to carbon atoms (**D** in Scheme 5.4).[283] Only mono(phosphanyl)pentaphospholanides are a structural motif known in the literature in for example hexaphosphine or the complex $[Cp^*Fe(\eta^4\text{-}P_5PH_2)]^-$, the product of the attack of $NaPH_2$ on **XXVII**.[77,284] Therefore **13**, **14** and **15** are the first examples for this type of P_7 ligand.

5.2.3 Further reactions of $[Cp^*Fe(\eta^4\text{-}P_5R)]^-$ with chlorophosphines and arsines (treasury)

By reaction of **XXVII** with MeLi in thf at -80 °C the anionic complex $[Cp^*Fe(\eta^4\text{-}P_5CH_3)]^-$ is formed *in situ* and further reacted with standard solutions of the chlorophosphines R_2PCl ($R = {}^t\!Bu, Mes, NEt_2$) and 5-chloro-5H-dibenzophosphole (Scheme 5.5). The resulting neutral complexes are extracted with a mixture of toluene and hexane from the oily residue which is formed upon removal of the solvent. Formation of the 1,1 substitution products endo-$[Cp^*Fe(\eta^4\text{-}1,1\text{-}CH_3,P(NEt_2)_2\text{-}P_5)]$ (**16**, endo according to the position of the $P(NEt_2)_2$ fragment in relation to the Cp^*Fe fragment) and endo-$Cp^*Fe(\eta^4\text{-}1,1\text{-}CH_3,P{}^t\!Bu\text{-}P_5)]$ (**17**) is observed for R = NEt_2 and ${}^t\!Bu$, respectively. For reactions with ${}^t\!Bu_2PCl$ also exo-1,2-substitution is observed in the complex $[Cp^*Fe(\eta^4\text{-}(1\text{-}P{}^t\!Bu_2\text{-}2\text{-}CH_3\text{-}P_5)]$ (**18**). The same structural motif is observed in $[Cp^*Fe(\eta^4\text{-}(1\text{-}PMes_2\text{-}2\text{-}CH_3\text{-}P_5)]$ (**21**) when Mes_2PCl is used in the reaction instead. For $(NEt_2)_2PCl$ and 5-chloro-5H-dibenzophosphole, respectively, highly asymmetric 1,2-substituted ligands as in **11a** and **11b** are observed in $[Cp^*Fe(\eta^{3:1}\text{-}1\text{-}CH_3\text{-}2\text{-}P(NEt_2)_2\text{-}P_5)]$ (**19**) and $[Cp^*Fe(\eta^{3:1}\text{-}1\text{-}CH_3\text{-}2\text{-}C_{12}H_8P\text{-}P_5)]$ (**20**). Unfortunately, it is not possible to isolate any of the above mentioned products by fractionated crystallisation and the complexes are not stable enough during chromatographic workup.

The best separation is achieved by multiple crystallisations of product mixtures of **16** and **19** and thus a 85,8 % pure sample of **19** contaminated with **16** is obtained (according to integration of the signals for P_A in the ^{31}P NMR spectrum of the sample). The two P_6 moieties in **16** and **19** are observed in the $^{31}P\{^1H\}$ NMR spectrum of the product mixture as an ALMM'XX' spin system for **16** (due to the C_S symmetry of the phosphorus ligand) and an ADEMNX spin system for **19**. Both spin systems have been simultaneously iteratively fitted and simulated in order to describe the spin systems properly with all observable coupling constants (figure 5.8). An ADMQVX spin system similar to the one of **19** is observed for **20** in the ^{31}P NMR spectrum of the respective reaction solution with 5-chloro-5H-dibenzophosphole. The complex is only formed in small quantities, while large amounts of the dibenzochlorophosphole react either to 5,5'-bi-5H-benzo[b]phosphindole or to 5-methyldibenzophosphole under the formation of **XXVII** (scheme 5.5). The ratio of the integrals of the multiplet of P_A of the ADHMQX spin system of **20** at 222.7 ppm and the singlet for 5,5'-bi-5H-benzo[b]phosphindole at -21 ppm[285] is 3:4. The ratio of the integrals of for P_A of **20** and the singlet assigned to 5-methyldibenzophosphole at -24.8 ppm[286] is 3:1. Spectroscopic data for the reactions with Mes_2PCl and ${}^t\!Bu_2PCl$ is inconclusive due to the obtained complex product mixtures and products from these reactions can only be



Scheme 5.5: Reaction of $Li[Cp^*Fe(\eta^4\text{-}P_5CH_3)]$ with the chlorophosphines R_2PCl ($R = {}^t\mathrm{Bu}, \mathrm{Mes}, \mathrm{NEt_2}$) and 5-chloro-5H-dibenzophosphole.

characterized by X-ray structure analysis (*vide infra*). In the $^{31}P\{^1H\}$ NMR spectra of the respective reaction solutions multiplets of complex spin systems of different reaction products are superimposed with each other. Therefore neither integration, iterative fitting and simulation nor $^{31}P\,^{31}P$ COSY NMR spectroscopy make it possible to fully analyse the regarding $^{31}P\{^1H\}$ NMR spectra (Supporting Information).

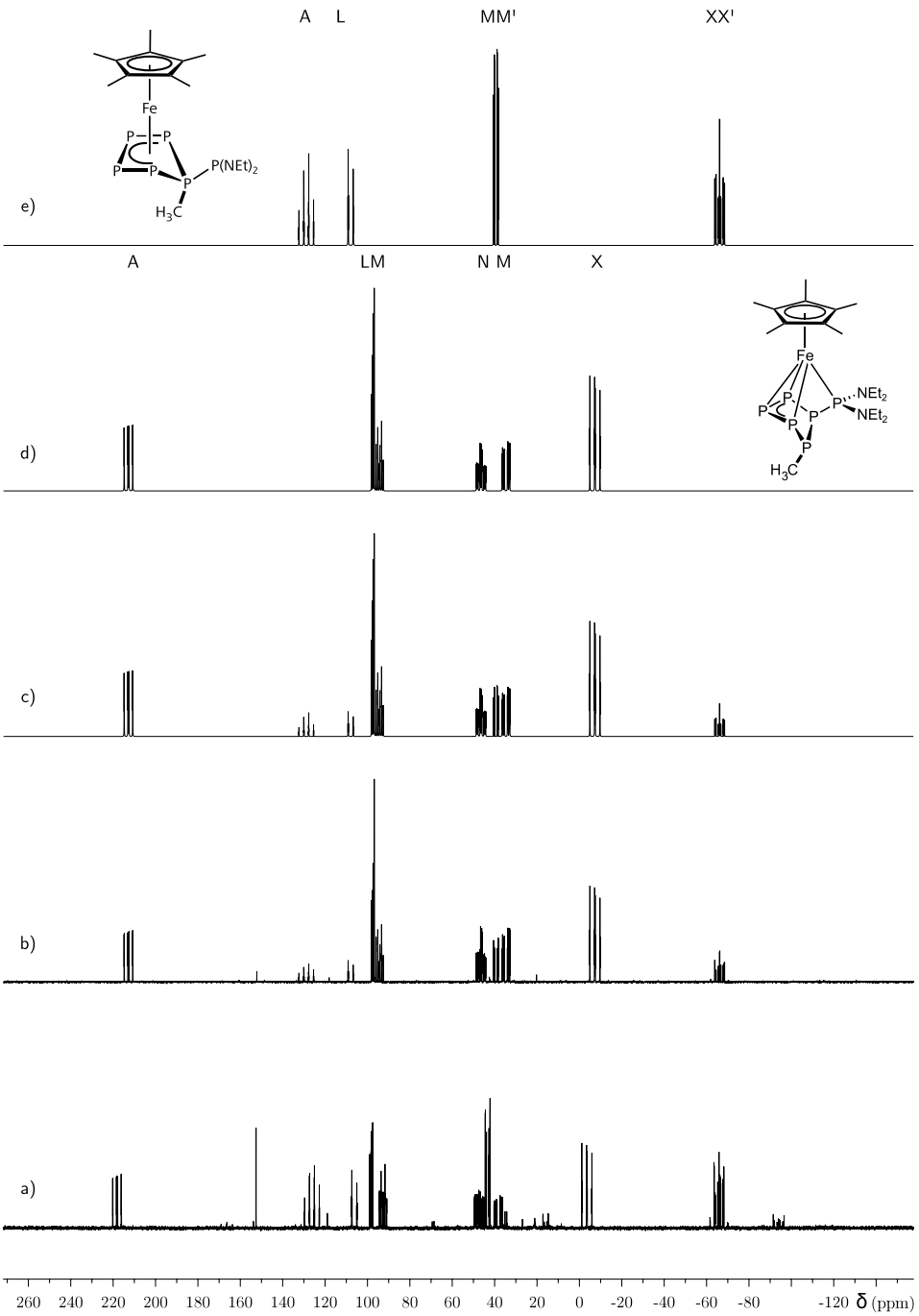


Figure 5.8: $^{31}P\{^{1}H\}$ NMR spectra of **16** and **19** as reaction mixture and mixture of isolated crystalline material with the simulation of the respective spectra and spin systems: a) spectrum of the crude reaction mixture immediately after the reaction in thf with D_2O capillary, b) spectrum of the crystalline product mixture after extraction and recrystallisation in CD_2Cl_2, c) simulated spectrum with both spin systems simultaneously fitted, d) the simulated ADEMNX spin system of **19**, e) the simulated ALMM'XX' spin system of **16**.

For both products of the reaction with $^{t}Bu_2PCl$ (the 1,1-substituted **18** and the 1,2 substituted **17**) as well as for the complexes **21** and **19**, crystals suitable for X-ray structure analysis were obtained by storing the respective extracts of the reaction mixture with addition of *n*-pentane at -30 °C for one week. The solid state structure of **17** is similar to the reported complex endo-$[Cp^*Fe(\eta^4\text{-}1,1\text{-}CH_3,PPh_2\text{-}P_5)]$ (**10a**; endo-PPh_2 relative to Cp^*Fe, Scheme 5.4) and the solid state structure of **19** is similar to the one of $[Cp^*Fe(\eta^{3:1}\text{-}(1\text{-}CH_3\text{-}2\text{-}PPh_2\text{-}P_5))]$ (**11**). The complexes **18** and **21** show a similar structural motifs which are unknown so far (figure 5.9): instead of the R_2P fragment coordinating to the iron atom as it is the case in **11** and **19**, it is bound in exo-position to the *cyclo*-P_5 ligand, which remains in an η^4 coordinating envelope conformation as observed for the starting material $[Cp^*Fe(\eta^4\text{-}P_5CH_3)]^-$. The methyl group is coplanar with the phosphorus atoms, coordinating to the iron atom (*vide infra*, figure 5.9).

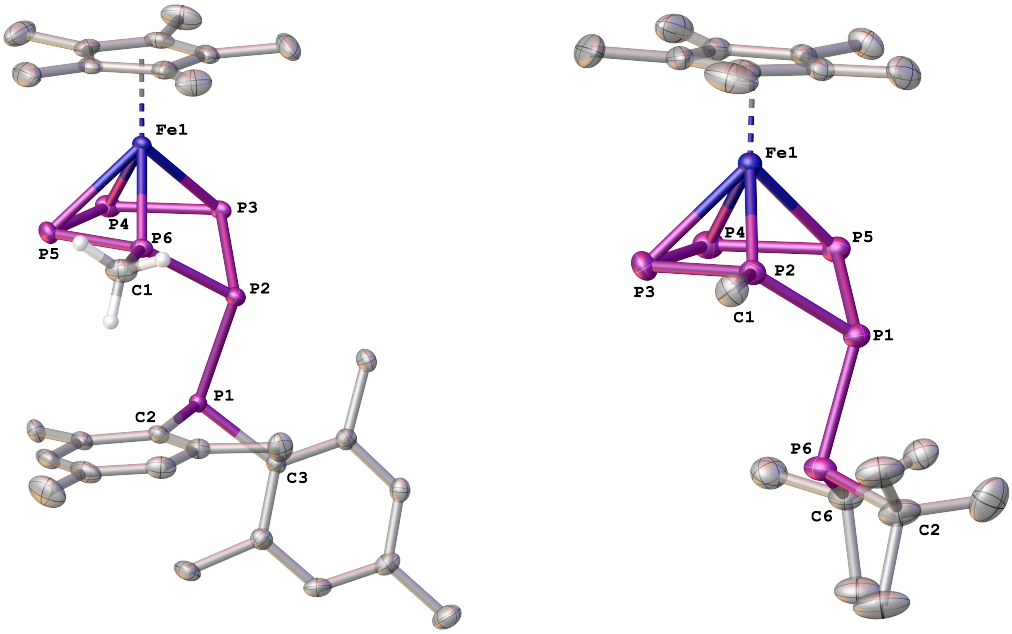


Figure 5.9: Molecular structures of **21** (left) and **18** (right) in the solid state. Hydrogen atoms are omitted for clarity. Selected bond lengths of **21**: Fe1-P6 2.1720(11), Fe1-P3 2.3174(11), Fe1-P5 2.3821(11), Fe1-P4 2.3554(12), P1-P2 2.2585(14), P1-C3 1.849(4), P1-C2 1.846(4), P6-P5 2.1304(14), P6-P2 2.1333(14), P6-C1 1.830(5), P3-P4 2.1602(15), P3-P2 2.2137(14), P5-P4 2.1342(16). Selected bond lengths of **18**: Fe1-P2 2.1616(5) Fe1-P5 2.3228(5) Fe1-P3 2.3982(6) Fe1-P4 2.3339(5), P2-P1 2.1244(7), P2-P3 2.1365(7), P2-C1 1.823(2), P1-P5 2.2342(6), P1-P6 2.2435(7), P5-P4 2.1641(7), P3-P4 2.1379(7), P6-C6 1.894(2), P6-C2 1.905(2).

The main difference in the solid state structures of **18** and **21** is the orientation of the organic substituents on the R_2P fragments: The mesityl substituents in **21** are arranged in a way, that the aromatic ring starting with C2 is coplanar with the mean plane of

the four phosphorus atoms in the polyphosphorus ligand coordinating to the Fe atom (P3, P4, P5 and P6; twist angle between mean planes: 2.3 °). This is due to a CH-π interaction of one of the protons (H1C) from the methyl group to the mesityl group. The methyl group is perfectly aligned with the centroid of the mesityl group. The distances of the Mes-centroid and the calculated methyl-proton of 2.659 Å and the methyl carbon atom of 3.451 Å are in good agreement with crystallographic examples (e.g., distance of aromatic centroid and carbon atom in CH-π contact of 3.56 Å in the $[\mathrm{Co(pyridoxy\text{-}l\text{-}phenylalaninato)_2}]^-$ anion) and respective calculations.[270–272,287]

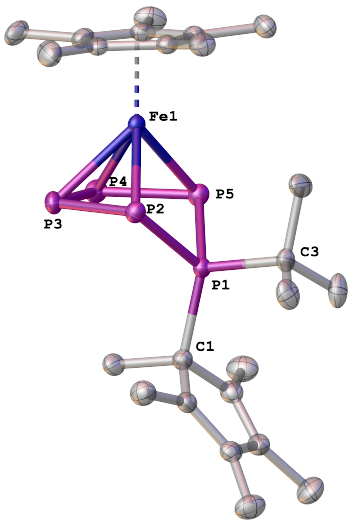
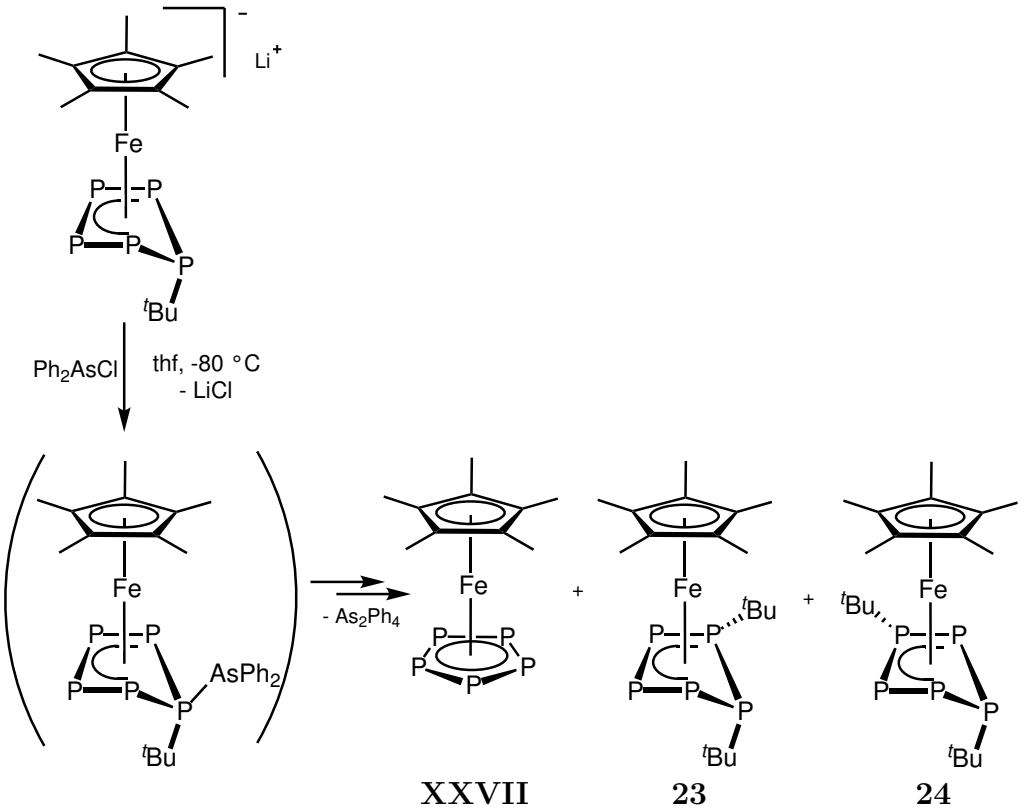


Figure 5.10: Structure of **22** in the solid state. Bond lengths and angles are given in the supporting information. Hydrogen atoms are omitted for clarity.

Investigating the reactivity of dichlorophosphines and phosphorus trichloride towards $[\mathrm{Cp^*Fe}(\eta^4\text{-}\mathrm{P_5R})]^-$ ($\mathrm{R} = \mathrm{CH_3}, {}^t\mathrm{Bu}$), the formation of the starting material **XXVII** alongside a complex mixture of multiple unidentifiable side products is observed. As for 5-chloro-5H-dibenzophosphole the competitive redox reactions seem to be preferred. The reaction of $[\mathrm{Cp^*Fe}(\eta^4\text{-}\mathrm{P_5}{}^t\mathrm{Bu})]^-$ with $\mathrm{Cp^*PCl_2}$ is the only one in this part of the study with any analytically valuable results. Although the $^{31}\mathrm{P}\{^1\mathrm{H}\}$ NMR spectra of the reaction mixture showed equivalent behaviour to the other di- and trihalogenides (signals for the starting material **XXVII** alongside a complex mixture of multiple unidentifiable side products), a few single crystals of $[\mathrm{Cp^*Fe}(\eta^4\text{-}1,1\text{-}{}^t\mathrm{Bu},(\mathrm{Cp^*})\text{-}\mathrm{P_5})]$ (**22**) could be obtained by layering of a *n*-pentane:o-difluorobenzene mixture of the crude product (which was extracted with acetonitrile from the residue of the reaction) with *n*-pentane at -30 °C. The solid state structure of **22** (*vide sinistre*, figure 5.10) shows, that the complex is only functionalized by the initial carbon nucleophile and $\mathrm{Cp^*}$. This is an additional piece of evidence for redox reactions concurring with the electrophilic addition, as observed for the mono-halogenated phosphines. Bond lengths and angles in **22** are similar to other, 1,1-diorgano-functionalized derivatives of **XXVII** such as $[\mathrm{Cp^*Fe}(\eta^4\text{-}(1,1\text{-}\mathrm{CH_3},({}^t\mathrm{Bu})\text{-}\mathrm{P_5}))]$.[76]

Last but not least the reactivity of $[\mathrm{Cp^*Fe}(\eta^4\text{-}\mathrm{P_5R})]^-$ $\mathrm{R} = \mathrm{Me}$, $({}^t\mathrm{Bu})$, synthesized *in situ* from **XXVII** and the respective organolithium compound, towards diphenylchloroarsine was investigated (*vide infra* scheme 5.6). For reactions of $[\mathrm{Cp^*Fe}(\eta^4\text{-}\mathrm{P_5CH_3})]^-$ with $\mathrm{Ph_2AsCl}$, $^{31}\mathrm{P}\{^1\mathrm{H}\}$ NMR spectra of freshly prepared re-

action solutions, measured immediately after letting the sample warm up to room temperature show some strongly broadened multiplets which can not be properly analysed due to the bad signal to noise ratio. These signals broaden more over the course of several hours, so that no fine coupling can be observed. The brown colour of the reaction solutions darkens significantly when stored at room temperature or at -30 °C in the dark over the course of one day. Attempts to crystallize any products only produced dark brown oils. For reactions with $[\mathrm{Cp^*Fe}(\eta^4\text{-}\mathrm{P_5}^t\mathrm{Bu})]^-$ the colour change to a dark



XXVII **23** **24**

Scheme 5.6: Reaction of $\mathrm{Li[Cp^*Fe}(\eta^4\text{-}\mathrm{P_5}^t\mathrm{Bu})]$ with $\mathrm{Ph_2AsCl}$. The supposed intermediary product before disproportionation into **XXVII**, **23** and **24** is shown in brackets.

brown is observed at about -10 °Cwhile letting the reaction solution heat up to room temperature. A singlet assigned to **XXVII** and two well resolved ADMNX spin systems are observed in the $^{31}\mathrm{P}\{^1\mathrm{H}\}$ NMR spectra of the reaction solution. This indicates the presence of two asymmetrically substituted *cyclo*-$\mathrm{P_5}$ units. After extraction with hexane and storing the solution at -30 °C for 18 hours, green crystals of **XXVII** and colourless crystals of $\mathrm{Ph_4As_2}$ are obtained and identified by X-ray diffraction experiments. After discarding the first crystal fraction (containing mostly **XXVII**) the solvent is removed and the resulting brown oil is re-dissolved in a small quantity of acetonitrile,

leaving some of the oil undissolved. A $^{31}P\{^{1}H\}$ NMR spectrum of this solution shows that both products could be partially separated by their difference in solubility since the ratio of the two products assigning from integration has shifted from 1:1 to 3:2. By storing the decanted solution at -30 °C for 18 hours dark brown crystals suitable for X-ray diffraction experiments are obtained. The solid state structure shows that both reaction products co-crystallize. The products are identified as $[Cp^*Fe(\eta^4\text{-}(1,3\text{-}^t Bu_2\text{-}P_5))]$ (**23**) and $[Cp^*Fe(\eta^4\text{-}(1,2\text{-}^t Bu_2\text{-}P_5))]$ (**24**, both **XXVII**, **23** and **24** are visible as a disordered molecule, supporting information figure 5.81 on page 246). The bond lengths and angles of **XXVII**, **23** and **24** are similar to the ones of the 1,2 substitution products **18** and **21** (*vide supra*). One of the ^{t}Bu groups is bound in exo conformation to the shifted P-atom of the envelope shaped phosphorus ligand, while the other ^{t}Bu group is coplanar with the η^4 coordinating phosphorus atoms of the ligand (see supporting information for solid state structures). In order to separate **23** and **24**, chromatographic

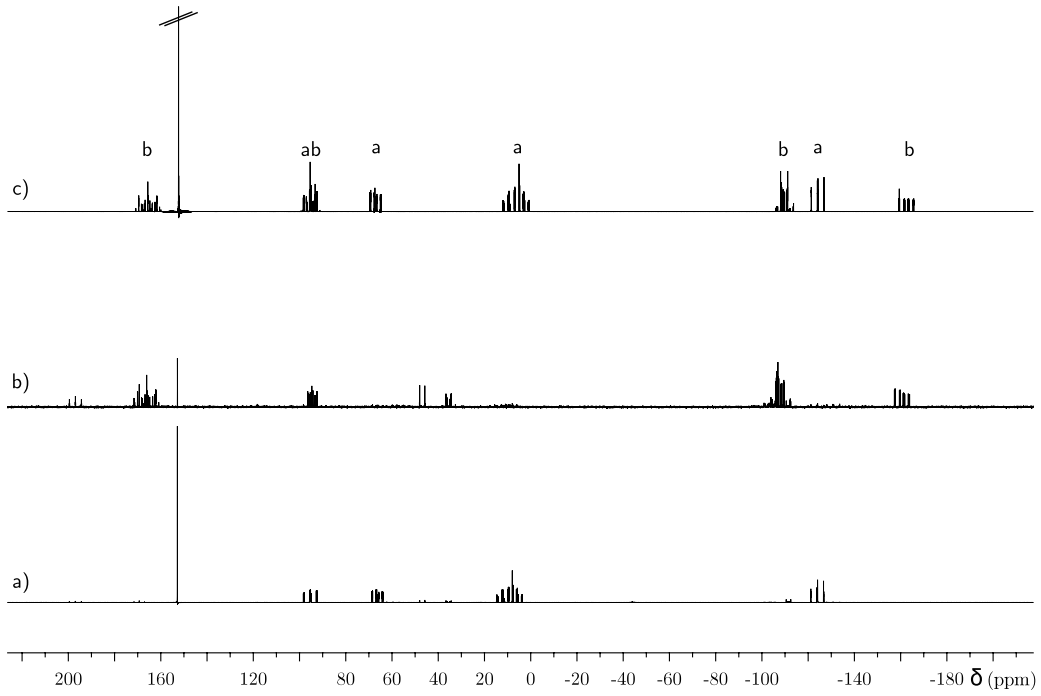


Figure 5.11: $^{31}P\{^{1}H\}$ NMR spectra of **23** and **24**. Before and after the column chromatography. a): Chromatography fraction 1, b): chromatography fraction 2 and c): NMR of the crystalline raw product after extraction with acetonitrile. The intense signal for **XXVII** in spectrum c) at 152 ppm could not be depicted in scale for better visibility of the multiplets from **23** and **24**. For better understanding the signals in the spectrum of the crystalline product mix c) is marked with the letters of the according spectrum from the chromatography fractions.

work up of the crystalline product mixture was performed (dry silica gel, d = 2 cm, l = 15 cm, *n*-hexane:dichloromethane 1:1). After a green fraction of **XXVII** a brown fraction of approximately 5 mL is collected immediately at the end of the first one. The last, dark brown fraction (approximately 15 mL) is a bit more separated from the first ones. Both product fractions contain enough material for $^{31}P\{^{1}H\}$ NMR spectroscopic analysis, which shows that the product mixture can partially be separated (*vide supra*, figure 5.11). Particularly the separation of the first product from **XXVII** is incomplete. Product fraction two is still a mixture of **23** and **24**. In order to exclude the possibility that an equilibrium of **23** and **24** in solution is the reason for the presence of both products in one chromatography fraction, a VT $^{31}P\{^{1}H\}$ NMR study was performed on some crystalline material before the column chromatographic work up. No dynamic process or equilibrium is observed at room temperature or -80 °C, respectively. The same sample was then remeasured after one week to ensure that there is no change in the ratio of **23** and **24** over a prolonged period of time at room temperature - also with no visible changes. In order to present an alternative pathway to products **23** and **24**, $[Cp^*Fe(\eta^4\text{-}P_5{}^tBu)]^-$ was quenched with ^tBuBr and ^tBuCl, but no evidence for the formation of **24** or **23** was observed in $^{31}P\{^{1}H\}$ NMR spectra of the reaction solutions, since no reaction occurred and all starting material was left.

5.3 Conclusion

By *in situ* generation of $Li[Cp^*Fe(\eta^4\text{-}P_5R)]$ $(R = Me,{}^t Bu)$ from $[Cp^*Fe(\eta^5\text{-}P_5)]$ with alkyl lithium compounds (MeLi or ^tBuLi) and quenching with different chlorophosphines R_2PCl $(R = Ph, Cy)$ new, phosphorus rich complexes are formed. For R = Cy endo- and exo-$[Cp^*Fe(\eta^4\text{-}1,1\text{-}CH_3,PCy_2\text{-}P_5)]$ (**12b** and **12a**, endo and exo regarding the PCy_2 group to the Cp^*Fe fragment) are obtained synthesized by thermal control of the reaction. For R = Ph the exclusive formation of endo-$[Cp^*Fe(\eta^4\text{-}1,1\text{-}CH_3,PPh_2\text{-}P_5)]$ (**10**) is observed at - 80 °C. At room temperature **10** quantitatively converts into $[Cp^*Fe(\eta^{3:1}\text{-}(1\text{-}CH_3\text{-}2\text{-}PPh_2\text{-}P_5))]$ (**11a**) by a 1,2 shift. The resulting polyphosphorus ligand is highly asymmetric and shows an increased distance of the *cyclo*-P_5 moiety to the central iron atom compared with the starting material **XXVII**.

Due to the selective formation of **11a** and **11b** these complexes were used for further substitution studies. By nucleophilic attack of ^tBuLi on $[Cp^*Fe(\eta^{3:1}\text{-}(1\text{-}R\text{-}2\text{-}PPh_2\text{-}P_5))]$ (R = Me: **11a**, R = ^tBu: **11b**) and quenching with Cy_2PCl two novel, highly functionalized P_7 moieties in $[Cp^*Fe(\eta^{1:1:1}\text{-}(1\text{-}{}^tBu\text{-}2\text{-}PPh_2\text{-}3\text{-}Me\text{-}4\text{-}PCy_2\text{-}P_5))]$ (**13**) and $[Cp^*Fe(\eta^{1:2}\text{-}(1\text{-}{}^tBu\text{-}2\text{-}PCy_2\text{-}3\text{-}Me\text{-}4\text{-}PPh_2\text{-}P_5))]$ (**14**) are formed in a complex prod-

uct mixture along with an unknown minor product. By variation of the sequence, in which order the substituents are introduced into **XXVII**, more insight into the influence of sterically demanding organic groups like $^t\mathrm{Bu}$ on the selectivity of the nucleophilic attack on **11** is given. This way also the connectivity of the functionalized polyphosphorus ligand in the otherwise not further characterizable minor product of the reactions is determined. By using $^t\mathrm{Bu_2PCl}$ instead of $\mathrm{Cy_2PCl}$ in the second one pot reaction sequence $[\mathrm{Cp^*Fe}(\eta^{1:2}\text{-}(1\text{-}^t\mathrm{Bu}\text{-}2\text{-}\mathrm{P}^t\mathrm{Bu}\text{-}3\text{-}\mathrm{Me}\text{-}4\text{-}\mathrm{PPh_2}\text{-}\mathrm{P_5}))]$ (**15**), the first 1,3-bis(phosphanyl)-pentaphospholanide iron complex is isolated as a pure compound which was fully characterized. Complex **15** represents an unique example for the highest number of functionalized phosphorus atoms of a *cyclo*-$\mathrm{P_5}$ ligand in a pentaphosphaferrocene derivative (4 out of 5).

Additional investigations with chlorophosphines and arsines were made. Yet these reactions did not yield pure compounds, so a qualitative analytical study was performed to gain more insight. Reaction of $\mathrm{Li}[\mathrm{Cp^*Fe}(\eta^4\text{-}\mathrm{P_5CH_3})]$ with $(\mathrm{NEt_2})_2\mathrm{PCl}$ yields endo-$[\mathrm{Cp^*Fe}(\eta^4\text{-}1,1\text{-}\mathrm{CH_3},\mathrm{P}(\mathrm{NEt_2})_2\text{-}\mathrm{P_5})]$ (**16**, endo arrangement according to the position of the $^t\mathrm{Bu_2P}$ fragment in relation to the $\mathrm{Cp^*Fe}$ fragment) and $[\mathrm{Cp^*Fe}(\eta^{3:1}\text{-}1\text{-}\mathrm{CH_3}\text{-}2\text{-}\mathrm{P}(\mathrm{NEt_2})_2\text{-}\mathrm{P_5})]$ (**19**). The identity of **19** is also confirmed by single crystal diffraction. Switching from $(\mathrm{NEt_2})_2\mathrm{PCl}$ to 5-chloro-5H-dibenzophosphole, only the known 1,2 substitution pattern is observed in $[\mathrm{Cp^*Fe}(\eta^{3:1}\text{-}1\text{-}\mathrm{CH_3}\text{-}2\text{-}\mathrm{C_{12}H_8P}\text{-}\mathrm{P_5})]$ (**20**) in the $^{31}\mathrm{P}\{^1\mathrm{H}\}$ NMR spectrum of the reaction solution alongside side products from redox reactions. When quenching with $^t\mathrm{Bu_2PCl}$ one reaction product with an endo-1,1 substitution pattern was identified as endo-$\mathrm{Cp^*Fe}(\eta^4\text{-}1,1\text{-}\mathrm{CH_3},\mathrm{P}^t\mathrm{Bu}\text{-}\mathrm{P_5})]$ (**17**) by X-ray diffraction experiments. With the same analytical method one other reaction product could be identified as $[\mathrm{Cp^*Fe}(\eta^4\text{-}(1\text{-}\mathrm{P}^t\mathrm{Bu_2}\text{-}2\text{-}\mathrm{CH_3}\text{-}\mathrm{P_5})]$ (**18**), showing a novel structural motif for group 14-15 element substituted derivatives of **XXVII** with the phosphine fragment in exo position (relative to $\mathrm{Cp^*Fe}$) and the methyl group in plane with the η^4 coordinating phosphorus atoms of the ligand. The same basic motif was observed when quenching $\mathrm{Li}[\mathrm{Cp^*Fe}(\eta^4\text{-}\mathrm{P_5CH_3})]$ with $\mathrm{Mes_2PCl}$. The only crystallographically identifiable reaction product was $[\mathrm{Cp^*Fe}(\eta^4\text{-}(1\text{-}\mathrm{PMes_2}\text{-}2\text{-}\mathrm{CH_3}\text{-}\mathrm{P_5})]$ (**21**). Last but not least the reactivity of $[\mathrm{Cp^*Fe}(\eta^4\text{-}\mathrm{P_5R})]^-$ $(\mathrm{R} = \mathrm{Me},^t\mathrm{Bu})$ towards $\mathrm{Ph_2AsCl}$ is investigated. For R = Me only extremely short lived products are observed in $^{31}\mathrm{P}\{^1\mathrm{H}\}$ NMR spectra of freshly prepared reaction solutions. For R = $^t\mathrm{Bu}$ disproportionation leads to the formation of **XXVII**, $\mathrm{As_2Ph_4}$ and the two 1,2 and 1,3 group 14 element substituted derivatives of **XXVII** $[\mathrm{Cp^*Fe}(\eta^4\text{-}(1,2\text{-}(^t\mathrm{Bu_2}\text{-}\mathrm{P_5})]$ (**23**) and $[\mathrm{Cp^*Fe}(\eta^4\text{-}(1,3\text{-}(^t\mathrm{Bu_2}\text{-}\mathrm{P_5})]$ (**24**).

With increasing number of functionalized phosphorus atoms of the *cyclo* $\mathrm{P_5}$ ligand in **XXVII**, the centroid of the *cyclo*-$\mathrm{P_5}$ unit increases its distance towards the central iron

atom and hapticity of the ligand decreases. This trend and the new synthetic pathway to highly functionalized, phosphorus rich complexes such as **15** could be utilized in future studies to find a route towards highly functionalized polyphosphines in a rather clean fashion by decomplexations.

5.4 Supporting information

5.4.1 General remarks

All manipulations were performed using standard schlenk techniques on a dual manifold schlenk line or a glove box under an atmosphere of dry argon. Traces of oxygen in the inert gas were removed by passing it over a BASF R 3-11 (CuO/$MgSiO_3$) catalyst. Residual moisture in the inert gas was removed, by passing it through concentrated H_2SO_4, orange gel and sicapent on dried pumice stone. All glassware was vigorously heated in dynamic vacuum before use and any teflon tubing was stored in an oven at 170 °C.

Toluene, diethylether, thf, dichloromethane, acetonitrile, hexane and pentane were purified and dried by the solvent purification system SPS-800 from mbraun. Deuterated solvents were dried and distilled over CaH_2.

MeLi (1.6 M in diethylether), ^{t}BuLi (1.7 M in pentane), PhLi (1.9 M in dibutylether), Mes_2PCl and Ph_2PCl were obtained from Sigma Aldrich. Cy_2PCl, $(NEt_2)_2PCl$, Cp^*PCl_2, $^tBu_2PCl$, 5-chloro-5H-dibenzophosphole and Ph_2AsCl were prepared according to literature procedures.[176,288–292] All chlorophosphines were distilled in an atmosphere of dry argon before being diluted with toluene to a standard solution.

NMR spectra were measured with a Bruker Avance 400 (^{1}H: 400.132 MHz; ^{13}C: 100.613 MHz; ^{31}P: 161.97 MHz) using special NMR tubes with a screw cap or a J. Young valve. Any working steps preparing samples for measurement at - 30 °C were performed at this temperature and the samples stored at - 30 °C until measured. The spin systems of the ^{31}P-NMR spectra were iteratively simulated/fitted with the DAISY package in TopSpin 3.2 from Bruker.

5.4.2 Experimental procedure and analytical data

Synthesis of $[\mathbf{Cp^*Fe(\eta^{3:1}\text{-}(1\text{-}R\text{-}2\text{-}PPh_2\text{-}P_5))}]$ ($\mathbf{R = Me, {}^tBu}$)

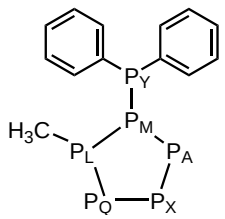
Data for 11a (R = Me)

To a solution of $[\mathrm{Cp^*Fe(\eta^5\text{-}P_5)}]$ (644 mg; 1.86 mmol) in thf 1.73 mL (1.86 mmol) of a standard solution of ^{t}BuLi in *n*-pentane ($\mathrm{c = 1.075\ mol\,L^{-1}}$) are slowly added at - 80 °C. After stirring the brown solution for 15 minutes, 7.44 mL (1.86 mmol) of a standard solution of $\mathrm{Ph_2PCl}$ in toluene ($\mathrm{c = 0.25\ mol\,L^{-1}}$) are added. After warming the dark green solution to room temperature, the solvent is removed and the residue re-dissolved in a 1:1 mixture of hexane and toluene. The off white precipitate is removed on a P4 glass frit and the solvent removed from the filtrate. The resulting dark green-brown oil is dissolved in 5 mL of thf and is slowly added to 130 mL of *n*-pentane. The precipitation of microcrystalline **11** is completed by storing the flask at - 30 °C for 20 hours. The solid is decanted from the solution and dried in vacuum to yield 750 mg (1.37 mmol; 74 %) of **11a**

Elemental analysis: expected for $\mathrm{C_{23}H_{28}P_6Fe}$: 5.17 % H, 50.58 % C, 34.03 % P, 10.22 % Fe. Found: 5.08 % H, 50.41 % C.

ESI-MS: $\frac{m}{z}$ = 1091.99 ($[\mathrm{M}]_2^+ = [\mathrm{Cp^*Fe(\eta^{3:1}\text{-}(1\text{-}CH_3\text{-}2\text{-}PPh_2\text{-}P_5))}]_2^+$

^{1}H NMR: ($\mathrm{CD_2Cl_2}$; 300 K): δ[ppm] = 0.86 (m, $\mathrm{C}H_3$, $^2\mathrm{J_{P_LH}} = 12$ Hz, $^3\mathrm{J_{P_AH}} = 6$ Hz, $^3\mathrm{J_{P_MH}} = 5$ Hz); 1.49 (s, 15 H, $\mathrm{C_5(C}H_3)_5$); 7.25 - 7.90 (m, 10H, $\mathrm{P}Ph_2$)



^{31}P$\{^1$H$\}$ NMR: ($\mathrm{CD_2Cl_2}$; 300 K): δ[ppm] = 219.2 (m, $\mathrm{P_A}$, $^1\mathrm{J_{P_AP_M}} = 294$ Hz, $^1\mathrm{J_{P_AP_X}} = 362$ Hz, $^2\mathrm{J_{P_AP_Q}} = 20$ Hz, $^2\mathrm{J_{P_AP_L}} = 4$ Hz); 72.7 (m; $\mathrm{P_L}$, $^1\mathrm{J_{P_LP_M}} = 289$ Hz, $^1\mathrm{J_{P_LP_Q}} = 139$ Hz, $^2\mathrm{J_{P_LP_X}} = 13$ Hz, $^2\mathrm{J_{P_LP_Y}} = 99$ Hz, $^2\mathrm{J_{P_LP_A}} = 4$ Hz), 62.8 (m, $\mathrm{P_M}$, $^1\mathrm{J_{P_MP_A}} = 294$ Hz, $^1\mathrm{J_{P_MP_L}} = 289$ Hz, $^1\mathrm{J_{P_MP_Y}} = 90$ Hz, $^2\mathrm{J_{P_MP_Q}} = 33$ Hz, $^2\mathrm{J_{P_MP_X}} = 16$ Hz); 39.9 (m, $\mathrm{P_Q}$, $^1\mathrm{J_{P_QP_X}} = 407$ Hz, $^1\mathrm{J_{P_QP_L}} = 139$ Hz, $^2\mathrm{J_{P_QP_M}} = 33$ Hz, $^2\mathrm{J_{P_QP_A}} = 20$ Hz, $^2\mathrm{J_{P_QP_Y}} = 6$ Hz); -13.9 (m, $\mathrm{P_X}$, $^1\mathrm{J_{P_XP_Q}} = 407$ Hz, $^1\mathrm{J_{P_XP_A}} = 362$ Hz, $^2\mathrm{J_{P_XP_M}} = 16$ Hz, $^2\mathrm{J_{P_XP_L}} = 13$ Hz, $^2\mathrm{J_{P_XP_Q}} = 6$ Hz); - 10.7 (m, $\mathrm{P_Y}$, $^1\mathrm{J_{P_YP_M}} = 90$ Hz, $^2\mathrm{J_{P_YP_L}} = 99$ Hz, $^2\mathrm{J_{P_YP_N}} = 6$ Hz, $^2\mathrm{J_{P_YP_X}} = 4$ Hz)

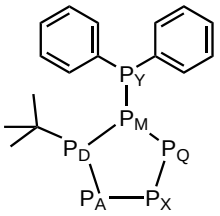
^{31}P NMR: (CD_2Cl_2; 300 K): δ[ppm] = 219.2 (m, P_A, $^1J_{P_AP_M} = 294$ Hz, $^1J_{P_AP_X} = 362$ Hz, $^2J_{P_AP_Q} = 20$ Hz, $^2J_{P_AP_L} = 4$ Hz, $^3J_{P_AH} = 6$ Hz); 72.7 (m; P_L, $^1J_{P_LP_M} = 289$ Hz, $^1J_{P_LP_Q} = 139$ Hz, $^2J_{P_LP_X} = 13$ Hz, $^2J_{P_LP_Y} = 99$ Hz, $^2J_{P_LP_A} = 4$ Hz, $^2J_{P_LH} = 12$ Hz), 62.8 (m, P_M, $^1J_{P_MP_A} = 294$ Hz, $^1J_{P_MP_L} = 289$ Hz, $^1J_{P_MP_Y} = 90$ Hz, $^2J_{P_MP_Q} = 33$ Hz, $^2J_{P_MP_X} = 16$ Hz, $^3J_{P_MH} = 5$ Hz); 39.9 (m, P_Q, $^1J_{P_QP_X} = 407$ Hz, $^1J_{P_QP_L} = 139$ Hz, $^2J_{P_QP_M} = 33$ Hz, $^2J_{P_QP_A} = 20$ Hz, $^2J_{P_QP_Y} = 6$ Hz); -13.9 (m, P_X, $^1J_{P_XP_Q} = 407$ Hz, $^1J_{P_XP_A} = 362$ Hz, $^2J_{P_XP_M} = 16$ Hz, $^2J_{P_XP_L} = 13$ Hz, $^2J_{P_XP_Q} = 6$ Hz); - 10.7 (m, P_Y, $^1J_{P_YP_M} = 90$ Hz, $^2J_{P_YP_L} = 99$ Hz, $^2J_{P_YP_N} = 6$ Hz, $^2J_{P_YP_X} = 4$ Hz)

Data for 11b (R = ^{t}Bu)

To a solution of $[Cp^*Fe(\eta^5\text{-}P_5)]$ (138 mg; 0.4 mmol) in thf 0.85 mL (0.4 mmol) of a standard solution of MeLi in *n*-pentane ($c = 0.473\ mol\,L^{-1}$) are slowly added at - 80 °C. After stirring the brown solution for 15 minutes, 1.6 mL (0.4 mmol) of a standard solution of Ph_2PCl in toluene ($c = 0.25\ mol\,L^{-1}$) are added. After warming the dark green solution to room temperature, the solvent is removed and the residue redissolved in a 1:1 mixture of *n*-hexane and dichloromethane. The off white precipitate is removed on a P4 glass frit and the solvent removed from the filtrate. Crystallisation sets in at room temperature if only litte dichloromethane is used and crystallisation is completed by storing the flask at - 30 °C for 20 hours. The dark brownish green crystals are decanted from the solution and dried in vacuum to yield 59 mg (0.1 mmol; 25 %) of **11b**.

Elemental analysis: expected for $C_{26}H_{34}P_6Fe$: 5.83 % H, 53.08 % C, 31.59 % P, 9.49 % Fe. Found: 6.33 % H, 52.82 % C.

^{1}H NMR: (CD_2Cl_2; 300 K): δ[ppm] = 0.82 (d, $C(CH_3)_3$, $^2J_{P_DH} = 13$ Hz); 1.48 (s, 15 H, $C_5(CH_3)_5$); 7.27(m, 2H, PPh_2); 7.34 to 7.46(m, 6H, PPh_2); 7.91(m, 2H, PPh_2)



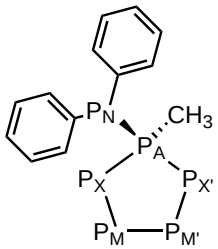
^{31}P{^{1}H} NMR: (CD_2Cl_2; 300 K): δ[ppm] = 174.5 (m, P_A, $^{1}J_{P_AP_D} = 351$ Hz, $^{1}J_{P_AP_X} = 355$ Hz, $^{2}J_{P_AP_Q} = 15$ Hz, $^{2}J_{P_AP_M} = 6$ Hz); 112.8 (m; P_D, $^{1}J_{P_DP_A} = 351$ Hz, $^{1}J_{P_DP_M} = 333$ Hz, $^{2}J_{P_DP_X} = 30$ Hz, $^{2}J_{P_DP_Y} = 104$ Hz, $^{2}J_{P_DP_Q} = 43$ Hz), 74.1 (m, P_M, $^{1}J_{P_MP_D} = 333$ Hz, $^{1}J_{P_MP_Q} = 131$ Hz, $^{1}J_{P_MP_Y} = 100$ Hz, $^{2}J_{P_MP_X} = 9$ Hz, $^{2}J_{P_MP_A} = 6$ Hz); 51.2 (m, P_Q, $^{1}J_{P_QP_X} = 415$ Hz, $^{1}J_{P_QP_M} = 131$ Hz, $^{2}J_{P_QP_A} = 15$ Hz, $^{2}J_{P_QP_D} = 43$ Hz); -4.4 (m, P_X, $^{1}J_{P_XP_Q} = 415$ Hz, $^{1}J_{P_XP_A} = 355$ Hz, $^{2}J_{P_XP_M} = 9$ Hz, $^{2}J_{P_XP_D} = 30$ Hz); - 11.2 (m, P_Y, $^{1}J_{P_YP_M} = 100$ Hz, $^{2}J_{P_YP_D} = 104$ Hz)

^{31}P NMR: Same signals as the $^{31}P\{^{1}H\}$ NMR except for additional coupling for 112.8 (m; P_D, $^{3}J_{P_DH} = 13$ Hz) and broadening of - 11.2 (m, P_Y) due to coupling with the phenyl groups.

Synthesis of endo-[Cp*Fe(η^4-(1-Me-1-PPh$_2$-P$_5$))]

To a solution of [Cp*Fe(η^5-P_5)] (644 mg; 1.86 mmol) in thf 1,73 mL (1.86 mmol) of a standard solution of MeLi in *n*-pentane ($c = 1.075\ mol\,L^{-1}$) are slowly added at - 80 °C . After stirring the brown solution for 15 minutes, 7.44 mL (1.86 mmol) of a standard solution of Ph_2PCl in toluene ($c = 0.25\ mol\,L^{-1}$) are added. After 1 hour of stirring, the flask is transferred to a cooling bath with a temperature of - 30 °C and the solvent removed in vacuum. The resulting dark green residue is suspended in hexane and dichloromethane is added until only small amounts of oily residue remain on the wall of the flask, always maintaining - 30 °C . The suspension is then allowed to settle and carefully decanted into a pre cooled flask. By carefully removing dichloromethane at - 60 °C in small increments, solid endo-[Cp*Fe(η^4-(1-Me-1-PPh_2-P_5))] (**10**) begins to precipitate, which is then redissolved at - 30 °C. After removing small amounts of dichloromethane, the solution is stored at - 30 °C in a freezer to yield crystals of **10** suitable for X-ray diffraction. The crystals then are washed with cold acetonitrile at - 30 °C and dissolved in cold CD_2Cl_2 for NMR studies.

^{1}H NMR: (CD_2Cl_2; 243 K): δ[ppm] = 0.41 (d, CH_3, $^{2}J_{P_AH} = 8.3$ Hz); 1.6 (s, 15 H, $C_5(CH_3)_5$); 7.39 - 7.67 (m, 10H, PPh_2)



^{31}P{^{1}H} NMR: (CD_2Cl_2; 243 K): δ[ppm] = 119.3 (m, P_A, $^1J_{P_AP_X} = ^1 J_{P_AP_{X'}} = 390$ Hz, $^1J_{P_AP_N} = 287$ Hz, $^2J_{P_AP_M} = ^2 J_{P_AP_{M'}} = 10$ Hz), 35.35 (m, $P_M, P_{M'}$, $^1J_{P_MP_{M'}} = 394$ Hz, $^1J_{P_MP_X} = ^1 J_{P_{M'}P_{X'}} = 374$ Hz, $^2J_{P_MP_{X'}} = ^2 J_{P_{M'}P_X} = -35$ Hz, $^2J_{P_AP_M} = ^2 J_{P_AP_{M'}} = \pm 10$ Hz, $^3J_{P_MP_N} = ^3 J_{P_{M'}P_N} = 8$ Hz),-17.1 (m, P_N, $^1J_{P_NP_A} = 287$ Hz, $^2J_{P_NP_X} = ^2 J_{P_NP_{X'}} = 66$ Hz, $^3J_{P_NP_M} = ^3 J_{P_NP_{M'}} = 8$ Hz), -99 (m, $P_X, P_{X'}$, $^1J_{P_XP_A} = ^1 J_{P_{X'}P_X} = 390$ Hz, $^1J_{P_XP_M} = ^1 J_{P_{X'}P_{M'}} = 374$ Hz, $^2J_{P_{X'}P_M} = ^2 J_{P_XP_{M'}} = -35$ Hz, $^2J_{P_XP_N} = ^2 J_{P_{X'}P_N} = 66$ Hz, $^2J_{P_XP_{X'}} = -14$ Hz)

^{31}P NMR: (CD_2Cl_2; 243 K): Same as the proton decoupled spectrum, expect for additional coupling of the signal at 119 ppm ($^2J_{P_AH} = 8.3$ Hz) and broadening of the signal at -17.1 ppm due to unresolved coupling of P_N with the phenyl groups.

Synthesis of endo-[Cp*Fe(η^4-(1-Me-1-PCy$_2$-P$_5$))]

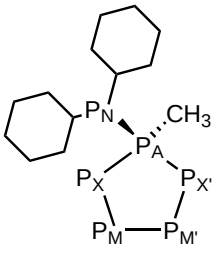
To 10 mL of a solution of [Cp*Fe(η^5-P_5)] (207 mg; 0.6 mmol) in thf, a standard solution of methyl lithium in diethylether (0.60 mL, $c = 1.038$ mol L^{-1}, 0.6 mmol) is added at - 80 °C. After stirring for 15 minutes and letting the reaction mixture warm to room temperature, a standard solution of Cy_2PCl in toluene (6 mL, $c = 0.1$ mol L^{-1}; 0.6 mmol) is added to the dark brown solution. The reaction mixture was stirred for 3 h and the solvent removed in vacuum. The green-brown residue is dissolved 15 mL of *n*-hexane and stored at - 30 °C for crystallisation. After one day dark green crystals of **12a** are decanted from the solution and dried in vacuum.

Yield: 68 mg (0.12 mmol; 20.3 %)

Elemental analysis: expected for $C_{23}H_{38}P_6Fe$: 7.22 % H, 49.48 % C, 33.29 % P, 10.00 % Fe. Found: 7.15 % H, 50.17 % C.

^{1}H NMR: (CD_2Cl_2, 300 K): δ[ppm] = 0.26 (d, 3 H, CH_3, $^2J_{P_AH} = 8.8$ Hz); 1,68 (s; 15 H; $C_5(CH_3)_5$); 0.83 to 1.84 (m, 22 H; C_6H_{11})

Due to a not further identifiable dynamic process multiplet MM' could not be properly fitted iteratively. Therefore small coupling constants are not reliable and only couplings up to ^{2}J are given.



^{31}P{^{1}H} NMR: (CD_2Cl_2; 300 K): δ[ppm] = 113.3 (m, P_A, $^1J_{P_AP_X} = ^1 J_{P_AP_{X'}} = 387$ Hz, $^1J_{P_AP_N} = 319$ Hz), 30.1 (m, $P_M, P_{M'}$, $^1J_{P_MP_{M'}} = 393$ Hz, $^1J_{P_MP_X} = ^1 J_{P_{M'}P_{X'}} = 372$ Hz, $^2J_{P_MP_{X'}} = ^2 J_{P_{M'}P_X} = -35$ Hz), -3.8 (m, P_N, $^1J_{P_NP_A} = 319$ Hz, $^2J_{P_NP_X} = ^2 J_{P_NP_{X'}} = -49$ Hz), -102.9 (m, $P_X, P_{X'}$, $^1J_{P_XP_A} = ^1 J_{P_{X'}P_X} = 387$ Hz, $^1J_{P_XP_M} = ^1 J_{P_{X'}P_{M'}} = 372$ Hz, $^2J_{P_{X'}P_M} = ^2J_{P_XP_{M'}} = -35$ Hz, $^2J_{P_XP_N} = ^2 J_{P_{X'}P_N} = -49$ Hz)

^{31}P NMR: (CD_2Cl_2; 300 K): Same as the proton decoupled spectrum, expect for additional coupling of the signal at 113.3 ppm ($^2J_{P_AH} = 8.8$ Hz) and broadening of the signal at -3.8 ppm due to unresolved coupling of P_N with the cyclohexyl substituents.

Synthesis of exo-[Cp*Fe(η^4-(1-Me-1-PCy$_2$-P$_5$))]

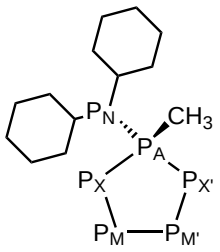
To a 10 mL solution of [Cp*Fe(η^5-P_5)] (138 mg; 0.4 mmol) in thf, a standard solution of methyl lithium in diethylether (0.39 mL, $c = 1.038\ mol\,L^{-1}$, 0.4 mmol) is added at 193 K. After stirring for 15 minutes a standard solution of Cy_2PCl in toluene (4 mL, $c = 0.1\ mol\,L^{-1}$; 0.4 mmol) to the dark brown solution. The reaction mixture is allowed to warm up to room temperature and stirred for 24 h. To the yellow-brown residue 15 mL of *n*-pentane are added and o-DFB added dropwise to the suspension until nearly all of the coloured residue is dissolved. After sedimentation, the solution is decanted from the brownish grey solid and stored at 243 K for crystallisation. After two days dark green crystals of **12b** are decanted from the solution and dried in vacuum.

Yield: 85 mg (0.15 mmol; 38 %)

Elemental analysis: expected for $C_{23}H_{38}P_6Fe$: 7.22 % H, 49.48 % C, 33.29 % P, 10.00 % Fe. Found: 7.77 % H, 49.79 % C.

ESI-MS: $\frac{m}{z}$ = 558 ($[M]^+ = [Cp^*Fe(\eta^4\text{-}(1\text{-}CH_3\text{-}2\text{-}PCy_2\text{-}P_5))]^+$

^{1}H NMR: (CD_2Cl_2, 300 K): δ[ppm] = 1.20 (brm; 11 H; C_6H_{11}); 1.61 (s; 15 H; $C_5(CH_3)_3$); 1.64 (brm; ; 11 H; C_6H_{11}); 2.50 (ddt; 3 H; CH_3; $^2J_{P_AH} = 8$ Hz; $^3J_{P_NH} = 7.5$ Hz; $^3J_{P_XH} = 6,3$ Hz; $^3J_{P_{X'}H} = 6.3$ Hz



^{31}P{^{1}H} NMR: (CD_2Cl_2; 300 K): δ[ppm] = 127.7 (m; P_A; $^{1}J_{P_AP_N} = 358$ Hz; $^{1}J_{P_AP_X} = 383$ Hz; $^{1}J_{P_AP_{X'}} = 388$ Hz; $^{2}J_{P_AP_M} = 13$ Hz; $^{2}J_{P_AP_{M'}} = 13$ Hz); 42.6 (m; P_M and $P_{M'}$; $^{1}J_{P_MP_X} = 408$ Hz; $^{1}J_{P_{M'}P_{X'}} = 399$ Hz; $^{1}J_{P_MP_{M'}} = 384$ Hz; $^{2}J_{P_MP_{X'}} = -44$ Hz; $^{2}J_{P_{M'}P_X} = -31$ Hz; $^{2}J_{P_AP_M} = 13$ Hz; $^{2}J_{P_AP_{M'}} = 13$ Hz); 30.0 (m; P_N; $^{1}J_{P_NP_A} = 358$ Hz; $^{2}J_{P_NP_X} = 14$ Hz; $^{2}J_{P_NP_{X'}} = 14$ Hz); -59.8 (m; P_X and $P_{X'}$; $^{1}J_{P_XP_A} = 383$ Hz; $^{1}J_{P_{X'}P_A} = 388$ Hz; $^{1}J_{P_XP_M} = 408$ Hz; $^{1}J_{P_{X'}P_{M'}} = 399$ Hz; $^{1}J_{P_XP_N} = 14$ Hz; $^{1}J_{P_{X'}P_N} = 14$ Hz)

^{31}P NMR: (CD_2Cl_2; 300 K): δ[ppm] = 127.7 (m; P_A; $^{1}J_{P_AP_N} = 358$ Hz; $^{1}J_{P_AP_X} = 383$ Hz; $^{1}J_{P_AP_{X'}} = 388$ Hz; $^{2}J_{P_AP_M} = 13$ Hz; $^{2}J_{P_AP_{M'}} = 13$ Hz; $^{2}J_{P_AH} = 8$ Hz); 42.6 (m; P_M and $P_{M'}$; $^{1}J_{P_MP_X} = 408$ Hz; $^{1}J_{P_{M'}P_{X'}} = 399$ Hz; $^{1}J_{P_MP_{M'}} = 384$ Hz; $^{2}J_{P_MP_{X'}} = -44$ Hz; $^{2}J_{P_{M'}P_X} = -31$ Hz; $^{2}J_{P_AP_M} = 13$ Hz; $^{2}J_{P_AP_{M'}} = 13$ Hz); 30.0 (m; P_N; $^{1}J_{P_NP_A} = 358$ Hz; $^{2}J_{P_NP_X} = 14$ Hz; $^{2}J_{P_NP_{X'}} = 14$ Hz; $^{2}J_{P_NH} = 7,5$ Hz); -59.8 (m; P_X and $P_{X'}$; $^{1}J_{P_XP_A} = 383$ Hz; $^{1}J_{P_{X'}P_A} = 388$ Hz; $^{1}J_{P_XP_M} = 408$ Hz; $^{1}J_{P_{X'}P_{M'}} = 399$ Hz; $^{1}J_{P_XP_N} = 14$ Hz; $^{1}J_{P_{X'}P_N} = 14$ Hz; $^{2}J_{P_XH} = 6$ Hz; $^{2}J_{P_{X'}H} = 6$ Hz

Synthesis of [Cp*Fe($\eta^{1:1:1}$-(1-t-Bu-2-PCy$_2$-3-Me-4-PPh$_2$-P$_5$))] and [Cp*Fe($\eta^{1:2}$-(1-t-Bu-2-PPh$_2$-3-Me-4-PCy$_2$-P$_5$))]

From 11a:

To a solution of **11a** (60 mg, 0.109 mmol) in thf at -80 °C , 0.55 mL of a standard solution of ^{t}BuLi in pentane (0.109 mmol, c=0.2 M) is slowly added with a syringe. After shortly stirring the dark brown solution, 0.9 mL of a standard solution of Cy_2PCl in toluene (0.109 mmol, c=0.121 M) is slowly added. After letting the intense red solution warm to room temperature, the solvent is removed in vacuum. The resulting oily residue is dissolved in pentane and filtrated over a P4 glass frit. By carefully removing pentane in an Ar-stream and storing at -30 °C crystallisation of [Cp*Fe($\eta^{1:2}$-(1-t-Bu-2-PCy$_2$-3-Me-4-PPh$_2$-P$_5$))] (**14**) and [Cp*Fe($\eta^{1:1:1}$-(1-t-Bu-2-PPh$_2$-3-Me-4-PCy$_2$-P$_5$))] (**13**) is induced. Co-crystallisation of both products is difficult to prevent and only crystals of **13** are suitable for picking by hand under a microscope in a glove box.

From 11b:

the procedure is equivalent to the synthesis from **11a**, except for the difference in starting materials (**11b** and MeLi) and that the resulting product solution is of a reddish brown colour. With these starting materials **13** is not formed.

Yield of picked crystals of **13**: 12.5 mg (0.014 mmol, 13 %)

ESI-MS: $\frac{m}{z}$ = 800.2 ($[\mathrm{M}]^+ = [\mathrm{Cp^*Fe(CH_3\text{-}PPh_2^tBuPCy_2P_5))}]^+$; 603 ($[\mathrm{M}]^+ - \mathrm{PCy_2}$); 213 ($\mathrm{PCy_2MeH^+}$)

NMR data for **13**:

^{1}H NMR: ($\mathrm{tol\text{-}d_8}$, 300 K): δ[ppm] = 1.64 (d, 9 H, $\mathrm{C}(\mathrm{C}H_3)_3$, $^3\mathrm{J_{PH}} = 11.8$ Hz); 1.00 to 2.06 (m; 22 H; Cy); 1.91 (s, 15 H; $\mathrm{C_5}(\mathrm{C}H_3)_3$); 2.26 (m, 3 H, $\mathrm{C}H_3$), 6.95 to 7.20 (m, 10 H, Ph)

Due to the overlap of the signals in the spectrum, the spin system could not be iteratively fitted and the signals could not be assigned to the corresponding phosphorus atoms (*vide infra* figure 5.36).

^{31}P$\{^1$H$\}$ NMR: ($\mathrm{tol\text{-}d_8}$; 300 K): δ[ppm] = 165.1 (m, 1 P), 61.7 (m, 1 P), 15.5 (m, 2 P), 10.8 (m, 1 P), -6.2 (m, 2 P)

^{31}P NMR: P-H coupling is not properly resolved and pronounced broadening can only be observed for the strongly overlapped signals at 15.5 ppm and 10.8 ppm.

Synthesis of $[\mathrm{Cp^*Fe}(\eta^{1:2}\text{-}(\mathbf{1\text{-}t\text{-}Bu\text{-}2\text{-}P^tBu_2\text{-}3\text{-}Me\text{-}4\text{-}PPh_2\text{-}P_5}))]$ (15)

To a solution of **11a** (109 mg, 0.2 mmol) in thf at -80 °C, 0.33 mL of a standard solution of $^t\mathrm{BuLi}$ in *n*-pentane (0.2 mmol, c=0.6 M) is slowly added with a syringe. After shortly stirring the dark brown solution, 0.4 mL of a standard solution of $^t\mathrm{Bu_2PCl}$ in toluene (0.2 mmol, c=0.5 M) is slowly added. After letting the brown solution warm to room temperature, the solvent is removed in vacuum. The resulting oily residue is dissolved in pentane and filtrated over a P4 glass frit and the resulting filtrate dried in vacuum. The residue is washed two times with 5 mL of acetonitrile and dissolved with a mixture of acetonitrile and diethylether. The ether is then evaporated by bubbling argon through

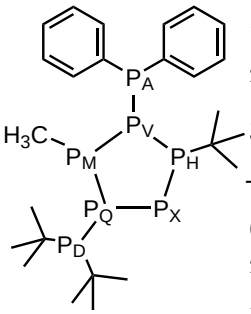
the solution. From this mixture crystals of $[Cp^*Fe(\eta^{1:2}\text{-}(1\text{-t-Bu-}2\text{-}P^tBu_2\text{-}3\text{-Me-}4\text{-}PPh_2\text{-}P_5))]$ (**15**) are formed upon storing at room temperature over night.

Crystalline yield: 47 mg (0.063 mmol; 38 %)

Elemental analysis: expected for $C_{35}H_{55}P_7Fe$: 7.40 % H, 56.16 % C, 28.96 % P, 7.46 % Fe. Found: 7.55 % H, 55.83 % C.

ESI-MS: $\frac{m}{z}$ = 748 ($[M]^+ = [Cp^*Fe(CH_3PPh_2^tBuP^tBu_2P_5))]^+$; 603 ($[M]^+ - P^tBu_2$)

^{1}H NMR: (CD_2Cl_2, 300 K): δ[ppm] = 0.09 (m, 3 H, CH_3, $^2J_{P_MH} = 8.7$ Hz); 1.33 (m; 18 H; $P_D{}^tBu_2$, $^3J_{P_DH} = 6.5$ Hz); 1.51 (s and d (superimposed), 15+9=24 H, $C_5(CH_3)_5$ and ^tBu, $^3J_{P_HH} = 11.7$ Hz), 7.21 to 8.01 (m, 10H, P_APh_2)



^{31}P{^{1}H}-NMR: (CD_2Cl_2; 300 K): δ[ppm] = 154.2 (m, P_A, $^1J_{P_AP_V} = 181$ Hz, $^1J_{P_AP_H} = 76$ Hz, $^2J_{P_AP_Q} = 23$ Hz, $^2J_{P_AP_X} = 12$ Hz), 58.6 (m, P_D, $^1J_{P_DP_Q} = 525$ Hz, $^2J_{P_DP_X} = 20$ Hz, $^2J_{P_DP_H} = 11.5$ Hz), 18.3 (m, P_H, $^1J_{P_HP_V} = 332$ Hz, $^1J_{P_HP_X} = 379$ Hz, $^2J_{P_HP_A} = 76$ Hz, $^2J_{P_HP_D} = 11$ Hz, $^2J_{P_HP_Q} = 19$ Hz), -5.4 (m, P_M, $^1J_{P_MP_Q} = 392$ Hz, $^1J_{P_MP_V} = 326$ Hz), -25.6 (m, P_Q, $^1J_{P_QP_X} = 460$ Hz, $^1J_{P_QP_D} = 525$ Hz, $^2J_{P_QP_A} = 23$ Hz, $^2J_{P_QP_H} = 19$ Hz, $^1J_{P_QP_V} = 16$ Hz), -64.9 (m, P_V, $^1J_{P_VP_M} = 325$ Hz, $^1J_{P_VP_H} = 332$ Hz, $^1J_{P_VP_A} = 181$ Hz, $^2J_{P_VP_Q} = 16$ Hz, $^2J_{P_VP_X} = 18$ Hz), -89.2 (m, P_X, $^1J_{P_XP_Q} = 460$ Hz, $^1J_{P_XP_H} = 379$ Hz, $^2J_{P_XP_D} = 20$ Hz, $^1J_{P_XP_A} = 12$ Hz)

^{31}P-NMR: (CD_2Cl_2; 300 K): Additional P-H couplings for the signals of P_D ($^2J_{P_Dt\text{-}Bu} = 11.2$ Hz) and P_V ($^2J_{P_VH} = 7.1$ Hz). Broadening for all other signals is observed due to additional P-H coupling. Complete iterative simulation of the proton coupled spin system was not possible due to limitations of the software for this many nuclei.

Reaction of Li[Cp*Fe(η^4-P$_5$CH$_3$)] with (NEt$_2$)$_2$PCl

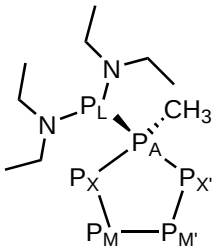
To a 10 mL solution of $[Cp^*Fe(\eta^5\text{-}P_5)]$ (138 mg; 0.4 mmol) in thf, a standard solution of methyl lithium in diethylether (0.39 mL, $c = 1.038\ mol\,L^{-1}$, 0.4 mmol) is added

at 193 K. After stirring for 15 minutes a standard solution of $(NEt_2)_2PCl$ in toluene (4 mL, $c = 0.1\ mol\,L^{-1}$; 0.4 mmol) to the dark brown solution. The reaction mixture is allowed to warm up to room temperature and stirred for 24 h. To brown residue after removing the solvent 15 mL of *n*-pentane are added and o-dfb dropped to the suspension until nearly all of the coloured residue is dissolved. After sedimentation, the solution is decanted from the brownish grey solid and stored at -30 °C for crystallisation. After two days brown crystals of **19** are decanted from the solution and dried in vacuum. The crystalline fraction contained 18 % **16**.

Yield: 92 mg (0.17 mmol; 42 %)

Analytical data for 16:

^{1}H NMR: (CD_2Cl_2; 300 K): δ[ppm] = 0.99 (t, 12 H, NCH_2CH_3); 1.62 (s, 15 H, $Cp(CH_3)_3$); 2.32 (m , 3 H, CH_3); 3.63 (m, 8 H, NCH_2CH_3).

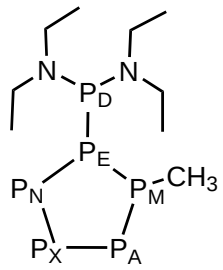


^{31}P{^{1}H} NMR: (CD_2Cl_2; 300 K): δ[ppm] = 128.8 (m, P_A, $^1J_{P_AP_L} = 385$ Hz, $^2J_{P_AP_M} = {}^2J_{P_AP'_M} = 12$ Hz, $^1J_{P_AP_X} = {}^1J_{P_AP_{X'}} = 368$ Hz); 107.9 (m, P_L, $^1J_{P_LP_A} = 385$ Hz, $^2J_{P_LP_X} = {}^2J_{P_LP_{X'}} = 20.5$ Hz); 39.4 (m, P_M and $P_{M'}$, $^1J_{P_MP_X} = {}^1J_{P_{M'}P_{X'}} = 283$ Hz, $^2J_{P_MP_{X'}} = {}^2J_{P_{M'}P_X} = -84$ Hz, $^2J_{P_MP_A} = {}^2J_{P_{M'}P_A} = 12$ Hz); -66.1 (m, P_X and $P_{X'}$, $^1J_{P_AP_X} = {}^1J_{P_AP_{X'}} = 368$ Hz, $^1J_{P_MP_X} = {}^1J_{P_{M'}P_{X'}} = 283$ Hz, $^2J_{P_MP_{X'}} = {}^2J_{P_{M'}P_X} = -84$ Hz, $^2J_{P_LP_X} = {}^2J_{P_LP_{X'}} = 20.5$ Hz)

^{31}P NMR: (CD_2Cl_2; 300 K): Same as the data from the $^{31}P\{^1H\}$ NMR except for broadening of all multipletts except MM'. For XX' a $^3J_{PH}$ coupling of 5.9 Hz can be observed.

Analytical data for 19:

^{1}H NMR: (CD_2Cl_2; 300 K): δ[ppm] = 0.92 (m, 3 H; (m , 3 H, CH_3)); 1.17 (t, 6 H, NCH_2CH_3); 1.31 (t, 6 H, NCH_2CH_3); 1.65 (s, 15 H, $Cp(CH_3)_3$); 2.8 to 3.28 (m, 8H, NCH_2CH_3).

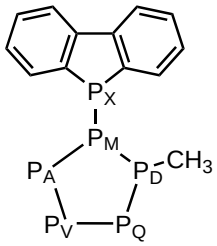


^{31}P{^{1}H} NMR: (CD_2Cl_2; 300 K): δ[ppm] = 212.7 (m, P_A, $^{1}J_{P_AP_X} = 364$ Hz, $^{1}J_{P_AP_M} = 289$ Hz, $^{2}J_{P_AP_N} = 16$ Hz, $^{1}J_{P_AP_E} = 5$ Hz); 97.4 (m, P_D, $^{2}J_{P_DP_E} = 124$ Hz, $^{1}J_{P_DP_M} = 91$ Hz); 94.3 (m, P_E, $^{2}J_{P_EP_M} = 294$ Hz, $^{1}J_{P_DP_E} = 294$ Hz, $^{2}J_{P_DP_N} = 137$ Hz, $^{2}J_{P_DP_X} = 12$ Hz); 46.4 (m, P_M, $^{1}J_{P_MP_A} = 289$ Hz, $^{1}J_{P_MP_E} = 294$ Hz, $^{1}J_{P_MP_D} = 91$ Hz, $^{2}J_{P_MP_N} = 40$ Hz, $^{2}J_{P_MP_X} = 13$ Hz); 34.6 (m, P_N, $^{1}J_{P_NP_D} = 137$ Hz, $^{1}J_{P_NP_X} = 408$ Hz, $^{2}J_{P_NP_A} = 17$ Hz, $^{2}J_{P_NP_M} = 40$ Hz); -7.3 (m, P_X, $^{1}J_{P_XP_A} = 364$ Hz, $^{1}J_{P_XP_N} = 408$ Hz, $^{2}J_{P_XP_E} = 12$ Hz, $^{2}J_{P_XP_M} = 13$ Hz)

^{31}P NMR: (CD_2Cl_2; 300 K): Same as the data from the $^{31}P\{^{1}H\}$ NMR except for broadening of all multipletts except X. For M a $^{3}J_{PH}$ coupling of 5.0 Hz can be observed.

Reaction of Li[Cp*Fe(η^4-P_5CH_3)] with 5-chloro-5H-dibenzophosphole

To a 10 mL solution of [Cp*Fe(η^5-P_5)] (138 mg; 0.4 mmol) in thf, a standard solution of methyl lithium in diethylether (0.39 mL, $c = 1.038\ mol\,L^{-1}$, 0.4 mmol) is added at 193 K. After stirring for 15 minutes a solution of 5-chloro-5H-dibenzophosphole (87 mg; 0.4 mmol) in 2 mL of thf to the dark brown solution. The dark green reaction mixture is allowed to warm up to room temperature and stirred for 24 h. The dark brown solution was reduced in volume and transferred into an NMR tube containing a D_2O capillary. After NMR analysis the sample was retrieved for crystallisation and isolation. No crystals or solid product could be isolated from the mixture.



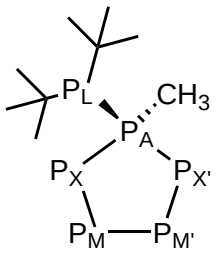
^{31}P{^{1}H} NMR: (CD_2Cl_2; 300 K): δ[ppm] = 222.6 (m, P_A, $^{1}J_{P_AP_M} = 274$ Hz, $^{1}J_{P_AP_V} = 365$ Hz, $^{2}J_{P_AP_D} = 8$ Hz, $^{2}J_{P_AP_Q} = 21$ Hz, $^{2}J_{P_AP_X} = 5$ Hz); 82.3 (m, P_D, $^{1}J_{P_DP_M} = 276$ Hz, $^{1}J_{P_DP_Q} = 132$ Hz, $^{2}J_{P_DP_V} = 15$ Hz, $^{2}J_{P_DP_X} = 100$ Hz, $^{2}J_{P_DP_A} = 8$ Hz); 57.3 (m, P_M, $^{1}J_{P_MP_A} = 274$ Hz, $^{1}J_{P_MP_D} = 276$ Hz, $^{2}J_{P_MP_Q} = 43$ Hz, $^{2}J_{P_MP_V} = 20$ Hz, $^{2}J_{P_MP_X} = 85$ Hz); 48.3 (m, P_Q, $^{1}J_{P_QP_V} = 404$ Hz, $^{1}J_{P_QP_D} = 132$ Hz, $^{2}J_{P_QP_A} = 21$ Hz, $^{2}J_{P_QP_M} = 43$ Hz); 1.5 (m, P_V, $^{1}J_{P_VP_A} = 365$ Hz, $^{1}J_{P_VP_Q} = 404$ Hz, $^{2}J_{P_VP_D} = 15$ Hz, $^{2}J_{P_VP_M} = 20$ Hz, $^{2}J_{P_VP_X} = 4$ Hz); -13.0 (m, P_X, $^{1}J_{P_XP_D} = 100$ Hz, $^{2}J_{P_XP_A} = 5$ Hz, $^{2}J_{P_XP_M} = 85$ Hz, $^{2}J_{P_XP_V} = 4$ Hz)

^{31}P NMR: (CD_2Cl_2; 300 K): Same as the data from the $^{31}P\{^{1}H\}$ NMR except for broadening of all multipletts except Q and V.

Reaction of Li[Cp*Fe(η^4-P_5CH_3)] with $^{t}Bu_2PCl$

To a 10 mL solution of [Cp*Fe(η^5-P_5)] (138 mg; 0.4 mmol) in thf, a standard solution of methyl lithium in diethylether (0.39 mL, $c = 1.038\ mol\,L^{-1}$, 0.4 mmol) is added at 193 K. After stirring for 15 minutes a 3.3 mL of a standard solution of $^{t}Bu_2PCl$ ($c = 1.22\ mol\,L^{-1}$, 0.4 mmol) are added to the dark brown solution. The reaction mixture is allowed to warm up to room temperature and stirred for 24 h. The brown solution was died in vacuum and the residue extracted three times with 2 mL of pentane. The brown solution was decanted from a green brown residue and stored at -30 °C for 24 hours to yield crystals of **18** in a yield of 31 mg (0.015 mmol, 4 %). The greenish residue was dissolved in a minimum amount of toluene. The solution was allowed to settle and decanted from the beige solids which precipitated upon addition of the solvent. A small amount of *n*-pentane was added greenish brown solution and stored at -30 °C for crystallisation. After several months a few crystals of **17** suitable for X-ray structure determination could be retrieved. The crystalline fraction of **18** was used for ^{31}P NMR spectroscopy. Due to a no further identifiable impurity or equilibrium in solution, the integrals of the respective NMR signals did not match with any of the described compounds. The crystalline fraction of **17** was not sufficient for further analysis, but the NMR signals for **17** can be determined by comparison of the crude reaction NMR and the ^{31}P NMR spectra of the crystalline fraction of **18**. The according ALMM'XX' spin system is well separated and resolved. Therefore analysis of the spin

system by iterative fitting and simulation was possible. NMR spectroscopic data for **17** could therefore be determined:



^{31}P$\{^1$H$\}$ NMR: (CD_2Cl_2; 300 K): δ[ppm] = 119.7 (m, P_A, $^1J_{P_AP_L} = 390$ Hz, $^2J_{P_AP_M} = ^2J_{P_AP'_M} = 11$ Hz, $^1J_{P_AP_X} = ^1J_{P_AP_{X'}} = 387$ Hz); 42.9 (m, P_L, $^1J_{P_LP_A} = 385$ Hz, $^2J_{P_LP_X} = ^2J_{P_LP_{X'}} = 34$ Hz, $^3J_{P_LP_M} = ^3J_{P_LP_{M'}} = 8$ Hz); 22.1 (m, P_M and $P_{M'}$, $^1J_{P_MP_{M'}} = 389$ Hz,$^1J_{P_MP_X} = ^1J_{P_{M'}P_{X'}} = 370$ Hz, $^2J_{P_MP_{X'}} = ^2J_{P_{M'}P_X} = -34$ Hz, $^2J_{P_MP_A} = ^2J_{P_{M'}P_A} = 11.2$ Hz); -95.6 (m, P_X and $P_{X'}$, $^1J_{P_AP_X} = ^1J_{P_AP_{X'}} = 387$ Hz, $^1J_{P_MP_X} = ^1J_{P_{M'}P_{X'}} = 370$ Hz, $^2J_{P_MP_{X'}} = ^2J_{P_{M'}P_X} = -34$ Hz, $^2J_{P_LP_X} = ^1J_{P_LP_{X'}} = 34$ Hz, $^1J_{P_XP_{X'}} = -21$ Hz)

^{31}P NMR: (CD_2Cl_2; 300 K): Same as the data from the $^{31}P\{^1H\}$ NMR except for broadening of multipletts A and L. For A a $^2J_{PH}$ coupling of 8.6 Hz can be observed.

Reaction of Li[Cp*Fe(η^4-P_5CH_3)] with Mes_2PCl

To a 10 mL solution of [Cp*Fe(η^5-P_5)] (138 mg; 0.4 mmol) in thf, a standard solution of methyl lithium in diethylether (0.39 mL, $c = 1.038\ mol\,L^{-1}$, 0.4 mmol) is added at 193 K. After stirring for 15 minutes a standard solution of Mes_2PCl in toluene (8 mL, $c = 0.05\ mol\,L^{-1}$; 0.4 mmol) to the dark brown solution. The dark green reaction mixture is allowed to warm up to room temperature and stirred for 24 h. After reducing the amount of solvent, the brown solution was analysed by ^{31}P NMR spectroscopy. After retrieving the sample and storing the solution over night at -30 °C , small needle shaped crystals were observed, not suitable for X-ray diffraction experiments. After redissolving the needles at -30 °C with thf and addition of some drops of pentane at room temperature, small brown needles and dark green block shaped crystals were retrieved, the latter being suitable for X-ray diffraction experiments. Any attempts to recrystallize the brown needles or to retrieve additional crystal fractions from the mother liquor failed so far.

Yield: 63 mg of the mixed crystalline fraction (0.03 mmol; 7.5 %)

The NMR spectra from this reaction could not be interpreted correctly, although different solvents were used (high impact on chemical shift) and an ^{31}P-^{31}P COSY NMR and multiple ^{31}P NMR spectra were recorded (*vide infra*).

Reaction of Li[Cp*Fe(η^4-P$_5$^{t}Bu)] with Cp*PCl$_2$

To a 10 mL solution of [Cp*Fe(η^5-P$_5$)] (138 mg; 0.4 mmol) in thf, a standard solution of tertbutyl lithium in pentane (0.85 mL, $c = 0.47\ \mathrm{mol\,L^{-1}}$, 0.4 mmol) is added at 193 K. After stirring for 15 minutes a standard solution of Cp*PCl$_2$ in toluene (2 mL, $c = 0.2\ \mathrm{mol\,L^{-1}}$; 0.4 mmol) to the dark brown solution. The reaction mixture is allowed to warm up to room temperature, stirred for 24 h and the solvent removed partially to get a concentrated solution for a crude reaction NMR. After washing with acetonitrile, the brown, oily residue was suspended in pentane and ortho difluoro benzene added until nearly all soluble material was dissolved. After decanting and storing the solution at -30 °C over several months a few small green-brown crystals of **22** suitable for x-ray diffraction could be retrieved.
yield: 63 mg of the mixed crystalline fraction (0.03 mmol; 7.5 %)

The NMR spectra from this reaction could not be interpreted correctly, since there are multiple redox processes involved in the reaction (*vide infra*). The products from these reactions could not be isolated or characterized except for **22**.

Reaction of Li[Cp*Fe(η^4-P$_5$CH$_3$)] with Ph$_2$AsCl

To 10 mL solution of [Cp*Fe(η^5-P$_5$)] (138 mg; 0.4 mmol) in thf, a standard solution of tertbutyl lithium in pentane (0.85 mL, $c = 0.47\ \mathrm{mol\,L^{-1}}$, 0.4 mmol) is added at 193 K. After stirring for 15 minutes 3 mL of a solution of Ph$_2$AsCl in toluene (0.4 mmol; 105 mg) to the dark brown solution. The reaction mixture is allowed to warm up to room temperature and stirred for 24 h. The solvent was removed in vacuum and the dark brown residue extracted with *n*-hexane. After allowing the off white precipitate to settle, the brown solution was decanted and stored at -30 °C until formation of green crystals of **XXVII** and colourless crystals of Ph$_4$As$_2$ suitable for X-ray diffraction experiments were observed. Decanting the cold solution from the crystal mixture, reducing slightly in volume and storing further at -30 °C yielded brown crystals of [Cp*Fe(η^4-(1,2-(^{t}Bu$_2$-P$_5$)] (**24**) with [Cp*Fe(η^4-(1,3-(^{t}Bu$_2$-P$_5$)] (**23**) cocrystalized. The crystalline product mixture was then separated in a small column chromatography set up (diameter 2 cm and length 15 cm of dry silica gel)using a 1:1 mixture of

dichloromethane and hexane as the mobile phase. After a first green fraction of **XXVII**, a second brown fraction followed at the end of the green one. Last a dark brown fraction could be retrieved. Both fractions were analysed by NMR spectroscopy to check if the separation was successful. Both fractions could be separated, but due to either less successful separation of **XXVII** and the first brown fraction or decomposition, both fractions show multiple impurities in the NMR spectra. Iterative fitting and simulation of the spectra was not possible due to some suspected dynamic processes or equilibria in solution which can to this point not be accounted for. This processes or equilibria make it impossible to fit the fine structure of the $^{31}\mathrm{P}$ NMR spectrum of fraction 1, but from the tentative simulation the ^{1}J couplings can be estimated. Additionally strong $^{3}J_{\mathrm{PH}}$ can be observed for two of the multiplets. From this it can be deducted, that the 1,2-substitution product **23** is the compound eluted in the first brown fraction.

Yield: 85 mg (0.14 mmol; 35 %)

^{1}H NMR: ($\mathrm{C_6D_6}$; 300 K): δ[ppm] = 0.67 (d, 9 H, $^{t}\mathrm{Bu}$, $^{3}\mathrm{J_{P_DH}} = 12.4$ Hz); 1.42 (d, 9 H, $^{t}\mathrm{Bu}$, $^{3}\mathrm{J_{P_AH}} = 15.7$ Hz); 0.67 (d, 15 H, $\mathrm{Cp^*}$)

^{31}P{^{1}H} NMR: ($\mathrm{C_6D_6}$; 300 K): δ[ppm] = 95.3 (m, $\mathrm{P_A}$, $^{1}\mathrm{J_{P_AP_D}} \approx 435$ Hz, $^{1}\mathrm{J_{P_AP_X}} \approx 470$ Hz); 66.4 (m, $^{1}\mathrm{J_{P_DP_A}} \approx 435$ Hz, $^{1}\mathrm{J_{P_DP_N}} \approx 305$ Hz); 11.7 (m, $\mathrm{P_M}$, $^{1}\mathrm{J_{P_MP_N}} \approx 339$ Hz, $^{1}\mathrm{J_{P_MP_X}} \approx 447$ Hz); 6.0 (m, $\mathrm{P_N}$, $^{1}\mathrm{J_{P_NP_D}} \approx 305$ Hz, $^{1}\mathrm{J_{P_NP_M}} \approx 339$ Hz); -123.9 (m, $\mathrm{P_X}$, $^{1}\mathrm{J_{P_XP_A}} \approx 470$ Hz, $^{1}\mathrm{J_{P_XP_M}} \approx 447$ Hz)

^{31}P NMR: ($\mathrm{C_6D_6}$; 300 K): Same as the data from the $^{31}\mathrm{P}\{^{1}\mathrm{H}\}$ NMR except for distinct fine splitting of signals A and D due to $^{3}J_{\mathrm{PH}}$ coupling (constants see ^{1}H NMR data)

5.4.3 NMR spectra and simulations of spin systems

NMR spectra of [Cp*Fe($\eta^{3:1}$-(1-Me-2-PPh$_2$-P$_5$))] (11a)

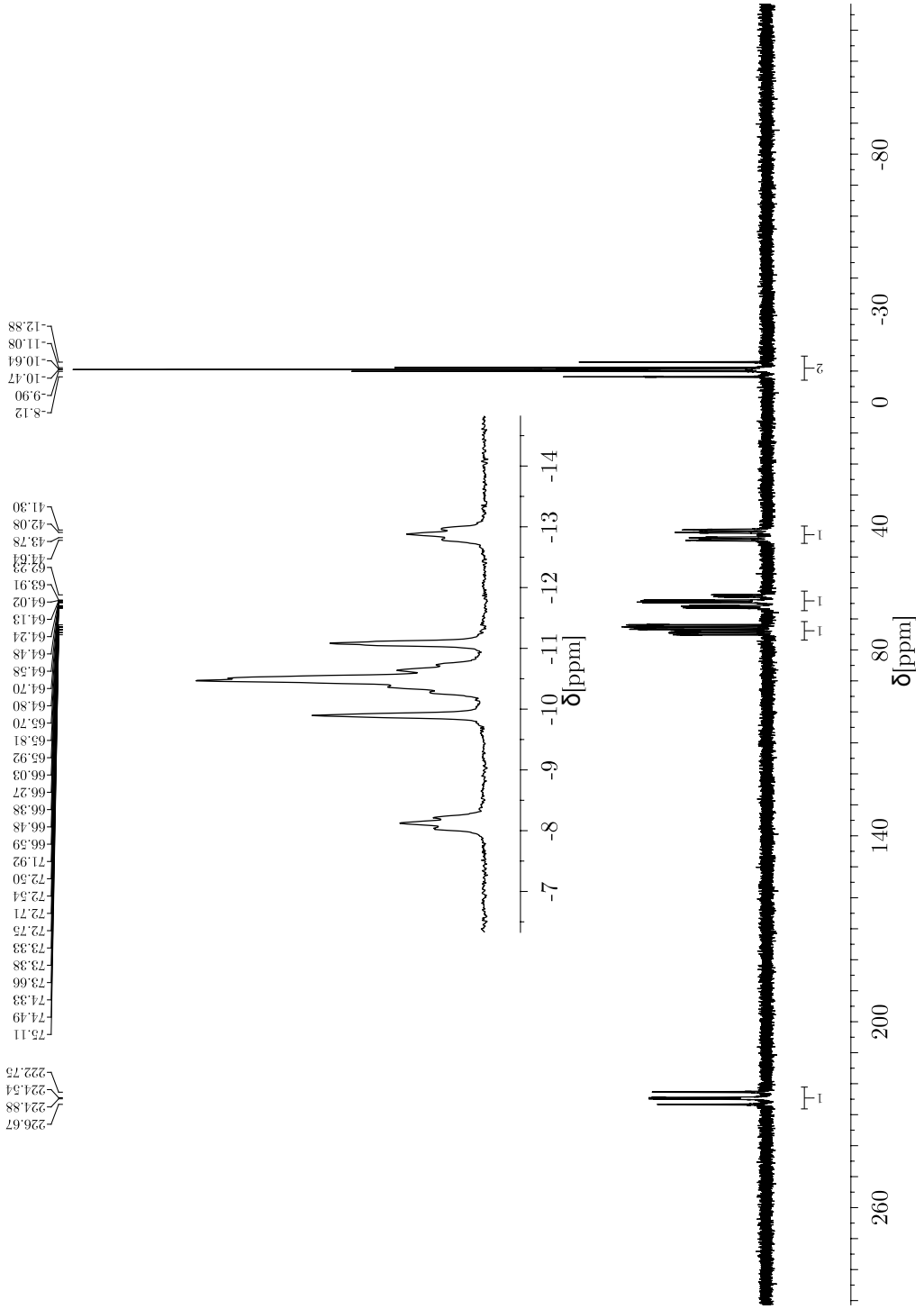


Figure 5.12: $^{31}P\{^1H\}$ NMR spectrum of [Cp*Fe($\eta^{3:1}$-(1-Me-2-PPh$_2$-P$_5$))] (**11a**) at room temperature in C_6D_6.

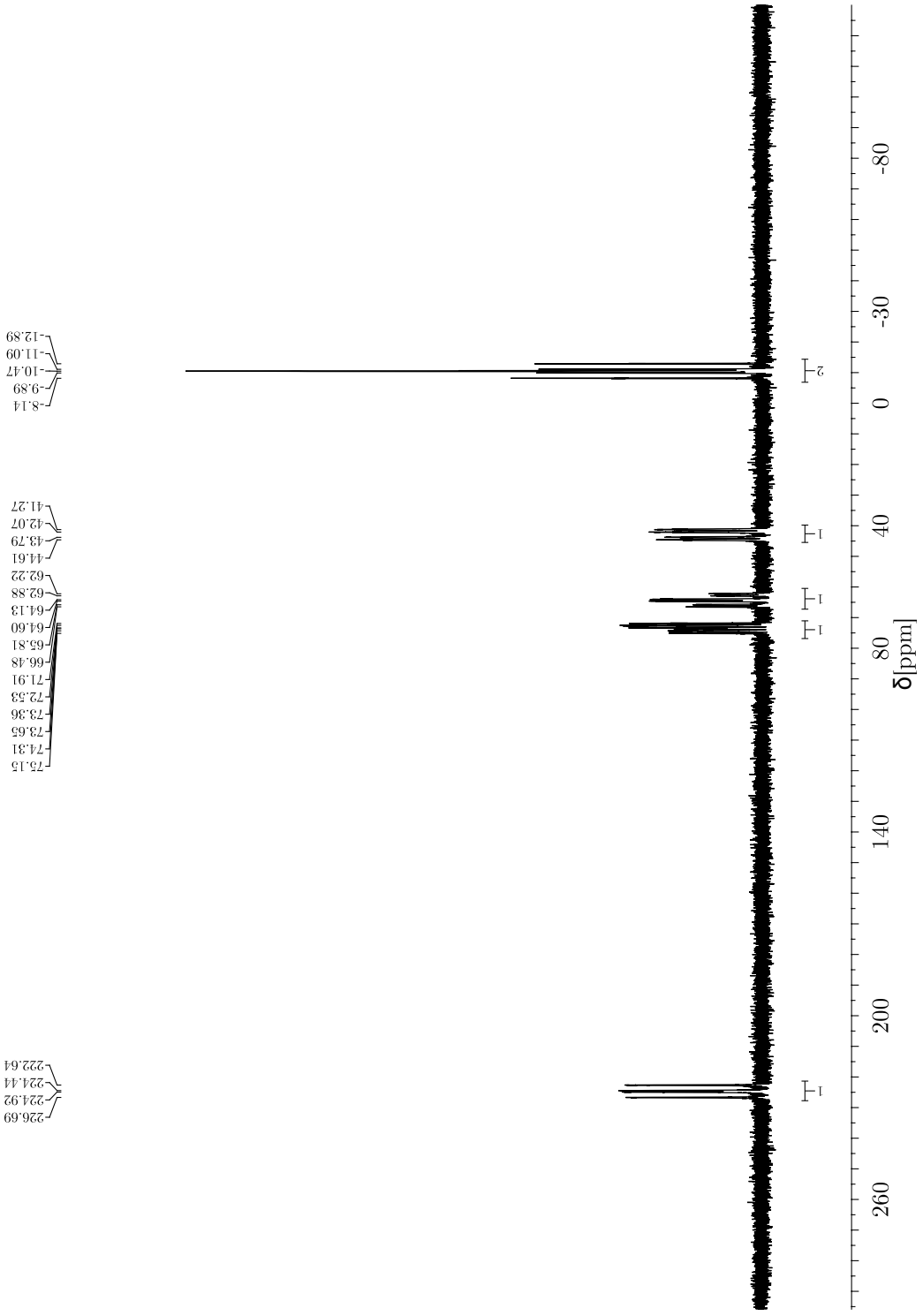


Figure 5.13: ^{31}P NMR spectrum of [Cp*Fe($\eta^{3:1}$-(1-Me-2-PPh$_2$-P$_5$))] (**11a**) at room temperature in C_6D_6.

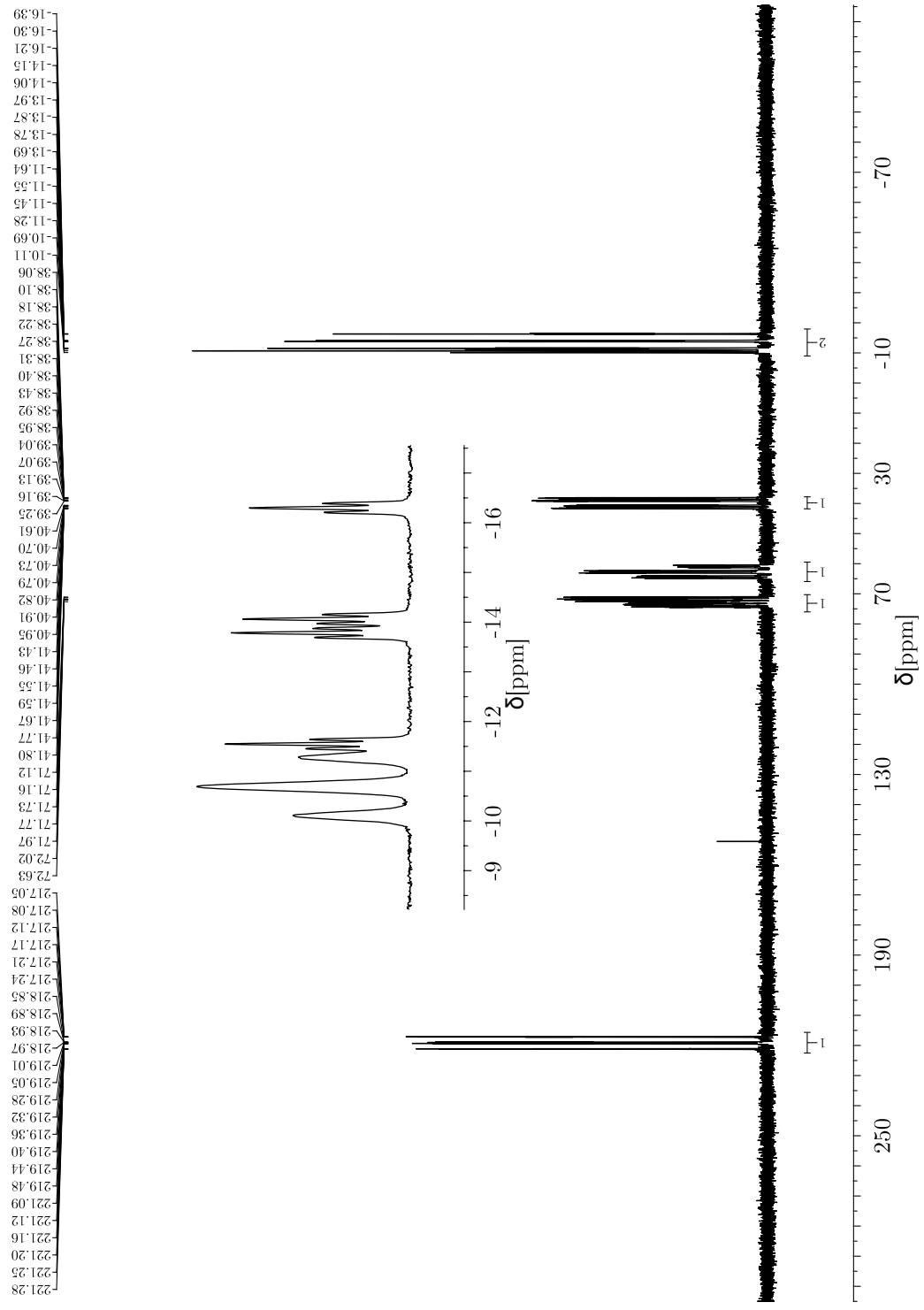


Figure 5.14: $^{31}P\{^{1}H\}$ NMR spectrum of [$Cp^*Fe(\eta^{3:1}$-(1-Me-2-PPh_2-P_5))] (**11a**) at room temperature in CD_2Cl_2. The singlet at 152 ppm can be assigned to residual **XXVII**.

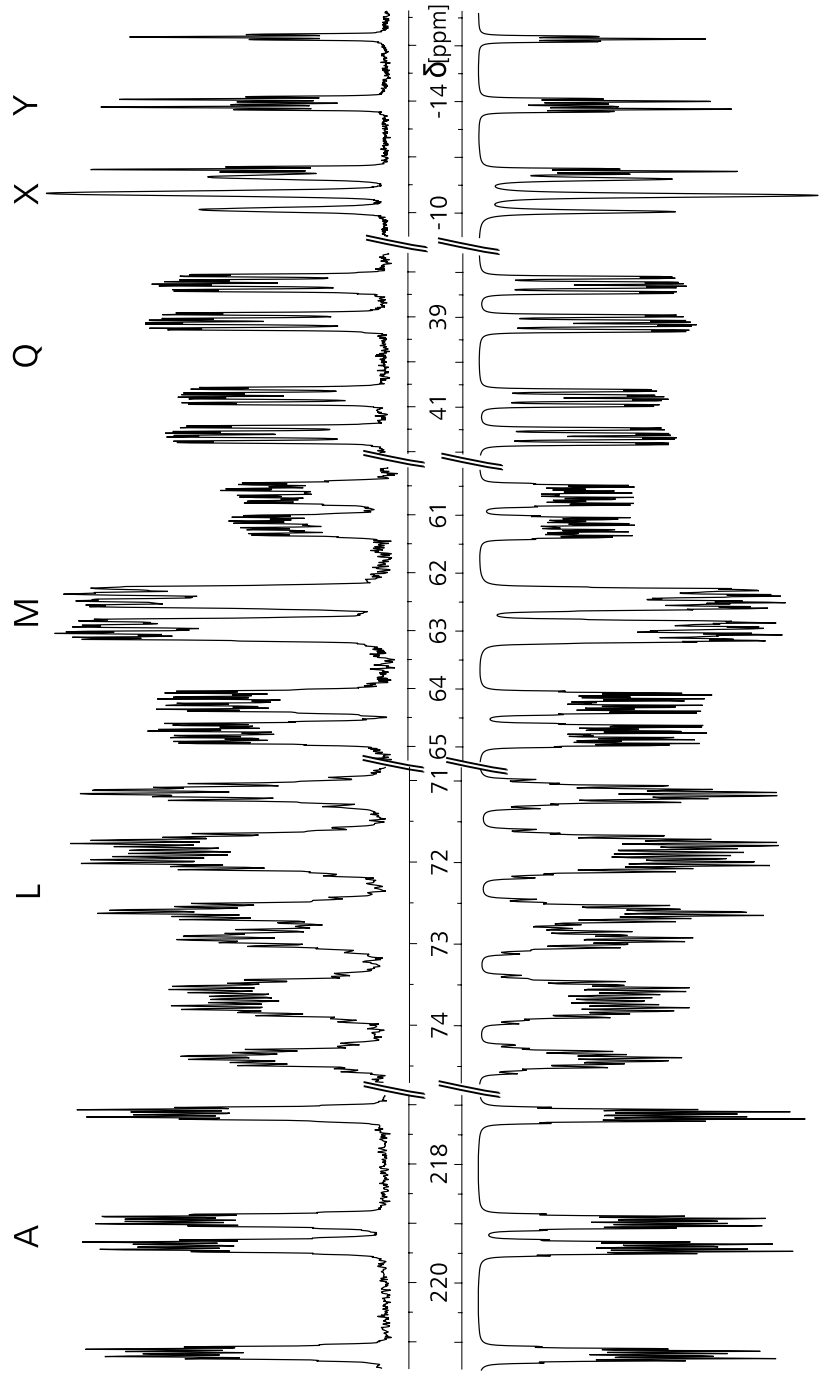


Figure 5.15: ^{31}P NMR spectrum (excerpts) of [Cp*Fe($\eta^{3:1}$-(1-Me-2-PPh$_2$-P$_5$))] (**11a**) at room temperature in CD_2Cl_2 with simulation of the spin system (inverted).

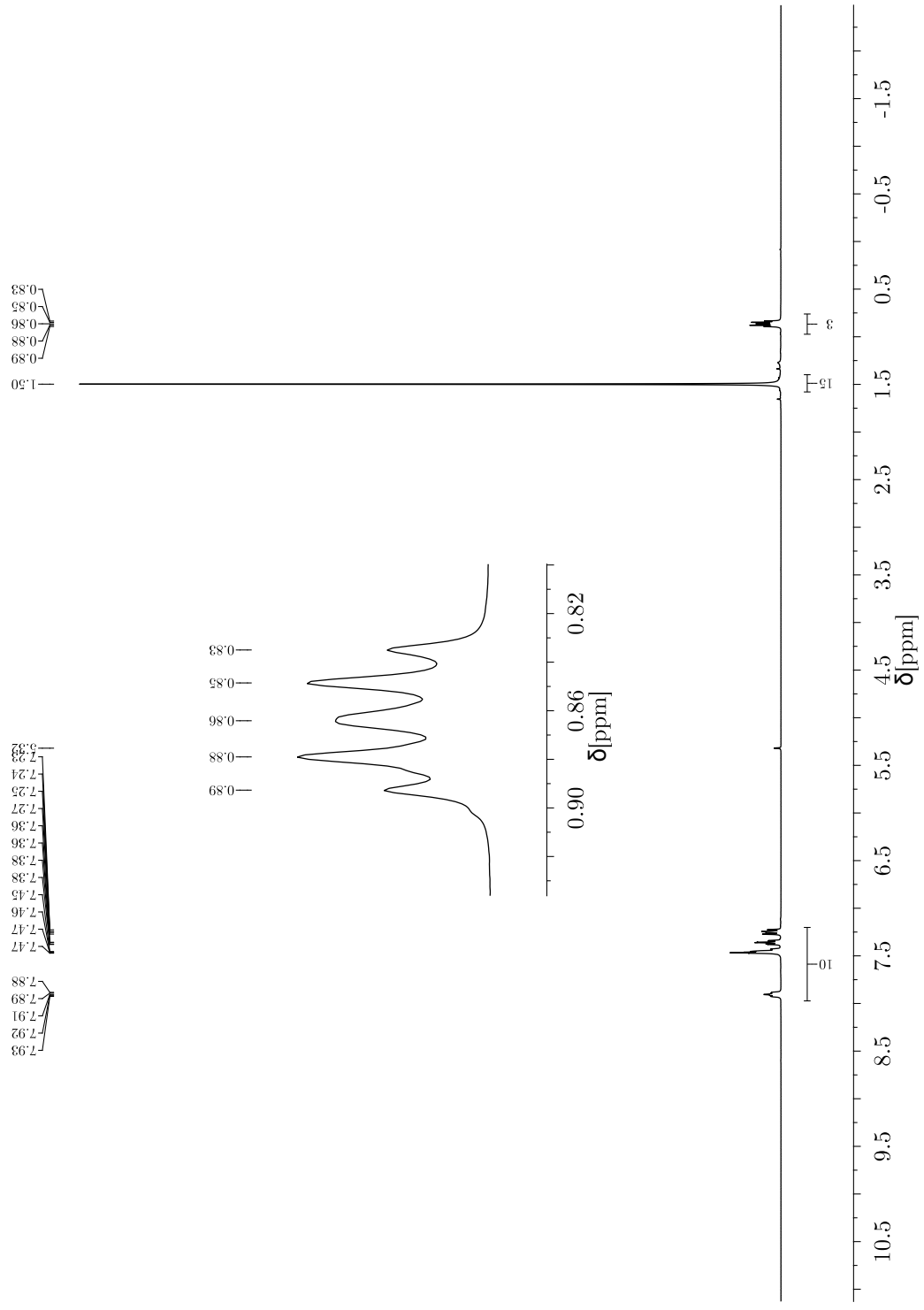


Figure 5.16: ^{1}H NMR spectrum of [Cp*Fe($\eta^{3:1}$-(1-Me-2-PPh$_2$-P$_5$))] (**11a**) at room temperature in CD_2Cl_2. The singulet at 5.32 ppm corresponds to residual CH_2Cl_2 from the deuterated solvent.

NMR spectra of [$Cp^*Fe(\eta^{3:1}$-(1-^{t}Bu-2-PPh_2-P_5))] (11b)

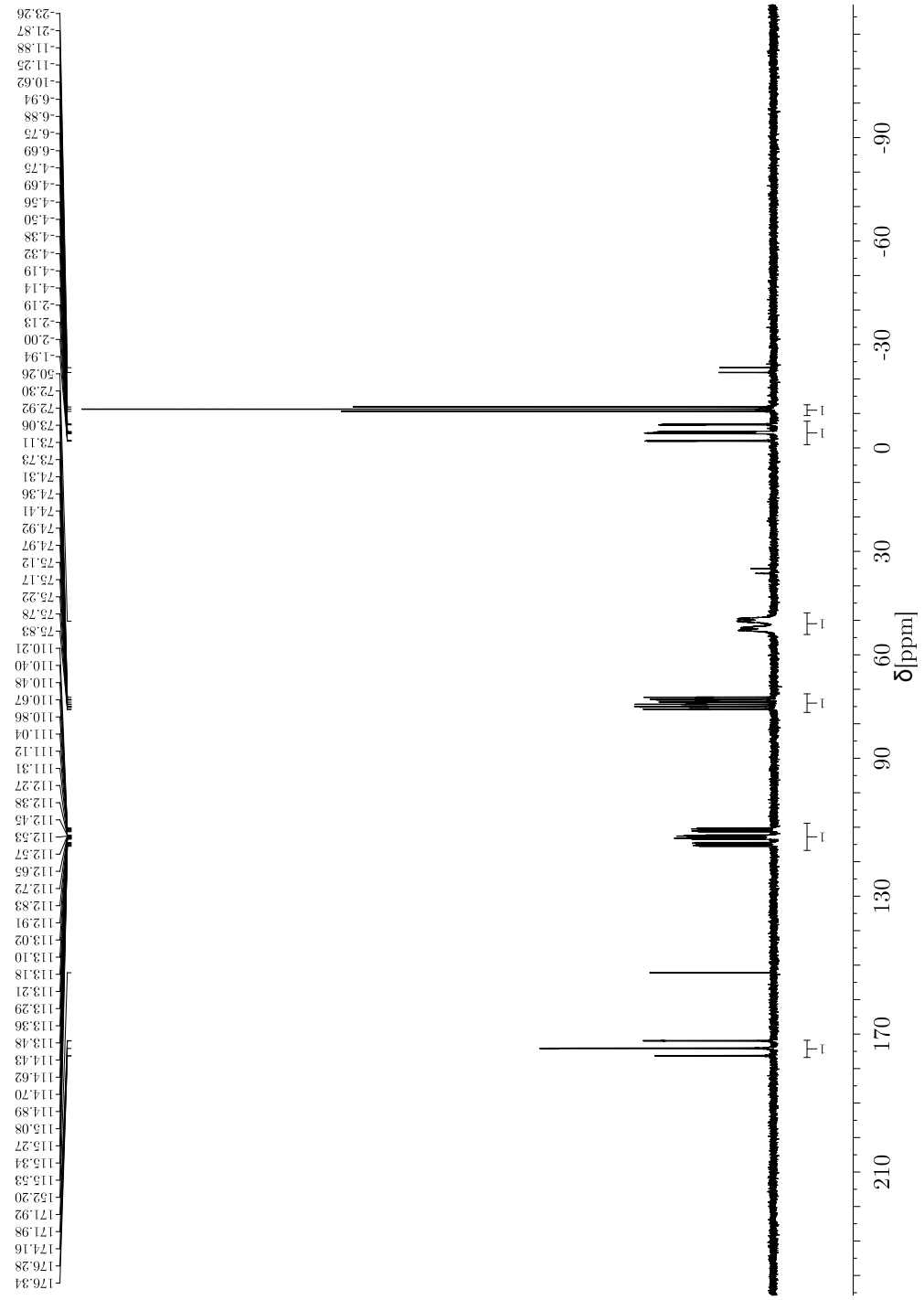


Figure 5.17: $^{31}P\{^1H\}$ NMR spectrum of [$Cp^*Fe(\eta^{3:1}$-(1-^{t}Bu-2-PPh_2-P_5))] (**11b**) at room temperature in CD_2Cl_2. The singlet at 152 ppm can be assigned to residual **XXVII**.

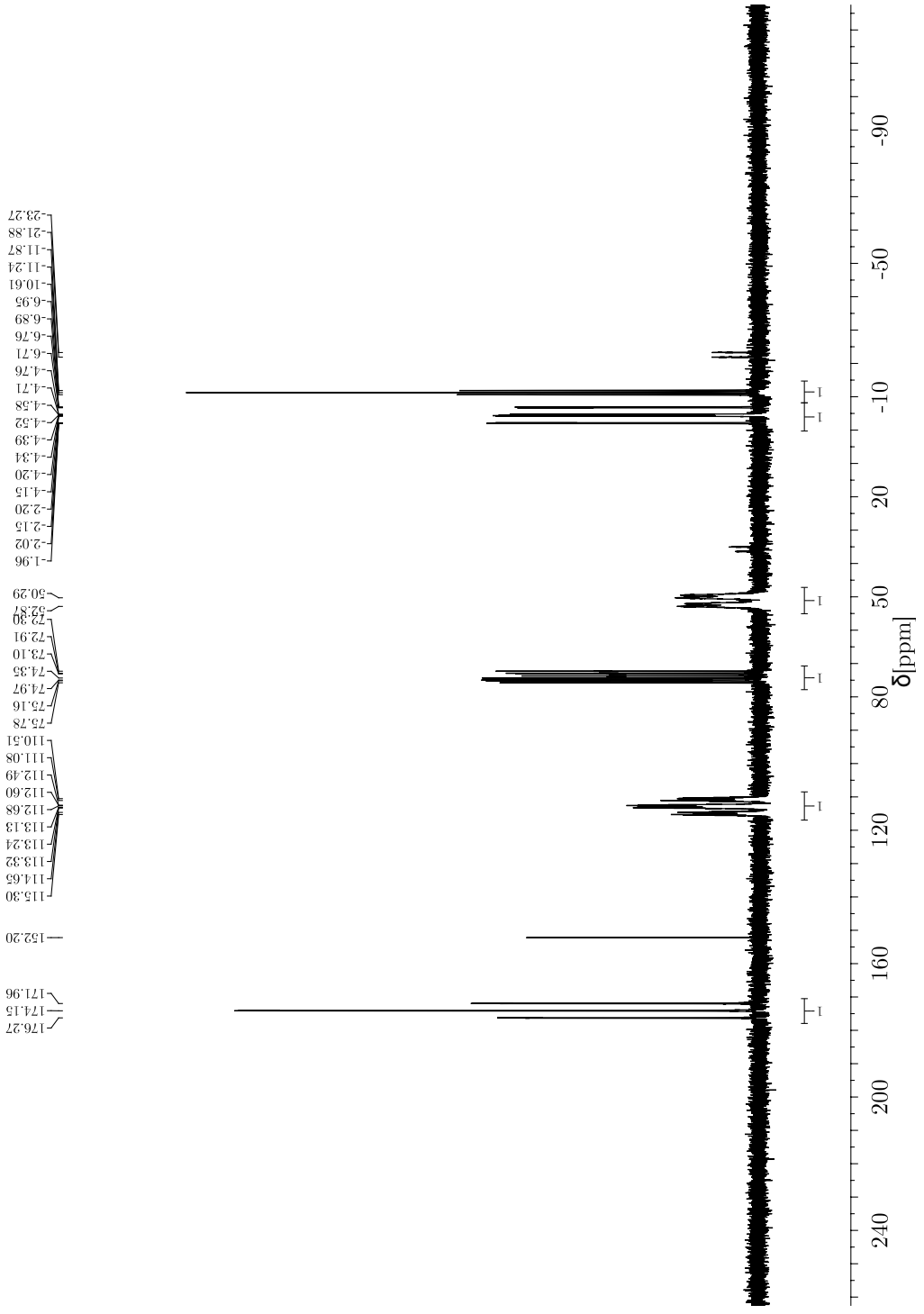


Figure 5.18: ^{31}P NMR spectrum of [Cp*Fe($\eta^{3:1}$-(1-^{t}Bu-2-PPh$_2$-P$_5$))] (**11b**) at room temperature in CD_2Cl_2. The singlet at 152 ppm can be assigned to residual **XXVII**.

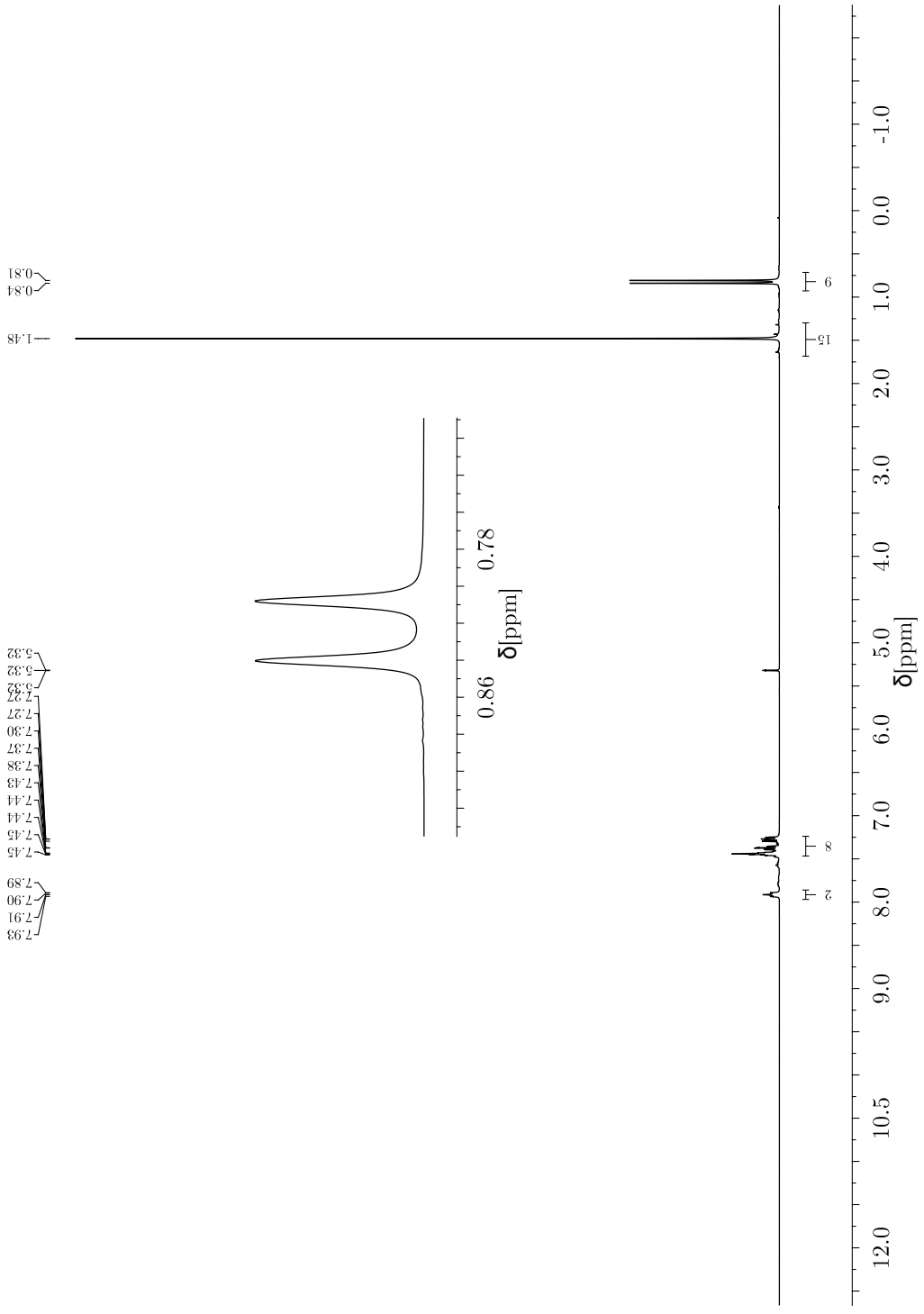


Figure 5.19: ^{1}H NMR spectrum of [Cp*Fe($\eta^{3:1}$-(1-^{t}Bu-2-PPh$_2$-P$_5$))] (**11b**) at room temperature in CD_2Cl_2. The singlet at 5.32 ppm corresponds to residual CH_2Cl_2 from the deuterated solvent.

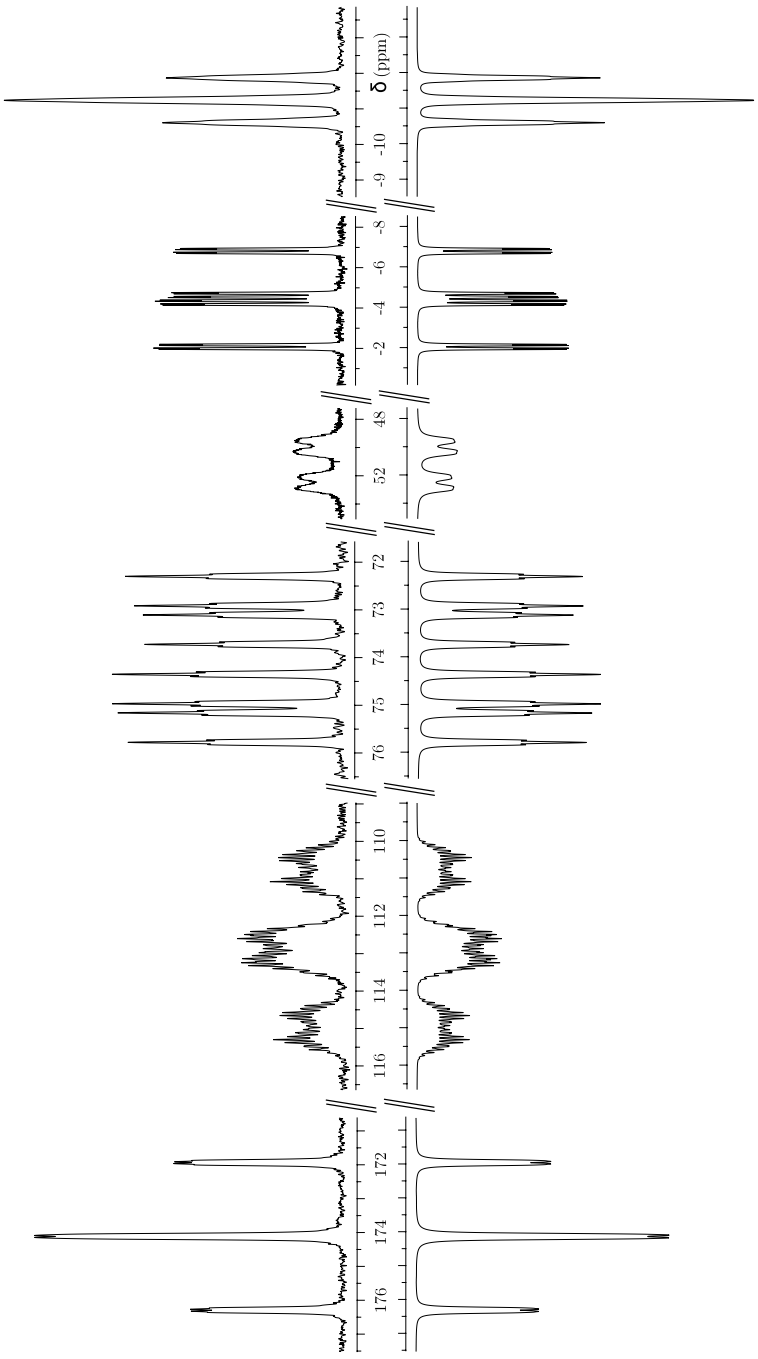


Figure 5.20: ^{31}P NMR spectrum (excerpts) of [Cp*Fe($\eta^{3:1}$-(1-^{t}Bu-2-PPh$_2$-P$_5$))] (**11b**) at room temperature in CD_2Cl_2 with simulation of the spin system (inverted).

[Cp*Fe(η^4-(1, 1-CH_3-PPh_2–P_5))] (10)

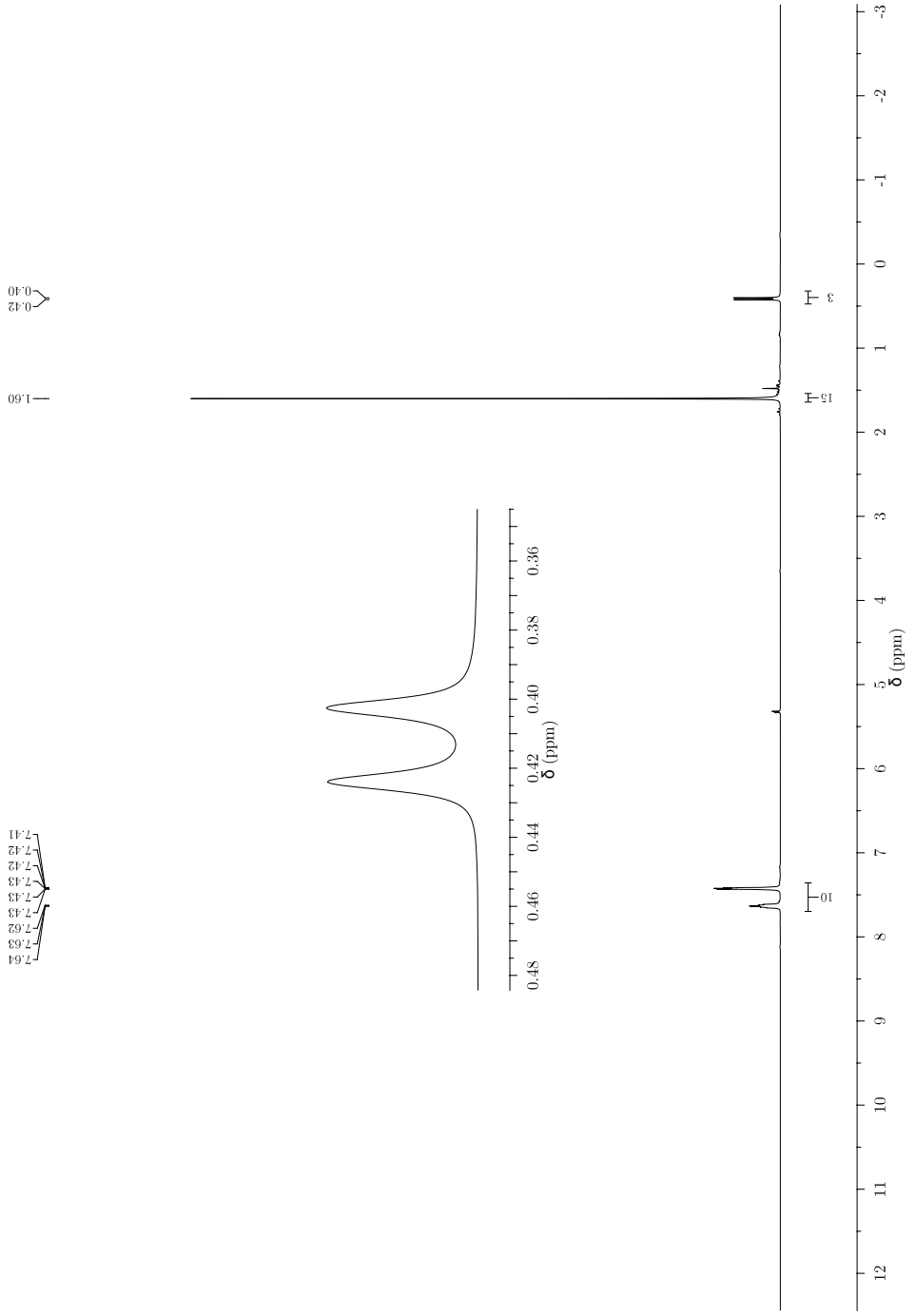


Figure 5.21: ^{1}H NMR spectrum of [Cp*Fe(η^4-(1, 1-CH_3-PPh_2–P_5))] (**10**) at -30 ℃ in CD_2Cl_2.

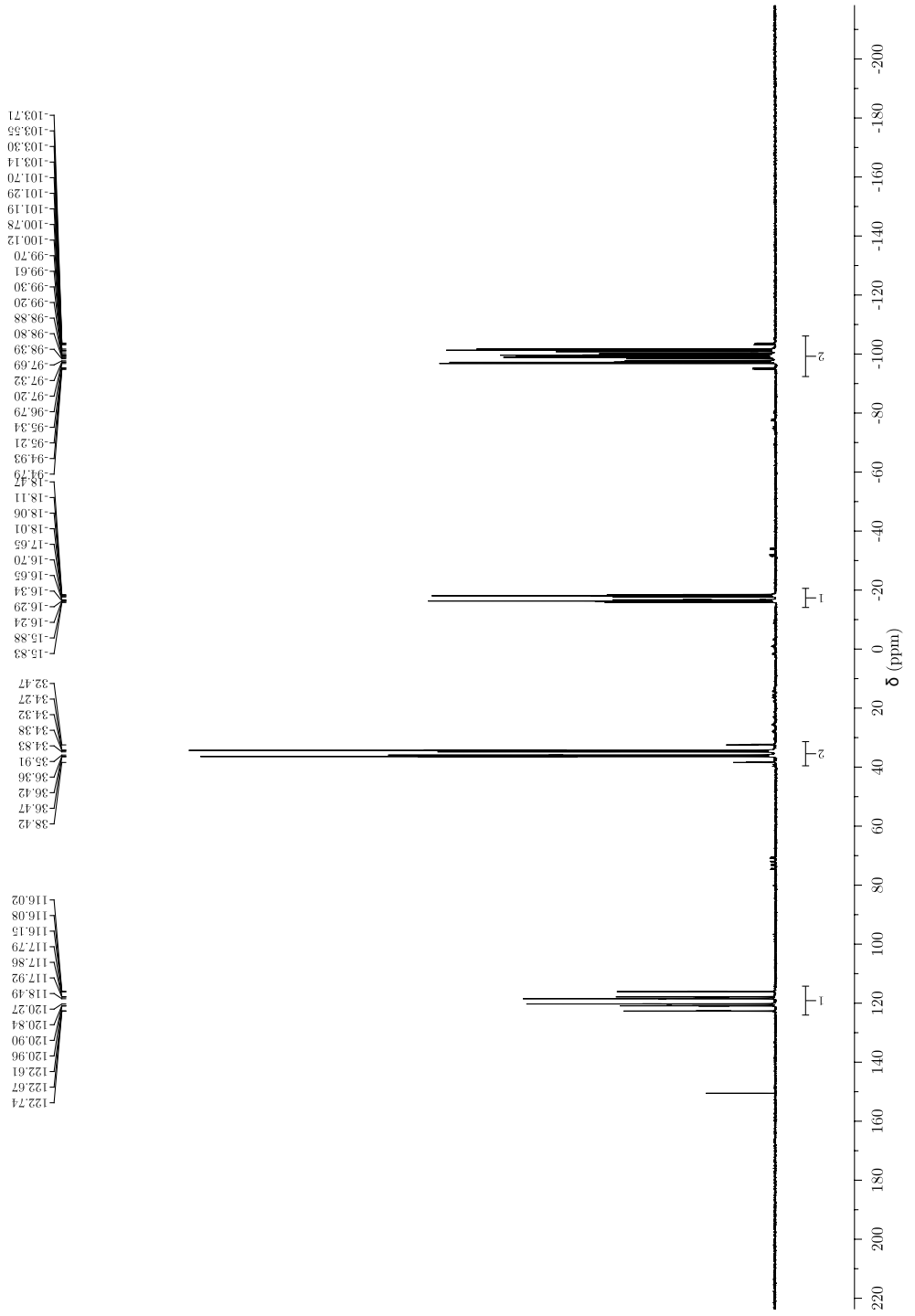


Figure 5.22: $^{31}P\{^{1}H\}$ NMR spectrum of [$Cp^*Fe(\eta^4$-$(1,1$-CH_3-PPh_2–$P_5))$] (**10**) at -30 ℃ in CD_2Cl_2. The singlet at 152 ppm can be assigned to residual **XXVII**.

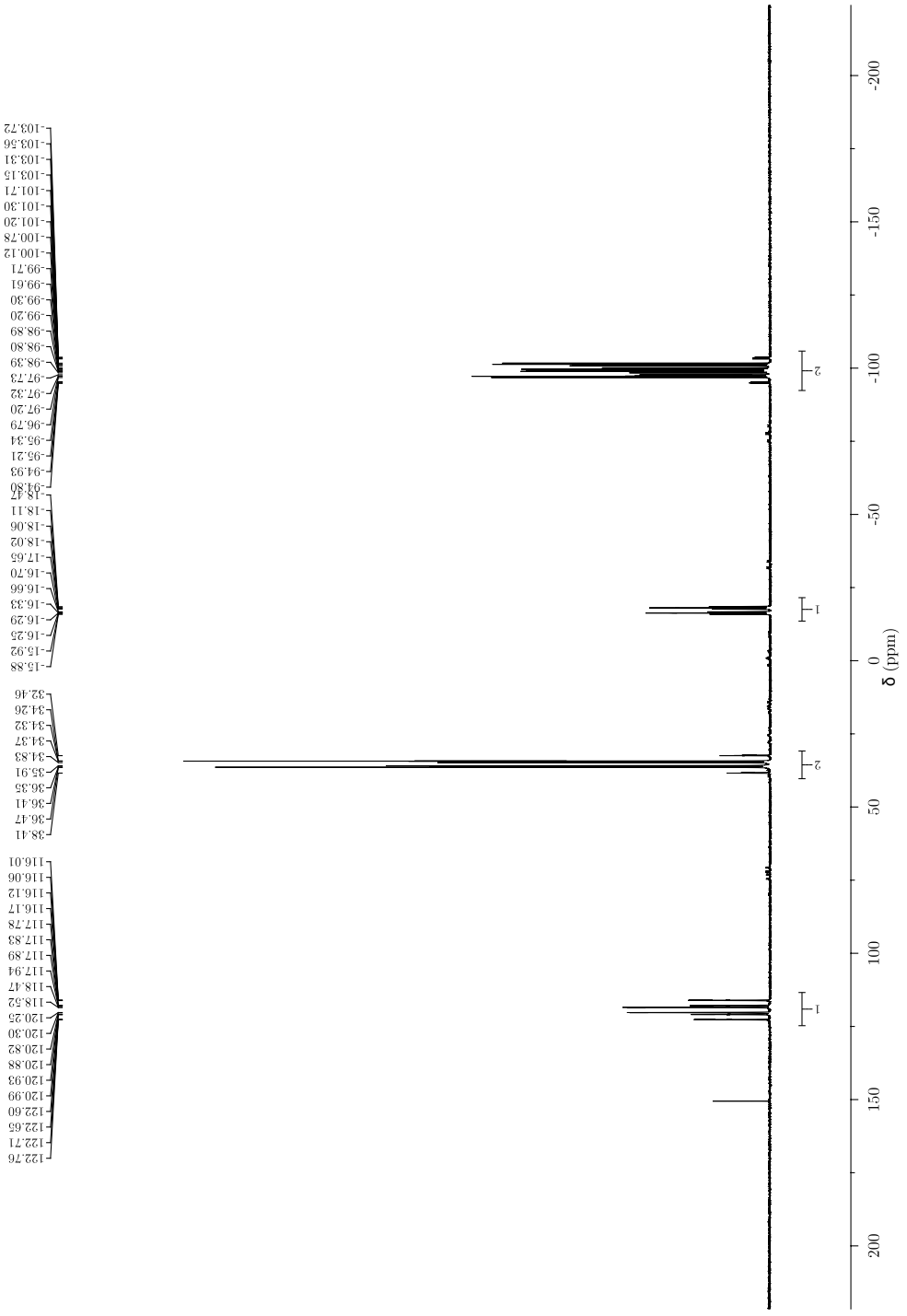


Figure 5.23: $^{31}P\{^{1}H\}$ NMR spectrum of [Cp*Fe(η^4-(1, 1-CH_3-PPh_2–P_5))] (**10**) at -30 ℃ in CD_2Cl_2. The singlet at 152 ppm can be assigned to residual **XXVII**.

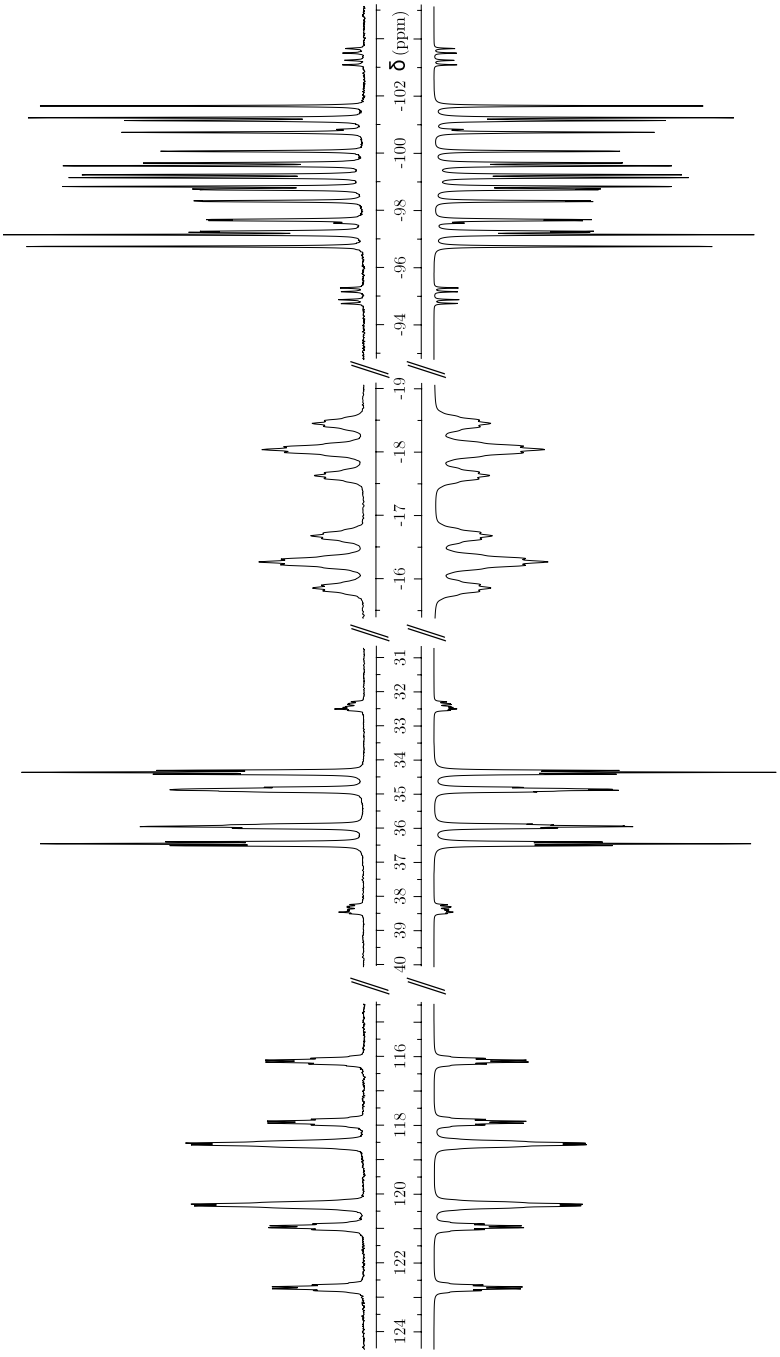


Figure 5.24: $^{31}P\{^{1}H\}$ NMR spectrum (excerpts) of [Cp*Fe(η^4-(1,1-CH_3-PPh_2–P_5))] (**10**) at -30 ℃ in CD_2Cl_2 with simulation of the spin system (inverted).

NMR spectra of endo-[Cp*Fe(η^4-(1-Me-1-PCy$_2$-P$_5$))] (12a)

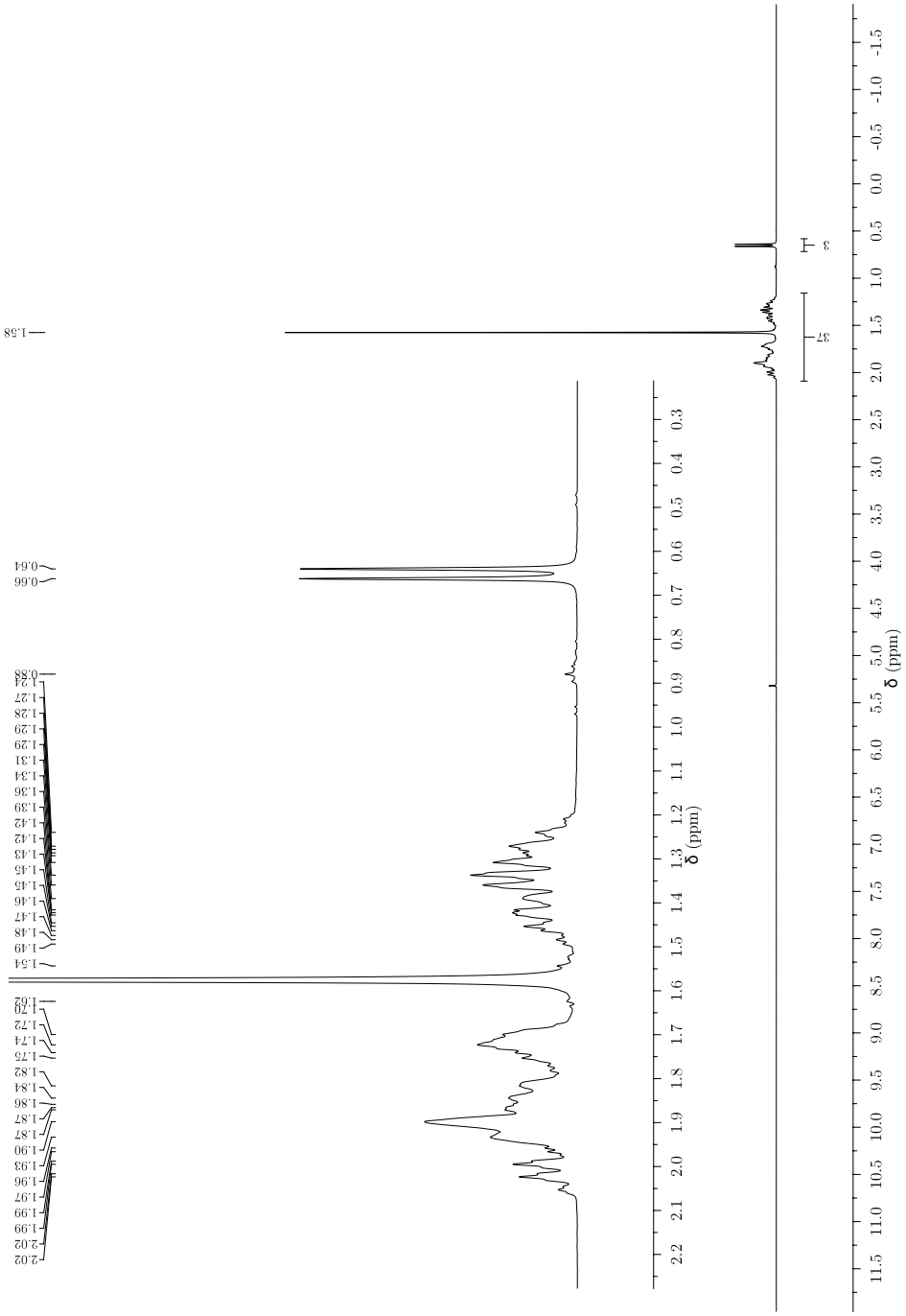


Figure 5.25: ^{1}H NMR spectrum of endo-[Cp*Fe(η^4-(1-Me-1-PCy$_2$-P$_5$))] (**12a**) at room temperature in CD_2Cl_2.

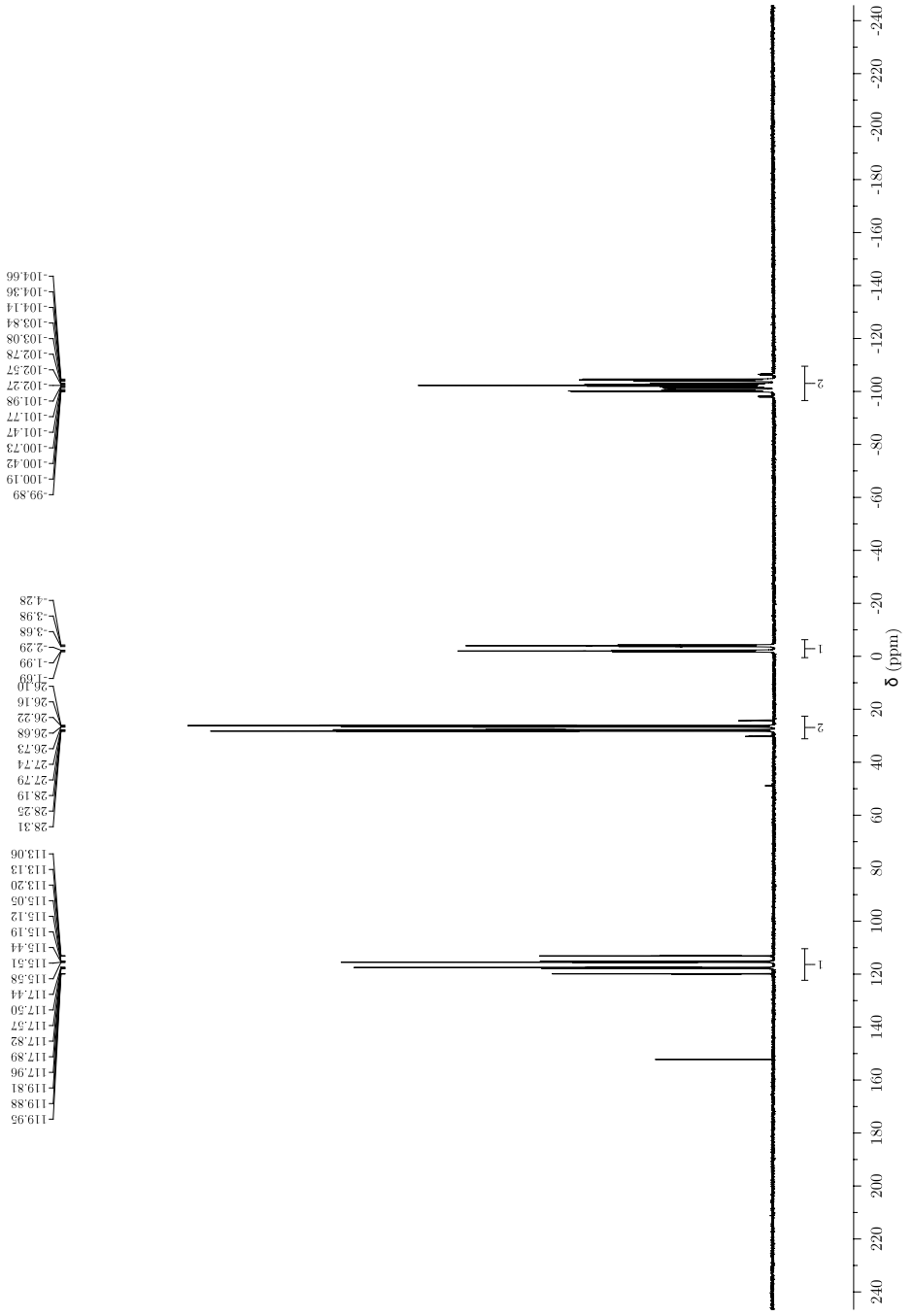


Figure 5.26: $^{31}P\{^{1}H\}$ NMR spectrum of endo-[Cp*Fe(η^4-(1-Me-1-PCy$_2$-P$_5$))] (**12a**) at room temperature in CD_2Cl_2. The singlet at 152 ppm can be assigned to residual **XXVII**.

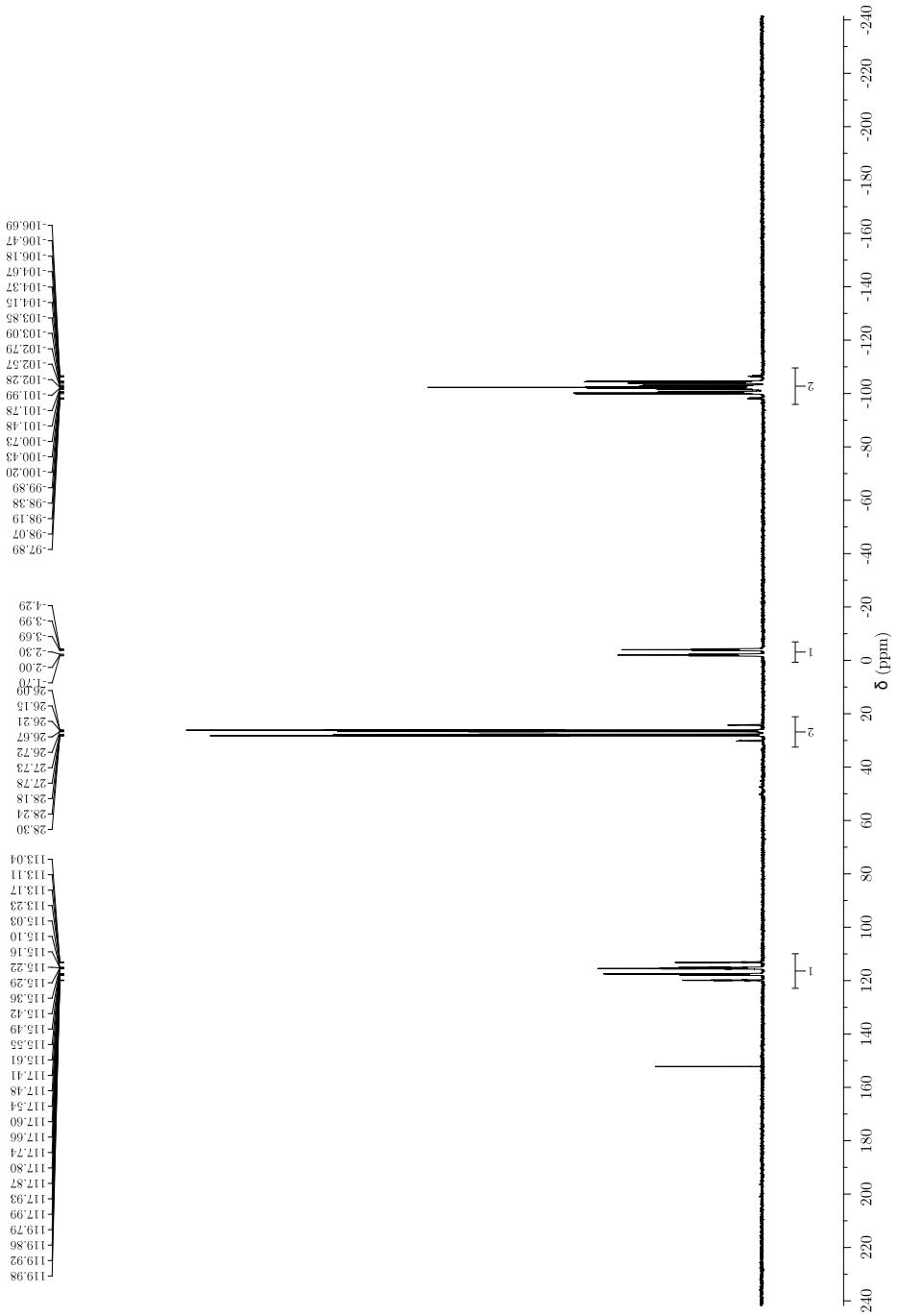


Figure 5.27: ^{31}P NMR spectrum of endo-[Cp*Fe(η^4-(1-Me-1-PCy$_2$-P$_5$))] (**12a**) at room temperature in CD_2Cl_2. The singlet at 152 ppm can be assigned to residual **XXVII**.

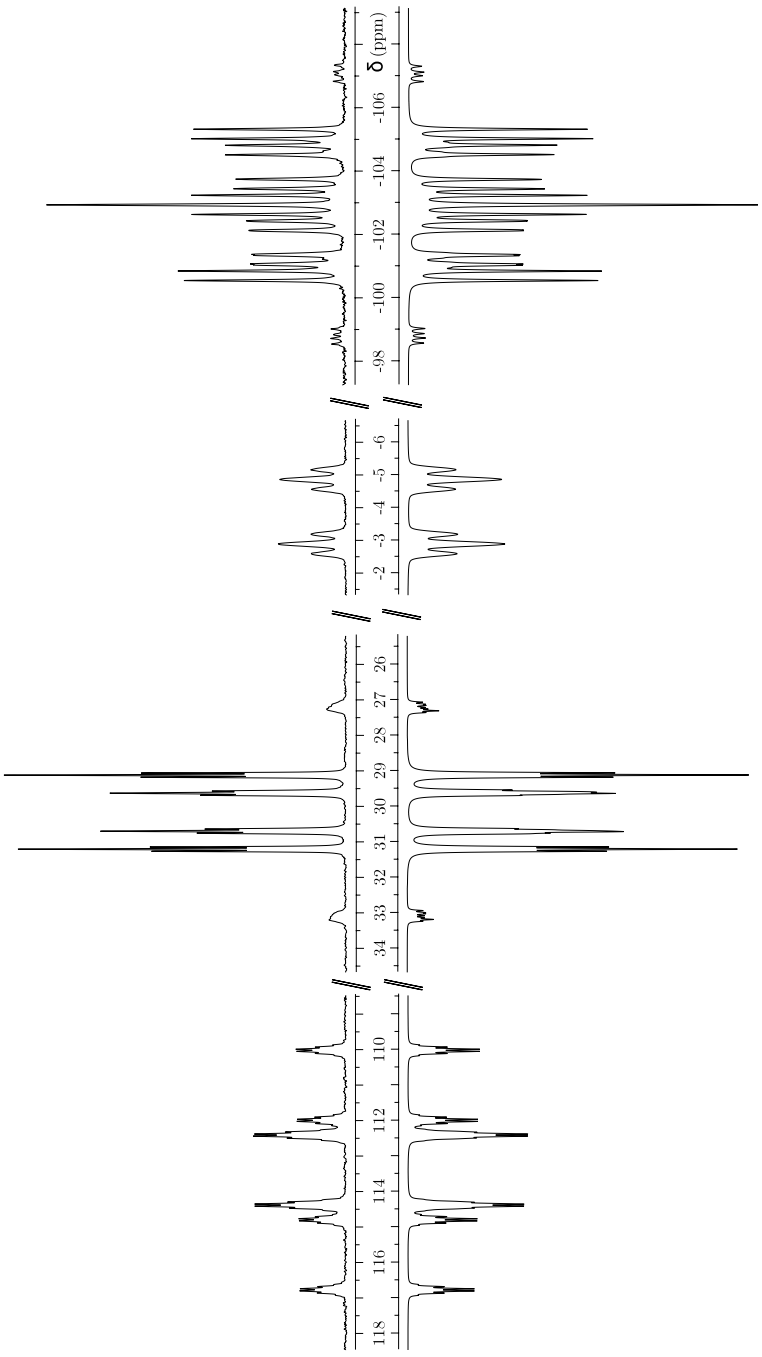


Figure 5.28: ^{31}P NMR spectrum (excerpts) of endo-[Cp*Fe(η^4-(1-Me-1-PCy$_2$-P$_5$))] (**12a**) at room temperature in CD_2Cl_2 with simulation of the spin system (inverted).

exo-[Cp*Fe(η^4-(1,1-CH$_3$-PCy$_2$–P$_5$))] (12b)

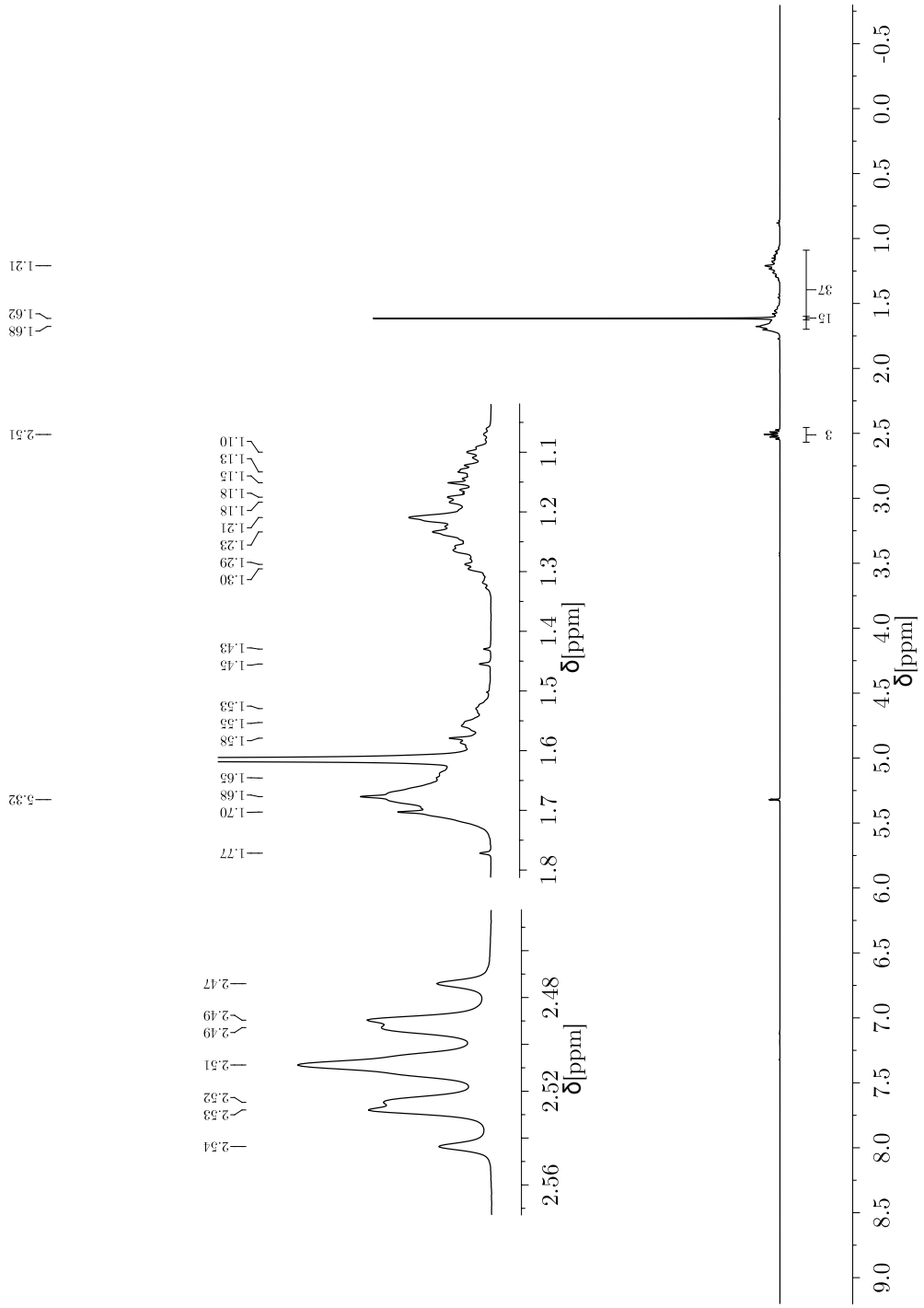


Figure 5.29: ^{1}H NMR spectrum of exo-[Cp*Fe(η^4-(1,1-CH$_3$-PCy$_2$–P$_5$))] (**12b**) at room temperature in CD_2Cl_2.

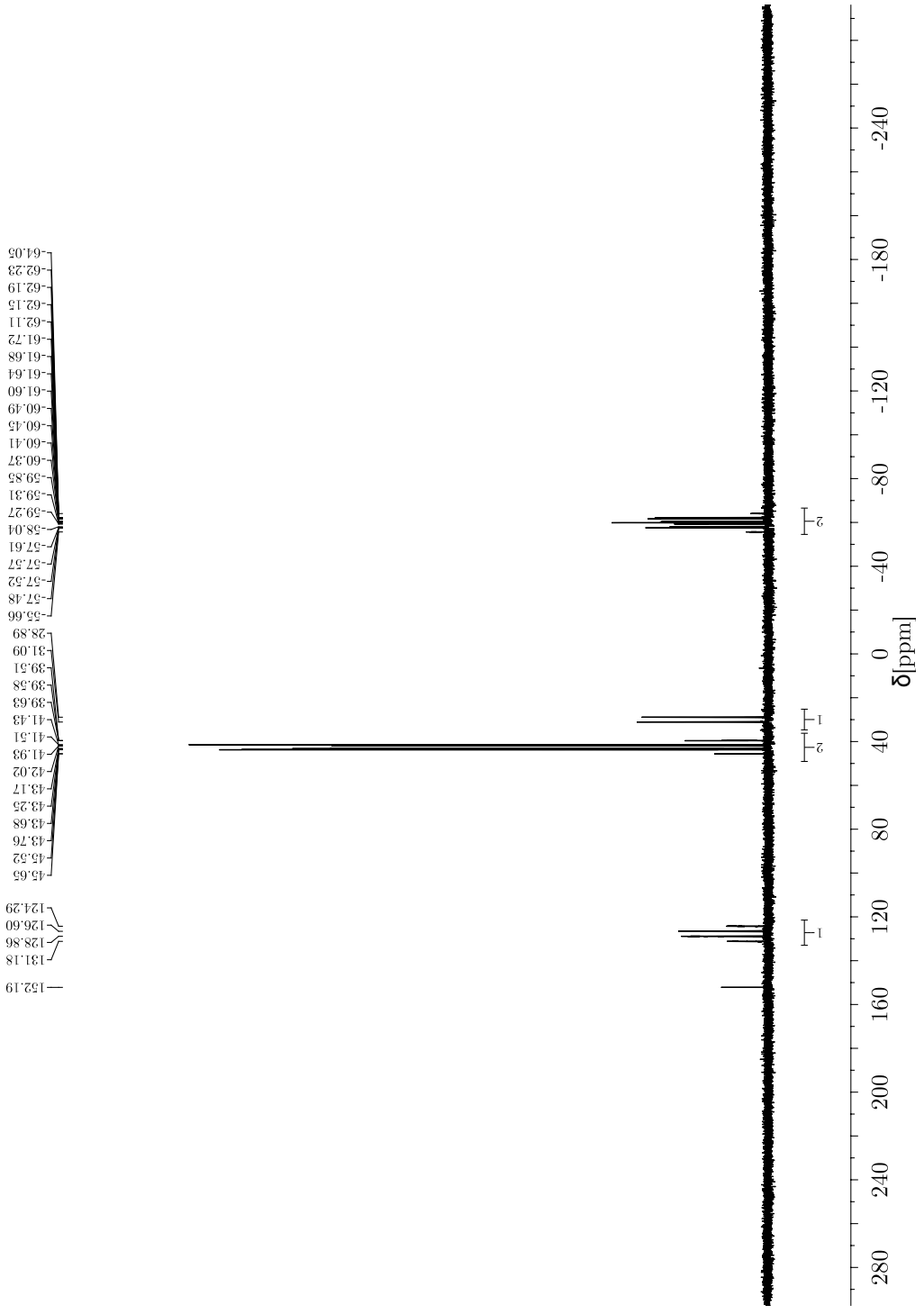


Figure 5.30: $^{31}P\{^{1}H\}$ NMR spectrum of exo-[$Cp^*Fe(\eta^4$-$(1,1$-CH_3-PCy_2–$P_5))$] (**12b**) at room temperature in CD_2Cl_2. The singlet at 152 ppm can be assigned to residual **XXVII**.

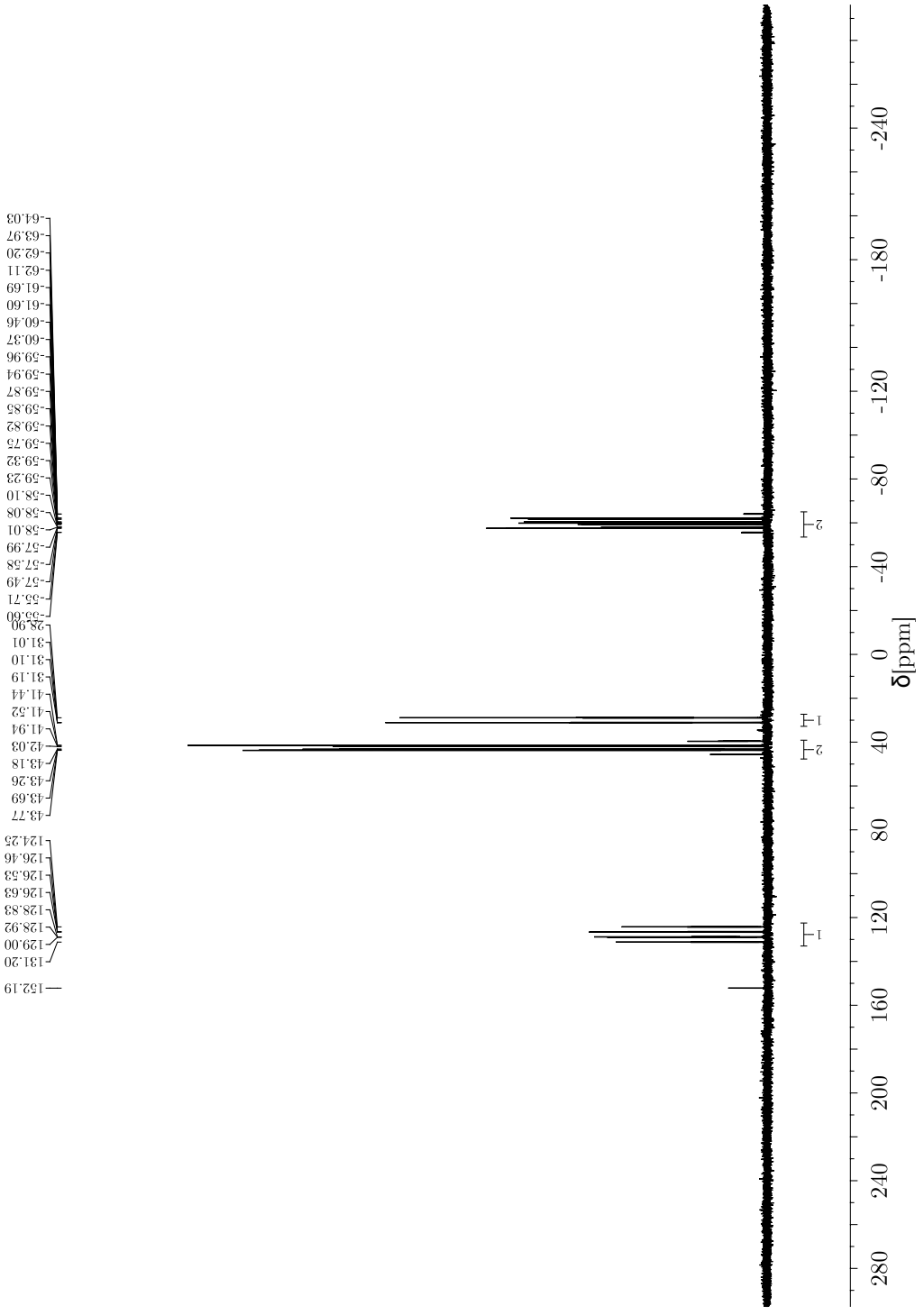


Figure 5.31: ^{31}P NMR spectrum of exo-[Cp*Fe(η^4-(1, 1-CH_3-PCy_2–P_5))] (**12b**) at room temperature in CD_2Cl_2. The singlet at 152 ppm can be assigned to residual **XXVII**.

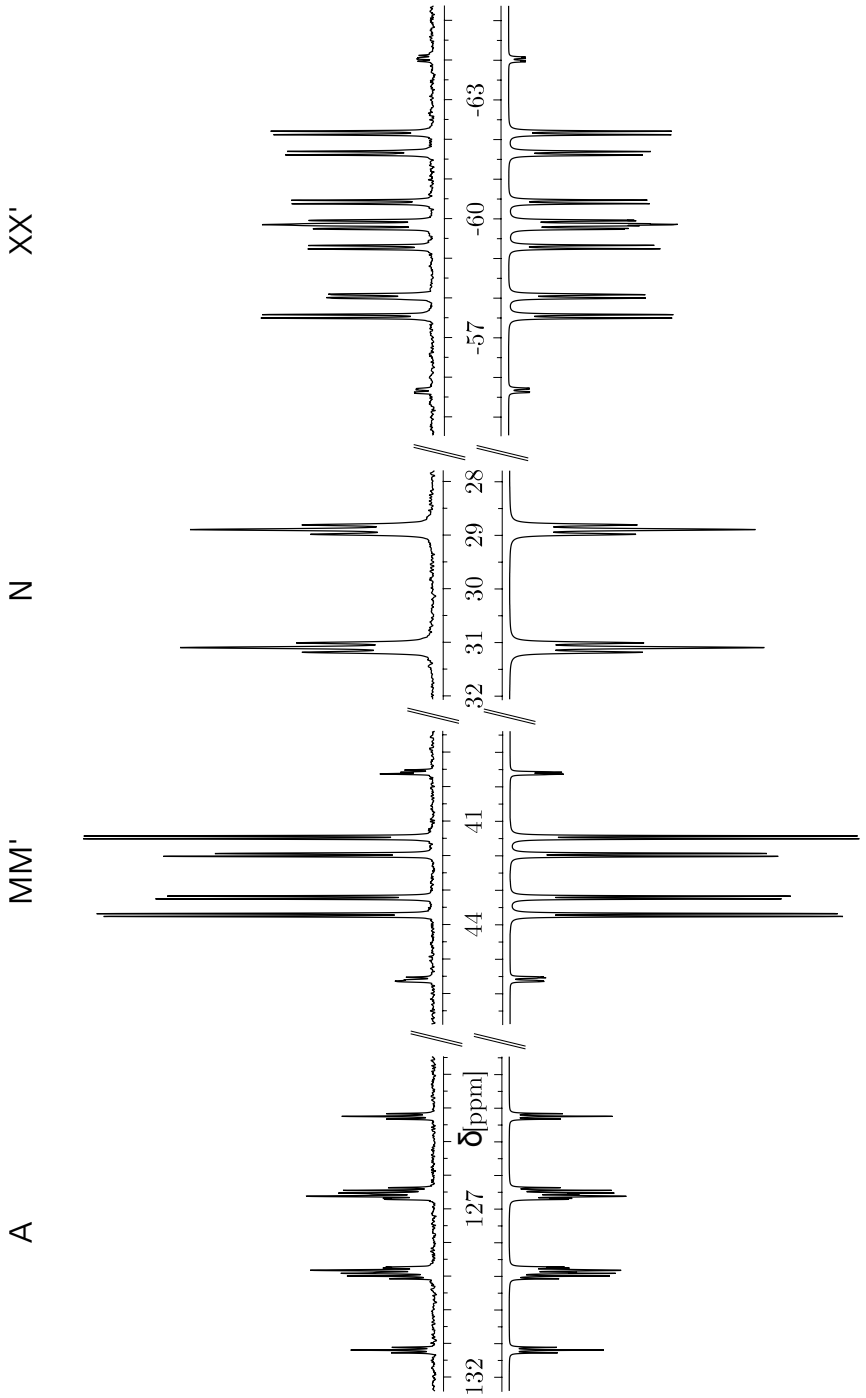


Figure 5.32: ^{31}P NMR spectrum (excerpts) of exo-[Cp*Fe(η^4-(1,1-CH_3-PCy_2–P_5))] (**12b**) at room temperature in CD_2Cl_2 with simulation of the spin system (inverted).

[Cp*Fe($\eta^{1:1:1}$-(1-^{t}Bu-2-PPh$_2$-3-Me-4-PCy$_2$-P$_5$))] (13)

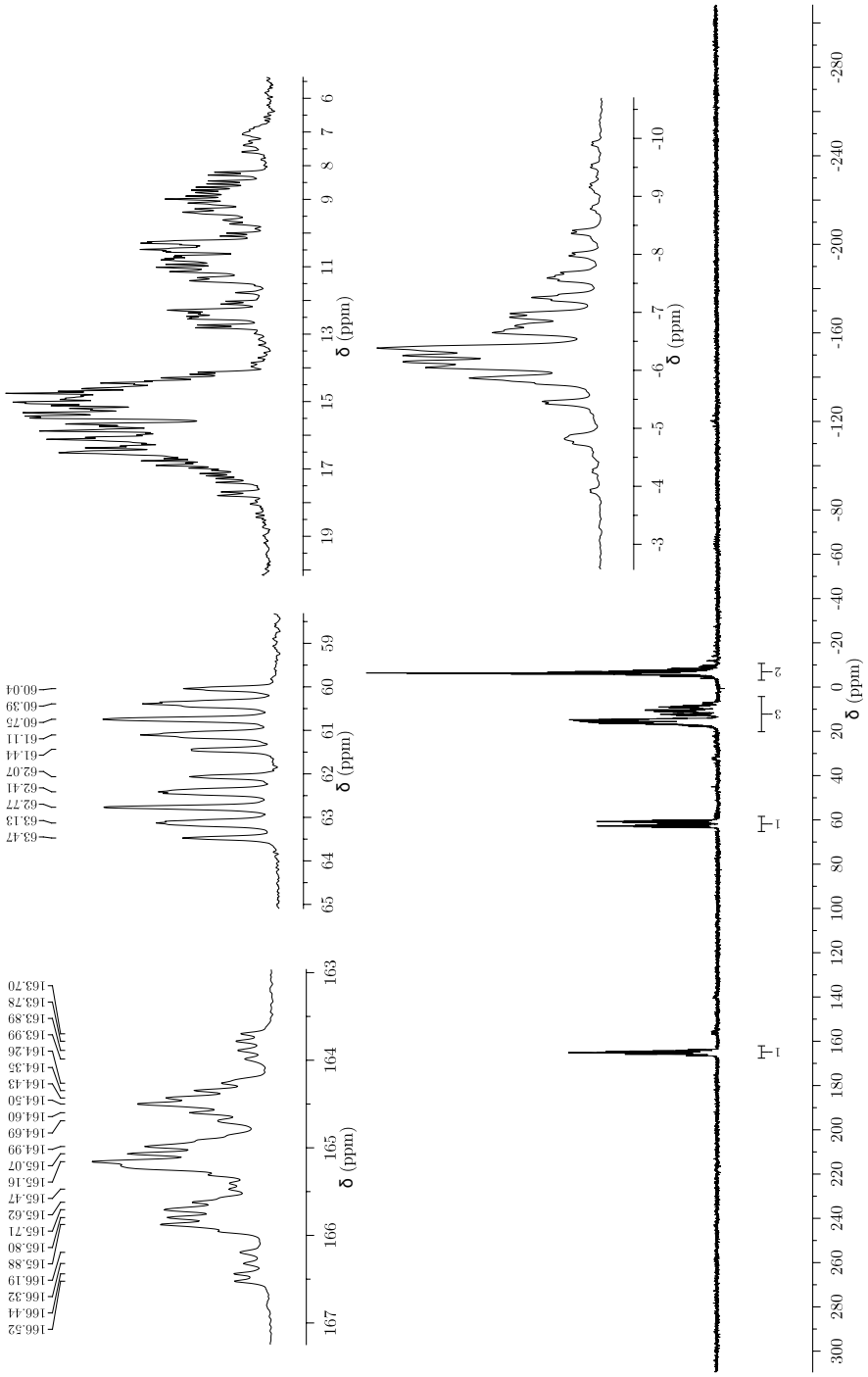


Figure 5.33: $^{31}P\{^1H\}$ NMR spectrum of [Cp*Fe($\eta^{1:1:1}$-(1-^{t}Bu-2-PPh$_2$-3-Me-4-PCy$_2$-P$_5$))] (**13**) at room temperature in toluene-d$_8$.

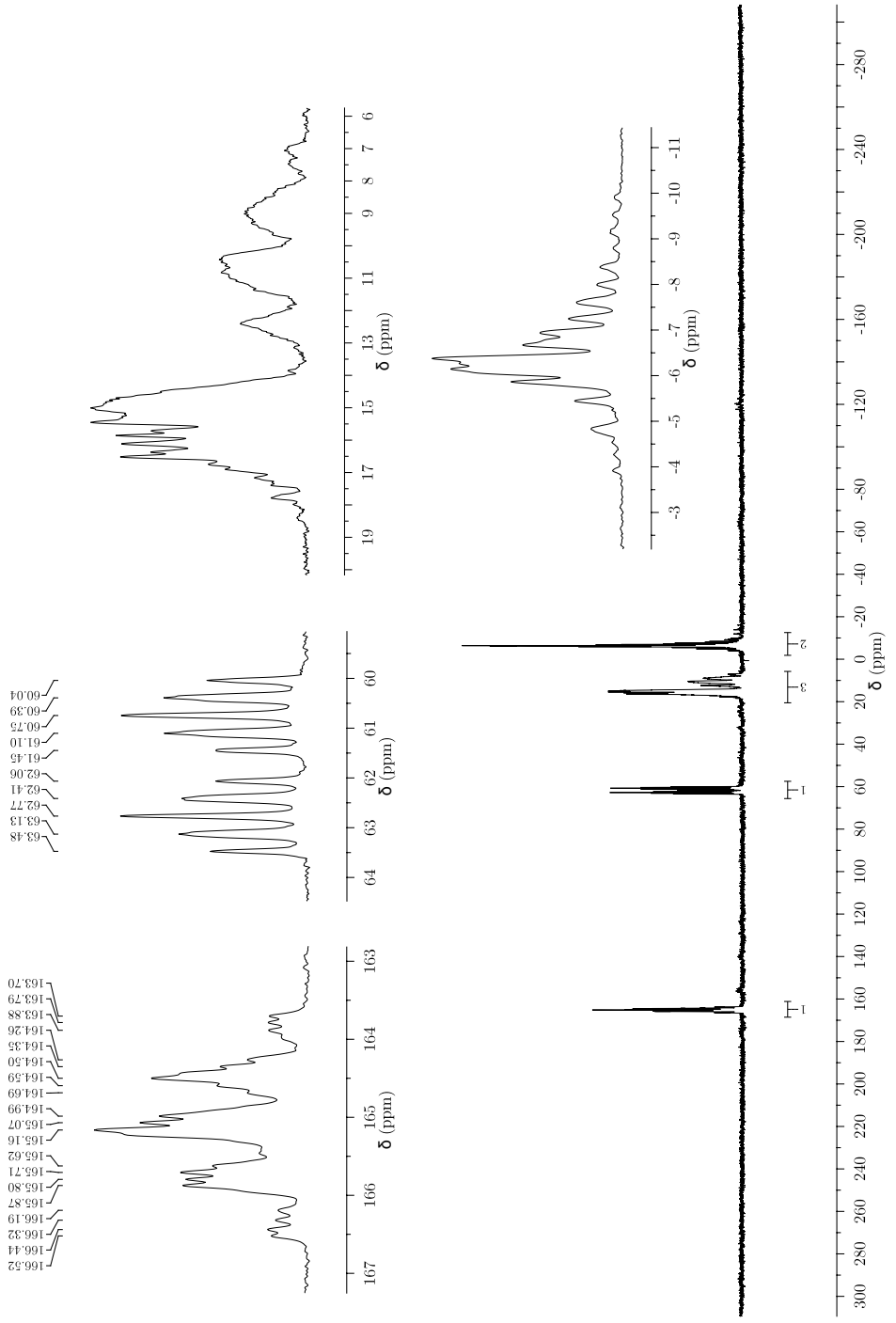


Figure 5.34: ^{31}P NMR spectrum of [Cp*Fe($\eta^{1:1:1}$-(1-^{t}Bu-2-PPh$_2$-3-Me-4-PCy$_2$-P$_5$))] (**13**) at room temperature in toluene-d$_8$.

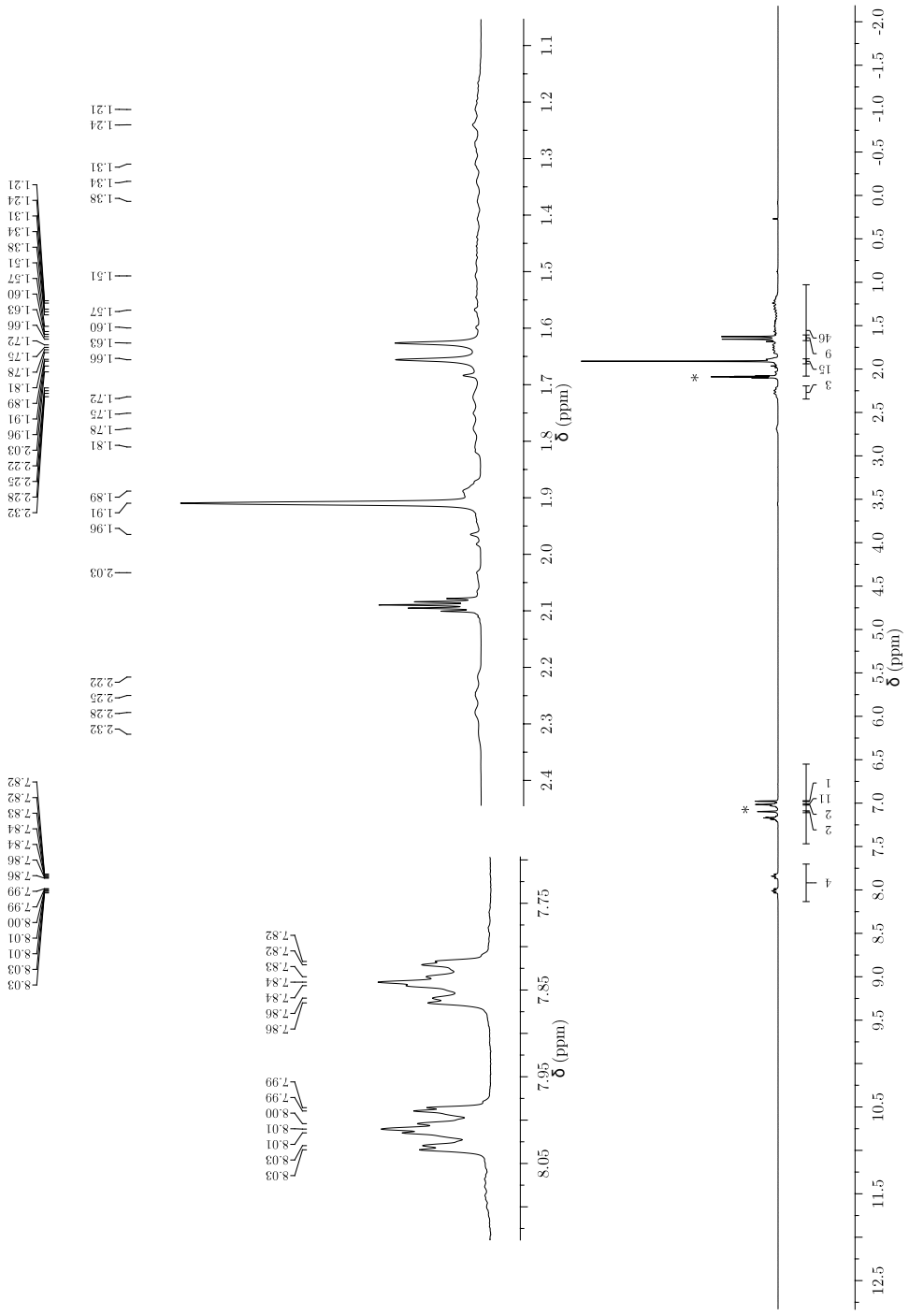


Figure 5.35: ^{1}H NMR spectrum of [Cp*Fe($\eta^{1:1:1}$-(1-^{t}Bu-2-PPh$_2$-3-Me-4-PCy$_2$-P$_5$))] (**13**) at room temperature in toluene-d$_8$. Solvent signals are marked with an asterisk.

[Cp*Fe($\eta^{1:1:1}$-(1-^{t}Bu-2-PPh$_2$-3-Me-4-PCy$_2$-P$_5$))] (13) and [Cp*Fe($\eta^{1:2}$-(1-^{t}Bu-2-PCy$_2$-3-Me-4-PPh$_2$-P$_5$))] (14) in the reaction solution.

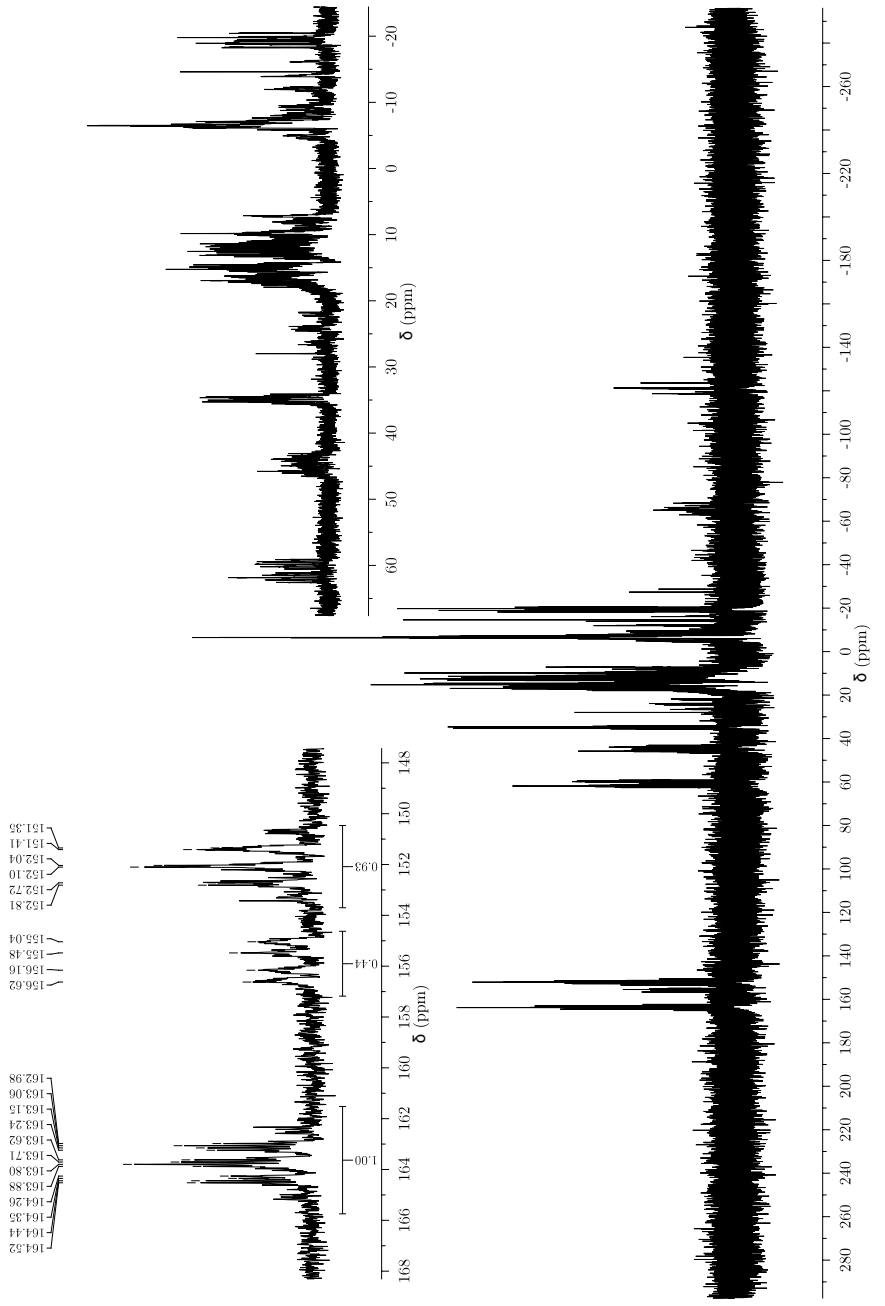


Figure 5.36: $^{31}P\{^1H\}$ NMR spectrum of the reaction solution from the reaction of **11a** with ^{t}BuLi and Cy_2PCl at room temperature in thf with D_2O capillary. With the three separated multiplets from 150 ppm to 165 ppm the ratios of the three reaction products can be roughly quantified.

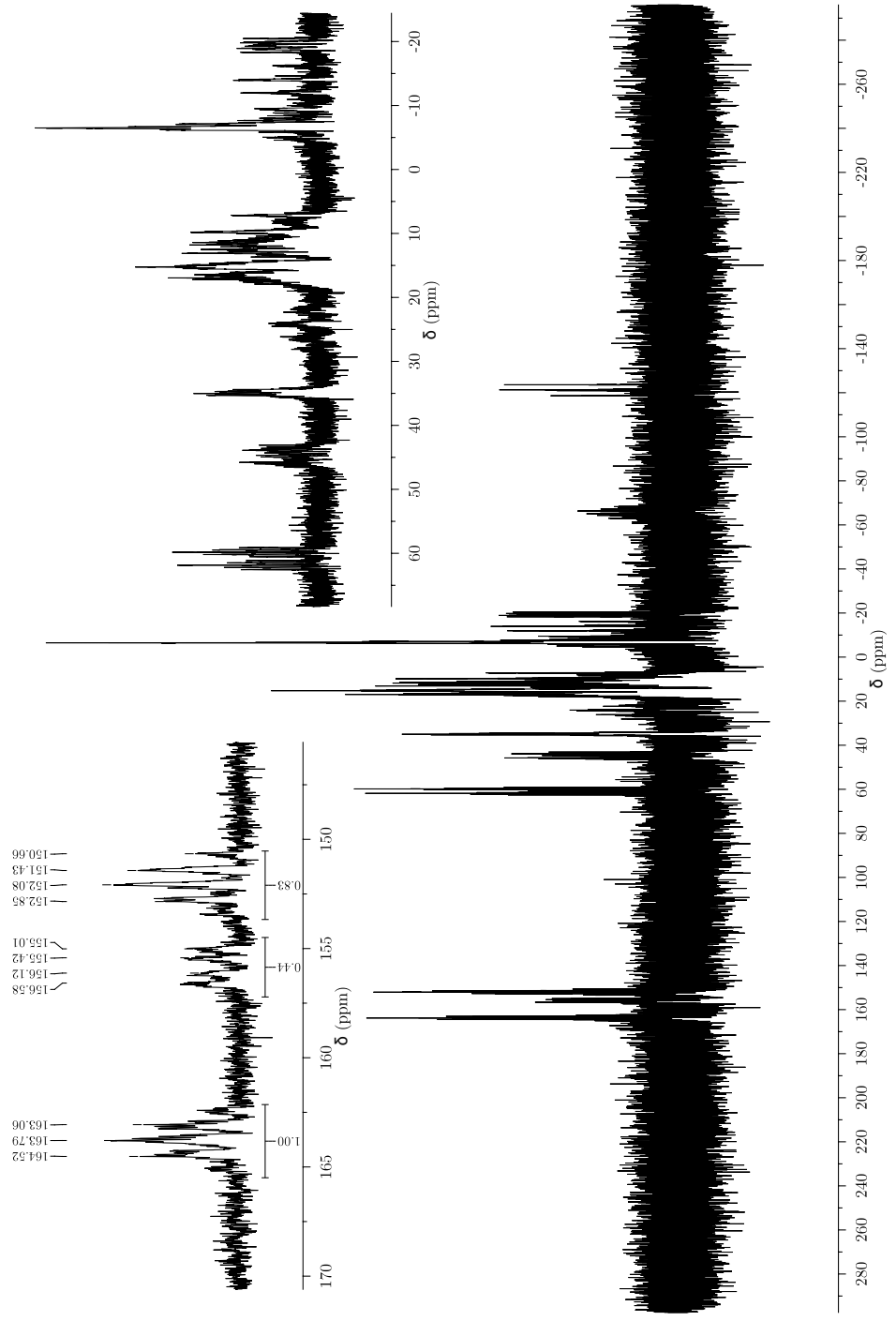


Figure 5.37: ^{31}P NMR spectrum of the reaction solution from the reaction of **11a** with ^{t}BuLi and Cy_2PCl at room temperature in thf with D_2O capillary.

NMR spectra of [Cp*Fe($\eta^{1:1:1}$-(1-^{t}Bu-2-P^{t}Bu$_2$-3-Me-4-PPh$_2$-P$_5$))] (15)

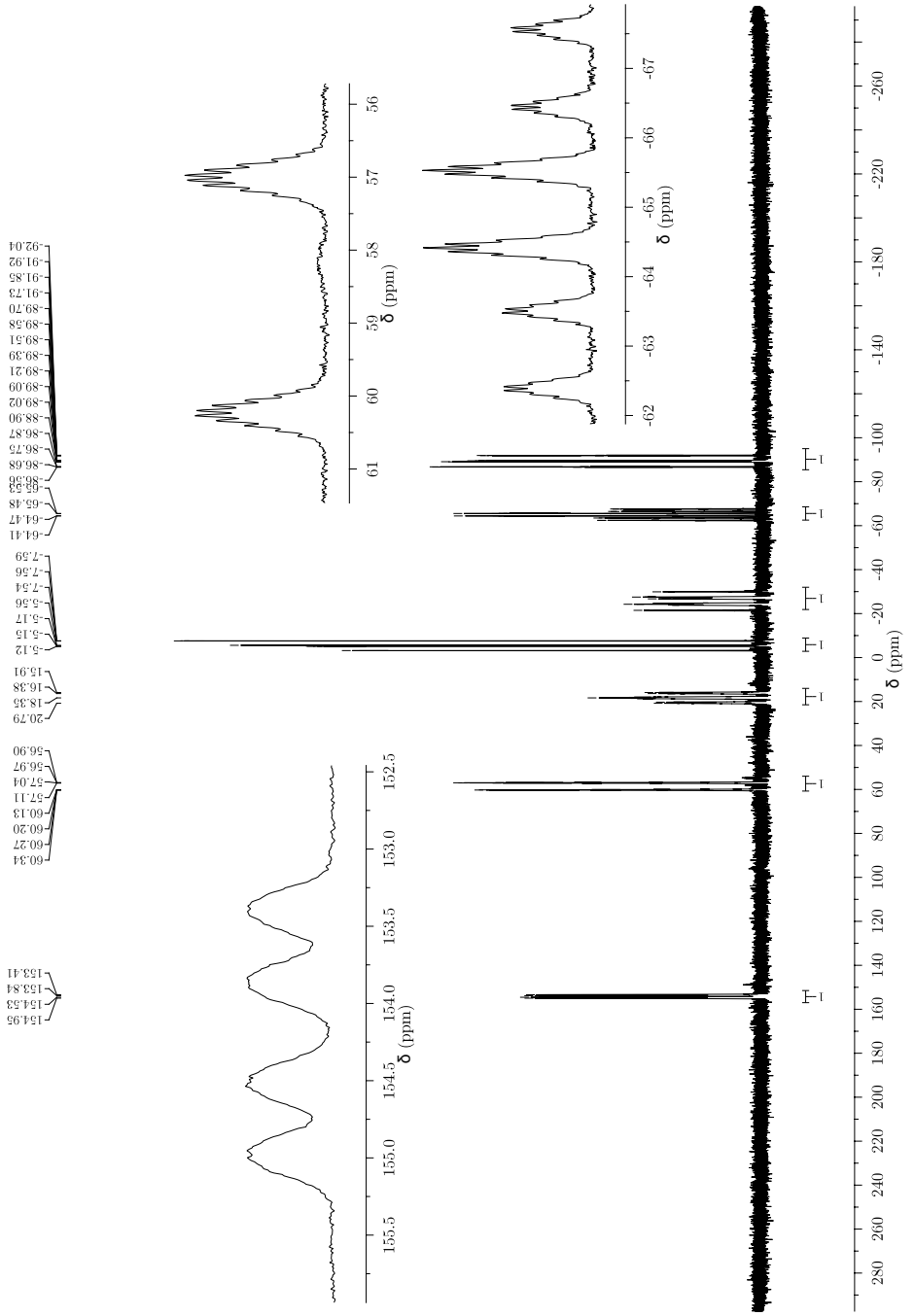


Figure 5.38: $^{31}P\{^1H\}$ NMR spectrum of [Cp*Fe($\eta^{1:1:1}$-(1-^{t}Bu-2-P^{t}Bu$_2$-3-Me-4 -PPh$_2$-P$_5$))] (**15**) at room temperature in CH_2Cl_2.

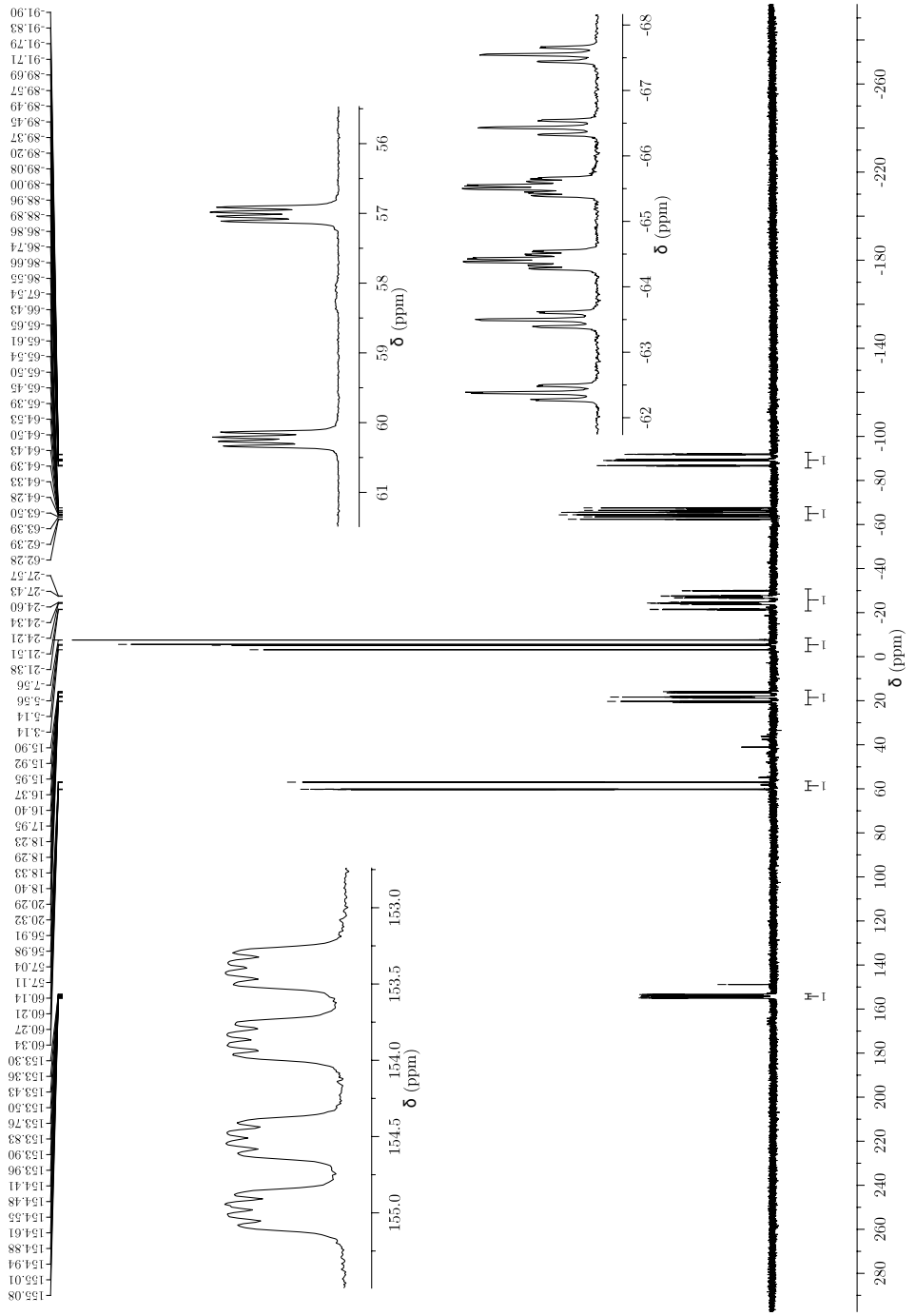


Figure 5.39: ^{31}P NMR spectrum of [Cp*Fe($\eta^{1:1:1}$-(1-^{t}Bu-2-P^{t}Bu$_2$-3-Me-4-PPh$_2$-P$_5$))] (**15**) at room temperature in CH_2Cl_2.

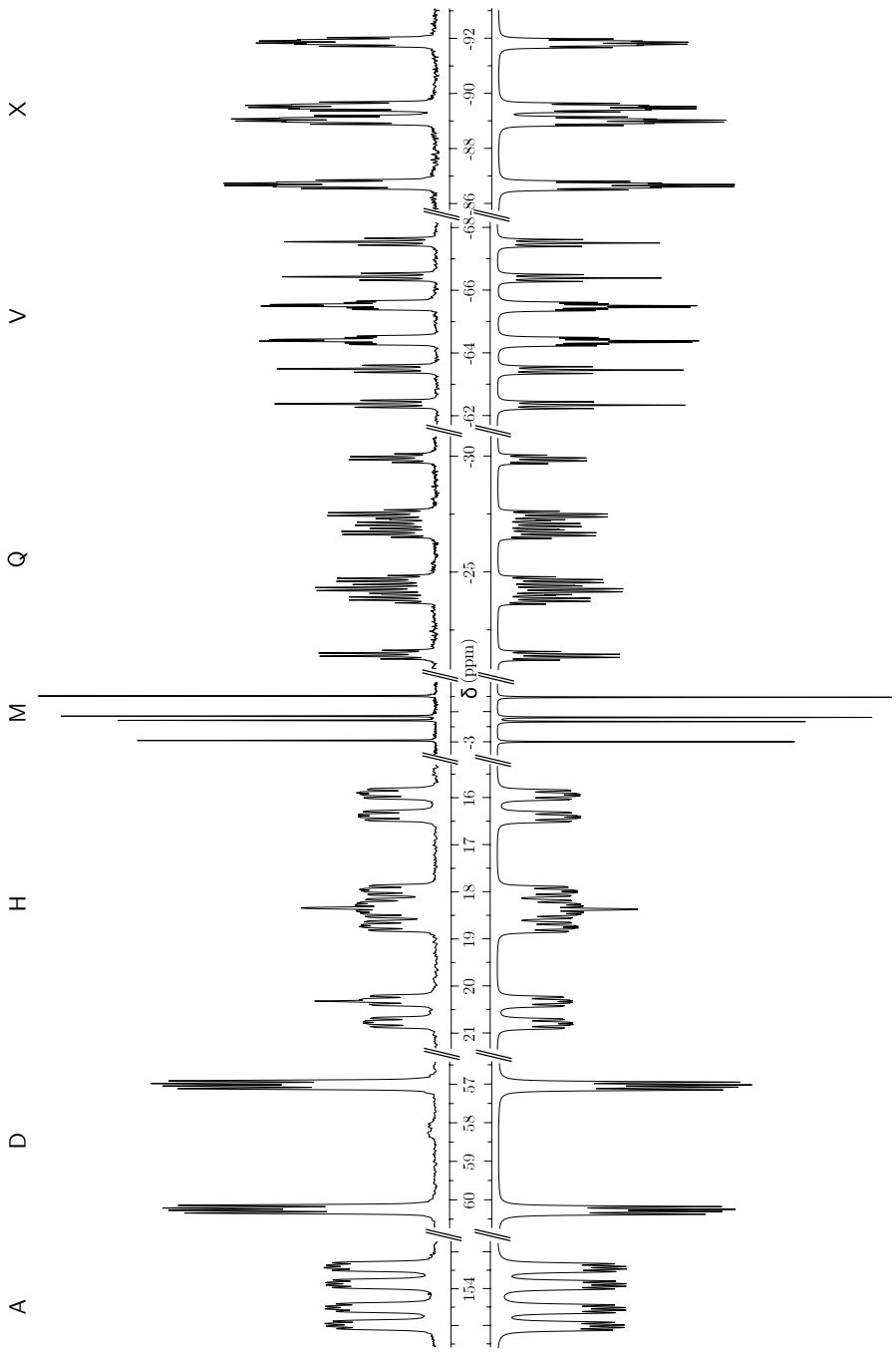


Figure 5.40: ^{31}P NMR spectrum (excerpts) of [Cp*Fe($\eta^{1:1:1}$-(1-^{t}Bu-2-P^{t}Bu$_2$-3-Me-4-PPh$_2$-P$_5$))] (**15**) at room temperature in CD_2Cl_2 with simulation of the spin system (inverted).

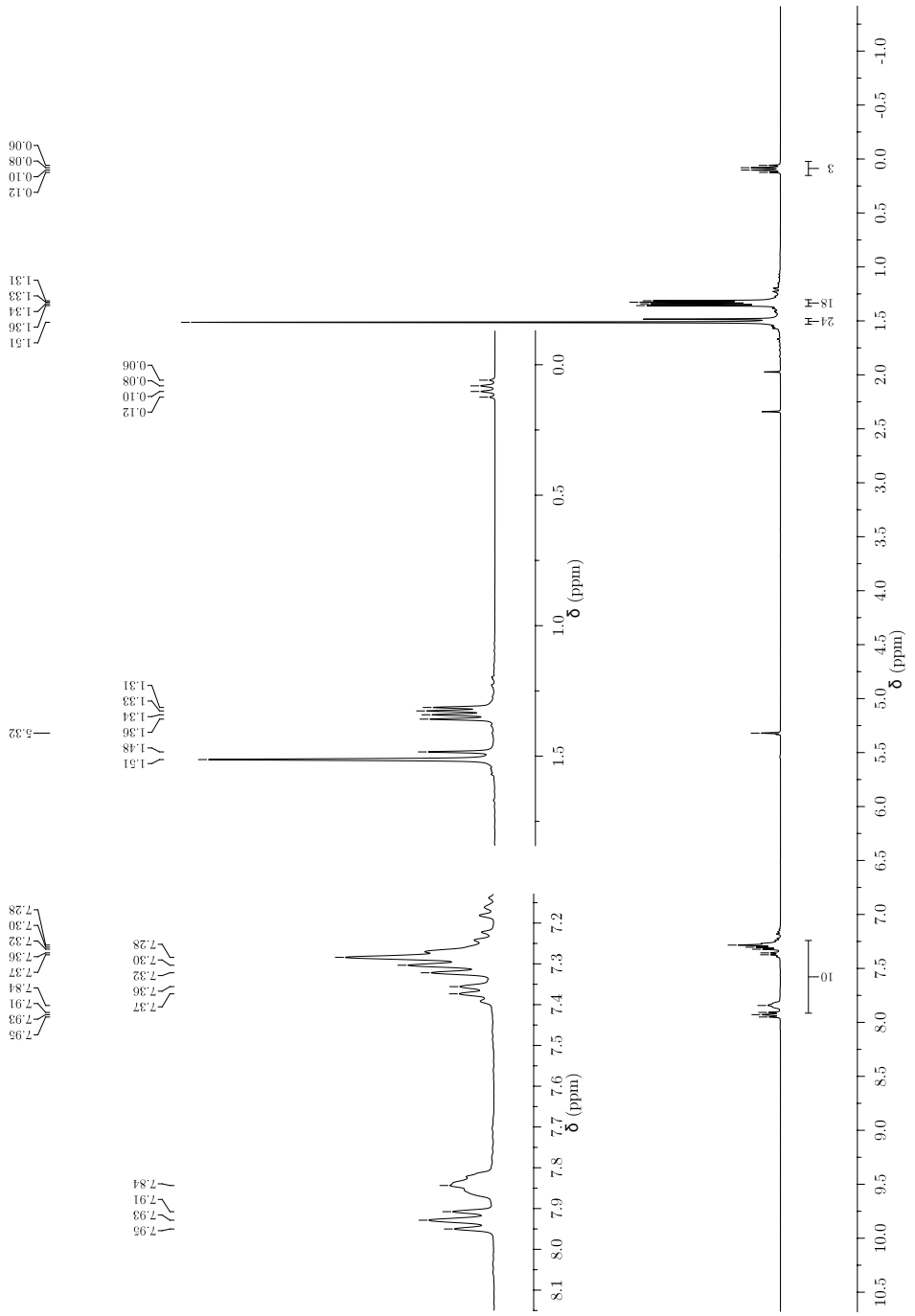


Figure 5.41: ^{1}H NMR spectrum of [Cp*Fe($\eta^{1:1:1}$-(1-^{t}Bu-2-P^{t}Bu$_2$-3-Me-4-PPh$_2$-P$_5$))] (**15**) at room temperature in CD_2Cl_2. The singulet at 5.32 ppm corresponds to residual CH_2Cl_2 from the deuterated solvent.

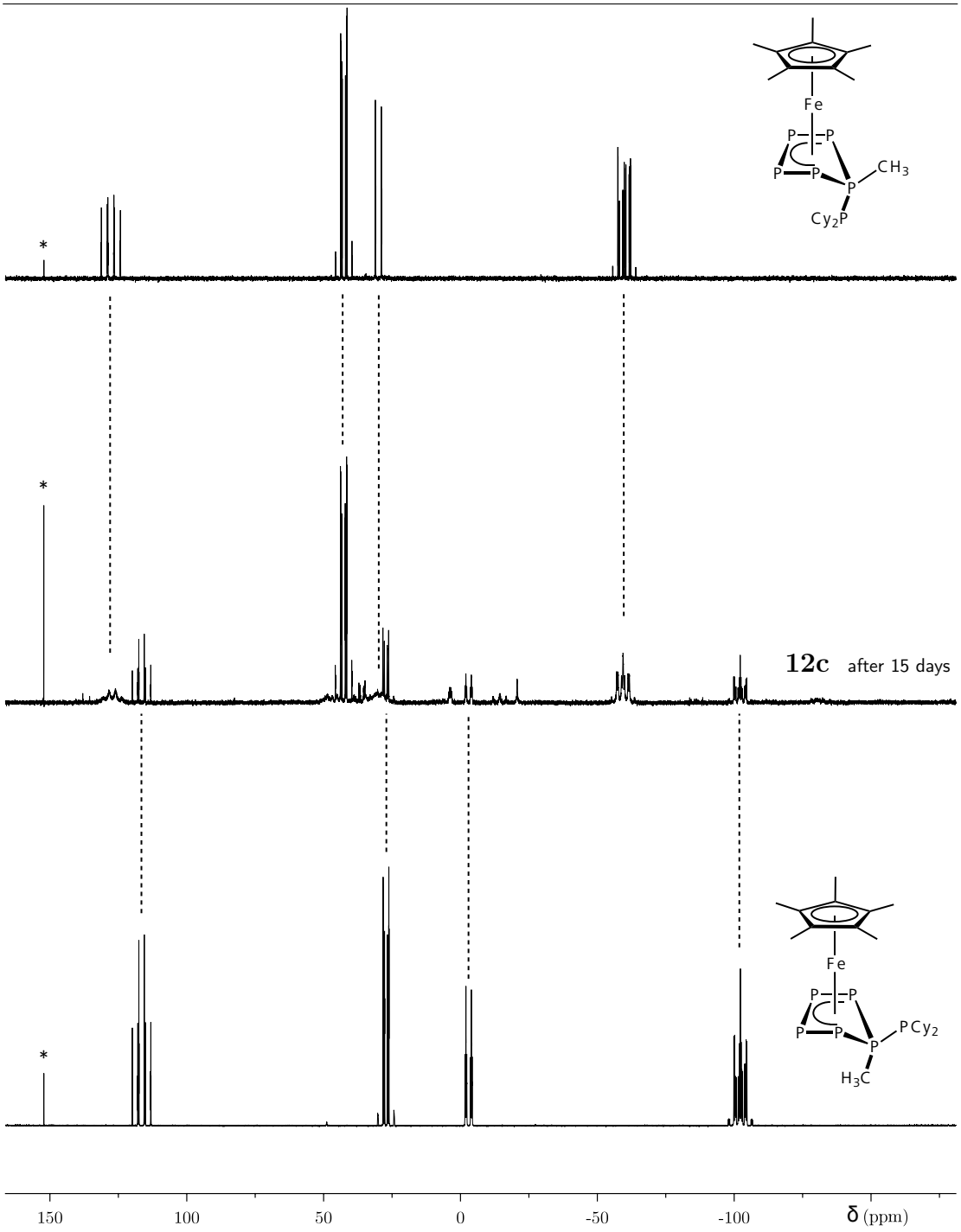


Figure 5.42: $^{31}P\{^{1}H\}$ NMR study on stability of **12a** in solution at room temperature. A solution of crystalline **12a** in CD_2Cl_2 shows a clean AMM'NXX' spin system (spectrum on the bottom) with only a minute trace of **XXVII** (marked with an asterisk). After storing this solution under inert conditions for half a month (spectrum in the middle), a conversion of the endo isomer **12a** to the exo isomer **12b** can be observed (the NMR of a sample of pure **12b** is depicted on the top). The ratio of **12b**:**12a** can be determined to be 2:1 by integration of the isolated XX' signals of the respective complex.

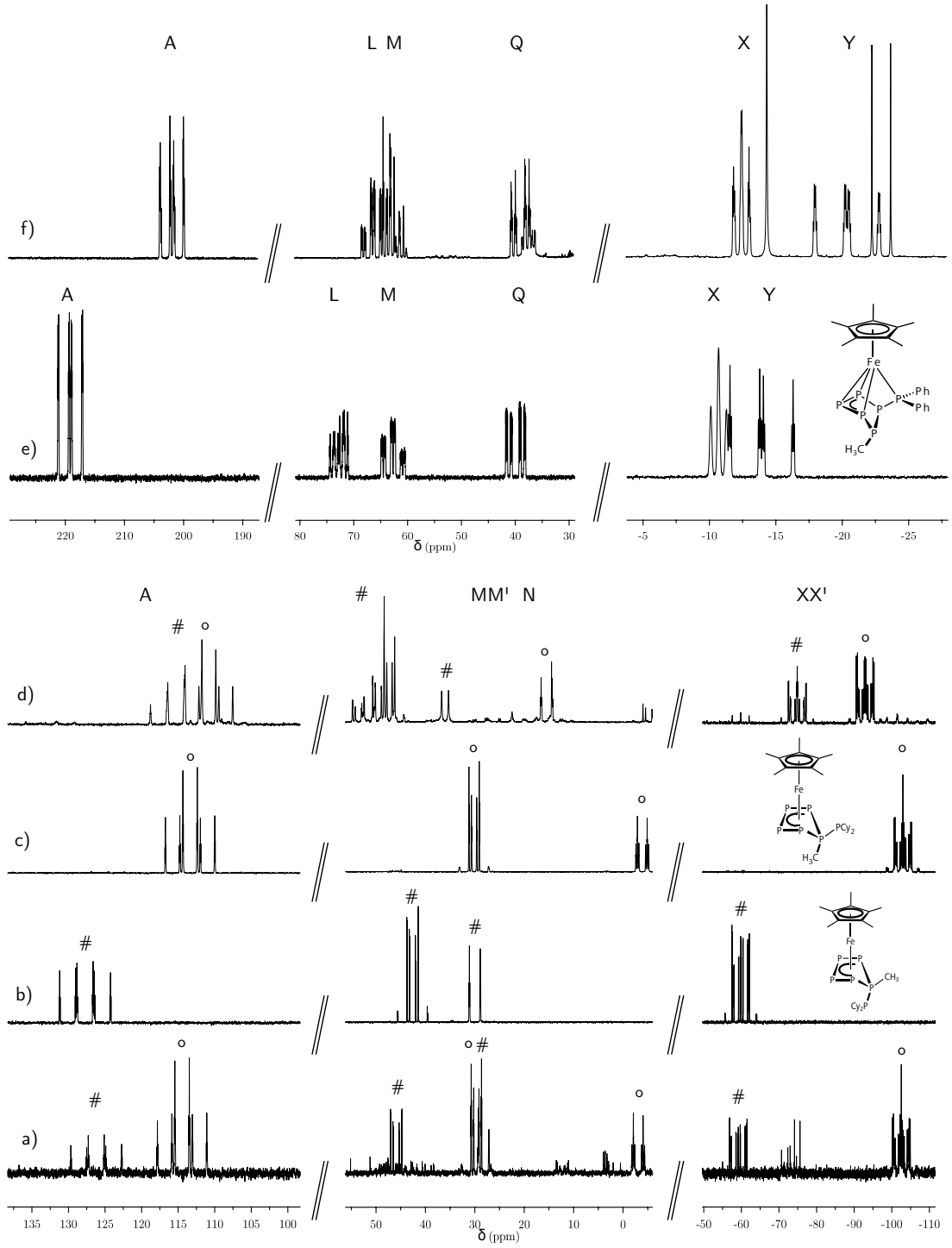


Figure 5.43: $^{31}P\{^{1}H\}$ NMR study on the influence of the steric bulk of the Cp ligand. a): crude NMR of the reaction of Li[Cp*Fe(η^4-P_5CH_3)] in thf with Cy_2PCl (reaction at - 80 °C), b): pure **12b** in CD_2Cl_2, c): pure **12a** in C_6D_6, d) crude NMR of the reaction of Li[Cp^{BIG}Fe(η^4-P_5CH_3)] in thf with Ph_2PCl (reaction at - 80 °C), e): pure **11a** in CD_2Cl_2, f): crude NMR of the reaction of Li[Cp″Fe(η^4-P_5CH_3)] in thf with Ph_2PCl (reaction at - 80 °C). To distinguish the isomers more easily signals of exo products are marked with # and of endo with o.

NMR spectra of the reaction of $[Cp^*Fe(\eta^4\text{-}P_5CH_3)]$ with $(NEt_2)_2PCl$

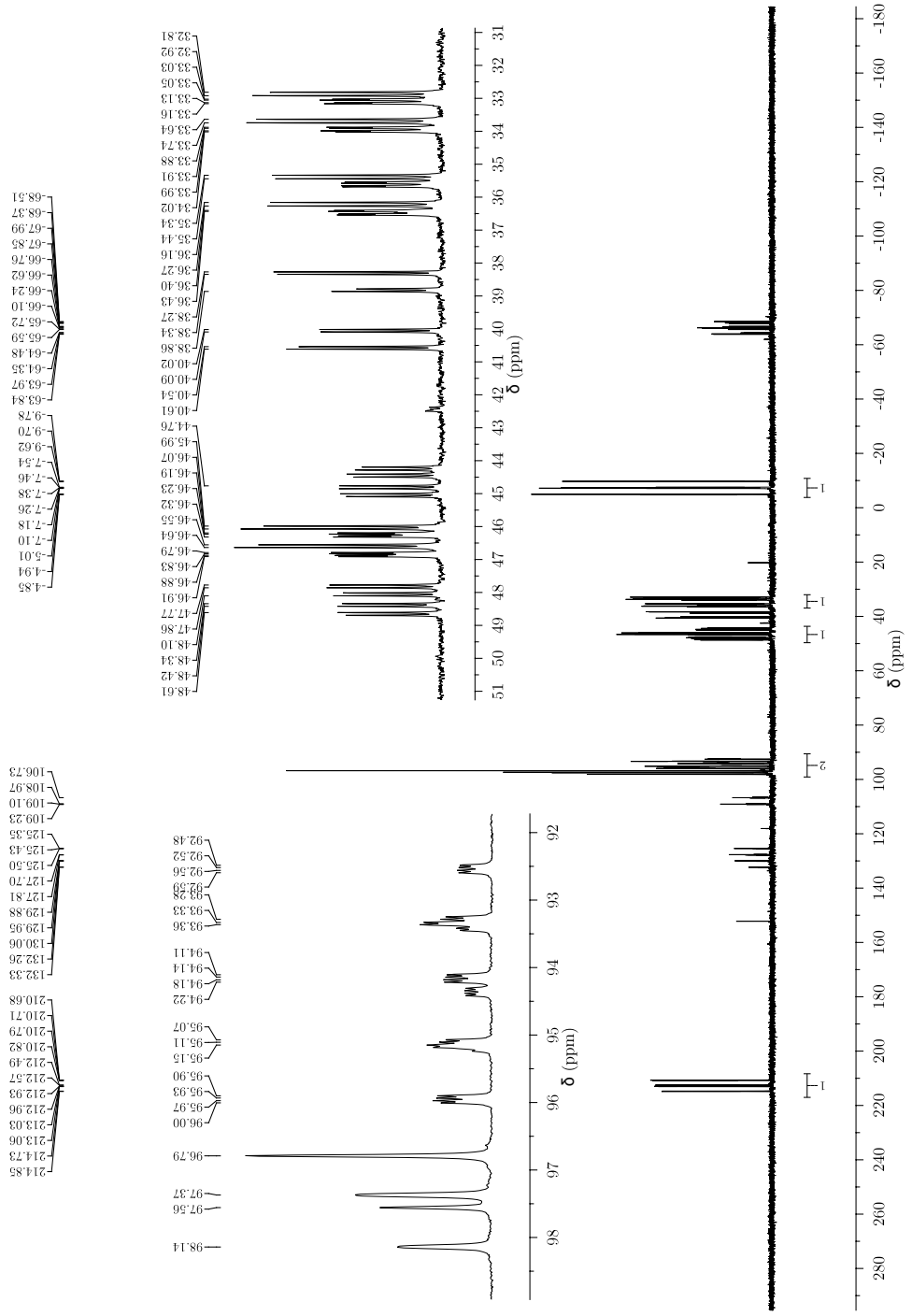


Figure 5.44: $^{31}P\{^1H\}$ NMR spectrum of the reaction of $[Cp^*Fe(\eta^4\text{-}P_5CH_3)]$ with $(NEt_2)_2PCl$ at room temperature in CD_2Cl_2 (crystalline product mix).

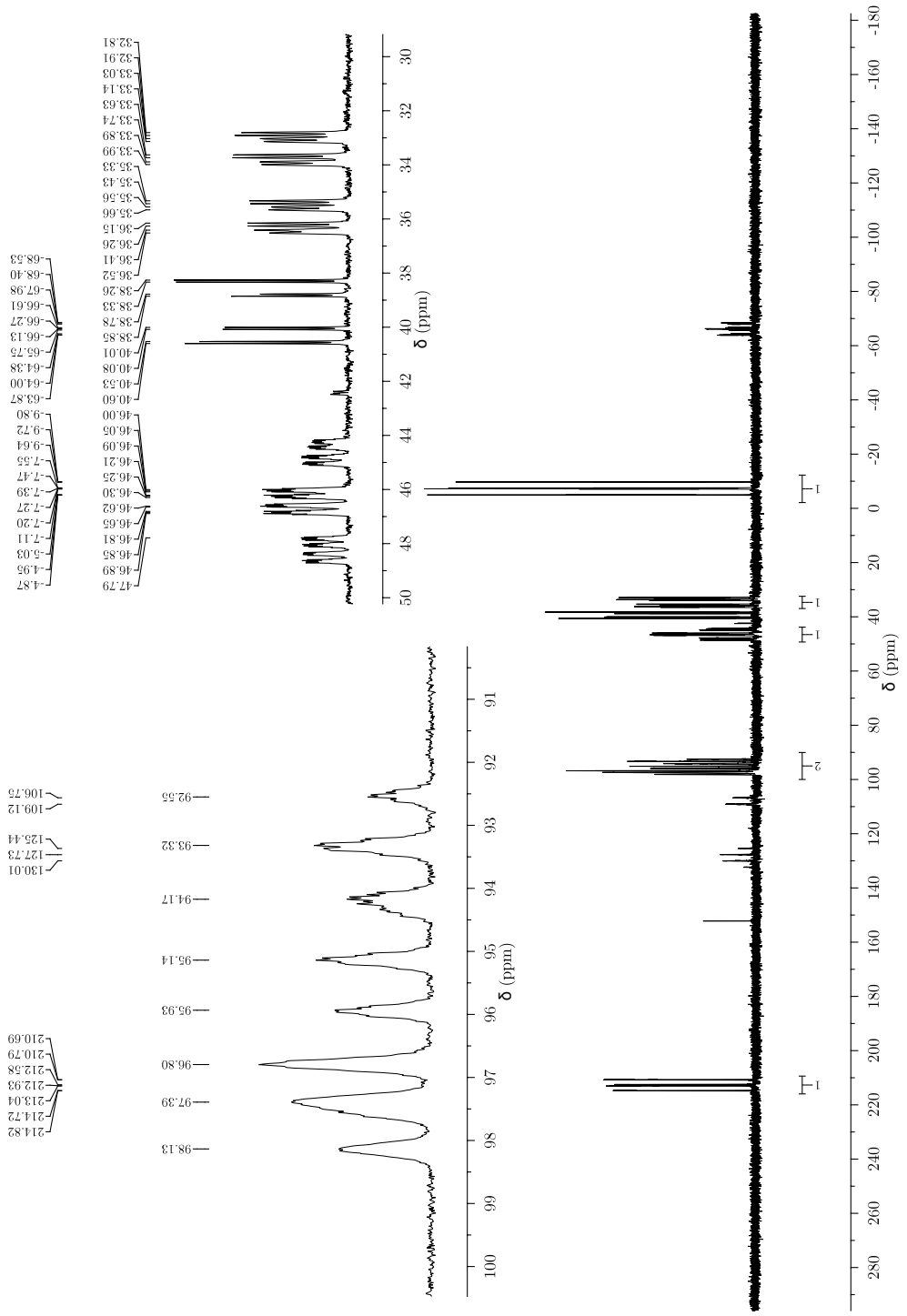


Figure 5.45: ^{31}P NMR spectrum of the reaction of [Cp*Fe(η^4-P_5CH_3)] with $(NEt_2)_2PCl$ at room temperature in CD_2Cl_2 (crystalline product mix).

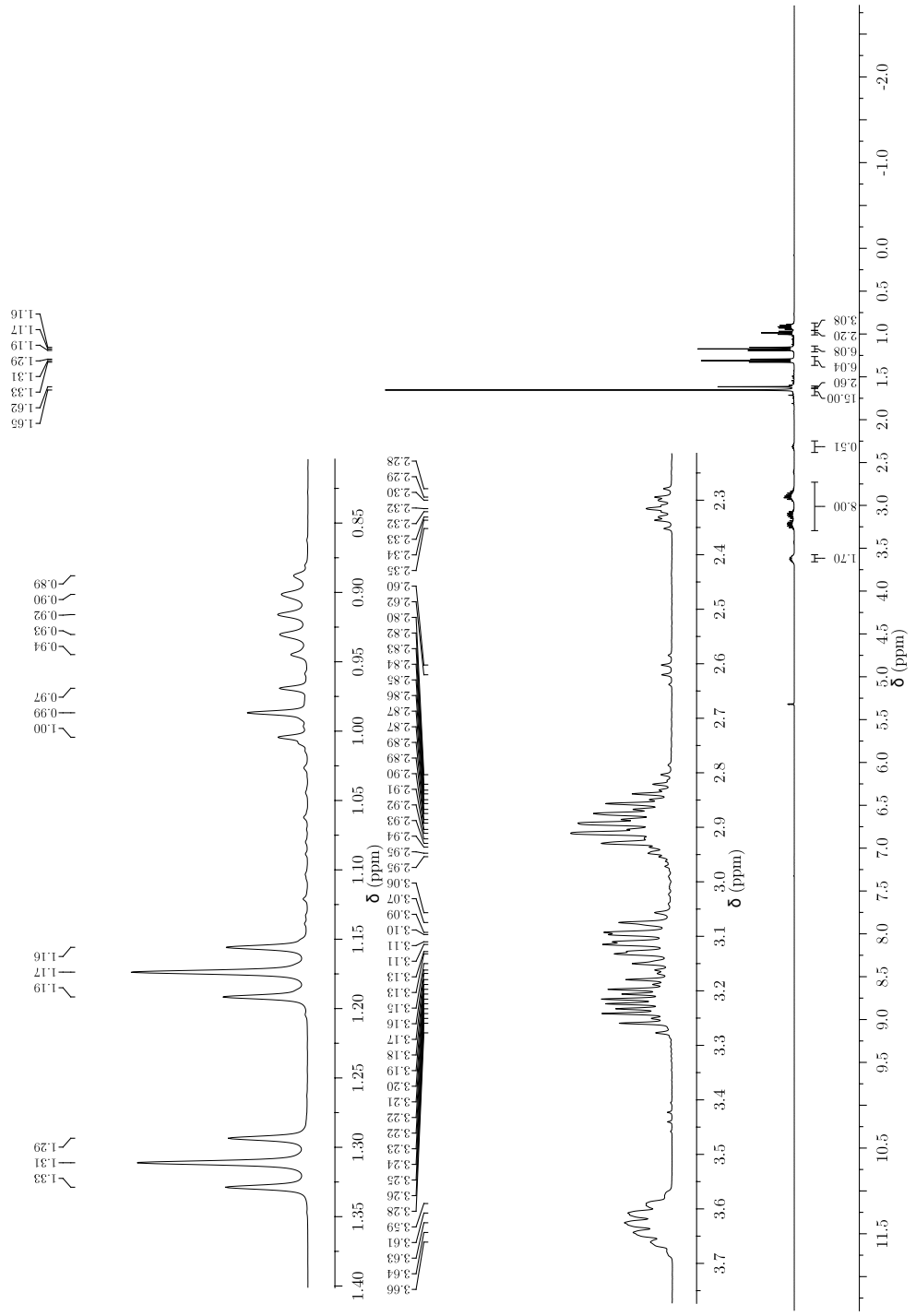


Figure 5.46: ^{1}H NMR spectrum of the reaction of [Cp*Fe(η^4-P_5CH_3)] with $(NEt_2)_2PCl$ at room temperature in CD_2Cl_2 (crystalline product mix).

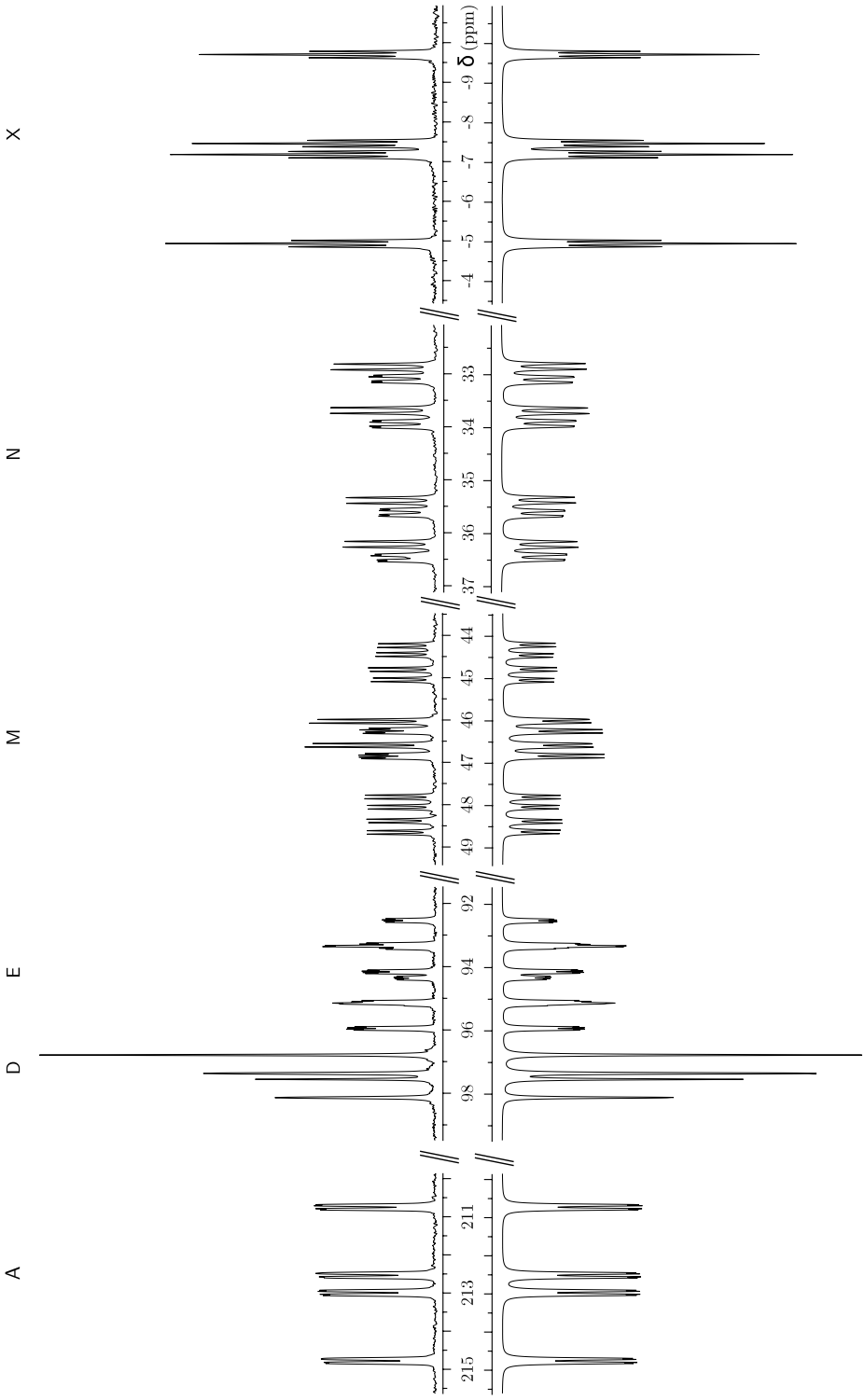


Figure 5.47: Excerpt of the $^{31}P\{^{1}H\}$ NMR spectrum of the reaction of $[Cp^*Fe(\eta^4\text{-}P_5CH_3)]$ with $(NEt_2)_2PCl$ in CD_2Cl_2 of the spin system of **19** with the simulation of the spin system shown inverted.

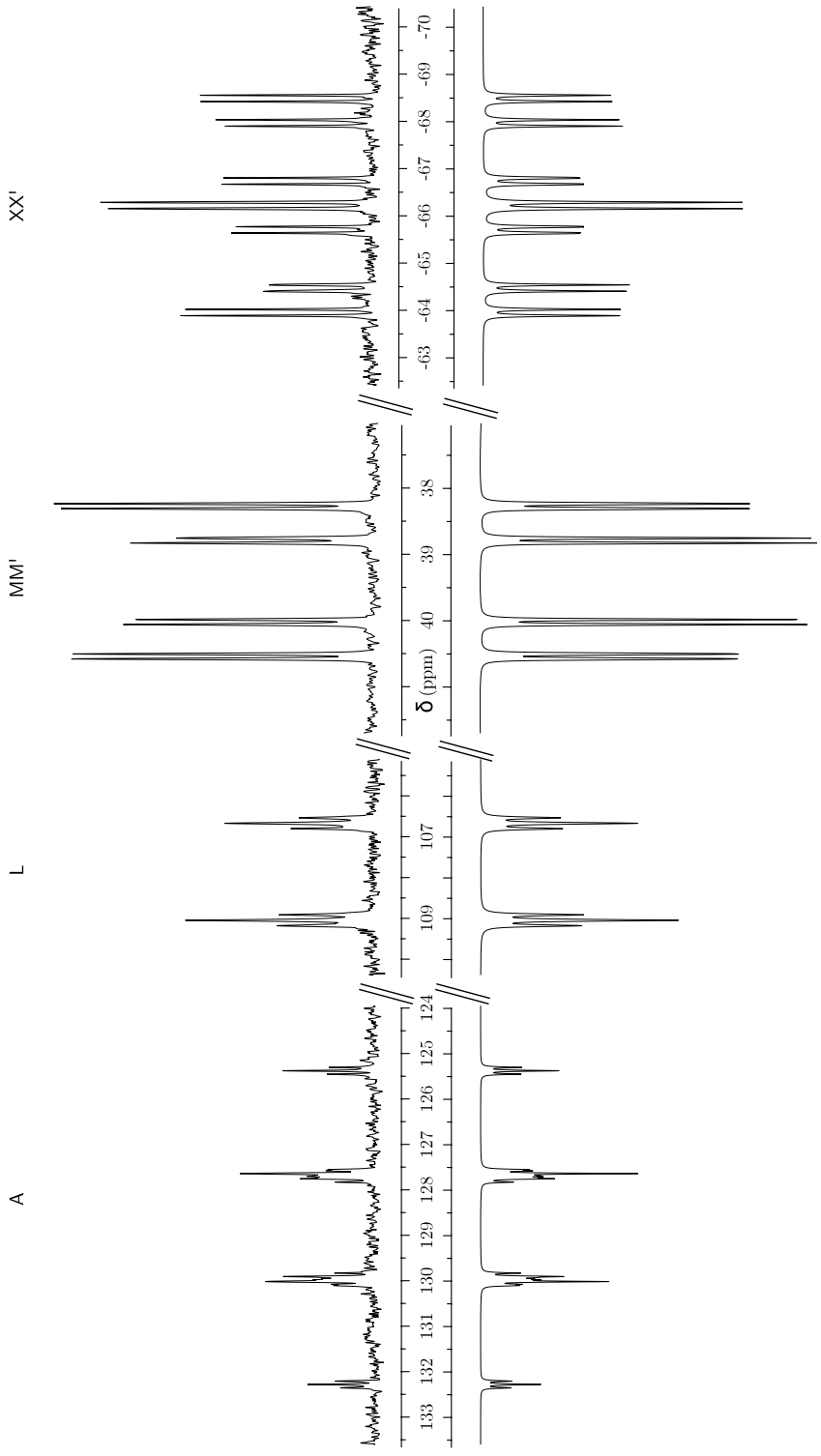


Figure 5.48: Excerpt of the $^{31}P\{^{1}H\}$ NMR spectrum of the reaction of $[Cp^*Fe(\eta^4\text{-}P_5CH_3)]$ with $(NEt_2)_2PCl$ in CD_2Cl_2 of the spin system of **16** with the simulation of the spin system shown inverted.

NMR spectra of [Cp*Fe($\eta^{3:1}$-1-CH_3-2-$C_{12}H_8$P-P_5)] (20)

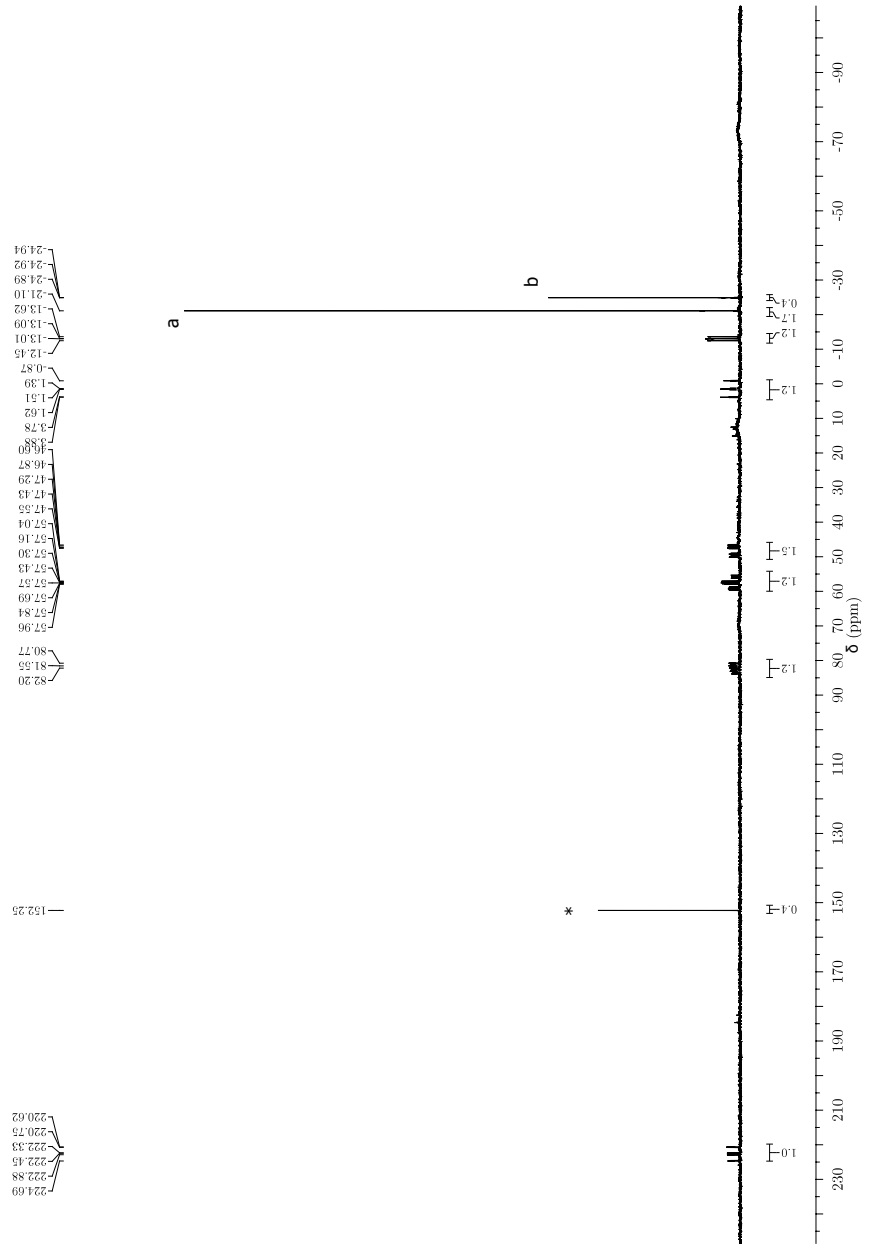


Figure 5.49: $^{31}P\{^1H\}$ NMR spectrum of [Cp*Fe($\eta^{3:1}$-1-CH_3-2-$C_{12}H_8$P-P_5)] (**20**) at room temperature in the reaction mixture (thf with D_2O capillary). Residual **XXVII** is marked with an asterisk, 5,5'-bi-5H-benzo[b]phosphindole with a and 5-methylbenzophosphole with b.

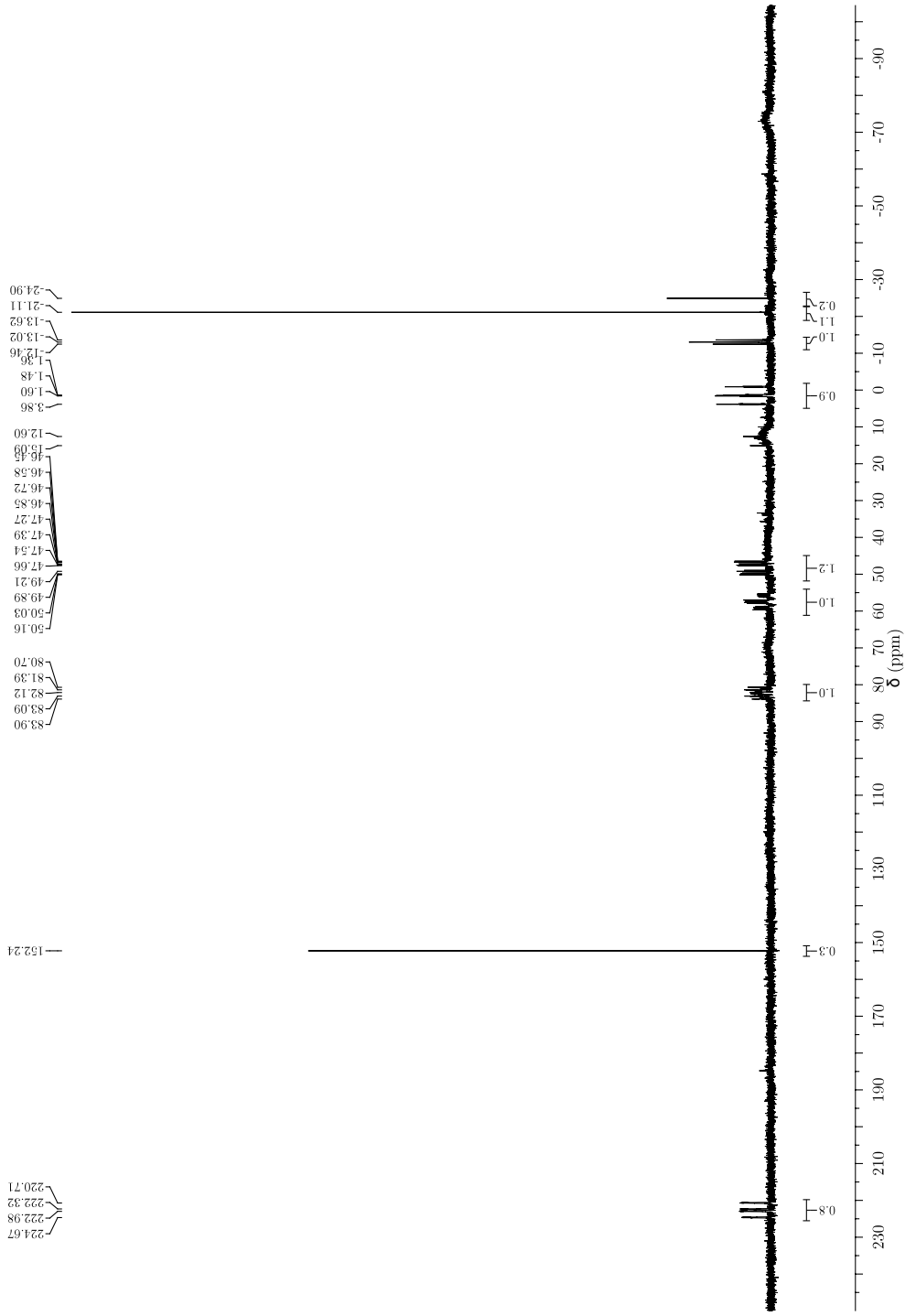


Figure 5.50: ^{31}P NMR spectrum of [Cp*Fe($\eta^{3:1}$-1-CH_3-2-$C_{12}H_8$P-P_5)] (**20**) at room temperature in the reaction mixture (thf with D_2O capillary).

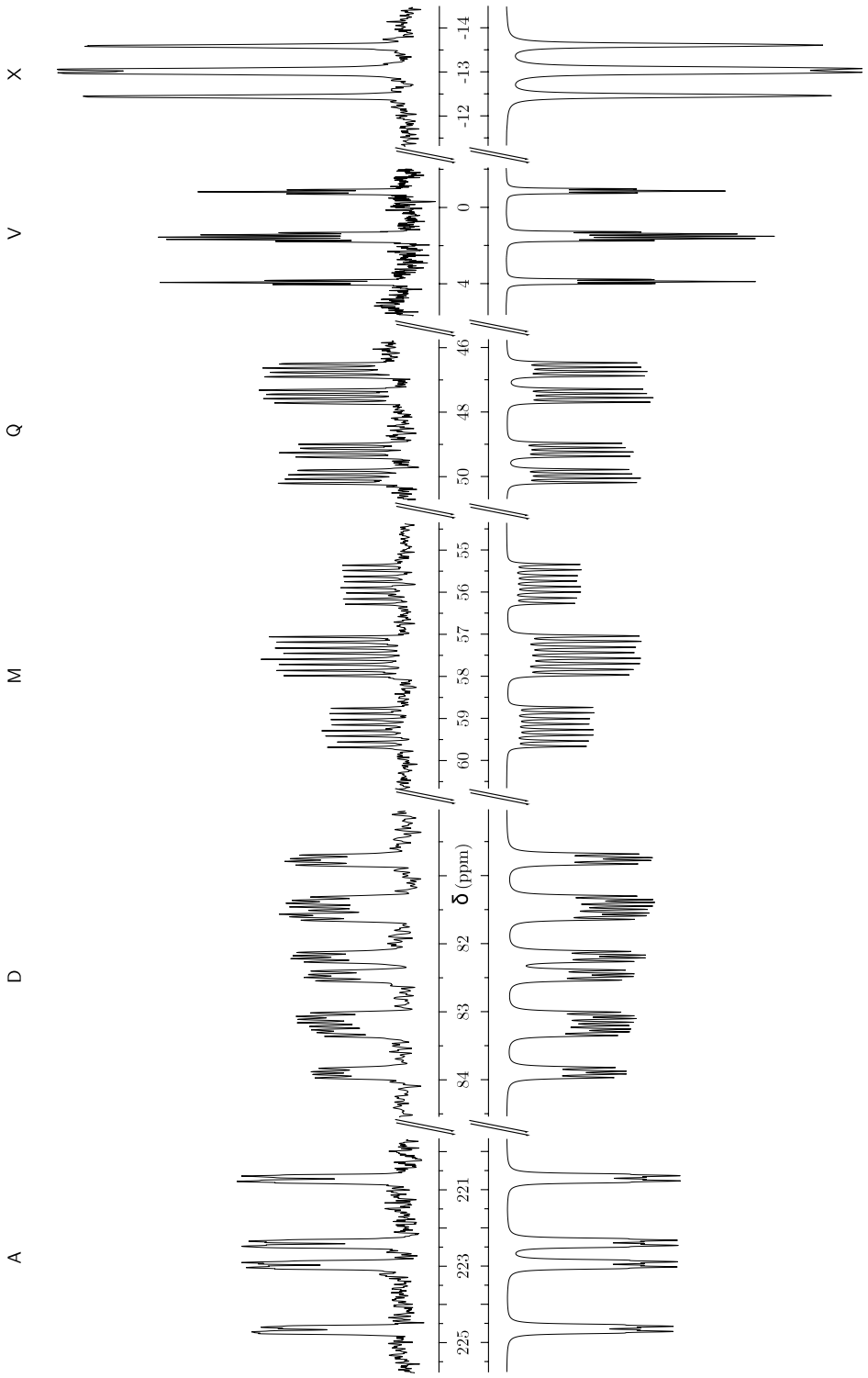


Figure 5.51: Excerpt of the $^{31}P\{^{1}H\}$ NMR spectrum of [Cp*Fe($\eta^{3:1}$-1-CH_3-2-$C_{12}H_8$P-P_5)] (**20**) in thf with D_2O capillary) with the simulation of the spin system shown inverted.

Reaction of Li[Cp*Fe(η^4-P_5CH_3)] with ^{t}Bu$_2$PCl

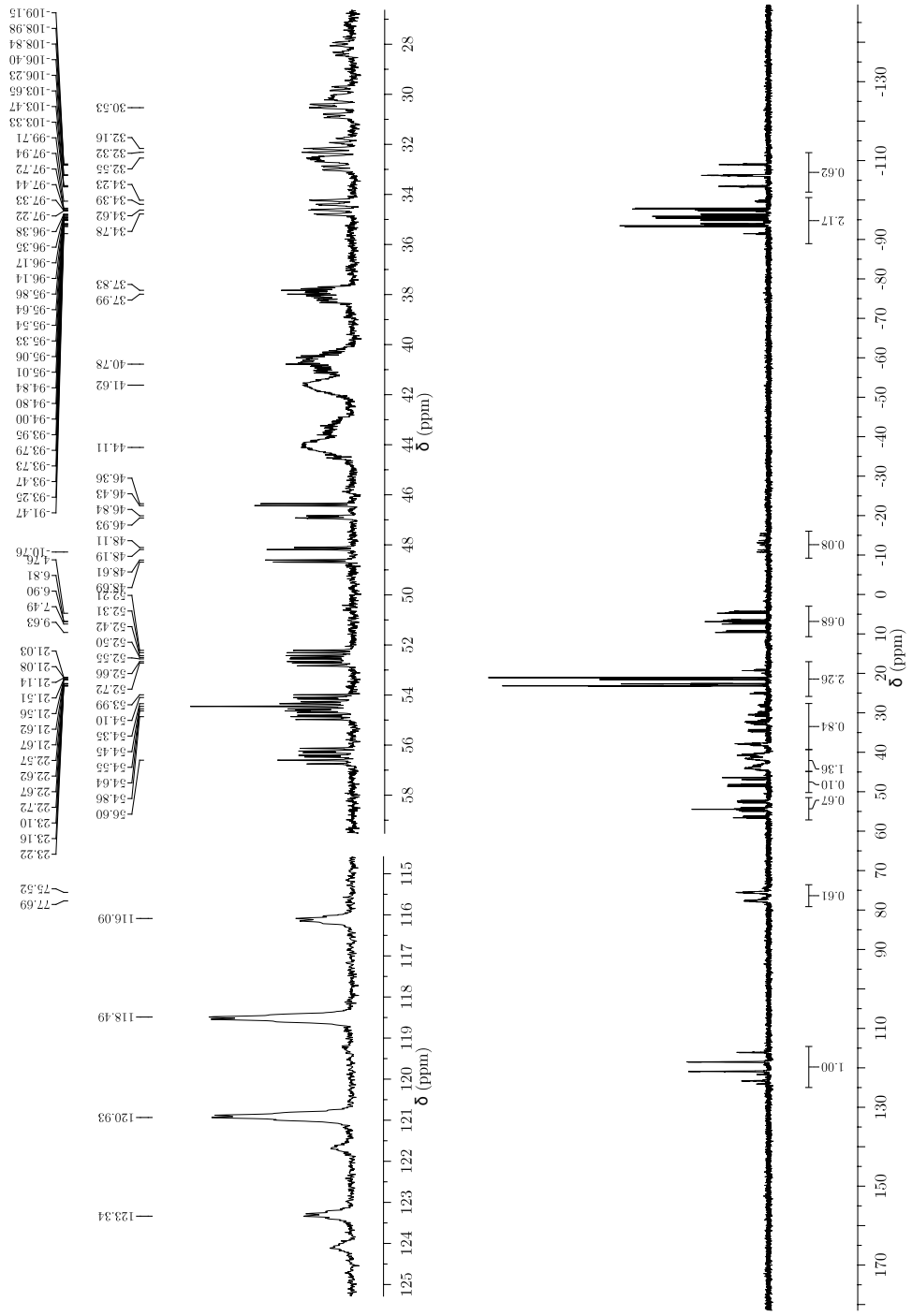


Figure 5.52: $^{31}P\{^1H\}$ NMR spectrum of the reaction mix of [Cp*Fe(η^4-P_5CH_3)] with ^{t}Bu$_2$PCl at room temperature in thf with D_2O capillary.

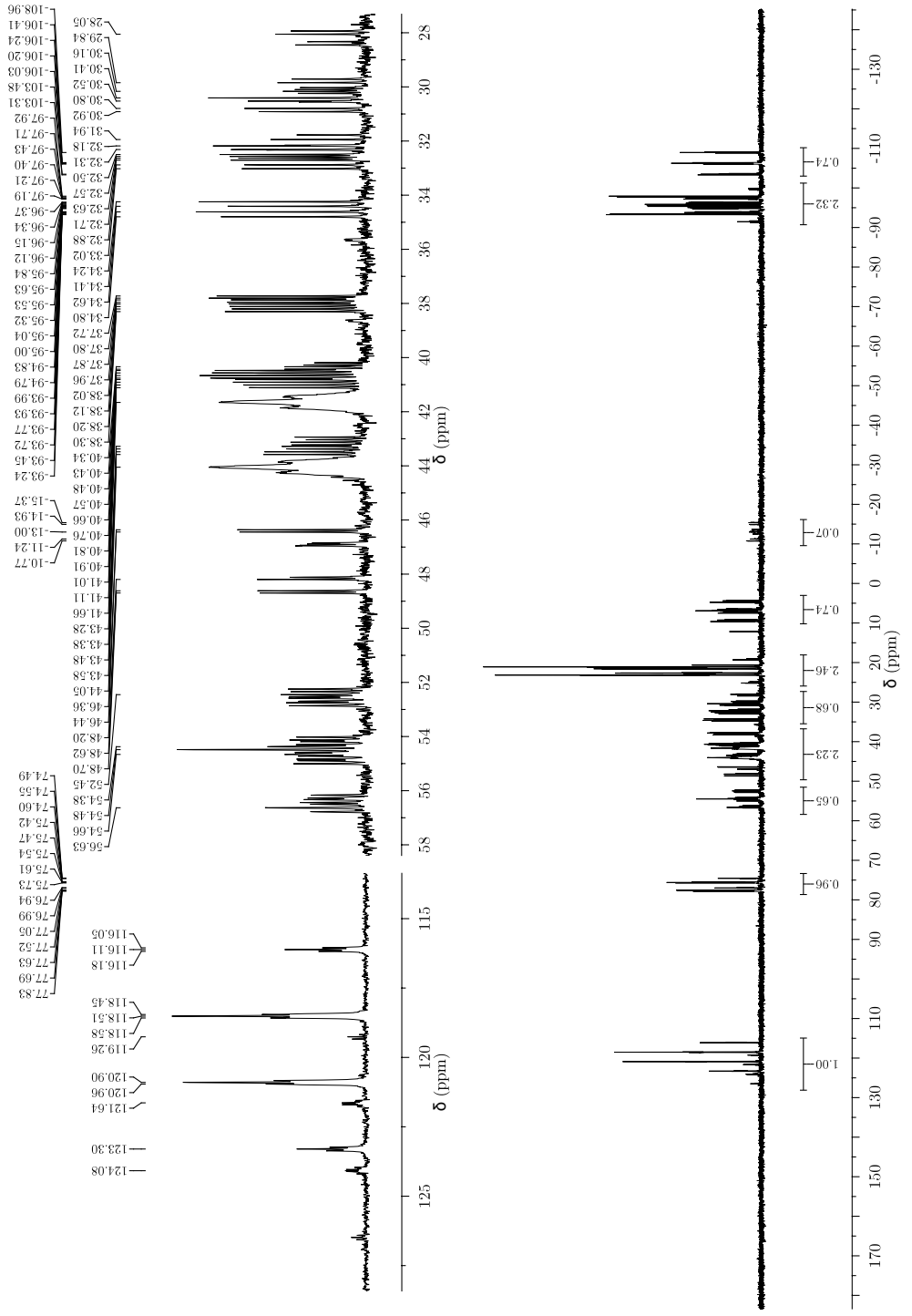


Figure 5.53: ^{31}P NMR spectrum of the reaction mix of [Cp*Fe(η^4-P_5CH_3)] with ^{t}Bu$_2$PCl at room temperature in thf with D_2O capillary.

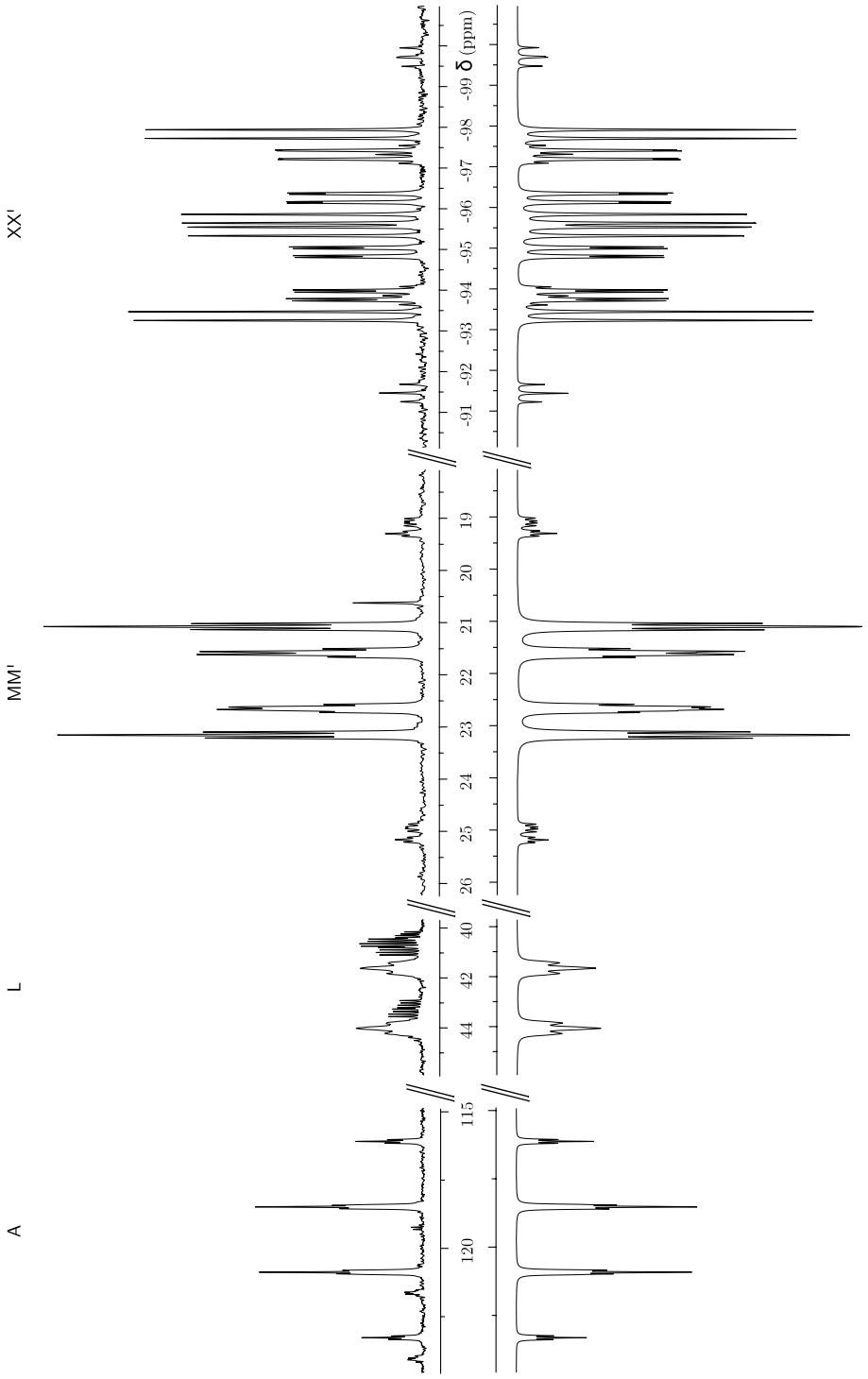


Figure 5.54: Excerpt of the $^{31}P\{^{1}H\}$ NMR spectrum of the reaction of [Cp*Fe(η^4-P_5CH_3)] with $^{t}Bu_2PCl$ in thf with D_2O capillary of the spin system of endo-Cp*Fe(η^4-1, 1-CH_3, P^{t}Bu-P_5 (**17**) with the simulation of the spin system shown inverted.

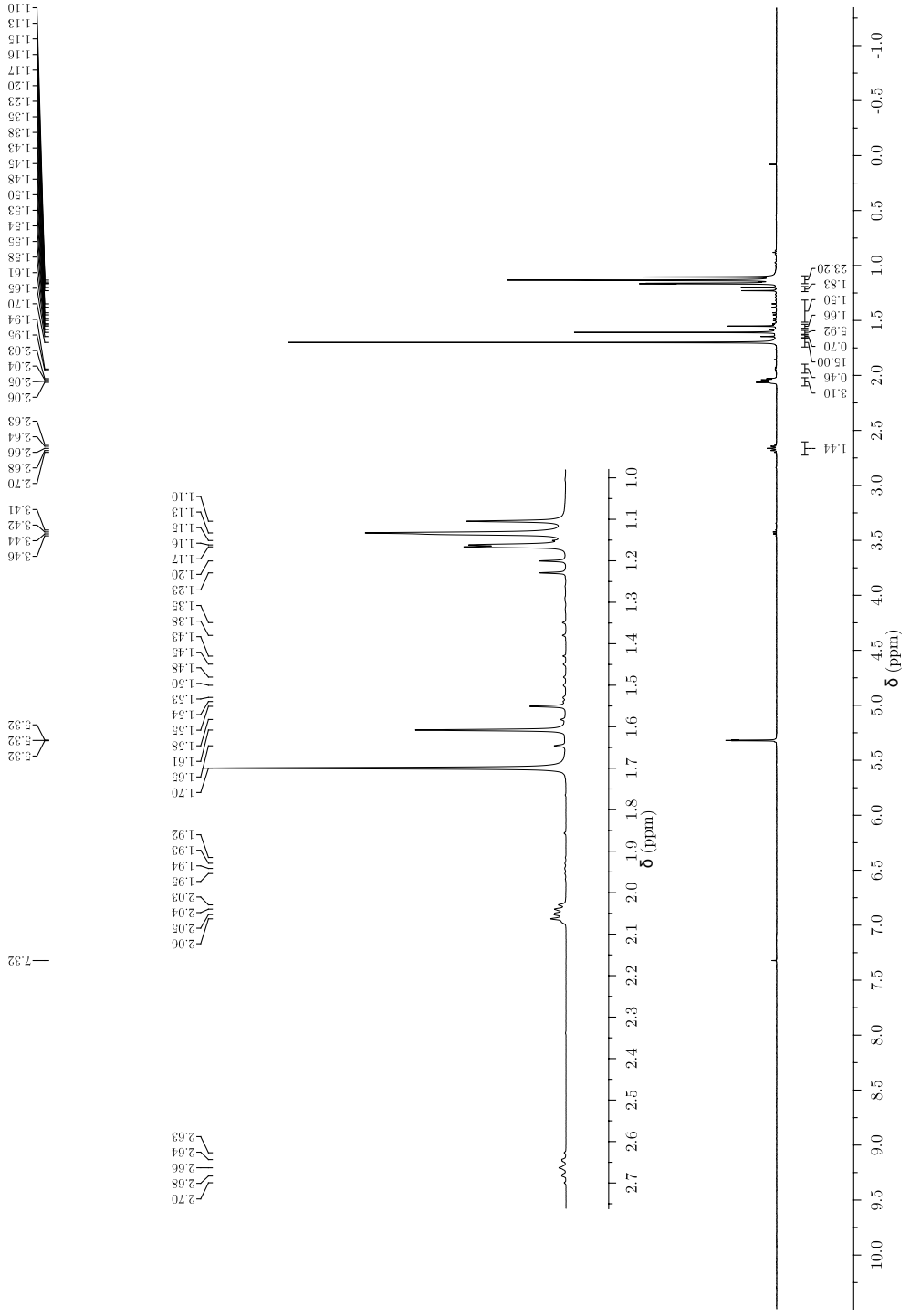


Figure 5.55: ^{1}H NMR spectrum of the reaction of [Cp*Fe(η^4-P_5CH_3)] with $^{t}Bu_2PCl$ at room temperature in CD_2Cl_2 (crystalline product mix).

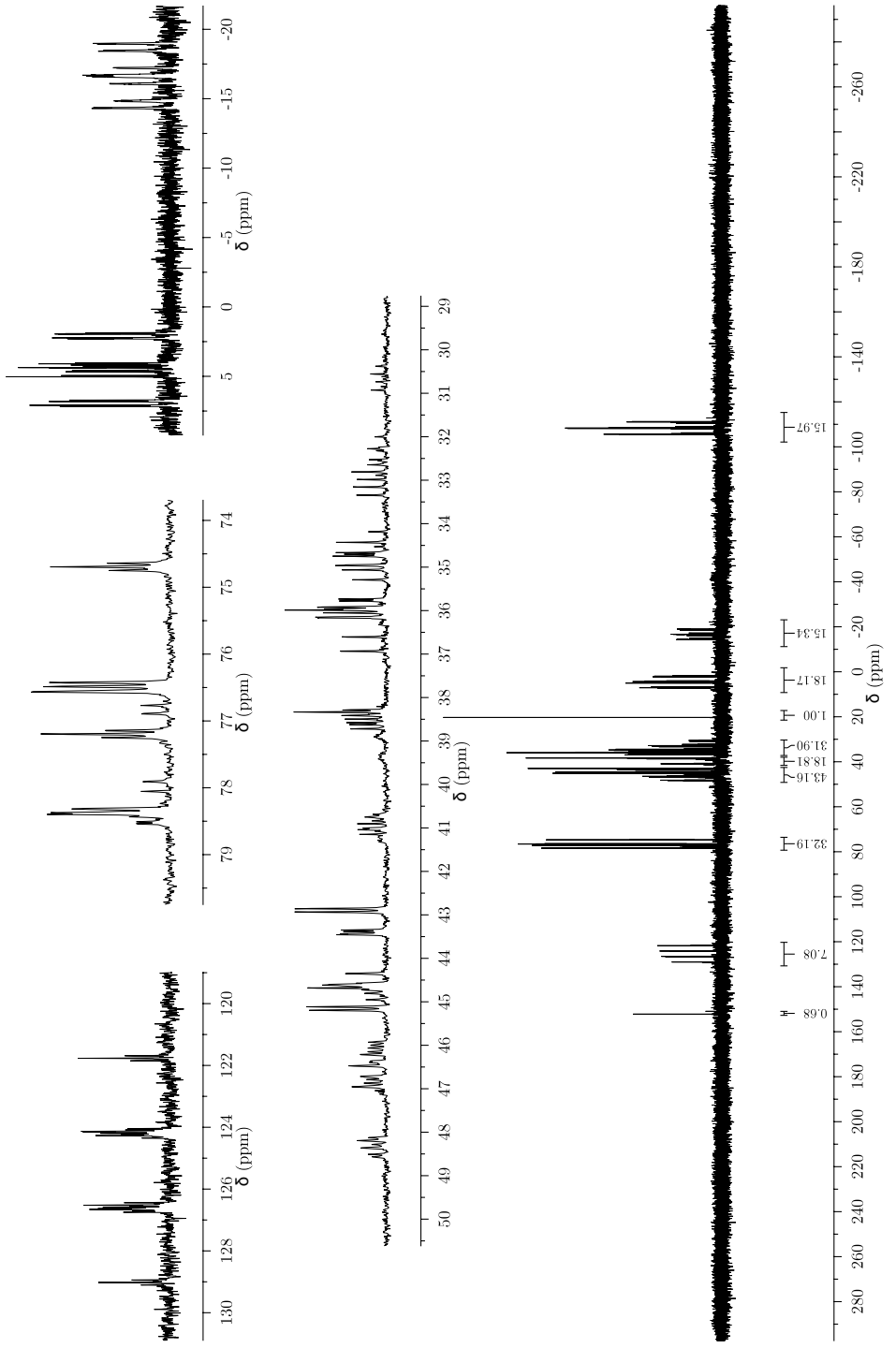


Figure 5.56: ^{31}P NMR spectrum of the reaction of [Cp*Fe(η^4-P_5CH_3)] with ^{t}Bu$_2$PCl at room temperature in CD_2Cl_2 (crystalline product mix).

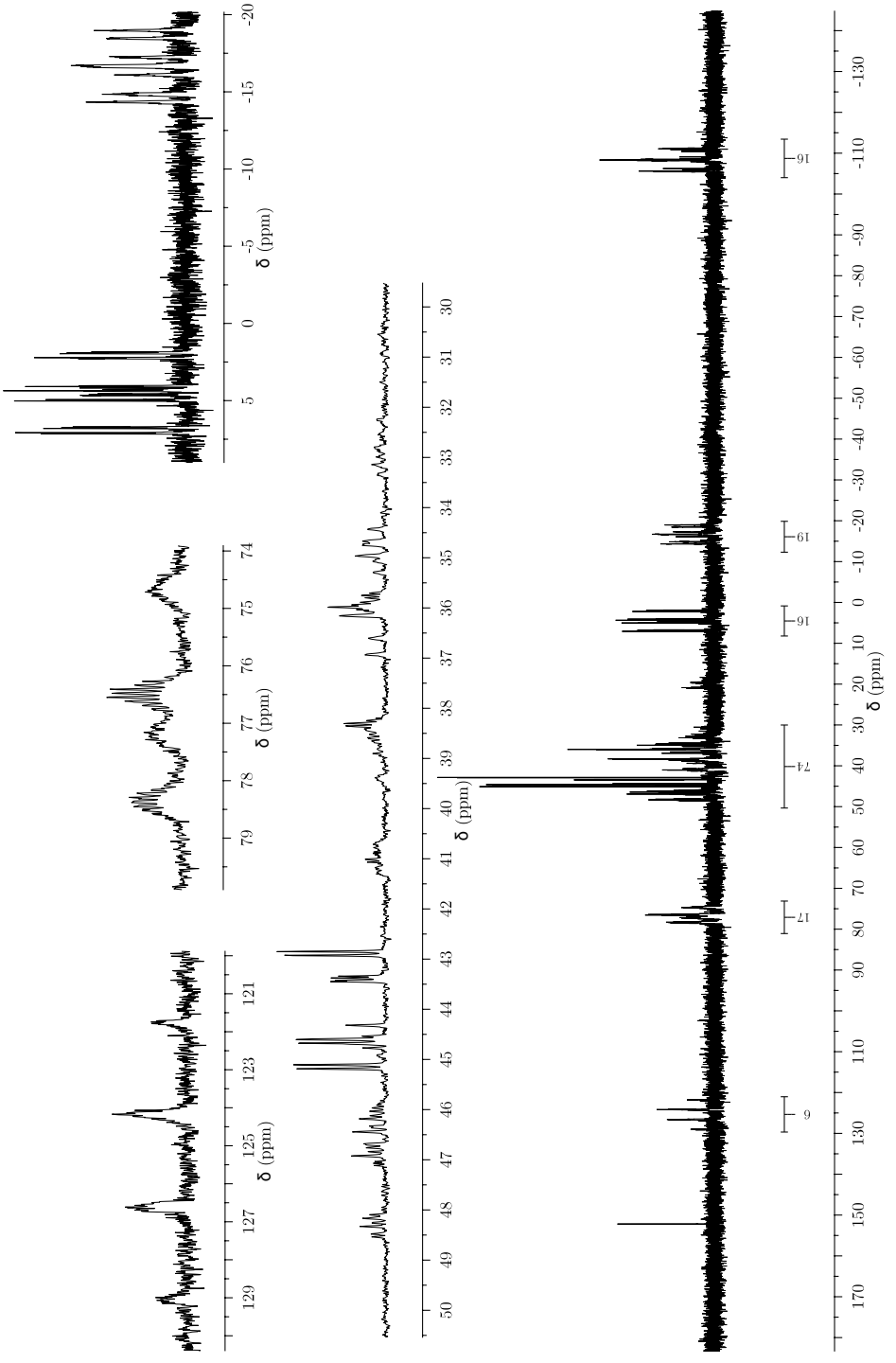


Figure 5.57: $^{31}P\{^{1}H\}$ NMR spectrum of the reaction of [Cp*Fe(η^4-P_5CH_3)] with $^{t}Bu_2PCl$ at room temperature in CD_2Cl_2 (crystalline product mix). The singulet at 152 ppm can be assigned to residual **XXVII**.

Reaction of Li[Cp*Fe(η^4-P_5CH_3)] with Mes_2PCl

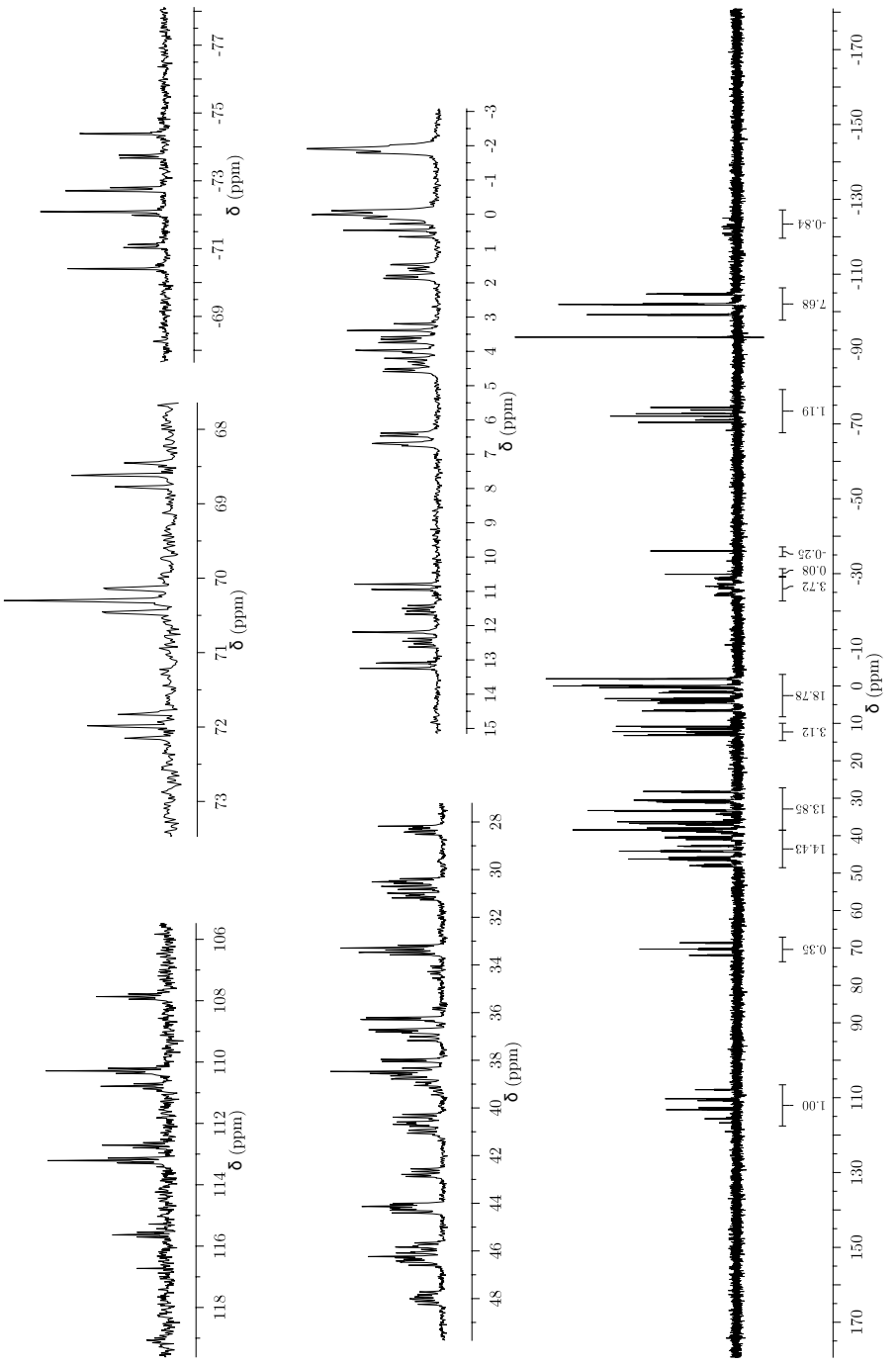


Figure 5.58: ^{31}P NMR spectrum of the reaction mix of [Cp*Fe(η^4-P_5CH_3)] with Mes_2PCl at room temperature in thf with D_2O capillary.

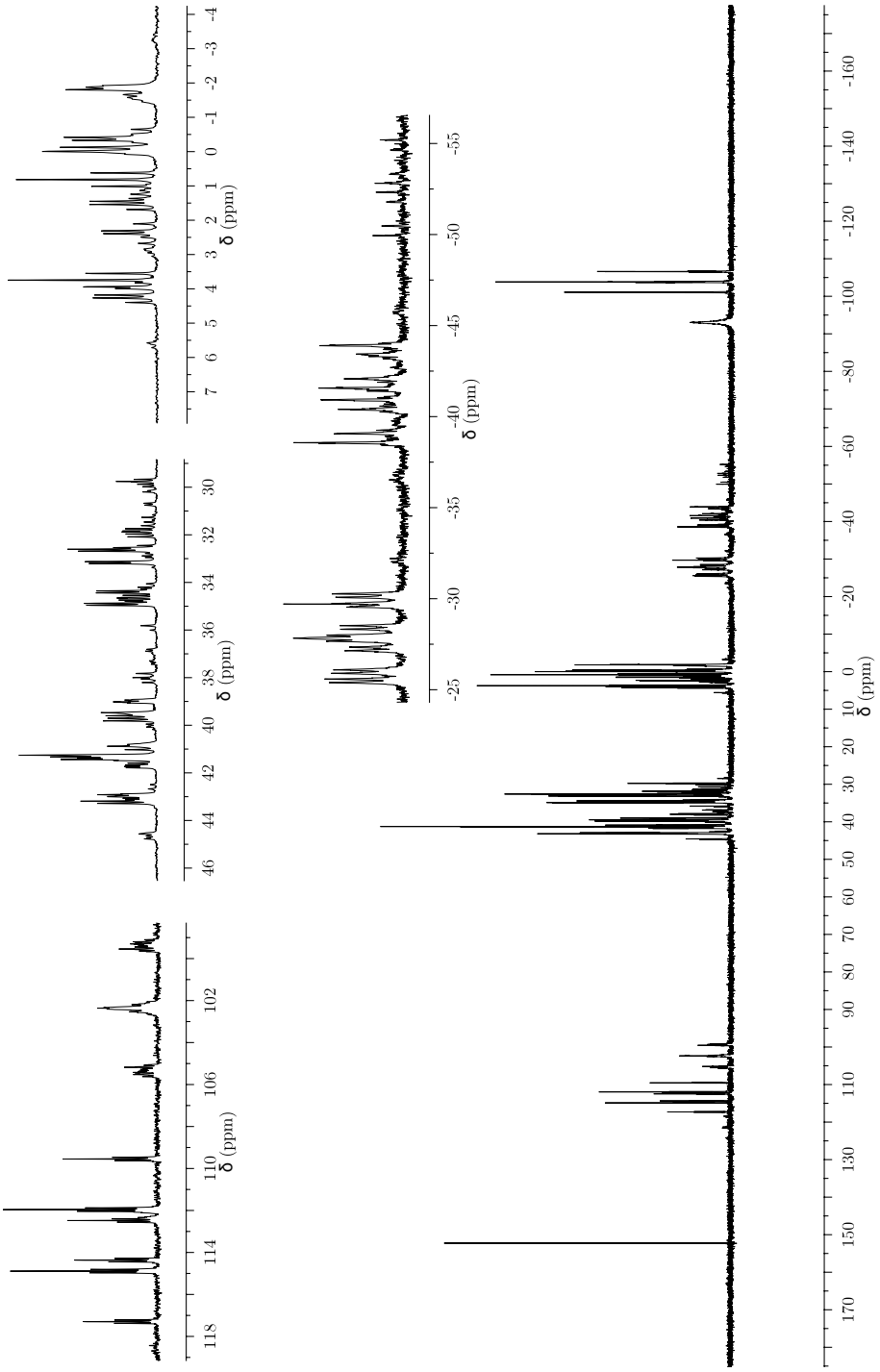


Figure 5.59: $^{31}P\{^{1}H\}$ NMR spectrum of the reaction of $[Cp^{*}Fe(\eta^{4}\text{-}P_5CH_3)]$ with $^{t}Bu_2PCl$ at room temperature in CD_2Cl_2 (crystalline product mix). The singulet at 152 ppm can be assigned to residual **XXVII**.

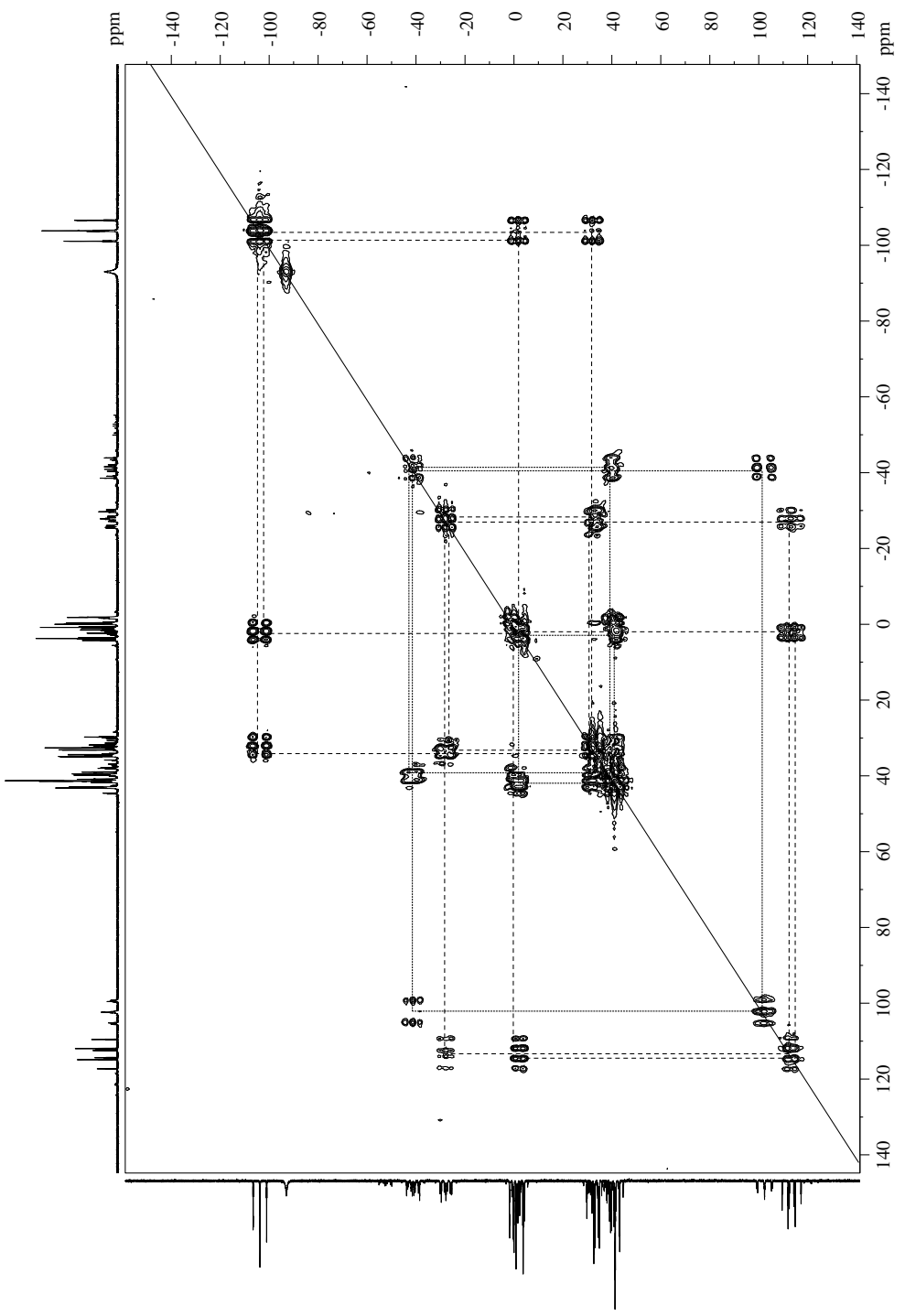


Figure 5.60: ^{31}P-^{31}P-COSY NMR spectrum in CD_2Cl_2 at 273 K of the reaction of [Cp*Fe(η^4-P_5CH_3)] with ^{t}Bu$_2$PCl at room temperature in CD_2Cl_2 (crystalline product mix). For easier understanding, the diagonal signals are connected via a solid line and the couplings between multiplets marked with dotted or dashed rectangles.

Reaction of Li[Cp*Fe(η^4-P$_5{}^t$Bu)] with Cp*PCl$_2$

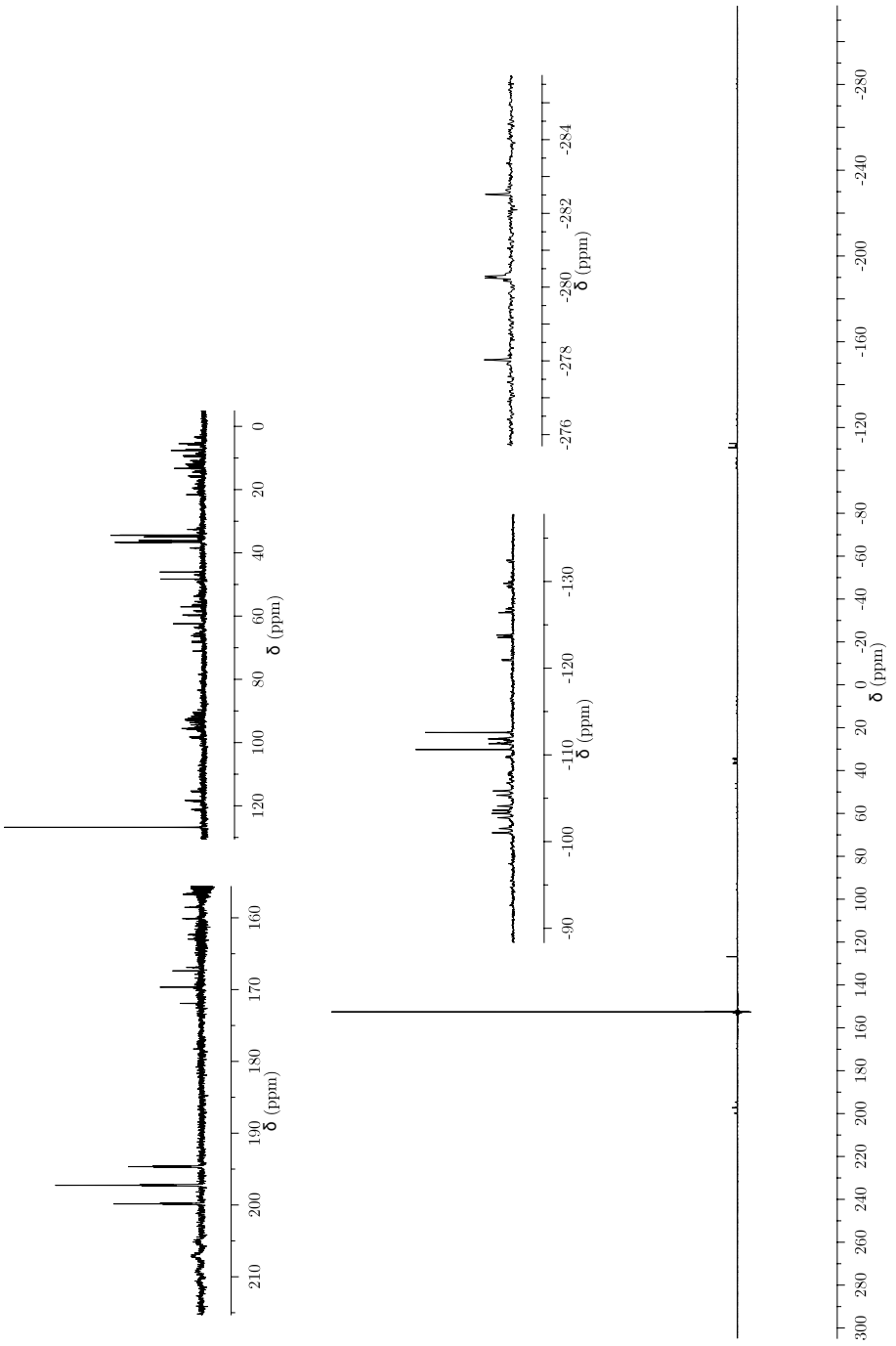


Figure 5.61: ^{31}P NMR spectrum of the reaction mix of Li[Cp*Fe(η^4-P$_5{}^t$Bu)] with Cp*PCl$_2$ at room temperature in thf with D_2O capillary.

Reaction of Li[Cp*Fe(η^4-P$_5$^{t}Bu)] with Ph_2AsCl_2

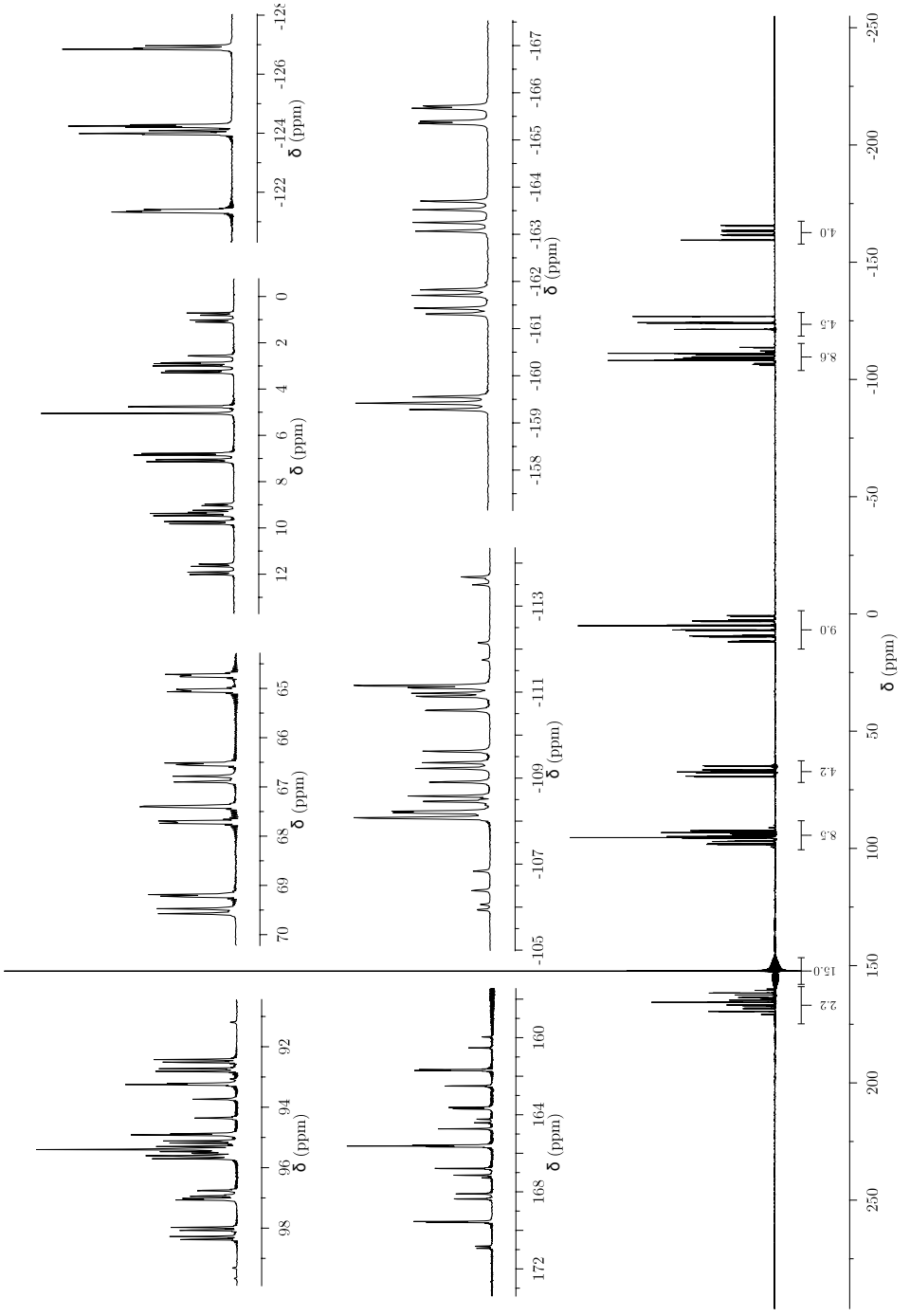


Figure 5.62: ^{31}P NMR spectrum of the reaction mix of Li[Cp*Fe(η^4-P$_5$^{t}Bu)] with Ph_2AsCl_2 at room temperature in in CD_2Cl_2.

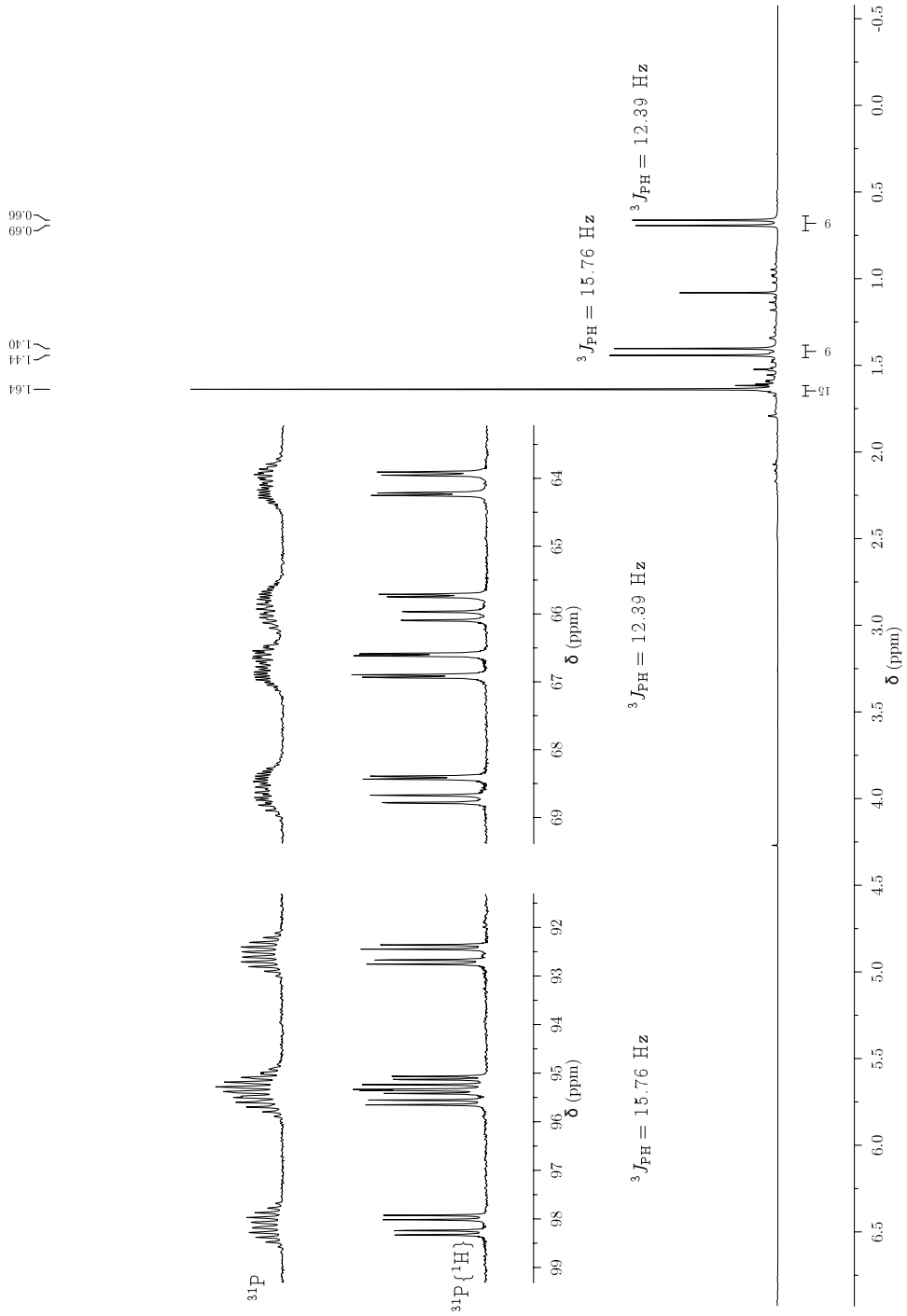


Figure 5.63: ^{1}H NMR spectrum of the first product fraction from the column chromatography of Li[Cp*Fe(η^4-P$_5$^{t}Bu)] with Ph_2AsCl_2 at room temperature in C_6D_6.

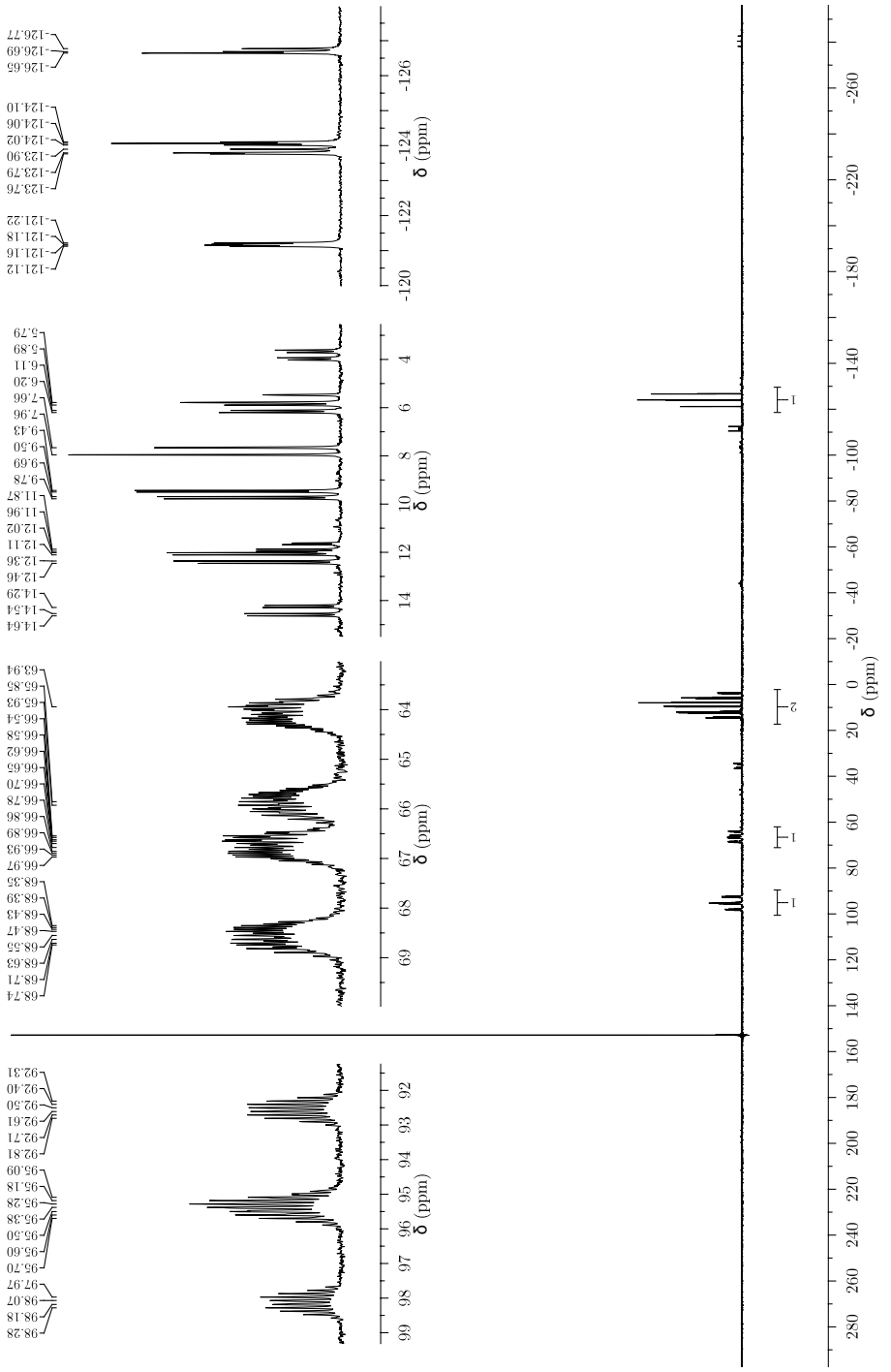


Figure 5.64: ^{31}P NMR spectrum of the first product fraction from the column chromatography of Li[Cp*Fe(η^4-P_5^tBu)] with Ph_2AsCl_2 at room temperature in C_6D_6.

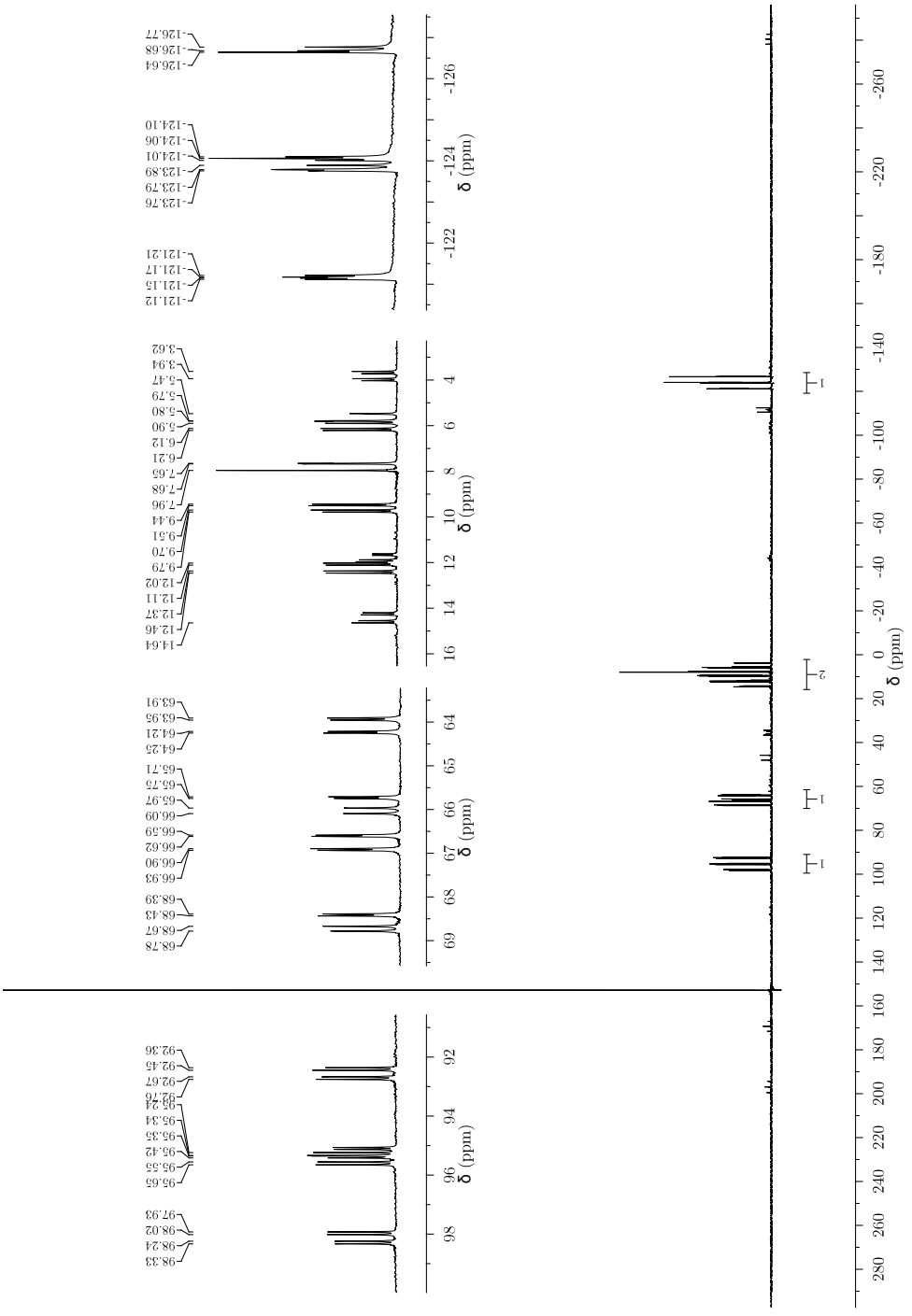


Figure 5.65: $^{31}P\{^{1}H\}$ NMR spectrum of the first product fraction from the column chromatography of Li[Cp*Fe(η^4-P$_5$^{t}Bu)] with Ph_2AsCl_2 at room temperature in C_6D_6. The singulet at 152 ppm can be assigned to residual **XXVII**.

5.4.4 Crystallographic details

General remarks

If not stated otherwise, crystals were transferred, at a constant flow of dry argon, from the schlenk flask into a cup filled with FOMBLIN (perfouroether). Suitable crystals were then mounted on a MiTeGen micro loop. Structures were solved with the ShelXT[177] solution program using dual methods and by using Olex2 1.5-alpha[178] as the graphical interface. The models were refined with ShelXL 2018/3[179] using full matrix least squares minimisation on F^2.

Crystallographic Data

Table 5.1: Crystallographic data for **10**, **11a** and **11b**:

Compound	**10**	**11a**	**11b**
Formula	$C_{23}H_{28}FeP_6$	$C_{23}H_{28}Fe_2P_6$	$C_{26}H_{34}Fe_2P_6$
$\rho_{calc.}/gcm^{-3}$	1.446	1.472	1.386
μ/mm^{-1}	8.509	8.660	5.616
Formula Weight	546.12	546.12	588.20
Colour	clear dark green	metallic dark black	clear dark brow
Shape	needle-shaped	block-shaped	block-shaped
$Size/mm^3$	$0.56 \times 0.12 \times 0.09$	$0.31 \times 0.22 \times 0.20$	$0.08 \times 0.04 \times 0.04$
T/K	123.00(10)	123.01(10)	122.99(10)
Crystal System	monoclinic	orthorhombic	monoclinic
Flack Parameter	n.a.	0.032(3)	n.a.
Hooft Parameter	n.a.	0.0028(16)	n.a.
Space Group	$P2_1/c$	$Pna2_1$	$P2_1/c$
a/Å	10.4687(6)	8.9126(2)	11.3790(3)
b/Å	15.6872(10)	17.2011(3)	10.3144(3)
c/Å	15.3249(10)	16.0790(3)	24.1083(7)
$\alpha/°$	90	90	90
$\beta/°$	94.581(6)	90	94.989(2)
$\gamma/°$	90	90	90
$V/Å^3$	2508.7(3)	2465.02(8)	2818.81(14)
Z	4	4	4
Z'	1	1	1
Wavelength/Å	1.54184	1.54184	1.39222
Radiation type	Cu K_α	Cu K_α	Cu K_β
$\theta_{min}/°$	4.039	3.763	3.521
$\theta_{max}/°$	67.178	76.223	60.133
Measured Refl's.	18786	16147	9772
Indep't Refl's	4436	4889	5459
Refl's $I \geq 2\sigma(I)$	3986	4825	4659
R_{int}	0.0582	0.0264	0.0277
Parameters	277	278	306
Restraints	0	1	0
Largest Peak	0.375	0.208	0.485
Deepest Hole	-0.495	-0.266	-0.346
GooF	1.040	1.044	1.039
wR2 (all data)	0.0949	0.0575	0.0859
wR2	0.0912	0.0572	0.0813
R1 (all data)	0.0414	0.0229	0.0489
R1	0.0364	0.0562	0.0379

Table 5.2: Crystallographic data for **12b**, **12a** and **13**:

Compound	**12b**	**12a**	**13**
Formula	$C_{23}H_{40}Fe_2P_6$	$C_{23}H_{40}FeP_6$	$C_{39}H_{59}FeP_7$
$\rho_{calc.}$/gcm^{-3}	1.385	1.338	1.316
μ/mm^{-1}	7.973	7.705	5.812
Formula Weight	558.22	558.22	800.50
Colour	dark green	metallic dark green	clear dark red
Shape	plate-shaped	block-shaped	block-shaped
Size/mm^3	$0.21 \times 0.13 \times 0.04$	$0.26 \times 0.21 \times 0.13$	$0.17 \times 0.11 \times 0.06$
T/K	122.9(3)	123.01(10)	123.00(10)
Crystal System	triclinic	triclinic	triclinic
Space Group	P-1	P-1	P-1
a/Å	8.4922(3)	9.5276(6)	10.3999(4)
b/Å	9.2804(3)	11.8971(8)	14.0095(5)
c/Å	18.5907(8)	13.5718(9)	14.2675(4)
α/°	81.447(3)	69.633(6)	78.608(3)
β/°	82.931(3)	78.755(5)	82.460(3)
γ/°	67.910(3)	75.336(5)	88.166(3)
V/Å^3	1338.90(9)	1385.50(17)	2020.12(12)
Z	2	2	2
Z'	1	1	1
Wavelength/Å	1.54184	1.54184	1.54184
Radiation type	Cu K_α	Cu K_α	Cu K_α
θ_{min}/°	4.824	4.047	3.218
θ_{max}/°	73.518	76.387	74.614
Measured Refl's.	14835	10294	28513
Indep't Refl's	5237	5570	8180
Refl's I $\geq 2\sigma$(I)	4944	5383	7884
R_{int}	0.0506	0.0219	0.0307
Parameters	277	397	433
Restraints	0	6	0
Largest Peak	0.794	0.281	0.421
Deepest Hole	-0.606	-0.372	-0.305
GooF	1.055	1.046	1.043
wR2 (all data)	0.1205	0.0769	0.0746
wR2	0.1177	0.0760	0.0733
R1 (all data)	0.0468	0.0303	0.0290
R1	0.0447	0.0292	0.0277

Table 5.3: Crystallographic data for **14** and **15**:

Compound	**14**	**15**
Formula	$C_{78}H_{118}Fe_2P_{14}$	$C_{35}H_{55}FeP_7$
$\rho_{calc.}$/gcm^{-3}	1.314	1.291
μ/mm^{-1}	5.803	6.060
Formula Weight	1601.00	748.43
Colour	clear light orange	dark red
Shape	needle-shaped	prism-shaped
Size/mm^3	$0.12 \times 0.02 \times 0.02$	$0.13 \times 0.07 \times 0.02$
T/K	100.00(10)	123.00(10)
Crystal System	orthorhombic	monoclinic
Space Group	$Pca2_1$	$P2_1/c$
a/Å	23.9115(6)	10.3372(2)
b/Å	10.4220(2)	36.5659(5)
c/Å	32.4732(12)	10.7066(2)
α/°	90	90
β/°	90	107.891(2)
γ/°	90	90
V/Å^3	8092.5(4)	3851.28(12)
Z	4	4
Z'	1	1
Wavelength/Å	1.54184	1.54184
Radiation type	Cu K_α	Cu K_α
θ_{min}/°	2.721	8.99
θ_{max}/°	65.089	133.976
Measured Refl's.	32992	37180
Indep't Refl's	12490	6813
Refl's I $\geq 2\sigma$(I)	8965	6813
R_{int}	0.0699	0.0547
Parameters	976	443
Restraints	237	10
Largest Peak	0.956	0.51
Deepest Hole	-0.608	-0.39
GooF	1.075	1.063
wR2 (all data)	0.1917	0.0895
wR2	0.1677	0.0875
R1 (all data)	0.1006	0.0363
R1	0.0663	0.0340

Table 5.4: Crystallographic data for **17**, **18** and **19**:

Compound	**17**	**18**	**19**
Formula	$C_{19}H_{36}FeP_6$	$C_{19}H_{36}FeP_6$	$C_{19}H_{38}FeN_2P_6$
$\rho_{calc.}/gcm^{-3}$	1.362	1.340	1.430
μ/mm^{-1}	8.589	6.236	6.325
Formula Weight	506.15	506.15	536.18
Colour	clear intense green	clear dark green	clear dark green
Shape	block-shaped	plate-shaped	block-shaped
Size/mm^3	$0.12 \times 0.05 \times 0.04$	$0.19 \times 0.14 \times 0.04$	$0.20 \times 0.16 \times 0.09$
T/K	122.99(10)	123.00(10)	123.01(10)
Crystal System	orthorhombic	monoclinic	monoclinic
Flack Parameter	0.020(10)	n.a.	n.a.
Hooft Parameter	n.a.	n.a.	n.a.
Space Group	$Pna2_1$	$P2_1/c$	$P2_1/c$
a/Å	20.3671(10)	12.2699(3)	16.4461(4)
b/Å	14.1783(7)	12.5118(3)	9.6469(2)
c/Å	8.5495(5)	16.9018(4)	16.1113(4)
$\alpha/^\circ$	90	90	90
$\beta/^\circ$	90	104.726(3)	103.046(2)
$\gamma/^\circ$	90	90	90
V/$Å^3$	2468.8(2)	2509.51(11)	2490.14(10)
Z	4	4	4
Z'	1	1	1
Wavelength/Å	1.54184	1.39222	1.39222
Radiation type	Cu K_α	Cu K_β	Cu K_β
$\theta_{min}/^\circ$	3.799	3.363	2.490
$\theta_{max}/^\circ$	73.215	66.004	74.790
Measured Refl's.	9969	11377	15348
Indep't Refl's	3208	5745	6759
Refl's $I \geq 2\sigma(I)$	3085	5281	6473
R_{int}	0.0600	0.0238	0.0215
Parameters	248	247	263
Restraints	55	0	0
Largest Peak	0.576	0.565	0.411
Deepest Hole	-0.498	-0.436	-0.587
GooF	1.035	1.029	1.057
wR2 (all data)	0.1128	0.0862	0.0702
wR2	0.1115	0.0832	0.0693
R1 (all data)	0.0481	0.0363	0.0270
R1	0.0461	0.0328	0.0258

Table 5.5: Crystallographic data for **21**, **22** and **23** and **24**:

Compound	**21**	**22**	**23** and **24**
Formula	$C_{29}H_{40}FeP_6$	$C_{24}H_{39}FeP_5$	$C_{18}H_{33}FeP_5$
$\rho_{calc.}$/gcm^{-3}	1.351	1.343	1.318
μ/mm^{-1}	6.957	7.448	8.459
Formula Weight	630.28	538.25	460.14
Colour	clear dark brown	clear light green	clear dark red
Shape	block-shaped	plate-shaped	block-shaped
Size/mm^3	$0.07 \times 0.04 \times 0.02$	$0.15 \times 0.08 \times 0.04$	$0.15 \times 0.08 \times 0.04$
T/K	122.9(2)	122.9(2)	122.94(15)
Crystal System	monoclinic	triclinic	monoclinic
Flack Parameter	0.088(5)	n.a.	n.a.
Hooft Parameter	0.0947(19)	n.a.	n.a.
Space Group	$P2_1$	$P\bar{1}$	$P2_1/c$
a/Å	8.85670(10)	8.4765(4)	14.8962(3)
b/Å	8.74590(10)	10.9668(5)	9.28010(10)
c/Å	20.0504(3)	15.4974(4)	17.7572(3)
α/°	90	74.289(3)	90
β/°	93.6940(10)	80.814(3)	109.141(2)
γ/°	90	74.675(4)	90
V/Å^3	1549.87(3)	1331.47(10)	2319.01(7)
Z	2	2	4
Z'	1	1	1
Wavelength/Å	1.54184	1.54184	1.54184
Radiation type	Cu K_α	Cu K_α	Cu K_α
θ_{min}/°	4.419	4.306	5.178
θ_{max}/°	73.845	74.106	74.395
Measured Refl's.	15358	9808	17406
Indep't Refl's	5847	5183	4702
Refl's I $\geq 2\sigma$(I)	5763	4579	4324
R_{int}	0.0374	0.0381	0.0340
Parameters	338	289	295
Restraints	1	0	69
Largest Peak	0.571	0.477	0.636
Deepest Hole	-0.683	-0.523	-0.466
GooF	1.046	1.013	1.053
wR2 (all data)	0.1104	0.1008	0.0827
wR2	0.1096	0.0966	0.0799
R1 (all data)	0.0414	0.0435	0.0357
R1	0.0408	0.0374	0.0319

[$\mathbf{Cp^*Fe(\eta^4\text{-}(1\text{-}Me\text{-}1\text{-}PPh_2\text{-}P_5))}$]

Crystals of [$Cp^*Fe(\eta^4$-(1-Me-1-PPh_2-P_5))] (**10**) were obtained by storing a saturated solution (*n*-hexane:dichloromethane 20:1) at 243 K for 24 hours. A clear dark green needle-shaped crystal with dimensions $0.56 \times 0.12 \times 0.09$ mm^3 was selected for the diffraction experiment. The crystal was kept at a steady T = 123.00(10) K during data collection. The structure solution was refined as a two component inversion twin (BASF 0.032(3)).

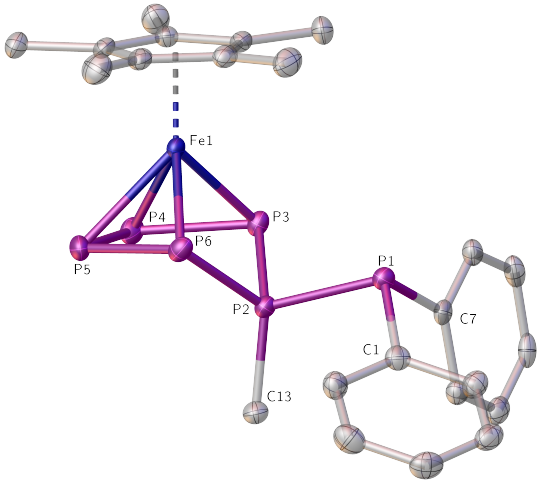


Figure 5.66: Molecular structure of **10** in the solid state. Hydrogen atoms are omitted for clarity. Selected bond lengths and angles: Fe1-P3 2.3178(7), Fe1-P6 2.3080(7), Fe1-P4 2.3318(7), Fe1-P5 2.3390(7), P2-P3 2.1433(8), P2-P1 2.2093(9), P2-P6 2.1535(8), P2-C13 1.821(3), P3-P4 2.1484(8), P1-C7 1.835(2), P1-C1 1.833(2), P6-P5 2.1540(9), P4-P5 2.1519(10), P3-Fe1-P4 55.04(2), P3-Fe1-P5 94.29(3), P6-Fe1-P3 88.58(3), P6-Fe1-P4 93.93(3), P6-Fe1-P5 55.23(2), P4-Fe1-P5 54.87(3), P3-P2-P1 101.47(3), P3-P2-P6 97.48(3), P6-P2-P1 105.55(3), C13-P2-P3 118.30(9), C13-P2-P1 111.43(9), C13-P2-P6 120.12(9), P2-P3-Fe1 86.73(3), P2-P3-P4 98.10(3), P4-P3-Fe1 62.81(2), C7-P1-P2 97.15(8), C1-P1-P2 102.55(8), C1-P1-C7 103.70(11), P2-P6-Fe1 86.74(3), P2-P6-P5 98.50(4), P5-P6-Fe1 63.12(3), P3-P4-Fe1 62.15(2), P3-P4-P5 105.10(3), P5-P4-Fe1 62.74(2), P6-P5-Fe1 61.66(2), P4-P5-Fe1 62.40(2), P4-P5-P6 103.93(3).

[$\mathbf{Cp^*Fe(\eta^{3:1}\text{-}(1\text{-}Me\text{-}2\text{-}PPh_2\text{-}P_5))}$]

Crystals of [$Cp^*Fe(\eta^{3:1}$-(1-Me-2-PPh_2-P_5))] (**11a**) were obtained by storing a saturated solution (*n*hexane:dichloromethane 20:1) at 243 K for 24 hours. A metallic dark black block-shaped-shaped crystal with dimensions $0.31 \times 0.22 \times 0.20$ mm^3 was selected for the diffraction experiment. The crystal was kept at a steady T = 123.01(10) K during data collection. The structure solution was refined as a two component inversion twin.

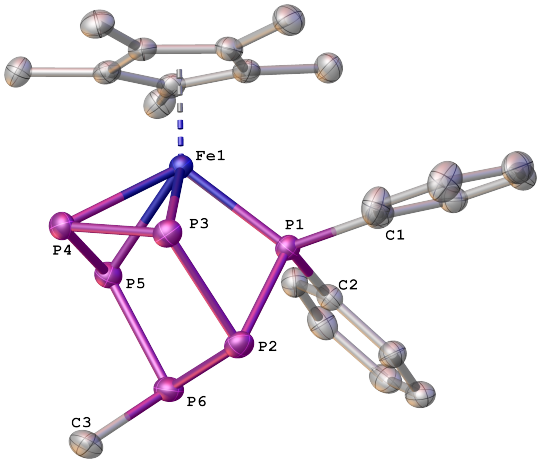


Figure 5.67: Molecular structure of **11a** in the solid state. Hydrogen atoms are omitted for clarity. Selected bond lengths and angles: Fe1-P1 2.1988(7), Fe1-P4 2.3544(7), Fe1-P5 2.3382(7), Fe1-P3 2.3724(7), P1-P2 2.1965(9), P1-C1 1.841(3), P1-C2 1.833(3), P4-P5 2.1359(9), P4-P3 2.1207(9), P2-P6 2.1868(10), P2-P3 2.2828(9), P5-P6 2.2090(9), P6-C3 1.845(3), P1-Fe1-P4 113.36(3), C3-P6-P2 100.75(12), P1-Fe1-P5 88.19(3), C3-P6-P5 102.51(11), P1-Fe1-P3 75.96(3), P4-P3-Fe1 62.91(3), P4-Fe1-P3 53.31(2), P4-P3-P2 106.79(4), P5-Fe1-P4 54.15(2), P2-P3-Fe1 92.62(3), P5-Fe1-P3 87.77(2), P2-P1-Fe1 99.98(3), C1-P1-Fe1 120.01(8), P2-P1-Fe1 99.98(3), C1-P1-Fe1 120.01(8), C1-P1-P2 102.45(9), C2-P1-Fe1 121.90(9), C2-P1-P2 106.99(8), C2-P1-C1 103.12(12), P5-P4-Fe1 62.54(3), P3-P4-Fe1 63.78(3), P3-P4-P5 100.20(4), P1-P2-P3 77.89(3), P6-P2-P1 88.64(3), P6-P2-P3 103.66(4), P4-P5-Fe1 63.31(3), P4-P5-P6 103.62(4), P6-P5-Fe1 107.35(3), P2-P6-P5 100.16(4).

[$\mathbf{Cp^*Fe(\eta^{3:1}\text{-}(1\text{-}^t Bu\text{-}2\text{-}PPh_2\text{-}P_5))}$]

Crystals of [$Cp^*Fe(\eta^{3:1}$-(1-t-Bu-2-PPh_2-P_5))] (**11b**) were obtained by storing a saturated solution (*n*hexane:dichloromethane 20:1) at 243 K for 24 hours. A clear dark brown block-shaped-shaped crystal with dimensions $0.08 \times 0.04 \times 0.04$ mm^3 was selected for the diffraction experiment. The crystal was kept at a steady T = 122.99(10) K during data collection.

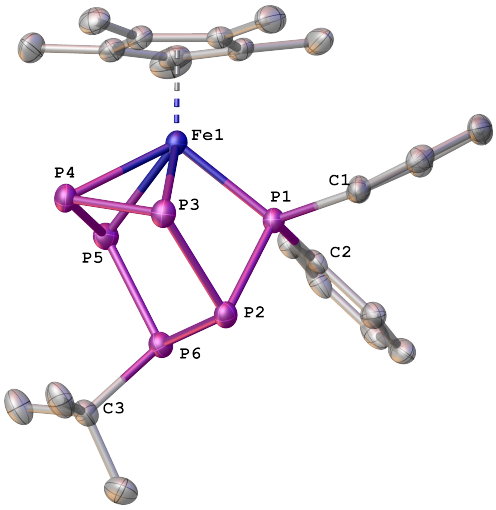


Figure 5.68: Molecular structure of **11b** in the solid state. Hydrogen atoms are omitted for clarity. Selected bond lengths and angles: Fe1-P1 2.2105(8), Fe1-P3 2.3717(9), Fe1-P4 2.3501(8), Fe1-P5 2.3450(8), P1-P2 2.1975(11), P1-C1 1.839(3), P1-C2 1.827(3), P2-P6 2.1930(10), P2-P3 2.2849(10), P6-P5 2.2025(11), P6-C3 1.901(3), P3-P4 2.1194(10), P4-P5 2.1436(11), P1-Fe1-P3 75.44(3), P1-Fe1-P4 113.33(3), P1-Fe1-P5 88.58(3), P4-Fe1-P3 53.34(3), P5-Fe1-P3 87.85(3), P5-Fe1-P4 54.33(3), P2-P1-Fe1 99.85(3), C1-P1-Fe1 117.27(9), C1-P1-P2 105.46(10), C2-P1-Fe1 125.08(10), C2-P1-P2 106.12(9), C2-P1-C1 101.21(12), P1-P2-P3 77.49(4), P6-P2-P1 88.18(4), P6-P2-P3 104.28(4), P2-P6-P5 100.23(4), C3-P6-P2 104.95(10), C3-P6-P5 108.14(10), P2-P3-Fe1 92.81(3), P4-P3-Fe1 62.81(3), P4-P3-P2 106.70(4), P3-P4-Fe1 63.85(3), P3-P4-P5 100.27(4), P5-P4-Fe1 62.71(3), P6-P5-Fe1 107.08(3), P4-P5-Fe1 62.96(3), P4-P5-P6 104.69(4).

exo-[Cp*Fe(η^4-(1-Me-1-PCy$_2$-P$_5$))]

Crystals of exo-[Cp*Fe(η^4-(1-Me-1-PCy$_2$-P$_5$))] (**12b**) were obtained by storing a saturated *n*-hexane solution at 243 K for 24 hours. A dark green plate-shaped crystal with dimensions $0.21 \times 0.13 \times 0.04$ mm^3 was selected for the diffraction experiment. The crystal was kept at a steady T = 122.9(3) K during data collection.

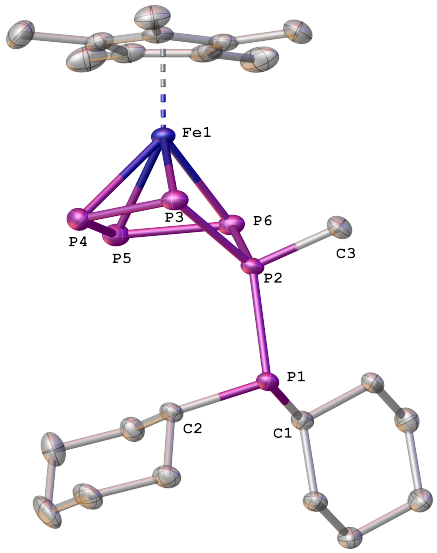


Figure 5.69: Molecular structure of **12b** in the solid state. Hydrogen atoms are omitted for clarity. Selected bond lengths and angles: Fe1-P6 2.3171(6), Fe1-P3 2.3177(7), Fe1-P4 2.3502(6), Fe1-P5 2.3379(6), P2-P1 2.2271(7), P2-P6 2.1610(8), P2-P3 2.1619(7), P2-C3 1.833(2), P1-C2 1.871(2), P1-C1 1.869(2), P6-P5 2.1389(8), P3-P4 2.1383(9), P4-P5 2.1495(9), P6-Fe1-P3 88.73(2), P6-Fe1-P4 93.52(2), P6-Fe1-P5 54.71(2), P3-Fe1-P4 54.52(2), P3-Fe1-P5 93.60(2), P5-Fe1-P4 54.58(2), P6-P2-P1 126.82(3), P6-P2-P3 97.12(3), P3-P2-P1 120.11(3), C3-P2-P1 101.33(9), C3-P2-P6 105.46(9), C3-P2-P3 103.35(8), C2-P1-P2 100.66(7), C1-P1-P2 101.04(7), C1-P1-C2 104.97(10), P2-P6-Fe1 86.21(3), P5-P6-Fe1 63.14(2), P5-P6-P2 101.52(3), P2-P3-Fe1 86.18(3), P4-P3-Fe1 63.51(2), P4-P3-P2 101.49(3), P3-P4-Fe1 61.96(2), P3-P4-P5 104.66(3), P5-P4-Fe1 62.42(2), P6-P5-Fe1 62.15(2), P6-P5-P4 104.91(3), P4-P5-Fe1 63.00(2).

endo-[$Cp^*Fe(\eta^4$-(1-Me-1-PCy_2-P_5))]

Crystals of endo-[$Cp^*Fe(\eta^4$-(1-Me-1-PCy_2-P_5))] (**12a**) were obtained by storing a saturated *n*-hexane solution at 243 K for 24 hours. A metallic dark green block-shaped crystal with dimensions $0.26 \times 0.21 \times 0.13$ mm^3 was selected for the diffraction experiment. The crystal was kept at a steady T = 123.01(10) K during data collection. Due to a ringflip of the cyclohexyl group of C1/C1' both cyclohexyl groups and the Phosphorus atoms P3, P4 and P5 are disordered. The parts are present in a 1:1 ratio. Atom numbers of the disordered part are marked with a dash. The SIMU restraint was used for refinement on C7 and C7'.

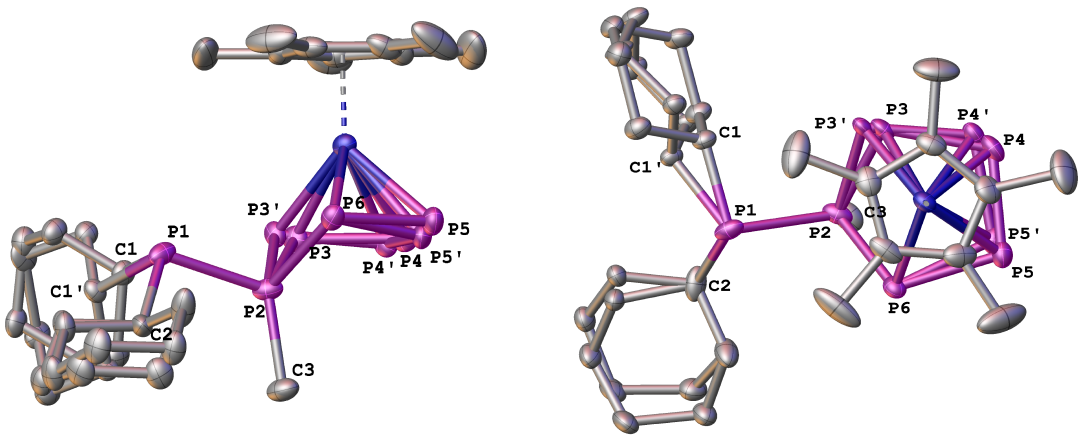


Figure 5.70: Disorder of the Molecular structure of **11b** in the solid state. Due to a ringflip of the cyclohexyl group of C1/C1' both cyclohexyl groups and the Phosphorus atoms P3, P4 and P5 are disordered. On the left side, the structure is depicted in the same angle as in figure 5.71, on the right side from below for better oversight. Both parts of the molecule are visible in a 1:1 ratio in the solid state structure.

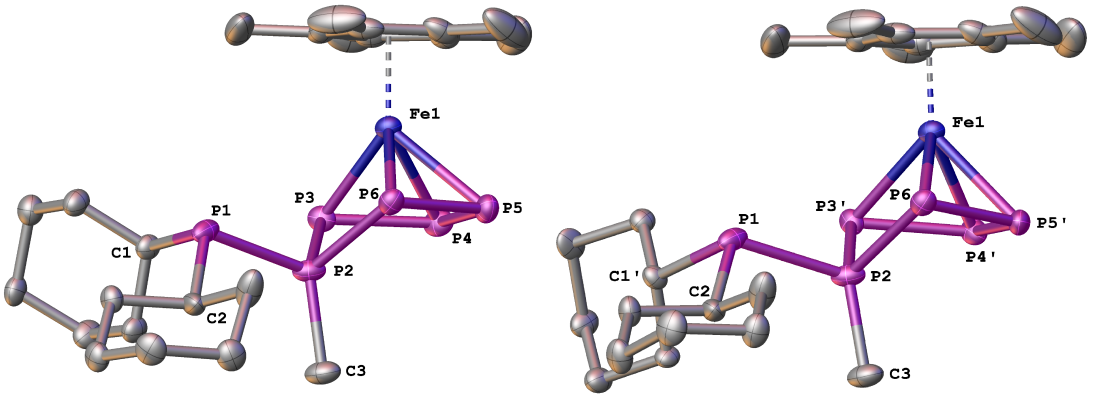


Figure 5.71: Molecular structures of the disordered parts of **12a** in the solid state. Hydrogen atoms are omitted for clarity. Selected bond lengths and angles: Fe1-P6 2.3175(5), Fe1-P3 2.257(4), Fe1-P5 2.369(4), Fe1-P4 2.330(3), Fe1-P4' 2.347(3), Fe1-P5' 2.318(3), Fe1-P3' 2.383(4), P2-P1 2.2076(6), P2-P6 2.1466(6), P2-P3 2.186(4), P2-C3 1.8278(18), P2-P3' 2.142(4), P1-C2 1.8649(19), P1-C1 1.883(3), P1-C1' 1.901(3), P6-P5 2.157(4), P6-P5' 2.128(4), P3-P4 2.136(3), P5-P4 2.141(4), P4'-P5' 2.146(4), P4'-P3' 2.145(3), P6-Fe1-P5 54.79(9), P6-Fe1-P4 92.70(8), P6-Fe1-P4' 94.51(8), P6-Fe1-P5' 54.65(9), P6-Fe1-P3' 88.31(9), P3-Fe1-P6 88.52(9), P3-Fe1-P5 94.65(10), P3-Fe1-P4 55.47(8), P4-Fe1-P5 54.20(9), P4'-Fe1-P3' 53.94(7), P5'-Fe1-P4' 54.77(9), P5'-Fe1-P3' 92.02(10), P6-P2-P1 102.64(2), P6-P2-P3 94.95(14), P3-P2-P1 109.6(2), C3-P2-P1 113.92(7), C3-P2-P6 116.46(7), C3-P2-P3 116.94(13), C3-P2-P3' 121.74(15), P3'-P2-P1 99.45(19), P3'-P2-P6 99.57(11), C2-P1-P2 100.26(6), C2-P1-C1 114.46(15), C2-P1-C1' 93.63(15), C1-P1-P2 94.28(13), C1'-P1-P2 110.69(13), P2-P6-Fe1 86.769(19), P2-P6-P5 104.8(2), P5-P6-Fe1 63.82(10), P5'-P6-Fe1 62.68(10), P5'-P6-P2 93.8(2), P2-P3-Fe1 87.34(13), P4-P3-Fe1 63.99(12), P4-P3-P2 102.8(2), P6-P5-Fe1 61.39(10), P4-P5-Fe1 61.98(12), P4-P5-P6 102.98(16), P3-P4-Fe1 60.54(14), P3-P4-P5 105.40(18), P5-P4-Fe1 63.82(13), P5'-P4'-Fe1 61.91(12), P3'-P4'-Fe1 63.87(14), P3'-P4'-P5' 104.02(19), P6-P5'-Fe1 62.67(9), P6-P5'-P4' 106.57(15), P4'-P5'-Fe1 63.32(12), P2-P3'-Fe1 85.25(13), P2-P3'-P4' 95.78(19), P4'-P3'-Fe1 62.20(12).

[$\mathbf{Cp^*Fe(\eta^{1:1:1}\text{-}(1\text{-}^t Bu\text{-}2\text{-}PCy_2\text{-}3\text{-}Me\text{-}4\text{-}PPh_2\text{-}P_5))}$]

Crystals of [$Cp^*Fe(\eta^{1:1:1}$-(1-t-Bu-2-PCy_2-3-Me-4-PPh_2-P_5))] (**13**) were obtained by storing a saturated pentane solution at 243 K for 24 hours. A clear intense red block-shaped crystal with dimensions $0.17 \times 0.11 \times 0.06$ mm^3 was selected for the diffraction experiment. The crystal was kept at a steady T = 123.00(10) K during data collection.

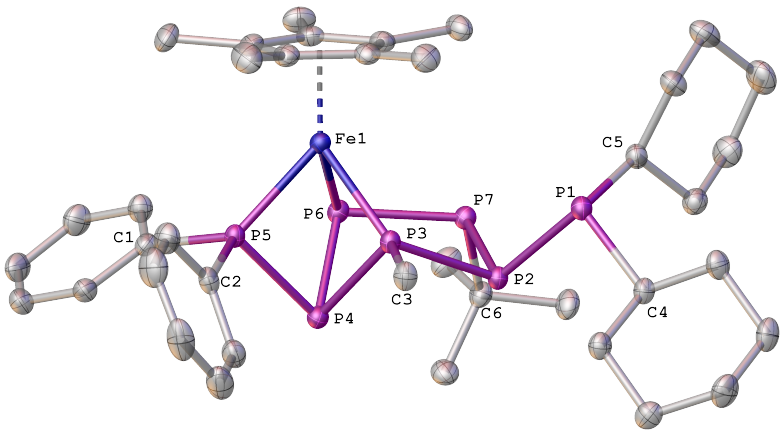


Figure 5.72: Molecular structure of **13** in the solid state. Hydrogen atoms are omitted for clarity. Selected bond lengths and angles: Fe1-P5 2.2116(4), Fe1-P3 2.1943(4), Fe1-P6 2.3141(4), P5-P4 2.2113(5), P5-C1 1.8390(16), P5-C2 1.8421(16), P2-P3 2.2217(5), P2-P7 2.1984(5), P2-P1 2.2337(5), P3-P4 2.2222(5), P3-C3 1.8393(16), P7-P6 2.2418(5), P7-C6 1.9008(16), P4-P6 2.2689(5), P1-C4 1.8719(16), P1-C5 1.8689(16), P5-Fe1-P6 77.809(15) P3-Fe1-P5 77.110(15), P3-Fe1-P6 75.086(15), P4-P5-Fe1 89.559(17), C1-P5-Fe1 125.74(5), C1-P5-P4 107.01(5), C1-P5-C2 102.48(7), C2-P5-Fe1 123.60(5), C2-P5-P4 103.77(5), P3-P2-P1 99.37(2), P7-P2-P3 91.293(19), P7-P2-P1 110.50(2), Fe1-P3-P2 125.12(2), Fe1-P3-P4 89.722(18), P2-P3-P4 93.317(19), C3-P3-Fe1 125.77(6), C3-P3-P2 101.99(5), C3-P3-P4 114.93(5), P2-P7-P6 99.53(2), C6-P7-P2 102.03(5), C6-P7-P6 105.65(5), P5-P4-P3 76.543(18), P5-P4-P6 78.779(18), P3-P4-P6 75.471(17), C4-P1-P2 95.54(5), C5-P1-P2 103.24(5), C5-P1-C4 104.65(7), P7-P6-Fe1 105.964(18), P7-P6-P4 101.18(2), P4-P6-Fe1 85.647(17).

$[\mathbf{Cp^*Fe(\eta^{1:2}\text{-}(1\text{-}^t Bu\text{-}2\text{-}PPh_2\text{-}3\text{-}Me\text{-}4\text{-}PCy_2\text{-}P_5))}]$

Tiny crystals of $[Cp^*Fe(\eta^{1:2}\text{-}(1\text{-t-Bu-2-}PPh_2\text{-3-Me-4-}PCy_2\text{-}P_5))]$ (**14**) were obtained by storing a saturated *n*-pentane at -30 °C for 2 weeks. A clear light orange needle-shaped crystal with dimensions $0.12 \times 0.02 \times 0.02\ mm^3$ was selected for the diffraction experiment. The crystal was kept at a steady T = 100.01(10) K during data collection. The two enantiomers of **14** are present in the asymmetric unit and each shows a disordered cyclohexyl group on P1 due to a ring flip. The parts of the disorder are present in a ratio of 3:1. The structure was solved as an inversion twin and the Flack parameter was refined to 0.468(11), which means that the crystal consists of a racemic mixture of both isomers. The restraint SIMU was used for moddeling the disordered cyclohexyl group of the atoms C52B, C51B, C55B, C54B, C54B, C53B, C53B, C52B, C17B and C17A in the proximity of P1. SADI was used on the former cyclohexyl groupand on C17B C18B C19B, C20B, C20A, C21A, C22B and C21B of the cyclohexyl groups on the other enantiomer.

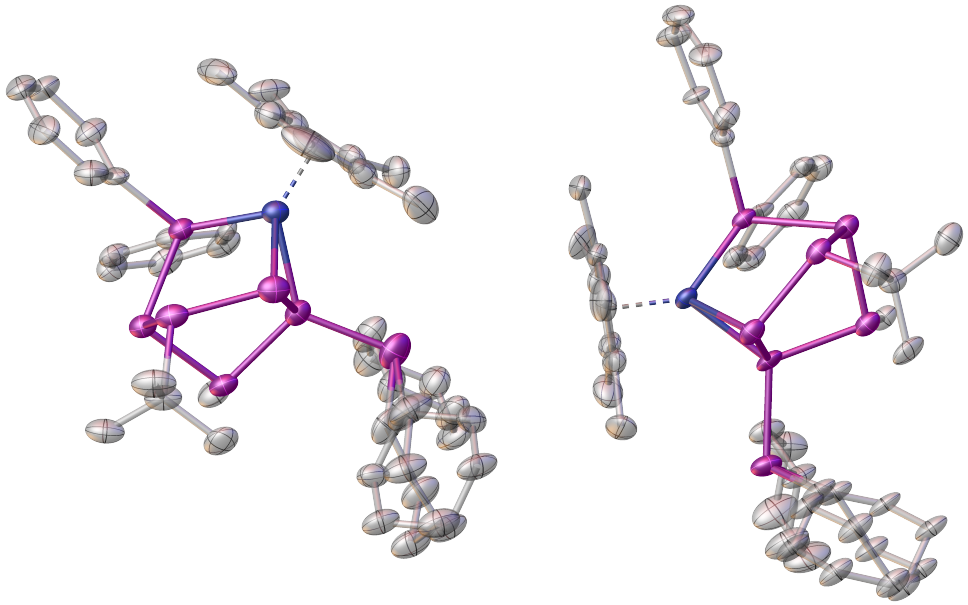


Figure 5.73: Molecular structure of **14** in the solid state (asymmetric unit).

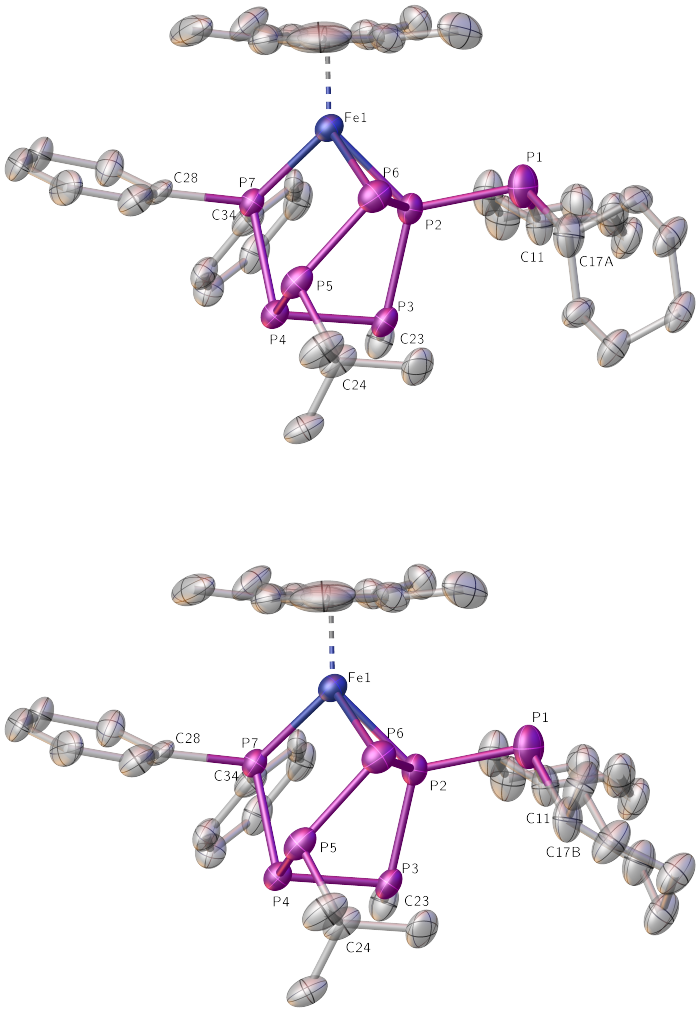


Figure 5.74: Molecular structure of **14** in the solid state showing the disorder of one of the cyclohexyl groups on P1. Hydrogen atoms are omitted for clarity. Selected bond lengths of **14**: Fe1-P7 2.166(4), Fe1-P2 2.203(4), Fe1-P6 2.307(4), P7-P4 2.262(5), P7-C34 1.857(12), P7-C28 1.836(13), P3-P4 2.193(5), P3-P2 2.232(5), P3-C23 1.873(12), P4-P5 2.193(4), P5-P6 2.221(6), P5-C24 1.908(14), P2-P6 2.163(5), P2-P1 2.208(6), P1-C11 1.881(14), P1-C17A 1.87(2), P1-C17B 1.88(3), P7-Fe1-P2 88.25(15), P7-Fe1-P6 97.76(15), P2-Fe1-P6 57.25(13), Fe1-P7-P4 112.80(16), C34-P7-Fe1 118.6(5), C34-P7-P4 96.0(4), C28-P7-Fe1 120.7(5), C28-P7-P4 102.7(5), C28-P7-C34 102.2(6), P4-P3-P2 95.49(17), C23-P3-P4 104.2(4), C23-P3-P2 110.9(5), P3-P4-P7 99.48(18), P3-P4-P5 96.11(18), P5-P4-P7 92.27(18), P4-P5-P6 102.44(18), C24-P5-P4 107.4(4), C24-P5-P6 111.0(5), Fe1-P2-P3 123.00(18), Fe1-P2-P1 124.5(2), P6-P2-Fe1 63.77(14), P6-P2-P3 101.43(19), P6-P2-P1 113.6(2), P1-P2-P3 112.1(2), P5-P6-Fe1 104.69(18), P2-P6-Fe1 58.97(13), P2-P6-P5 104.20(19), C11-P1-P2 101.5(5), C11-P1-C17B 99.4(17), C17A-P1-P2 105.5(10), C17A-P1-C11 112.7(11), C17B-P1-P2 99.6(19).

[$\mathbf{Cp^*Fe(\eta^{1:2}\text{-}(1\text{-}^t Bu\text{-}2\text{-}PPh_2\text{-}3\text{-}Me\text{-}4\text{-}P^tBu_2\text{-}P_5))}$]

Tiny crystals of [$Cp^*Fe(\eta^{1:2}$-(1-^{t}Bu-2-PPh_2-3-Me-4-P^tBu_2-P_5))] (**15**) were obtained by slowly evaporating diethyl ether from a solution of **15** in an acetonitrile-diethyl ether mixture and storing the resulting solution at room temperature over night. A dark red prism-shaped crystal with dimensions $0.13 \times 0.17 \times 0.02\ mm^3$ was selected for the diffraction experiment. The crystal was kept at a steady T = 123.00(10) K during data collection. The ^{t}Bu group of C6/C6' is disordered due to a rotation of the group with an occupation of 0.625 and 0.374, respectively of the parts. The restraint SADI was used on the C atoms of the mentioned ^{t}Bu group and P3.

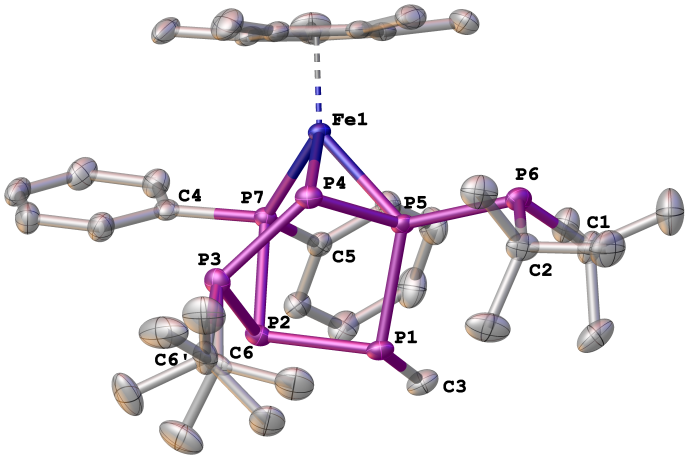


Figure 5.75: Molecular structure of **15** in the solid state showing the disorder of one of the cyclohexyl groups on P1. Hydrogen atoms are omitted for clarity. Selected bond lengths of **15**: Fe1-P5 2.2393(6), Fe1-P7 2.1735(6), Fe1-P4 2.2928(6), P5-P1 2.2465(7), P5-P6 2.2379(7), P5-P4 2.1639(7), P7-P2 2.2582(7), P7-C5 1.844(2), P7-C4 1.853(2), P1-P2 2.1917(8), P1-C3 1.864(2), P2-P3 2.1956(8), P6-C2 1.906(2), P6-C1 1.900(3), P4-P3 2.1987(8), P3-C6 1.892(8), P3-C6' 1.909(11), P5-Fe1-P4 57.02(2), P7-Fe1-P5 87.78(2), P7-Fe1-P4 98.51(2), Fe1-P5-P1 121.82(3), P6-P5-Fe1 123.47(3), P6-P5-P1 114.48(3), P4-P5-Fe1 62.73(2), P4-P5-P1 101.05(3), P4-P5-P6 112.11(3), Fe1-P7-P2 112.39(3), C5-P7-Fe1 116.16(7), C5-P7-P2 98.87(7), C5-P7-C4 99.95(10), C4-P7-Fe1 125.03(7), C4-P7-P2 100.37(7), P2-P1-P5 95.67(3), C3-P1-P5 112.19(8), C3-P1-P2 100.94(8), P1-P2-P7 99.41(3), P1-P2-P3 98.23(3), P3-P2-P7 89.95(3), C2-P6-P5 108.17(8), C1-P6-P5 104.09(8), C1-P6-C2 110.42(11), P5-P4-Fe1 60.24(2), P5-P4-P3 105.39(3), P3-P4-Fe1 101.79(3), P2-P3-P4 102.93(3), C6-P3-P2 109.6(3), C6-P3-P4 113.3(3), C6'-P3-P2 104.7(4), C6'-P3-P4 110.9(4).

$[\mathbf{Cp^*Fe(\eta^4\text{-}(1,1\text{-}P^tBu_2\text{-}CH_3\text{-}P_5)}]$

Crystals of $[Cp^*Fe(\eta^4\text{-}(1,1\text{-}P^tBu_2\text{-}CH_3\text{-}P_5)]$ (**17**) were obtained by storing a saturated toluene:*n*-pentane mixture at 243 K for one month. A clear dark red irregular-shaped crystal with dimensions $0.12 \times 0.05 \times 0.04\ mm^3$ was selected for the diffraction experiment. The crystal was kept at a steady T = 122.99(10) K during data collection.

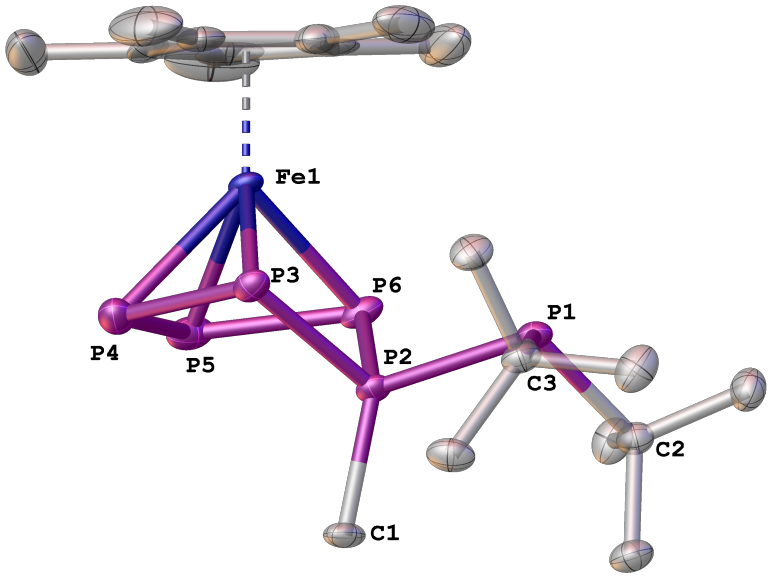


Figure 5.76: Molecular structures of **17** in the solid state. Hydrogen atoms are omitted for clarity. Selected bond lengths and angles: Fe1-P6 2.3131(14), Fe1-P5 2.3413(18), Fe1-P3 2.3034(14), Fe1-P4 2.3461(19), P1-P2 2.219(2), P1-C3 1.900(5), P1-C2 1.924(6), P2-P6 2.1753(17), P2-P3 2.1621(18), P2-C1 1.826(5), P6-P5 2.146(2), P5-P4 2.145(2), P3-P4 2.146(2), P6-Fe1-P5 54.91(6), P6-Fe1-P4 93.40(6), P5-Fe1-P4 54.46(6), P3-Fe1-P6 87.94(5), P3-Fe1-P5 93.60(6), P3-Fe1-P4 54.97(6), C3-P1-P2 103.51(19), C3-P1-C2 110.9(2), C2-P1-P2 103.57(18), P6-P2-P1 104.78(8), P3-P2-P1 106.87(8), P3-P2-P6 95.29(7), C1-P2-P1 116.9(2), C1-P2-P6 115.4(2), C1-P2-P3 115.0(2), P2-P6-Fe1 87.76(6), P5-P6-Fe1 63.21(6), P5-P6-P2 99.57(8), P6-P5-Fe1 61.88(6), P4-P5-Fe1 62.88(6), P4-P5-P6 104.42(8), P2-P3-Fe1 88.32(6), P4-P3-Fe1 63.52(6), P4-P3-P2 99.68(8), P5-P4-Fe1 62.65(6), P5-P4-P3 104.19(8), P3-P4-Fe1 61.50(6).

[$\mathbf{Cp^*Fe(\eta^4\text{-}(1\text{-}P^tBu_2\text{-}2\text{-}CH_3\text{-}P_5)}$]

Crystals of [$Cp^*Fe(\eta^4$-(1-P^tBu_2-2-CH_3-P_5)] (**18**) were obtained by storing a saturated toluene:*n*-pentane mixture at 243 K for one month. A clear dark red irregular-shaped crystal with dimensions $0.19 \times 0.14 \times 0.04$ mm^3 was selected for the diffraction experiment. The crystal was kept at a steady T = 123.00(10) K during data collection.

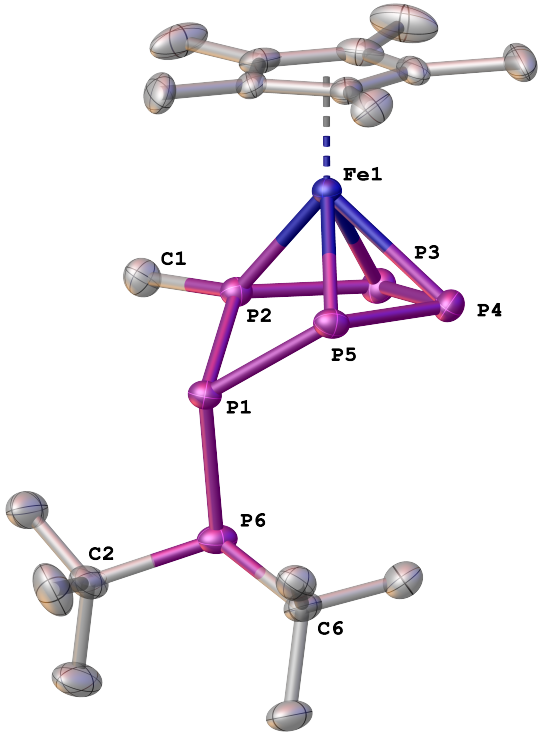


Figure 5.77: Molecular structures of **18** in the solid state. Hydrogen atoms are omitted for clarity. Selected bond lengths and angles: Fe1-P2 2.1616(5) Fe1-P5 2.3228(5) Fe1-P3 2.3982(6) Fe1-P4 2.3339(5), P2-P1 2.1244(7), P2-P3 2.1365(7), P2-C1 1.823(2), P1-P5 2.2342(6), P1-P6 2.2435(7), P5-P4 2.1641(7), P3-P4 2.1379(7), P6-C6 1.894(2), P6-C2 1.905(2), P2-Fe1-P5 78.030(19), P2-Fe1-P3 55.589(19), P2-Fe1-P4 88.830(19), P5-Fe1-P3 91.36(2), P5-Fe1-P4 55.383(19), P4-Fe1-P3 53.694(18), P1-P2-Fe1 102.36(2), P1-P2-P3 119.19(3), P3-P2-Fe1 67.83(2), C1-P2-Fe1 132.95(8), C1-P2-P1 114.35(7), C1-P2-P3 113.42(7), P2-P1-P5 80.79(2), P2-P1-P6 106.11(3), P5-P1-P6 121.58(3), P1-P5-Fe1 94.22(2), P4-P5-Fe1 62.570(19), P4-P5-P1 111.84(3), P2-P3-Fe1 56.583(18), P2-P3-P4 94.89(3), P4-P3-Fe1 61.616(19), P5-P4-Fe1 62.047(19), P3-P4-Fe1 64.690(19), P3-P4-P5 103.49(3), C6-P6-P1 103.41(7), C6-P6-C2 110.56(10), C2-P6-P1 98.51(7).

[$\mathbf{Cp^*Fe(\eta^{3:1}\text{-}(1\text{-}Me\text{-}2\text{-}P(NEt_2)_2\text{-}P_5))}$]

Crystals of [$Cp^*Fe(\eta^{3:1}$-(1-Me-2-P$(NEt_2)_2$-P_5))] (**19**) were obtained by storing a saturated dichloromethane:*n*-pentane solution at 243 K for one night. A clear dark green block-shaped crystal with dimensions $0.20 \times 0.16 \times 0.09$ mm^3 was selected for the diffraction experiment. The crystal was kept at a steady T = 123.01(10) K during data collection.

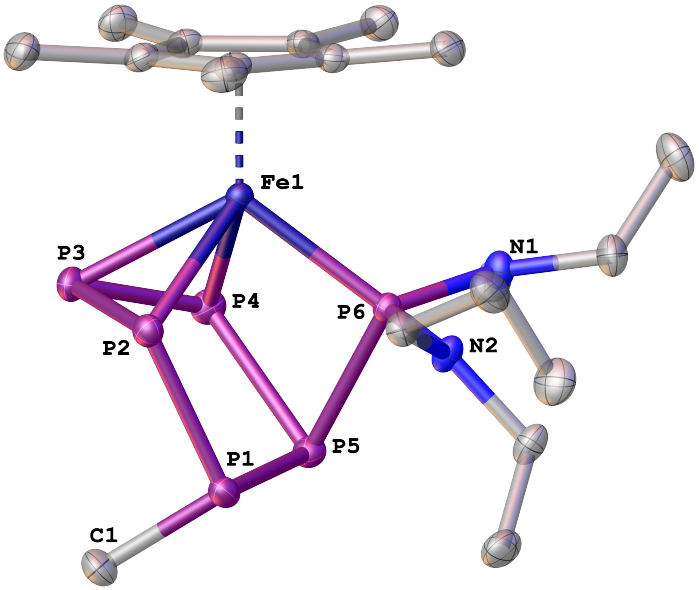


Figure 5.78: Molecular structures of **19** in the solid state. Hydrogen atoms are omitted for clarity. Selected bond lengths and angles: Fe1-P6 2.2212(3), Fe1-P2 2.3119(4), Fe1-P3 2.3583(4), Fe1-P4 2.3651(4), P6-P5 2.2433(4),, P6-N2 1.6780(11), P6-N1 1.7062(11), P1-P2 2.2052(4), P1-P5 2.1833(5), P1-C1 1.8465(14), P2-P3 2.1429(4), P5-P4 2.2715(5), P3-P4 2.1184(5), N2-C8 1.4677(15), N2-C6 1.4772(16), N1-C4 1.4715(16), N1-C2 1.4673(16), P6-Fe1-P2 88.573(12), P6-Fe1-P3 114.235(13), P6-Fe1-P4 76.822(12), P2-Fe1-P3 54.615(12), P2-Fe1-P4 88.305(13), P3-Fe1-P4 53.294(12), Fe1-P6-P5 98.184(15), N2-P6-Fe1 121.65(4), N2-P6-P5 109.09(4), N2-P6-N1 101.85(5), N1-P6-Fe1 119.06(4), N1-P6-P5 105.86(4), P5-P1-P2 101.147(17), C1-P1-P2 99.52(5), C1-P1-P5 103.02(5), P1-P2-Fe1 107.078(16), P3-P2-Fe1 63.794(13), P3-P2-P1 102.242(18), P6-P5-P4 78.339(15), P1-P5-P6 87.596(16), P1-P5-P4 102.672(18), P2-P3-Fe1 61.591(12), P4-P3-Fe1 63.517(13), P4-P3-P2 99.736(18), P5-P4-Fe1 93.369(14), P3-P4-Fe1 63.189(13), P3-P4-P5 107.277(18).

[$\mathbf{Cp^*Fe(\eta^4\text{-}(1\text{-}PMes_2\text{-}2\text{-}CH_3\text{-}P_5)}$]

Crystals of [$Cp^*Fe(\eta^4$-(1-$PMes_2$-2-CH_3-P_5)] (**21**) were obtained by storing a saturated thf solution at 243 K for one month. A clear dark red irregular-shaped crystal with dimensions $0.07 \times 0.04 \times 0.02$ mm^3 was selected for the diffraction experiment. The crystal was kept at a steady T = 122.9(2) K during data collection.

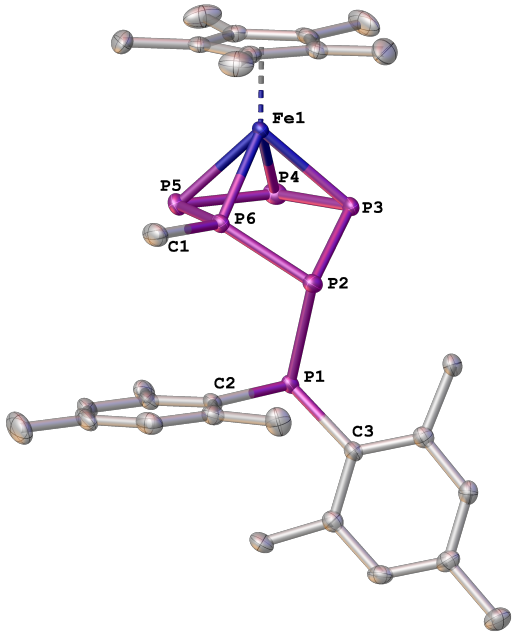


Figure 5.79: Molecular structures of **21** in the solid state. Hydrogen atoms are omitted for clarity. Selected bond lengths and angles: Fe1-P6 2.1720(11), Fe1-P3 2.3174(11), Fe1-P5 2.3821(11), Fe1-P4 2.3554(12), P1-P2 2.2585(14), P1-C3 1.849(4), P1-C2 1.846(4), P6-P5 2.1304(14), P6-P2 2.1333(14), P6-C1 1.830(5), P3-P4 2.1602(15), P3-P2 2.2137(14), P5-P4 2.1342(16), P6-Fe1-P3 79.24(4), P6-Fe1-P5 55.55(4), P6-Fe1-P4 87.86(4), P3-Fe1-P5 92.61(4), P3-Fe1-P4 55.06(4), P4-Fe1-P5 53.55(4), C3-P1-P2 110.39(13), C2-P1-P2 93.46(14), C2-P1-C3 104.67(18), P5-P6-Fe1 67.23(4), P5-P6-P2 118.63(6), P2-P6-Fe1 100.27(5), C1-P6-Fe1 130.41(17), C1-P6-P5 114.19(17), C1-P6-P2 117.31(16), P4-P3-Fe1 63.36(4), P4-P3-P2 109.71(6), P2-P3-Fe1 93.63(5), P6-P5-Fe1 57.22(4), P6-P5-P4 94.99(6), P4-P5-Fe1 62.59(4), P3-P4-Fe1 61.57(4), P5-P4-Fe1 63.87(4), P5-P4-P3 104.61(6), P6-P2-P1 105.98(6), P6-P2-P3 82.44(5), P3-P2-P1 109.31(6).

[$\mathbf{Cp^*Fe(\eta^4\text{-}(1,1\text{-}Cp^*\text{-}CH_3\text{-}P_5)}$]

Crystals of [$Cp^*Fe(\eta^4$-$(1,1$-Cp^*-CH_3-$P_5)$] (**22**) were obtained by storing a saturated o-difluorobenzene:*n*-pentane solution at 243 K for more than one month. A clear light green plate-shaped crystal with dimensions $0.15 \times 0.08 \times 0.04$ mm^3 was selected for the diffraction experiment. The crystal was kept at a steady T = 122.9(2) K during data collection.

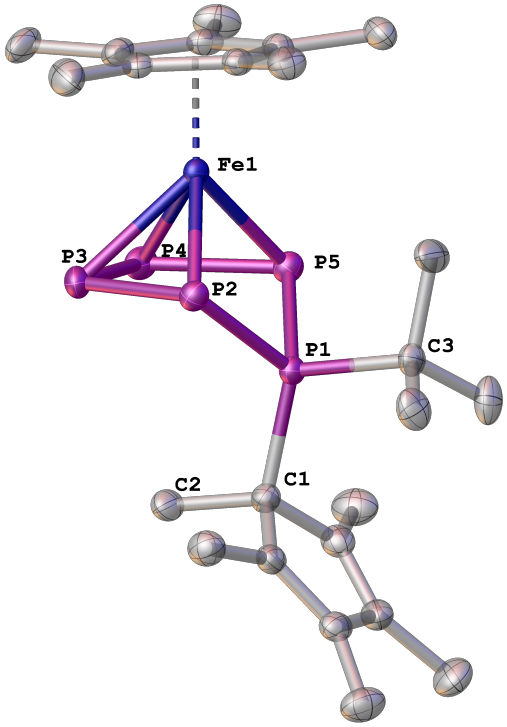


Figure 5.80: Molecular structures of **22** in the solid state. Hydrogen atoms are omitted for clarity. Selected bond lengths and angles: Fe1-P5 2.3273(7), Fe1-P2 2.3268(7), Fe1-P4 2.3285(7), Fe1-P3 2.3194(7), P1-P5 2.1793(8), P1-P2 2.1733(8), P1-C1 1.900(2), P1-C3 1.888(2), P5-P4 2.1408(8), P2-P3 2.1438(8), P4-P3 2.1552(9), P5-Fe1-P4 54.75(2), P2-Fe1-P5 86.86(2), P2-Fe1-P4 93.61(2), P3-Fe1-P5 93.48(2), P3-Fe1-P2 54.96(2), P3-Fe1-P4 55.25(2), P2-P1-P5 94.63(3), C1-P1-P5 119.71(8), C1-P1-P2 117.45(8), C3-P1-P5 106.24(8), C3-P1-P2 107.25(8), C3-P1-C1 109.98(10), P1-P5-Fe1 88.86(3), P4-P5-Fe1 62.65(2), P4-P5-P1 100.50(3), P1-P2-Fe1 89.02(3), P3-P2-Fe1 62.34(2), P3-P2-P1 100.38(3), P5-P4-Fe1 62.60(2), P5-P4-P3 103.94(3), P3-P4-Fe1 62.16(2), P2-P3-Fe1 62.70(2), P2-P3-P4 104.27(3), P4-P3-Fe1 62.59(2), C2-C1-P1 109.04(16).

$[\mathbf{Cp^*Fe(\eta^4\text{-}(1,2\text{-}(^t Bu_2\text{-}P_5)})]$ and $[\mathbf{Cp^*Fe(\eta^4\text{-}(1,3\text{-}(^t Bu_2\text{-}P_5)})]$

Crystals of $[Cp^*Fe(\eta^4\text{-}(1,3\text{-}(^tBu_2\text{-}P_5)]$ (**24**) and $[Cp^*Fe(\eta^4\text{-}(1,2\text{-}(^tBu_2\text{-}P_5)]$ (**23**) were obtained by storing a saturated *n*-hexane solution at 213 K for one month. A clear dark red block-shaped crystal with dimensions $0.15 \times 0.08 \times 0.04\ mm^3$ was selected for the diffraction experiment. The crystal was kept at a steady T = 122.94(15) K during data collection. The two compounds co-crystallize and are observed as a disorder of the envelope structure of the *cyclo*-P_5 ligand with **23** present in the ASU with 12 % occupancy.

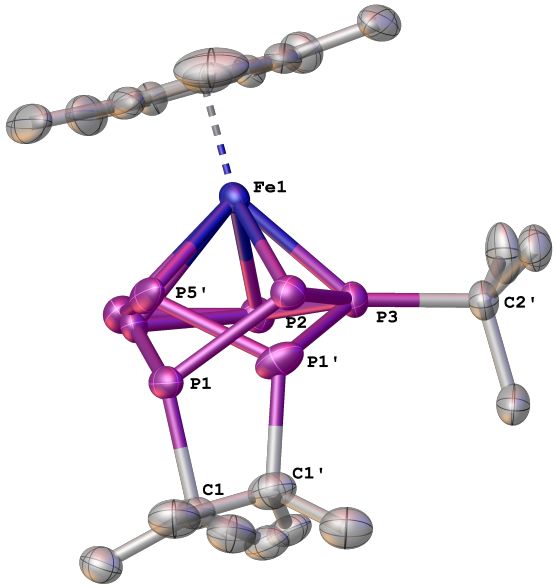


Figure 5.81: Disordered solid state structure of cocrystalized $[Cp^*Fe(\eta^4\text{-}(1,2\text{-}(^tBu_2\text{-}P_5)]$ and $[Cp^*Fe(\eta^4\text{-}(1,3\text{-}(^tBu_2\text{-}P_5)]$

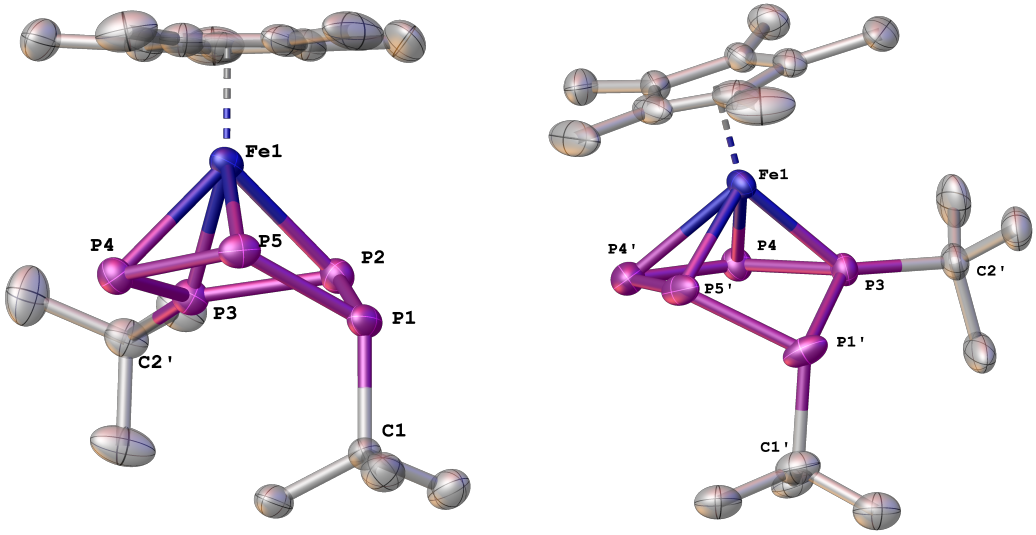


Figure 5.82: Molecular structures of **24** (left) and **23** (right) in the solid state. Hydrogen atoms are omitted for clarity. Selected bond lengths: Fe1-P3 2.2107(6), Fe1-P4 2.3672(6), Fe1-P5 2.3328(10), Fe1-P2 2.3872(7), Fe1-P5' 2.220(7), Fe1-P4' 2.465(16), P3-P4 2.1029(7), P3-P2 2.1010(7), P3-C2' 1.868(2), P3-P1' 2.321(8), P4-P5 2.1542(11), P4-P4' 2.046(17), P5-P1 2.1751(12), P1-P2 2.1640(8), P1-C1 1.888(2), P1'-P5' 2.165(11), P1'-C1' 1.85(3), P5'-P4' 2.190(19), P3-Fe1-P4 54.563(19), P3-Fe1-P5 87.30(3), P3-Fe1-P2 54.22(2), P3-Fe1-P5' 92.01(19), P3-Fe1-P4' 92.3(4), P4-Fe1-P2 95.77(2), P4-Fe1-P4' 50.0(4), P5-Fe1-P4 54.55(3), P5-Fe1-P2 83.93(3), P5'-Fe1-P4 91.7(2), P5'-Fe1-P4' 55.4(5), Fe1-P3-P1' 82.8(2), P4-P3-Fe1 66.51(2), P4-P3-P1' 106.8(2), P2-P3-Fe1 67.18(2), P2-P3-P4 114.06(3), C2'-P3-Fe1 139.26(7), C2'-P3-P4 119.86(8), C2'-P3-P2 125.96(8), C2'-P3-P1' 125.7(2), P3-P4-Fe1 58.93(2), P3-P4-P5 94.94(4), P5-P4-Fe1 61.91(3), P4'-P4-Fe1 67.5(5), P4'-P4-P3 108.9(5), P4-P5-Fe1 63.54(3), P4-P5-P1 112.71(5), P1-P5-Fe1 90.06(4), P2-P1-P5 93.35(4), C1-P1-P5 114.53(8), C1-P1-P2 113.39(8), P3-P2-Fe1 58.60(2), P3-P2-P1 102.27(3), P1-P2-Fe1 88.90(3), P5'-P1'-P3 90.5(3), C1'-P1'-P3 114.7(7), C1'-P1'-P5' 112.3(8), P1'-P5'-Fe1 86.2(3), P1'-P5'-P4' 110.7(6), P4'-P5'-Fe1 68.0(5), P4-P4'-Fe1 62.5(4), P4-P4'-P5' 102.0(7), P5'-P4'-Fe1 56.6(4).

5.4.5 Details on quantum chemical calculations

The geometry optimizations were initiated from the coordinates taken from the crystal structure coordinates of the compounds **10**, **11a**, **12b** and **12a**. All structure optimizations were carried out using the ORCA package.[181] The geometry optimizations have been done without any constraints and frequency calculations were also performed on all the optimized geometries to ensure that the optimized geometries did not have any imaginary frequencies. Geometry optimizations have been carried out using the density functional method TPSS/D4/CPM(THF)[293–296] functional. The basis set was def2-TZVP.[183,193] Single point energies for calculating the relative energies were recalculated using the ωB97X-D4/CPM(THF)[294–297] functional and the def2-TZVPPD[298] basis set.

Table 5.6: Free energies and enthalpies of isomers for $[Cp^*(\eta^4\text{-}P_5CH_3)]^-$ (Energies given in Hartree:

Compound	exo-$[Cp*(\eta^4\text{-}P_5CH_3)]^-$		$[Cp*(\eta^4\text{-}P_5CH_3)]^-$-TS		endo-$[Cp*(\eta^4\text{-}P_5CH_3)]^-$	
Method	TPSS	wB96X-D4	TPSS	wB96X-D4	TPSS	wB96X-D4
SCF Energy	-3401.3774	-3401.308875	-3401.335627	-3401.257502	-3401.370756	-3401.303187
Total correction	0.28771065	0.28771065	0.28650284	0.28650284	0.28780814	0.28780814
E_0	-3401.0896889	-3401.0211641	-3401.0491242	-3400.9709995	-3401.0829482	-3401.0153785
Thermal Enthalpy correction	0.0009442	0.0009442	0.0009442	0.0009442	0.0009442	0.0009442
H	-3401.0887446	-3401.0202199	-3401.0481800	-3400.9700553	-3401.0820040	-3401.0144343
S	0.07145098	0.07145098	0.07145304	0.07145304	0.07114333	0.07114333
G	-3401.1601956	-3401.0916709	-3401.1196330	-3401.0415083	-3401.1531474	-3401.0855776
ΔG_0 [kJ/mol]	0	0	106	132	19	16

Table 5.7: Free energies and enthalpies for the 1,2-migration in and isomers of **10** and **11a** (Energies given in Hartree:

Compound	**10**		TS of 1,2-migration **10** to **11a**		**11a**		exo-**10**		exo-**10**-isomer	
Method	TPSS	wB96X-D4	TPSS	wB96X-D4	TPSS	wB96X-D4	TPSS	wB96X-D4	TPSS	wB96X-D4
SCF Energy	-4206.266412	-4206.294325	-4206.213124	-4206.204323	-4206.284565	-4206.313136	-4206.266655	-4206.289912	-4206.264306	-4206.290965
Total correction	0.48186122	0.48186122	0.48016738	0.48016738	0.48251824	0.48251824	0.482488	0.482488	0.48211314	0.48211314
E_0	-4205.784551	-4205.812464	-4205.732957	-4205.724156	-4205.802047	-4205.830618	-4205.784167	-4205.784167	-4205.782193	-4205.808852
Thermal Enthalpy correction	0.00094421	0.00094421	0.00094421	0.00094421	0.00094421	0.00094421	0.00094421	0.00094421	0.00094421	0.00094421
H	-4205.783607	-4205.81152	-4205.732013	-4205.723212	-4205.801102	-4205.829674	-4205.783223	-4205.783223	-4205.781249	-4205.807907
S	0.09595861	0.09595861	0.09412228	0.09412228	0.09314696	0.09314696	0.09568296	0.09568296	0.09644237	0.09644237
G	-4205.879566	-4205.907478274	-4205.826135	-4205.817334	-4205.894249	-4205.922821	-4205.878906	-4205.902163	-4205.877691	-4205.90435
$G - E_{el}$	0.386846820		0.3869893		0.39031549		0.38774925		0.38661498	
ΔG_0 [kJ/mol]		0		237		-40		14		8

Table 5.8: Free energies and enthalpies for the 1,2-migration in and isomers of **12a** and **12b** (Energies given in Hartree:

Compound	**12a**		TS of 1,2-migration		Cy-1,2-mig.		**12b**-isomer		**12b**	
Method	TPSS	wB96X-D4	TPSS	wB96X-D4	TPSS	wB96X-D4	TPSS	wB96X-D4	TPSS	wB96X-D4
SCF Energy	-4213.517903	-4213.618352	-4213.456317	-4213.520256	-4213.516762	-4213.613855	-4213.519879	-4213.616323	-4213.514773	-4213.614544
Total correction	0.6213877	0.6213877	0.61916389	0.61916389	0.62220339	0.62220339	0.62152077	0.62152077	0.62158697	0.62158697
E_0	-4212.896516	-4212.996965	-4212.837153	-4212.901092	-4212.894559	-4212.991651	-4212.898358	-4212.994803	-4212.893186	-4212.992957
Thermal Enthalpy correction	0.00094421	0.00094421	0.00094421	0.00094421	0.00094421	0.00094421	0.00094421	0.00094421	0.00094421	0.00094421
H	-4212.895571	-4212.996021	-4212.836209	-4212.900148	-4212.893615	-4212.990707	-4212.897414	-4212.993858	-4212.892242	-4212.992013
S	0.10054385	0.10054385	0.09899191	0.09899191	0.09830552	0.09830552	0.10031884	0.10031884	0.10076271	0.10076271
G	-4212.996115	-4213.096564407	-4212.935201	-4212.99914	-4212.99192	-4213.089013	-4212.997733	-4213.094177	-4212.993005	-4213.092776
$G - E_{el}$	0.521788060		0.52111619		0.52484208		0.52214614		0.52176846	
ΔG_0 [kJ/mol]		0		256		20		6		10

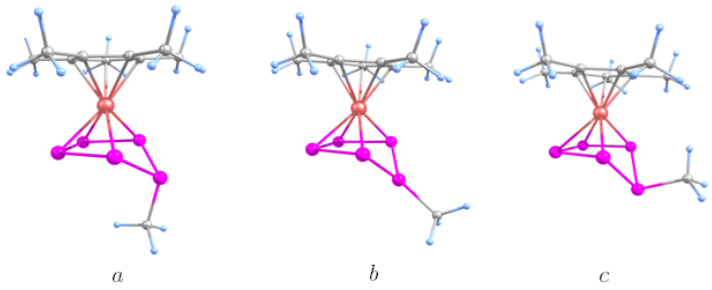


Figure 5.83: Optimized geometries for isomers for exo-$[Cp*(\eta^4\text{-}P_5CH_3)]^-$ (a), $[Cp*(\eta^4\text{-}P_5CH_3)]^-$-TS (b) and endo-$[Cp*(\eta^4\text{-}P_5CH_3)]^-$ (c).

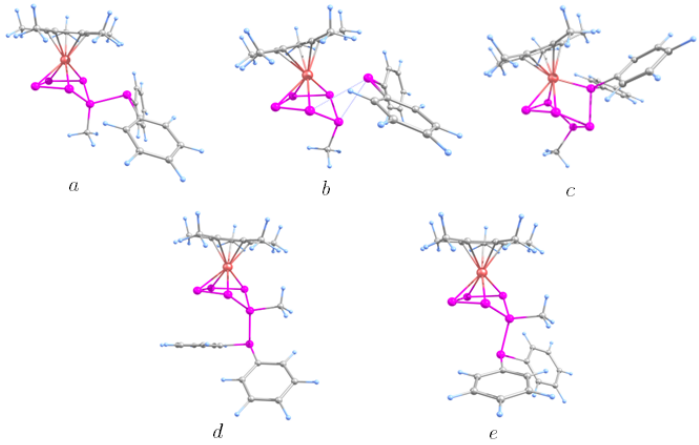


Figure 5.84: Optimized geometries for **10** (a), TS of 1,2-migration **10** to **11a** (b), **11a** (c), exo-**10** (d) and exo-**10**-isomer (e).

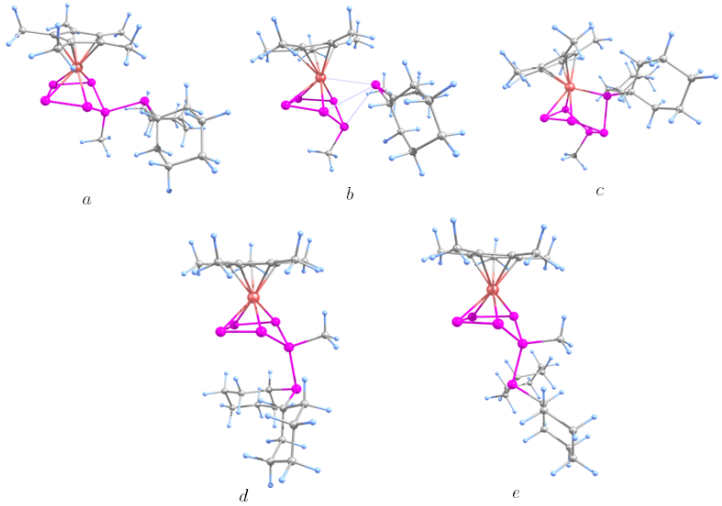


Figure 5.85: Optimized geometries for **12a** (a), TS of 1,2-migration (b), Cy-1,2-mig. (c), **12b**-isomer (d) and **12b** (e).

Cartesian coordinates for exo-$[Cp^*(\eta^4\text{-}P_5CH_3)]^-$

Fe	4.41997348188497	4.78690187310134	8.31842372956938	H	5.20857647681774	3.68028736002860	12.23787323378546
P	5.34328615261648	7.79888388796505	8.43074817461669	H	5.13024613705957	5.36842327406170	11.70355714475195
P	3.47945880826113	6.84638408534090	7.85889707275975	C	3.78484843138807	1.91155530543409	7.11018106590094
P	6.43122617176481	5.92184130750176	8.39199705489020	H	4.77907337390282	1.78882074863305	6.67028708803910
P	3.89920118031774	5.53536004710246	6.18407378107157	H	3.12342236051204	2.30692322510507	6.33341418747408
P	5.91754179515303	4.90390743391879	6.54816534669501	H	3.41561320045025	0.91668366432925	7.39597391005420
C	3.83209096649326	2.82948323965169	8.29208038053365	C	2.38188408689593	5.25632110599025	10.79970170648859
C	4.94324468082102	2.99569933849601	9.19326934826114	H	3.00962439545170	6.00644116113576	11.28927832835037
C	4.55062241799649	3.93234522197388	10.20996761335833	H	1.85812788187366	4.69052753374562	11.58351016413581
C	3.20179889646682	4.33774648421661	9.94722364055244	H	1.63088802571209	5.78303797780136	10.20452589657531
C	2.75193585070055	3.65647506924179	8.76536625512497	C	1.38741809781862	3.76933069002396	8.16006527409092
C	5.93935625270111	8.91189546454497	7.05753732934142	H	1.00049407088776	4.78949637370780	8.25168951127048
C	6.26699787000293	2.30097763217740	9.11557613279953	H	0.67636100254732	3.09525871130611	8.65814103746031
H	6.28359196525559	1.40660067633306	9.75432170653175	H	1.40829384596222	3.51319755478936	7.09696290965291
H	7.07523589237995	2.96173443844488	9.44622235802917	H	5.27499438292765	9.78042632467755	6.98255208299658
H	6.48840097665613	1.98807545450963	8.09109600780699	H	5.94764935977069	8.37514876698487	6.10338537374145
C	5.37940456633036	4.35224412371801	11.38443035531282	H	6.95183842130240	9.26198776307729	7.28906790682722
H	6.44531072491691	4.32584654592987	11.14284101814912				

Cartesian coordinates for exo-endo-TS of $[Cp^*(\eta^4\text{-}P_5CH_3)]^-$

Fe	0.13376866155949	0.07280613611583	-0.66936315942548	H	1.10101526408023	-0.51733030594351	3.32668472877598
P	1.13868228819436	2.93625863972566	-1.27026614618596	H	1.07807794494763	1.07042224067688	2.53950225625023
P	-0.80259840763736	2.05397928261204	-1.25234255411733	C	-0.64612571667661	-2.94360037584494	-1.42885686456975
P	2.14220625264147	1.12015689083084	-0.77665730057067	H	0.30957047151458	-3.11358238803828	-1.93494860788915
P	-0.51584704810920	0.50658254473363	-2.84158848201755	H	-1.37603621770518	-2.64904040621756	-2.18920207556637
P	1.50448135763605	-0.13772802719094	-2.51144589650301	H	-0.97526490994067	-3.89717542604522	-0.99321570241787
C	-0.51190353745041	-1.88518054711745	-0.38002737619672	C	-1.74665403122809	0.90327970241800	1.85062666490572
C	0.65905626397315	-1.62364512690301	0.41041396060909	H	-1.08198742871278	1.69984799309259	2.19868669117318
C	0.35622927595639	-0.54150666421921	1.31132088011411	H	-2.22570181326567	0.45674730477040	2.73398991546088
C	-0.99519096766584	-0.13627286836940	1.07655785732270	H	-2.52968457094907	1.36047534909044	1.23939438867741
C	-1.53460269996590	-0.96279088122443	0.02848825917439	C	-2.93144106882551	-0.88748082653993	-0.50463888870783
C	1.64832979090578	4.70269047214996	-0.98434569918922	H	-3.28802316506973	0.14797496088892	-0.52143001486856
C	1.95822427810808	-2.36559126448790	0.34850147582050	H	-3.62642901055798	-1.47050017523054	0.11606581285399
H	1.99365569890649	-3.16874221030548	1.09811103594219	H	-2.98297197278018	-1.27522469425580	-1.52636123435376
H	2.80190124738141	-1.69391095964143	0.54054036388021	H	1.01250229830033	5.34192918506766	-1.60571934917823
H	2.10640673439859	-2.81590630984273	-0.63764576813646	H	2.68487677467238	4.81266430017166	-1.31971806074271
C	1.26179966906948	0.00469803886197	2.37241748849959	H	1.56697095480806	5.01073899901079	0.06121761671164
H	2.31270733948621	-0.11604258279949	2.09525378446481				

Cartesian coordinates for endo-$[Cp^*(\eta^4\text{-}P_5CH_3)]^-$

Fe	4.39732434445128	4.77647536352847	8.38341707307924	H	5.22058988373819	3.53686500583542	12.25940816313356
P	5.43617074553915	7.95781862287789	8.18502178837790	H	5.11137595986405	5.24440586083716	11.79409257931585
P	3.51671379210013	6.85152163674907	8.02179847853970	C	3.74839742397599	1.93507854666302	7.09521560441335
P	6.34495892549683	5.95914197611938	8.51852078065486	H	4.74030507012472	1.82400996058431	6.64674717541961
P	3.87109296275221	5.62096804601344	6.29377286565562	H	3.08371641116120	2.35496764506453	6.33388411131841
P	5.92205901801722	4.97732656906389	6.65155192591833	H	3.37894323894594	0.93175990238655	7.34964113383551
C	3.80303700236974	2.81696022313327	8.30417482860629	C	2.36848262302472	5.17713104864706	10.88326349018268
C	4.91847828714204	2.95408535700472	9.20555367816735	H	3.00299595284531	5.88882489295712	11.41960980854776
C	4.53395157919548	3.86343134773116	10.24967067405556	H	1.81475477758638	4.58944306226005	11.62952903592924
C	3.18461910889296	4.28139914601587	10.00370691135782	H	1.64179625338120	5.75019553410938	10.29986640218573
C	2.72713660447547	3.63234292791978	8.80661384499660	C	1.36035052844899	3.76869006129624	8.21009133635783
C	5.25850433083474	8.41199501412765	9.99679676934982	H	0.97636452846819	4.78603221338999	8.33826768860244
C	6.24112202440361	2.26032133560566	9.09845503650610	H	0.64793962035163	3.08036312900404	8.68633850058115
H	6.26018640110751	1.34316163033499	9.70398616257622	H	1.37673049901752	3.54967637434537	7.13857203328348
H	7.05229626873178	2.90686788172515	9.44940688841280	H	4.57035922506372	9.25856257676814	10.08918236350569
H	6.45790568577671	1.98487165251364	8.06226446898721	H	6.23509833932782	8.71344139953291	10.38932252370670
C	5.37047312828610	4.24525167907613	11.43197591922023	H	4.87601865966106	7.56931094310297	10.58582464676225
H	6.43422079544026	4.24522143367535	11.17789530845677				

Cartesian coordinates for 10

Fe	5.31496959630317	10.27590714437857	2.89459735114859	H	10.52670792115411	10.37316345370896	7.58393279821370
P	8.31593852101960	10.41247349763596	3.33555344591734	C	9.76965278757733	9.24688138175237	5.89974533987431
P	6.86461585757136	11.97412984656027	3.04763648015141	C	10.80237887966078	7.07282981238165	5.57381766521075
P	8.45167673529775	10.47257323254880	5.54626858563093	H	10.87454785694693	6.14817777633026	5.00773853250509
P	7.01529012569845	8.73530107938735	2.96778872784310	C	3.58324896320127	7.58186290037483	2.84541685611798
P	6.16866278416155	11.43910593162865	1.07555815047612	H	3.59483470691381	7.48302089168270	1.75648319632825
P	6.27414690056111	9.29048932772809	1.01800723105283	H	2.63686269528694	7.16399616472628	3.21442236181824
C	3.31125537672098	10.16356958634897	2.49284138965712	H	4.39653760825617	6.97253238566096	3.25177774953073
C	4.17391413797138	10.91249445944898	4.51995849314192	C	2.65109462224961	10.13940513915313	1.14981873692968
C	9.32532283319343	12.08094752280553	5.69132843637884	H	2.88357263083242	11.04445802136871	0.58143605571329
C	10.69684268987153	12.25888863004349	5.45785815355387	H	1.55971021538956	10.07811267866105	1.25665251030102
H	11.32231560771180	11.40576483511626	5.21427854806423	H	2.98115894485289	9.27703528306150	0.56364184057373
C	8.53602784964096	13.19432624756114	6.01563464287573	C	9.96644417750938	10.51673307268017	2.54626749661879
H	7.47362241899403	13.06141201328741	6.20084895704908	H	9.81547948166862	10.46792767160721	1.46418242696344
C	11.26457760331671	13.52853818646989	5.54407784639623	H	10.59211525826283	9.68198147586123	2.87493529731591
H	12.32788120621852	13.65623474865837	5.36019451382275	H	10.43273544062808	11.46863063017777	2.81504580377111
C	3.58489811893341	11.33772006319869	3.28023428775857	C	4.56689126830821	11.79638564124498	5.66274855969037
C	4.26002809289449	9.48280924786049	4.50621213321462	H	5.43094021488504	11.38791093726923	6.19414668999161
C	3.72347212262193	9.01451699447342	3.25692393777661	H	3.73676804364018	11.88339478655434	6.37702161116732
C	11.52706019643008	8.48158052803436	7.39342551043956	H	4.82262923339731	12.80189838023726	5.31806680627278
H	12.16572201988504	8.65856896355843	8.25456385655090	C	4.76024713126580	8.63044136821023	5.63079834787096
C	10.47024314456421	14.63404837926713	5.85945596619540	H	5.12951038973562	7.66865445178183	5.26538596965973
H	10.91598914079236	15.62267563969279	5.92461320119935	H	3.95040370907121	8.43210390142855	6.34632305131996
C	9.10515788046238	14.46515460800552	6.09534986842668	H	5.57371482028972	9.12653406061287	6.16791372750283
H	8.48379205884771	15.32021426318127	6.34642606592605	C	3.27297773042568	12.75197886044120	2.89969256225050
C	11.63408459946676	7.28989771450371	6.67301569360235	H	4.01412198406113	13.44455812137464	3.31056481693303
H	12.35796129715106	6.53577448682515	6.96858544224376	H	2.28847111337912	13.04816993507581	3.28610777520659
C	9.87319540640847	8.04077896849533	5.19250292613774	H	3.26081254162993	12.87341804698721	1.81314820300205
H	9.22369275366217	7.84696386503602	4.34216482187570				
C	10.60107255314691	9.45134275785168	7.01386254683836				

Cartesian coordinates for TS of 1,2-migration 10 to 11a

Fe	-1.18242053519584	-0.16436881002383	-1.29030538590428	C	3.21324492366676	-0.91703580144275	2.17557599752836
P	1.88511992296026	0.03203831893766	-1.56859213157827	H	3.49884014637283	0.10097453111733	2.41562040347429
P	0.35789427098439	1.57808842903584	-1.56570028687880	C	2.00052391110597	-1.17044911860900	1.50480673663494
P	0.75756777842460	0.10677433377687	1.12838719574662	C	2.49204366085334	-3.55774756192136	1.63557813981842
P	0.52911322364236	-1.64913492697514	-1.75109631210734	H	2.20196057394239	-4.58375985427539	1.42480502710569
P	-0.82218713786463	1.06438784271407	-3.27642367968680	C	-2.85621181870529	-2.93482236882652	-1.41070183451885
P	-0.67277411806145	-1.06005125248568	-3.42249175729911	H	-2.76874426912175	-3.02483716031275	-2.49736684945488
C	-3.23518949671437	-0.37448109573957	-1.75479732212618	H	-3.81426920455227	-3.37748127022263	-1.10840270851816
C	-2.50009703875067	0.41453159831157	0.29031200445957	H	-2.05420257610018	-3.52110484773155	-0.95385152155580
C	1.69147695690500	1.66983838961213	1.34292591257095	C	-3.90976520332913	-0.42624036965596	-3.08612242281707
C	2.97998700755611	1.94620367217563	0.85483281450981	H	-3.69104858925075	0.46801210298170	-3.67680465659721
H	3.49173940446155	1.20082887294689	0.25271317109610	H	-4.99690215022353	-0.48072021591202	-2.93981142036247
C	1.03674347144666	2.66512452561422	2.08948410218065	H	-3.59845406294968	-1.30167808160862	-3.66163192522890
H	0.04305960204993	2.47143989175687	2.48114673454215	C	2.90519078375172	0.18338712383849	-3.11365307960395
C	3.59754324818037	3.16504050875921	1.11701892697673	H	2.26813850924990	0.23299942377846	-4.00162517046249
H	4.59637726005091	3.35681086028758	0.73401243789696	H	3.57103499298979	-0.68330293958150	-3.18273420201913
C	-3.04063992897792	0.81014445865525	-0.96739408531584	H	3.51222124471796	1.09241752454659	-3.04285483025993
C	-2.34409582775168	-1.01916657342777	0.28203728610071	C	-2.33220253164459	1.31955101816947	1.46560029531454
C	-2.78992098739042	-1.50316192607028	-0.98471810606342	H	-1.64705265006451	0.89543623211419	2.20184775997018
C	4.05005536030341	-1.96436755127707	2.55702519312868	H	-3.30705528750427	1.46329123247790	1.95175541020784
H	4.97969309210867	-1.74272724204201	3.07508391610924	H	-1.96383465405074	2.30432037220992	1.16410445607769
C	2.93142945687461	4.14647881055643	1.85826856350114	C	-1.97148500370773	-1.86763417755450	1.45379277640914
H	3.40946907193363	5.10319766234060	2.05001545553019	H	-1.60982114507507	-2.84935147713764	1.13891678807924
C	1.64921239368778	3.89283922302284	2.34424708609607	H	-2.85781394686793	-2.02282423517630	2.08403401389571
H	1.12347622339153	4.64765658597094	2.92266081090662	H	-1.20631117551788	-1.38591999769859	2.06878981766948
C	3.70286310801366	-3.28812047594834	2.27925473136087	C	-3.42688243335116	2.20246152599329	-1.35157887302953
H	4.36274939841334	-4.10078461456319	2.56974104384209	H	-2.73466883820315	2.93464222355902	-0.92598706987304
C	1.64967977031487	-2.51466589872206	1.26382001367144	H	-4.43307696480835	2.43153661197999	-0.97610831089513
H	0.70985862723650	-2.73928578472132	0.77017451696468	H	-3.43117981985586	2.32477172242239	-2.43763559722017

Cartesian coordinates for 11a

Fe	6.02768454049631	8.55612327105339	2.42694669213749	C	6.25383887359876	7.17222818233320	6.65269010116735
P	8.25380023503801	11.32560460039797	3.40229772987521	H	5.53430681984123	7.93808321999229	6.92218276009540
P	6.54405115875853	10.78970625143002	2.08864625234936	C	7.06255891804045	7.33477414666674	5.51957393362943
P	6.87293254631520	8.79185277171294	4.42370036993515	C	8.11564876403347	5.20123205163203	6.00547204709046
P	8.95667114311309	9.31615168596848	3.94825450133798	H	8.84682752672774	4.43963050623417	5.74938305058264
P	7.42521103813211	9.35816063539215	0.74313282439906	C	5.40040869065249	5.44487316530865	3.20567750328583
P	8.30960816487351	8.03807303286615	2.16158442578954	H	6.38171197078871	5.11225643715860	2.85558502296543
C	5.21799273552969	7.09123962959413	1.19992763892189	H	4.67109300642302	4.66473835377201	2.94832731526221
C	3.93291634792192	8.77066213979212	2.17227158324258	H	5.43729983379039	5.52275848834241	4.29371029574243
C	6.27928867034358	10.08162153926590	5.57198702926976	C	5.93341699171820	6.25941708994628	0.18376758071825
C	6.94494618843908	10.31414645832768	6.78507205831805	H	6.35281960836640	6.88327140474104	-0.61055264365629
H	7.77789060510485	9.68051071552432	7.07747480220365	H	5.24195483146822	5.54033336249270	-0.27477971723725
C	5.22417157190504	10.91444242885297	5.19421913878285	H	6.75083126523821	5.69652729251712	0.64328321288860
H	4.73250615134782	10.74466513769568	4.24215777548416	C	9.53984390803355	11.82163981920302	2.15263196147473
C	6.54686942764585	11.36327416404214	7.60808840309382	H	9.71197710875518	11.03356172088522	1.41367723100551
H	7.06753713076103	11.54205378882223	8.54477626102834	H	10.47072359373945	12.05988059902390	2.67689658954550
C	4.54832894930748	8.34639584567216	0.95213106050812	H	9.18369017343501	12.72208620233387	1.64203882104776
C	4.20574213536413	7.78136399219340	3.16772564417008	C	3.04202713150147	9.96530391879992	2.31654604577637
C	5.00346494044798	6.73871437025005	2.56890944171645	H	2.81759564083125	10.17345491269361	3.36525646070718
C	6.37028214580247	6.03256206484925	7.44907903070433	H	2.08877958955345	9.78337862456461	1.80303460589577
H	5.73539049135678	5.92296900546534	8.32397738555672	H	3.49369204602196	10.85864858324437	1.87356045700368
C	5.48435384351715	12.18990921598196	7.22735204889210	C	3.59617835408623	7.74039308899795	4.53376531963013
H	5.17874759631728	13.00993908477672	7.87121328021581	H	4.14702451234736	7.07443916817812	5.19936494152934
C	4.82320116775282	11.96495126242294	6.02065288627028	H	2.57010815807776	7.35685406431862	4.45687442382347
H	4.00159242165777	12.60825208922671	5.71841900219913	H	3.54666125028524	8.73014980857863	4.99366638859885
C	7.29906946433354	5.04300681151715	7.12742801433017	C	4.37309086356138	9.02721965698845	-0.36968254263751
H	7.39100986577405	4.15662288815560	7.74876394247938	H	4.42944388803851	10.11514183265429	-0.26665622665075
C	7.99668971606934	6.33615363731804	5.20736997282591	H	3.38361223907775	8.78072414989979	-0.77781088414458
H	8.63243043809225	6.43865640151036	4.33206825065974	H	5.12954032844764	8.71032549541927	-1.09056179683756

Cartesian coordinates for exo-10

Fe	5.40196210265893	10.22678619892163	2.36806747879614	C	11.25392488536073	9.50634515154463	6.75703883217805
P	7.99818995350253	10.18142355218812	3.91571728305111	H	11.36615469797948	10.48002206032652	7.22434234654873
P	6.71720095087837	8.57115987319959	3.28616783533830	C	10.06664634348475	9.18222212379283	6.08229856901595
P	8.61973790513325	10.30109376236213	6.07924297707623	C	10.97958577558920	6.98246857115876	5.59607690300800
P	6.78021068191896	11.83726825554648	3.29762017296325	H	10.86492623775351	6.00071639272650	5.14482799239704
P	4.95797892594355	9.14963758975784	4.38497739329152	C	3.89388984869228	12.83732499431627	1.26875553417265
P	4.99853764908504	11.31026774464047	4.38734857887056	H	3.22927584306907	12.93875686120518	2.13092830114434
C	3.56747622663277	10.24423498973323	1.46471410688709	H	3.36164851152113	13.20833956513925	0.38252486028041
C	5.51984238319670	9.54237484708022	0.40736328214885	H	4.76178391015452	13.48433639787468	1.43000770498998
C	9.29892289688337	11.99297158789057	5.92356538102886	C	2.22410966468757	10.23545529367853	2.12487228536959
C	10.54136484717007	12.32031038882152	5.35796843602265	H	2.09518676162200	9.34232687640156	2.74276491938783
H	11.21705241702936	11.53501772990228	5.03421939256399	H	1.42389426509410	10.24563280033005	1.37268630877506
C	8.44045908791849	13.02816175260180	6.32913643312094	H	2.09536246392071	11.11191640312622	2.76630997796725
H	7.47622717661660	12.78268807878806	6.76656825384106	C	9.48490573719836	10.15653024207033	2.84321754710612
C	10.91733088203003	13.65378834234947	5.21292793786598	H	9.15187580368536	10.07468633462787	1.80492723266891
H	11.88347797370923	13.89550445623938	4.77827266784368	H	10.10972994942664	9.29933971399251	3.10377231261223
C	4.31272070369107	9.08580475321909	1.04285194117066	H	10.04535871719230	11.08339004511391	2.98072734777895
C	5.51828517167750	10.97515604258184	0.42626977179969	C	6.56142042336049	8.67701944523728	-0.23150637656165
C	4.31220013066092	11.41335176810571	1.07451378332005	H	7.55431126042947	9.12977841207490	-0.15834143821063
C	12.29434938884845	8.58098211873291	6.83791143261389	H	6.33458300940535	8.53434555514752	-1.29699158824960
H	13.20838366123197	8.84806233697523	7.36150447109525	H	6.60072017972736	7.69072143091595	0.23824989117960
C	10.05508961653789	14.67736643711347	5.61618238242500	C	6.55573435381224	11.85912979227283	-0.19328591555030
H	10.35171768897939	15.71583624492730	5.49826327134365	H	6.61103089486173	12.82537301402549	0.31499782813148
C	8.81500642445074	14.36224622142049	6.17213497744208	H	6.31072045724563	12.04652818372907	-1.24776348840951
H	8.14017897614164	15.15271572312941	6.48823770289170	H	7.54609878459785	11.39677377596940	-0.15710732122386
C	12.16500239241604	7.32002314607677	6.25269977738750	C	3.89229291673259	7.65760180988250	1.19811093318135
H	12.97876880805313	6.60307911815274	6.31432692876541	H	4.75973079675347	7.00383929738424	1.33194271154557
C	9.93497295251096	7.90153857205484	5.51893059991329	H	3.34978367454645	7.31436070134934	0.30697365569549
H	9.01105429779720	7.61828129534288	5.01858959592210	H	3.23626450879087	7.53237511972951	2.06389539327023

Cartesian coordinates for exo-10-isomer

Fe	7.61614757815073	12.24290182736571	1.41173728777320	C	11.41670887015558	9.58367555358372	6.43252690615076
P	8.26880814113949	10.47089960830112	3.75355430788787	H	11.59897304132933	10.62370617469817	6.67892890974803
P	6.47013975252063	11.55967054951547	3.28750849496581	C	10.13951917958366	9.16460149287195	6.03075557734642
P	8.66230948636818	10.24403618742682	5.95993449827749	C	10.98012960317413	6.88612572684385	5.86241515813941
P	9.56452996378316	11.32410790563034	2.24707619488414	H	10.79951694241973	5.83607496660952	5.64937952783559
P	7.21862509212470	13.57416326813507	3.29019449062132	C	9.57147397628075	12.96579374607447	-1.03065568356011
P	9.23924019452088	13.41975797250799	2.57375493049170	H	9.88551097768274	13.93918499069042	-0.64428240347465
C	7.16919730953614	13.51050738951384	-0.13372403075978	H	9.58199667370042	13.01685641892471	-2.12782685024492
C	6.33739976863460	11.34213799123007	0.03240513229542	H	10.31492169983091	12.22264885541666	-0.72560604575848
C	9.24712670049302	11.95436715820562	6.22250317948758	C	7.25856809616205	15.00471769553963	-0.13913391061184
C	10.38128697246110	12.50772028887643	5.60838403469090	H	6.60001035889810	15.44041997810626	0.61740443608885
H	10.99885669817232	11.90011973561933	4.95606873503939	H	6.96387257269344	15.40644133141343	-1.11784890056801
C	8.43785043424171	12.77422212495158	7.02254180627061	H	8.27930677214130	15.33795139984393	0.06889374451265
H	7.55083912204320	12.35642437762272	7.49174112403368	C	7.95695386164044	8.75431800097200	3.18384881290154
C	10.70886452349598	13.84632215749981	5.81170158498601	H	7.58174909993388	8.80149697748677	2.15959287575109
H	11.58842569217811	14.26330929564325	5.32963675006003	H	7.21485578775587	8.28329673226507	3.83293101754382
C	6.00985924226475	12.73136694343516	0.21392053399555	H	8.88864258814285	8.18542186449782	3.21021810440541
C	7.69074567315379	11.26087645043011	-0.42779911812731	C	5.39470607232924	10.19268271137842	0.20884293084284
C	8.20761964053686	12.59864327912297	-0.53553282961068	H	5.92883720525302	9.27028042220237	0.45164396617999
C	12.46171856398500	8.66533499326621	6.53851043429074	H	4.83277838533292	10.01913169905343	-0.71912566704756
H	13.44340957517503	9.00873684366477	6.85365777121986	H	4.67284270092537	10.38934245400053	1.00604675873415
C	9.89601647889386	14.65482309579961	6.60860406783512	C	8.42028774829805	10.01148870386906	-0.81187677776855
H	10.14839241945621	15.70122724678589	6.75615048866706	H	9.49510672805848	10.11096376842336	-0.63804743470582
C	8.75675568702524	14.11909647296686	7.21033516728593	H	8.26976350767552	9.79886477397482	-1.87915327318009
H	8.11779812162864	14.74509584486321	7.82673979563580	H	8.06118719919963	9.14816398415491	-0.24569024298825
C	12.25317012216401	7.31785254452002	6.24231258745724	C	4.67799710811612	13.26256772842141	0.64370958637661
H	13.07122073479699	6.60737738972224	6.31993933599372	H	4.19449378702483	12.58450077393248	1.35396744150505
C	9.93121628339157	7.79740804727680	5.77104528433772	H	4.00905148555290	13.37225981333116	-0.22049376003679
H	8.93791568499504	7.44183172819317	5.51094698757147	H	4.77690854837705	14.24103913932647	1.12145436432500

Cartesian coordinates for 12a

Fe	4.31968972911790	4.78260945934624	8.24451561047909	H	6.69955168505851	4.38039292702621	10.78556517209348
P	5.32628949063090	7.63118735470593	8.02816419773139	H	5.61293076151632	3.74528427950456	12.03406465274236
P	5.47756271916532	8.23701933929742	10.16220971346226	H	5.44687016510621	5.42134881302679	11.48091489739440
P	3.32296532542692	6.84584083641050	7.99104019897401	C	3.56767388454513	1.88371574609919	7.14808322896268
P	3.42305641435192	5.58240224829466	6.24751151305107	H	4.49620379412053	1.76347485261821	6.58314669849196
P	5.45548127598206	4.87443157752717	6.21743268942496	H	2.80118049447556	2.25752146633536	6.46287890188525
P	6.38675891379729	5.76388973914437	7.94622764549649	H	3.25235192205969	0.89150597314294	7.49808981063713
C	5.77058633291157	8.95607603204136	6.83199921978639	C	10.03758733921640	8.39066542154630	11.49597725891126
H	5.15228197221933	9.84252947701185	6.99599602263026	H	11.06518408362956	8.04997193437977	11.67189640497049
H	5.57604708831306	8.55403562569555	5.83330557520341	H	9.96646927970663	9.41309487631095	11.89463367946840
H	6.82836797732469	9.21468630606340	6.92567408941138	C	2.60971939348887	5.23366505620573	10.97048169344217
C	3.75753126210334	2.81487473534147	8.30438225912310	H	3.27264235949808	6.02283545607185	11.33634286279060
C	4.97627633708041	3.00997630857633	9.04709747065830	H	2.24685826978474	4.66430265375160	11.83727983212591
C	4.70546453806513	3.94961307718643	10.10380378462485	H	1.74698924722460	5.70818944469991	10.49513391804740
C	3.32441240898899	4.32391378312784	10.02132080119247	C	1.29890069916802	3.69599498191163	8.49883477101375
C	2.73556772269164	3.62431302333610	8.91439217626299	H	0.88433643705716	4.69279127843378	8.67708448177561
C	3.81260590567556	10.36794793981385	9.52684282255971	H	0.69617288891580	2.97682841244638	9.06993111960232
H	3.13857524617833	9.96253054888949	10.29434275543923	H	1.18466361940423	3.46509169471441	7.43641987991412
H	3.56808064654393	9.84604787384673	8.59377701794671	C	7.30300730616274	7.94261821548881	10.46913273357625
C	5.26686842358246	10.08590717028249	9.94912680632364	H	7.43513455732262	6.91082449471872	10.10864572492410
H	5.94828301610722	10.45034798740966	9.16962437276443	C	3.56318481959038	11.87323430830683	9.36691249244724
C	9.04563103985427	7.48871419404198	12.24145731529776	H	2.51869633297751	12.04565022133545	9.08059589468542
H	9.25018383825812	7.50253676289890	13.31895363787285	H	4.18903620042440	12.25719796651968	8.54878603935081
H	9.17288724348362	6.45093970802719	11.90165611534520	C	7.59590425715752	7.92489529409528	11.98310236331934
C	8.28936206995614	8.84050225855869	9.71326156835516	H	7.44051430775978	8.92392143868644	12.40856012303594
H	8.09134254387254	8.79478121806562	8.63699702524995	H	6.89681958549633	7.24837974748694	12.48855053963346
H	8.15298264140599	9.88487613543047	10.02282824395376	C	5.33391458200492	12.33667365514543	11.10660697204142
C	5.58801806333092	10.82889118002988	11.25928290540846	H	5.55032129936184	12.84152672924454	12.05597790363690
H	4.95990603251002	10.42647755737050	12.06664483914411	H	6.03319597266643	12.74097934352399	10.36100392711653
H	6.63022647600439	10.66174160287235	11.54770656776114	C	3.89607923903351	12.62668974981272	10.66028870876439
C	6.28580401335506	2.32977462621945	8.79695674152528	H	3.75301236282454	13.70504013293563	10.52056971844788
H	6.37004653524695	1.41494198907042	9.39879371872119	H	3.20021137485545	12.31026163800420	11.45052068097046
H	7.12382605383475	2.98196112154776	9.06243239244021	C	9.73844323948209	8.41173318076759	9.99178812332151
H	6.39166059705692	2.05364174930377	7.74400659617726	H	9.89736664602534	7.40625768759724	9.57711227957265
C	5.67068415159637	4.40184682333100	11.15480544292458	H	10.43034754685402	9.08660155798753	9.47311765816244

Cartesian coordinates for TS of 1,2-migration

Fe	-0.77937396549111	-1.85420749427296	-1.25712729382484	H	1.21235835051567	-2.87910143697144	1.50002179793643
P	0.76762212498280	0.57815435578506	-2.44771788109469	H	-0.08264748377758	-3.39709003456900	2.59172020049262
P	0.19989448943488	0.40072450902252	0.46917453903146	H	0.15672776285807	-1.66977062819762	2.26261914286188
P	-1.34189429509259	0.07087024809856	-2.43032406066575	C	-2.32468920188163	-4.60342021695294	-2.20954288289149
P	-1.43938290954703	-1.75216815324635	-3.53884829615699	H	-1.46643620561283	-4.97705333208804	-2.77579249152620
P	0.40437911365268	-2.73156342141480	-3.12043846607459	H	-3.01949147120845	-4.13413073956000	-2.90964986925765
P	1.43284004506752	-1.39678292520424	-1.80849764639363	H	-2.82821766435550	-5.46333105136978	-1.74731952179961
C	1.30516768466521	0.83758745714635	-4.21001860454551	C	4.66505511058608	1.73795746522505	1.55192677248380
H	0.84263112941512	1.75610145967155	-4.58708768026616	H	5.76131827780813	1.70515362566296	1.58208225599150
H	1.01429063418325	-0.00778194193660	-4.84069783648153	H	4.35067429697431	2.56332272832562	2.20737258437404
H	2.39376380715046	0.95730841025074	-4.23133093981463	C	-2.56825603094587	-1.04870088407758	1.47342807645505
C	-1.90172082449091	-3.65128641742870	-1.13944829249759	H	-1.78254258628464	-0.47493243760631	1.97116002000854
C	-0.71599338425485	-3.77338652718655	-0.33855224734907	H	-3.13587636756755	-1.59008777156535	2.24307162947455
C	-0.76946943562901	-2.77539845692779	0.67531698617963	H	-3.25201832212240	-0.35637006518630	0.97683952495453
C	-1.99700158717190	-2.03481130616106	0.51006475712661	C	-4.01516765593685	-2.11264807748961	-1.13082549322059
C	-2.68028705241562	-2.55820968672691	-0.62539730154463	H	-4.16496195974551	-1.04441933084921	-0.95175911525679
C	-1.92552140557275	2.31684579352431	0.03147076380323	H	-4.81938489971085	-2.65823464977184	-0.61987980753181
H	-2.51741356254102	1.76658619301921	0.77461570126416	H	-4.11014783150101	-2.29564331656607	-2.20497440087593
H	-2.15258551859326	1.87813478997360	-0.94377294311313	C	2.06977927156871	0.70321477357456	0.56822010144412
C	-0.43421832959686	2.16559465759518	0.36101141630021	H	2.50333105937711	-0.09778304102078	-0.04771989550353
H	0.15589903605413	2.71935788365464	-0.37949195405364	C	-2.34506771406495	3.79408344298063	0.04237980646319
C	4.08055875564955	0.42392920630990	2.08222284346991	H	-3.41136158282792	3.87704298359454	-0.20290573134573
H	4.40408448909210	0.25044799703570	3.11640159508376	H	-1.79291401921393	4.32799168816886	-0.74442601996879
H	4.46274716114650	-0.41208040486771	1.47912223745730	C	2.54456307852842	0.42145726628335	2.01445518925677
C	2.64345190646164	2.02755878434666	0.05491111099190	H	2.14905209622226	1.18503916322448	2.69664468999930
H	2.31243718110873	2.19523535220296	-0.97710667437223	H	2.15476396132785	-0.54328632865327	2.35554877664357
H	2.26994405008367	2.86574239146160	0.65607870422240	C	-0.59077719884948	4.25909041541941	1.79375336550323
C	-0.19077280153155	2.77348527589784	1.76682106397848	H	-0.40646862989055	4.66614684317840	2.79594651106342
H	-0.79363711738805	2.21885754546738	2.49935773129604	H	0.05293682554283	4.81306389328718	1.09623570436645
H	0.85403226906031	2.67012801150562	2.07070188725991	C	-2.05876883574524	4.44803191064046	1.39856675022816
C	0.33626053411001	-4.82779738560651	-0.46676456096369	H	-2.31241672564718	5.51512157209050	1.37229981423400
H	0.11749448946260	-5.66037886209125	0.21532060543530	H	-2.69823154324186	3.98393125020942	2.16327491633384
H	1.32339217739005	-4.43381768329975	-0.20721838270128	C	4.17825208848909	2.01652373978332	0.12432326029735
H	0.38086649081753	-5.22274849084393	-1.48463116521386	H	4.56459108445536	1.23832476039154	-0.54941871425036
C	0.18723718259954	-2.66595736355943	1.81716149184785	H	4.57271810360609	2.97623201925999	-0.23295815505857

Cartesian coordinates for Cy-1,2-mig.

Fe	4.44029317265693	4.69392943113723	8.20878302061185	C	5.15077501695487	1.46695808744548	8.69811840405271
P	5.65529498122494	8.07957172786022	7.45497377535293	H	4.58238994884555	0.60579162442837	8.32735348108161
P	6.45704812836305	5.39616385336176	8.96126816126216	H	5.55451981922870	1.19602390961398	9.67636604755731
P	3.82882274778674	6.88214080135456	7.76891001660476	H	5.98727396366605	1.62674203585925	8.01071463589950
P	3.87351467208510	5.53167419079658	6.09608859624822	C	4.59759065408105	3.38264929389759	11.29028607107937
P	5.84400044395321	4.75608161390483	6.31414740040299	H	5.62053591993050	3.00883159070126	11.26599221945570
P	7.09370452688160	6.47484762864406	7.13701770443436	H	3.99681552292958	2.67546621674845	11.87815239303016
C	5.43561792328928	8.71340603147438	5.71891029697313	H	4.59101162170051	4.33735097161661	11.82036589256245
H	4.58011289829791	9.39612064207409	5.70976862318722	C	3.12833656247371	2.28191707581848	6.48076794898635
H	5.25239144112374	7.89576856361309	5.01543231389951	H	4.09729586623420	1.99424149029436	6.06207255892576
H	6.33191987948134	9.26937805376571	5.42638221484672	H	2.61039270689799	2.90328739157609	5.74615202813708
C	3.29338446193876	3.00126391474433	7.78197961143992	H	2.54060028549338	1.36628959600413	6.63180027313682
C	4.24309891539273	2.66053918915670	8.78927233874823	C	10.43615371449991	2.77197287122064	9.62448032361066
C	3.99700484210854	3.51255477950657	9.92532780263674	H	11.22589219438389	2.05941915111309	9.35671640005915
C	2.89178474385743	4.36747797956176	9.61958872759972	H	10.66009295741234	3.13479939084588	10.63806689721236
C	2.44534542207149	4.04884505554451	8.29805956762011	C	2.19457310136973	5.31343232405282	10.54554957243928
C	5.38505145674645	7.25040352488420	10.82239126721118	H	2.80821153893415	5.55787476139616	11.41516344277850
H	4.67597038801587	6.48963012704462	11.16642878369789	H	1.26300951246844	4.86056113715498	10.91068266100757
H	4.93304873895254	7.72786196727402	9.94978495385104	H	1.93631268514222	6.24614523106808	10.03471908847421
C	6.70009120947272	6.55440872481467	10.43908597754955	C	1.20495757051211	4.59525230816559	7.66283368321428
H	7.40163741804807	7.31222089507655	10.06036053698780	H	1.10087144501726	5.66883132661940	7.84934104822441
C	9.06985941750343	2.07765135788021	9.63012509622196	H	0.32624261445381	4.09416353476450	8.09096840779273
H	9.05801621594849	1.25866450282388	10.35978972796419	H	1.19923733379138	4.43272437515378	6.58256489553979
H	8.88341169478346	1.63307216990145	8.64208869445190	C	7.94256542437255	4.22661996970988	8.94520761275179
C	9.30566206757735	4.94645210038201	8.97675490873103	H	7.82874587557980	3.77824741574445	7.94448478164612
H	9.31926108640901	5.77366897062116	8.25995949005924	C	5.59804223647381	8.29857242754264	11.92168821918605
H	9.48015437919088	5.37638091464915	9.96992767897451	H	4.63566888939531	8.75904321232114	12.17648280819667
C	7.31912039293977	5.90989473727321	11.69316953290974	H	6.24390618029615	9.09821737741914	11.53207119027724
H	6.65298017276909	5.12826878224358	12.07571085463827	C	7.94100763606300	3.06855617419402	9.95294576182227
H	8.27237793161906	5.43393772534580	11.45842375557240	H	8.07910786844463	3.45043445533727	10.96968202188012

H	6.98567399698461	2.54973041806173	9.92731247920040	H	6.43956532961200	8.45178086715058	13.92008726852006
C	7.54610923731537	6.96414690683720	12.78878232241797	H	5.55016020747316	6.95716061785983	13.61363645507827
H	7.98725601092021	6.48034134388444	13.66904032325161	C	10.43778321479632	3.95893039573499	8.65453310505704
H	8.27715079966339	7.70178513852808	12.42787822004228	H	10.30870106276693	3.59088857713272	7.62680657745999
C	6.24571847092800	7.68065889909087	13.16448154363406	H	11.40110036000317	4.48237792717621	8.69056130962919

Cartesian coordinates for 12b-isomer

Fe	6.05163262492754	4.56349680054592	15.63466680478681	H	9.32752683866252	4.12437439053878	9.17435534266743
P	7.85315198796361	6.21376759778437	13.82246466451656	H	7.60487834982243	4.45966320148234	9.36065875824642
P	8.24934907858899	7.82984589552815	12.31825402376445	C	6.98111858316826	10.33414976015862	12.24079596274598
P	6.79719271266687	4.35350990710709	13.46566475789309	H	7.90737290374334	10.68717187196659	12.70943036583110
P	6.93708923930894	6.69335085124322	15.72142893293622	H	7.12456431858668	10.40359630463820	11.15361334861478
P	4.85047931833901	6.51073803339152	15.24424826747318	C	4.23352223652971	9.24634946842492	12.44197394389075
P	4.75819871051067	4.96244694489076	13.74748567375706	H	3.30729161962109	8.88200628266840	11.98066257420145
C	5.67282575716152	4.26616156420078	17.64212483588609	H	4.10388136027754	9.16586160242758	13.53056639832978
C	6.71834549022467	8.86626145948665	12.63273342844570	C	5.79900117936279	11.22157043923459	12.65786008290483
H	6.61268659146075	8.83032669527616	13.72908049896031	H	5.72526761771720	11.22160548235190	13.75480574946596
C	7.01754100231529	3.85270451610136	17.34419305602512	H	5.98405430778501	12.25755234797049	12.34801807905592
C	7.87501156842443	6.85881064812193	10.76344658831682	C	3.28259125989874	3.55683837171578	16.84380926182816
H	6.86334220174063	6.44094270313506	10.84996099417398	H	2.93708272528716	4.56667875456349	17.08272527369595
C	4.77757168954405	3.48975488642346	16.82449810238907	H	2.87326337360890	2.87117362225804	17.59772688132996
C	7.93555061314124	7.79977671297247	9.54441673005414	H	2.86574493016832	3.27820865627561	15.87179699274868
H	7.22158088566848	8.62253539210157	9.65722772045581	C	5.27845698133574	5.28868112230035	18.66115311384243
H	8.93666646918531	8.25089940086112	9.49394605150272	H	6.01637985606158	6.09503259234944	18.72165223647534
C	7.65226437402824	7.03193349468914	8.24527115536200	H	5.20206276231781	4.83211767880156	19.65725147037249
H	6.62251246037491	6.64843601707762	8.27263491843313	H	4.30940748248772	5.73290829499635	18.41797663862432
H	7.71696369745134	7.71674274432820	7.39084342258437	C	4.47954116613603	10.71237975682679	12.06323295622489
C	6.95701222725797	2.82326489543851	16.35065968030403	H	3.64532321526903	11.33856349645535	12.40263830049151
C	8.87220319331452	5.70081080495000	10.58869180776523	H	4.52070737956172	10.79932521667767	10.96764267950337
H	9.89572110478335	6.10130997105985	10.57231726548019	C	8.25562235419192	4.35109034887051	18.02208062366552
H	8.80811725570447	5.00887701034978	11.43707659744799	H	9.13080807907595	4.26147100248770	17.37304553179854
C	5.57484461992427	2.59349632847500	16.02880996039626	H	8.45140670312948	3.76407043553997	18.93000248213177
C	5.40970634175304	8.35736057363502	12.01566890295484	H	8.15431829092158	5.39920111725919	18.31648439826391
H	5.22811666833076	7.32188042312987	12.32199583638140	C	8.11898649012864	2.05282293792185	15.80554190000401
H	5.48812728601680	8.36677940104729	10.92116966699416	H	7.92863000015832	1.71959181545840	14.78175163647800
C	8.62745812196368	5.86134208535933	8.06928022790161	H	8.30294581158668	1.16137151501966	16.42084746691109
H	8.38743422133400	5.29956331960158	7.15835202483853	H	9.03337910168799	2.65198256466920	15.80603114913233
H	9.64579712364345	6.25657081889357	7.94353032852566	C	5.06322043394753	1.56738527195102	15.06602499530631
C	9.55740810437150	5.68255363673580	14.26351551146329	H	4.08983794165899	1.85727723247006	14.66108512180810
H	10.06645396869442	5.31832576119275	13.36774502260042	H	4.94903212064113	0.59427934576327	15.56237260271420
H	9.50355169617107	4.88881366563681	15.01138340807336	H	5.75460816240685	1.43460275650270	14.22812201464769
H	10.10149220655825	6.54211847809087	14.66247307361385				
C	8.59456345020580	4.93233550213932	9.28880372358585				

Cartesian coordinates for 12b

Fe	4.26626888213142	4.66097836219897	7.47826349254731	C	8.91519471758619	7.52251258927862	12.47296498436815
P	5.01649939835818	7.43754962393494	8.55630472964047	H	9.20735046985521	7.65691101725038	13.52166219667085
P	5.30206903575945	8.43658187452342	10.53809361610920	H	8.89528431828436	6.44071644141907	12.27892730162156
P	6.21001405290649	5.67911451093801	8.16896492133932	C	8.11629095097761	8.60251460153345	9.83030672718708
P	5.26485715316364	4.32708848039273	9.55095088020278	H	7.82905031956439	8.43757337463098	8.78568840792776
P	3.18166705831105	4.90298235511337	9.52058728157769	H	8.12727256009084	9.68778953327316	9.99329546415390
P	3.09993529659114	6.53948253504096	8.12884562654743	C	5.81149711899764	11.13952981540528	11.15461751007225
C	5.35632773087034	8.56652813934407	7.14301849305335	H	5.21481882992296	10.96440060301105	12.06095157465404
H	4.65662982947623	9.40439394135865	7.14473395315950	H	6.84894616732909	10.88954924987680	11.39765189427423
H	5.22640170946893	7.98395841329372	6.22618673197458	C	1.34298966844349	3.66237957352408	6.60771983827135
H	6.38052777812597	8.94062812070307	7.20168914237466	H	0.83383066099045	3.08992516381735	5.82055218999514
C	3.78382288920067	2.75798762321767	6.90191446975039	H	0.92357387776057	4.67334346456204	6.60708222861635
C	2.82057703054197	3.68690955045936	6.37007867366447	H	1.10659488122696	3.19870727958275	7.56932118999282
C	3.52176293755321	4.62058112676942	5.53144293787298	C	2.90172058037085	5.72259855358867	4.72998247576577
C	4.91083883563692	4.27004939011614	5.53740554533513	H	1.99271600510230	6.09961341328300	5.20619231035658
C	5.07728301227340	3.11638347373491	6.37981052048210	H	2.63165914304576	5.35771555674651	3.72942622208595
C	3.83925902197225	10.61949134200277	9.67066420346799	H	3.59337821562353	6.56058746241698	4.60498238094155
H	3.20689142806763	10.44275196915937	10.55188802899623	C	3.48336581500011	1.58857731077026	7.78683619446543
H	3.44590154644501	9.97735775204238	8.87330365988933	H	2.61319828708866	1.78796044951635	8.41854983037857
C	5.28973905157065	10.23500033115329	10.02246724263205	H	4.33044534819236	1.36150024472007	8.44050362804379
H	5.92955412703179	10.37688815668828	9.14271867646087	H	3.26850984314004	0.69354402457420	7.18767366848712

C	9.93920314468573	8.18469613371166	11.54238217597812	H	2.70200175289530	12.34802871204372	9.02801739298953
H	10.93306639912197	7.74857327571451	11.70039874066705	H	4.32593686750985	12.25246708517558	8.34126978073744
H	10.01511054283918	9.25330694273883	11.79092346280292	C	7.50828331255862	8.09540754051090	12.24848764440403
C	5.98717060373598	4.94165959337806	4.74255114587573	H	7.50014763106526	9.15544078222233	12.53294355206027
H	5.78079959763954	6.00796755877774	4.61503951655056	H	6.77970724639871	7.58530605606953	12.88927414626680
H	6.05781090863603	4.49157098438188	3.74274692880896	C	5.71610958443219	12.61946973627342	10.75122873953739
H	6.96175333992294	4.83795989435557	5.22685612545586	H	6.07666401461548	13.24846462638038	11.57422080222580
C	6.36641951915224	2.39820984066493	6.63168094194011	H	6.38160359397101	12.79759863577766	9.89463276601429
H	7.20987436378003	3.09584343599511	6.64874063232477	C	4.28259668615182	13.00782693679369	10.36880483732074
H	6.56097045234937	1.65983791525108	5.84213523485156	H	4.24567014549769	14.05657060918640	10.05020888477192
H	6.34339822069025	1.87085374675579	7.58928884250144	H	3.63662060449440	12.91712876446709	11.25371665727246
C	7.09595954388129	7.94573404558467	10.76990284427988	C	9.52316889752712	8.03583382844899	10.07369837677588
H	7.07393644250325	6.86709102807704	10.54670175594799	H	9.52893513140874	6.97116077845872	9.80057855013248
C	3.74352096552119	12.09492993118602	9.26012547819430	H	10.24373146296439	8.53988579765122	9.41790823390254

Chapter 6

Synthons for group 2 metals - An updated synthesis of group 2 anthracenides and their use as reducing agents for polypnictogenide ligand complexes.

This chapter was written as a manuscript ready for submission. Conceptualisation, writing of the manuscript, preparation of compounds, electroanalytical measurements (including evaluation of the data) and analytic samples as well as evaluation of all analytic data was done by Martin Weber. X-Ray diffraction measurements were performed and evaluated by Martin Weber and partially checked by Michael Seidl. Supervision, writing review, project administration and funding acquisition: Manfred Scheer

Abstract

By using an improved synthetic pathway, the anthracenides of the group 2 metals Ca, Sr and Ba are straightforward accessible for subsequent organometallic synthesis. These highly reactive compounds are slightly soluble in tetrahydrofurane and can be used as synthons for group 2 metals due to the lability of the anthracene ligand. These features are used to investigate their reactivity towards the $\mathrm{P_n}$ ligand complexes $[\mathrm{Cp^*Fe(\eta^5\text{-}P_5)}]$ and $[\mathrm{Cp^*Fe(\eta^{3:1}\text{-}(1\text{-}CH_3\text{-}2\text{-}PPh_2\text{-}P_5))}]$, respectively. The resulting products $[\mathrm{Cp^*Fe(\mu,\eta^{4:3}\text{-}P_5)Mg(thf)_3}]$ and $[\mathrm{Cp^*Fe(\mu,\eta^{3:3:4}\text{-}(1\text{-}CH_3\text{-}2\text{-}PPh_2\text{-}P_5)_2)Mg(thf)_4}]$ are the first examples for molecular polypnictogenides of magnesium

soluble in carbon based solvents without a stabilisation from N-donor ligands. The P_{12} ligand in the latter complex is the first example for a 2,2'-diphosphanyl substituted decaphosphadihydrofulvalen shaped structural motif (dodecaphospha-2,2'-dimethyl-[1,1'-bi(cyclopentadien)]diyl). The complexes $[Cp^*Fe(\mu,\eta^{4:3}\text{-}P_5)Sr(thf)_4]_2 \cdot (thf)_2$ and $[Cp^*Fe(\mu,\eta^{3:2:2}\text{-}(1\text{-}CH_3\text{-}2\text{-}PPh_2\text{-}P_5))Sr(thf)_3]_2$ represent the first examples for molecular polypnictogen compounds of strontium stable in carbon based solvents.

6.1 Introduction

In the past years the chemistry of the earth alkaline metals Mg, Ca, Sr and Ba has experienced a revival.[125,129,299,300] Beryllium is somewhat excluded from this revival due to its different chemical behaviour and difficult handling because of its toxicity.[301,302] Recent studies focus on group 2 metals stabilized by N-donor ligands as in the case of the Mg(I) species $[^{Dipp}BDIMg]_2$ (BDI = β-diketiminate , Dipp = diisopropylphenyl).[130,132,239,303–306] Especially the heavier metals Ca, Sr and Ba are less well explored than Mg. Activation of heavy group 2 metals is mandatory due to passivation effects and high melting and boiling points of the metals, prohibiting e.g. the formation of metal mirrors it is commonly done for Na or K. These challenges in working with alkaline earth metals are more pronounced for the heavier metals.[307–309] For Mg different techniques for activation are known and the use of e.g. Grignard reagents is rather usual in modern laboratory synthesis. A rather special form of activation is the formation of magnesium anthracenide (MgA) upon heating magnesium turnings in a saturated solution of anthracene in thf for a prolonged period of time, with small amounts of MeI added for initial activation.[310] The formed anthracenide can be directly used as a highly reactive synthon for Mg(0), forming anthracene when reacting with a suitable substrate. It should be mentioned, that anthracene is a not-innocent ligand and can influence the reactivity and sometimes can participate in reactions.[311–315] Although its solubility is low and the use of donor solvents like thf is mandatory, the advantage of MgA as a Mg(0) synthon in metal organic chemistry is that at least parts of the anthracenide are in solution. This way no reactions are taking place directly on the metal surfaces.
For the higher homologues of Mg, the anthracenides are also known. However their synthesis can be regarded as rather challenging and require ball milling in mineral oil and large amounts of starting materials, while only giving bad to moderate yields with low purities of the respective anthracene compounds.[316] A reason for this is the less electron donating nature of the heavier earth alkaline metals and passivation effects on the metal surface as well as decreased solubility and higher reactivity of the formed

products.[316] Thus bulky, electron donating ligands are usually required to stabilize the organometallic compounds of Ca, Sr and Ba. The need for ligands with high sterically demand also applies to the 1,3-bisketiminate ligands required to stabilize the respective Sr or Ba compounds $[^{DNPP}BDISrH]_2$ (DNPP = 1,3-di(pentan-3-yl)-benzene) and $[^{DNPP}BDIBaN(SiMe_3)_2]$.[130,131] Cleavage of ethers like thf used as solvents is observed for all alkaline earth anthracenide compounds upon moderately heating them and Sr and Ba compounds begin to form amides upon dissolution in liquid ammonia.[317]

Due to these challenges the reactivity of such group 2 metal compounds towards the elements of group 15 is nearly unexplored. In the past polyphosphides of Ca, Sr and Ba were only known to exist in the solid state or in liquid ammonia as a solvent.[137–148] Until recently only three molecular polyphosphide of Mg, soluble in hydrocarbons, were known: $[\{^{Dipp}BDIMg\}_2(\mu,\eta^{1:1:1:1}\text{-}^{n}Bu_2P_4)]$, $[\{^{Dipp}BDIMg\}_2(\mu,\eta^{1:1:1:1}\text{-}^{n}Bu_2P_8)]$ and $[\{^{Dipp}BDIMg\}_3(\mu_3\eta^{1:1:1:1:1:1}\text{-}P_7]$.[132] Our group reported the first supramolecular aggregate of the polyphosphorus ligand complex $[Cp^*Fe(\eta^5\text{-}P_5)]$ (**XXVII**) and the Mg(I) species $[^{Dipp}BDIMg]_2$ as well as the first molecular Ca polyphosphides (chapter 4).[198] No molecular polyphosphides of Sr or Ba are known to this date, making the Sr diphosphanylsiloxanide $[\{P_2(^{i}Pr_2Si)_2O\}_2\{Sr(dme)_2\}_2]$ the only existing molecular diphosphide of Sr soluble in hydrocarbons.[242] After our investigations on the first molecular group 2 polyphosphide ligands the question arose how group 2 metals without N-Donor ligands would behave as reduction agents. Therefore, we report an updated synthetic pathway to the heavier group 2 anthracenides and their use as reducing agents.

For the investigations pentaphosphaferrocene $[Cp^*Fe(\eta^5\text{-}P_5)]$ (**XXVII**) and its functionalized derivative $[Cp^*Fe(\eta^{3:1}\text{-}(1\text{-}CH_3\text{-}2\text{-}PPh_2\text{-}P_5))]$ (**11a**, Chapter 5) are chosen. The redox chemistry of **XXVII** was first investigated by electrochemical studies which could show two ECEC processes (a reaction cascade: **E**lectrochemical oxidation or reduction, **C**hemical reaction e.g. dimerisation, **E**lectrochemical reduction or oxidation, another **C**hemical reaction e.g. decay of the dimer) in the cyclic voltammogram of **XXVII** indicating the formation of dimeric oxidation and reduction products.[74] Our group was able to proof the identity of these products by reduction of **XXVII** with potassium to $[K(dme)_2K(dme)][\{Cp^*Fe\}_2(\mu,\eta^{4:4}\text{-}P_{10})]$ and oxidation with thianthrenium salts to $[\{Cp^*Fe\}_2(\mu,\eta^{4:4}\text{-}P_{10})][SbF_6]_2$.[75] Furthermore, the dicationic species $[K(dme)K(\text{di-benzo-}[18]\text{crown-}6)][Cp^*Fe(\eta^4\text{-}P_5)]$ was identified.[173] Other reagents for the reduction of **XXVII** like $[(DIP_2pyr)SmI(thf)_3]$ (DIP_2pyr =2,5-bis{*N*-(2,6-diisopropylphenyl)-iminomethyl}pyrrolyl) or carbon nucleophiles like RLi (R= Me, ^{t}Bu) or $[(^{Dipp}BDI\text{-}Mg(CH_3))_2]$ ($^{Dipp}BDI = \{[2,6\text{-}^{i}Pr_2C_6H_3NCMe]_2CH\}^-$) also give a similar structured product, with an η^4 coordination mode and one phosphorus atom bent out of the plane of the former *cyclo*-P_5 ligand.[174,198,216]

6.2 Results on the synthesis of alkaline earth metal anthracenides

From the existing literature procedure for the synthesis of the earth alkaline metal anthracenides it is evident that activation of the group 2 metal and its fine dispersion as a powder is a crucial step for a feasible synthesis route.[316] Ball milling of earth alkaline metals suspended in mineral oils introduces multiple possible sources of contamination and reducing yields as well as the purity of the final products. In contrast, the dissolution in liquid ammonia seems to be a relatively easy way to convert lumps of Ca, Sr or Ba into a powder or microporous solid. A small amount of ammonia is condensed onto the metal and removed after most of the metal is dissolved, as described by *Westerhausen* for the synthesis of grignard reagents of the heavier group 2 metals.[318] This also eliminates the necessity of further activating the finely dispersed metal in solution with e.g. MeI (as done by *Bönnemann et al.*)[316] as long as not even trace amounts of water or oxygen get into contact with the metal before the antracenide begins to form (visible by vibrant colours, *vide infra*). Therefore a synthesis route (Figure 6.1) was designed in which not even standard inert gas from the schlenkline was applied, but where thf and anthracene are added in high vacuum (Supporting Information).

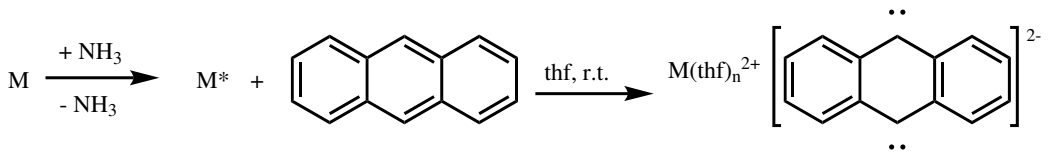


Figure 6.1: Generalized activation and reaction pathway to earth alkaline metal anthracenides according to the novel synthetic pathway.

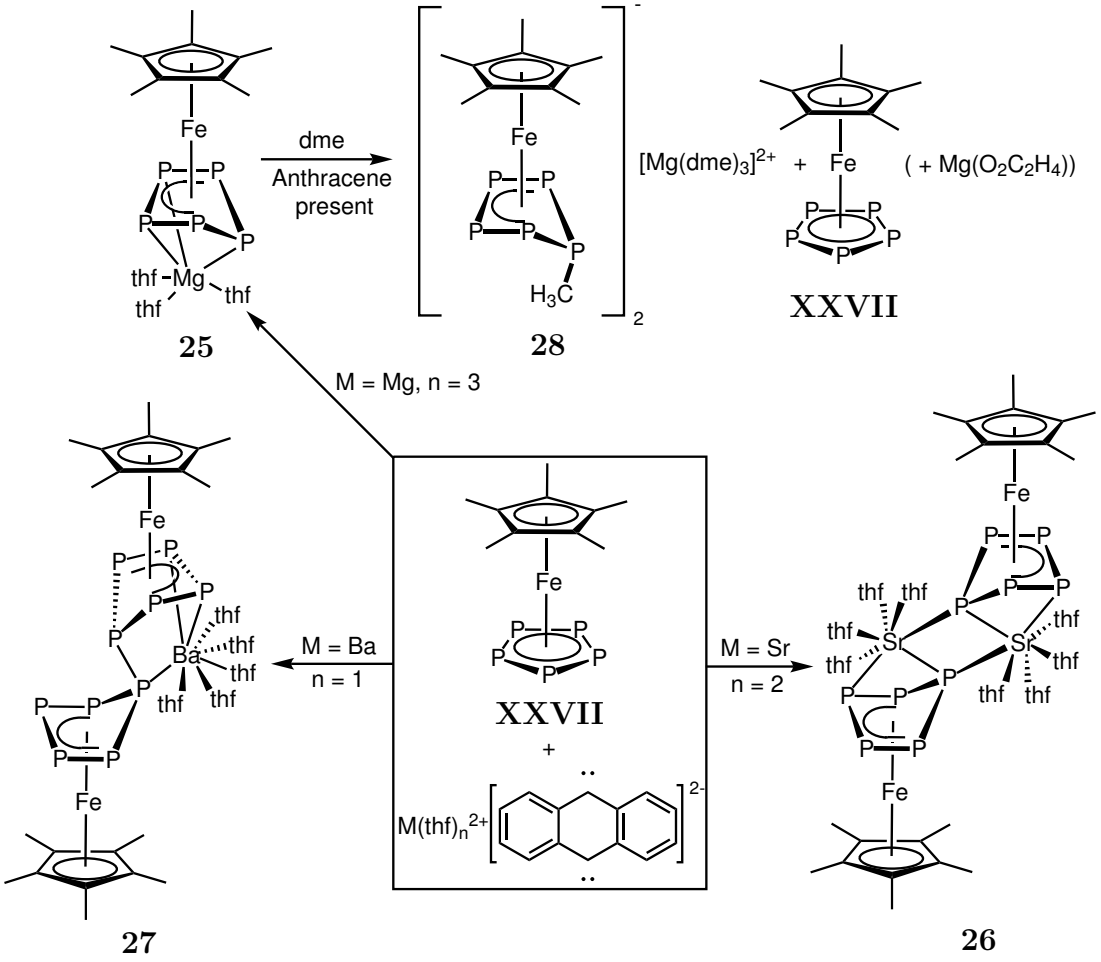
After activation of the metal and adding anthracene and a stirring bar, thf (dried and stored over potassium mirror/benzophenone) is condensed onto the solid mixture (cooled in liquid nitrogen). The valve is closed while the flask is still under vacuum and brought up to room temperature. For Sr and Ba, the reaction starts during the period of one hour of vigorous stirring. The start of the reaction is indicated by the appearance of a colour change of the reaction mixture (intense colour of the suspension: violet for Sr, dark blue in the case of Ba). If no colour change is observed during the first hour, the reaction mixture (still under vacuum) should be activated by an ultrasonic bath. At this point dry argon is carefully added to the flask. After all metal powder is consumed the reaction is assumed to be finished and the liquid is decanted. The remaining powder is washed three times with cold pentane yielding intensely coloured, fine, homogeneous powders as they are reported in the literature.[316] For Ca, the activation was more un-

reliable and the synthesis of CaA is additionally difficult because of the possibility to also form the dianthracenide CaA2. Therefore the dianthracenide is deliberately synthesized and a small amount of MeI added to the reaction mixture. Yet the reaction still took longer and required prolonged activation in the ultrasonic bath. The colour of the solution varies in the case of Ca during the reaction from brown to green containing a brownish grey powder which is turning deep violet (the colour reported for $\mathrm{CaA_2}$;[316] CaA is reported to be of a brownish orange colour) when washed with pentane, dried in vacuum and isolated.

6.3 Reactivity of alkaline earth metal anthracenides towards pentaphosphaferrocene

In order to use the anthracene compounds of Mg, Ca, Sr and Ba as reducing agents for pentaphosphaferrocene, two equivalents of the respective powderous anthracene compound are mixed with crystalline $[\mathrm{Cp^*Fe}(\eta^5\text{-}\mathrm{P_5})]$ (**XXVII**) in a dry schlenk flask. The flask is then cooled in a bath of liquid nitrogen and thf, which is stored on potassium mirror, is directly condensed onto the solid reaction mixture. While the reaction mixture is slowly heated to room temperature the flask is shaken vigorously to assure perfect mixing. The reaction starts immediately upon melting of the solvent, visible as the mixture turns brown in colour. After stirring the resulting brown suspension at room temperature for 5 minutes, the solids are allowed to settle and the clear, dark brown solution is decanted into another flask. Storing the solutions at -30 °C yields crystalline products in up to one week. For the anthracene compounds of Mg and Sr the compounds $[\mathrm{Cp^*Fe}(\mu,\eta^{4:3}\text{-}\mathrm{P_5})\mathrm{Mg(thf)_3}]$ (**25**, Scheme 6.1 on page 263) and $[\mathrm{Cp^*Fe}(\mu,\eta^{4:3}\text{-}\mathrm{P_5})\mathrm{Sr(thf)_4}]_2\cdot(\mathrm{thf})_2$ (**26**) could be isolated and fully characterized. Complex **25** is the first example for a molecular polyphosphide of magnesium without a N-donor ligand and **26** is the first example of a molecular, hydrocarbon soluble polyphosphide of strontium. The pentaphosphaferrocene **XXVII** reacted with both $[\mathrm{Ba(thf)A}]$ and $[\mathrm{CaA_2(thf)_6}]$, visible in the distinct colour change and the absence of signals for **XXVII** in the $^{31}\mathrm{P}$ NMR spectra of the respective reaction solutions. Yet no product could be isolated or identified for the reaction with $[\mathrm{CaA_2(thf)_6}]$. $^{31}\mathrm{P}$ NMR spectra of the reaction mixtures with $[\mathrm{Ba(thf)A}]$ show an extremely broadened AMM'XX' spin system, fitting to an expected twofold reduction product of **XXVII** (*vide infra*). If the solution is stored at room temperature for longer than 4 hours, the signals will no longer be visible and the colour of the solution changes to a brighter brown. The same behaviour is observed at 0 °C over the course of 2-3 days or at

-30 °C over the course of 1-2 weeks, maintaining temperatures below 0 °C throughout the reaction time. Using slightly less than two equivalents of $[\mathrm{Ba(thf)A}]$ and handling the reaction mixture at -10 °C a few crystals of $[\{\mathrm{Cp^*Fe}\}_2(\mu,\eta^{4:4:3:3}\text{-}\mathrm{P_{10}})\mathrm{Ba(thf_3)}]$ (**27**, Scheme 6.1), suitable for tentative X-ray structure determination were obtained after storing the solution at -30 °C for 2 weeks.



Scheme 6.1: Reaction of **XXVII** with the earth alkali metal anthracenides $\mathrm{M(thf)_nA}$ ($\mathrm{M = Mg(n = 3)}$, $\mathrm{Sr(n = 2)}$, $\mathrm{Ba(n = 1)}$). All reactions were performed by condensation of thf onto the mixture of solid starting materials cooled with liquid nitrogen and warming to room temperature.

Both **25** and **26** (Scheme 6.1) show an AMM'XX' spin system in their $^{31}\mathrm{P}$ NMR spectra, expected for the C_S symmetric $\mathrm{P_5}$ ligand in envelope conformation. In contrast to the 1,3-bisketiminate stabilized magnesium compound $[(^{\mathrm{Dipp}}\mathrm{BDI\text{-}Mg})_2(\mu,\eta^{4:2:1}\text{-}\mathrm{P_5})(\mathrm{FeCp^*})]$,[198] **25** does not show any dynamic process for the coordination

of the magnesium atom to the P_5 ligand.[198] The signals of **26** are slightly broadened in comparison to **25** but still resolved well enough for iterative fitting and simulation of the spin system. Due to the higher basicity of Sr, the signal of multiplet A is significantly shifted down field and chemical shifts are similar to the ones of [K(dme)K(dibenzo-[18]crown-6)][Cp*Fe(η_4-P_5)].[173] The relatively strong down field shift of the MM' multiplett in the ^{31}P NMR spectrum of **25** (50 ppm compared to the shift of -3 ppm for the respective multiplet in the spectrum of **26**) can be explained by a rather strong coordination of the Mg atom to the respective phosphorus atoms.

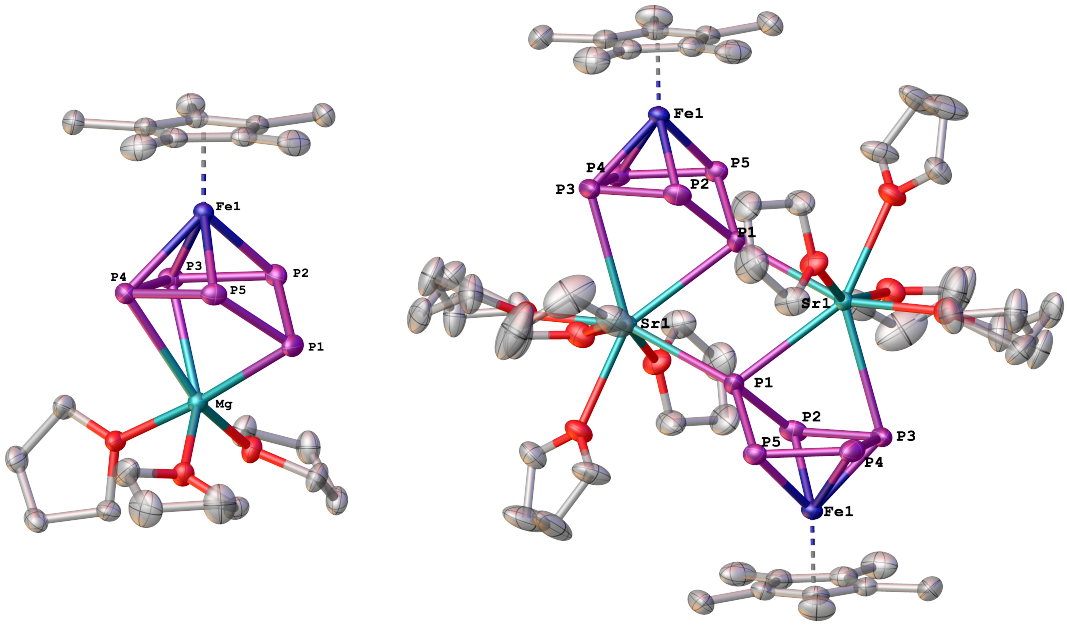


Figure 6.2: Molecular structures of **25** (left) and **26** (right) in the solid state. Selected bond lengths of **25**: Fe1-P4 2.3121(5), Fe1-P5 2.2586(5), Fe1-P3 2.2980(5), Fe1-P2 2.2624(5), P4-P5 2.2177(6), P4-P3 2.1709(6), P4-Mg 2.8388(7), P5-P1 2.1755(6), P5-Mg 3.1619(7), P3-P2 2.2233(6), P3-Mg 2.7791(7), P1-P2 2.1772(6), P1-Mg 2.5626(7), P2-Mg 3.0748(7). Selected bond lengths of **26**: Fe1-P5 2.2720(8), Fe1-P2 2.2826(7), Fe1-P4 2.3222(8), Fe1-P3 2.2901(8), Sr1-P2 3.4128(8), Sr1-P1[1] 3.1174(7), Sr1-P1 3.0794(7), Sr1-P4 3.7466(8), Sr1-P3 3.1775(7), P5-P1 2.1625(9), P5-P4 2.1972(10), P2-P1 2.1733(11), P2-P3 2.2164(11), P4-P3 2.1491(13).

The solid state structure of **25** (Figure 6.2, left) confirms the P_5^{2-} moiety with the Mg atom coordinating to the phosphorus atom bent out of plane (P1), as well as the two P atoms on the opposite side (P3 and P4). The fact that the bond Mg-P1 (2.5626(7) Å) is significantly shorter than Mg-P3 (2.7791(7) Å) and Mg-P4 (2.8388(7) Å) can be explained by a stronger coordination of Mg to P1, as observed for the chemical shifts of the respective signals in the ^{31}P NMR spectrum of **25** (*vide supra*). The distance of the Mg atom to the centroid of the surface, produced by P2, P3, P5 and P5 is 2.4380(6) Å.

The bond lengths and angles of the P_5^{2-} moiety in **25** and **26** are similar to the ones observed in similar complexes like $[K(dme)K(dibenzo\text{-}[18]crown\text{-}6)][Cp^*Fe(\eta_4\text{-}P_5)]$.[173] The bond lengths of Sr to P1 (3.0794(7) Å) and to the P1 atom of the other moiety in the dimeric solid state structure of **26** (3.1174(7) Å) only differ by 0.038 Å and are both comparable to the Sr-P bond lengths in $[\{P_2(^iPr_2Si)_2O\}_2\{Sr(dme)_2\}_2]$ (3.1086(11) Å and 3.1271(11) Å).[242] The distance of the Sr atoms to the mean plane of the *cyclo*-P_5 ligand in **26** is 3.0683(4) Å. Both the $Sr\cdots Sr$ distance of 5.1062(4) Å and the distance of both P1 atoms (3.5110(14) Å) are to large for a $Sr\cdots Sr$ or $P\cdots P$ interaction.
It was also tested if it is possible to reduce **XXVII** with earth alkaline metals with and without small amounts of anthracene present in the reaction mixture. The metals were first activated with liquid ammonia as described above. After months of stirring, the formation of a dark oily residue in the case of Sr (anthracene present) and no reactions at all are observed for Mg, Ca and Ba.
In order to improve the yields of the crystallisation of **25**, dimethoxyethane (dme) was used as a solvent for extraction of the crude reaction mixture. Surprisingly a colour change was observed and the ^{31}P NMR spectrum of the solution showed a different reaction product together with the starting material **XXVII** in a 1:1 ratio. After X-ray diffraction experiments on some crystals obtained from the solution the product of the reaction could be identified as $[Cp^*Fe(\eta^4\text{-}P_5CH_3)]_2[Mg(dme)_3]\cdot(dme)$ (**28**). The formation of **28** and **XXVII** in a 1:1 ratio can be explained by a disproportionation reaction and cleavage of the ether groups in dme. The chemical shifts as well as the coupling constants of the AMM'XX' spin system in the ^{31}P NMR spectrum of **28** are identical with spectra of $[Cp^*Fe(\eta^4\text{-}P_5CH_3)]^-$, the product from the nucleophilic methylation of **XXVII** with LiMe.[77] Since the methyl groups are cleaved of the solvent, magnesium ethylenglycoxide has to be formed in order to balance the reaction equation (Scheme 6.1). Repeating the experiment by dissolving neat **25** in neat dme in the absence of anthracene did not result in any cleavage of the ether bonds in dme.

6.4 Investigations on the redox chemistry of $[\mathbf{Cp^*Fe(\eta^{3:1}\text{-}(1\text{-}CH_3\text{-}2\text{-}PPh_2\text{-}P_5))}]$

The cyclic voltrammogram of $[Cp^*Fe(\eta^{3:1}\text{-}(1\text{-}CH_3\text{-}2\text{-}PPh_2\text{-}P_5))]$ (**11a**) reveals a similar behaviour as it is known for **XXVII**,[74] but with lower reduction and oxidation potentials: Both oxidation and reduction are not-coulomb reversible one electron processes (Figure 6.3). The chemical and electrochemical behaviour of the resulting 17 valence electron (VE) oxidation product **11a**$^+$ and the 19 VE reduction product [**11a**]$^-$ are best classified as two ECEC processes (*vide supra* in introduction): After the one electron oxidation at A (529 mV, Figure 6.3) of **11a** to [**11a**]$^+$, dimerisation of the 17 VE complex to $[\mathbf{11a}]_2^{2+}$ is too fast to detect the coulomb reversible reduction of [**11a**]$^+$ back to **11a** even at high scan rates (1000 mVs^{-1}). The dimer $[\mathbf{11a}]_2^{2+}$ is then reduced back to **11a**, observed in wave B (-19 mV, Figure 6.3) of the single product reduction. The same basic description is applicable for the respective one electron reduction at -1600 mV (peak C in Figure 6.3) and the oxidation of the formed dimer $[\mathbf{11a}]_2^{2-}$ observed as peak D (915 mV).

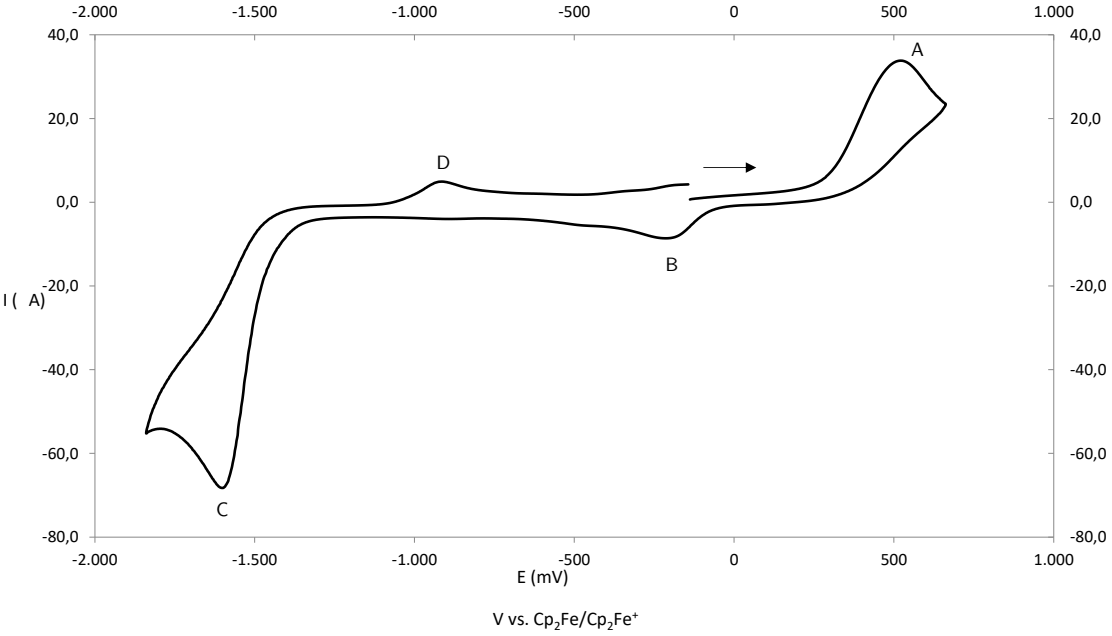
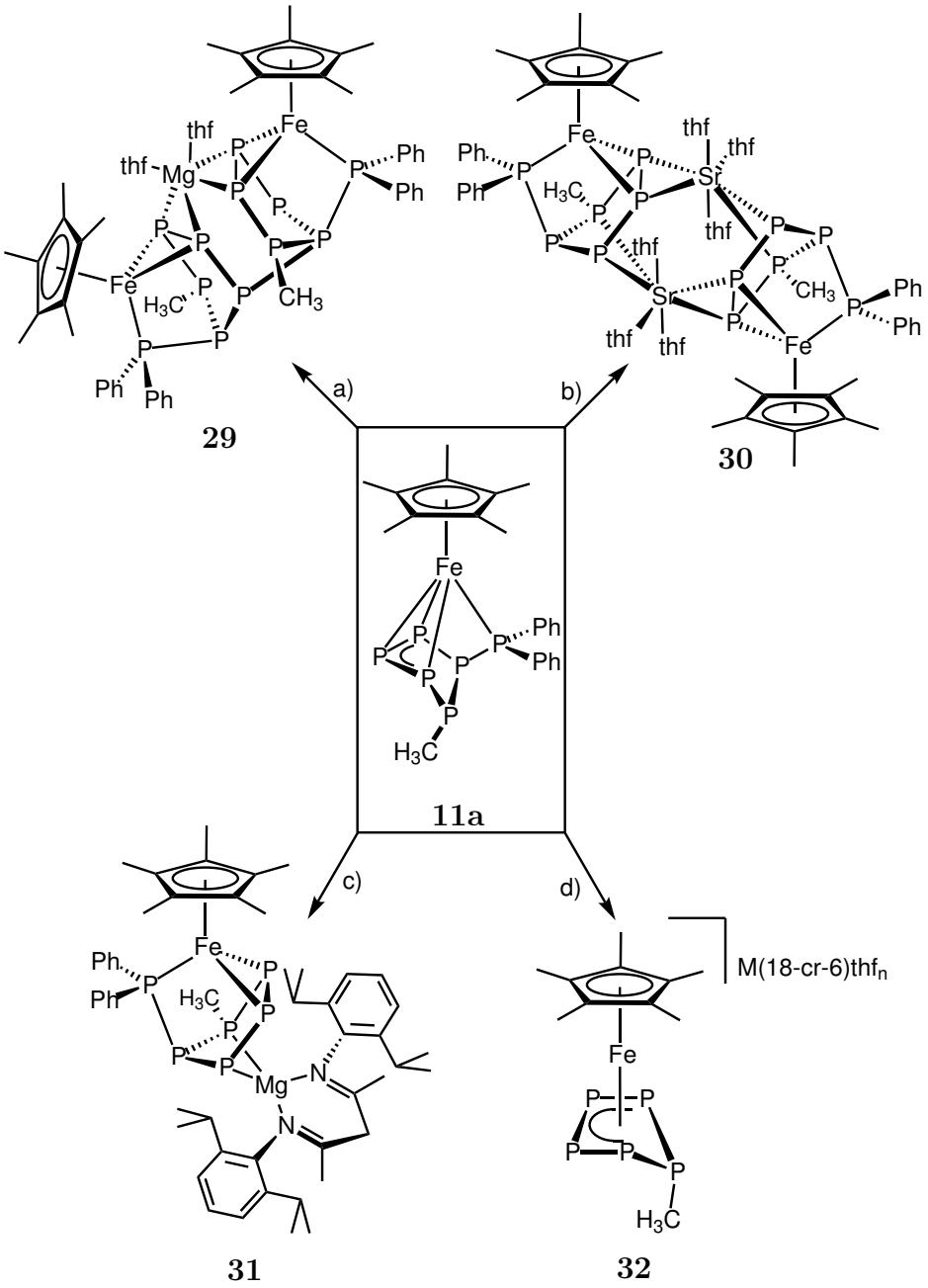


Figure 6.3: Cyclic voltammogram of **11a** in dichloromethane.

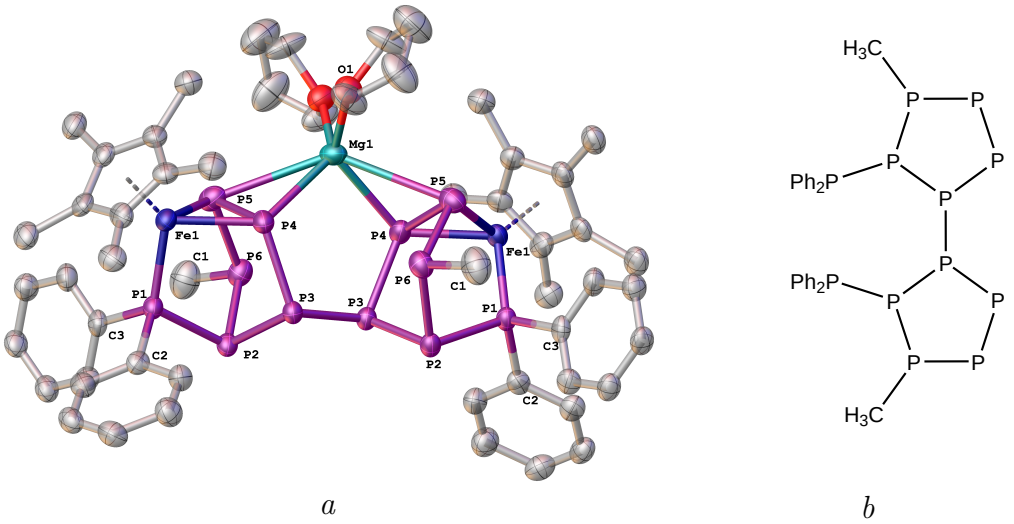
When complex **11a** is reacted with MgA or SrA in the experimental set-up as used for **XXVII** (*vide supra*), crystals of $[Cp^*Fe(\mu_3, \eta^{3:3:4}\text{-}(1\text{-}CH_3\text{-}2\text{-}PPh_2\text{-}P_5)_2)Mg(thf)_4]$ (**29**) and $[Cp^*Fe(\mu, \eta^{3:2:2}\text{-}(1\text{-}CH_3\text{-}2\text{-}PPh_2\text{-}P_5))Sr(thf)_3]_2$ (**30**, 6.2)) are obtained by storing the respective thf solutions at -30 °C for 1 week.



Scheme 6.2: Reaction of **11a** with several reducing agents: a) with one or two equivalents of MgA in thf at approximately -108 ℃ (thf condensed and frozen onto solid starting materials), b) with one or two equivalents of SrA in thf at approximately -108 ℃ (thf condensed and frozen onto solid starting materials), c) with [(^{DIPP}BDI)Mg]$_2$ at -80 ℃ in toluene, and d) over potassium or sodium mirror in thf at room temperature.

The solid state structures of **29** and **30** (Figure 6.4) show a central metallo-nortricyclan structural motif. In **29** a new P-P bond is formed between two units of onefold reduced **11a**. The resulting P_{12}^{2-} ligand can be described as a dodecaphospha-2,2'-dimethyl-

[1,1'-bi(cyclopentadien)]diyl ligand and is the first example for this 2,2'-diphosphanyl substituted decaphosphadihydrofulvalen shaped structural motif for a P_{12} moiety. The Mg-P bonds in **29** are not of the same length, but differ by 0.5 Å (2.575(3) Å and 3.048(2) Å). The P-P bonds and angles in **29** are in agreement with reported complexes with the same basic structural motif (*vide supra*, chapter 5). The length of the newly formed bond P3-P3[1] (2.222(3) Å) is comparable to the other P-P bonds in **29**. Complex **29** is identical with $[\mathbf{11a}]_2^{2-}$, the product of the reductive ECEC process postulated from the cyclic voltammetry measurements (*vide supra*).



a *b*

Figure 6.4: Molecular structure of **29** in the solid state (*a*) and schematic depiction of the novel dodecaphospha-2,2'-dimethyl-[1,1'-bi(cyclopentadien)]diyl ligand (*b*) for easier understanding. Hydrogen atoms are omitted for clarity. Selected bond lengths: Fe1-P1 2.1495(19), Fe1-P4 2.2614(18), Fe1-P5 2.258(2), P3-P3[1] 2.222(3), P3-P2 2.200(2), P3-P4 2.227(2), P1-P2 2.254(2), P1-C3 1.836(7), P1-C2 1.857(7), P2-P6 2.191(3), P6-P5 2.227(3), P6-C1 1.832(9), P4-P5 2.204(3), P4-Mg1 2.575(3), P5-Mg1 3.048(2).

In contrast, the solid state structure of **30** (Figure 6.5) is best described as a dimer of the dianion of **11a** with strontium coordinating two units of the twofold reduced complex. The central structural motif is identical with the one in **29** but without a P-P bond formation between two units of the complex. Using MgA as reducing agent for **11a** so far only produced **29**. SrA seems to be the more powerful reducing agent, resulting in the twofold reduction of **11a** and therefore not resulting in P-P bond formation. A ^{31}P NMR study was performed in order to investigate the reducing strength of the anthracenides towards **11a** more closely. Less than one equivalent of the anthracenides shows both **11a** and the respective onefold reduction product $[\mathbf{11a}]_2^{2-}$ in the ^{31}P NMR of the reaction solutions. If two equivalents of the respective anthracenide are used

instead, **11a** and **29** are present in the ^{31}P NMR of the reaction solution in a 1:1.8 mixture for MgA and only signals attributed to **30** are observed using SrA. Thus the reducing power of MgA is only sufficient to form **29** in an equilibrium with the starting material while the reducing power of SrA is sufficient to reduce **11a** completely to the twofold reduction product **30**.

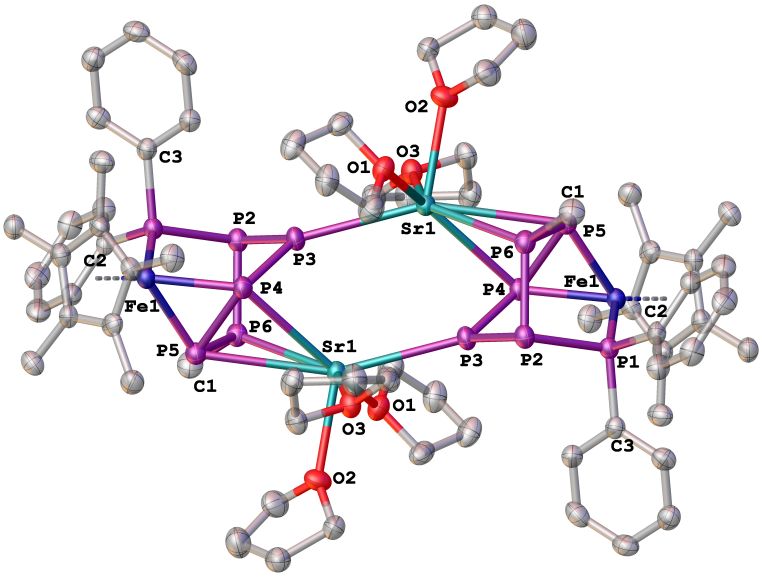


Figure 6.5: Molecular structure of **30** in the solid state. Hydrogen atoms are omitted for clarity. Selected bond lengths: Sr1-Sr11 4.3803(7), Sr1-P41 3.1204(11), Sr1-P51 3.2807(11), Sr1-P3 3.1088(11), Sr1-P3^1 3.2416(12), Sr1-P6^1 3.1697(12), Fe1-P4 2.2640(12), Fe1-P5 2.2779(13), Fe1-P1 2.1405(12), P4-P5 2.2040(15), P4-P3 2.2243(15), P5-P6 2.2292(16), P1-P2 2.2756(15), P1-C2 1.843(4), P1-C3 1.847(4), P2-P3 2.1685(16), P2-P6 2.1851(16), P6-C1 1.856(5).

Since the reduction products of **XXVII** with alkaline metal mirrors are already known, the use of sodium and potassium mirror for the reduction of **11a** are tested. After several attempts crystals of $[Cp^*Fe(\eta^4\text{-}(P_5CH_3))][K(18\text{-cr-}6)(thf)_2]$ (**32**) are obtained as the only product (Scheme 6.2). This concludes, that reduction of **11a** leads to decomposition of **11a** with $[Cp^*Fe(\eta^4\text{-}P_5CH_3)]^-$ as the ultimate product. In contrast, the anthracene compounds, although highly reactive, are not showing any signs of decomposition of the starting material. In order to investigate the influence of sterically demanding N-donor ligands, **11a** was reacted with the Mg(I) dimer $[(^{DIPP}BDI)Mg]_2$. Upon reduction of **11a** with $[(^{DIPP}BDI)Mg]_2$ in toluene at room temperature, and storing the orange-brown solution at -30 °C for two weeks, a few orange crystals of $[Cp^*Fe\{\mu_2,\eta^{1:2:2}\text{-}(1\text{-}CH_3\text{-}2\text{-}PPh_2\text{-}P_5)\}Mg(^{DIPP}BDI)]$ (**31**) are obtained alongside amorphous brown solids and brown oil. The ^{31}P NMR spectrum of the mother liquor shows

a complex product mix which could not be separated by any means so far. Also **31** sows a metallo-nortricyclan structural motif similar.
The formation of **31** corresponds to the single electron reduction of **11a** to $[Cp^*Fe(\eta^{1:2}\text{-}(1\text{-}CH_3\text{-}2\text{-}PPh_2\text{-}P_5))]^-$, the product postulated by cyclic voltammetry. This species should not be stable itself and should dimerize to form the above mentioned P_{12}^{2-} dianion. In the case of **31** this is not possible due to the more covalent nature of the $^{DIPP}BDIMg-P$ bond and the steric shielding of the β-diketiminate ligand and the phenyl groups in the backbone of the ligand. Due to the small amount of **31** in a complicated reaction mixture, isolation and full spectroscopic characterisation of this compound has not yet been successful.

6.5 Conclusion

By activation of the alkaline earth metals Ca, Sr and Ba with liquid ammonia an improved synthesis of the corresponding anthracene compounds of these metals is found. Since the synthesis pathway does not rely on ball milling under mineral oil or large amounts of starting materials, it can be easily performed by using standard schlenk techniques. In order to explore the reactivity of earth alkaline metal compounds without sterically demanding and stabilizing N-donor ligands and to proof the identity and quality of the products obtained, they were reacted with pentaphosphaferrocene $[Cp^*Fe(\eta^5\text{-}P_5)]$ (**XXVII**). For the anthracene compound of Mg the complex $[Cp^*Fe(\mu,\eta^{4:3}\text{-}P_5)Mg(thf)_3]$ (**25**) was obtained and fully characterized. It represents the first molecular polyphosphide of magnesium soluble in carbon based solvents without N-donor ligands. Reaction of **XXVII** with the anthracene compound of Sr yields $[Cp^*Fe(\mu,\eta^{4:3}\text{-}P_5)Sr(thf)_4]_2 \cdot (thf)_2$ (**26**), the first molecular polyphosphide compound of strontium. Although the dianthracenide of Ca reacts with **XXVII**, detected by the colour change observed upon addition, no products of this reaction could be isolated or identified. For the anthracene compound of Ba formation of an extremely temperature sensitive product was observed in ^{31}P NMR spectra of the freshly prepared reaction solutions. This short lived product could not be isolated but trace amounts of $[\{Cp^*Fe\}_2(\mu,\eta^{4:4:3:3}\text{-}P_{10})Ba(thf_3)]$ (**27**), the first molecular polyphosphide compound of barium, were obtained, when using less than two equivalents of BaA in the reaction.
The anthracenides of Mg and Sr also proof to be valuable in the exploration of the redox chemistry of the recently reported complex $[Cp^*Fe(\eta^{3:1}\text{-}(1\text{-}CH_3\text{-}2\text{-}PPh_2\text{-}P_5))]$ (**11a**). Cyclic voltammetry of **11a** gave similar results for **11a** as for **XXVII**: reduction and oxidation of **11a** are identified as one electron processes followed by dimerisation

of the 17 VE oxidation- or the 19 VE reduction product, respectively. The alkali metals Na and K did proof the be too harsh as reduction agents for **11a** and decomposition of the starting material is observed. Reduction with $[(^{\mathrm{DIPP}}\mathrm{BDI})\mathrm{Mg}]_2$ produced mixtures of different products of which only one could be identified by X-ray diffraction experiments as $[\mathrm{Cp^*Fe}\{\mu_2,\eta^{1:2:2}\text{-}(1\text{-}\mathrm{CH_3}\text{-}2\text{-}\mathrm{PPh_2}\text{-}\mathrm{P_5})\}\mathrm{Mg}(^{\mathrm{DIPP}}\mathrm{BDI})]$ (**31**). This product represents the one electron reduction of **11a** without subsequent dimerisation, which is not possible due to the sterically demanding N donor ligand in $[(^{\mathrm{DIPP}}\mathrm{BDI})\mathrm{Mg}]_2$. Only the anthracenide of Mg was suitable to perform an onefold reduction of **11a** with a subsequent dimerisation by P-P bond formation to $[\mathrm{Cp^*Fe}(\mu_3,\eta^{3:3:4}\text{-}(1\text{-}\mathrm{CH_3}\text{-}2\text{-}\mathrm{PPh_2}\text{-}\mathrm{P_5})_2)\mathrm{Mg(thf)_4}]$ (**29**). Complex **29** shows a so far unprecedented, functionalized dodecaphospha-2,2'-dimethyl-[1,1'-bi(cyclopentadien)]diyl ligand. The twofold reduction to $[\mathrm{Cp^*Fe}(\mu,\eta^{3:2:2}\text{-}(1\text{-}\mathrm{CH_3}\text{-}2\text{-}\mathrm{PPh_2}\text{-}\mathrm{P_5}))\mathrm{Sr(thf)_3}]_2$ (**30**) is observed when the anthracenide of Sr is used for the reduction of **11a** instead. Comparison of the reactivity of **11a** towards $[\mathrm{Mg}(\eta^2\text{-}\mathrm{C_{14}H_{10}})(\mathrm{thf})_3]$ and $[(^{\mathrm{DIPP}}\mathrm{BDI})\mathrm{Mg}]_2$ shows that stabilisation of Mg by bulky donor ligands is not required to form stable polyphosphides in solution. Bulky ligands like the β-diketiminate ligands in $[(^{\mathrm{DIPP}}\mathrm{BDI})\mathrm{Mg}]_2$ can even hinder further reactions such as dimerisation due to their high sterical demand.

These results show the value of the anthracene compounds of the alkaline earth metals as synthons for the metals themselves. This provides an easier access to the metals Mg, Ca, Sr and Ba as reducing agents for researchers who are not specialized in working with these metals. The availability of these compounds broadens the range of available reducing agents in general. The use of special reducing agents can be necessary, as shown for **11a**, to adapt reduction potential and basicity to the requirements of the compound in question. By this way, products are obtainable that cannot be synthesised using standard reducing agents.

6.6 Supporting information

6.6.1 General techniques and materials

All manipulations were performed using standard schlenk techniques on a dual manifold schlenk line or a glove box under an atmosphere of dry argon. Traces of oxygen in the inert gas were removed by passing it over a BASF R 3-11 (CuO/$MgSiO_3$) catalyst. Residual moisture in the inert gas was removed, by passing it through concentrated H_2SO_4, orange gel and sicapent on dried pumice stone. All glassware was vigorously heated in vacuum before use and any teflon tubing was stored in an oven at 170 °C.
Thf, toluene and *n*-pentane were purified and dried by the solvent purification system SPS-800 from mbraun. Deuterated solvents and dme were dried and distilled over CaH_2. Thf was additionally dried by storing it over a potassium mirror with benzophenone present as an indicator.
Mg turnings were acquired from Merck (suitable for grignard reactions), Ca, Sr and Ba were obtained from Onyxmet. Ca granules were used as delivered. Sr and Ba were removed from mineral oil, washed with pentane and dried in vacuum. Dendritic Sr was put in the ultrasonic bath for a short period of time while suspended in pentane to remove small pieces of Sr with an oxide layer on the surface of the metal. Dendritic Sr and the solid cube of Ba were cut in an glovebox using a wire stripper. $[Cp^*Fe(\eta^5\text{-}P_5)]$, $[Cp^*Fe(\eta^4\text{-}(1\text{-}Me\text{-}1\text{-}PPh_2\text{-}P_5))]$ and $[(^{DIPP}BDI)Mg]_2$ were synthesized according to literature procedures.[69,262]
Cyclic voltammetry of $[Cp^*Fe(\eta^4\text{-}(1\text{-}Me\text{-}1\text{-}PPh_2\text{-}P_5))]$ was performed in o-difluorobenzene using a glassy carbon working electrode, a platinum counter electrode and bare silver wire as reference electrode. For referencing the potentials, ferrocene was used as an internal standard. As conducting salt tetrabutylammoniumhexafluorophosphate, recrystallized five times from ethanol and dried at 120 °C in high vacuum for two days was used.
NMR spectra were measured with a Bruker Avance 400 (^{1}H: 400.132 MHz; ^{13}C: 100.613 MHz; ^{31}P: 161.97 MHz) using special NMR tubes with a screw cap or a J. Young valve. The spin systems of the ^{31}P NMR spectra were simulated with the DAISY package in TopSpin 3.2 from Bruker using the data from 2D-NMR spectra to assign the multiplets to the corresponding compounds and get more information about the connectivity of the phosphorus framework.

6.6.2 Experimental details

Updated synthesis of $[\mathbf{Mg}(\eta^2\text{-}\mathbf{C_{14}H_{10}})(\mathbf{thf})_3]$

A large schlenk flask with a teflon valve containing 267 mg of magnesium turnings (11 mmol) was evacuated and heated vigorously until all water was removed from the metal surface (visible as constant vacuum of $1 \cdot 10^{-3}$ mbar while heating). After the metal has cooled to room temperature 2 g of anthracene (11.2 mmol) and a stirring bar are added in the Ar atmosphere of a glovebox. On the schlenkline the flask is evacuated and cooled with liquid nitrogen. Using the schlenklines vacuum line, 100 mL of dry thf, stored over potassium mirror are condensed onto the solid reaction mixture. After thawing the solvent and stirring at room temperature for 15 minutes the reaction mixture is activated in an ultrasonic bath for 10 minutes. Then the reaction mixture is heated to 50 °C with a water bath while stirring vigorously. If the reaction does not start in at least 20 minutes (visible by the green colour of the solution), the ultrasonic treatment is repeated until the solution is turning dark green and orange solids begin to precipitate. The reaction mixture is stirred at 50 °C for 4h and at room temperature for 3 weeks to ensure that the reaction is complete. After letting the orange solid settle the dark green solution is decanted. After cooling the slurry with liquid nitrogen, thf is condensed onto the mix and thawed again in order to wash the reaction mixture with dry thf. This is repeated for at least three times before drying the orange, powdery magnesium anthracenide for multiple hours in high vacuum. The dry product should react pyrophoric if removed from the inert gas atmosphere.

Yield: 3.4 g (8.1 mmol, 73 %)

Since analysis of the product apart from physical appearance proofs to be difficult due to the high sensitivity and low solubility it was used as a pure product in the following reactions.

Updated synthesis of $[\mathbf{Ca}(\mathbf{C_{14}H_{10}})_2(\mathbf{thf})_6]$

A large schlenk flask with a teflon valve containing 0.5 g of calcium granules (12.5 mmol) is cooled to -50 °C and ammonia condensed onto the metal until no solid lumps are visible. The ammonia is carefully removed by letting the flask warm to room temperature slowly. The last traces of ammonia are removed from the resulting yellowish golden metal powder deposit by drying in high vacuum for 10 minutes. A schlenk flask with a core for the glass fitting containing 4.5 g of anthracene (25 mmol)

and a very small stirring bar is connected to the flask containing the metal powder and evacuated for 10 minutes. The whole apparatus is then tilted back while the teflon valve is opened in order to allow all of the anthracene and the stirring bar to fall into the flask containing the metal powder. The lower flask is then cooled with nitrogen and 150 mL of dry thf, stored over potassium mirror is condensed onto the solid reaction mixture. After condensation the teflon valve is closed, the small flask removed and the solvent allowed to thaw. Sill under high vacuum, the reaction mixture is activated in an ultrasonic bath until a colour change of the solvent is visible (either bluish brown, green or violet). After activation the reaction mixture remains for 10 more minutes in the ultrasonic bath, making sure that temperatures do not rise above 40 °C. The reaction mixture is stirred for 1 month to ensure that the reaction was complete. After the dark brown, grey or violet solid is completely settled the greyish brown (it may also appear to be almost black) solution is decanted. The solid is washed three times with pentane at 0 °C and dried in high vacuum. At least upon drying the fine powder should turn a dark, intense violet colour. If the product is dry it should react pyrophoric if removed from the inert gas atmosphere.

Yield: 5.3 g (6.4 mmol, 52 %)
Since analysis of the product apart from physical appearance proofs difficult due to the high sensitivity and low solubility it was used as pure product in the following reactions.

Updated synthesis of $[\mathbf{Sr(C_{14}H_{10})(thf)_2}]$

A large schlenk flask with a teflon valve containing 0.7 g of strontium metal (7.9 mmol) is cooled to -50 °C and ammonia condensed onto the metal until no solid lumps are visible. The ammonia is carefully removed by letting the flask heat to room temperature slowly. The last traces of ammonia are removed from the resulting yellowish golden metal powder deposit by drying in high vacuum for 10 minutes. A schlenk flask with a core for the glass fitting containing 1.336 g of anthracene (7.6 mmol) and a very small stirring bar is connected to the flask containing the metal powder and evacuated for 10 minutes. The whole apparatus is then tilted back while the teflon valve is opened in order to allow all of the anthracene and the stirring bar to fall into the flask containing the metal powder. The lower flask is then cooled with nitrogen and 100 mL of dry thf, stored over potassium mirror is condensed onto the solid reaction mixture. After condensation the teflon valve is closed, the small flask removed and the solvent allowed to thaw. Sill under high vacuum, the reaction mixture is activated in an ultrasonic bath un-

til a colour change of the solvent is visible (intense violet). After activation the reaction mixture remains for 10 more minutes in the ultrasonic bath, making sure that temperatures do not rise above 40 °C. The reaction mixture is stirred for 11 days to ensure that the reaction is complete. After the dark violet solid is completely settled the solution is decanted and discarded. The solid is washed three times with pentane at 0 °C and dried in high vacuum. If the product is dry it should react pyrophoric if removed from the inert gas atmosphere.

Yield: 2.05 g (4.99 mmol, 63 %)

Since analysis of the product apart from physical appearance proofs to be difficult due to the high sensitivity and low solubility it was used as a pure product in the following reactions.

Updated synthesis of $[\mathbf{Ba(C_{14}H_{10})(thf)}]$

A large schlenk flask with a teflon valve containing 460 mg of barium metal (3.3 mmol) is cooled to -50 °C and ammonia condensed onto the metal until no solid lumps are visible. The ammonia is carefully removed by letting the flask heat to room temperature slowly. The last traces of ammonia are removed from the resulting yellowish golden metal powder deposit by drying in high vacuum for 10 minutes. A schlenk flask with a core for the glass fitting containing 570 mg of anthracene (3.2 mmol) and a very small stirring bar is connected to the flask containing the metal powder and evacuated for 10 minutes. The whole apparatus is then tilted back while the teflon valve is opened in order to allow all of the anthracene and the stirring bar to fall into the flask containing the metal powder. The lower flask is then cooled with nitrogen and 80 mL of dry thf, stored over potassium mirror is condensed onto the solid reaction mixture. After condensation the teflon valve is closed, the small flask removed and the solvent allowed to thaw. Sill under high vacuum, the reaction mixture is activated in an ultrasonic bath until a colour change of the solvent is visible (intense blue). After activation the reaction mixture remains for 10 more minutes in the ultrasonic bath, making sure that temperatures do not rise above 40 °C. The reaction mixture is stirred for 11 days to ensure that the reaction is complete. After the dark blue solid is completely settled the solution is decanted and discarded. The solid is washed three times with pentane at 0 °C and dried in high vacuum. If the product is dry it should react pyrophoric if removed from the inert gas atmosphere.

Yield: 350 mg (0.9 mmol, 28 %)

Since analysis of the product apart from physical appearance proofs to be difficult due to the high sensitivity and low solubility it was used as a pure product in the following reactions.

Synthesis of $[\mathbf{Cp^*Fe(\mu,\eta^{4:3}\text{-}P_5)Mg(thf)_3}]$ (25)

A flask containing 103 mg of $[Cp^*Fe(\eta^5\text{-}P_5)]$ (0.3 mmol) and 125 mg of $[Mg(\eta^2\text{-}C_{14}H_{10})(thf)_3]$ (0.3 mmol) as well as a small stirring bar is evacuated and cooled in liquid nitrogen. After condensing 10 mL of thf onto the solid reaction mixture, the flask is allowed to warm up to room temperature slowly while stirring vigorously as soon as possible. The dark brown reaction mixture is stirred for 10 minutes at room temperature and the solids allowed to settle. After carefully decanting the dark brown solution into a very well dried flask, the volume of solvent is carefully removed until solids start to form in the cold. After storing the solution at -30 °C over night a first batch of dark brown crystals of $[Cp^*Fe(\mu,\eta^{4:3}\text{-}P_5)Mg(thf)_3]$ (**25**) suitable for x-ray diffraction experiments are retrieved. After decanting the solution from the crystals and drying them in high vacuum for 2 hours, the solution is reduced in volume and stored at -30 °C again to yield a second batch of crystals.

Crystalline yield: 54 mg (0.1 mmol, 33%)

Elemental analysis: expected for $C_{35}H_{55}P_7Fe$: 6.70 % H, 45.05 % C, 8.18 % O, 4.14 % Mg, 26.40 % P, 9.52 % Fe. Found: 6.63 % H, 44.87 % C.

^{1}H-NMR: ($thf-d8$, 300 K): δ[ppm] = 1.24 (s, 15 H, Cp^*); 1.73 (m and brs; 24 H; thf); 3.57 (m and brs; 24 H; thf)

^{31}P-NMR: ($thf-d8$; 300 K): 119.3 (m, P_A, $^1J_{P_AP_M} = {}^1J_{P_AP_{M'}} = 240$ Hz, $^2J_{P_AP_X} = {}^2J_{P_AP_{X'}} = 7$ Hz), 50.3 (m, P_M and $P_{M'}$, $^1J_{P_AP_M} = {}^1J_{P_AP_{M'}} = 240$ Hz, $^1J_{P_MP_X} = {}^1J_{P_{M'}P_{X'}} = 272$ Hz, $^2J_{P_MP_{X'}} = {}^2J_{P_{M'}P_X} = -78$ Hz, $^2J_{P_MP_{M'}} = 20$ Hz), -40.3 (m,P_X and $P_{X'}$, $^1J_{P_XP_{X'}} = 343$ Hz, $^1J_{P_MP_X} = {}^1J_{P_{M'}P_{X'}} = 272$ Hz, $^2J_{P_MP_{X'}} = {}^2J_{P_{M'}P_X} = -78$ Hz, $^2J_{P_AP_X} = {}^2J_{P_AP_{X'}} = 7$ Hz)

Synthesis of $[\mathbf{Cp^*Fe(\mu,\eta^{4:3}\text{-}P_5)Sr(thf)_4]_2 \cdot (thf)_2}$ (26)

A flask containing 103 mg of $[Cp^*Fe(\eta^5\text{-}P_5)]$ (0.3 mmol) and 130 mg of $[Sr(C_{14}H_{10})(thf)_2]$ (0.32 mmol) as well as a small stirring bar is evacuated and cooled in liquid nitrogen. After condensing 10 mL of thf onto the solid reaction mixture, the flask is allowed to warm up to room temperature slowly while stirring vigorously as soon as possible. The dark brown reaction mixture is stirred for 10 minutes at room temperature and the solids allowed to settle. After carefully decanting the dark brown solution into a very well dried flask, the volume of solvent is carefully removed until solids start to form in the cold. After storing the solution at -30 °C over night a first batch of dark brown crystals of $[Cp^*Fe(\mu,\eta^{4:3}\text{-}P_5)Sr(thf)_4]_2 \cdot (thf)_2$ (**26**) suitable for x-ray diffraction experiments are retrieved. After decanting the solution from the crystals and drying them in high vacuum for 2 hours, the solution is reduced in volume and stored at -30 °C again to yield a second batch of crystals.

Crystalline yield: 122 mg (0.18 mmol, 60%)

^{1}H-NMR: ($thf-d8$, 300 K): δ[ppm] = 1.20 (s, 15 H, Cp^*); 1.73 (m and brs; 8 H; thf); 3.57 (m and brs; 8 H; thf)

^{31}P-NMR: ($thf-d8$; 300 K): 150.7 (m, P_A, $^1J_{P_AP_M} = {}^1J_{P_AP_{M'}} = 296$ Hz, $^2J_{P_AP_X} = {}^2J_{P_AP_{X'}} = 22$ Hz), -3.6 (m, P_M and $P_{M'}$, $^1J_{P_AP_M} = {}^1J_{P_AP_{M'}} = 296$ Hz, $^1J_{P_MP_X} = {}^1J_{P_{M'}P_{X'}} = 207$ Hz, $^2J_{P_MP_{X'}} = {}^2J_{P_{M'}P_X} = -91$ Hz, $^2J_{P_MP_{M'}} = 10$ Hz), -51.8 (m,P_X and $P_{X'}$, $^2J_{P_XP_{X'}} = 14$ Hz, $^1J_{P_MP_X} = {}^1J_{P_{M'}P_{X'}} = 207$ Hz, $^2J_{P_MP_{X'}} = {}^2J_{P_{M'}P_X} = -91$ Hz, $^2J_{P_AP_X} = {}^2J_{P_AP_{X'}} = 22$ Hz)

Reaction of $[\mathbf{Cp^*Fe(\eta^4\text{-}(1\text{-}Me\text{-}1\text{-}PPh_2\text{-}P_5))}]$ with $[\mathbf{(nacnac^{DIPP})Mg]_2}$

Onto a solution of $[Cp^*Fe(\eta^4\text{-}(1\text{-}Me\text{-}1\text{-}PPh_2\text{-}P_5))]$ (35 mg, 0.1 mmol) in 6 mL of toluene $[(nacnac^{DIPP})Mg]_2$ (88 mg, 0.1 mmol) dissolved in 4 mL of toluene is added at -80 °C. After stirring the brown reaction mixture at room temperature over night the colour changes to a brownish red. ^{31}P NMR spectra of the reaction solution (with D_2O capillary) are silent. After adding pentane to the reaction solution the red solution is decanted from the precipitating solids. After storing the solution at -30 °C for 4 months, some orange crystals of $[\{Cp^*Fe\}(\mu,\eta^{3:1},\eta^{1:1}\text{-}(1\text{-}Me\text{-}2\text{-}PPh_2\text{-}P_5))\{^{Dipp}BDI\text{-}Mg\}]$ (**31**) suitable of x-ray structure determination are observed alongside amorphous brown solids and oils.

Yield: cannot be determined

Synthesis of $[\mathbf{Cp^*Fe(\mu_3,\eta^{3:3:4}\text{-}(1\text{-}CH_3\text{-}2\text{-}PPh_2\text{-}P_5)_2)Mg(thf)_4}]$ (29)

A flask containing 109 mg of $[Cp^*Fe(\eta^4\text{-}(1\text{-}Me\text{-}1\text{-}PPh_2\text{-}P_5))]$ (0.2 mmol) and 88 mg of $[Mg(\eta^2\text{-}C_{14}H10)(thf)_3]$ (0.21 mmol) as well as a small stirring bar is evacuated and cooled in liquid nitrogen. After condensing 10 mL of thf onto the solid reaction mixture, the flask is allowed to warm up to room temperature slowly while stirring vigorously as soon as possible. The reddish brown reaction mixture is stirred for 10 minutes at room temperature and the solids allowed to settle. After carefully decanting the solution into a very well dried flask, the volume of solvent is carefully removed until solids start to form in the cold. After storing the solution at -30 °C over night dark brown crystals of $[Cp^*Fe(\mu_3,\eta^{3:3:4}\text{-}(1\text{-}CH_3\text{-}2\text{-}PPh_2\text{-}P_5)_2)Mg(thf)_4]$ (**29**) suitable for x-ray diffraction experiments are retrieved.

Crystalline yield: 38 mg (0.03 mmol, 30%)

^{31}P NMR: (thf with D_2O capillary; 300 K): 189.4 (m, $P_{AA'}$), 33.4 (m, $P_{GG'}$), -11.0 (m, $P_{MM'}$), -40.8 (m, $P_{QQ'}$), -83.3 (m, $P_{UU'}$), -122.7 (m, $P_{XX'}$)

Due to software limitations of a maximum number of 10 nuclei, the expected AA'GG'MM'QQ'UU'XX' spin system of **29** could not be iteratively fitted and simulated, so that coupling constants cannot be determined reliably.

Synthesis of $[\mathbf{Cp^*Fe(\mu,\eta^{3:2:2}\text{-}(1\text{-}CH_3\text{-}2\text{-}PPh_2\text{-}P_5))Sr(thf)_3]_2}$ (30)

A flask containing 109 mg of $[Cp^*Fe(\eta^4\text{-}(1\text{-}Me\text{-}1\text{-}PPh_2\text{-}P_5))]$ (0.2 mmol) and 86 mg of $[Sr(C_{14}H_{10})(thf)_2]$ (0.21 mmol) as well as a small stirring bar is evacuated and cooled in liquid nitrogen. After condensing 10 mL of thf onto the solid reaction mixture, the flask is allowed to warm up to room temperature slowly while stirring vigorously as soon as possible. The reddish brown reaction mixture is stirred for 10 minutes at room temperature and the solids allowed to settle. After carefully decanting the solution into a very well dried flask, the volume of solvent is carefully removed until solids start to form in the cold. After storing the solution at -30 °C over night dark brown crystals of $[Cp^*Fe(\mu,\eta^{3:2:2}\text{-}(1\text{-}CH_3\text{-}2\text{-}PPh_2\text{-}P_5))Sr(thf)_3]_2$ (**30**) suitable for x-ray diffraction experiments are retrieved.

Crystalline yield: 48 mg (0.03 mmol, 29%)

^{31}P NMR: (thf with D_2O capillary; 300 K): 189.4 (d, P_A, $^1J_{PP} = 201$ Hz), 33.8 (brm, P_D), -11.0 (t, P_G, $^1J_{PP} = 321$ Hz), -40.8 (brq, P_M), -83.3 (brt, P_Q), -122.7 (brm, P_X)

Due to the extreme broadening of the signals, coupling constants were not determined for all nuclei.

6.6.3 NMR spectra

NMR spectra of $[\mathbf{Cp^*Fe(\mu,\eta^{4:3}\text{-}P_5)Mg(thf)_3}]$ (25)

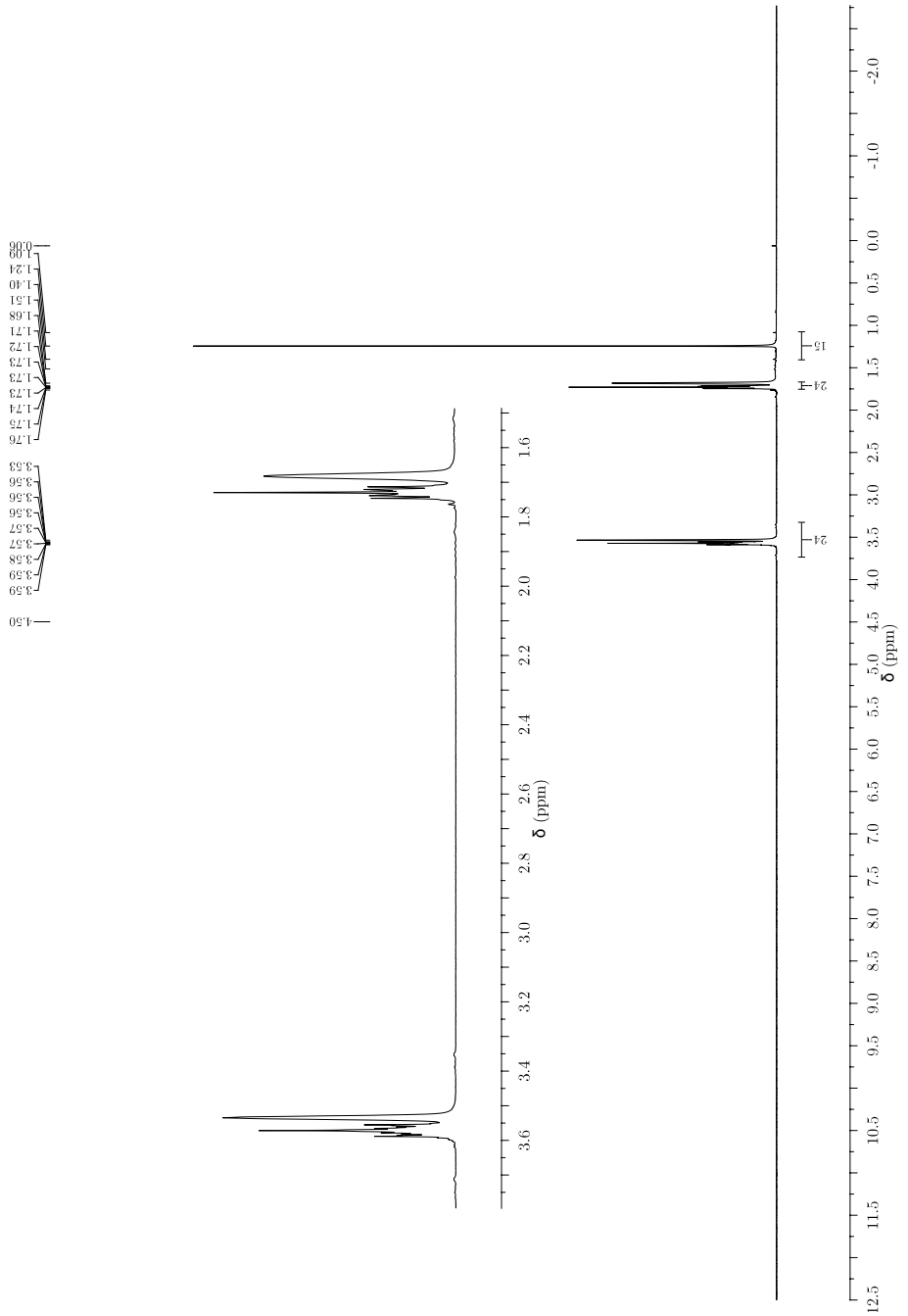


Figure 6.6: ^{1}H NMR spectrum of $[Cp^*Fe(\mu,\eta^{4:3}\text{-}P_5)Mg(thf)_3]$ (**25**) at room temperature in thf-d_8.

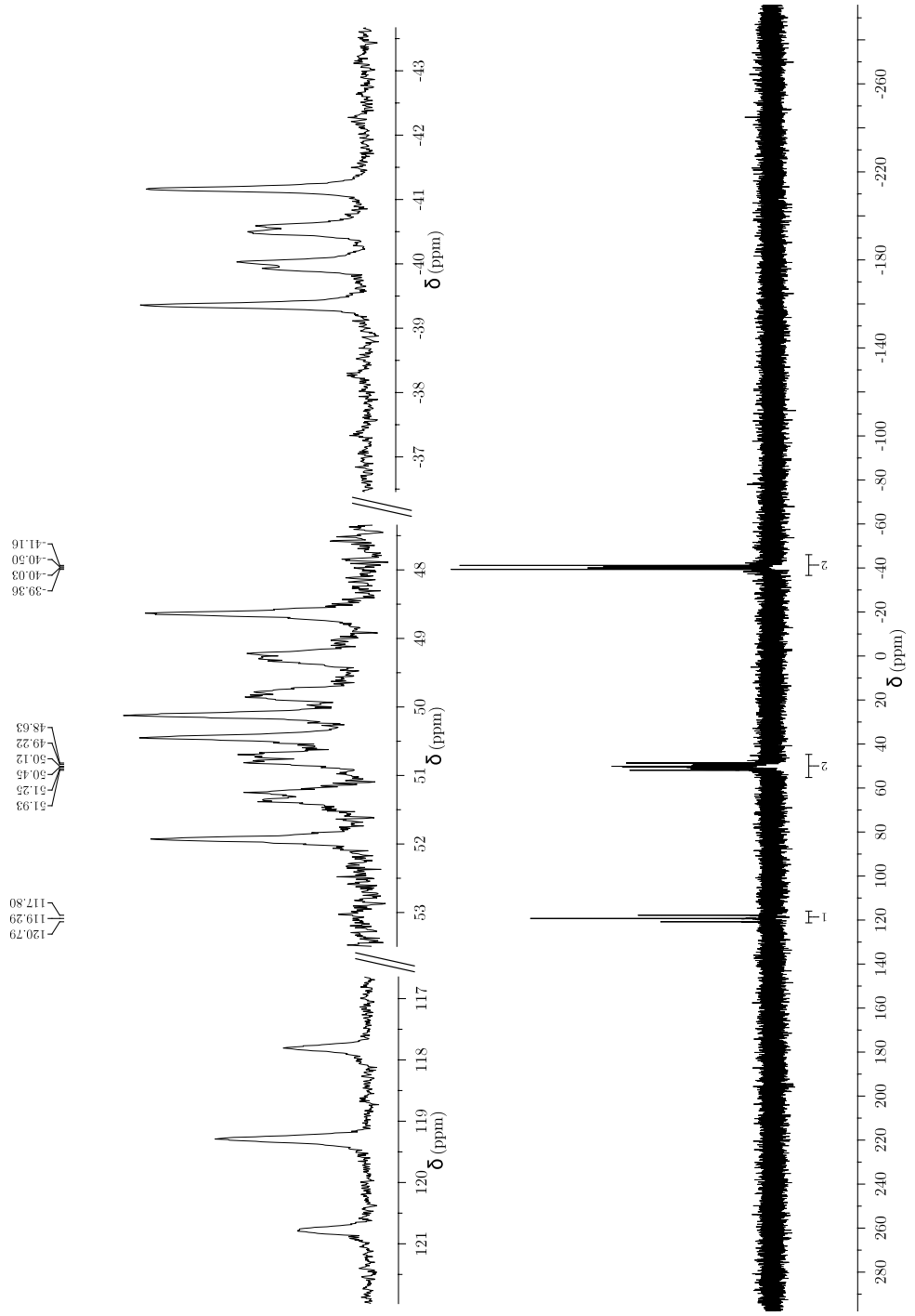


Figure 6.7: ^{31}P NMR spectrum of [Cp*Fe($\mu, \eta^{4:3}$-P_5)Mg(thf)$_3$] (**25**) at room temperature in thf-d_8.

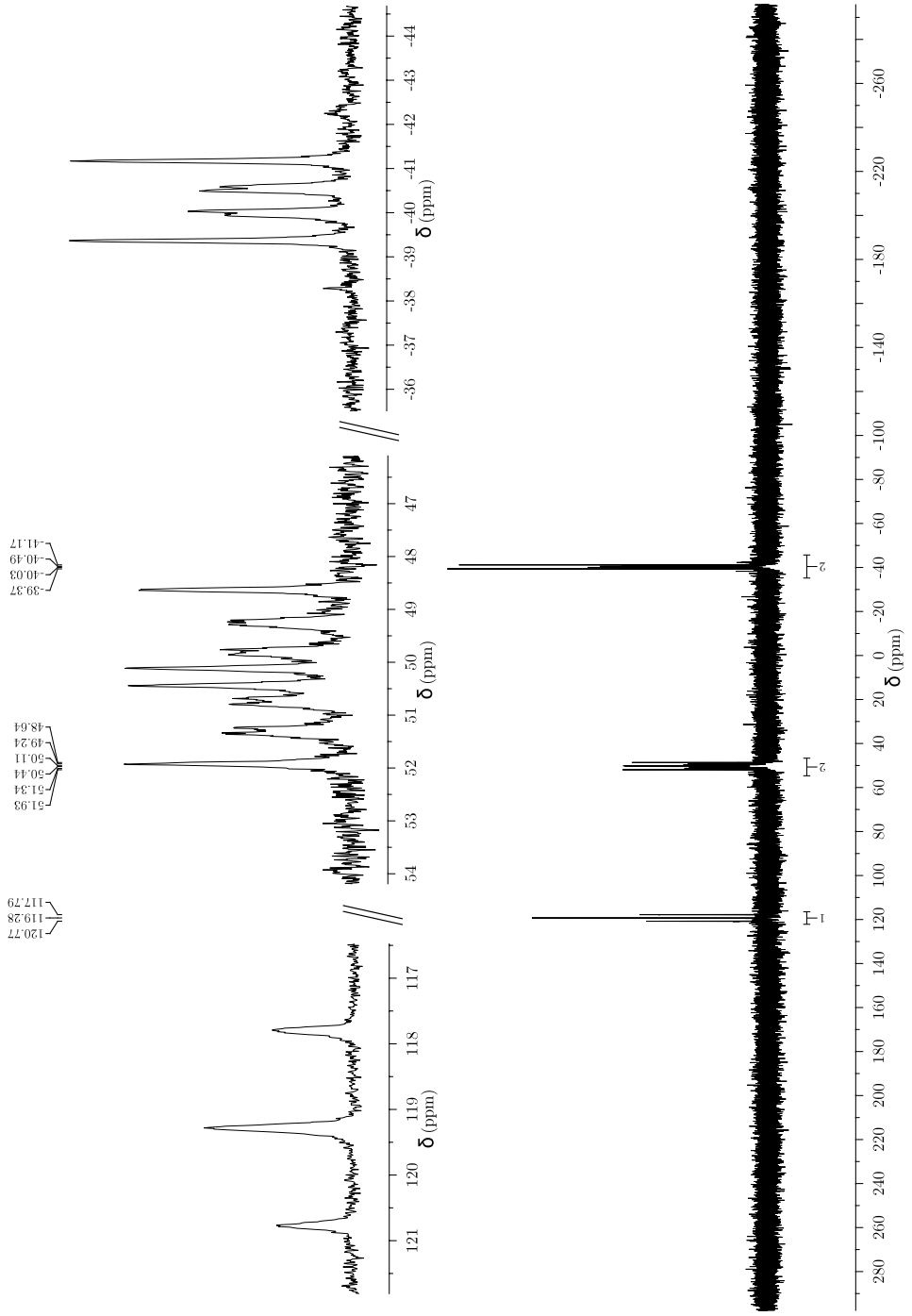


Figure 6.8: ^{31}P NMR spectrum of [Cp*Fe($\mu, \eta^{4:3}$-P_5)Mg(thf)$_3$] (**25**) at room temperature in thf-d$_8$.

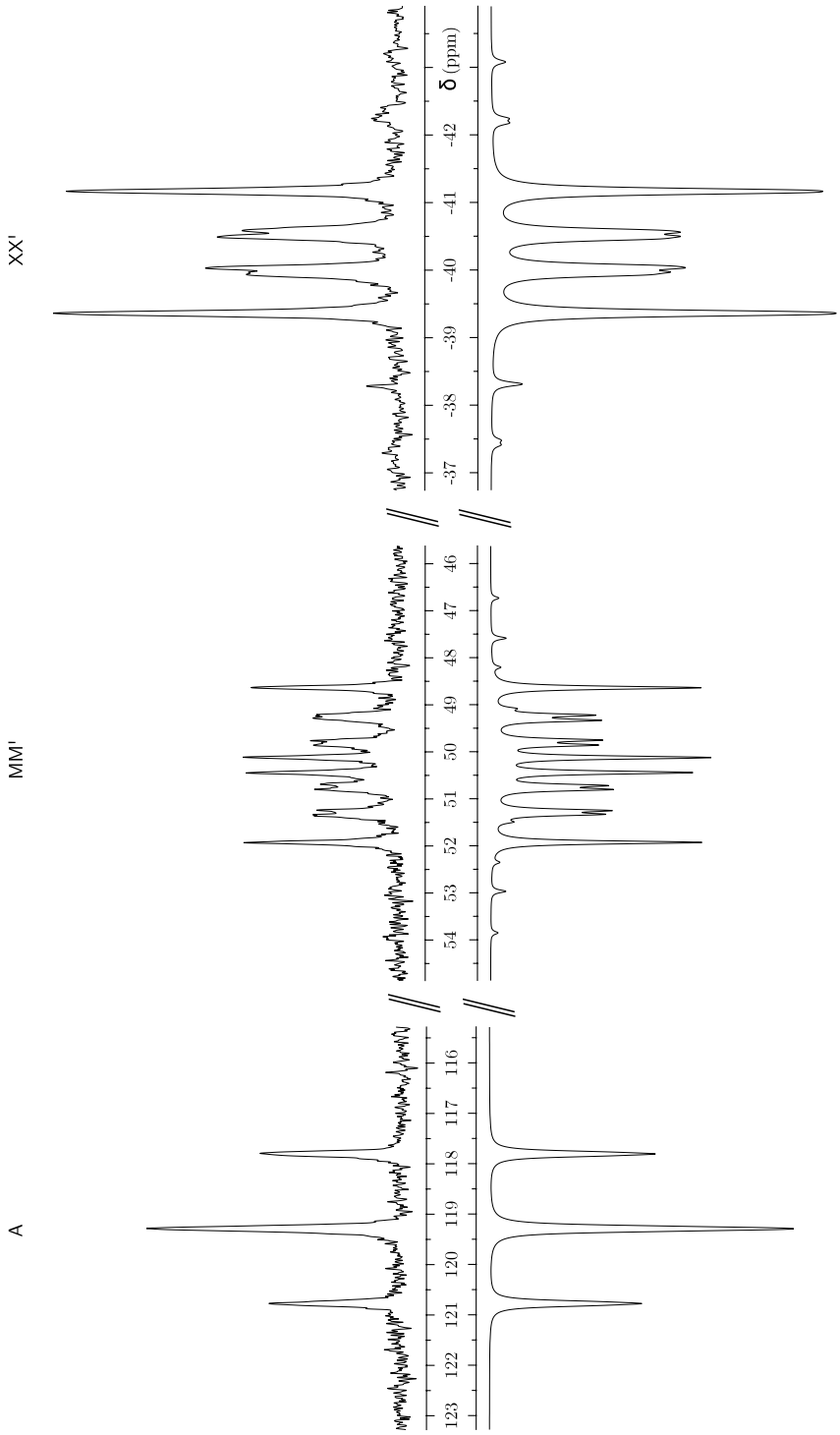


Figure 6.9: Excerpt with simulation of the ^{31}P NMR spectrum of $[Cp^*Fe(\mu,\eta^{4:3}\text{-}P_5)Mg(thf)_3]$ (**25**) in thf-d_8 with simulation of the spin system of **25** shown inverted.

NMR spectra of $[Cp^*Fe(\eta^4\text{-}P_5CH_3)]_2[Mg(dme)_3](dme)$ (28)

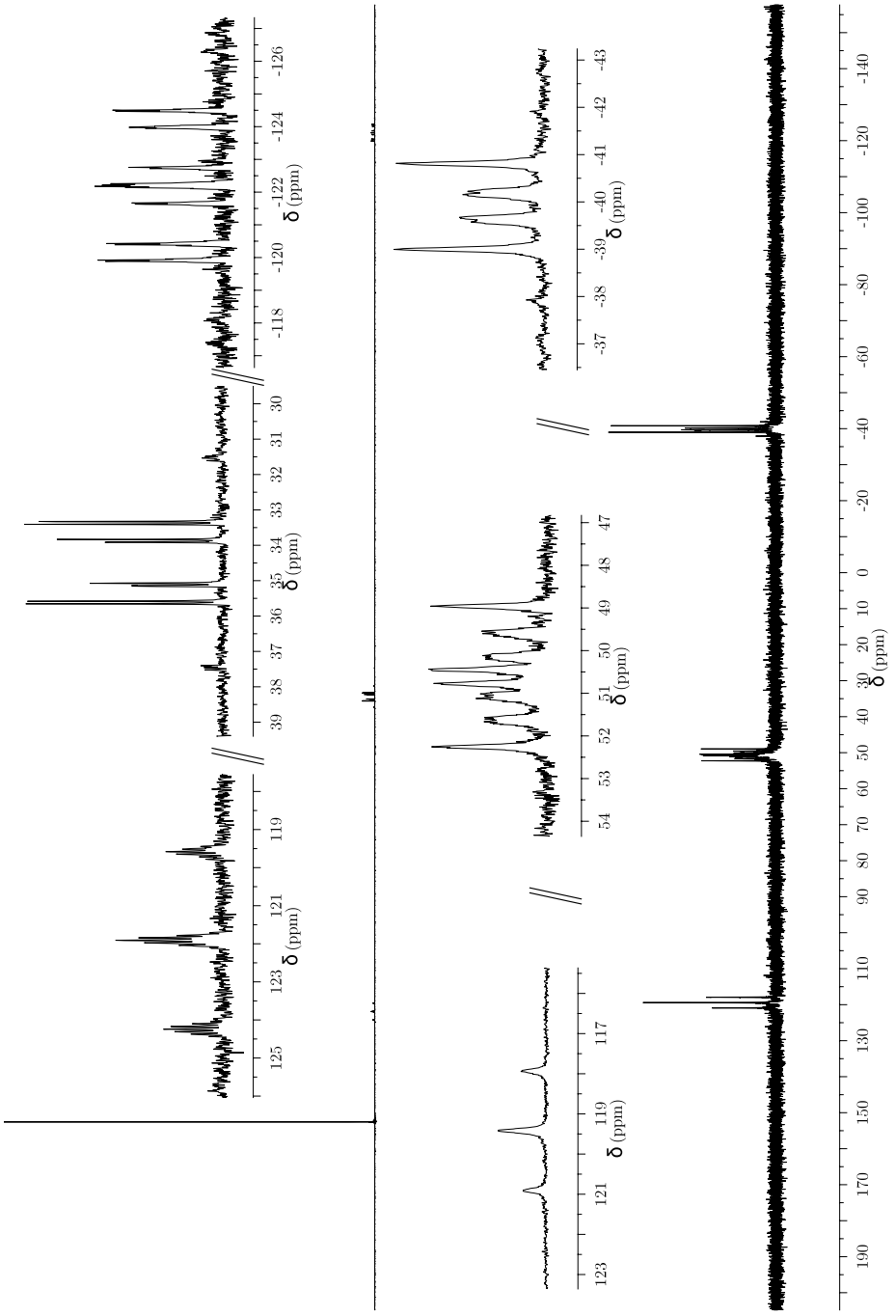


Figure 6.10: $^{31}P\{^1H\}$ NMR spectrum of $[Cp^*Fe(\eta^4\text{-}P_5CH_3)]_2[Mg(dme)_3](dme)$ (**28**) at room temperature in thf with D_2O capillary.

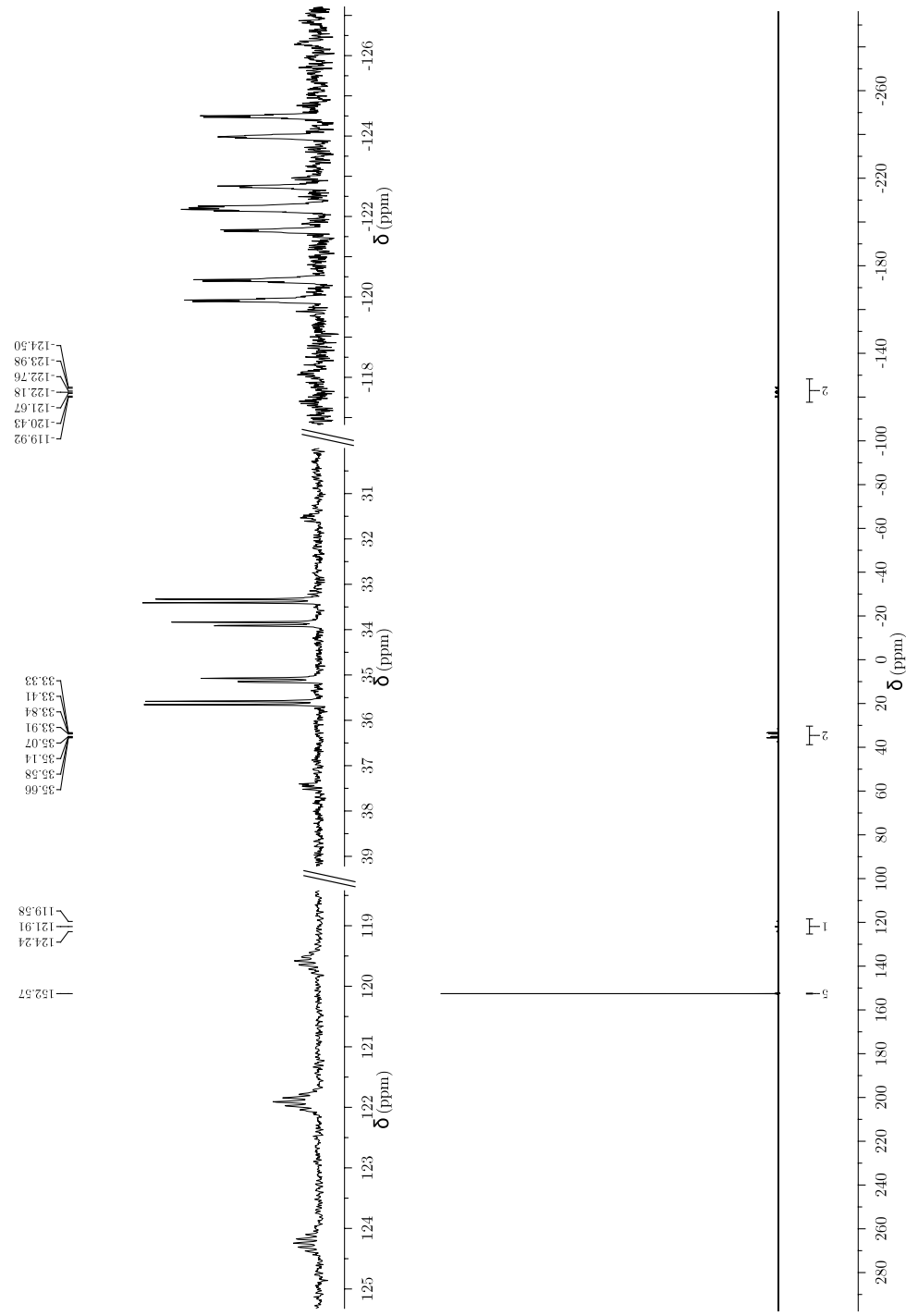


Figure 6.11: ^{31}P NMR spectrum of a reaction mixture containing 1:1 [Cp*Fe(η^4-P_5CH_3)]$_2$[Mg(dme)$_3$](dme) (**28**) and **XXVII** in at room temperature in thf with D_2O capillary.

NMR spectra of $[\mathbf{Cp^*Fe}(\mu,\eta^{\mathbf{4:3}}\text{-}\mathbf{P_5})\mathbf{Sr(thf)_4}]_\mathbf{2}\cdot\mathbf{(thf)_2}$ (26)

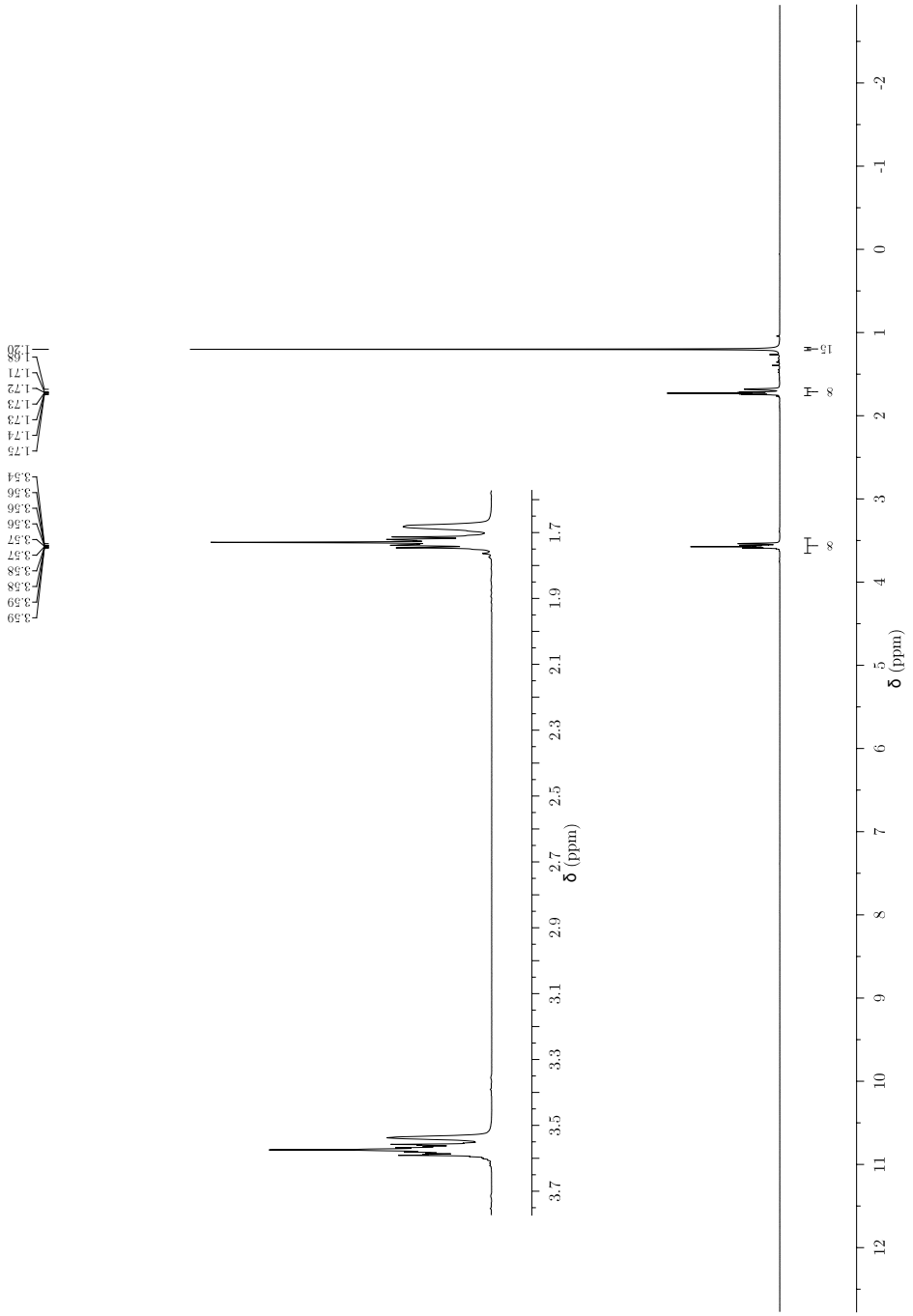


Figure 6.12: ^{1}H NMR spectrum of $[Cp^*Fe(\mu,\eta^{4:3}\text{-}P_5)Sr(thf)_4]_2\cdot(thf)_2$ (**26**) at room temperature in thf-d_8.

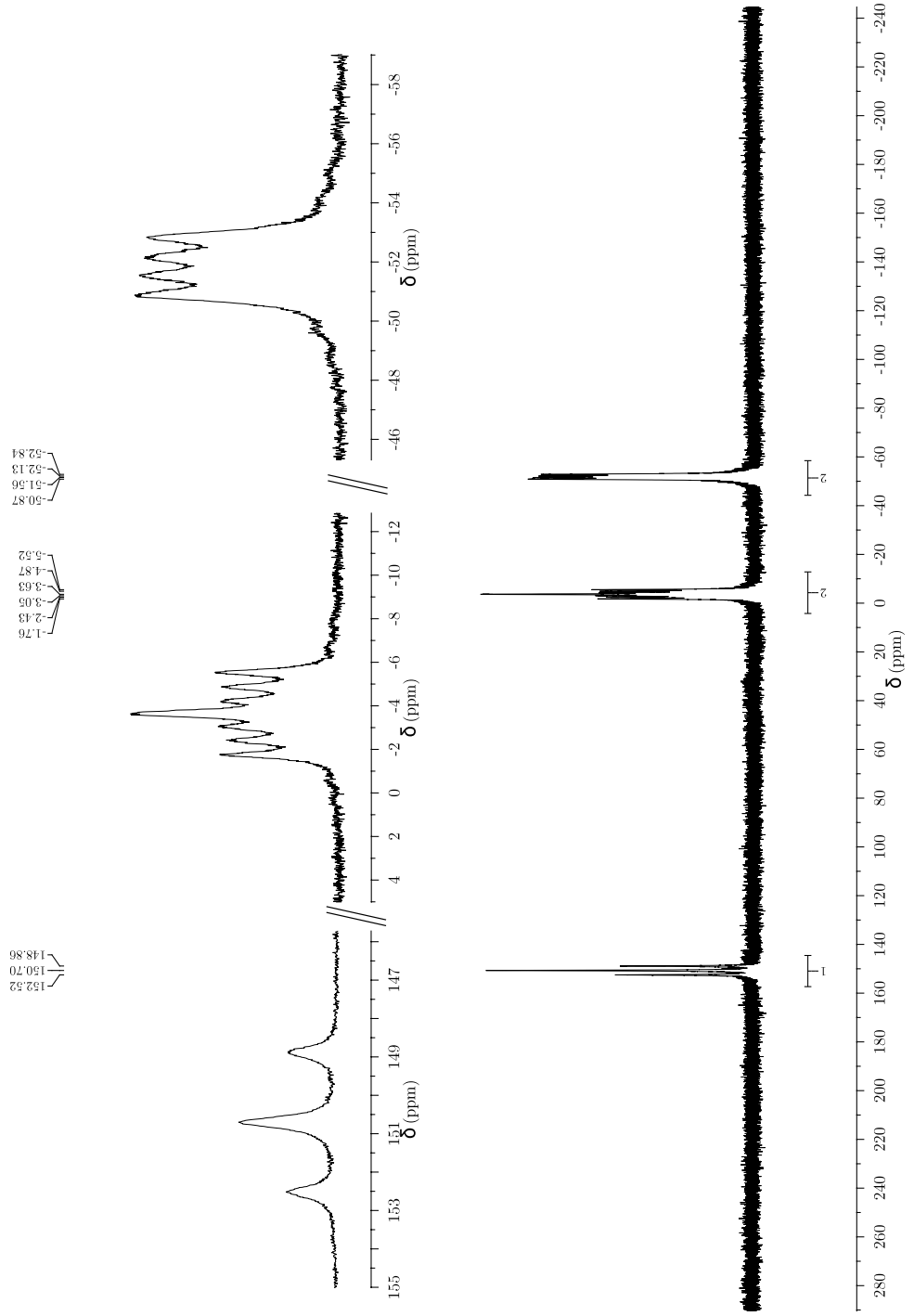


Figure 6.13: $^{31}P\{^{1}H\}$ NMR spectrum of $[Cp^{*}Fe(\mu,\eta^{4:3}\text{-}P_5)Sr(thf)_4]_2 \cdot (thf)_2$ (**26**) at room temperature in thf-d_8.

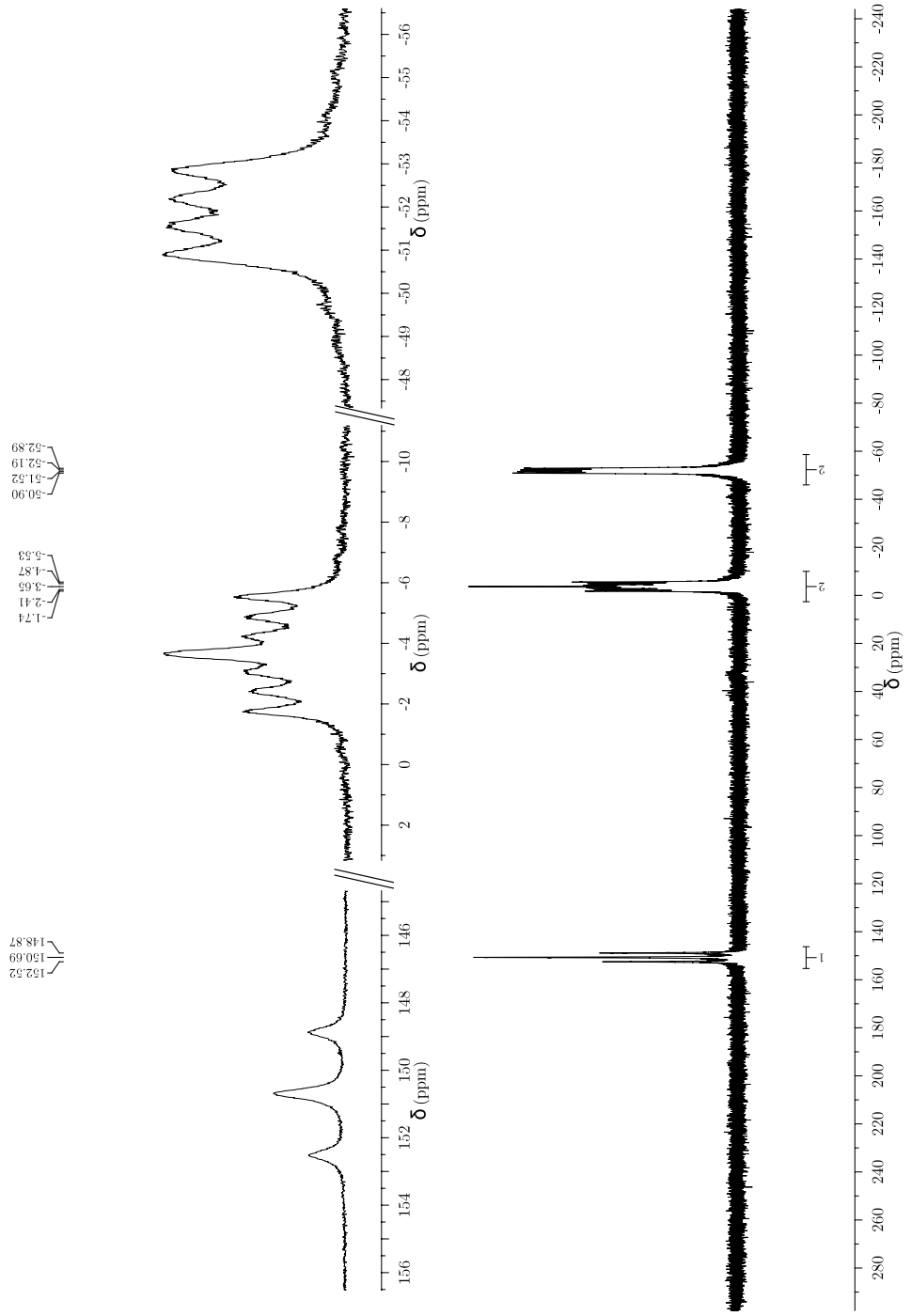


Figure 6.14: ^{31}P NMR spectrum of $[Cp^*Fe(\mu,\eta^{4:3}\text{-}P_5)Sr(thf)_4]_2 \cdot (thf)_2$ (**26**) at room temperature in thf-d_8.

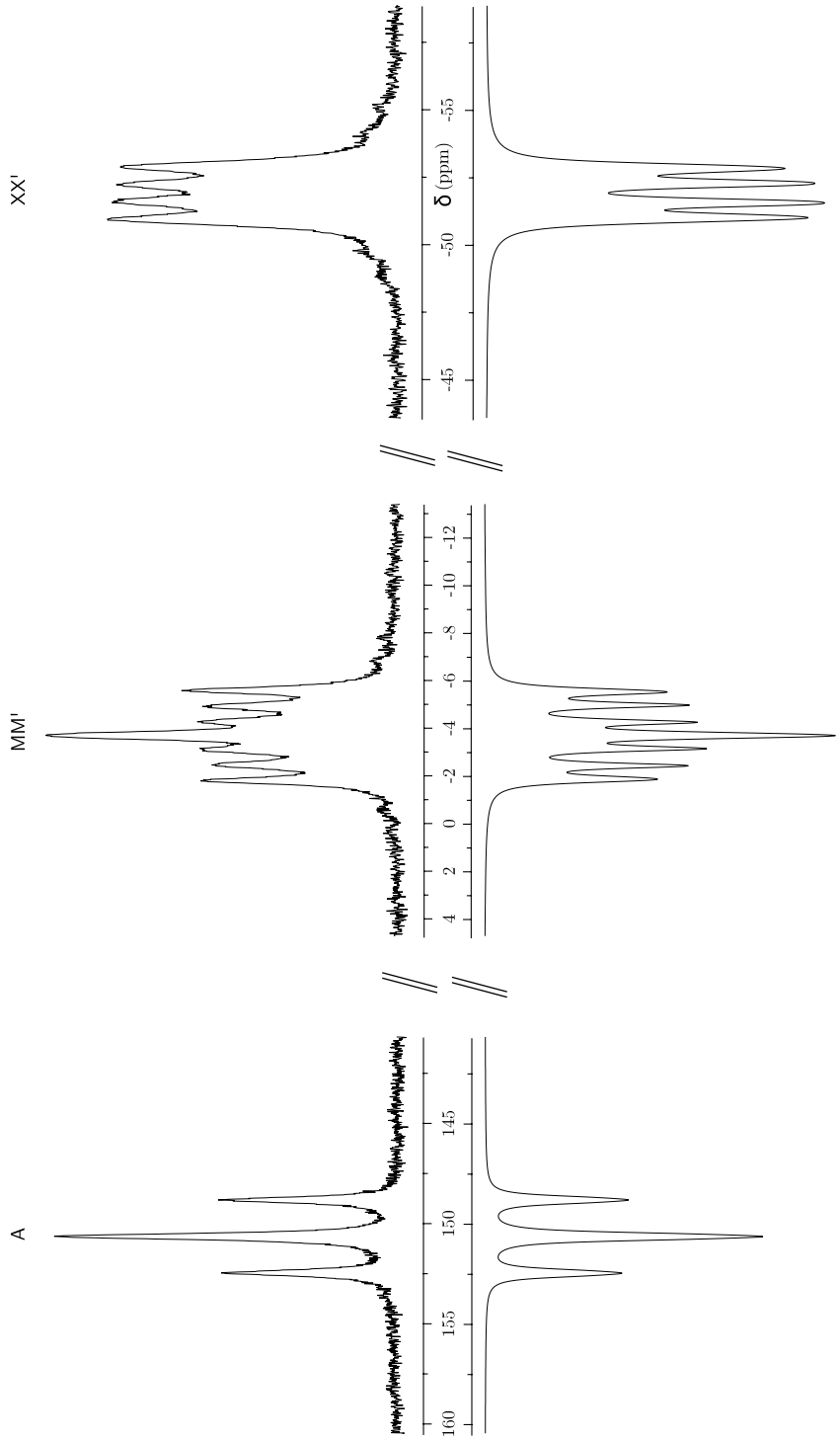


Figure 6.15: Excerpt with simulation of the ^{31}P NMR spectrum of $[Cp^*Fe(\mu,\eta^{4:3}\text{-}P_5)Sr(thf)_4]_2 \cdot (thf)_2$ (**26**) at room temperature in thf-d_8 with simulation of the spin system of **25** shown inverted.

NMR spectra of $\{Cp^*Fe\}_2(\mu_2\eta^{4:4:3:3}\text{-}P_{10})Ba(thf_3)]$ (27)

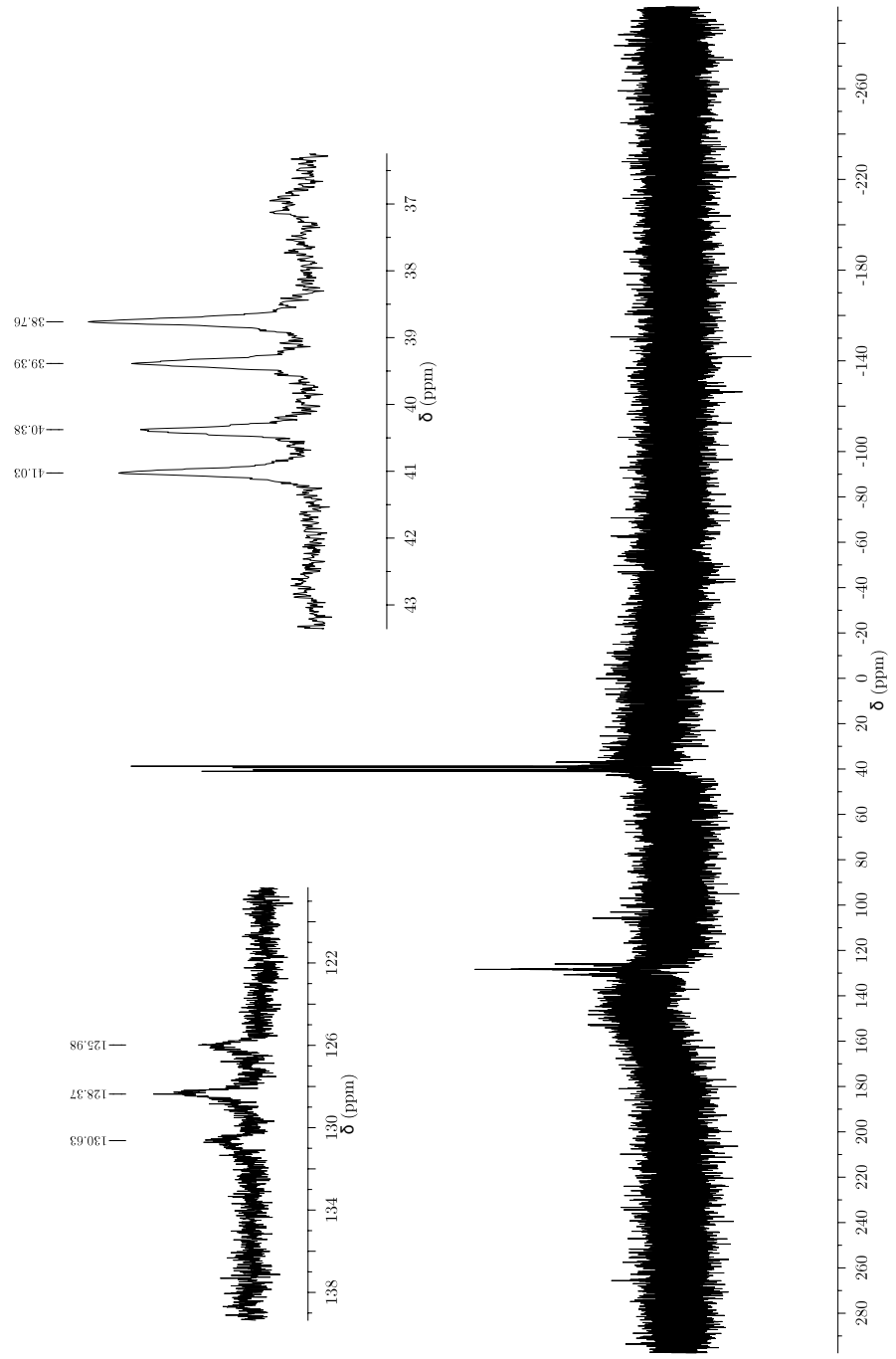


Figure 6.16: ^{31}P NMR spectrum of $[\{Cp^*Fe\}_2(\mu_2\eta^{4:4:3:3}\text{-}P_{10})Ba(thf_3)]$ (**27**) in the reaction solution at room temperature (thf and D_2O capillary).

NMR spectra of [Cp*Fe($\mu_3, \eta^{3:3:4}$-(1-CH_3-2-PPh_2-P_5)$_2$)Mg(thf)$_4$] (29)

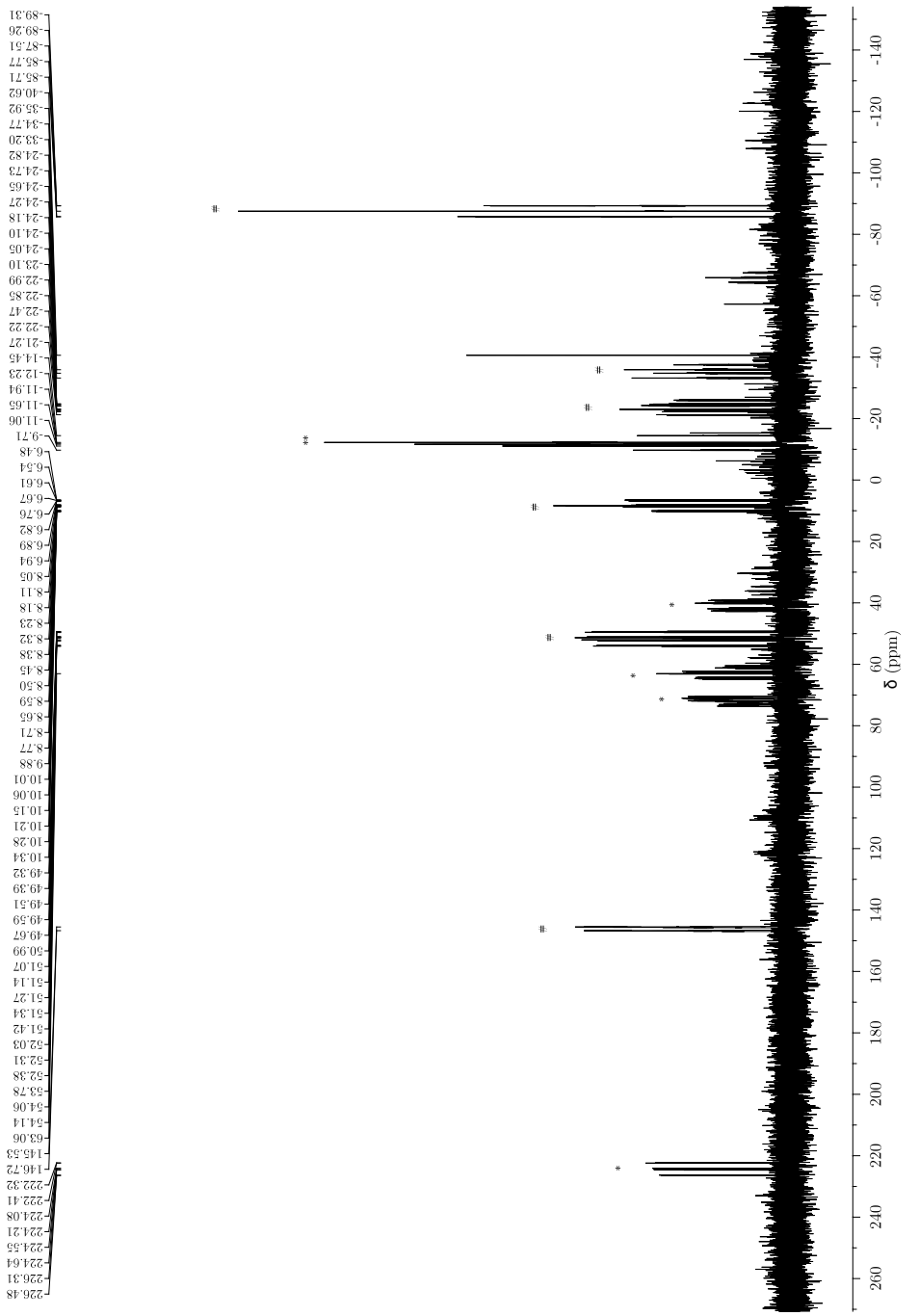


Figure 6.17: ^{31}P NMR spectrum of [Cp*Fe($\mu_3, \eta^{3:3:4}$-(1-CH_3-2-PPh_2-P_5)$_2$)Mg(thf)$_4$] (**29**) in the reaction solution with the starting material **11a** still present at room temperature (thf and D_2O capillary). For the reaction 10 equivalents of MgA were used. Signals of the starting material **11a** are marked with an asterisk and signals of **29** with # .

NMR spectra of $[\mathbf{Cp^*Fe(\mu,\eta^{3:2:2}\text{-}(1\text{-}CH_3\text{-}2\text{-}PPh_2\text{-}P_5))Sr(thf)_3]_2}$ (30)

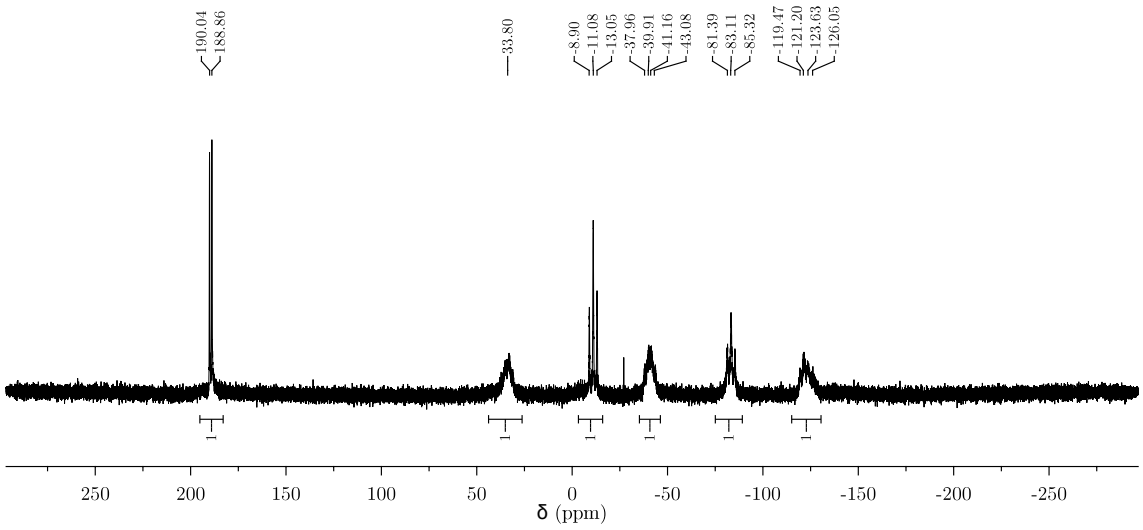


Figure 6.18: ^{31}P NMR spectrum of $[Cp^*Fe(\mu,\eta^{3:2:2}\text{-}(1\text{-}CH_3\text{-}2\text{-}PPh_2\text{-}P_5))Sr(thf)_3]_2$ (**30**) in the reaction solution at room temperature (thf and D_2O capillary). For the reaction 5 equivalents of SrA were used.

6.6.4 Crystallographic details

General remarks

If not stated otherwise, crystals were picked directly from the flask under a constant flow of dry argon. Suitable crystals were then mounted on a Mylar loop in degassed mineral oil. Structures were solved with the ShelXT[177] solution program using dual methods and by using Olex2 1.5-alpha[178] as the graphical interface. The models were refined with ShelXL 2018/3[179] using full matrix least squares minimisation on F^2.

Crystallographic data

Table 6.1: Crystallographic data for **25**, **26** and **27**:

Compound	**25**	**26**	**27**
Formula	$C_{22}H_{39}FeMgO_3P_5$	$C_{60}H_{110}O_{10}P_{10}Fe_2Sr_2$	$C_{40}H_{66}Fe_2MgP_{10}O_5Ba$
$\rho_{calc.}/gcm^{-3}$	1.304	1.407	1.382
μ/mm^{-1}	6.951	1.097	1.509
Formula Weight	586.54	1588.11	1185.57
Colour	dark green	dark black	dark brown
Shape	octahedral-shaped	block-shaped	rhombohedral-shaped
$Size/mm^3$	$0.43 \times 0.28 \times 0.23$	$0.45 \times 0.3 \times 0.23$	$0.11 \times 0.08 \times 0.05$
T/K	123.00(10)	140.00(10)	133.00(10)
Crystal System	orthorhombic	monoclinic	orthorhombic
Space Group	Pbcn	$P2_1/n$	$Pca2_1$
a/Å	31.9024(4)	12.3561(3)	27.7184(7)
b/Å	11.25500(10)	15.5150(3)	40.4538(12)
c/Å	16.6438(2)	20.0866(5)	20.3254(4)
$\alpha/^\circ$	90	90	90
$\beta/^\circ$	90	103.304(2)	90
$\gamma/^\circ$	90	90	90
$V/Å^3$	5976.15(12)	3747.36(15)	22791.2(10)
Z	8	2	16
Z'	1	0.5	4
Wavelength/Å	1.54184	0.56087	0.71073
Radiation type	Cu K_α	Ag K_α	Mo K_α
$\theta_{min}/^\circ$	4.165	2.229	1.781
$\theta_{max}/^\circ$	74.403	26.155	25.681
Measured Refl's.	21198	54177	100266
Indep't Refl's	6012	12345	36899
Refl's $I \geq 2\sigma(I)$	5567	9256	28429
R_{int}	0.0275	0.0613	0.1007
Parameters	294	403	2659
Restraints	0	0	3884
Largest Peak	0.419	1.259	4.315
Deepest Hole	-0.415	-1.072	-2.990
GooF	1.017	1.035	1.070
wR2 (all data)	0.0790	0.1281	0.2868
wR2	0.0770	0.1106	0.2679
R1 (all data)	0.0329	0.0711	0.1217
R1	0.0300	0.0472	0.1014

Table 6.2: Crystallographic data for **28** and **29** :

Compound	**28**	**29**
Formula	$C_{38}H_{76}Fe_2MgO_8P_{10}$	$C_{54}H_{72}Fe_2MgP_{12}O_2$
$\rho_{calc.}/gcm^{-3}$	1.317	1.195
μ/mm^{-1}	7.333	6.262
Formula Weight	1106.69	1260.76
Colour	dark brown	clear intense brown
Shape	irregular-shaped	plate-shaped
Size/mm^3	$0.28 \times 0.14 \times 0.13$	$0.06 \times 0.05 \times 0.02$
T/K	122.98(11)	123.00(10)
Crystal System	monoclinic	tetragonal
Space Group	$P2_1/c$	$P4_32_12$
a/Å	10.5512(6)	10.73460(10)
b/Å	14.2205(7)	10.73460(10)
c/Å	37.349(2)	60.8000(8)
$\alpha/^\circ$	90	90
$\beta/^\circ$	95.224(5)	90
$\gamma/^\circ$	90	90
V/$Å^3$	5580.7(5)	7006.08(16)
Z	4	4
Z'	2	1
Wavelength/Å	1.54184	1.54184
Radiation type	Cu K_α	Cu K_α
$\theta_{min}/^\circ$	2.376	4.182
$\theta_{max}/^\circ$	74.069	75.105
Measured Refl's.	24832	30565
Indep't Refl's	10987	6848
Refl's I $\geq 2\sigma$(I)	7378	5884
R_{int}	0.0670	0.0496
Parameters	761	328
Restraints	945	0
Largest Peak	0.630	0.454
Deepest Hole	-0.672	-0.319
GooF	1.058	1.044
wR2 (all data)	0.2633	0.1399
wR2	0.2244	0.1349
R1 (all data)	0.1112	0.0665
R1	0.0835	0.0571

Table 6.3: Crystallographic data for **30** and **31**:

Compound	**30**	**31**
Formula	$C_{78}H_{120}O_8P_{12}Fe_2Sr_2$	$C_{109}H_{150}Fe_2Mg_2N_4P_{12}$
$\rho_{calc.}$/gcm^{-3}	1.430	1.242
μ/mm^{-1}	6.774	4.251
Formula Weight	1844.31	2048.28
Colour	dark red	clear dark red
Shape	needle-shaped	irregular-shaped
Size/mm^3	$0.18 \times 0.02 \times 0.02$	$0.09 \times 0.07 \times 0.05$
T/K	123.01(10)	122.97(10)
Crystal System	monoclinic	monoclinic
Flack Parameter	n.a.	n.a.
Hooft Parameter	n.a.	n.a.
Space Group	$P2_1/n$	$P2_1/c$
a/Å	10.7954(2)	14.4098(4)
b/Å	20.3376(3)	21.0640(5)
c/Å	19.5093(3)	18.1097(5)
α/°	90	90
β/°	90.3120(10)	95.055(2)
γ/°	90	90
V/Å^3	4283.25(12)	5475.4(2)
Z	2	2
Z'	0.5	0.5
Wavelength/Å	1.54184	1.54184
Radiation type	Cu K_α	Cu K_α
θ_{min}/°	6.278	3.726
θ_{max}/°	130.26	73.426
Measured Refl's.	19764	19828
Indep't Refl's	6956	10428
Refl's I $\geq 2\sigma$(I)	5595	7687
R_{int}	0.0624	0.0464
Parameters	512	652
Restraints	160	105
Largest Peak	0.893	0.450
Deepest Hole	-0.925	-0.652
GooF	1.061	1.050
wR2 (all data)	0.1387	0.1364
wR2	0.1300	0.1170
R1 (all data)	0.0624	0.0833
R1	0.0490	0.0554

$[\mathbf{Cp^*Fe(\mu,\eta^{4:3}\text{-}P_5)Mg(thf)_3}$

Crystals of $[Cp^*Fe(\mu,\eta^{4:3}\text{-}P_5)Mg(thf)_3$ (**25**) were obtained by storing a saturated thf solution at -30 °C for two days. A dark green red octahedral-shaped crystal with dimensions $0.43 \times 0.28 \times 0.23$ mm^3 was selected for the diffraction experiment. The crystal was kept at a steady T = 123.00(10) K during data collection.

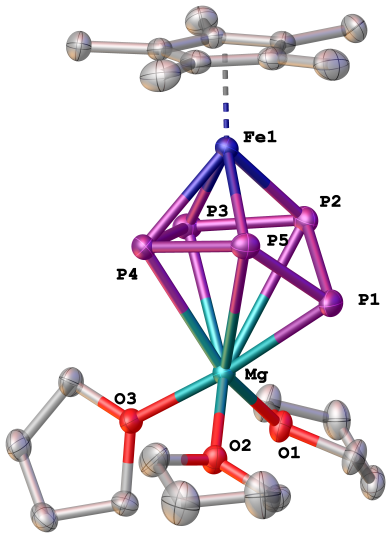


Figure 6.19: Molecular structures of (**25**) in the solid state. Hydrogen atoms are omitted for clarity. Selected bond lengths and angles: Fe1-P4 2.3121(5), Fe1-P5 2.2586(5), Fe1-P3 2.2980(5), Fe1-P2 2.2624(5), P4-P5 2.2177(6), P4-P3 2.1709(6), P4-Mg 2.8388(7), P5-P1 2.1755(6), P5-Mg 3.1619(7), P3-P2 2.2233(6), P3-Mg 2.7791(7), P1-P2 2.1772(6), P1-Mg 2.5626(7), P2-Mg 3.0748(7), Mg-O1 2.0525(13), Mg-O3 2.0985(12), Mg-O2 2.0586(13), P5-Fe1-P4 58.035(17), P5-Fe1-P3 94.975(17), P5-Fe1-P2 81.107(18), P3-Fe1-P4 56.184(17), P2-Fe1-P4 94.804(18), P2-Fe1-P3 58.351(18), Fe1-P4-Mg 100.153(19), P5-P4-Fe1 59.773(17), P5-P4-Mg 76.31(2), P3-P4-Fe1 61.578(17), P3-P4-P5 99.88(2), P3-P4-Mg 65.82(2), Fe1-P5-Mg 92.488(17), P4-P5-Fe1 62.191(17), P4-P5-Mg 60.730(18), P1-P5-Fe1 96.60(2), P1-P5-P4 109.38(2), P1-P5-Mg 53.602(17), Fe1-P3-Mg 102.272(19), P4-P3-Fe1 62.238(17), P4-P3-P2 100.05(2), P4-P3-Mg 68.73(2), P2-P3-Fe1 60.024(17), P2-P3-Mg 74.94(2), P5-P1-P2 84.95(2), P5-P1-Mg 83.29(2), P2-P1-Mg 80.44(2), Fe1-P2-Mg 94.723(18), P3-P2-Fe1 61.625(17), P3-P2-Mg 60.780(18), P1-P2-Fe1 96.44(2), P1-P2-P3 109.37(2), P1-P2-Mg 55.269(17), P4-Mg-P5 42.958(14), P4-Mg-P2 69.293(17), P3-Mg-P4 45.449(16), P3-Mg-P5 68.510(16), P3-Mg-P2 44.285(15), P1-Mg-P4 83.00(2), P1-Mg-P5 43.105(15), P1-Mg-P3 84.38(2), P1-Mg-P2 44.287(16,) P2-Mg-P5 56.217(15), O1-Mg-P4 152.24(4), O1-Mg-P5 140.26(4), O1-Mg-P3 106.86(4), O1-Mg-P1 97.97(4), O1-Mg-P2 91.97(4), O1-Mg-O3 85.89(5), O1-Mg-O2 102.55(5), O3-Mg-P4 91.96(4), O3-Mg-P5 132.46(4), O3-Mg-P3 91.19(4), O3-Mg-P1 174.80(4), O3-Mg-P2 132.46(4), O2-Mg-P4 104.91(4), O2-Mg-P5 91.76(4), O2-Mg-P3 150.18(4), O2-Mg-P1 96.41(4), O2-Mg-P2 140.04(4), O2-Mg-O3 86.08(5).

$[\mathbf{Cp^*Fe(\eta^4\text{-}P_5CH_3)]_2[Mg(dme)_3](dme)}$

Crystals of $[Cp^*Fe(\eta^4\text{-}P_5CH_3)]_2[Mg(dme)_3](dme)$ (**28**) were obtained by storing a saturated dme solution at -30 °C for three weeks. A clear dark brown irregular-shaped crystal with dimensions $0.28 \times 0.14 \times 0.13\ mm^3$ was selected for the diffraction experiment. The crystal was kept at a steady T = 122.98(11) K during data collection. The structure of (**28**) is heavily disordered in one of the $[Cp^*Fe(\eta^4\text{-}P_5CH_3)]$ units with the parts being occupied to 60 % and 40 % respectively (figure 6.21).

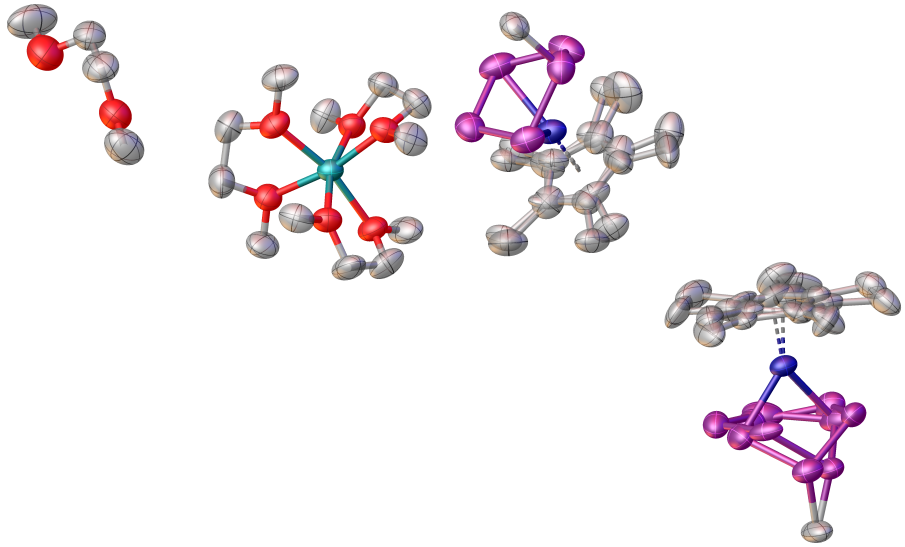


Figure 6.20: Asymmetric unit of the molecular structure of **28** in the solid state.

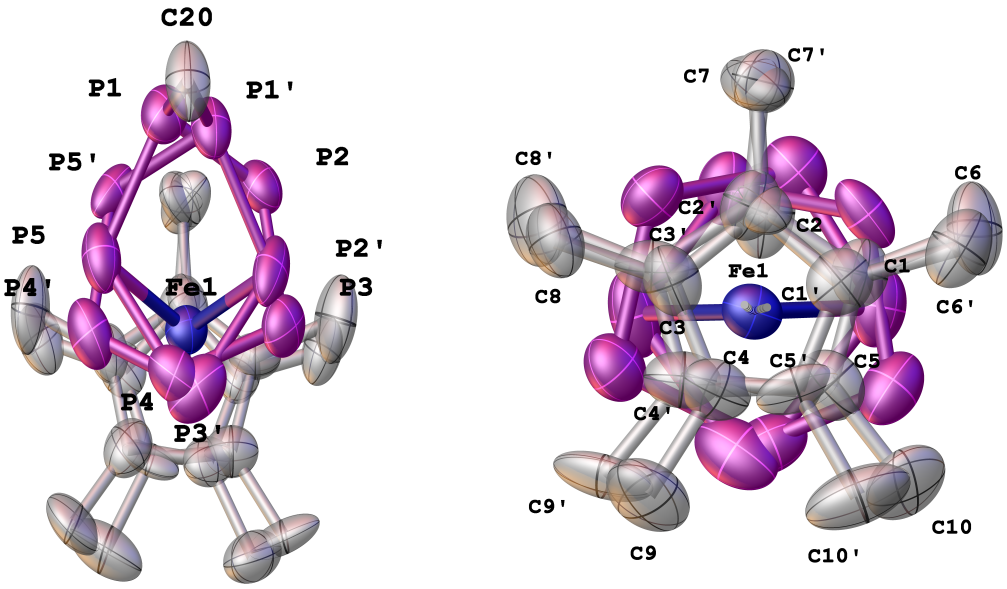


Figure 6.21: Molecular structure of **28** in the solid state. Hydrogen atoms are omitted for clarity. Selected bond lengths and angles: Fe1-P5 2.299(2), Fe1-C2 2.074(13), Fe1-C1 2.108(14), Fe1-C3 2.078(15), Fe1-C4 2.062(15), Fe1-C5 2.085(16), Fe1-P2' 2.260(7), Fe1-C5' 2.120(17), Fe1-C4' 2.07(2), Fe1-C3' 2.08(2), Fe1-C2' 2.05(2), Fe1-C1' 2.11(2), P4-P3 2.132(7), P4-P5 2.150(7), P3-P2 2.127(4), P2-P1 2.160(4), P1-P5 2.173(4), P1-C20 1.888(7), P4'-P3' 2.073(16), P4'-P5' 2.151(11), P3'-P2' 2.125(16), P2'-P1' 2.147(12), P1'-P5' 2.157(8), P3-P4-Fe1 63.05(17), P3-P4-P5 102.8(2), P5-P4-Fe1 61.61(17), P4-P3-Fe1 62.60(19), P2-P3-Fe1 62.88(10), P2-P3-P4 103.7(2), P3-P2-Fe1 62.98(9), P3-P2-P1 107.95(15), P1-P2-Fe1 89.86(11), P2-P1-P5 91.89(12), C20-P1-P2 109.2(3), C20-P1-P5 107.7(3), P4-P5-Fe1 63.01(19), P4-P5-P1 107.34(19), P1-P5-Fe1 90.53(13), P3'-P4'-Fe1 61.4(6), P3'-P4'-P5' 103.7(6), P5'-P4'-Fe1 61.1(2), P4'-P3'-Fe1 66.7(5), P4'-P3'-P2' 104.4(7), P2'-P3'-Fe1 61.0(5), P3'-P2'-Fe1 63.7(6), P3'-P2'-P1' 107.2(6), P1'-P2'-Fe1 90.2(4), C20-P1'-P2' 117.9(6), C20-P1'-P5' 109.7(4), P2'-P1'-P5' 92.7(3), P4'-P5'-Fe1 65.2(2), P4'-P5'-P1' 105.5(3), P1'-P5'-Fe1 87.9(3).

$[\mathbf{Cp^*Fe(\mu,\eta^{4:3}\text{-}P_5)Sr(thf)_4]_2(thf)_2}$

Crystals of $[Cp^*Fe(\mu,\eta^{4:3}\text{-}P_5)Sr(thf)_4]_2(thf)_2$ (**26**) were obtained by storing a saturated thf solution at -30 °C for one day. A dark black block-shaped crystal with dimensions $0.45 \times 0.30 \times 0.23\ mm^3$ was selected for the diffraction experiment. The crystal was kept at a steady T = 140.00(10) K during data collection with a Ag source to prevent decomposition of the crystal.

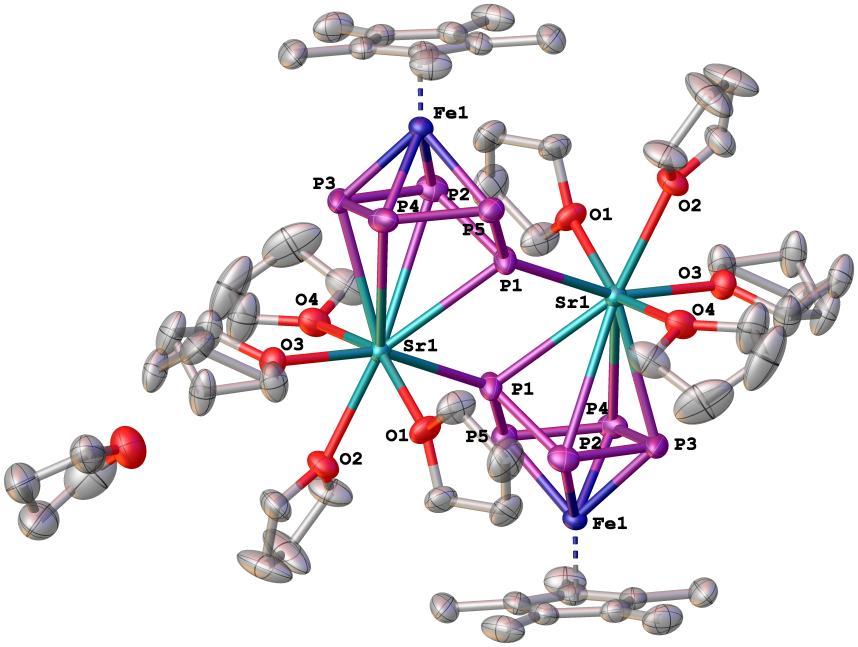


Figure 6.22: Molecular structures of $[Cp^*Fe(\mu,\eta^{4:3}\text{-}P_5)Sr(thf)_4]_2(thf)_2$ (**26**) in the solid state. Hydrogen atoms are omitted for clarity. Selected bond lengths and angles: Sr1-P2 3.4128(8), Sr1-P1^1 3.1174(7), Sr1-P1 3.0794(7), Sr1-P4 3.7466(8), Sr1-P3 3.1775(7), Sr1-O3 2.5729(18), Sr1-O4 2.573(2), Sr1-O1 2.5521(19), Sr1-O2 2.6228(19), Fe1-P5 2.2720(8), Fe1-P2 2.2826(7), Fe1-P4 2.3222(8), Fe1-P3 2.2901(8), P5-P1 2.1625(9), P5-P4 2.1972(10), P2-P1 2.1733(11), P2-P3 2.2164(11), P4-P3 2.1491(13), P2-Sr1-P4 55.415(16), P1^1-Sr1-P2 85.278(19), P1-Sr1-P2 38.69(2), P1-Sr1-P1^1 69.02(2), P1-Sr1-P4 60.231(17), P1^1-Sr1-P4 129.253(18), P1-Sr1-P3 68.423(18), P1^1-Sr1-P3 123.84(2), P3-Sr1-P2 39.100(19), P3-Sr1-P4 34.95(2), O3-Sr1-P2 113.67(5), O3-Sr1-P1 130.89(5), O3-Sr1-P1^1 159.37(5), O3-Sr1-P4 70.88(5), O3-Sr1-P3 74.57(5), O3-Sr1-O2 73.43(6), O4-Sr1-P2 80.97(5), O4-Sr1-P1^1 80.95(5), O4-Sr1-P1 111.92(5), O4-Sr1-P4 117.42(5), O4-Sr1-P3 82.64(5), O4-Sr1-O3 93.59(7), O4-Sr1-O2 75.51(7), O1-Sr1-P2 124.18(5), O1-Sr1-P1^1 95.37(5), O1-Sr1-P1 89.84(5), O1-Sr1-P4 84.57(5), O1-Sr1-P3 119.20(5), O1-Sr1-O3 80.95(7), O1-Sr1-O4 154.42(7), O1-Sr1-O2 78.98(7), O2-Sr1-P2 155.91(5), O2-Sr1-P1^1 85.94(5), O2-Sr1-P1 151.57(5), O2-Sr1-P4 142.55(5), O2-Sr1-P3 139.65(5), P5-Fe1-P2 80.50(3), P5-Fe1-P4 57.13(3), P5-Fe1-P3 94.44(3), P2-Fe1-P4 93.06(3), P2-Fe1-P3 57.99(3), P3-Fe1-P4 55.54(3), P1-P5-Fe1 97.18(4), P1-P5-P4 105.62(4), P4-P5-Fe1 62.58(3), Fe1-P2-Sr1 111.25(3), P1-P2-Sr1 62.33(3), P1-P2-Fe1 96.56(3), P1-P2-P3 106.57(4), P3-P2-Sr1 64.71(3), P3-P2-Fe1 61.18(3), Sr1-P1-Sr1^1 110.98(2), P5-P1-Sr1^1 141.95(4), P5-P1-Sr1 105.23(3), P5-P1-P2 85.48(3), P2-P1-Sr1^1 112.21(4), P2-P1-Sr1 78.98(3), Fe1-P4-Sr1 100.18(3), P5-P4-Sr1 85.79(3), P5-P4-Fe1 60.28(3), P3-P4-Sr1 57.89(2), P3-P4-Fe1 61.48(3), P3-P4-P5 100.78(4), Fe1-P3-Sr1 119.48(3), P2-P3-Sr1 76.19(3), P2-P3-Fe1 60.84(3), P4-P3-Sr1 87.16(3), P4-P3-Fe1 62.99(3), P4-P3-P2 99.90(4).

$[\{\mathbf{Cp^*Fe}\}_\mathbf{2}(\mu,\eta^{\mathbf{4:4:3:3}}\text{-}\mathbf{P_{10}})\mathbf{Ba(thf_3)}]$

Crystals of $[\{Cp^*Fe\}_2(\mu,\eta^{4:4:3:3}\text{-}P_{10})Ba(thf_3)]$ (**27**) were obtained by storing a saturated thf solution at -30 °C for three weeks. A dark irregular shaped crystal with dimensions $0.11 \times 0.08 \times 0.05\ mm^3$ was selected for the diffraction experiment. Although an Mo source was used and the sample carefully cooled from room temperature to 133 K on the goniometer head, the diffraction pattern shows signs of decomposition of the crystal in frames of the end of the measurement. The quality of the measurement is only sufficient to determine the heavy atom framework of the respective compound **27** tentatively and bondlengths cannot be determined with absolute certainty. The asymmetric unit consists of 4 molecules of **27**, one being heavily disordered. The disorder could only be solved for isotropic phosphorus atoms in the case of this molecule. All units of **27** show different coordination modes of the Ba atom to the P_{10} ligand.

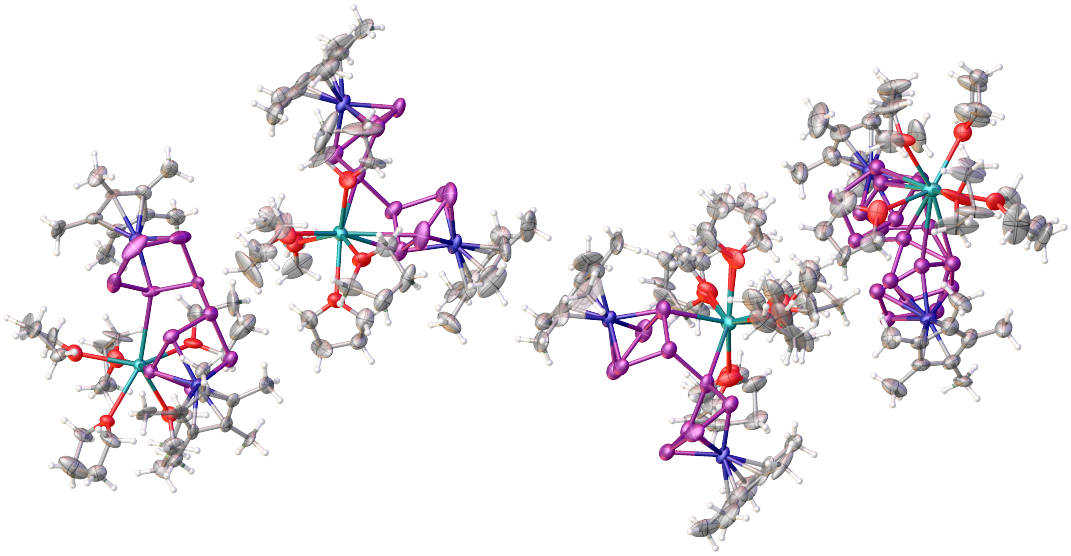


Figure 6.23: Tentative solution of the molecular structures of **27** in the solid state. Bond lengths and angles are not reliable and the solution only shows the connectivity of the heavy atom framework in **27**. The unit of **27** on the right is heavily disordered and the highest peak as well as the deepest hole in the electron density of the model is located at this moiety.

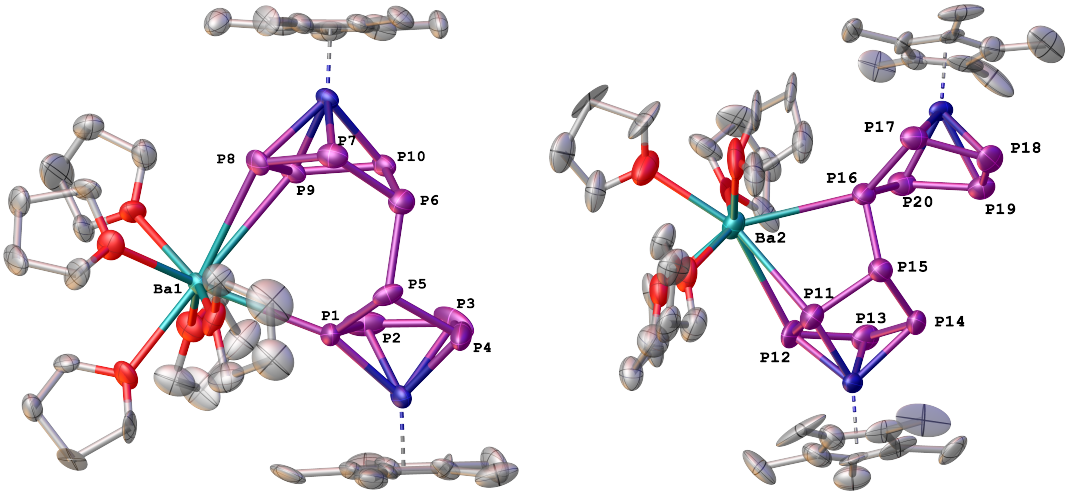


Figure 6.24: Excerpts from the molecular structure of **27** in the solid state. Two of the moieties, present in the asymmetric unit, which show different coordination modes of the Ba atom and the P_{10}^{2-} unit in **27**. Selected, tentatively estimated bond lengths and angles: Ba1-P9 3.557(5), Ba1-P8 3.339(5), Ba1-P1 3.320(5), Ba2-P16 3.526(6), Ba2-P12 3.547(8), Ba2-P11 3.210(7), P9-P10 2.154(7), P9-P8 2.164(7), P10-P6 2.146(8), P8-P7 2.145(8), P1-P2 2.106(9), P1-P5 2.192(8), P7-P6 2.174(8), P20-P16 2.193(10), P20-P19 2.110(10), P14-P13 2.131(9) , P14-P15 2.143(10) , P16-P17 2.180(8) , P16-P15 2.236(9) , P6-P5 2.209(7) , P19-P18 2.127(11), P2-P3 2.120(13), P4-P5 2.177(8) , P4-P3 2.148(13) , P12-P11 2.244(12) , P8-Ba1-P9 36.39(11), P1-Ba1-P9 71.51(12), P1-Ba1-P8 84.48(13), P16-Ba2-P12 74.26(15), P11-Ba2-P16 64.65(16), P11-Ba2-P12 38.38(19), P10-P9-Ba1 129.3(2) , P6-P10-P9 106.9(3), P10-P9-P8 103.8(3), P8-P9-Ba1 66.31(18), P9-P8-Ba1 77.3(2) , P7-P8-Ba1 126.3(3), P7-P8-P9 102.8(3), P2-P1-Ba1 107.1(3), P2-P1-P5 108.8(3), P5-P1-Ba1 115.9(2), P8-P7-P6 108.1(3), P20-P16-Ba2 123.4(3), P20-P16-P15 113.2(4), P17-P16-Ba2 133.8(3), P17-P16-P20 92.0(3) , P17-P16-P15 107.3(3), P15-P16-Ba2 86.5(2) , P10-P6-P7 93.8(3) , P10-P6-P5 116.2(3), P7-P6-P5 109.8(3), P18-P17-P16 105.7(4), P14-P15-P16 112.5(4), P14-P15-P11 91.0(3) , P11-P15-P16 110.5(4), P20-P19-P18 104.2(4), P1-P2-P3 103.4(4), P3-P4-P5 107.0(4), P1-P5-P6 116.6(3), P4-P5-P1 90.8(3) , P4-P5-P6 106.5(3), P13-P12-Ba2 126.8(3), P13-P12-P11 101.1(4), P11-P12-Ba2 62.6(3), P15-P11-Ba2 96.2(3) , P19-P18-P17 103.6(4), P2-P3-P4 103.5(3).

$[\{\mathbf{Cp^*Fe}\}(\mu,\eta^{\mathbf{3:1}},\eta^{\mathbf{1:1}}\text{-}(\mathbf{1\text{-}Me\text{-}2\text{-}PPh_2\text{-}P_5}))\{^{\mathbf{Dipp}}\mathbf{BDI\text{-}Mg}\}]$

Crystals of $[\{Cp^*Fe\}(\mu,\eta^{3:1},\eta^{1:1}\text{-}(1\text{-Me-2-}PPh_2\text{-}P_5))\{^{Dipp}BDI\text{-Mg}\}]$ (**31**) were obtained by storing a saturated pentane solution at 243 K for one month. A clear dark red irregular-shaped crystal with dimensions $0.09 \times 0.07 \times 0.05$ mm^3 was selected for the diffraction experiment. The crystal was kept at a steady T = 122.97(10) K during data collection. The Structure of **31** is disordered in one of the isopropyl groups of the ^{Dipp}BDI- ligand. The parts are visible in a 1:1 ratio. Atom numbers of the disordered part are marked with a dash.

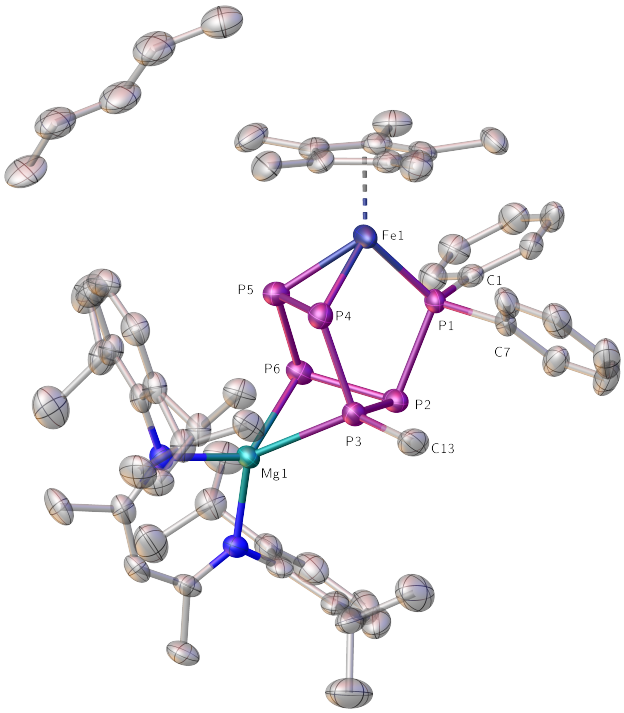


Figure 6.25: Molecular structures of **31** in the solid state. Hydrogen atoms are omitted for clarity. Selected bond lengths and angles: Fe1-P1 2.1585(11), Fe1-P4 2.2768(12), Fe1-P5 2.2706(12), P1-P2 2.2502(13), P1-C1 1.832(4), P1-C7 1.839(4), P2-P3 2.1832(14), P2-P6 2.1895(14), P3-P4 2.2223(14), P3-Mg1 2.6374(15), P3-C13 1.844(4), P6-P5 2.2117(14), P6-Mg1 2.5738(15), P4-P5 2.1596(14), Mg1-N2 2.027(3), Mg1-N1 2.044(3), P1-Fe1-P4 93.48(4), P1-Fe1-P5 96.05(4), P5-Fe1-P4 56.71(4), Fe1-P1-P2 113.34(5), C1-P1-Fe1 116.83(12), C1-P1-P2 104.65(13), C1-P1-C7 103.57(18), C7-P1-Fe1 116.94(14), C7-P1-P2 99.35(13), P3-P2-P1 95.30(5), P3-P2-P6 89.57(5), P6-P2-P1 98.26(5), P2-P3-P4 104.55(5), P2-P3-Mg1 87.61(5), P4-P3-Mg1 99.56(5), C13-P3-P2 113.64(16), C13-P3-P4 108.46(15), C13-P3-Mg1 138.11(15), P2-P6-P5 100.12(5), P2-P6-Mg1 89.11(5), P5-P6-Mg1 90.92(5), P3-P4-Fe1 112.23(5), P5-P4-Fe1 61.50(4), P5-P4-P3 95.13(5), P6-P5-Fe1 112.29(5), P4-P5-Fe1 61.79(4), P4-P5-P6 108.70(5), P6-Mg1-P3 72.46(4), N2-Mg1-P3 126.11(10), N2-Mg1-P6 115.61(10), N2-Mg1-N1 94.22(13), N1-Mg1-P3 120.87(10), N1-Mg1-P6 131.08(10).

$[\mathbf{Cp^*Fe(\mu_3,\eta^{3:3:4}\text{-}(1\text{-}CH_3\text{-}2\text{-}PPh_2\text{-}P_5)_2)Mg(thf)_4}]$

Crystals of $[Cp^*Fe(\mu_3,\eta^{3:3:4}\text{-}(1\text{-}CH_3\text{-}2\text{-}PPh_2\text{-}P_5)_2)Mg(thf)_4]$ (**29**) were obtained by storing a saturated thf solution at -30 °C for two weeks. A clear intense brown plate-shaped crystal with dimensions $0.06 \times 0.05 \times 0.02$ mm^3 was selected for the diffraction experiment. The crystal was kept at a steady T = 123.00(10) K during data collection.

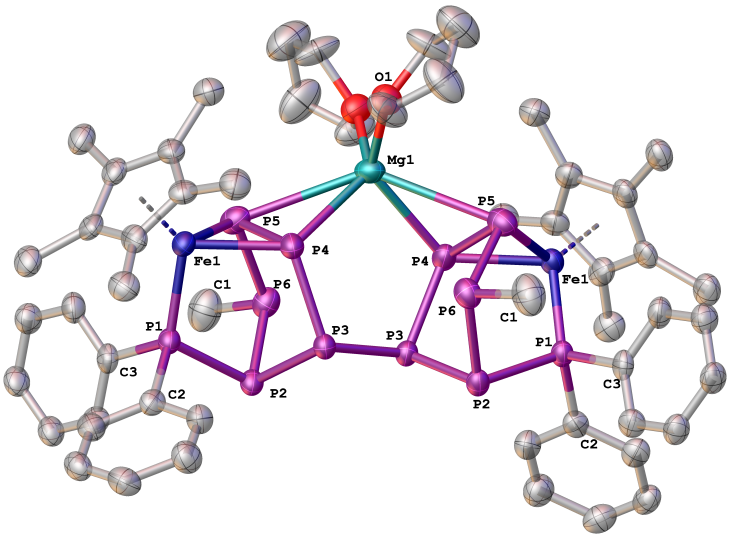


Figure 6.26: Molecular structures of (**29**) in the solid state. Hydrogen atoms are omitted for clarity. Selected bond lengths and angles: Fe1-P1 2.1495(19), Fe1-P4 2.2614(18), Fe1-P5 2.258(2), P3-P3^1 2.222(3), P3-P2 2.200(2), P3-P4 2.227(2), P1-P2 2.254(2), P1-C3 1.836(7), P1-C2 1.857(7), P2-P6 2.191(3), P6-P5 2.227(3), P6-C1 1.832(9), P4-P5 2.204(3), P4-Mg1 2.575(3), P5-Mg1 3.048(2), Mg1-O1 2.043(6), Mg1-O1^1 2.043(6), P1-Fe1-P4 96.06(7), P1-Fe1-P5 91.49(8), P5-Fe1-P4 58.36(7), P3^1-P3-P4 111.73(6), P2-P3-P3^1 96.36(11), P2-P3-P4 100.46(9), Fe1-P1-P2 113.95(8), C3-P1-Fe1 119.3(2), C3-P1-P2 96.3(2), C3-P1-C2 101.8(3), C2-P1-Fe1 118.5(2), C2-P1-P2 103.7(2), P3-P2-P1 94.06(8), P6-P2-P3 92.63(9), P6-P2-P1 97.85(9), P2-P6-P5 101.29(10), C1-P6-P2 106.5(3), C1-P6-P5 105.4(3), Fe1-P4-Mg1 130.67(9), P3-P4-Fe1 109.41(8), P3-P4-Mg1 109.03(9), P5-P4-Fe1 60.75(7), P5-P4-P3 107.81(10), P5-P4-Mg1 78.82(8), Fe1-P5-Mg1 111.07(8), P6-P5-Fe1 116.52(10), P6-P5-Mg1 95.48(8), P4-P5-Fe1 60.89(7), P4-P5-P6 96.29(9), P4-P5-Mg1 56.00(7), P4^1-Mg1-P4 97.88(13), P4^1-Mg1-P5^1 45.18(6), P4-Mg1-P5 45.18(6), P4-Mg1-P51 104.58(10), P4^1-Mg1-P5 104.58(10), P5-Mg1-P5^1 139.65(13), O1-Mg1-P4 104.03(15), O1^1-Mg1-P4 131.40(14), O1^1-Mg1-P4^1 104.03(15), O1-Mg1-P4^1 131.40(14), O1-Mg1-P5^1 87.11(14), O1^1-Mg1-P5 87.11(14), O1-Mg1-P5 121.67(14), O1^1-Mg1-P5^1 121.67(14), O1^1-Mg1-O1 93.1(3).

$[\mathbf{Cp^*Fe(\mu,\eta^{3:2:2}\text{-}(1\text{-}CH_3\text{-}2\text{-}PPh_2\text{-}P_5))Sr(thf)_3]_2}$

Crystals of $[Cp^*Fe(\mu,\eta^{3:2:2}\text{-}(1\text{-}CH_3\text{-}2\text{-}PPh_2\text{-}P_5))Sr(thf)_3]_2$ (**30**) were obtained by storing a saturated thf solution at -30 °C for one week. A dark needle-shaped crystal with dimensions $0.18 \times 0.02 \times 0.02$ mm^3 was selected for the diffraction experiment.

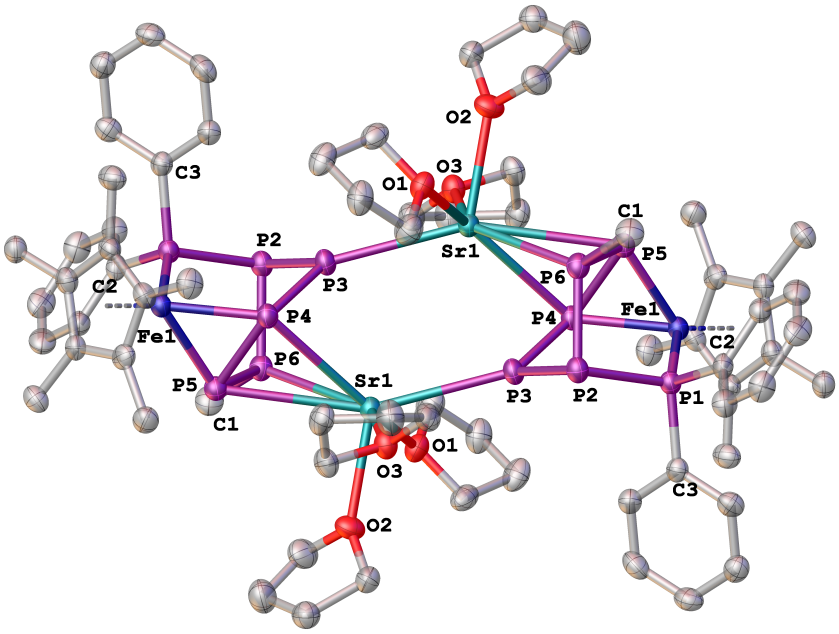


Figure 6.27: Molecular structures of **30** in the solid state. Hydrogen atoms are omitted for clarity. Selected bond lengths and angles: Sr1-Sr11 4.3803(7), Sr1-P41 3.1204(11), Sr1-P51 3.2807(11), Sr1-P3 3.1088(11), Sr1-P3^1 3.2416(12), Sr1-P6^1 3.1697(12), Sr1-O1 2.522(3), Sr1-O3 2.561(3), Sr1-O2 2.538(3), Fe1-P4 2.2640(12), Fe1-P5 2.2779(13), Fe1-P1 2.1405(12), P4-P5 2.2040(15), P4-P3 2.2243(15), P5-P6 2.2292(16), P1-P2 2.2756(15), P1-C2 1.843(4), P1-C3 1.847(4), P2-P3 2.1685(16), P2-P6 2.1851(16), P6-C1 1.856(5), P4^1-Sr1-Sr1^1 77.87(2), P4^1-Sr1-P5^1 40.18(3), P4^1-Sr1-P3^1 40.87(3), P4^1-Sr1-P6^1 63.59(3), P5^1-Sr1-Sr1^1 110.56(2), P3^1-Sr1-Sr1^1 45.142(19), P3-Sr1-Sr1^1 47.66(2), P3-Sr1-P4^1 119.50(3), P3-Sr1-P5^1 157.83(3), P3^1-Sr1-P5^1 65.57(3), P3-Sr1-P3^1 92.80(3), P3-Sr1-P6^1 131.90(3), P6^1-Sr1-Sr1^1 94.30(2), P6^1-Sr1-P5^1 40.39(3), P6^1-Sr1-P3^1 57.38(3), O1-Sr1-Sr1^1 94.05(7), O1-Sr1-P4^1 141.48(7), O1-Sr1-P5^1 114.56(7), O1-Sr1-P3 75.93(7), O1-Sr1-P3^1 109.18(7), O1-Sr1-P6^1 79.84(7), O1-Sr1-O3 132.12(10), O1-Sr1-O2 73.12(10), O3-Sr1-Sr1^1 104.14(7), O3-Sr1-P4^1 86.09(7), O3-Sr1-P5^1 99.93(7), O3-Sr1-P3 84.41(7), O3-Sr1-P3^1 115.06(7), O3-Sr1-P6^1 140.32(7), O2-Sr1-Sr1^1 161.16(7), O2-Sr1-P4^1 120.77(8), O2-Sr1-P5^1 87.63(8), O2-Sr1-P3 114.46(8), O2-Sr1-P3^1 151.85(8), O2-Sr1-P6^1 96.84(8), O2-Sr1-O3 76.40(10), P4-Fe1-P5 58.06(4), P1-Fe1-P4 93.94(5), P1-Fe1-P5 92.01(5), Fe1-P4-Sr1^1 134.94(5), P5-P4-Sr1^1 73.83(4), P5-P4-Fe1 61.29(4), P5-P4-P3 105.81(6), P3-P4-Sr1^1 72.49(4), P3-P4-Fe1 114.78(6), Fe1-P5-Sr1^1 126.50(4), P4-P5-Sr1^1 65.99(4), P4-P5-Fe1 60.65(4), P4-P5-P6 96.77(6), P6-P5-Sr1^1 67.13(4), P6-P5-Fe1 114.79(6), Fe1-P1-P2 114.92(6), C2-P1-Fe1 120.55(14), C2-P1-P2 95.94(14), C2-P1-C3 102.3(2), C3-P1-Fe1 116.41(14), C3-P1-P2 103.52(13), P3-P2-P1 97.85(6), P3-P2-P6 90.01(6), P6-P2-P1 95.74(6), Sr1-P3-Sr1^1 87.20(3), P4-P3-Sr1^1 66.64(4), P4-P3-Sr1 128.29(5), P2-P3-Sr1 130.15(5), P2-P3-Sr1^1 104.54(5), P2-P3-P4 100.16(6), P5-P6-Sr1^1 72.48(4), P2-P6-Sr1^1 106.43(5), P2-P6-P5 102.76(6), C1-P6-Sr1^1 141.16(17), C1-P6-P5 108.35(16), C1-P6-P2 110.92(18).

Chapter 7

Supramolecular aggregates of $[Cp^*Fe(\eta^{3:1}\text{-}(1\text{-}CH_3\text{-}2\text{-}PPh_2\text{-}P_5))]$

This chapter was written as a manuscript ready for submission. Conceptualisation, writing of the manuscript, preparation of compounds and analytic samples as well as evaluation of all analytic data was done by Martin Weber. X-Ray diffraction measurements were performed and evaluated by Martin Weber and partially checked by Michael Seidl. Supervision, writing review, project administration and funding acquisition: Manfred Scheer

7.1 Introduction

In the past, the chemistry of the pentaphosphaferrocene $[Cp^*Fe(\eta^5\text{-}P_5)]$ (**XXVII**) was extensively studied by our working group. The remarkable versatile reactivity of **XXVII** includes reversible redox reactions, functionalisation with main group nucleophiles and electrophiles and the use as a multidentate donating ligand in coordination chemistry.[69,72,73,76–79,173,198,216] When coinage metal salts such as Cu(I) halogenides or silver salts are reacted with **XXVII**, supramolecular aggregates are formed by self assembly.[80–90] Due to its symmetric nature and the free electron pairs on each phosphorus atom, fullerene-like supramolecular spheres are formed by reaction of Cu(I) halogenides with **XXVII**.[80,81,83–87,89] Some of these supramolecular compounds are capable of host-guest chemistry by incorporating small molecules like P_4, As_4, carborane or the complex **XXVII** it self and releasing these molecules upon dissolution.[80,82,85,86] Reaction of **XXVII** with copper, silver or thallium salts can also yield 1-, 2- or three dimensional coordination polymers.[90] All these reactions base on self assembly of the supramolecular structures and are therefore depending on the parameters of the reaction

set-up like solvents, concentrations or the used crystallisation method. When using solvents like acetonitrile, which can also act as N-donor ligands, the results may vary from reactions performed e.g., in dichloromethane or o-difluorobenzene. This affinity of the used copper or silver salts to N-donor ligands can also be exploited by using organic nitriles as linkers deliberately. By using such three component self-assembly systems, aforementioned supramolecular spheres can also be linked together to form a three dimensional polymer.[89]

Coordination of coinage metals to the *cyclo*-P_5 ligand in **XXVII** does usually not lead to a change in the geometry of the ligand, as it is the case for oxidation, reduction or functionalisation with nucleophiles or electrophiles (resulting in an envelope conformation of the ligand of **XXVII**).[77–79,82,173,198] Since self assembly of the known supramolecular aggregates of **XXVII** is highly depending on the symmetry of the starting material, the question arises if P_n ligands of a lower symmetry can also form similar aggregates by self assembly. Investigations of other P_n ligands so far involved simple, highly symmetric polyphosphorus ligands like *cyclo*-P_n (n = 3, 4) or the resulting coordination compounds can not be considered supramolecular, as it is the case for coordination compounds starting from $[\{Cp'''Fe(CO)_2\}_2(\mu,\eta^{1:1}\text{-}P_4)]$ (**VIIIa**).[67,68,151–154,319,320] The recent report of $[Cp^*Fe(\eta^{3:1}\text{-}(1\text{-}CH_3\text{-}2\text{-}PPh_2\text{-}P_5))]$ (**11a**) offers multiple opportunities in this regard: On the one hand, the functionalized polyphosphorus ligand in **11a** is highly asymmetric, compared to the C_5 symmetry of **XXVII** or C_S symmetry of the ligand in functionalized derivatives of **XXVII** $[Cp^*Fe(\eta^4\text{-}P_5RR')]$. This makes the lonepairs on the phosphorus atoms of the ligand in **11a** more accessible in all three spatial dimensions. In addition, the the Me and PPh_2 functionalized phosphorus atoms in **11a** should be more electron rich, which should make coordination to electron deficient coinage metal salts more likely. The organic substituents in **11a** also have a great influence on the polarity of the molecule. On the other hand, relatively high yields and good solubility make **11a** perfectly suitable to perform the necessary number of reaction or crystallisation studies, since the outcome of those experiments depend greatly on these parameters, and different supramolecular aggregates may be formed under different conditions. Additionally the question arises if the PPh_2 fragment, coordinating to the iron center of **11a**, can coordinate to other electron deficient metal centres. Herein we report the use of **11a** as a novel building block for supramolecular aggregates with the coinage metal salts $Ag[SbF_6]$ and $Cu[X]$ (X = Cl, Br).

7.2 Results

Reacting the complex $[Cp^*Fe(\eta^{3:1}\text{-}(1\text{-}CH_3\text{-}2\text{-}PPh_2\text{-}P_5))]$ (**11a**) with $Ag[SbF_6]$ in o-DFB, DCM or acetonitrile at room temperature results in deep red solutions or suspensions containing brown powders in the case of o-DFB and DCM as solvents. The powderous products could not not be identified by any means so far. Reactions in acetonitrile yield the one dimensional polymer $[Cp^*Fe\{\mu_5,\eta^{1:3:1:1}\text{-}(1\text{-}CH_3\text{-}2\text{-}PPh_2\text{-}P_5)\}(Ag(MeCN))_2]_n[SbF_6]_{2n}$ (**33**) upon storing the concentrated acetonitrile-toluene mixture of a layering experiment at -30 °C for a month in the form of dark red crystals suitable for X-ray diffraction experiments. For reactions of **11a** with the Cu(I) halogenides, the respective halogenide is dissolved in acetonitrile and layered onto a solution of the complex. In the case of CuCl, by using relatively concentrated solutions the novel supramolecular wheel $[(Cp^*Fe\{\mu_5,\eta^{1:3:1:1:1:1}\text{-}(1\text{-}CH_3\text{-}2\text{-}PPh_2\text{-}P_5)\})(CuCl)(Cu(\mu_2\text{-}Cl))]_8$ (**34**) is obtained. Using a more diluted system for layering, very small amounts of $[\{CuCl\{(Cp^*Fe\{\mu_5,\eta^{1:3:1:1:1}\text{-}(1\text{-}CH_3\text{-}2\text{-}PPh_2\text{-}P_5)\}(CuCl(MeCN))\}_3)\}_2Cl][Cl]$ (**35**) are observed. The to **35** structurally identical supramolecular aggregate $[\{CuBr\{(Cp^*Fe\{\mu_5,\eta^{1:3:1:1:1}\text{-}(1\text{-}CH_3\text{-}2\text{-}PPh_2\text{-}P_5)\}(CuBr(MeCN))\}_3)\}_2Br][Br]$ (**36**) is obtained in larger amounts by using CuBr in a more concentrated layering system. Although **11a** does react with CuI (colour change from olive green to red-brown), only small amounts of amorphous , unidentifiable material is observed. Upon reaction of **11a** with the coinage metal salts Ag[OTf], AgCN, $[Ag(MeCN)_4][BF_4]$, $[Cu(MeCN)_4][BF_4]$, [Ag(tol)][OTf] or thallium (I) salts as $Tl[PF_6]$ with **11a**, no formation of supramolecular aggregates or otherwise identifiable products is observed: While all silver and copper salts do react with **11a**, observable as a colour change from olive green to red or brown, the thallium salts do not react with **11a** at all.

The solid state structure of **33** is built up by syndiotactically arranged units of **11a** linked by two Ag(MeCN) fragments forming a P_4Ag_2 six membered ring. Due to the asymmetric nature of **11a** as a subunit of **33**, this six membered rings are not planar and the polymer describes a waveform instead of being strictly linear (Figure 7.1). The structure of the subunits of **11a** remains unchanged compared to the solid state structure of the pure complex. Due to the ALMQXY spin system in the ^{31}P NMR spectrum of **11a** and the pronounced broadening of the signals of this moiety in coordination compounds, NMR spectra of **33** only show a extremely broad signal from 70 ppm to -17 ppm in the ^{31}P NMR spectra. Therefore NMR spectroscopy is not suitable for the characterisation of supramolecular aggregates of complex **11a**, since the polymer **33** is the compound with the highest solubility of the compounds presented in this work, and the intensity of the broad signals is to low for any kind of interpretation, although the

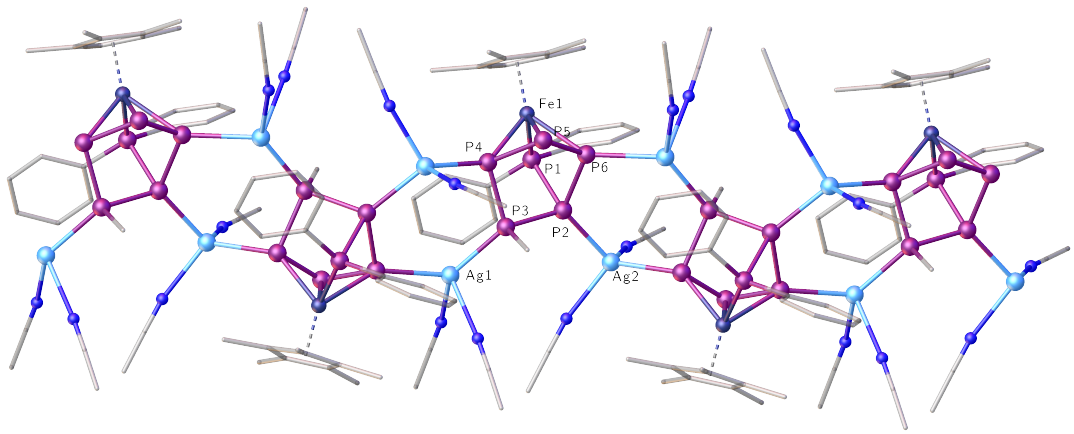


Figure 7.1: Structure of the one dimensional polymer **33** in the solid state. Hydrogen atoms, solvent molecules and counter ions are omitted for clarity.

solution of the sample measured was saturated with **33**. In order to check if possible dynamic processes in solution are responsible for this extreme broadening, VT NMR or MAS NMR studies have to be performed.

For $[(Cp^*Fe\{\mu_5,\eta^{1:3:1:1:1:1}\text{-}(1\text{-}CH_3\text{-}2\text{-}PPh_2\text{-}P_5)\})(CuCl)(Cu(\mu_2\text{-}Cl))]_8$ (**34**) the production of single crystals suitable for X-ray analysis proofs to be difficult. Crystallisation of **34** only occurs in close proximity of the phase boundary when both phases begin to mix. After 2-3 days, further mixing of the layers will not increase the amount of **34**, but the crystals are beginning to disappear and crystal quality declines. Samples, which are prepared for measurements with synchrotron radiation are not sufficiently stable for transportation, so measurements have to be performed at least 2 days after preparation of the sample. Crystals of **34** contain large amounts of acetonitrile and crack if cooled too rapidly. During measurements with powerful Cu_α sources, crystals of **34** start to decompose in a few hours and Mo or Ag sources do not result in improved data acquisition before the crystals decompose. After multiple attempts a measurement on crystals of **34** with satisfactory quality indicators of the structure solution ($R_1 = 9.46$ %, $wR_2 = 26.32$ % and a goodness of fit = 0.894) was performed.

The supramolecular aggregate consists of 8 units of **11a** (Figure 7.2). The syndiotactically arranged units are connected to each other by two CuCl molecules for each complex, forming a P_4Cu_2 six membered ring, comparable to the P_4Ag_2 rings in **33**. The six membered rings in **34** are also not planar. The Cp^* ligands are not coplanar to the plane, which is defined by the supramolecular ring, but are slightly tilted towards the middle of the annular structure (angle between mean plane of the inner, coplanar copper atoms of **34** and the mean plane of a Cp^* ligand: 18.3 °). The chlorine atoms of the outer CuCl units are directed away from the center of the structure, while the Cl atoms, bridg-

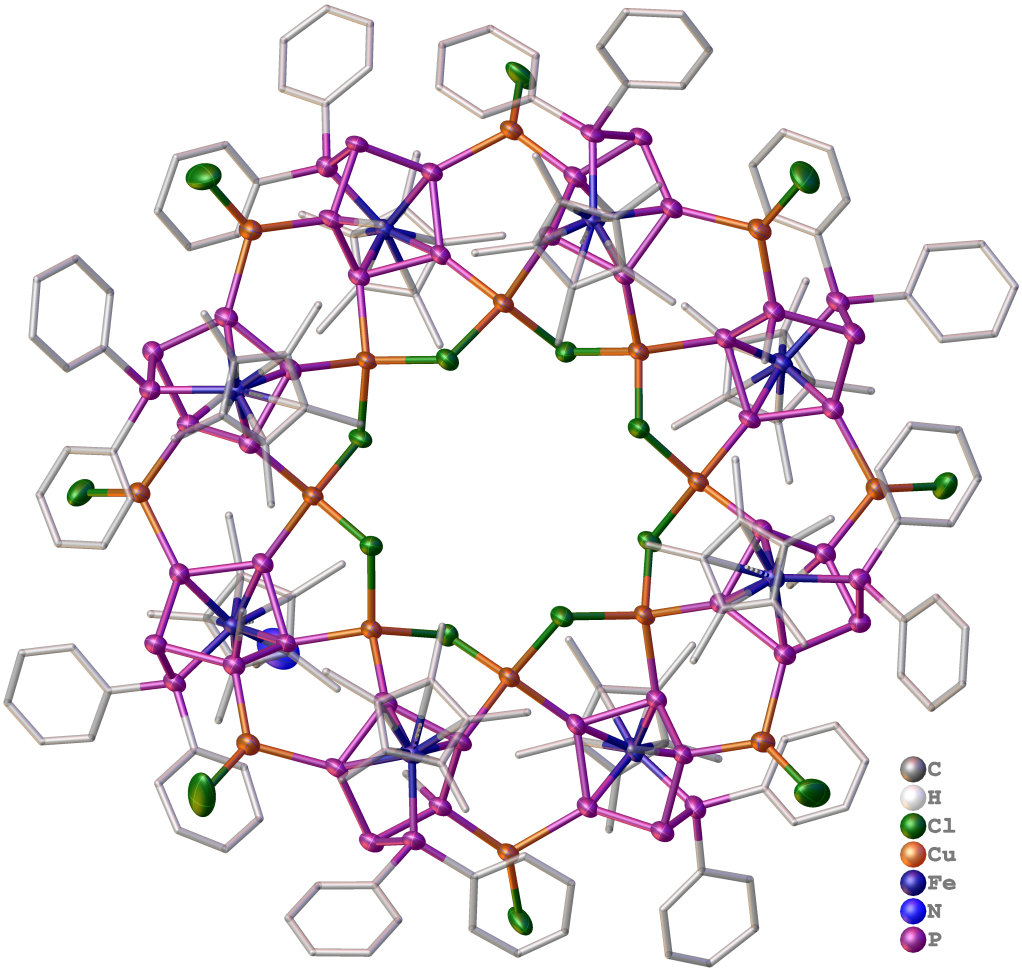


Figure 7.2: Molecular structure of the annular supramolecule **34** in the solid state. Hydrogen atoms, solvent molecules and counter ions are omitted for clarity.

ing the inner Cu atoms are facing towards the center. The inner copper atoms are coplanar, while the corresponding chlorine atoms are arranged alternately above and below this plane. The distance of two opposite, inner Cl atoms is 7.737 Å and the distance of the corresponding copper atoms amounts to 9.712 Å. This creates a large enough opening in the structure to allow acetonitrile molecules to be located right in the center of the structure, which are nearly orthogonal to the mean plane of **34** (Figure 7.9 on page 321, supporting information). The whole supramolecular aggregate is approximately 31 Å in diameter (distance of the two H atoms, furthest apart (H07T and H07U: 29.1782(10) Å) with the van der Waals radii of H added). The annular structure of **34** is the first example for a supramolecular wheel consisting of a coinage metal salt and a polypnictogen ligand complex. Compared to the only other supramolecular wheel known for P_n ligand complexes, the tetrameric $[(^{Dipp}BDI\text{-}Mg)_4(\mu\text{-}\eta^{4:1:1}\text{-}P_5(CH_3))_4(FeCp^*)_4)]$ (**5**), **34** is the largest supramolecular aggregate of this type to this date.[198]

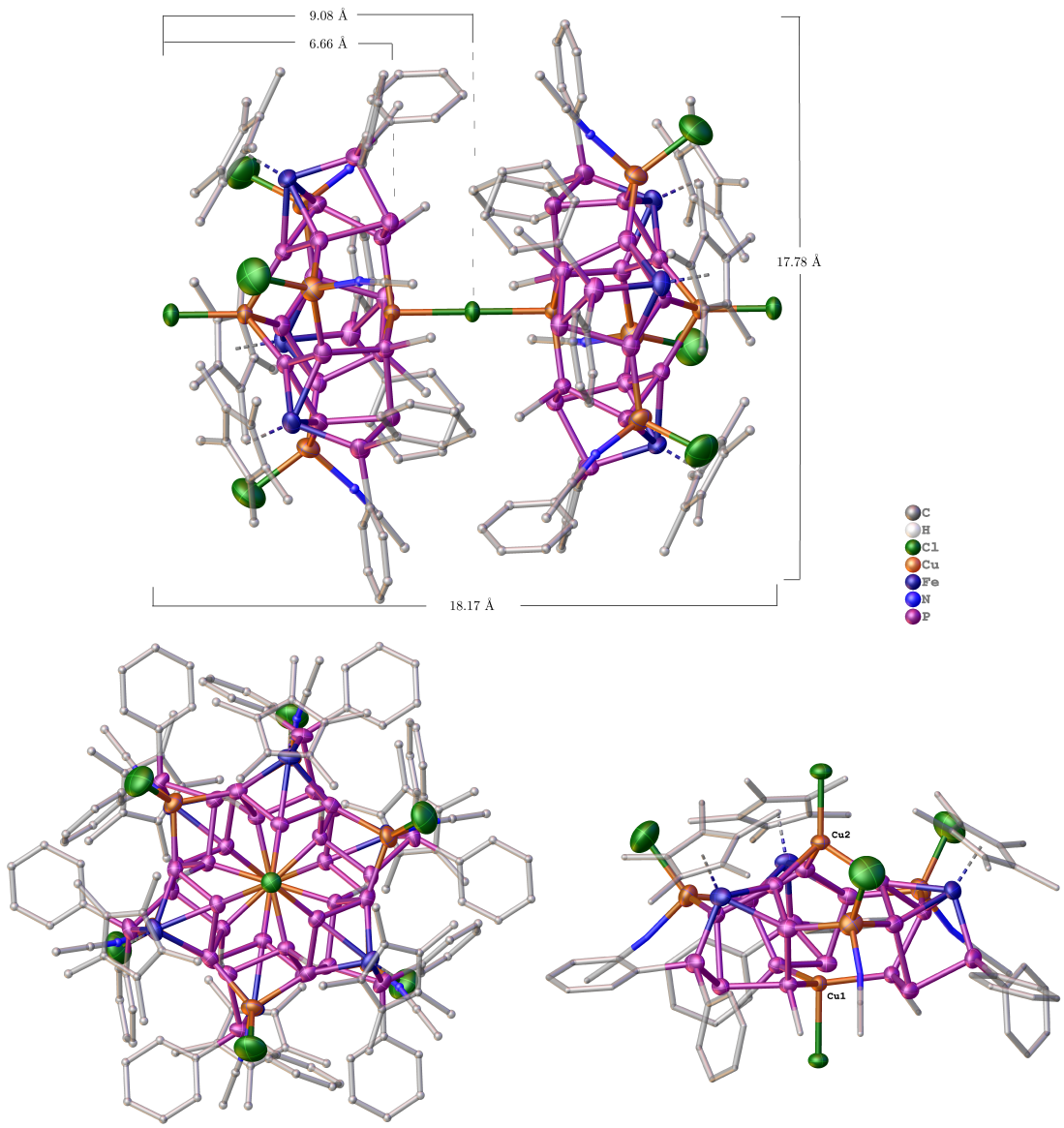


Figure 7.3: Structure of the discrete supramolecular aggregate **35** in the solid state. Hydrogen atoms, solvent molecules and counter ions are omitted for clarity. On the bottom left, the aggregate is shown along side the C_3 axes of the trimeric subunits. On the bottom right one of these subunits is shown in more detail, revealing the different coordination modes of Cu in the molecule.

When the experiment is performed with more diluted solutions of CuCl and **11a**, only few crystals of **34** are formed and will disappear again after some days. But after complete mixing of the layered phases, a few crystals of the supramolecular aggregate $[\{CuCl\{(Cp^*Fe\{\mu_5,\eta^{1:3:1:1:1}\text{-}(1\text{-}CH_3\text{-}2\text{-}PPh_2\text{-}P_5)\}(CuCl(MeCN))\}_3)\}_2Cl][Cl]$ (**35**), suitable for X-ray structure determination are observed. If CuBr is used instead of CuCl, the isostructural supramolecule $[\{CuBr\{(Cp^*Fe\{\mu_5,\eta^{1:3:1:1:1}\text{-}(1\text{-}CH_3\text{-}2\text{-}PPh_2\text{-}P_5)\}$

$(CuBr(MeCN))\}_3)\}_2Br][Br]$ (**36**) is formed in larger amounts than **35**. The aggregates **35** and **36** consist of two cationic, trimeric subunits linked by a chlorine (**35**) or bromine (**36**) atom. These subunits consist of three moieties of **11a** linked by the respective copper halide. Since only one counter ion is coordinating to two copper centres, the aggregates **35** and **36** are cationic with a chloride or bromide counter ion, respectively. The symmetry elements in **35** and **36** are described as followed: The trimeric units at each end are C_3 symmetric and the whole structure has an inversion centre in the bridging halogenide in the center of the structure. As for **33** and **34** the building blocks of **11a** remain unchanged in their geometry in **35** and **36**. The geometry of the trimeric units in **35** and **36** are quite remarkable (Figure 7.3): While the CuX on the outside ends of the molecule (bottom right side in Figure 7.3, the CuCl unit of Cu2 on the top end of the trimeric unit) is coordinated tetrahedrally to the three units of the complex **11a**, the central Cu atom bound to the bridging halogenide ion (Cu1) is coordinated by the phosphorus atoms of the complex almost trigonal planar (distance of Cu1 and the centroid of the plane formed by the phosphorus atoms coordinating to the copper atom = 0.2686(11) Å). This coordination mode of Cu1 and the elongation of the Cu1-Cl bond (2.4222(3) Å) compared to Cu2-Cl (2.2332(6) Å) indicate, that Cu1 is best described as a Cu^+ ion.[321,322] This also explains the presence of a X^- counter ion in the solid state structures of **35** and **36**: Two Cu^+ ions are coordinating to the central Cl^- or Br^- ion in the inversion center of the aggregates, which are therefore themselves cationic. The remaining CuX units in **35** and **36** are coordinated by one acetonitrile molecule each. yet, not all acetonitrile molecules are fully occupied in the X-ray structure models of **35** and **36**, since disorder with halogen atoms is observed. The structural motifs of these supramolecular aggregates have not been observed for a coordination compound of a P_n ligand complex so far.

7.3 Conclusion

Due to the highly asymmetric nature of the the functionalized $\mathrm{P_n}$ ligand in the complex $[\mathrm{Cp^*Fe}(\eta^{3:1}\text{-}(1\text{-}\mathrm{CH_3}\text{-}2\text{-}\mathrm{PPh_2}\text{-}\mathrm{P_5}))]$ (**11a**), supramolecular aggregates of so far unknown structural motifs are formed by the reactions with the coinage metal salts $\mathrm{Ag[SbF_6]}$ and CuX ($\mathrm{X = Cl, Br}$). While reaction with $\mathrm{Ag[SbF_6]}$ in acetonitrile yields the one dimensional polymer $[\mathrm{Cp^*Fe}\{\mu_5, \eta^{1:3:1:1}\text{-}(1\text{-}\mathrm{CH_3}\text{-}2\text{-}\mathrm{PPh_2}\text{-}\mathrm{P_5})\}(\mathrm{Ag(MeCN))_2}]_\mathrm{n}$ $[\mathrm{SbF_6}]_{2\mathrm{n}}$ (**33**), reactions of **11a** with the copper (I) halogenides produces discrete, supramolecular aggregates: Both CuCl and CuBr form the isostructural aggregates $[\{\mathrm{CuX}\{(\mathrm{Cp^*Fe}\{\mu_5, \eta^{1:3:1:1:1}\text{-}(1\text{-}\mathrm{CH_3}\text{-}2\text{-}\mathrm{PPh_2}\text{-}\mathrm{P_5})\}(\mathrm{CuX(MeCN))}\}_3)\}_2\mathrm{X}][\mathrm{X}]$ (X = Cl: **35**, X = Br: (**36**). These molecules are C_S symmetric and consist of two trimeric units of **11a** linked with CuX and a bridging halogen atom in the inversion centre of the molecule. Both **35** and **36** are the first examples for this structural motif. For CuCl the extremely sensitive and shortlived annular supramolecule $[(\mathrm{Cp^*Fe}\{\mu_5, \eta^{1:3:1:1:1:1}\text{-}(1\text{-}\mathrm{CH_3}\text{-}2\text{-}\mathrm{PPh_2}\text{-}\mathrm{P_5})\})(\mathrm{CuCl})(\mathrm{Cu}(\mu_2\text{-}\mathrm{Cl}))]_8$ (**34**) could be observed and represents the largest supramolecular wheel of a polypnictogen-ligand-complex coordination compound.

7.4 Supporting information

7.4.1 General techniques and materials

All manipulations were performed using standard schlenk techniques on a dual manifold schlenk line or a glove box under an atmosphere of dry argon. Traces of oxygen in the inert gas were removed by passing it over a BASF R 3-11 (CuO/$MgSiO_3$) catalyst. Residual moisture in the inert gas was removed, by passing it through concentrated H_2SO_4, orange gel and sicapent on dried pumice stone. All glassware was vigorously heated in dynamic vacuum before use and any teflon tubing was stored in an oven at 170 °C.

Toluene, dichloromethane and acetonitrile were purified and dried by the solvent purification system SPS-800 from mbraun. Deuterated acetonitrile was dried over multiple batches of dried molecular sieve before use.

All copper and Silver salts were obtained from Sigma Aldrich. $[Cp^*Fe(\eta^{3:1}\text{-}(1\text{-}CH_3\text{-}2\text{-}PPh_2\text{-}P_5))]$ (**11a**) was prepared according to literature procedures (chapter 5.4.2).

NMR spectra were measured with a Bruker Avance 400 (^{1}H: 400.132 MHz; ^{13}C: 100.613 MHz; ^{31}P: 161.97 MHz) using special NMR tubes with a screw cap or a J. Young valve.

7.4.2 Experimental Details

Synthesis of $[\mathbf{Cp^*Fe\{\mu_5,\eta^{1:3:1:1}\text{-}(1\text{-}CH_3\text{-}2\text{-}PPh_2\text{-}P_5)\}(Ag(MeCN))_2]_n[SbF_6]_{2n}}$

Onto a solution of $[Cp^*Fe(\eta^{3:1}\text{-}(1\text{-}CH_3\text{-}2\text{-}PPh_2\text{-}P_5))]$ (**11a**, 27 mg, 0.05 mmol) in toluene (10 mL), a solution of $AgSbF_6$ (34 mg, 0.1 mmol) in acetonitrile (10 mL) is layered. After complete mixing, the solvent is removed in vacuum from the red solution. After storing 4 mL of the concentrated reaction solution at -30 °C for one week, dark red crystals of the one dimensional polymer $[Cp^*Fe\{\mu_5,\eta^{1:3:1:1}\text{-}(1\text{-}CH_3\text{-}2\text{-}PPh_2\text{-}P_5)\}(Ag(MeCN))_2]_n[SbF_6]_{2n}$ (**33**) are obtained.

Yield: 8 mg (0.006 mmol, 12 %)

Elemental Analysis: Expected for $[FeAg_2C_{25}H_{31}Sb_2P_6F_{12}N]_n$: 2.45 % H, 23.56 % C, 1.09 % N, 17.89 % F, 14.58 % P, 4.38 % Fe, 16.93 % Ag, 19.11 % Sb. Found: 2.63 % H, 23.47 % C, 1.42 % N. This accounts for the loss of some acetonitrile molecules upon washing with n-pentane and drying in a high vacuum for 6 hours.

NMR psectra of concentrated solutions of **33** in deuterated acetonitrile show extreme broadening of any signals. Therefore no multiplets or integrals can be doubtlessly assigned.

^{1}H-NMR: ($MeCN$-d_3, 300 K): δ[ppm] = 1.51 (br, Cp^*); 7.61 (br; Ph)
Signals from the methyl groups are not visible in the spectrum due to the extreme broadening.
^{31}P-NMR: ($MeCN$-d_3; 300 K): 128.9 (br), 18.1 (m), 9.5 (br), -157.7 (br)

Synthesis of $[\{\mathbf{CuX}\{(\mathbf{Cp^*Fe}\{\mu_5,\eta^{1:3:1:1:1}\text{-}(\mathbf{1\text{-}CH_3\text{-}2\text{-}PPh_2\text{-}P_5})\}(\mathbf{CuX}(\mathbf{MeCN}))\}_3)\}_2\mathbf{X}][\mathbf{X}]$ ($\mathbf{X = Cl, Br}$)

Onto a solution of $[Cp^*Fe(\eta^{3:1}\text{-}(1\text{-}CH_3\text{-}2\text{-}PPh_2\text{-}P_5))]$ (**11a**, 27 mg, 0.05 mmol) in toluene (20 mL), a solution of CuX (X = Cl: 10 mg, 0.1 mmol, X = Br: 12 mg, 0.1 mmol) in acetonitrile (20 mL) is layered. After complete mixing small black crystals of the cationic supramolecular aggregates $[Cp^*Fe\{\mu_5,\eta^{1:3:1:1}\text{-}(1\text{-}CH_3\text{-}2\text{-}PPh_2\text{-}P_5)\}(Ag(MeCN))_2]_n[SbF_6]_{2n}$ (**33**) are obtained.

Yield for X = Cl: cannot be determined (only few crystals)
Yield for X = Br: 12 mg (0.0025 mmol, 15 %)
Elemental analysis for X = Br: Expected for $C_{150}H_{174}P_{36}Fe_6Cu_{12}Br_{12}N_2$: 3.39 % H, 34.80 % C, 0.54 % N, 21.54 % P, 6.47 % Fe, 14.73 % Cu, 18.52 % Br. Found: 3.58 % H, 35.19 % C, 0.16 % N. This accounts for 2 acetonitrile molecules still present in the compound after washing with n-pentane and drying in a high vacuum for 6 hours.

Synthesis of $[(\mathbf{Cp^*Fe}\{\mu_5,\eta^{1:3:1:1:1:1}\text{-}(\mathbf{1\text{-}CH_3\text{-}2\text{-}PPh_2\text{-}P_5})\})(\mathbf{CuCl})(\mathbf{Cu}(\mu_2\text{-}\mathbf{Cl}))]_8$

Onto a solution of $[Cp^*Fe(\eta^{3:1}\text{-}(1\text{-}CH_3\text{-}2\text{-}PPh_2\text{-}P_5))]$ (**11a**, 27 mg, 0.05 mmol) in toluene (10 mL), a solution of $CuCl$ (10 mg, 0.1 mmol) in acetonitrile (10 mL) is layered. After one day, highly sensitive, black crystals of the supramolecular wheel $[(Cp^*Fe\{\mu_5,\eta^{1:3:1:1:1:1}\text{-}(1\text{-}CH_3\text{-}2\text{-}PPh_2\text{-}P_5)\})(CuCl)(Cu(\mu_2\text{-}Cl))]_8$ (**34**) are observed. Upon isolating and drying, the crystals completely decompose.

Yield: cannot be determined

7.4.3 NMR spectra

NMR spectra of $[\mathbf{Cp^*Fe\{\mu_5,\eta^{1:3:1:1}\text{-}(1\text{-}CH_3\text{-}2\text{-}PPh_2\text{-}P_5)\}(Ag(MeCN))_2]_n[SbF_6]_{2n}}$ (33)

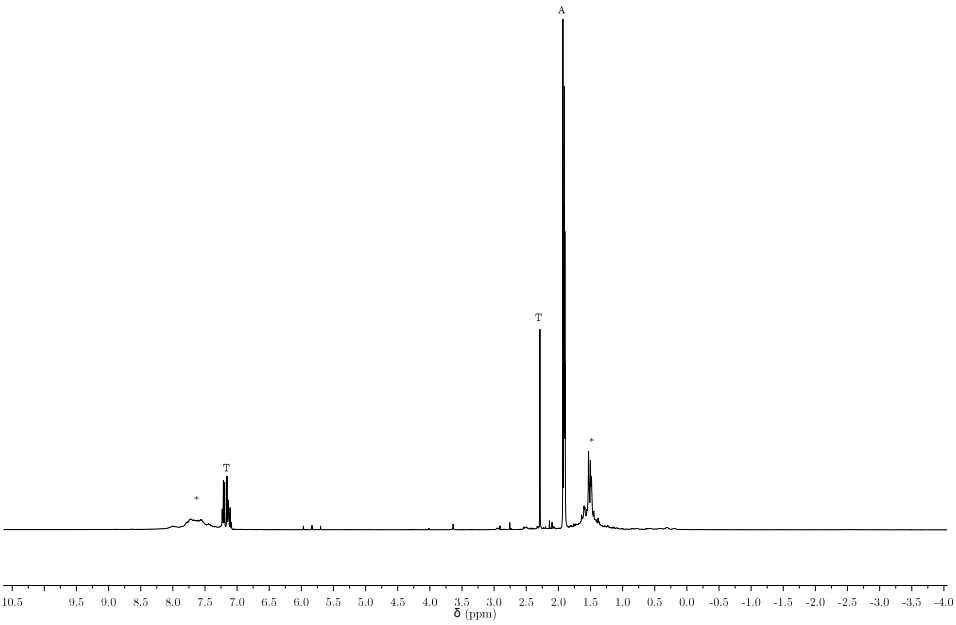


Figure 7.4: ^{1}H NMR spectrum of $[Cp^*Fe\{\mu_5,\eta^{1:3:1:1}\text{-}(1\text{-}CH_3\text{-}2\text{-}PPh_2\text{-}P_5)\}(Ag(MeCN))_2]_n[SbF_6]_{2n}$ (**33**) in deuterated acetonitrile (solvent residue A). Traces of toluene (T) are visible in the spectrum along side the extremely broadened signals of **33**, marked with an asterisk.

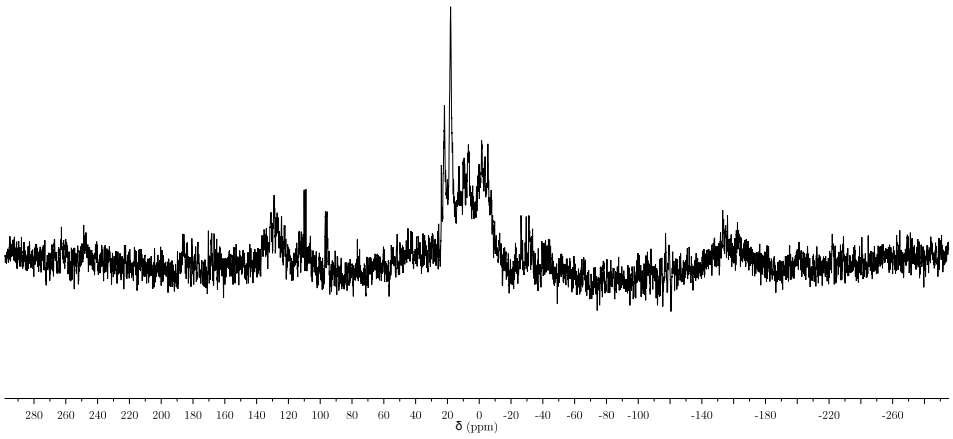


Figure 7.5: ^{31}P NMR spectrum of [Cp*Fe{$\mu_5, \eta^{1:3:1:1}$-(1-CH_3-2-PPh_2-P_5)}$(Ag(MeCN))_2]_n[SbF_6]_{2n}$ (**33**) in deuterated acetonitrile. The signals of **33** are extremely broadened and barely visible, with the exception of parts of a multiplett at 18 ppm, superimposed by an extremely broadened signal.

7.4.4 Crystallographic details

General remarks

If not stated otherwise, crystals were picked directly from the flask under a constant flow of dry argon. Suitable crystals were then mounted on a Mylar loop in degassed mineral oil. Structures were solved with the ShelXT[177] solution program using dual methods and by using Olex2 1.5-alpha[178] as the graphical interface. The models were refined with ShelXL 2018/3[179] using full matrix least squares minimisation on F^2.

Crystallographic data

Table 7.1: Crystallographic data for **33** and **34**:

Compound	**33**	**34**
Formula	$C_{77}H_{100}Ag_4F_{24}Fe2N_{12}P_{12}Sb_4$	$C_{188}H_{226}C_{l16}Cu_{16}Fe_8N_2P_{48}$
$\rho_{calc.}/gcm^{-3}$	1.878	1.248
μ/mm^{-1}	6.951	1.790
Formula Weight	3051.50	6030.89
Colour	clear brownish orange	dark brown
Shape	rect. prism-shaped	plate-shaped
$Size/mm^3$	$0.18 \times 0.05 \times 0.03$	$0.07 \times 0.06 \times 0.01$
T/K	100.01(10)	136(5)
Crystal System	monoclinic	monoclinic
Space Group	$P2_1/n$	$P2_1/n$
a/Å	13.55010(10)	34.4544(12)
b/Å	12.94710(10)	26.5210(13)
c/Å	30.7634(3)	35.1287(13)
$\alpha/^\circ$	90	90
$\beta/^\circ$	91.0540(10)	90.128(3)
$\gamma/^\circ$	90	90
$V/Å^3$	5396.05(8)	32099(2)
Z	2	4
Z'	0.5	1
Wavelength/Å	1.54184	0.71073
Radiation type	Cu K_α	Mo K_α
$\theta_{min}/^\circ$	2.873	1.992
$\theta_{max}/^\circ$	74.483	23.256
Measured Refl's.	65401	134937
Indep't Refl's	10838	44813
Refl's $I \geq 2\sigma(I)$	8901	20551
R_{int}	0.0445	0.1681
Parameters	717	2557
Restraints	346	126
Largest Peak	1.657	1.625
Deepest Hole	-1.939	-0.842
GooF	1.073	0.934
wR2 (all data)	0.1642	0.2466
wR2	0.1570	0.2085
R1 (all data)	0.0694	0.1632
R1	0.0581	0.0902

Table 7.2: Crystallographic data for **35** and **36**:

Compound	**35**	**36**
Formula	$C_{75}H_{93}Cl_{6.93}P_{18}Fe_3Cu_5N_{1.57}$	$Br_{5.15}C_{91.1}Cu_{5.15}Fe_3H_{114.65}N_{7.55}P_{18}$
$\rho_{calc.}$/gcm^{-3}	1.527	1.575
μ/mm^{-1}	9.236	8.615
Formula Weight	2304.97	2779.22
Colour	dark brown	clear dark brown
Shape	irregular-shaped	rhombohedral-shaped
Size/mm^3	$0.21 \times 0.12 \times 0.11$	$0.21 \times 0.11 \times 0.07$
T/K	123.00(10)	123.01(10)
Crystal System	cubic	orthorhombic
Space Group	Pa-3	Pbca
a/Å	27.16960(10)	31.9723(4)
b/Å	27.16960(10)	22.7693(3)
c/Å	27.16960(10)	32.1906(3)
α/°	90	90
β/°	90	90
γ/°	90	90
V/Å^3	20056.3(2)	23434.3(4)
Z	8	8
Z'	0.3333333	1
Wavelength/Å	1.54184	1.54184
Radiation type	Cu K_α	Cu K_α
θ_{min}/°	2.817	3.378
θ_{max}/°	74.920	73.013
Measured Refl's.	47531	74159
Indep't Refl's	6838	22137
Refl's I $\geq 2\sigma$(I)	5946	20195
R_{int}	0.0603	0.0167
Parameters	352	1381
Restraints	13	394
Largest Peak	1.237	1.193
Deepest Hole	-1.068	-0.839
GooF	1.043	1.091
wR2 (all data)	0.1825	0.1304
wR2	0.1785	0.1284
R1 (all data)	0.0649	0.0515
R1	0.0594	0.0478

$[\mathbf{Cp^*Fe\{\mu_{2,2},\eta^{1:3:1:1}\text{-}(1\text{-}CH_3\text{-}2\text{-}PPh_2\text{-}P_5)\}(Ag(MeCN))_2]_n[SbF_6]_{2n}}$

Crystals of $[Cp^*Fe\{\mu_{2,2},\eta^{1:3:1:1}\text{-}(1\text{-}CH_3\text{-}2\text{-}PPh_2\text{-}P_5)\}(Ag(MeCN))_2]_n[SbF_6]_{2n}$ **(33)** were obtained by storing a saturated toluene solution at -30 °C for 2 weeks. A clear brownish orange rectangular prism-shaped crystal with dimensions $0.18 \times 0.05 \times 0.03$ mm^3 was selected for the diffraction experiment. The crystal was kept at a steady T = 100.01(10) K during data collection. One of the $[SbF_6]^-$-counter ions was disoreded.

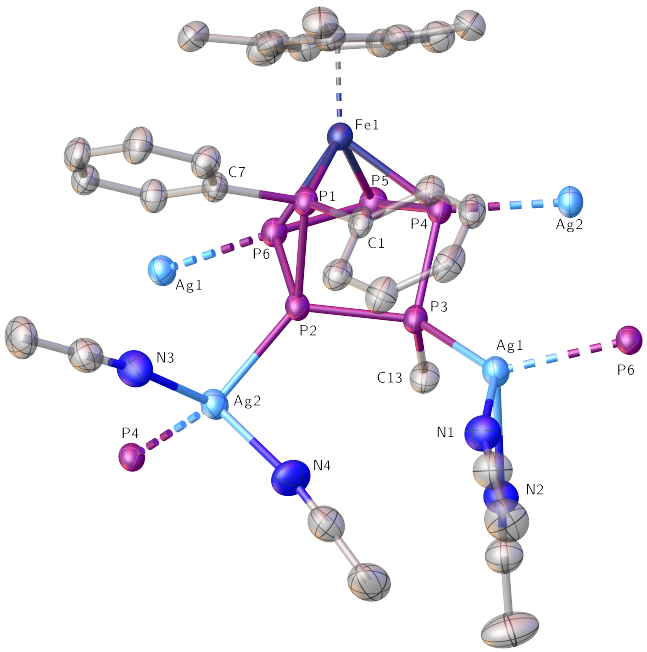


Figure 7.6: Detail of the molecular structure of **33** in the solid state showing the connectivity in the one dimensional polymer chain. Hydrogen atoms are omitted for clarity.

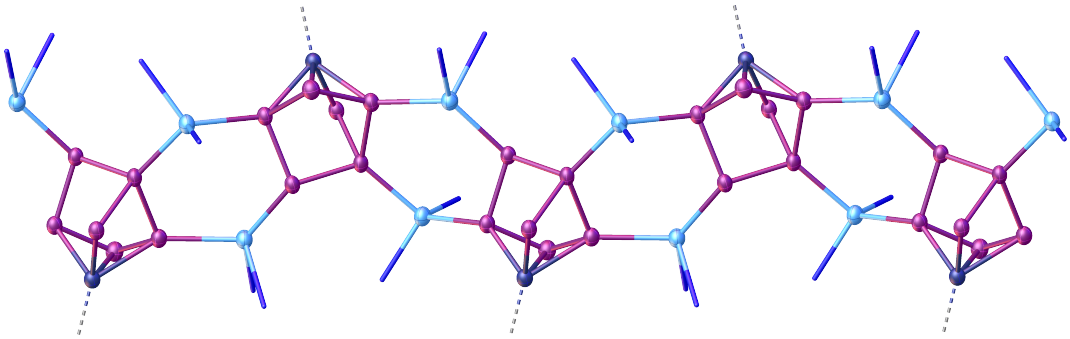


Figure 7.7: Heavy atom backbone of the molecular structure of **33** in the solid state.. Hydrogen and carbon atoms are omitted for clarity.

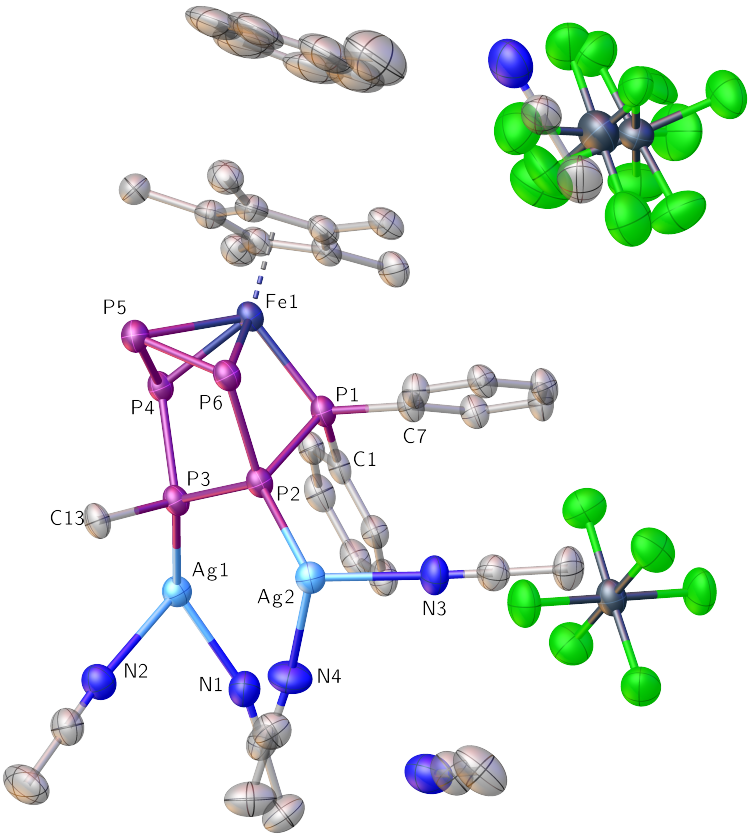


Figure 7.8: Molecular structure of **33** in the solid state. Hydrogen atoms are omitted for clarity. Selected bond lengths and angles: Ag2-P4^{1} 2.4597(16), Ag2-P2 2.4475(17), Ag2-N3 2.302(6), Ag2-N4 2.303(7), Ag1-P6^{2} 2.5273(17), Ag1-P3 2.4437(17), Ag1-N1 2.263(7), Ag1-N2 2.549(7), Fe1-P1 2.223(2), Fe1-P4 2.2855(18), Fe1-P6 2.3652(19), Fe1-P5 2.3841(19), P1-P2 2.203(2), P1-C1 1.814(7), P1-C7 1.824(7), P4-P3 2.207(2), P4-P5 2.147(2), P2-P6 2.238(2), P2-P3 2.193(2), P6-P5 2.131(2), P3-C13 1.834(6), P2-Ag2-P4^{1} 120.45(6), N3-Ag2-P4^{1} 101.44(18), N3-Ag2-P2 111.94(18), N3-Ag2-N4 100.5(3), N4-Ag2-P4^{1} 120.1(2), N4-Ag2-P2 100.9(2), P6^{2}-Ag1-N2 101.01(16), P3-Ag1-P6^{2} 122.22(6), P3-Ag1-N2 95.51(17), N1-Ag1-P6^{2} 100.45(19), N1-Ag1-P3 136.29(18), N1-Ag1-N2 84.3(2), P1-Fe1-P4 88.63(7), P1-Fe1-P6 77.53(7), P1-Fe1-P5 116.31(7), P4-Fe1-P6 86.35(7), P4-Fe1-P5 54.69(6), P6-Fe1-P5 53.31(6), P2-P1-Fe1 96.86(8), C1-P1-Fe1 125.8(2), C1-P1-P2 103.2(2), C1-P1-C7 104.4(3), C7-P1-Fe1 118.6(2), C7-P1-P2 104.1(2), Fe1-P4-Ag2^{2} 140.25(8), P3-P4-Ag2^{2} 108.35(8), P3-P4-Fe1 110.56(8), P5-P4-Ag2^{2} 113.61(8), P5-P4-Fe1 65.00(7), P5-P4-P3 102.73(9), P1-P2-Ag2 124.57(8), P1-P2-P6 80.68(8), P6-P2-Ag2 121.94(8), P3-P2-Ag2 123.90(8), P3-P2-P1 93.40(8), P3-P2-P6 101.84(9), Fe1-P6-Ag1^{1} 147.19(8), P2-P6-Ag1^{1} 111.74(8), P2-P6-Fe1 91.99(8), P5-P6-Ag1^{1} 123.44(9), P5-P6-Fe1 63.80(7), P5-P6-P2 109.44(9), P4-P3-Ag1 118.44(8), P2-P3-Ag1 126.94(9), P2-P3-P4 97.12(9), C13-P3-Ag1 105.5(2), C13-P3-P4 103.8(3), C13-P3-P2 102.0(2), P4-P5-Fe1 60.32(6), P6-P5-Fe1 62.89(7), P6-P5-P4 96.17(9).

$[(\mathbf{Cp^*Fe\{\mu_5,\eta^{1:3:1:1:1:1}\text{-}(1\text{-}CH_3\text{-}2\text{-}PPh_2\text{-}P_5)\}})(\mathbf{CuCl})(\mathbf{Cu(\mu_2\text{-}Cl)})]_8$

Crystals of $[(Cp^*Fe\{\mu_5,\eta^{1:3:1:1:1:1}\text{-}(1\text{-}CH_3\text{-}2\text{-}PPh_2\text{-}P_5)\})(CuCl)(Cu(\mu_2\text{-}Cl))]_8$ (**34**) were obtained as mentioned in the experimental details (*vide supra*). A dark brown plate-shaped crystal with dimensions $0.07 \times 0.06 \times 0.01\ mm^3$ was selected for the diffraction experiment. The crystal was kept at a steady T = 136(5) K during data collection. Crystals of **34** decompose easily due to the loss of solvent (toluene and acetonitrile) while selecting a suitable crystal under the microscope. All crystals showed pronounced radiation damage after 1.5 to 2 h of measurement with a Cu_{K_α} source and after 4 to 5 hours with a Mo_{K_α} source (both radiation sources with a rotating anode and being rather powerful). Less intense Ag_{K_α} sources showed insufficient diffraction. After approxiamtely 60 crystals and multiple attempts to get a complete measurement, the here presented measurement proofed to be the most complete with the least amount of damage on the crystal during measurement. In the asymmetric unit, 32 molecules of acetonitrile are present in total. Two of these molecules were modelled, while the rest was accounted for using a solvent mask. One of the modelled solvent molecules is located in the center of the annular structure of **34**.

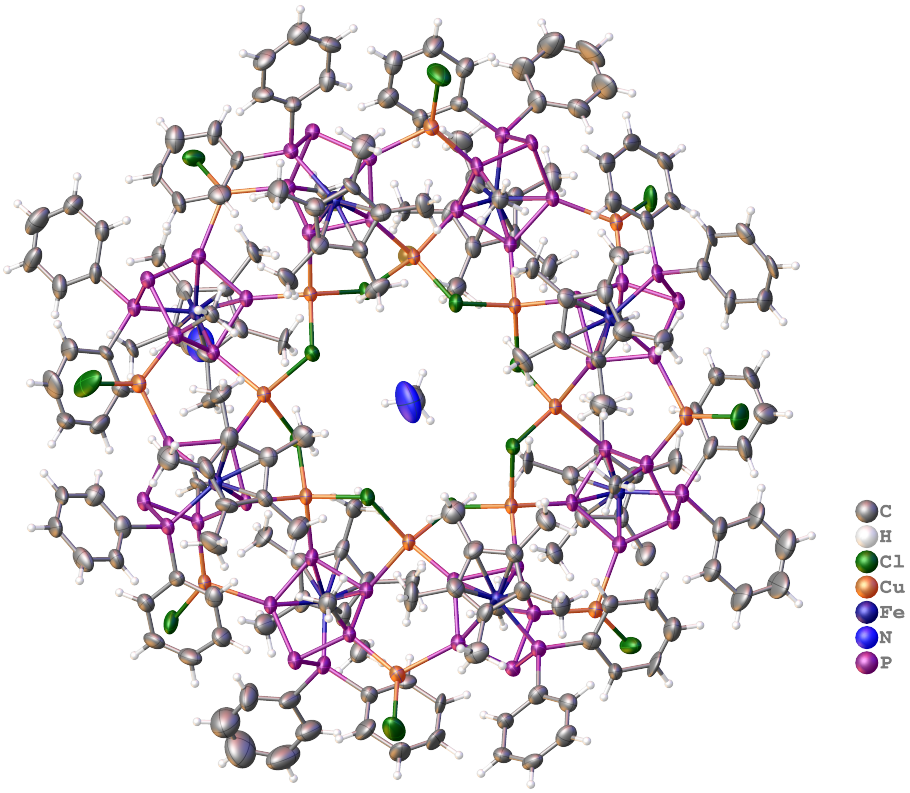


Figure 7.9: Molecular structure of **34** in the solid state. Average P-Cu distance (for the outer Cu atoms) 2.3103(4) Å. Average CuCl distance for the same Cu atoms: 2.1753(5) Å. Average P-Cu distance (for the inner Cu atoms) 2.3455(4) Å. Average CuCl distance for the same Cu atoms: 2.3132(4) Å. Bond lengths and angles for subunits of **11a** are similar to the free complex.

$[\{\mathbf{CuCl}\{(\mathbf{Cp^*Fe}\{\mu_{3,2,2},\eta^{1:3:1:1:1}\text{-}(\mathbf{1\text{-}CH_3\text{-}2\text{-}PPh_2\text{-}P_5})\}(\mathbf{CuCl(MeCN)})\}_3)\}_2\mathbf{Cl}][\mathbf{Cl}]$

Crystals of $[\{CuCl\{(Cp^*Fe\{\mu_5,\eta^{1:3:1:1:1}\text{-}(1\text{-}CH_3\text{-}2\text{-}PPh_2\text{-}P_5)\}(CuCl(MeCN))\}_3)\}_2Cl][Cl]$ (**35**) were obtained as described in the experimental details (*vide supra*). A dark brown rectangular irregular-shaped crystal with dimensions $0.21\times 0.12\times 0.11$ mm^3 was selected for the diffraction experiment. The crystal was kept at a steady T = 123.00(10) K during data collection. The Cl counter ion is disordered and one position on Cu3.

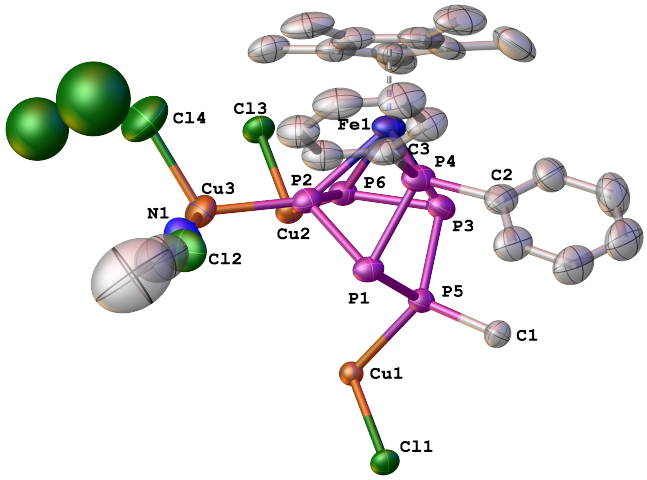


Figure 7.10: Asymmetric unit in the Molecular structure of **33** in the solid state. Hydrogen atoms are omitted for clarity. Selected bond lengths and angles: Cu2-Cl4 2.4224(8) Cu2-P6 2.2938(9) Cu2-P61 2.2939(9) Cu2-P62 2.2939(9), Cu1-Cl3 2.2219(17), Cu1-P42 2.3074(10), Cu1-P4 2.3073(10), Cu1-P41 2.3074(10), Cu3-P3 2.2766(12), Cu3-P51 2.2702(12), Cu3-Cl2 2.2782(19), Cu3-Cl1 2.297(3), Fe-P4 2.3309(11), Fe-P3 2.3467(12), Fe-P5 2.3157(12), Fe-P1 2.2204(12), P6-P2 2.1834(13), P6-P5 2.2196(13), P6-C1 1.837(4), P4-P3 2.1308(14), P4-P5 2.1279(14), P2-P3 2.2638(13), P2-P1 2.2112(14), P1-C2 1.832(5), P1-C3 1.829(5), P6-Cu2-Cl4 96.72(3), Cl3-Cu1-P4 120.30(3), P3-Cu3-Cl2 115.11(7), P3-Cu3-Cl1 110.31(8), Cl2-Cu3-Cl1 100.67(10), P4-Fe-P3 54.20(4), P5-Fe-P4 54.51(4), P5-Fe-P3 87.33(4), P1-Fe-P4 113.68(4), P1-Fe-P3 75.84(4), P1-Fe-P5 86.37(4), P2-P6-Cu2 99.83(4), P2-P6-P5 99.95(5), P5-P6-Cu2 123.61(5), C1-P6-Cu2 114.63(13), C1-P6-P2 108.45(14), C1-P6-P5 107.93(14), Cu1-P4-Fe 152.77(5), P3-P4-Cu1 127.84(5), P3-P4-Fe 63.28(4), P5-P4-Cu1 128.89(5), P5-P4-Fe 62.38(4), P5-P4-P3 98.21(5), P6-P2-P3 94.04(5), P6-P2-P1 97.27(5), P1-P2-P3 77.74(5), Cu3-P3-Fe 144.68(5), P4-P3-Cu3 120.50(5), P4-P3-Fe 62.52(4), P4-P3-P2 108.68(5), P2-P3-Cu3 114.46(5), P2-P3-Fe 94.68(5), P6-P5-Fe 109.87(5), P4-P5-Fe 63.11(4), P4-P5-P6 91.75(5), P2-P1-Fe 99.85(5), C2-P1-Fe 123.85(19), C2-P1-P2 105.83(15), C3-P1-Fe 118.95(15), C3-P1-P2 101.86(17), C3-P1-C2 103.5(2).

$[\{\mathbf{CuBr}\{(\mathbf{Cp^*Fe}\{\mu_{\mathbf{3,2,2}},\eta^{\mathbf{1:3:1:1:1}}\text{-}(\mathbf{1\text{-}CH_3\text{-}2\text{-}PPh_2\text{-}P_5})\}(\mathbf{CuBr(MeCN)})\}_{\mathbf{3}})\}_{\mathbf{2}}\mathbf{Br}][\mathbf{Br}]$

Crystals of $[\{CuBr\{(Cp^*Fe\{\mu_{3,2,2},\eta^{1:3:1:1:1}\text{-}(1\text{-}CH_3\text{-}2\text{-}PPh_2\text{-}P_5)\}(CuBr(MeCN))\}_3)\}_2Br][Br]$ (**36**) were obtained by layering a toluene solution of **11a** with a acetonitrile solution of CuBr at room temperature. A clear dark brown rhombohedral-shaped crystal with dimensions $0.21 \times 0.11 \times 0.07$ mm^3 was selected for the diffraction experiment. The crystal was kept at a steady T = 123.01(10) K during data collection. A solvent mask was calculated and 808 electrons were found in a volume of 3808 Å^3 in one void per unit cell. This is consistent with the presence of 4.5 acetonitrile molecules per asymmetric unit, which account for 792 electrons per unit cell.

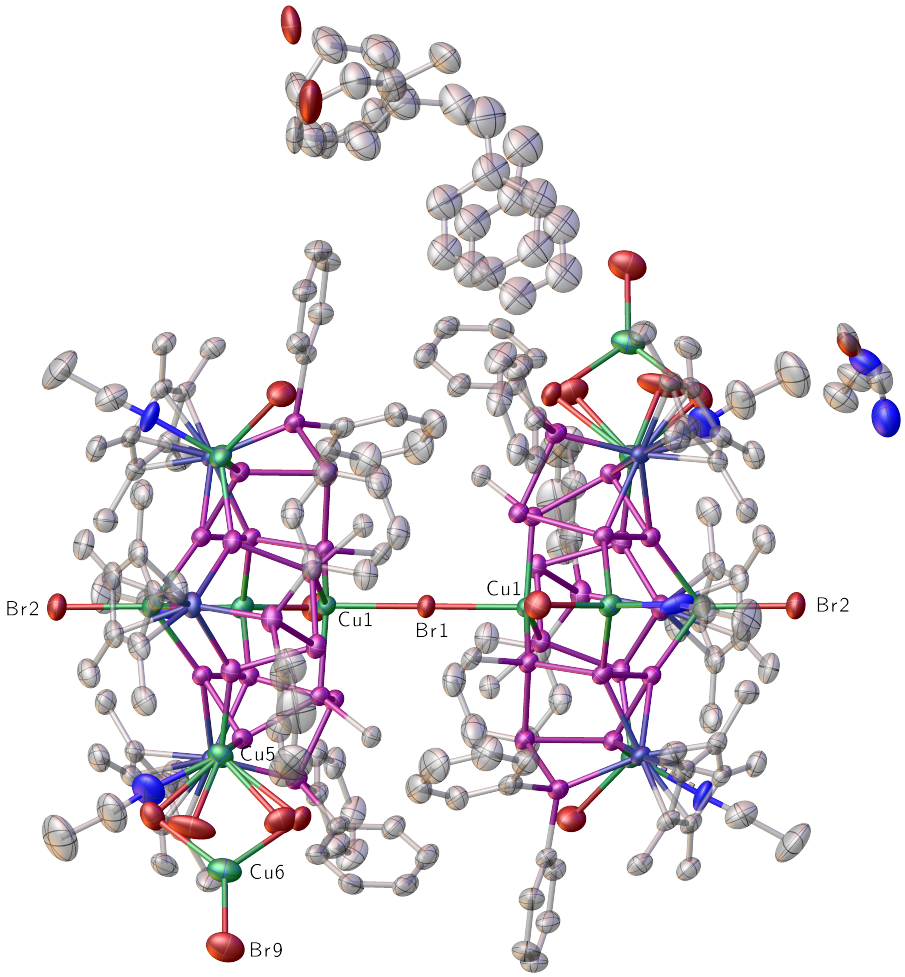


Figure 7.11: Molecular structure of **36** in the solid state showing the discrete molecule with the symmetry generated counterpart. Hydrogen atoms are omitted for clarity.

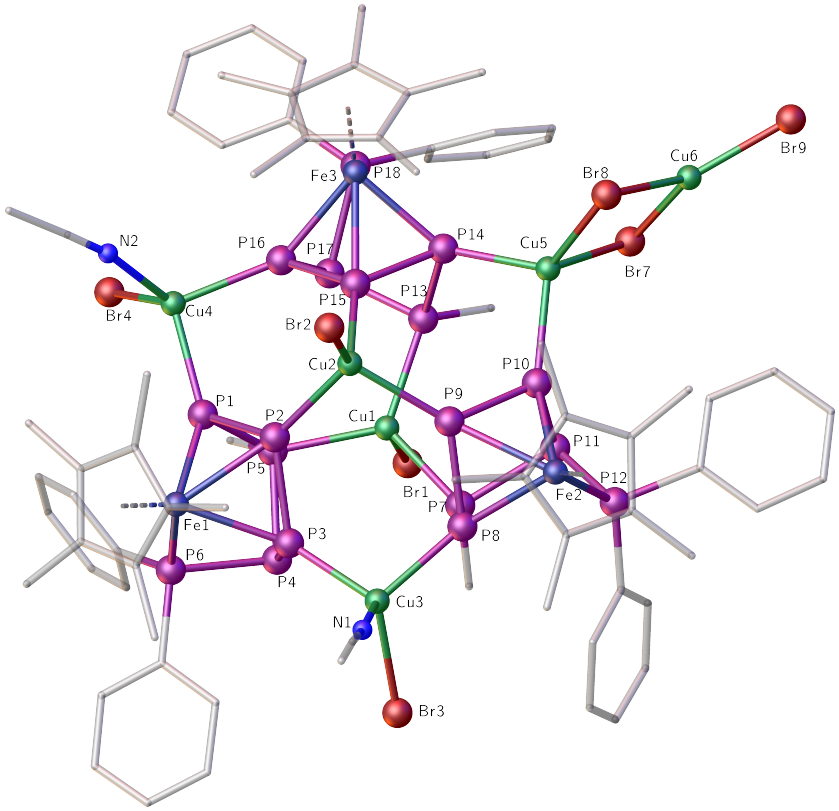


Figure 7.12: Molecular structure of **36** in the solid state. Hydrogen atoms and disordered atoms are omitted for clarity. Bond lengths are similar to the isostructural Cl substituted **35**. Average Cu-Br distance (excluding the Cu1-Br1 bond): 2.3962(6) Å. Cu1-Br1 = 2.4999(6) Å.

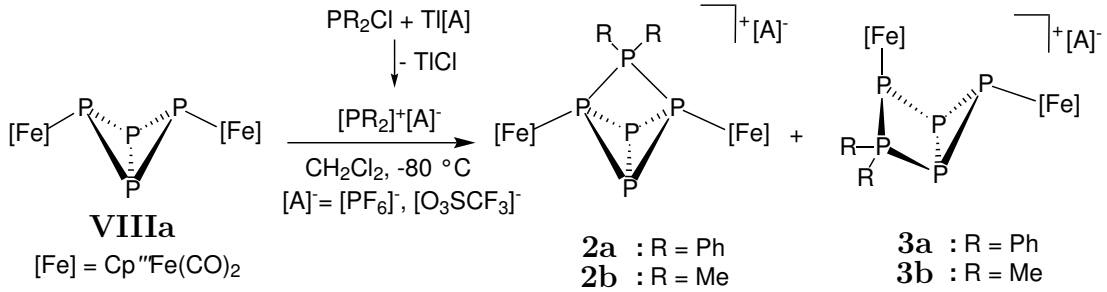
Chapter 8

Conclusion

In this work the functionalisation of iron based polyphosphorus complexes with electrophilic $\mathrm{P_1}$ building blocks as well as the reactivity of group 2 metal compounds towards polyphosphorus ligand complexes was investigated.
For the functionalisation of $\mathrm{P_n}$ ligand complexes with *in situ* generated phosphenium ions, the $\mathrm{P_4}$ butterfly complex $[\{\mathrm{Cp'''Fe(CO)_2}\}_2(\mu,\eta^{1:1}\text{-}\mathrm{P_4})]$ (**VIIIa**) was chosen for first investigations, since its highest occupied molecular orbitals are located at the wingtip atoms of the butterfly motif, which has made coordination to Lewis acidic transition metal compounds possible in the past.[68]
Upon attack of carbon based nucleophiles on the sandwich complex $[\mathrm{Cp^*Fe}(\eta^5\text{-}\mathrm{P_5})]$ (**XXVII**) and subsequent reaction of an electrophilic $\mathrm{P_1}$ reagents, neutral compounds with novel $\mathrm{P_6}$ moieties are obtained. The reactivity of the resulting products was further explored.
The second area of research explored in this thesis was the reactivity of $\mathrm{P_n}$ ligand complexes towards reagents of the alkaline earth metals. The chemistry of polyphosphorus compounds and group 2 metal compounds in classic carbon based solvents was almost unexplored. Since the metals themselves are relatively hard to react and organometallic compounds of Ca, Sr and Ba are extremely sensitive and hard to stabilize, enormous synthetic challenges arose. In one chapter of this work bisketiminate stabilized magnesium and calcium reagents were used as reducing agents on **XXVII**. The reactivity of the anthracene compounds of Mg, Ca, Sr and Ba on **XXVII** was studied in order to provide insight into this type of chemistry without the use of bulky, electron donating ligands to stabilize the products of the reactions. For the heavier homologues of Mg, a new synthetic pathway to the anthracenides was presented.

8.1 Reactivity of [{Cp‴Fe(CO)$_2$}$_2$(μ,$\eta^{1:1}$-P$_4$)] towards phosphenium ions

The phospha[1.1.0]bicyclobutane (also called "butterfly") ligand in [{Cp‴Fe(CO)$_2$}$_2$ (μ,$\eta^{1:1}$-P$_4$)] (**VIIIa**) represents the structural motif obtained after the opening of one P-P bond of white phosphorus. In the recent past it was shown that this bond opening can be achieved by the insertion of phosphenium ions ([R$_2$P]$^+$ (R = alkyl, aryl) into the P$_4$ tetrahedron.[100] In total, three phosphenium ions can react with white phosphorus in this manner. Due to their extremely high reactivity, phosphenium ions have to be generated *in situ* from a chlorophosphine and a suitable halogen abstracting agent such as GaCl$_3$, silver(I) or thallium(I) salts.[95,159] Complex **VIIIa** is known to react readily with Lewis acidic transition metal compounds e.g, coinage metal salts or Fe, Ni, Zn or Ru compounds.[68,151] Therefore, it was feasible to investigate the reactivity of **VIIIa** towards *in situ* generated phosphenium ions.

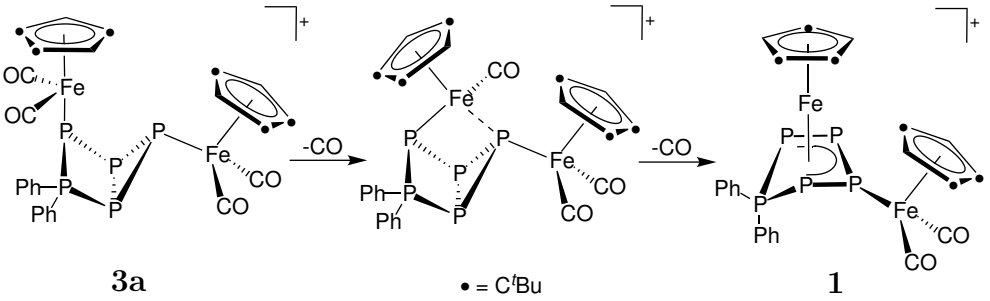


Scheme 8.1: Reaction of **VIII** with in situ generated phosphenium ions.

Despite multiple attempts, no products could be isolated or observed in the ^{31}P NMR spectra of the reaction solutions at room temperature, when the reaction depicted in Scheme 8.1 was performed in dichloromethane at -80 °C. A low temperature NMR study was conducted to gain more insight. By analysis of the ^{31}P ^{31}P COSY NMR spectrum as well as iterative fitting and simulation of the two superimposed, complex spin systems observable at -80 °C, the connectivity of the phosphorus frameworks in the products **2a**, **2b**, **3a** and **3b**, depicted in Scheme 8.1, were predicted. Upon warming the solutions to room temperature, the products began to decompose at -60 °C according to VT NMR studies. After multiple reactions, performed with different solvents, halogen abstractors, and variation of the reaction parameters, small amounts of crystalline **3a** were obtained, providing proof to the postulated phosphorus framework.

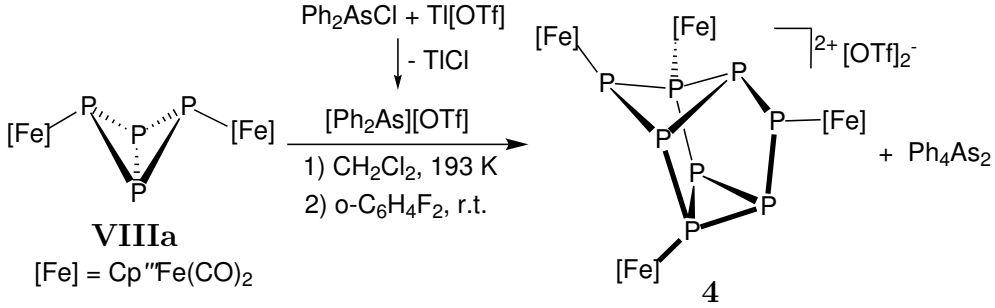
It was also possible to obtain small amounts of crystals (suitable for structure determination with synchrotron radiation) of one of the decomposition products: Via a pathway observed by mass spectrometry and supported by DFT calculations , **3a** reacts to **1** un-

der the extrusion of two equivalents of CO gas, as shown in Scheme 8.2 (*vide infra*). Complex **1** shows a similar structural motif as a twofold functionalized pentaphosphaferrocene of the type $[Cp^*Fe(\eta^5\text{-}P_5R_2)]$ with a $[Cp'''Fe(CO)_2]$ fragment coordinating to the *cyclo*-P_5 ligand in 1,3 position to the functionalized phosphorus atom bent out of plane.



Scheme 8.2: Stepwise decarbonylation of **3a** to **1**.

Diphenylarsenium ions were generated *in situ* and reacted with **VIIIa** in the same manner as the respective phosphenium ions. By ^{31}P NMR spectroscopy the formation of two products was observed in freshly prepared reaction solutions. Prediction of the connectivity of the P_4As frameworks was not possible since ^{75}As is not suitable for high resolution NMR spectroscopy (the extreme quadropole broadening of the nucleus only allows for measurement of simple, highly symmetric As containing molecules in solution[323]) At room temperature the products disproportionate into Ph_4As_2 and **4**, the formal oxidation product of $[\{Cp'''Fe(CO)_2\}_2(\mu,\eta^{1:1}\text{-}P_4)]$ (Scheme 8.3), which has not been known to this date.



Scheme 8.3: Reaction of **VIIIa** with in situ generated arsenium ions.

In conclusion, it is possible to functionalize **VIIIa** with phosphenium ions and expand the phospha[1.1.0]bicyclobutane ligand with this P_1 building block. Yet the products are not stable above -60 °C in dichloromethane solutions and thus could not be isolated but only described by elaborate NMR studies and X-ray structure determination. The reaction of **VIIIa** with *in situ* prepared $[Ph_2As][OTf]$ resulted in the formal oxidation of **VIIIa** due to disproportionation of the initial reaction products at room temperature.

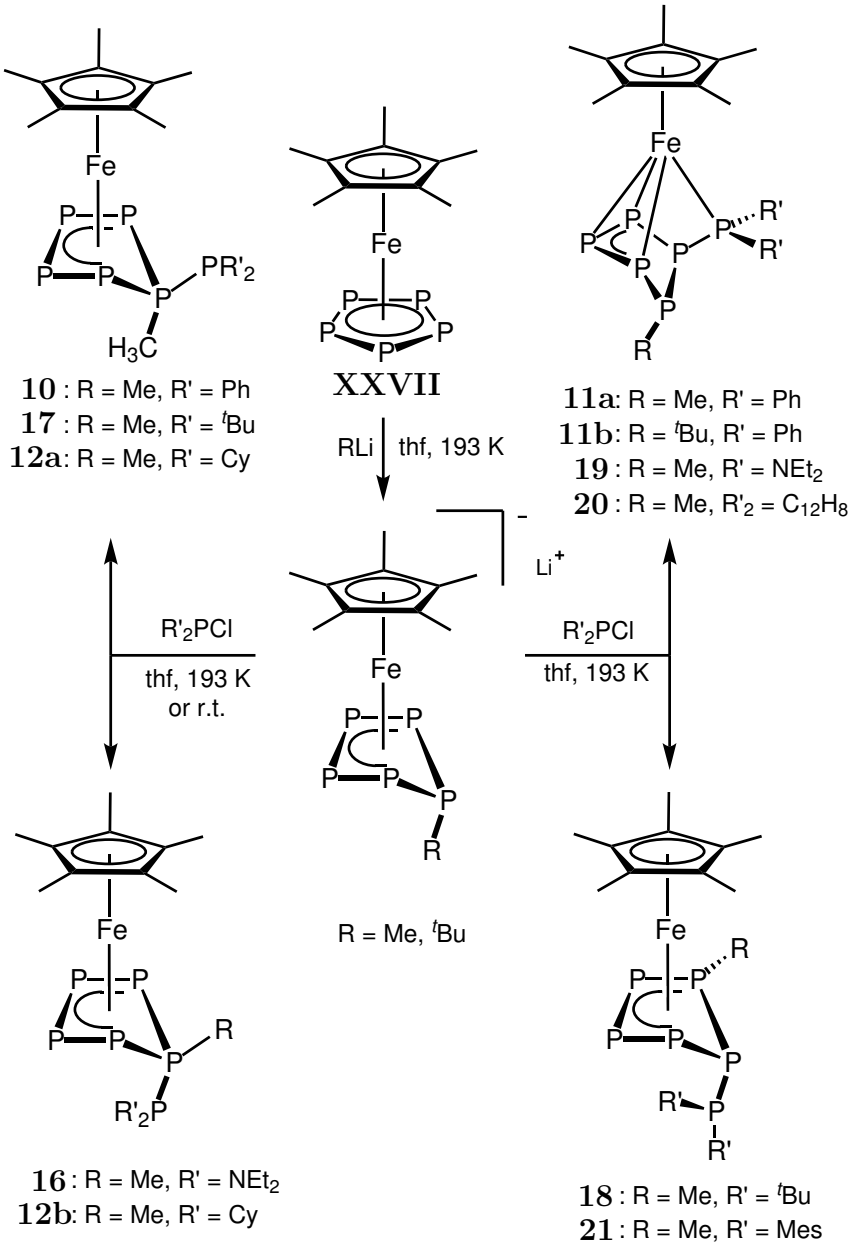
8.2 Consecutive functionalisation of $[Cp^*Fe(\eta^5\text{-}P_5)]$ with carbon nucleophiles and phosphorus electrophiles.

The functionalisation of the *cyclo*-P_5 ligand in $[Cp^*Fe(\eta^5\text{-}P_5)]$ (**XXVII**) with carbon nucleophiles and subsequent quenching of the anionic products $[Cp^*Fe(\eta^4\text{-}P_5R)]^-$ with carbon electrophiles gives neutral, 1,1-functionalized products.[77] These can be used to synthesize asymmetrical substituted phosphines in a selective and clean manner.[76] Also the functionalisation of **XXVII** with main group electrophiles is possible.[78] However both nucleophilic and electrophilic attack of P_1 building blocks on **XXVII** prove to be difficult.[77,78] Therefore quenching $[Cp^*Fe(\eta^4\text{-}P_5R)]^-$, the products of the attack of carbon nucleophiles on **XXVII**, with chlorophosphines was investigated as a feasible synthetic pathway for the P_1 functionalisation of **XXVII**.

The anionic complexes $[Cp^*Fe(\eta^4\text{-}P_5R)]^-$ $(R = Me, {}^tBu)$ were generated *in situ* by addition of the respective organo-lithium compound to **XXVII** at -80 °C in thf. To the resulting dark brown reaction solution, the chlorophosphines R_2PCl (R = Ph, Cy, Me, Mes, $N(Et_2)_2$, ${}^tBu$) and 5-chloro-5H-dibenzophosphole were added to the reaction mixture at either -80 °C or room temperature, depending on the respective phosphine (Scheme 8.4). Selective reactions were observed for Ph_2PCl and Cy_2PCl, while the other phosphines gave complex product mixtures. Unfortunately these products could not be separated chromatographically or by fractionated crystallisation. However, the products from this mixtures were characterized by ^{31}P NMR spectroscopy and/or X-ray structure determination (Scheme 8.4, page 329).

Upon reaction of $[Cp^*Fe(\eta^4\text{-}P_5CH_3)]^-$ with Cy_2PCl at -80 °C in thf, a mixture of endo- and exo-$[Cp^*Fe(\eta^4\text{-}1,1\text{-}CH_3,PCy_2\text{-}P_5)]$ (**12**, endo and exo regarding the PCy_2 group to the Cp^*Fe fragment) was observed in the ^{31}P NMR spectrum of the reaction solution at room temperature as two AMM'NXX' spin systems. The exo isomer **12b** was crystallized from this reaction solution as a clean product. Adding Cy_2PCl at room temperature to the reaction mixture changed the ratio of the mixture and the endo isomer **12a** was crystallized as the main product.

The reaction of $[Cp^*Fe(\eta^4\text{-}P_5CH_3)]^-$ with Ph_2PCl yielded endo-$[Cp^*Fe(\eta^4\text{-}1,1\text{-}CH_3,PPh_2\text{-}P_5)]$ (**10**; endo-PPh_2 relative to Cp^*Fe, isostructural to **12a**) at -80 °C. Compound **10** is not stable at room temperature and converts by a 1,2 shift to the novel complex $[Cp^*Fe(\eta^{3:1}\text{-}(1\text{-}CH_3\text{-}2\text{-}PPh_2\text{-}P_5))]$ (**11a**), which was isolated in 75 % crystalline yield. The conversion of **10** into **11a** was also observed by variable temperature ^{31}P NMR spectroscopy: Samples of crystalline **10**, dissolved in CD_2Cl_2 at -30 °C,

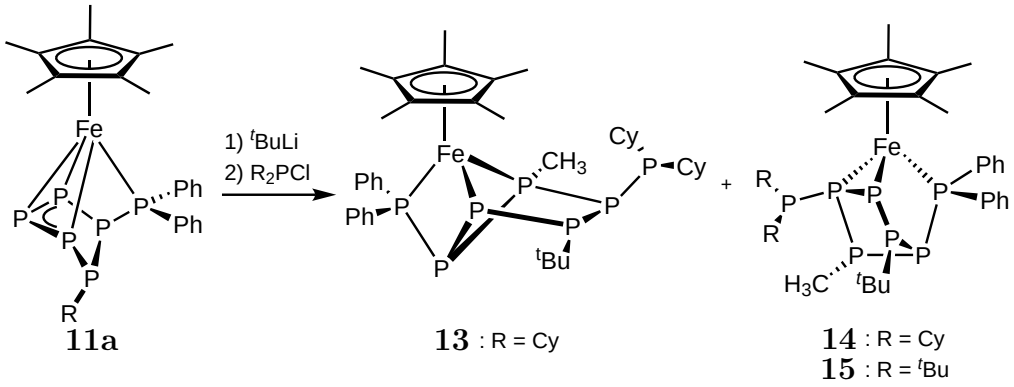


Scheme 8.4: Products from quenching $[Cp^*Fe(\eta^4\text{-}P_5R)]^-$ (R = Me, ^{t}Bu, generated *in situ*) with different chlorophosphines.

show an AMM'NXX' spin system in the ^{31}P NMR spectrum due to the C_S symmetry of the ligand. When heating the sample slowly to room temperature, conversion of **11a** is beginning at 0 °C and is complete after 30 hours at room temperature. The ADMQVX spin system of the highly asymmetric ligand in **11a** remains the only signal visible in the spectrum. Complex **11a** is the first isolated example of a 1,2 functionalized pentaphosphaferrocene. Due to this fact and the relatively easy accessibility of the compound, the reactivity of **11a** was further investigated.

8.2.1 Reactivity of the complex [Cp*Fe($\eta^{3:1}$-(1-Me-2-PPh$_2$-P$_5$))]

Since functionalisation of **XXVII** with carbon nucleophiles and Ph_2PCl produced the novel 1,2-substituted complex **11a** quantitatively, the question arose if **11a** can be further functionalized, maximizing the number of substituted phosphorus atoms in the *cyclo*-P_5 ligand of **XXVII**.
Solutions of **11a** were reacted with different carbon-based nucleophiles such as MeLi, ^{t}BuLi, PhLi and the respective grignard reagents at -80 °C and room temperature in thf. Of these nucleophiles, ^{t}BuLi shows the highest regioselectivity for the nucleophilic attack according to ^{31}P NMR spectra of the reaction solution (all three unsubstituted phosphorus atoms in **11a** may be attacked by the nucleophile). So far, these anionic complexes could not be isolated, but quenching the reaction by the addition of another chlorophosphine such as Cy_2PCl or $^tBu_2PCl$ resulted in stable products, which were isolated and fully characterized.



Scheme 8.5: Reaction of **VIII** with in situ generated phosphenium ions.

When quenching **11a** after *in situ* attack of ^{t}Bu with Cy_2PCl two main products of the reaction were isolated as a mixture of crystalline products. By X-ray structure determination the products were identified as [Cp*Fe($\eta^{1:1:1}$-(1-^{t}Bu-2-PPh$_2$-3-Me-4-PCy$_2$-P$_5$))] (**13**) and [Cp*Fe($\eta^{1:2}$-(1-^{t}Bu-2-PCy$_2$-3-Me-4-PPh$_2$-P$_5$))] (**14**, scheme 8.5). By picking crystals of **13** under the microscope in a glove box and recording NMR spectra of solutions of these crystals, it was possible to partially interpret the complex ^{31}P NMR spectrum of the product mixture. Since the signals of **13** are superimposed into a few sets of multiplets in the spectrum of the pure compound as well as the reaction mixture, the coupling patterns could not be completely analysed. In order to find another synthetic pathway to **13** and **14** with a higher selectivity, a comparative reaction study with the ^{t}Bu substituted **11b** was conducted. In these reactions the complex **14** could be identified as the main product alongside a so far uncharacterized side product, which is also observed in the reactions with **11a**. Due to the absence of **13** in ^{31}P NMR spectra

of the reaction solutions and the fact that the same products are formed from different starting materials, the connectivity of the phosphorus framework in the side product was determined. Using the same reaction setup but $^tBu_2PCl$ to quench the reaction of **11a** with ^{t}BuLi, $[Cp^*Fe(\eta^{1:2}\text{-}(1\text{-}^t\text{Bu-}2\text{-P}^t\text{Bu-}3\text{-Me-}4\text{-PPh}_2\text{-P}_5))]$ (**15**), the ^{t}Bu derivative of **14** was isolated and fully characterized as a pure compound. The P_7 ligands in **13**, **14** and **15** are the first examples for a 1,3-bis(phosphanyl)pentaphospholanide structural motif.

8.2.2 Supramolecular aggregates of the complex $[\mathbf{Cp^*Fe}(\eta^{\mathbf{3:1}}\text{-}(\mathbf{1\text{-}Me\text{-}2\text{-}PPh_2\text{-}P_5}))]$

In the past, the pentaphosphaferrocene **XXVII** was successfully used by our group for the synthesis of supramolecular aggregates.[83] These are formed by self-assembly reactions when a P_n ligand complex is reacted with coinage metal salts such as Cu(I) halogenides or silver salts. Thus, the complexes used for supramolecular self-assembly in the past always featured highly symmetrical *cyclo*-P_n ligands. Also the solubility of the starting materials has a great influence on the outcome of the self-assembly reaction. The reactivity of functionalized P_n ligand complexes such as the novel synthesized complex $[Cp^*Fe(\eta^{3:1}\text{-}(1\text{-}CH_3\text{-}2\text{-}PPh_2\text{-}P_5))]$ (**11a**) towards coinage metal salts should lead to new structural motifs in supramolecular aggregates. Herein it was investigated if **11a** is feasible as a building block in supramolecular chemistry.

Layering of **11a** in toluene with the silver salt $Ag[SbF_6]$ in acetonitrile gives the syndiotactic, one dimensional polymer $[Cp^*Fe\{\mu_5,\eta^{1:3:1:1}\text{-}(1\text{-}CH_3\text{-}2\text{-}PPh_2\text{-}P_5)\}(Ag(MeCN))_2]_n[SbF_6]_{2n}$ (**33**, Figure 8.1, top) upon crystallisation from the concentrated reaction mixture at -30 °C. Other silver salts show a colour change upon reaction with **11a** but no supramolecular aggregates could be isolated far.

Layering of **11a** (in toluene) with CuCl (in acetonitrile) in a layering reaction gives the novel supramolecular wheel $[(Cp^*Fe\{\mu_5,\eta^{1:3:1:1:1:1}\text{-}(1\text{-}CH_3\text{-}2\text{-}PPh_2\text{-}P_5)\})_8(CuCl)_8(Cu(\mu_2\text{-}Cl))_8]$ (**34**, Figure 8.1, bottom left) in the form of short lived, extremely sensitive crystals. The aggregate contains 8 units of **11a**, syndiotacticly arranged and linked by two CuCl units each. With a diameter of 30 Å, **34** represents the largest known annular supramolecular aggregate of a P_n-ligand complex. Attempts to find more suitable reaction setups for the synthesis of larger amounts of **34** with a better crystal quality was not successful so far, but using a more diluted system for the layering reaction and a longer reaction time, small amounts of crystalline $[\{CuCl\{(Cp^*Fe\{\mu_5,\eta^{1:3:1:1:1}\text{-}(1\text{-}CH_3\text{-}2\text{-}PPh_2\text{-}P_5)\}(CuCl(MeCN))\}_3)\}_2Cl][Cl]$ (**35**, Figure 8.1, bottom right) are observed and characterized by X-ray diffraction experiments. The aggregate consists of

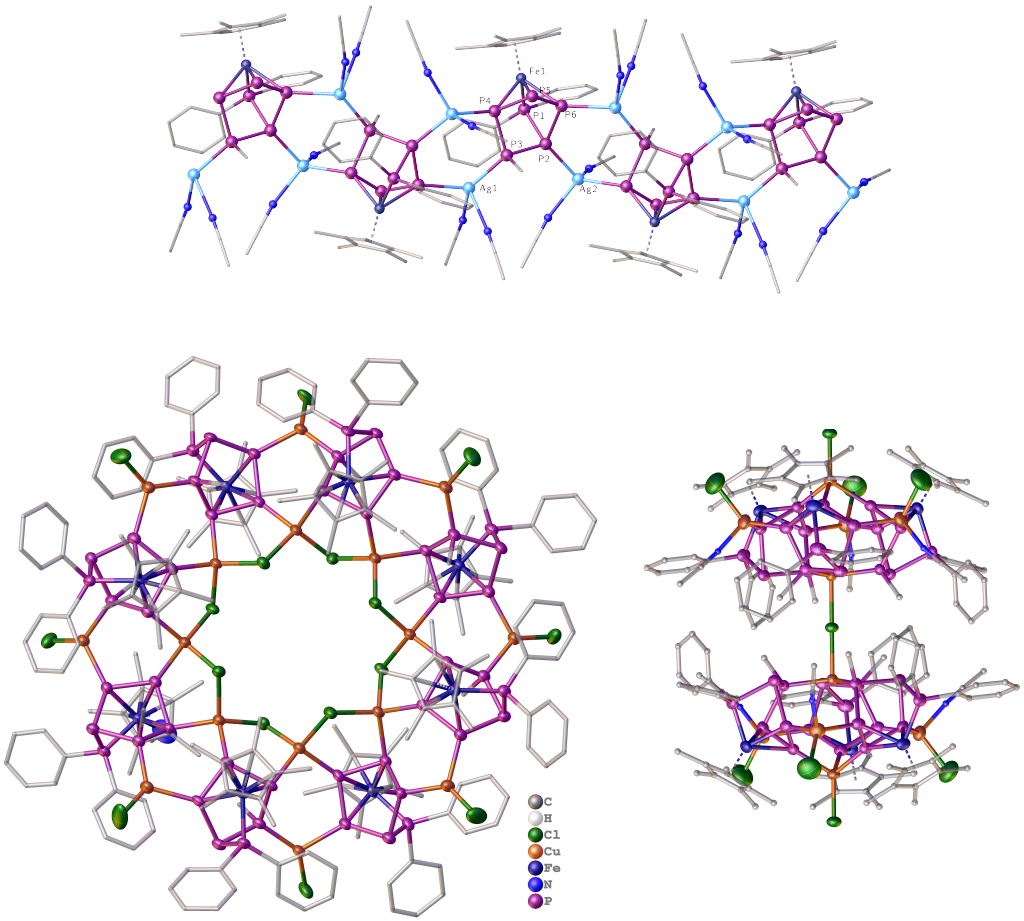


Figure 8.1: Solid state structures of supramolecular aggregates obtained from **11a** and Ag[SbF_6] as well as CuCl, respectively, in layering reactions. Hydrogen atoms, solvent molecules and counter ions are omitted for clarity. Top: **33**, bottom: left **34**, right **35**.

two identical, trimeric units of **11a** and CuCl, linked by a chloride ion, located in the inversion centre of the structure. The trimeric units are themselves cationic, also visible in the trigonal planar coordination mode of one of the Cu atoms, indicating the existence of Cu^+ ions, which is also supported by the long Cu-Cl distance to the chloride ion in the centre. A second chloride ion is not coordinating and acts as a counter ion for the monocationic aggregate. Reaction of **11a** with CuBr gives the isostructural [{CuBr{(Cp*Fe{μ_5,$\eta^{1:3:1:1:1}$-(1-CH_3-2-PPh_2-P_5)}(CuBr(MeCN))}$_3$)}$_2$Br][Br] (**36**) in larger amounts than obtained for **35**.

In conclusion, it was shown that **11a** is suitable as a building block in supramolecular chemistry. The asymmetric nature of **11a** and organic substituents apparently have a great influence on the geometries formed during the self-assembly of supramolecular aggregates with coinage metal salts.

8.3 Reactivity of group 2 metal compounds towards P_n-ligand complexes

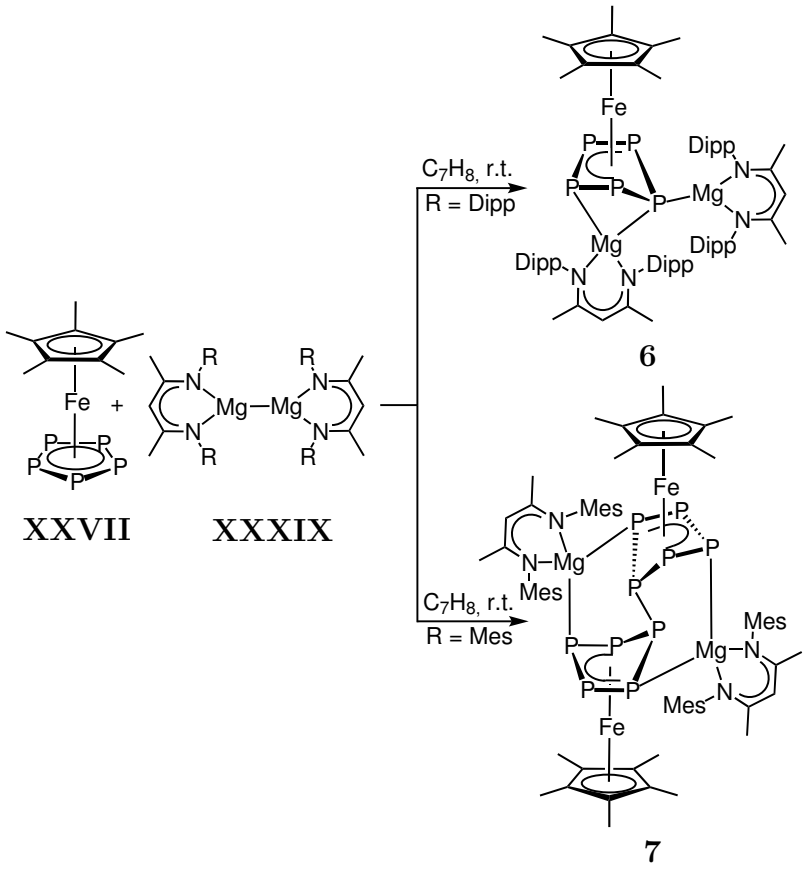
The organometallic chemistry of the heavy alkaline earth metals Ca, Sr and Ba is not as well explored as it is for magnesium. This is even more pronounced for the chemistry of the polypnictogenides of these metals. Group 2-15 element compounds are usually only accessible in solid state chemistry or as Zintl phases soluble in liquid ammonia. The organometallic compounds of the alkaline earth metals themselves provide several challenges in synthesis and handling. On the one hand, due to passivation of the surface the metals Ca, Sr and Ba are relatively uncreative and have to be activated in most cases. On the other hand, the organometallic compounds of these metals are extremely reactive and are seldom stable at room temperature without sterically demanding and donating ligands such as bis-ketiminates. By using the latter N-donor-ligands, some group 2 element reagents became more accessible in the recent past and first results of their reactivity towards white phosphorus were investigated.[132] Therefore the study of the reactivity of these alkaline earth compounds towards P_n ligand complexes can contribute to this almost unexplored field of organometallic and main group element chemistry.

8.3.1 Reactivity of bisketiminate stabilized Mg and Ca compounds towards $[Cp^*Fe(\eta^5\text{-}P_5)]$

The reactivity of the dimeric Mg(I) compound $[^{R}BDIMg]_2$ ($R = Dipp$ (**XXXIX**)) was studied in the recent past by many researchers and **XXXIX** has proven to be a powerful reducing agent. In the past our group showed that the pentaphosphaferrocene $[Cp^*Fe(\eta^5\text{-}P_5)]$ (**XXVII**) is reduced by alkaline metals to its dimeric monoanion and its dianiion.[173] The pentaphosphaferrocene can also be attacked by main group nucleophiles like organolithium compounds.[77] Herein, the reactivity of this complex towards **XXXIX**, its methyl compound $[^{Dipp}BDIMgCH_3]_2$, the mesityl substituted derivative of **XXXIX**, $[^{Mes}BDIMg]_2$, and the bis-ketiminate stabilized calcium hydride compound $[^{Mes}BDICaH]_2$ was explored.

When **XXVII** is reacted with **XXXIX** in toluene at room temperature the compound $[(^{Dipp}BDI\text{-}Mg)_2(\mu\text{-}\eta^{4:2:1}\text{-}P_5)(FeCp^*)]$ (**6**) is formed exclusively (Scheme 8.6). The structure of **37** is similar to the reported $[K(dme)K(dibenzo\text{-}[18]crown\text{-}6)][Cp^*Fe(\eta_4\text{-}P_5)]$. Any attempts to synthesize the dimeric $P_{10}{}^{2-}$ product by using **XXXIX** and an excess of **XXVII** in the reaction only resulted in the formation of **6** with unreacted

XXVII in the ^{31}P NMR spectrum of the respective reaction solutions. Only by using the mesityl substituted $[^{Mes}BDIMg]_2$ as reducing agent instead of **XXXIX** this structural motif is observed in $[(^{Mes}BDI\text{-}Mg)_2(\mu,\eta^{4:4:2:2}\text{-}P_{10})(FeCp^*)_2]$ (**7**, Scheme 8.6). Both **6** and **7** are highly soluble in apolar solvents such as *n*-hexane or *n*-pentane, which also distinguishes them from the respective potassium compounds.



Scheme 8.6: Reaction of **XXVII** with Mg(I) compounds.

The reaction of **XXVII** with the organomagnesium compound $[^{Dipp}BDIMgCH_3]_2$ results in the first example of a discrete cyclic tetrameric assembly of a polypnictogen complex: $[(^{Dipp}BDI\text{-}Mg)_4(\mu\text{-}\eta^{4:1:1}\text{-}P_5(CH_3))_4(FeCp^*)_4)]$ (**5**, Figure 8.2). The formation of this tetrameric species is only observed in the solid state: According to diffusion ordered NMR spectroscopy (DOSY NMR), the hydrodynamic radius of the species in solution is more comparable to **6**. Also the well resolved AMM'XX' system visible in the ^{31}P NMR spectra gives evidence to a C_S symmetric *cyclo*-P_5 ligand in envelope conformation without another $^{Dipp}BDI\text{-}Mg$ coordinating to the ligand (resolved on the NMR time scale) as it would be required for the assembly of tetrameric **5** or a dimeric species.

Last but not least the reactivity of $[^{Mes}BDICaH]_2$ towards **XXVII** and white phosphorus was studied. Reaction with the latter gives the Zintl ion $[(^{Dipp}BDI\text{-}Ca)_3(\mu,\eta^{2:2:2}\text{-}P_7)]$

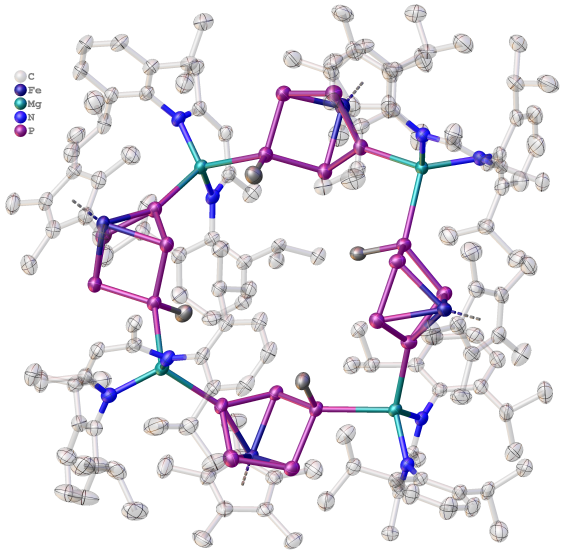
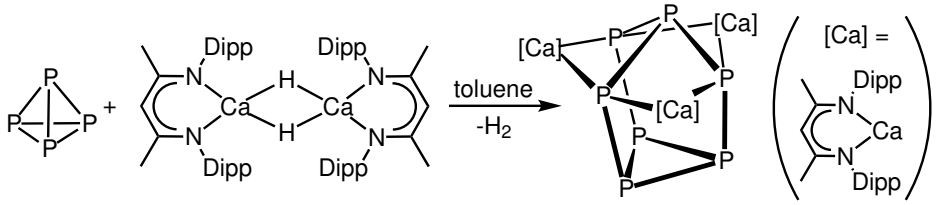


Figure 8.2: Structure of tetrameric [(^{Dipp}BDI-Mg)$_4$(μ-$\eta^{4:1:1}$-$P_5(CH_3)$)$_4$(FeCp*)$_4$)] (**5**) in the solid state. Hydrogen atoms are omitted for clarity.

(**9**, Scheme 8.7), the first polyphosphide of calcium soluble and stable in hydrocarbon based solvents. Also in the reaction of [^{Mes}BDICaH]$_2$ towards **XXVII** no hydride transfer but the formation of [(^{Dipp}BDI-Ca)$_2$(μ, $\eta^{4:4:3:3}$-P_{10})(FeCp*)$_2$] (**8**) is observed. In the solid state structure of **8**, however, the two units of **XXVII** are not twisted in relation to each other, as is the case with **7** or the respective product from the reduction of **XXVII** with potassium, [{K(dme)$_2$}{K(dme)}(μ, η^4-P_{10})(FeCp*)$_2$].



9

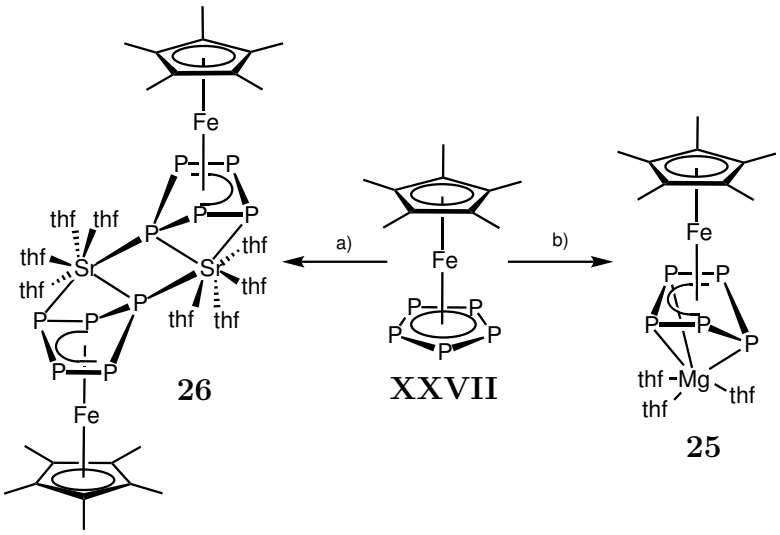
Scheme 8.7: Synthesis of [(^{Dipp}BDI-Ca)$_3$(μ, $\eta^{2:2:2}$-P_7)] (**9**).

These results show that the use of group 2 metal reagents in the chemistry of polyphosphorus compounds and complexes can lead to new, unexpected structural motifs and properties (such as high solubility in apolar solvents) of the products formed.

8.3.2 Reactivity of group 2 anthracene compounds towards polyphosphorus ligand complexes

The bis-ketiminate ligands used in the recently discovered alkaline earth metal compounds (see section 8.3.1) are not innocent ligands and can strongly influence the re-

activity and properties of the formed polyphosphorus compounds. Additionally, the respective Sr and Ba compounds require a more specialized ligand design and are harder to handle due to their high reactivity. Especially for Ba compounds at room temperature, possible ether cleavage makes it difficult to work with this compounds in usual solvents such as thf or diethyl ether. As a synthon for the group 2 metals, the anthracene (A) compounds of the respective alkaline earth metals can be used. Since synthesis of these compounds require large amounts of metals and ball milling according to the literature, a new preparative method has to be devised in order to obtain these compounds for reactivity studies with the standard equipment of an organometallic laboratory.[316]

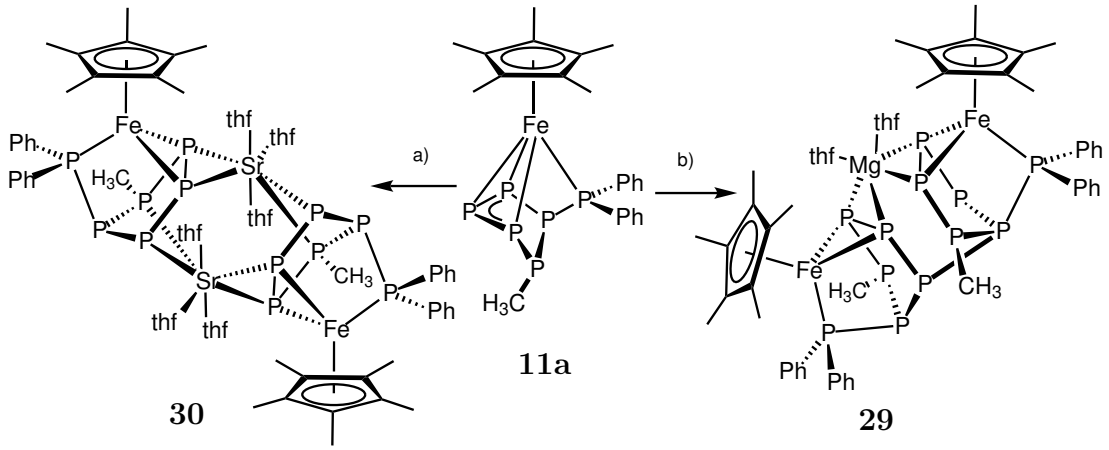


Scheme 8.8: Reaction of **XXVII** with a) [SrA(thf)$_2$] and b) [MgA(thf)$_3$] in thf as described in the text (*vide infra*).

In this thesis, instead of grinding and activating the metals with MeI, the dissolution in small amounts of liquid ammonia, directly condensed onto Ca, Sr or Ba, respectively, provided a more straight forward access to highly reactive metal powders after evaporation of ammonia. These powders are then reacted with anthracene in thf within an atmosphere of thf to yield the respective, intensely coloured anthracene compounds as fine powders. Reacting the anthracene compounds of Mg and Sr with the pentaphosphaferrocene [Cp*Fe(η^5-P_5)] (**XXVII**) by condensing thf onto a mixture of the solid starting materials yields the complexes [Cp*Fe($\mu, \eta^{4:3}$-P_5)Mg(thf)$_3$] (**25**) and [Cp*Fe($\mu, \eta^{4:3}$-P_5)Sr(thf)$_4$]$_2 \cdot$ (thf)$_2$ (**26**), the latter being the first example of a polyphosphorus compound of strontium observable in solution to this date (Scheme 8.8). For Ca no product formation but only a colour change of the reaction solution is observed when the respective dianthracene compound [CaA$_2$(thf)$_6$] is reacted with **XXVII** in the same manner (no conversion of the starting material **XXVII** according to ^{31}P NMR spectra of the reaction solution). The anthracene compound of Ba does react

with **XXVII** under the formation of a highly temperature sensitive product which could not be isolated so far. Only trace amounts of $[\{Cp^*Fe\}_2(\mu,\eta^{4:4:3:3}\text{-}P_{10})Ba(thf_3)]$ (**27**) were formed when using more than two equivalents of **XXVII** in the reaction.

The newly accessible group 2 anthracene compounds where also used to explore the redox chemistry of the highly functionalized pentaphosphaferrocene derivative $[Cp^*Fe(\eta^{3:1}\text{-}(1\text{-}CH_3\text{-}2\text{-}PPh_2\text{-}P_5))]$ (**11a**). Cyclic voltammetry shows that **11a** has a similar redox chemistry as **XXVII**. Therefore it should be possible to reduce **11a** to its dianion or the dimeric form of the monoanion, as reported for **XXVII**.[173] Upon reaction with sodium or potassium as reducing agents, **11a** is partially decomposed and $[Cp^*Fe(\eta^4\text{-}P_5CH_3)]^-$ is formed. Using the bis-ketiminate stabilized, dimeric Mg(I) compound $[^{Dipp}BDIMg]_2$ (**XXXIX**) as a reducing agent produces trace amounts of $[Cp^*Fe\{\mu_2,\eta^{1:2:2}\text{-}(1\text{-}CH_3\text{-}2\text{-}PPh_2\text{-}P_5)\}Mg(^{DIPP}BDI)]$ (**31**). Although **31** is a desired target of this synthesis, **XXXIX** is not suitable as a reducing agent for this reaction either: Unidentifiable side products are formed during the reaction and cannot be separated from the reaction mixture. Therefore **31** cannot be isolated as a pure compound. Only when using the anthracene compounds of Mg and Sr, the complex **11a** is reduced in a controlled manner (Scheme 8.9). Reaction with strontium anthracenide gives the dianion of **11a** in $[Cp^*Fe(\mu,\eta^{3:2:2}\text{-}(1\text{-}CH_3\text{-}2\text{-}PPh_2\text{-}P_5))Sr(thf)_3]_2$ (**30**) and the reaction with magnesium anthracenide the dimer of the monoanion with a P-P bond formation in $[Cp^*Fe(\mu_3,\eta^{3:3:4}\text{-}(1\text{-}CH_3\text{-}2\text{-}PPh_2\text{-}P_5)_2)Mg(thf)_4]$ (**29**). The ligand in the latter compound is the first example for a dodecaphospha-2,2'-dimethyl-[1,1'-bi(cyclopentadiene)]-diyl ligand known to this date.



Scheme 8.9: Reaction of **11a** with a) $[SrA(thf)_2]$ and b) $[MgA(thf)_3]$ in thf as described in the text (*vide supra*).

Appendix

List of compounds

I	$[(np_3)Ni(\eta^1\text{-}P_4)]$
II	$[W(CO)_3(PCy_3)_2(\eta^1\text{-}P_4)]$
III	$[(triphos)Re(CO)_2(\eta^1\text{-}P_4)][OTf]$
IV	$[Ag(\eta^2\text{-}P_4)_2][TEF]$
V	$[L_2RhCl(\eta^{1:1}\text{-}P_4)]$
VI	$sMes_2P_4$
VII	[*cis*, *trans*-$DmpP_4Dmp$]
VIIIa	$[\{Cp'''Fe(CO)_2\}_2(\mu,\eta^{1:1}\text{-}P_4)]$
VIIIb	$[\{Cp''Fe(CO)_2\}_2(\mu,\eta^{1:1}\text{-}P_4)]$
IX	$[Cp^*Nb(CO)_2(\eta^4\text{-}P_4)]$
X	$[\{Zr(L_{PN})\}_2(\mu,\eta^{4:4}\text{-}P_4)]$
XI	$[\{Cp''Fe\}(\mu,\eta^{4:1}\text{-}P_4)\{Fe(CO)_2Cp''\}]$
XII	$[\{Cp''Fe\}_2(\mu,\eta^{4:4}\text{-}P_4)]$
XIII	$[(^{Cy}CAAC)_3P_4]$
XIV	$[(^tBuCN(Cy)_2)_2P_4]$
XVa	$[Cp'''Fe(CO)_2]_2$
XVb	$[Cp''Fe(CO)_2]_2$
XVI	$[Cp'''Fe(CO)_2Br]$
XVII	$[\{Cp''Fe(CO)_2\}(\mu,\eta^{1:1:1}\text{-}P_4)\{\mu\text{-}\{Cp''Fe(CO)\}]$
XVIII	$[\{Cp''Fe\}(\eta^5\text{-}P_4\{Cp''Fe(CO)\})]$

XIX	$[\{\{Cp'''Fe(CO)_2\}_2(\mu_3,\eta^{1:1:1:1}\text{-}P_4)\}_2Cu][BF_4]$
XX	$[\{Cp'''Fe(CO)_2\}_2(\mu_3,\eta^{1:1:2}\text{-}P_4)\{Cu(MeCN)\}][BF_4]$
XXI	$[\{\{Cp'''Fe(CO)_2\}_2(\mu_3,\eta^{1:1:1:1}\text{-}P_4)\}_2Ag][PF_6]$
XXII	$[\{Cp'''Fe(CO)_2\}_2(\mu_3,\eta^{1:1:2}\text{-}P_4)\{Au(PPh_3)\}][PF_6]$
XXIII	$[\{Cp'''Fe(CO)_2\}_2(\mu_3,\eta^{1:1:2}\text{-}P_4)\{FeBr_2\}]$
XXIV	$[\{(Cp'''Fe(CO)_2)_2(\mu_3,\eta^{1:1:4}\text{-}P_4)\}_2Fe][PF_6]_2$
XXV	$[\{Cp'''Fe(CO)_2\}_2(\mu_3,\eta^{1:1:4}\text{-}P_4)\{Cp'''Fe\}][PF_6]$
XXVI	$[\{Cp'''Fe(CO)_2\}_2(\mu_3,\eta^{1:1:2}\text{-}P_4)\{Cp'''Fe(CO)\}][PF_6]$
XXVII	$[Cp^*Fe(\eta^5\text{-}P_5)]$
XXVIII	$[Cp^*Fe(\mu,\eta^{5:5}\text{-}P_{10})][SbF_6]$
XXIX	$[K(dme)_2K(dme)][Cp^*Fe(\mu,\eta^{4:4}\text{-}P_{10})]$
XXX	$[K(dme)K(dibenzo\text{-}[18]crown\text{-}6)][Cp^*Fe(\eta^4\text{-}P_5)]$
XXXI	$[Ph_2P-PPh_2Cl][GaCl_4]$
XXXII	$[(ClPh_2P)^+-(PPh_2Cl)^-]$
XXXIII	$[(C_4Et_4)P-PPh_3]^+$
XXXIV	$[(NMesCH_2CH_2NMes)P-PMe_3]^+$
XXXV	$[Ph_2P_5]^+$
XXXVI	$[Ph_4P_6]^{2+}$
XXXVII	$[Ph_6P_7]^{3+}$
XXXVIII	$[(diox)_2Ca\{CH(SiMe_3)_2\}_2]$
XXXIX	$[^{Dipp}BDIMg]_2$
XL	$[^{Dipp}BDIMgH]_2$
XLI	$[^{Dipp}BDICaH]_2$
XLII	$[^{DNPP}BDISrH]_2$
XLIII	$[^{DNPP}BDIBaN(SiMe_3)_2]$
1	$[\{Cp'''Fe\}(\mu,\eta^{4:1}\text{-}P_5(C_6H_5)_2)\{Cp'''(CO)_2Fe\}][PF_6]$
2a	**VIIIa** $+ [PPh_2]^+$: bicyclo[1.1.0]-tetraphosphabutane motif
2b	**VIIIa** $+ [PMe_2]^+$: bicyclo[1.1.0]-tetraphosphabutane motif

3a	$[\{Cp'''Fe(CO)_2\}_2(\mu,\eta^{1:1}\text{-}P_5Ph_2)][PF_6]$
3b	$[\{Cp'''Fe(CO)_2\}_2(\mu,\eta^{1:1}\text{-}P_5Me_2)][PF_6]$
4	$[\{Cp'''Fe(CO)_2\}_4(\mu_4\eta^{1:1:1:1}\text{-}P_8)]\ [OTf]_2$
5	$[(^{Dipp}BDI\text{-}Mg)_4(\mu,\eta^{4:1:1}\text{-}P_5(CH_3))_4(FeCp^*)_4)]$
6	$[(^{Dipp}BDI\text{-}Mg)_4(\mu,\eta^{4:1:1}\text{-}P_5(CH_3))_4(FeCp^*)_4)]$
7	$[(^{Mes}BDI\text{-}Mg)_2(\mu,\eta^{4:4:2:2}\text{-}P_{10})(FeCp^*)_2]$
8	$[(^{Dipp}BDI\text{-}Ca)_2(\mu,\eta^{4:4:3:3}\text{-}P_{10})(FeCp^*)_2]$
9	$[(^{Dipp}BDI\text{-}Ca)_3(\mu,\eta^{2:2:2}\text{-}P_7)]$
10a	endo-$[Cp^*Fe(\eta^4\text{-}1,1\text{-}CH_3,PPh_2\text{-}P_5)]$
11a	$[Cp^*Fe(\eta^{3:1}\text{-}(1\text{-}CH_3\text{-}2\text{-}PPh_2\text{-}P_5))]$
11b	$[Cp^*Fe(\eta^{3:1}\text{-}(1\text{-}^t\text{Bu-}2\text{-}PPh_2\text{-}P_5))]$
12a	endo-$[Cp^*Fe(\eta^4\text{-}1,1\text{-}CH_3,PCy_2\text{-}P_5)]$
12b	exo-$[Cp^*Fe(\eta^4\text{-}1,1\text{-}CH_3,PCy_2\text{-}P_5)]$
13	$[Cp^*Fe(\eta^{1:1:1}\text{-}(1\text{-}^t\text{Bu-}2\text{-}PPh_2\text{-}3\text{-Me-}4\text{-}PCy_2\text{-}P_5))]$
14	$[Cp^*Fe(\eta^{1:2}\text{-}(1\text{-}^t\text{Bu-}2\text{-}PCy_2\text{-}3\text{-Me-}4\text{-}PPh_2\text{-}P_5))]$
15	$[Cp^*Fe(\eta^{1:2}\text{-}(1\text{-}^t\text{Bu-}2\text{-P}^t\text{Bu-}3\text{-Me-}4\text{-}PPh_2\text{-}P_5))]$
16	endo-$[Cp^*Fe(\eta^4\text{-}1,1\text{-}CH_3,P(NEt_2)_2\text{-}P_5)]$
17	endo-$[Cp^*Fe(\eta^4\text{-}1,1\text{-}CH_3,P^t\text{Bu-}P_5)]$
18	$[Cp^*Fe(\eta^4\text{-}(1\text{-P}^t\text{Bu}_2\text{-}2\text{-}CH_3\text{-}P_5)]$
19	$[Cp^*Fe(\eta^{3:1}\text{-}1\text{-}CH_3\text{-}2\text{-}P(NEt_2)_2\text{-}P_5)]$
20	$[Cp^*Fe(\eta^{3:1}\text{-}1\text{-}CH_3\text{-}2\text{-}C_{12}H_8P\text{-}P_5)]$
21	$[Cp^*Fe(\eta^4\text{-}(1\text{-}PMes_2\text{-}2\text{-}CH_3\text{-}P_5)]$
22	$[Cp^*Fe(\eta^4\text{-}1,1\text{-}^t\text{Bu},(Cp^*)\text{-}P_5)]$
23	$[Cp^*Fe(\eta^4\text{-}(1,2\text{-}(^t\text{Bu}_2\text{-}P_5)]$
24	$[Cp^*Fe(\eta^4\text{-}(1,3\text{-}(^t\text{Bu}_2\text{-}P_5)]$
25	$[Cp^*Fe(\mu,\eta^{4:3}\text{-}P_5)Mg(thf)_3]$
26	$[Cp^*Fe(\mu,\eta^{4:3}\text{-}P_5)Sr(thf)_4]_2\cdot(thf)_2$

27 $[\{Cp^*Fe\}_2(\mu,\eta^{4:4:3:3}\text{-}P_{10})Ba(thf_3)]$

28 $[Cp^*Fe(\eta^4\text{-}P_5CH_3)]_2[Mg(dme)_3]\cdot(dme)$

29 $[Cp^*Fe(\mu_3,\eta^{3:3:4}\text{-}(1\text{-}CH_3\text{-}2\text{-}PPh_2\text{-}P_5)_2)Mg(thf)_4]$

30 $[Cp^*Fe(\mu,\eta^{3:2:2}\text{-}(1\text{-}CH_3\text{-}2\text{-}PPh_2\text{-}P_5))Sr(thf)_3]_2$

31 $[Cp^*Fe\{\mu_2,\eta^{1:2:2}\text{-}(1\text{-}CH_3\text{-}2\text{-}PPh_2\text{-}P_5)\}Mg(^{DIPP}BDI)]$

32 $[Cp^*Fe(\eta^4\text{-}(P_5CH_3))][K(18\text{-cr-}6)(thf)_2]$

33 $[Cp^*Fe\{\mu_5,\eta^{1:3:1:1}\text{-}(1\text{-}CH_3\text{-}2\text{-}PPh_2\text{-}P_5)\}(Ag(MeCN))_2]_n[SbF_6]_{2n}$

34 $[(Cp^*Fe\{\mu_5,\eta^{1:3:1:1:1:1}\text{-}(1\text{-}CH_3\text{-}2\text{-}PPh_2\text{-}P_5)\})(CuCl)(Cu(\mu_2\text{-}Cl))]_8$

35 $[\{CuCl\{(Cp^*Fe\{\mu_5,\eta^{1:3:1:1:1}\text{-}(1\text{-}CH_3\text{-}2\text{-}PPh_2\text{-}P_5)\}(CuCl(MeCN))\}_3)\}_2Cl][Cl]$

36 $[\{CuBr\{(Cp^*Fe\{\mu_5,\eta^{1:3:1:1:1}\text{-}(1\text{-}CH_3\text{-}2\text{-}PPh_2\text{-}P_5)\}(CuBr(MeCN))\}_3)\}_2Br][Br]$

List of abbreviations

dme	dimethoxyethane	thf	tetrahydrofurane
o-dfb	ortho-difluorobenzene	diox	dioxane
tol	toluene	tht	tetrahydrothiophene
Ph	phenyl group	Mes	mesityl group
Et	ethyl group	sMes	1,3,5-tritertbutylbenzene
Me	methyl group	^{i}Pr	isopropyl group
^{t}Bu	tertbutyl group	Cy	cyclohexyl group
cod	1,5-cyclooctadiene	np	tris(2-diphenyl-
Dmp	2,6-dimesitylphenyl	BDI	β-diketiminate
triphos	1,1,1-tris(diphenyl-		phosphinoethyl)amine
	phosphinomethyl)-ethane	CAAC	cyclic alkylaminocarbene
DDP	(2,6-diisopropylphenyl)(4-((2,6-diiso-	TMEDA	tetramethylethylenediamine
	propylphenyl)imino)pent-2-en-2-yl)amide	PNHNHP	N,N-bis(2-(diphenyl-phos-
DIPP	diisopropylphenyl		phino)phenyl)ethane-1,2-diaine
DNPP	dineopentylphenyl	OTf	$[OSO_2CF_3]^-$
TEF	$Al\{OC(CF_3)_3\}_4$	Cp*	pentamethylcyclopentadiene
Cp”	1,3-ditertbutyl-cyclopentadiene	Cp”’	1,2,4-tritertbutyl-cyclopentadiene
Cp^{BIG}	$C_5(C_6H_4(C_4H_9))_5)$	A	anthracene
DIP_2pyr	2,5-bis{*N*-(2,6-diisopropylphenyl)-	NMR	nuclear magnetic resonance
	iminomethyl}pyrrolyl	pd	pseudo doublet
s	singlet	d	doublet
t	triplet	br	broad signal
m	multiplet	pt	pseudo triplet
DOSY	diffusion ordered Spectroscopy	COSY	homonuclear correlation
DSTE	double stimulated echo	MS	mass spectrometry
ESI	electrospray ionization	IR	infrared spectroscopy
HOMO	highest molecular orbital	DFT	density functional theory
CV	cyclic voltammetry	SQV	square wave voltammetry
LUMO	lowest molecular orbital	M	$mol\ L^{-1}$
Å	Angstrom = 10^{-10} m		

List of Figures

1.1 Historic apparatus for the synthesis of white phosphorus. Phosphorus vapour from *a* is condensed in the copper tubing *b* and collected in a bottle filled with water.[7] 12
1.2 Structures of complexes **I**, **II**, **III** and **IV** with the structural motif **A**. . . 16
1.3 Structures of the complexes **V**, **VI**, **VII** and **VIII**. 17
1.4 Structures of selected complexes bearing a *cyclo*-P_4 unit (structural motif **C**). 17
1.5 DFT calculation on the complex $[\{CpFe(CO)_2\}_2(\mu,\eta^{1:1}\text{-}P_4)]$. 20
1.6 Coordination compounds of **VIIIa** with Lewis acidic coinage metal salts. 20
1.7 Example for a supramolecular aggregate of **XXVII**. 25
1.8 Stabilisation of diaminosubstituted phosphenium ions. 26
1.9 Some examples of earth alkaline metal compounds, stabilized by bulky and electron donating ligands. 31

3.1 Cationic parts of the molecular structures of **3a** (a) and **1** (b) in the solid state. 40
3.2 Simulated spin systems of **2a** and **3a**. 41
3.3 $^{31}P\{^1H\}$-VT-NMR-spectrum from the reaction of **VIII** with $[Ph_2P]^+$. . 42
3.4 Cationic part of the molecular structure of **4** in the solid state. 43
3.5 $^{31}P\{^1H\}$ VT NMR spectrum from the reaction of **VIIIa** with $[Ph_2P][OTf]$. 53
3.6 $^{31}P\{^1H\}$ NMR spectrum from the reaction of **VIIIa** with $[Ph_2P][OTf]$. 54
3.7 $^{31}P\{^1H\}$ NMR spectrum from the reaction of **VIIIa** with $[Ph_2P][OTf]$. 55
3.8 ^{31}P-^{31}P COSY NMR spectrum of **2a** and **3a** at -80 °C. 56
3.9 Simulation of the spin systems in the $^{31}P\{^1H\}$ NMR spectrum of compounds **2a** and **3a**. 57
3.10 $^{31}P\{^1H\}$ VT NMR spectrum of the reaction of **VIIIa** with $[Me_2P][OTf]$. 58
3.11 $^{31}P\{^1H\}$ NMR spectrum from the reaction of **VIIIa** with $[Me_2P][OTf]$. 59
3.12 ^{31}P-^{31}P COSY NMR spectrum of **2b** and **3b** at -80 °C. 60

3.13 Simulation of the spin systems in the $^{31}P\{^{1}H\}$ NMR spectrum of compounds **2b** and **3b** 61
3.14 Simulation (inverted) of the $^{31}\{^{1}H\}$ NMR spectrum of **1**. 62
3.15 $^{31}P\{^{1}H\}$ NMR spectrum from the reaction of **VIIIa** with $[Ph_2P][PF_6]$. . 62
3.16 ^{31}P-^{31}P COSY NMR spectrum of **1** at room temperature. 63
3.17 Simulation of the $^{31}P\{^{1}H\}$ NMR spectrum of coordination mode 1 and 2 of $[Ph_2As][OTf]$ on **VIIIa**. 64
3.18 Comparison of the $^{31}P\{^{1}H\}$ NMR spectrum of coordination mode 1 and 2 of $[Ph_2As][OTf]$ on **VIIIa** at 193 K and room temperature. 64
3.19 $^{31}P\{^{1}H\}$ NMR spectrum from the reaction of **VIIIa** with $[Ph_2As][OTf]$. 65
3.20 ^{31}P-^{31}P COSY NMR spectrum of **4** at 273 K. 66
3.21 ^{31}P VT NMR spectrum of **4**. 67
3.22 ^{31}P NMR spectrum of **4**. 68
3.23 ^{1}H NMR spectrum of **4** in CD_2Cl_2 at room temperature. 69
3.24 Molecular structure of **3a** in the solid state. 72
3.25 Molecular structure of **1** in the solid state. 73
3.26 Molecular structure of **4** in the solid state. 74

4.1 Molecular structure of complex **5** (left) in the solid state (the isopropyl groups are omitted for clarity) and a view of the monomeric section of complex **5** (right). Hydrogen atoms are omitted for clarity. Selected bond lengths and angles are given in the Supporting Information. 85
4.2 Molecular structure of complex **6** in the solid state. Hydrogen atoms are removed for clarity. Selected bond lengths and angles are given in the Supporting Information. 86
4.3 Molecular structure of complex **7** in the solid state. Hydrogen atoms and the non-coordinating solvent molecules are removed for clarity. Selected bond distances and angles are given in the Supporting Information. 89
4.4 Molecular structure of complex **8** in the solid state. Hydrogen atoms and the non-coordinating solvent molecules are removed for clarity. Selected bond distances and angles are given in the Supporting Information. 91
4.5 Synthesis of complex **9** 91
4.6 Molecular structure of complex **9** (left) in the solid state. 93
4.7 UB97D optimized geometries of complex **7** and complex **8**. 94
4.8 QTAIM analysis of complex **7** and complex **8**. 95
4.9 ^{1}H NMR (400 MHz, 300 K, C_6D_6) spectrum of complex **5** taken from an *in situ* experiment. 102

4.10 $^{13}C\{^{1}H\}$ NMR spectrum (100 MHz, 298 K, C_6D_6) of complex **5** taken from an in situ experiment. The resonance for $Cp(CH_3)$ of both complex **5** and excess $[Cp^*Fe(\eta^5\text{-}P_5)]$ is at the same position at 10.6 ppm. Also, the peak at 10.6 ppm is slightly broad indicating presence of more than one peak. 103
4.11 ^{1}H NMR (400 MHz, 300 K, C_6D_6) spectrum of complex **6**. 103
4.12 Variable temperature ^{1}H NMR (400 MHz, toluene-d_8) spectrum of complex **6**. 104
4.13 ^{1}H NMR (400 MHz, 233 K, toluene-d_8) spectrum of complex **6**. 104
4.14 Cutout of aliphatic section of ^{1}H NMR (400 MHz, 233 K, toluene-d_8) spectrum of complex **6**. 105
4.15 Cutout of aliphatic section of ^{1}H NMR (400 MHz, 233 K, toluene-d_8) spectrum of complex **6**. 105
4.16 $^{31}P\{^{1}H\}$ NMR (400 MHz, 300 K, toluene-d_8) spectrum of complex **6**. . 106
4.17 Variable temperature $^{31}P\{^{1}H\}$ NMR (400 MHz, toluene-d_8) spectrum of complex **6**. 106
4.18 $^{31}P\{^{1}H\}$ NMR (400 MHz, 233 K, toluene-d_8) spectrum of complex **6**. . 107
4.19 ^{1}H NMR (400 MHz, 233 K, C_6D_6) spectrum of complex **7**. + = residual toluene 107
4.20 $^{31}P\{^{1}H\}$ NMR (162 MHz, 298 K, toluene-d_8) spectrum of complex **7**. . 108
4.21 Variable temperature $^{31}P\{^{1}H\}$ NMR (162 MHz, toluene-d_8) spectrum of complex **7**. 108
4.22 $^{13}C\{^{1}H\}$ NMR spectrum (100 MHz, 298 K, toluene-d_8) of complex **7**. . 109
4.23 ^{1}H NMR (400 MHz, 300 K, C_6D_6) spectrum of complex **8**. $*$ = residual toluene 109
4.24 $^{31}P\{^{1}H\}$ NMR (162 MHz, 298 K, toluene-d_8) spectrum of complex **8**. . 110
4.25 Variable temperature $^{31}P\{^{1}H\}$ NMR (162 MHz, toluene-d_8) spectrum of complex **8**. 110
4.26 $^{13}C\{^{1}H\}$ NMR spectrum (100 MHz, 298 K, C_6D_6) of complex **8**. . . . 111
4.27 ^{1}H NMR (400 MHz, 300 K, C_6D_6) spectrum of complex **9**. 111
4.28 $^{31}P\{^{1}H\}$ NMR (162 MHz, 298 K, toluene-d_8) spectrum of NMR scale reaction between $[(^{Dipp}BDI\text{-}Ca\text{-}H)_2]$ and P_4. 112
4.29 $^{31}P\{^{1}H\}$ NMR (162 MHz, 298 K, toluene-d_8) spectrum of complex **9**. . 112
4.30 Variable temperature $^{31}P\{^{1}H\}$ NMR (162 MHz, toluene-d_8) spectrum of complex **9**. 113
4.31 $^{31}P\{^{1}H\}$ NMR (162 MHz, toluene-d_8) spectrum of complex **9**. 113
4.32 $^{13}C\{^{1}H\}$ NMR spectrum (100 MHz, 298 K, C_6D_6) of complex **9**. . . . 114

4.33 ^{31}P NMR of the reaction solution (toluene with D_2O capillary) with simulation (inverted) of the spin system. The singlet at 152 ppm is attributed to residual pentaphosphaferrocene, while the monomeric form of **5** shows up as an AMM'XX' spin system. 115
4.34 ^{31}P NMR spectra (experiment top, simulation bottom) of compound **6** in toluene-d_8 at 233 K, showing the ADMOX spin system of **6**. 116
4.35 Molecular structure of **5** in the solid state. 122
4.36 Molecular structure of **6** in the solid state. 122
4.37 Molecular structure of **7** in the solid state. 123
4.38 Molecular structure of **8** in the solid state. 123
4.39 Molecular structure of **9** in the solid state. 124
4.40 UB97D optimized geometries of complex **8**. 125
4.41 Selected Kohn-Sham orbitals (top view) of UB97D/6-31G**/LANL2DZ optimized geometry of complex **7**. 125
4.42 Selected Kohn-Sham orbitals (top view) of UB97D/6-31G**/LANL2DZ optimized geometry of complex **8**. 126

5.1 General depiction of a nucleophilic attack on **XXVII** with consecutive quenching by an electrophile (right) and attack of an electrophile (left). The 1,1 functionalized compound is utilized to synthesize asymmetrically substituted phosphines, while **XXVII** is regenerated from the reaction mixture by reaction with more white phosphorus (Bn = CH_2Ph = CH_2-C_6H_5). 133
5.2 ^{31}P NMR spectrum of **11a** in CD_2Cl_2 at room temperature. 135
5.3 VT ^{31}P $\{^1H\}$ NMR spectra of **10a** in CD_2Cl_2. 136
5.4 Molecular structures of **10a** and **11a** in the solid state. 138
5.5 Molecular structures of **12b** and **12a** in the solid state. 139
5.6 Molecular structures of **13** and **14** in the solid state. 143
5.7 $^{31}P\{^1H\}$ NMR spectrum of **15** in C_6D_6 at room temperature. 145
5.8 $^{31}P\{^1H\}$ NMR spectra of **16** and **19** in reaction and crystalline mixture. 149
5.9 Molecular structures of **18** and **21** in the solid state. 150
5.10 Structure of **22** in the solid state. 151
5.11 $^{31}P\{^1H\}$ NMR spectra of **23** and **24**. 153
5.12 $^{31}P\{^1H\}$ NMR spectrum of $[Cp^*Fe(\eta^{3:1}$-(1-Me-2-PPh_2-P_5))] (**11a**) at room temperature in C_6D_6. 171
5.13 ^{31}P NMR spectrum of $[Cp^*Fe(\eta^{3:1}$-(1-Me-2-PPh_2-P_5))] (**11a**) at room temperature in C_6D_6. 172

5.14 $^{31}P\{^{1}H\}$ NMR spectrum of $[Cp^{*}Fe(\eta^{3:1}\text{-}(1\text{-Me-2-}PPh_2\text{-}P_5))]$ (**11a**) at room temperature in CD_2Cl_2. 173
5.15 ^{31}P NMR spectrum (excerpts) of $[Cp^{*}Fe(\eta^{3:1}\text{-}(1\text{-Me-2-}PPh_2\text{-}P_5))]$ (**11a**) at room temperature in CD_2Cl_2 with simulation of the spin system. . . . 174
5.16 ^{1}H NMR spectrum of $[Cp^{*}Fe(\eta^{3:1}\text{-}(1\text{-Me-2-}PPh_2\text{-}P_5))]$ (**11a**) at room temperature in CD_2Cl_2. 175
5.17 $^{31}P\{^{1}H\}$ NMR spectrum of $[Cp^{*}Fe(\eta^{3:1}\text{-}(1\text{-}^{t}Bu\text{-2-}PPh_2\text{-}P_5))]$ (**11b**) at room temperature in CD_2Cl_2. The singlet at 152 ppm can be assigned to residual **XXVII**. 176
5.18 ^{31}P NMR spectrum of $[Cp^{*}Fe(\eta^{3:1}\text{-}(1\text{-}^{t}Bu\text{-2-}PPh_2\text{-}P_5))]$ (**11b**) at room temperature in CD_2Cl_2. The singlet at 152 ppm can be assigned to residual **XXVII**. 177
5.19 ^{1}H NMR spectrum of $[Cp^{*}Fe(\eta^{3:1}\text{-}(1\text{-}^{t}Bu\text{-2-}PPh_2\text{-}P_5))]$ (**11b**) at room temperature in CD_2Cl_2. 178
5.20 ^{31}P NMR spectrum (excerpts) of $[Cp^{*}Fe(\eta^{3:1}\text{-}(1\text{-}^{t}Bu\text{-2-}PPh_2\text{-}P_5))]$ (**11b**) at room temperature in CD_2Cl_2 with simulation of the spin system. . . . 179
5.21 ^{1}H NMR spectrum of $[Cp^{*}Fe(\eta^{4}\text{-}(1,1\text{-}CH_3\text{-}PPh_2\text{–}P_5))]$ (**10**) at -30 °C in CD_2Cl_2. 180
5.22 $^{31}P\{^{1}H\}$ NMR spectrum of $[Cp^{*}Fe(\eta^{4}\text{-}(1,1\text{-}CH_3\text{-}PPh_2\text{–}P_5))]$ (**10**) at -30 °C in CD_2Cl_2. The singlet at 152 ppm can be assigned to residual **XXVII**. 181
5.23 $^{31}P\{^{1}H\}$ NMR spectrum of $[Cp^{*}Fe(\eta^{4}\text{-}(1,1\text{-}CH_3\text{-}PPh_2\text{–}P_5))]$ (**10**) at -30 °C in CD_2Cl_2. 182
5.24 $^{31}P\{^{1}H\}$ NMR spectrum (excerpts) of $[Cp^{*}Fe(\eta^{4}\text{-}(1,1\text{-}CH_3\text{-}PPh_2\text{–}P_5))]$ (**10**) at -30 °C in CD_2Cl_2 with simulation of the spin system. 183
5.25 ^{1}H NMR spectrum of endo-$[Cp^{*}Fe(\eta^{4}\text{-}(1\text{-Me-1-}PCy_2\text{-}P_5))]$ (**12a**) at room temperature in CD_2Cl_2. 184
5.26 $^{31}P\{^{1}H\}$ NMR spectrum of endo-$[Cp^{*}Fe(\eta^{4}\text{-}(1\text{-Me-1-}PCy_2\text{-}P_5))]$ (**12a**) at room temperature in CD_2Cl_2. The singlet at 152 ppm can be assigned to residual **XXVII**. 185
5.27 ^{31}P NMR spectrum of endo-$[Cp^{*}Fe(\eta^{4}\text{-}(1\text{-Me-1-}PCy_2\text{-}P_5))]$ (**12a**) at room temperature in CD_2Cl_2. The singlet at 152 ppm can be assigned to residual **XXVII**. 186
5.28 ^{31}P NMR spectrum (excerpts) of endo-$[Cp^{*}Fe(\eta^{4}\text{-}(1\text{-Me-1-}PCy_2\text{-}P_5))]$ (**12a**) at room temperature in CD_2Cl_2 with simulation of the spin system. 187
5.29 ^{1}H NMR spectrum of exo-$[Cp^{*}Fe(\eta^{4}\text{-}(1,1\text{-}CH_3\text{-}PCy_2\text{–}P_5))]$ (**12b**) at room temperature in CD_2Cl_2. 188

5.30 $^{31}P\{^1H\}$ NMR spectrum of exo-[$Cp^*Fe(\eta^4$-(1, 1-CH_3-PCy_2–P_5))] (**12b**) at room temperature in CD_2Cl_2. The singlet at 152 ppm can be assigned to residual **XXVII**. 189
5.31 ^{31}P NMR spectrum of exo-[$Cp^*Fe(\eta^4$-(1, 1-CH_3-PCy_2–P_5))] (**12b**) at room temperature in CD_2Cl_2. The singlet at 152 ppm can be assigned to residual **XXVII**. 190
5.32 ^{31}P NMR spectrum (excerpts) of exo-[$Cp^*Fe(\eta^4$-(1, 1-CH_3-PCy_2–P_5))] (**12b**) at room temperature in CD_2Cl_2 with simulation of the spin system. 191
5.33 $^{31}P\{^1H\}$ NMR spectrum of [$Cp^*Fe(\eta^{1:1:1}$-(1-^{t}Bu-2-PPh_2-3-Me-4-PCy_2-P_5))] (**13**) at room temperature in toluene-d_8. 192
5.34 ^{31}P NMR spectrum of [$Cp^*Fe(\eta^{1:1:1}$-(1-^{t}Bu-2-PPh_2-3-Me-4-PCy_2-P_5))] (**13**) at room temperature in toluene-d_8. 193
5.35 ^1H NMR spectrum of [$Cp^*Fe(\eta^{1:1:1}$-(1-^{t}Bu-2-PPh_2-3-Me-4-PCy_2-P_5))] (**13**) at room temperature in toluene-d_8. 194
5.36 $^{31}P\{^1H\}$ NMR spectrum of the reaction solution from the reaction of **11a** with ^{t}BuLi and Cy_2PCl at room temperature in thf with D_2O capillary. With the three separated multiplets from 150 ppm to 165 ppm the ratios of the three reaction products can be roughly quantified. . . . 195
5.37 ^{31}P NMR spectrum of the reaction solution from the reaction of **11a** with ^{t}BuLi and Cy_2PCl at room temperature in thf with D_2O capillary. 196
5.38 $^{31}P\{^1H\}$ NMR spectrum of [$Cp^*Fe(\eta^{1:1:1}$-(1-^{t}Bu-2-P^{t}Bu$_2$-3-Me-4 -PPh_2-P_5))] (**15**) at room temperature in CH_2Cl_2. 197
5.39 ^{31}P NMR spectrum of [$Cp^*Fe(\eta^{1:1:1}$-(1-^{t}Bu-2-P^{t}Bu$_2$-3-Me-4-PPh_2-P_5))] (**15**) at room temperature in CH_2Cl_2. 198
5.40 ^{31}P NMR spectrum (excerpts) of [$Cp^*Fe(\eta^{1:1:1}$-(1-^{t}Bu-2-P^{t}Bu$_2$-3-Me-4-PPh_2-P_5))] (**15**) at room temperature in CD_2Cl_2 with simulation of the spin system. 199
5.41 ^1H NMR spectrum of [$Cp^*Fe(\eta^{1:1:1}$-(1-^{t}Bu-2-P^{t}Bu$_2$-3-Me-4-PPh_2-P_5))] (**15**) at room temperature in CH_2Cl_2. 200
5.42 $^{31}P\{^1H\}$ NMR study on stability of **12a** in solution at room temperature. 201
5.43 $^{31}P\{^1H\}$ NMR study on the influence of the steric bulk of the Cp ligand. 202
5.44 $^{31}P\{^1H\}$ NMR spectrum of the reaction of [$Cp^*Fe(\eta^4$-P_5CH_3)] with $(NEt_2)_2PCl$ at room temperature in CD_2Cl_2 (crystalline product mix). . 203
5.45 ^{31}P NMR spectrum of the reaction of [$Cp^*Fe(\eta^4$-P_5CH_3)] with $(NEt_2)_2PCl$ at room temperature in CD_2Cl_2 (crystalline product mix). . 204
5.46 ^1H NMR spectrum of the reaction of [$Cp^*Fe(\eta^4$-P_5CH_3)] with $(NEt_2)_2PCl$ at room temperature in CD_2Cl_2 (crystalline product mix). . 205

5.47 Excerpt with simulation of the $^{31}P\{^{1}H\}$ NMR spectrum of the reaction of $[Cp^{*}Fe(\eta^{4}\text{-}P_5CH_3)]$ with $(NEt_2)_2PCl$ in CD_2Cl_2 of the spin system of **19**. 206
5.48 Excerpt with simulation of the $^{31}P\{^{1}H\}$ NMR spectrum of the reaction of $[Cp^{*}Fe(\eta^{4}\text{-}P_5CH_3)]$ with $(NEt_2)_2PCl$ in CD_2Cl_2 of the spin system of **16**. 207
5.49 $^{31}P\{^{1}H\}$ NMR spectrum of $[Cp^{*}Fe(\eta^{3:1}\text{-}1\text{-}CH_3\text{-}2\text{-}C_{12}H_8P\text{-}P_5)]$ (**20**). . . 208
5.50 ^{31}P NMR spectrum of $[Cp^{*}Fe(\eta^{3:1}\text{-}1\text{-}CH_3\text{-}2\text{-}C_{12}H_8P\text{-}P_5)]$ (**20**). 209
5.51 Excerpt with simulation of the $^{31}P\{^{1}H\}$ NMR spectrum of (**20**) in thf with D_2O capillary). 210
5.52 $^{31}P\{^{1}H\}$ NMR spectrum of the reaction mix of $[Cp^{*}Fe(\eta^{4}\text{-}P_5CH_3)]$ with $^{t}Bu_2PCl$ at room temperature in thf with D_2O capillary. 211
5.53 ^{31}P NMR spectrum of the reaction mix of $[Cp^{*}Fe(\eta^{4}\text{-}P_5CH_3)]$ with $^{t}Bu_2PCl$ at room temperature in thf with D_2O capillary. 212
5.54 Excerpt with simulation of the $^{31}P\{^{1}H\}$ NMR spectrum of the reaction of $[Cp^{*}Fe(\eta^{4}\text{-}P_5CH_3)]$ with $^{t}Bu_2PCl$ in thf with D_2O capillary of the spin system of **17**. 213
5.55 ^{1}H NMR spectrum of the reaction of $[Cp^{*}Fe(\eta^{4}\text{-}P_5CH_3)]$ with $^{t}Bu_2PCl$ at room temperature in CD_2Cl_2 (crystalline product mix). 214
5.56 ^{31}P NMR spectrum of the reaction of $[Cp^{*}Fe(\eta^{4}\text{-}P_5CH_3)]$ with $^{t}Bu_2PCl$ at room temperature in CD_2Cl_2 (crystalline product mix). 215
5.57 $^{31}P\{^{1}H\}$ NMR spectrum of the reaction of $[Cp^{*}Fe(\eta^{4}\text{-}P_5CH_3)]$ with $^{t}Bu_2PCl$ at room temperature in CD_2Cl_2 (crystalline product mix). . . . 216
5.58 ^{31}P NMR spectrum of the reaction mix of $[Cp^{*}Fe(\eta^{4}\text{-}P_5CH_3)]$ with Mes_2PCl at room temperature in thf with D_2O capillary. 217
5.59 $^{31}P\{^{1}H\}$ NMR spectrum of the reaction of $[Cp^{*}Fe(\eta^{4}\text{-}P_5CH_3)]$ with $^{t}Bu_2PCl$ at room temperature in CD_2Cl_2 (crystalline product mix). . . . 218
5.60 ^{31}P-^{31}P-COSY NMR spectrum of the reaction of $[Cp^{*}Fe(\eta^{4}\text{-}P_5CH_3)]$ with $^{t}Bu_2PCl$ at room temperature in CD_2Cl_2 (crystalline product mix). 219
5.61 ^{31}P NMR spectrum of the reaction mix of $Li[Cp^{*}Fe(\eta^{4}\text{-}P_5{}^{t}Bu)]$ with $Cp^{*}PCl_2$ at room temperature in thf with D_2O capillary. 220
5.62 ^{31}P NMR spectrum of the reaction mix of $Li[Cp^{*}Fe(\eta^{4}\text{-}P_5{}^{t}Bu)]$ with Ph_2AsCl_2 at room temperature in in CD_2Cl_2. 221
5.63 ^{1}H NMR spectrum of the first product fraction from the column chromatography of $Li[Cp^{*}Fe(\eta^{4}\text{-}P_5{}^{t}Bu)]$ with Ph_2AsCl_2 at room temperature in C_6D_6. 222

5.64 ^{31}P NMR spectrum of the first product fraction from the column chromatography of Li[Cp*Fe(η^4-P$_5^t$Bu)] with Ph_2AsCl_2 at room temperature in C_6D_6. 223
5.65 ^{31}P{^{1}H} NMR spectrum of the first product fraction from the column chromatography of Li[Cp*Fe(η^4-P$_5^t$Bu)] with Ph_2AsCl_2 at room temperature in C_6D_6. 224
5.66 Molecular structure of **10** in the solid state. 231
5.67 Molecular structure of **11a** in the solid state. 232
5.68 Molecular structure of **11b** in the solid state. 233
5.69 Molecular structure of **12b** in the solid state. 234
5.70 Disorder of the Molecular structure of **11b** in the solid state. 235
5.71 Molecular structure of **12a** in the solid state. 236
5.72 Molecular structure of **13** in the solid state. 237
5.73 Molecular structure of **14** in the solid state (asymmetric unit). 238
5.74 Molecular structure of **14** in the solid state. 239
5.75 Molecular structure of **15** in the solid state. 240
5.76 Molecular structure of **17** in the solid state. 241
5.77 Molecular structure of **18** in the solid state. 242
5.78 Molecular structure of **19** in the solid state. 243
5.79 Molecular structure of **21** in the solid state. 244
5.80 Molecular structure of **22** in the solid state. 245
5.81 Disordered solid state structure of cocrystalized [Cp*Fe(η^4-(1, 2-(^{t}Bu$_2$-P$_5$)] and [Cp*Fe(η^4-(1, 3-(^{t}Bu$_2$-P$_5$)] 246
5.82 Molecular structures of **24** and **23** in the solid state. 247
5.83 Optimized geometries for isomers for [Cp*(η^4-P$_5$CH$_3$)]$^-$. 250
5.84 Optimized geometries for isomers for **11a**. 250
5.85 Optimized geometries for isomers for **12a** and **12b**. 250

6.1 Generalized activation and reaction pathway to earth alkaline metal anthracenides according to the novel synthetic pathway. 261
6.2 Molecular structures of **25** and **26** in the solid state. 264
6.3 Cyclic voltammogram of **11a** in dichloromethane 266
6.4 Molecular structure of **29** in the solid state. 268
6.5 Molecular structure of **30** in the solid state. 269
6.6 ^{1}H NMR spectrum of [Cp*Fe($\mu, \eta^{4:3}$-P$_5$)Mg(thf)$_3$] (**25**) at room temperature in thf-d$_8$. 280

6.7 ^{31}P NMR spectrum of $[Cp^*Fe(\mu,\eta^{4:3}\text{-}P_5)Mg(thf)_3]$ (**25**) at room temperature in thf-d_8. 281
6.8 ^{31}P NMR spectrum of $[Cp^*Fe(\mu,\eta^{4:3}\text{-}P_5)Mg(thf)_3]$ (**25**) at room temperature in thf-d_8. 282
6.9 Excerpt with simulation of the ^{31}P NMR spectrum of $[Cp^*Fe(\mu,\eta^{4:3}\text{-}P_5)Mg(thf)_3]$ (**25**) in thf-d_8 with simulation of the spin system. 283
6.10 $^{31}P\{^1H\}$ NMR spectrum of $[Cp^*Fe(\eta^4\text{-}P_5CH_3)]_2[Mg(dme)_3](dme)$ (**28**) at room temperature in thf with D_2O capillary. 284
6.11 ^{31}P NMR spectrum of a reaction mixture containing 1:1 $[Cp^*Fe(\eta^4\text{-}P_5CH_3)]_2[Mg(dme)_3](dme)$ (**28**) and **XXVII** in at room temperature in thf with D_2O capillary. 285
6.12 ^{1}H NMR spectrum of $[Cp^*Fe(\mu,\eta^{4:3}\text{-}P_5)Sr(thf)_4]_2\cdot(thf)_2$ (**26**) at room temperature in thf-d_8. 286
6.13 $^{31}P\{^1H\}$ NMR spectrum of $[Cp^*Fe(\mu,\eta^{4:3}\text{-}P_5)Sr(thf)_4]_2\cdot(thf)_2$ (**26**) at room temperature in thf-d_8. 287
6.14 ^{31}P NMR spectrum of $[Cp^*Fe(\mu,\eta^{4:3}\text{-}P_5)Sr(thf)_4]_2\cdot(thf)_2$ (**26**) at room temperature in thf-d_8. 288
6.15 Excerpt with simulation of the ^{31}P NMR spectrum of of $[Cp^*Fe(\mu,\eta^{4:3}\text{-}P_5)Sr(thf)_4]_2\cdot(thf)_2$ (**26**) at room temperature in thf-d_8 with simulation of the spin system. 289
6.16 ^{31}P NMR spectrum of $[\{Cp^*Fe\}_2(\mu_2\eta^{4:4:3:3}\text{-}P_{10})Ba(thf_3)]$ (**27**) in the reaction solution at room temperature (thf and D_2O capillary). 290
6.17 ^{31}P NMR spectrum of $[Cp^*Fe(\mu_3,\eta^{3:3:4}\text{-}(1\text{-}CH_3\text{-}2\text{-}PPh_2\text{-}P_5)_2)Mg(thf)_4]$ (**29**) in the reaction solution with the starting material **11a** still present at room temperature (thf and D_2O capillary) 291
6.18 ^{31}P NMR spectrum of $[Cp^*Fe(\mu,\eta^{3:2:2}\text{-}(1\text{-}CH_3\text{-}2\text{-}PPh_2\text{-}P_5))Sr(thf)_3]_2$ (**30**) in the reaction solution at room temperature (thf and D_2O capillary). For the reaction 5 equivalents of SrA were used. 292
6.19 Molecular structure of (**25**) in the solid state. 296
6.20 Asymmetric unit of the molecular structure of **28** in the solid state. . . . 297
6.21 Molecular structure of **28**. 298
6.22 Molecular structure of $[Cp^*Fe(\mu,\eta^{4:3}\text{-}P_5)Sr(thf)_4]_2(thf)_2$ (**26**) in the solid state. 299
6.23 Molecular structure of **27** in the solid state. 300
6.24 Excerpt from the molecular structure of **27** in the solid state. 301
6.25 Molecular structure of **31** in the solid state. 302
6.26 Molecular structure of (**29**) in the solid state. 303

6.27 Molecular structure of **30** in the solid state. 304

7.1 Structure of **33** in the solid state. 308
7.2 Molecular structure of **34** in the solid state. 309
7.3 Structure of **35** in the solid state. 310
7.4 ^{1}H NMR spectrum of $[Cp^{*}Fe\{\mu_5,\eta^{1:3:1:1}\text{-}(1\text{-}CH_3\text{-}2\text{-}PPh_2\text{-}P_5)\}(Ag(MeCN))_2]_n[SbF_6]_{2n}$ (**33**) in deuterated acetonitrile (solvent residue A). Traces of toluene (T) are visible in the spectrum along side the extremely broadened signals of **33**, marked with an asterisk. 315
7.5 ^{31}P NMR spectrum of $[Cp^{*}Fe\{\mu_5,\eta^{1:3:1:1}\text{-}(1\text{-}CH_3\text{-}2\text{-}PPh_2\text{-}P_5)\}(Ag(MeCN))_2]_n[SbF_6]_{2n}$ (**33**) in deuterated acetonitrile. The signals of **33** are extremely broadened and barely visible, with the exception of parts of a multiplett at 18 ppm, superimposed by an extremely broadened signal. 316
7.6 Detail of the molecular structure of **33** in the solid state. 319
7.7 Heavy atom backbone of the molecular structure of **33** in the solid state. 319
7.8 Molecular structure of **33** in the solid state. 320
7.9 Molecular structure of **34** in the solid state. 321
7.10 Molecular structure of **35** in the solid state. 322
7.11 Molecular structure of **36** in the solid state. 323
7.12 Molecular structure of **36** in the solid state with bond lenghts and angles. 324

8.1 Supramolecular aggregates of **11a**. 332
8.2 Structure of tetrameric **5**. 335

List of schemes

1.1 Overview of the conditions for phase transitions of the allotropes of phosphorus.[5] . . . 13
1.2 Industrial pathway of the synthesis of organophosphorus compounds. . 14
1.3 Stepwise activation of the P_4 tetrahedron, neglecting the charge. . . . 15
1.4 Synthesis of **VIIIa** over **XVa** (dme = dimethoxyethane). 18
1.5 Follow-up complexes of the decarbonylation of **VIIIb** to **XI**, **XII**, **XVII** and **XVIII**. 19
1.6 Reaction of **VIIIa** with Fe(II)-based Lewis acids. 21
1.7 Reduction and oxidation products of **XXVII**.[74,75] 22
1.8 Cyclic reaction pathway to asymmetrically substituted phosphines by consecutive functionalisation of **XXVII**. 23
1.9 Reactivity of **XXVII** towards main group electrophiles. 24
1.10 Preparation of phosphenium ions by halogen abstraction. 26
1.11 Possible reaction mechanisms for the formation of the phosphanylphosphonium salt **XXXI**.[96] 27
1.12 Exchange PPh_3 in **XXXIII** and exchange PMe_3 in **XXXIV**. 27
1.13 Insertion of the phosphenium ion $[Ph_2P]^+$ into the P_4 tetrahedron. . . . 28
1.14 Insertion of phosphenium ion $[R_2P]^+$ into $[Cp'''Ni(\eta^3\text{-}P_3)]$. 29
1.15 Reaction of reactive transition metal complex fragments with **XXXV**. . 29
1.16 Synthesis of the first molecular polyphosphides of a group 2 element observed in solution by *Hill et al.*.[132] 32

3.1 Selected compounds with a tetraphosphabicyclo[1.1.0] motif.[51,58,100] . 37
3.2 Reaction of **VIIIa** with in situ generated pnictogenium ions yielding the compounds mentioned in this paper. 39
3.3 Relative energies of starting material **VIIIa** and $[PPh_2]^+$, **3a** and its decarbonylation to **1** on the BP86/def2(SV(P) level. 44

4.1 (a) TM mediated P_4 functionalization and its further use as ligands and as phosphorus source, (b) group 2 complexes as reductant for organic substrates, (c) overview of this work. 82
4.2 Synthesis of the Mg-Fe organo-polyphosphide supramolecular complex **5**. 84
4.3 Synthesis of complex **6**. 86
4.4 Synthesis of complex **7**. 89
4.5 Synthesis of complex **8**. 90

5.1 *In situ* generation of $Li[Cp^*Fe(\eta^4\text{-}P_5R)]$ ($R = Me,\ ^tBu$) and quenching with R'_2PCl ($R' = Ph,\ Cy$). 134
5.2 Calculated energy profiles for the transition of the exo into the endo isomer of $Li[Cp^*Fe(\eta^4\text{-}P_5CH_3)]$. 140
5.3 Nucleophilic attack on **11a** (with MeLi) and **11b** (with t-BuLi). 142
5.4 Structures of P_7 moieties known in literature in comparison with the results from this work. 146
5.5 Reaction of $Li[Cp^*Fe(\eta^4\text{-}P_5CH_3)]$ with the chlorophosphines R_2PCl ($R = {}^tBu, Mes, NEt_2$) and 5-chloro-5H-dibenzophosphole. 148
5.6 Reaction of $Li[Cp^*Fe(\eta^4\text{-}P_5{}^tBu)]$ with Ph_2AsCl. 152

6.1 Reaction of **XXVII** with the earth alkali metal anthracenides. 263
6.2 Reaction of **11a** with several reducing agents. 267

8.1 Reaction of **VIII** with in situ generated phosphenium ions. 326
8.2 Stepwise decarbonylation of **3a** to **1**. 327
8.3 Reaction of **VIIIa** with in situ generated arsenium ions. 327
8.4 Products from quenching $[Cp^*Fe(\eta^4\text{-}P_5R)]^-$ ($R = Me, {}^tBu$, generated *in situ*) with different chlorophosphines. 329
8.5 Reaction of **VIII** with in situ generated phosphenium ions. 330
8.6 Reaction of **XXVII** with Mg(I) compounds. 334
8.7 Synthesis of $[(^{Dipp}BDI\text{-}Ca)_3(\mu, \eta^{2:2:2}\text{-}P_7)]$ (**9**). 335
8.8 Reaction of **XXVII** with $[SrA(thf)_2]$ and $[MgA(thf)_3]$. 336
8.9 Reaction of **11a** with $[SrA(thf)_2]$ and $[MgA(thf)_3]$. 337

List of Tables

3.1 $^{31}P\{^{1}H\}$ NMR data of **2a**: (CD_2Cl_2; 193 K): 50
3.2 $^{31}P\{^{1}H\}$ NMR data of **3a**: (CD_2Cl_2; 193 K): 50
3.3 $^{31}P\{^{1}H\}$ NMR data of **2b**: (CD_2Cl_2; 193 K): 50
3.4 $^{31}P\{^{1}H\}$ NMR data of **3b**: (CD_2Cl_2; 193 K): 51
3.5 $^{31}P\{^{1}H\}$ NMR data of **1**: (CD_2Cl_2; 300 K): 51
3.6 $^{31}P\{^{1}H\}$ NMR data of coordination mode 1 of $[Ph_2As][OTf]$ on **VIIIa** from the simulation (in CD_2Cl_2 at -80 °C). 51
3.7 $^{31}P\{^{1}H\}$ NMR data of coordination mode 2 of $[Ph_2As][OTf]$ on **VIII** from the simulation (in CD_2Cl_2 at -80 °C). 52
3.8 ^{31}P NMR data of **4**: (CD_2Cl_2; 273 K): 52
3.9 Crystallographic data for **1**, **3a** and **4**: 71
3.10 **VIIIa**, **2a**, **3a**, the decarbonlyated form of **3a**, **1**, CO and $[Ph_2P]^+$ (T=298,15 K; Energies are given in Hartree) 75

4.1 Topological parameters of electron density: electron density [$\rho(r)$], its Laplacian distribution [$\nabla^2\rho(r)$], potential energy density [$V(r)$], and kinetic energy density [$G(r)$] at the selected bond critical points (3,-1). All parameters are in atomic units (a.u). 95
4.2 Chemical shifts and coupling constants of the AMM'XX' spin system in the ^{31}P-NMR spectrum of **5** shown in figure 4.33. The multiplets are assigned to the phosphorus atoms in the simplified excerpt of the tetrameric structure in the solid phase shown in figure 4.35. 115
4.3 Chemical shifts and coupling constants of the ADMOX spin system in the $^{31}P\{^{1}H\}$-NMR spectrum of **6** at -40 °C (in toluene-d8) and assignment of the P atoms from the solid state structure to the spin system. . . 116
4.4 Results of the DOSY measurements at 298 K and 600 MHz in C_6D_6 . . 118
4.5 Crystallographic data for **5**, **6** and **7**: 120
4.6 Crystallographic data for **8** and **9**: 121

4.7 Free energies and enthalpies of Complexes **7Mg**, **8Ca**,**7Ca** and **8Mg**: . . 126

5.1 Crystallographic data for **10**, **11a** and **11b**: 226
5.2 Crystallographic data for **12b**, **12a** and **13**: 227
5.3 Crystallographic data for **14** and **15**: 228
5.4 Crystallographic data for **17**, **18** and **19**: 229
5.5 Crystallographic data for **21**, **22** and **23** and **24**: 230
5.6 Free energies and enthalpies of isomers for $[\mathrm{Cp^*}(\eta^4\text{-}\mathrm{P_5CH_3})]^-$ (Energies given in Hartree: 248
5.7 Free energies and enthalpies for the 1,2-migration in and isomers of **10** and **11a** (Energies given in Hartree: 249
5.8 Free energies and enthalpies for the 1,2-migration in and isomers of **12a** and **12b** (Energies given in Hartree: 249

6.1 Crystallographic data for **25**, **26** and **27**: 293
6.2 Crystallographic data for **28** and **29** : 294
6.3 Crystallographic data for **30** and **31**: 295

7.1 Crystallographic data for **33** and **34**: 317
7.2 Crystallographic data for **35** and **36**: 318

Bibliography

[1] R. Hooke, *Lectures and collections made by Robert Hooke*, John Martyn, **1635-1703**.

[2] R. Boyle, Robert Boyle's way of making phosphorus, From The Royal Society, CLP/11i/21, **1680**.

[3] G. W. Leibniz, *Miscellanea Berolinensia ad incrementum scientiarum*, *Vol. 1*, Historia inventionis phosphori, J. C. Papen, Berlin, **1710**, pp. 91–98.

[4] J. R. Partington, *Science Progress* **1936**, *30*, 402–412.

[5] A. F. Hollemann, N. Wiberg, E. Wiberg, *Lehrbuch der Anorganischen Chemie*, 102. Auflage, Walter de Gruyter, **2007**.

[6] K. Ashley, D. Cordell, D. Mavinic, *Chemosphere* **2011**, *84*, 737–746.

[7] E. Mitscherlich, *Lehrbuch der Chemie - 1. Band: Die Metalloide*, 4. Auflage, E.S. Mittler, Berlin, **1844**.

[8] C. W. Scheele, *Der Königl. Schwedischen Akademie der Wissenschaften neue Abhandlungen aus der Naturlehre aus dem Jahre 1771*, Untersuchung des Flussspats und dessen Säure, H. H. Holle, Leipzig, **1773**, pp. 122–139.

[9] *Nature* **1880**, *21*, translation from swedish article, 518–521.

[10] A. Lennartson, *The Chemical Works of Carl Wilhelm Scheele*, 1st Ed., Springer, **2017**.

[11] C. W. Scheele, *Nya lärda tidningar* **1774**, *1*, german translation in "Nachgelassene Briefe und Aufzeichnungen", 108–110.

[12] C. W. Scheele, A. Nordenskiöld, *Nachgelassene Briefe und Aufzeichnungen*, 1st Ed., Letter from Scheele to Gahn from 1770, P. A. Norstedt & söner, Stockholm, **1892**, pp. 37–50.

[13] L. Rosenstein, *J. Am. Chem. Soc.* **1920**, *42*, 883–889.

[14] J. Plutnar, Z. Sofer, M. Pumera, *RSC Adv.* **2020**, *10*, 36452–36458.

[15] A. K. Greaves, R. J. Letcher, *Bull. Environ. Contam. Toxicol.* **2017**, *98*, 2–7.

[16] I. van der Veen, J. de Boer, *Chemosphere* **2012**, *88*, 1119–1153.

[17] M. Venier, A. Dove, K. Romanak, S. Backus, R. Hites, *Environ. Sci. Technol.* **2014**, *48*, 9563–9572.

[18] A. Abu-Qare, M. Abou-Donia, *Food Chem. Toxicol.* **2002**, *40*, 1327–1333.

[19] J. Downing, M. Smith in *Comprehensive Coordination Chemistry II*, (Eds.: J. A. McCleverty, T. J. Meyer), Pergamon, Oxford, **2003**, pp. 253–296.

[20] A. L. Clevenger, R. M. Stolley, J. Aderibigbe, J. Louie, *Chem. Rev.* **2020**, *120*, 6124–6196.

[21] G. R. F. Orton, B. S. Pilgrim, N. R. Champness, *Chem. Soc. Rev.* **2021**, *50*, 4411–4431.

[22] D. H. Valentine Jr, J. H. Hillhouse, *Synthesis* **2003**, *2003*, 0317–0334.

[23] B. M. Cossairt, N. A. Piro, C. C. Cummins, *Chem. Rev.* **2010**, *110*, 4164–4177.

[24] M. Scheer, G. Balázs, A. Seitz, *Chem. Rev.* **2010**, *110*, 4236–4256.

[25] M. Caporali, L. Gonsalvi, A. Rossin, M. Peruzzini, *Chem. Rev.* **2010**, *110*, 4178–4235.

[26] S. Khan, S. S. Sen, H. W. Roesky, *Chem. Commun.* **2012**, *48*, 2169–2179.

[27] J. E. Borger, M. K. Jongkind, A. W. Ehlers, M. Lutz, J. C. Slootweg, K. Lammertsma, *ChemistryOpen* **2017**, *6*, 350–353.

[28] L. Giusti, V. R. Landaeta, M. Vanni, J. A. Kelly, R. Wolf, M. Caporali, *Coord. Chem. Rev.* **2021**, *441*, 213927.

[29] M. Till, J. Cammarata, R. Wolf, D. J. Scott, *Chem. Commun.* **2022**, *58*, 8986–8989.

[30] M. Till, V. Streitferdt, D. J. Scott, M. Mende, R. M. Gschwind, R. Wolf, *Chem. Commun.* **2022**, *58*, 1100–1103.

[31] R. Rothfelder, V. Streitferdt, U. Lennert, J. Cammarata, D. J. Scott, K. Zeitler, R. M. Gschwind, R. Wolf, *Angew. Chem. Int. Ed.* **2021**, *60*, 24650–24658.

[32] J. Cammarata, D. J. Scott, R. Wolf, *Chem. Eur. J.*, *28*, e202202456.

[33] M. Donath, K. Schwedtmann, T. Schneider, F. Hennersdorf, A. Bauzá, A. Frontera, J. J. Weigand, *Nat. Chem.* **2022**, *14*, 384–391.

[34] P. B. Arockiam, U. Lennert, C. Graf, R. Rothfelder, D. J. Scott, T. G. Fischer, K. Zeitler, R. Wolf, *Chem. Eur. J.* **2020**, *26*, 16374–16382.

[35] U. Lennert, P. B. Arockiam, V. Streitferdt, D. J. Scott, C. Rödl, R. M. Gschwind, R. Wolf, *Nat. Chem.* **2019**, *2*, 1101–1106.

[36] S. K. Ghosh, C. C. Cummins, J. A. Gladysz, *Org. Chem. Front.* **2018**, *5*, 3421–3429.

[37] B. M. Cossairt, C. C. Cummins, *New J. Chem.* **2010**, *34*, 1533–1536.

[38] D. G. Yakhvarov, E. V. Gorbachuk, R. M. Kagirov, O. G. Sinyashin, *Russ. Chem. Bull.* **2012**, *61*, 1300–1312.

[39] D. Sarkar, C. Weetman, D. Munz, S. Inoue, *Angew. Chem. Int. Ed.* **2021**, *60*, 3519–3523.

[40] D. J. Scott, J. Cammarata, M. Schimpf, R. Wolf, *Nat. Chem.* **2021**, *13*, 458–464.

[41] M. Baudler, *Angew. Chem. Int. Ed.* **1987**, *26*, 419–441.

[42] M. Baudler, *Angew. Chem. Int. Ed.* **1982**, *21*, 492–512.

[43] M. Baudler, M. Warnau, D. Koch, *Chem. Ber.* **1978**, *111*, 3838–3842.

[44] M. Baudler, C. Gruner, *Z. Naturforsch. B* **1976**, *31*, 1311–1312.

[45] A. Zheng, S.-B. Liu, F. Deng, *Chem. Rev.* **2017**, *117*, 12475–12531.

[46] A. Dransfeld, P. v. Ragué Schleyer, *Magn. Reson. Chem.* **1998**, *36*, S29–S43.

[47] I. Y. Chernyshov, M. V. Vener, I. G. Shenderovich, *J. Chem. Phys.* **2019**, *150*, 144706.

[48] J. G. J. Raj, *Rev. Inorg. Chem.* **2015**, *35*, 25–56.

[49] K. Moedritzer, L. Maier, L. C. D. Groenweghe, *J. Chem. Eng. Data* . **1962**, *7*, 307–310.

[50] L. Tang, J. R. Norton, *Macromolecules* **2004**, *37*, 241–243.

[51] A. P. Ginsberg, W. E. Lindsell, *J. Am. Chem. Soc.* **1971**, *93*, 2082–2084.

[52] P. Dapporto, S. Midollini, L. Sacconi, *Angew. Chem. Int. Ed.* **1979**, *18*, 469–469.

[53] T. Gröer, G. Baum, M. Scheer, *Organometallics* **1998**, *17*, 5916–5919.

[54] M. Peruzzini, L. Marvelli, A. Romerosa, R. Rossi, F. Vizza, F. Zanobini, *Eur. J. Inorg. Chem.* **1999**, *1999*, 931–933.

[55] I. Krossing, L. van Wüllen, *Chem. Eur. J.* **2002**, *8*, 700–711.

[56] R. Riedel, H.-D. Hausen, E. Fluck, *Angew. Chem.* **1985**, *97*, 1050–1050.

[57] B. M. Cossairt, C. C. Cummins, *New J. Chem.* **2010**, *34*, 1533–1536.

[58] O. J. Scherer, T. Hilt, G. Wolmershäuser, *Organometallics* **1998**, *17*, 4110–4112.

[59] O. J. Scherer, G. Schwarz, G. Wolmershäuser, *Z. Anorg. Allg. Chem.* **1995**, *622*, 951–957.

[60] O. J. Scherer, J. Vondung, G. Wolmershäuser, *Angew. Chem. Int. Ed.* **1989**, *28*, 1355–1357.

[61] W. W. Seidel, O. T. Summerscales, B. O. Patrick, M. D. Fryzuk, *Angew. Chem.* **2008**, *121*, 121–123.

[62] J. D. Masuda, W. W. Schoeller, B. Donnadieu, G. Bertrand, *Angew. Chem. Int. Ed.* **2007**, *46*, 7052–7055.

[63] O. Back, G. Kuchenbeiser, B. Donnadieu, G. Bertrand, *Angew. Chem. Int. Ed.* **2009**, *48*, 5530–5533.

[64] C. Schwarzmaier, A. Y. Timoshkin, G. Balázs, M. Scheer, *Angew. Chem. Int. Ed.* **2014**, *53*, 9077–9081.

[65] M. D. Eberl, Dissertation, Universität Regensburg, **2011**.

[66] C. Schwarzmaier, Dissertation, Universität Regensburg, **2012**.

[67] C. Schwarzmaier, S. Heinl, G. Balázs, M. Scheer, *Angew. Chem. Int. Ed.* **2015**, *54*, 13116–13121.

[68] J. Müller, S. Heinl, C. Schwarzmaier, G. Balázs, M. Keilwerth, K. Meyer, M. Scheer, *Angew. Chem.* **2017**, *129*, 7418–7423.

[69] O. J. Scherer, T. Brück, *Angew. Chem. Int. Ed.* **1987**, *26*, 59–59.

[70] F. Dielmann, R. Merkle, S. Heinl, M. Scheer, *Z. Naturforsch. B* **2009**, *64*, 3–10.

[71] O. J. Scherer, T. Brück, G. Wolmershäuser, *Chem. Ber.* **1989**, *122*, 2049–2054.

[72] M. Fleischmann, J. S. Jones, F. P. Gabbaï, M. Scheer, *Chem. Sci.* **2015**, *6*, 132–139.

[73] C. Heinl, E. Peresypkina, G. Balázs, E. Mädl, A. V. Virovets, M. Scheer, *Chem. Eur. J.* **2021**, *27*, 7542–7548.

[74] R. F. Winter, W. E. Geiger, *Organometallics* **1999**, *18*, 1827–1833.

[75] M. V. Butovskiy, G. Balázs, M. Bodensteiner, E. V. Peresypkina, A. V. Virovets, J. Sutter, M. Scheer, *Angew. Chem. Int. Ed.* **2013**, *52*, 2972–2976.

[76] S. Reichl, E. Mädl, F. Riedlberger, M. Piesch, G. Balázs, M. Seidl, M. Scheer, *Nat. Commun.* **2021**, *12*, 5774.

[77] E. Mädl, M. V. Butovskii, G. Balázs, E. V. Peresypkina, A. V. Virovets, M. Seidl, M. Scheer, *Angew. Chem. Int. Ed.* **2014**, *53*, 7643–7646.

[78] C. Riesinger, G. Balázs, M. Bodensteiner, M. Scheer, *Angew. Chem. Int. Ed.* **2020**, *59*, 23879–23884.

[79] C. Riesinger, G. Balázs, M. Seidl, M. Scheer, *Chem. Sci.* **2021**, *12*, 13037–13044.

[80] M. Scheer, A. Schindler, C. Gröger, A. Virovets, E. Peresypkina, *Angew. Chem. Int. Ed.* **2009**, *48*, 5046–5049.

[81] C. Heindl, E. V. Peresypkina, A. V. Virovets, W. Kremer, M. Scheer, *J. Am. Chem. Soc.* **2015**, *137*, 10938–10941.

[82] E. Peresypkina, C. Heindl, A. Virovets, H. Brake, E. Mädl, M. Scheer, *Chem. Eur. J.* **2018**, *24*, 2503–2508.

[83] J. Bai, A. V. Virovets, M. Scheer, *Science* **2003**, *300*, 781–783.

[84] F. Dielmann, M. Fleischmann, C. Heindl, E. V. Peresypkina, A. V. Virovets, R. M. Gschwind, M. Scheer, *Chem. Eur. J.* **2015**, *21*, 6208–6214.

[85] A. Schindler, C. Heindl, G. Balázs, C. Gröger, A. V. Virovets, E. V. Peresypkina, M. Scheer, *Chem. Eur. J.* **2012**, *18*, 829–835.

[86] M. Scheer, A. Schindler, R. Merkle, B. P. Johnson, M. Linseis, R. Winter, C. E. Anson, A. V. Virovets, *J. Am. Chem. Soc.* **2007**, *129*, 13386–13387.

[87] C. Heindl, E. Peresypkina, A. V. Virovets, I. S. Bushmarinov, M. G. Medvedev, B. Krämer, B. Dittrich, M. Scheer, *Angew. Chem. Int. Ed.* **2017**, *56*, 13237–13243.

[88] E. Peresypkina, A. Virovets, M. Scheer, *Cryst. Growth Des.* **2016**, *16*, 2335–2341.

[89] E. Peresypkina, K. Grill, B. Hiltl, A. V. Virovets, W. Kremer, J. Hilgert, W. Tremel, M. Scheer, *Angew. Chem. Int. Ed.* **2021**, *60*, 12132–12142.

[90] M. Scheer, L. J. Gregoriades, A. V. Virovets, W. Kunz, R. Neueder, I. Krossing, *Angew. Chem. Int. Ed.* **2006**, *45*, 5689–5693.

[91] A. H. Cowley, R. A. Kemp, *Chem. Rev.* **1985**, *85*, 367–382.

[92] A. H. Cowley, M. C. Cushner, J. S. Szobota, *J. Am. Chem. Soc.* **1978**, *100*, 7784–7786.

[93] D. Gudat, *Coord. Chem. Rev.* **1997**, *163*, 71–106.

[94] C. A. Dyker, N. Burford, *Chem. Asian J.* **2007**, *3*, 28–36.

[95] N. Burford, T. S. Cameron, D. J. LeBlanc, P. Losier, S. Sereda, G. Wu, *Organometallics* **1997**, *16*, 4712–4717.

[96] M. H. Holthausen, J. J. Weigand, *Chem. Soc. Rev.* **2014**, *43*, 6639–6657.

[97] N. Burford, T. S. Cameron, P. J. Ragogna, E. Ocando-Mavarez, M. Gee, R. McDonald, R. E. Wasylishen, *J. Am. Chem. Soc.* **2001**, *123*, 7947–7948.

[98] J. M. Slattery, C. Fish, M. Green, T. N. Hooper, J. C. Jeffery, R. J. Kilby, J. M. Lynam, J. E. McGrady, D. A. Pantazis, C. A. Russell, C. E. Willans, *Chem. Eur. J.* **2007**, *13*, 6967–6974.

[99] M. B. Abrams, B. L. Scott, R. T. Baker, *Organometallics* **2000**, *19*, 4944–4956.

[100] J. Weigand, M. Holthausen, R. Fröhlich, *Angew. Chem. Int. Ed.* **2009**, *48*, 295–298.

[101] J. J. Weigand, N. Burford, M. D. Lumsden, A. Decken, *Angew. Chem. Int. Ed.* **2006**, *45*, 6733–6737.

[102] S. S. Chitnis, E. MacDonald, N. Burford, U. Werner-Zwanziger, R. McDonald, *Chem. Commun.* **2012**, *48*, 7359–7361.

[103] J. M. F. Braddock, G. E. Coates, *J. Chem. Soc.* **1961**, 3208–3211.

[104] K. A. Porter, A. C. Willis, J. Zank, S. B. Wild, *Inorg. Chem* **2002**, *41*, 6380–6386.

[105] H. Althaus, H. J. Breunig, E. Lork, *Chem. Commun.* **1999**, 1971–1972.

[106] N. L. Kilah, S. Petrie, R. Stranger, J. W. Wielandt, A. C. Willis, S. B. Wild, *Organometallics* **2007**, *26*, 6106–6113.

[107] C. Riesinger, L. Dütsch, G. Balázs, M. Bodensteiner, M. Scheer, *Chem. Eur. J.* **2020**, *26*, 17165–17170.

[108] A. K. Adhikari, C. G. P. Ziegler, K. Schwedtmann, C. Taube, J. J. Weigand, R. Wolf, *Angew. Chem. Int. Ed.* **2019**, *58*, 18584–18590.

[109] J. A. Wanklyn, *Liebigs Ann. Chem.* **1866**, *140*, 353–356.

[110] V. Grignard, *Ann. Chim.* **1901**, *24*, 433–490.

[111] W. Schlenk, W. Schlenk jun., *Ber. Dtsch. Chem. Ges* **1929**, *62*, 920–924.

[112] R. Fischer, H. Görls, P. R. Meisinger, R. Suxdorf, M. Westerhausen, *Chem. Eur. J.* **2019**, *25*, 12830–12841.

[113] E. Beckmann, *Chem. Ber.* **1905**, *38*, 904–906.

[114] H. Gilman, F. Schulze, *J. Am. Chem. Soc.* **1926**, *48*, 2463–2467.

[115] K. Mochida, T. Yamanishi, *J. Organomet. Chem.* **1987**, *332*, 247–252.

[116] K. Mochida, S.-i. Ogura, T. Yamanishi, *Bull. Chem. Soc. Jpn.* **1986**, *59*, 2633–2634.

[117] M. Chastrette, R. Gauthier, *J. Organomet. Chem.* **1974**, *71*, 11–15.

[118] N. Kawabata, H. Nakamura, S. Yamashita, *J. Org. Chem.* **1973**, *38*, 3403–3406.

[119] D. Bryce-Smith, A. C. Skinner, *J. Chem. Soc.* **1963**, 577–585.

[120] D. A. J. Payne, R. T. Sanderson, *J. Am. Chem. Soc.* **1958**, *80*, 5324–5324.

[121] B. Wakefield in *Alkyl Derivatives of the Group II Metals*, (Eds.: H. Emeléus, A. Sharpe), Advances in Inorganic Chemistry and Radiochemistry, Academic Press, **1968**, pp. 341–425.

[122] F. Hart, A. Massey, M. S. Saran, *J. Organomet. Chem.* **1970**, *21*, 147–154.

[123] F. Kaufmann, A. Geraudelle, B. Kaempf, F. Schué, A. Deluzarche, A. Maillard, *J. Organomet. Chem.* **1970**, *24*, 13–31.

[124] F. G. N. Cloke, P. B. Hitchcock, M. F. Lappert, G. A. Lawless, B. Royo, *J. Chem. Soc., Chem. Commun.* **1991**, 724–726.

[125] B. M. Wolf, C. Stuhl, C. Maichle-Mössmer, R. Anwander, *J. Am. Chem. Soc.* **2018**, *140*, 2373–2383.

[126] S. P. Green, C. Jones, A. Stasch, *Science* **2007**, *318*, 1754–1757.

[127] A. Stasch, C. Jones, *Dalton Trans.* **2011**, *40*, 5659–5672.

[128] C. Jones, *Nat. Rev. Chem.* **2017**, *1*, 1–9.

[129] M. R. Crimmin, A. G. M. Barrett, M. S. Hill, P. B. Hitchcock, P. A. Procopiou, *Organometallics* **2007**, *26*, 2953–2956.

[130] B. Rösch, T. X. Gentner, H. Elsen, C. A. Fischer, J. Langer, M. Wiesinger, S. Harder, *Angew. Chem. Int. Ed.* **2019**, *58*, 5396–5401.

[131] T. X. Gentner, B. Rösch, K. Thum, J. Langer, G. Ballmann, J. Pahl, W. A. Donaubauer, F. Hampel, S. Harder, *Organometallics* **2019**, *38*, 2485–2493.

[132] M. Arrowsmith, M. S. Hill, A. L. Johnson, G. Kociok-Köhn, M. F. Mahon, *Angew. Chem. Int. Ed.* **2015**, *54*, 7882–7885.

[133] M. Westerhausen, H.-D. Hausen, W. Schwarz, *Z. anorg. allg.* **1995**, *621*, 877–888.

[134] M. Westerhausen, E. Markus M., W. Schwarz, *J. Organomet. Chem.* **1995**, *491*, 83–90.

[135] M. Westerhausen, M. H. Digeser, H. Nöth, J. Knizek, *Z. anorg. allg.* **1998**, *624*, 215–220.

[136] S. Blair, K. Izod, W. Clegg, R. W. Harrington, *Inorg. Chem.* **2004**, *43*, 8526–8531.

[137] S. Gärtner, N. Korber in *Zintl Ions: Principles and Recent Developments*, Springer Berlin Heidelberg, Berlin, Heidelberg, **2011**, pp. 25–57.

[138] W. Dahlmann, H. G. v. Schnering, *Naturwissenschaften* **1972**, *59*, 420.

[139] W. Dahlmann, H. G. v. Schnering, *Naturwissenschaften* **1973**, *60*, 429.

[140] H.-G. von Schnering, M. Wittmann, D. Sommer, *Z. anorg. allg.* **1984**, *510*, 61–71.

[141] B. Eisenmann, U. Rößler, *Z. anorg. allg.* **2003**, *629*, 459–462.

[142] N. Korber, J. Daniels, *Z. anorg. allg.* **1999**, *625*, 189–191.

[143] N. Korber, J. Daniels, *Z. anorg. allg.* **1996**, *622*, 1833–1838.

[144] N. Korber, J. Daniels, *Inorg. Chem.* **1997**, *36*, 4906–4908.

[145] M. Westerhausen, M. Krofta, A. Pfitzner, *Inorg. Chem.* **1999**, *38*, 598–599.

[146] J.-A. Dolyniuk, K. Kovnir, *Crystals* **2013**, *3*, 431–442.

[147] A. Haffner, V. Weippert, D. Johrendt, *Z. anorg. allg.* **2020**, *646*, 120–124.

[148] M. Westerhausen, C. Birg, M. Krofta, P. Mayer, T. Seifert, H. Nöth, A. Pfitzner, T. Nilges, H.-J. Deiseroth, *Z. anorg. allg.* **2000**, *626*, 1073–1080.

[149] M. Weber, G. Balázs, A. V. Virovets, E. Peresypkina, M. Scheer, *Molecules* **2021**, *26*.

[150] C. Schwarzmaier, A. Y. Timoshkin, G. Balázs, M. Scheer, *Angew. Chem. Int. Ed.* **2014**, *53*, 9077–9081.

[151] J. Müller, M. Scheer, *Chem. Eur. J.* **2021**, *27*, 3675–3681.

[152] J. Müller, G. Balázs, M. Scheer, *Chem. Commun.* **2021**, *57*, 2257–2260.

[153] R. Grünbauer, C. Schwarzmaier, M. Eberl, G. Balázs, M. Scheer, *Inorg. Chim. Acta* **2021**, *518*, 120234.

[154] C. Schwarzmaier, S. Heinl, G. Balázs, M. Scheer, *Angew. Chem. Int. Ed.* **2015**, *54*, 13116–13121.

[155] C. Schwarzmeier, PhD thesis, University of Regensburg, **2012**.

[156] S. Reichl, R. Grünbauer, G. Balázs, M. Scheer, *Chem. Commun.* **2021**, *57*, 3383–3386.

[157] R. Grünbauer, G. Balázs, M. Scheer, *Chem. Eur. J.* **2020**, *26*, 11722–11726.

[158] N. Burford, P. J. Ragogna, R. McDonald, M. J. Ferguson, *J. Am. Chem. Soc.* **2003**, *125*, 14404–14410.

[159] J. J. Weigand, N. Burford, R. J. Davidson, T. S. Cameron, P. Seelheim, *J. Am. Chem. Soc.* **2009**, *131*, 17943–17953.

[160] I. Krossing, I. Raabe, *Angew. Chem. Int. Ed.* **2001**, *40*, 4406–4409.

[161] N. L. Kilah, S. Petrie, R. Stranger, J. W. Wielandt, A. C. Willis, S. B. Wild, *Organometallics* **2007**, *26*, 6106–6113.

[162] H. J. Bernstein, J. A. Pople, W. G. Schneider, *Can. J. Chem.* **1957**, *35*, 67–83.

[163] F. Hennersdorf, J. J. Weigand, *Angew. Chem. Int. Ed.* **2017**, *56*, 7858–7862.

[164] M. E. Barr, B. R. Adams, R. R. Weller, L. F. Dahl, *J. Am. Chem. Soc.* **1991**, *113*, 3052–3060.

[165] V. L. Deringer, C. J. Pickard, D. M. Proserpio, *Angew. Chem. Int. Ed.* **2020**, *59*, 15880–15885.

[166] E. Mädl, G. Balázs, E. V. Peresypkina, M. Scheer, *Angew. Chem. Int. Ed.* **2016**, *55*, 7702–7707.

[167] M. Scheer, U. Becker, E. Matern, *Chem. Ber.* **1996**, *129*, 721–724.

[168] F. Hennersdorf, J. Frötschel, J. J. Weigand, *J. Am. Chem. Soc.* **2017**, *139*, 14592–14604.

[169] F. Spitzer, C. Graßl, G. Balázs, E. M. Zolnhofer, K. Meyer, M. Scheer, *Angew. Chem. Int. Ed.* **2016**, *55*, 4340–4344.

[170] W. Huang, P. L. Diaconescu, *Chem. Commun.* **2012**, *48*, 2216–2218.

[171] S. N. Konchenko, N. A. Pushkarevsky, M. T. Gamer, R. Köppe, H. Schnöckel, P. W. Roesky, *J. Am. Chem. Soc.* **2009**, *131*, 5740–5741.

[172] H.-W. Lerner, G. Margraf, L. Kaufmann, J. W. Bats, M. Bolte, M. Wagner, *Eur. J. Inorg. Chem.* **2005**, *2005*, 1932–1939.

[173] M. V. Butovskiy, G. Balázs, M. Bodensteiner, E. V. Peresypkina, A. V. Virovets, J. Sutter, M. Scheer, *Angew. Chem. Int. Ed.* **2013**, *52*, 2972–2976.

[174] E. Mädl, M. V. Butovskii, G. Balázs, E. V. Peresypkina, A. V. Virovets, M. Seidl, M. Scheer, *Angew. Chem. Int. Ed.* **2014**, *53*, 7643–7646.

[175] I. Krossing, *Chem. Eur. J.* **2001**, *7*, 490–502.

[176] W. R. Cullen, J. Trotter, *Can. J. Chem.* **1961**, *39*, 2602–2603.

[177] G. M. Sheldrick, *Acta Crystallogr. Sect. A* **2015**, *71*, 3–8.

[178] O. V. Dolomanov, L. J. Bourhis, R. J. Gildea, J. A. K. Howard, H. Puschmann, *J. Appl. Crystallogr.* **2009**, *42*, 339–341.

[179] G. M. Sheldrick, *Acta Crystallogr. Sect. C* **2015**, *71*, 3–8.

[180] A. Burkhardt, T. Pakendorf, B. Reime, J. Meyer, P. Fischer, N. Stübe, S. Panneerselvam, O. Lorbeer, K. Stachnik, M. Warmer, P. Rödig, D. Göries, A. Meents, . *Eur. Phys. J. Plus* **2016**, *131*, 56–64.

[181] F. Neese, F. Wennmohs, U. Becker, C. Riplinger, *J. Chem. Phys.* **2020**, *152*, 224108.

[182] A. D. Becke, *Phys. Rev. A* **1988**, *38*, 3098–3100.

[183] F. Weigend, R. Ahlrichs, *Phys. Chem. Chem. Phys.* **2005**, *7*, 3297–3305.

[184] M. D. Hanwell, D. E. Curtis, D. C. Lonie, T. Vandermeersch, E. Zurek, G. R. Hutchison, *J. Cheminformatics* **2012**, *4*, 17.

[185] K. Eichkorn, O. Treutler, H. Öhm, M. Häser, R. Ahlrichs, *Chem. Phys. Lett.* **1995**, *242*, 652–660.

[186] K. Eichkorn, F. Weigend, O. Treutler, R. Ahlrichs, *Theor. Chem. Acc.* **1997**, *97*, 119–124.

[187] A. D. Becke, *J. Chem. Phys.* **1993**, *98*, 5648–5652.

[188] C. Lee, W. Yang, R. G. Parr, *Phys. Rev. B* **1988**, *37*, 785–789.

[189] S. H. Vosko, L. Wilk, M. Nusair, *Can. J. Phys.* **1980**, *58*, 1200–1211.

[190] J. C. Slater, *Phys. Rev.* **1951**, *81*, 385–390.

[191] A. Schäfer, C. Huber, R. Ahlrichs, *J. Chem. Phys.* **1994**, *100*, 5829–5835.

[192] K. Eichkorn, F. Weigend, O. Treutler, R. Ahlrichs, *Theor. Chem. Acc.* **1997**, *97*, 119–124.

[193] F. Weigend, *Phys. Chem. Chem. Phys.* **2006**, *8*, 1057–1065.

[194] F. Furche, R. Ahlrichs, C. Hättig, W. Klopper, M. Sierka, F. Weigend, *Wiley Interdiscip. Rev.-Comput. Mol. Sci.* **2014**, *4*, 91–100.

[195] R. Ahlrichs, M. Bär, M. Häser, H. Horn, C. Kölmel, *Chem. Phys. Lett.* **1989**, *162*, 165–169.

[196] O. Treutler, R. Ahlrichs, *J. Chem. Phys.* **1995**, *102*, 346–354.

[197] M. Sierka, A. Hogekamp, R. Ahlrichs, *J. Chem. Phys.* **2003**, *118*, 9136–9148.

[198] R. Yadav, M. Weber, A. K. Singh, L. Münzfeld, J. Gramüller, R. M. Gschwind, M. Scheer, P. W. Roesky, *Eur. J. Chem.* **2021**, *27*, 14128–14137.

[199] D. H. R. Barton, J. Zhu, *J. Am. Chem. Soc.* **1993**, *115*, 2071–2072.

[200] D. H. Barton, R. A. Vonder Embse, *Tetrahedron* **1998**, *54*, 12475–12496.

[201] Y. H. Budnikova, D. G. Yakhvarov, O. G. Sinyashin, *J. Organomet. Chem.* **2005**, *690*, 2416–2425.

[202] B. M. Cossairt, C. C. Cummins, *New J. Chem.* **2010**, *34*, 1533–1536.

[203] J. E. Borger, A. W. Ehlers, J. C. Slootweg, K. Lammertsma, *Chem. Eur. J.* **2017**, *23*, 11738–11746.

[204] S. K. Ghosh, C. C. Cummins, J. A. Gladysz, *Org. Chem. Front.* **2018**, *5*, 3421–3429.

[205] U. Lennert, P. B. Arockiam, V. Streitferdt, D. J. Scott, C. Rödl, R. M. Gschwind, R. Wolf, *Nat. Catal.* **2019**, *2*, 1101–1106.

[206] G. Lu, J. Chen, X. Huangfu, X. Li, M. Fang, G. Tang, Y. Zhao, *Org. Chem. Front.* **2019**, *6*, 190–194.

[207] D. E. Corbridge, *Phosphorus: chemistry, biochemistry and technology*, CRC press, **2013**.

[208] L. Xu, Y. Chi, S. Du, W.-X. Zhang, Z. Xi, *Angew. Chem. Int. Ed.* **2016**, *55*, 9187–9190.

[209] S. Du, J. Yin, Y. Chi, L. Xu, W.-X. Zhang, *Angew. Chem. Int. Ed.* **2017**, *56*, 15886–15890.

[210] S. Du, J. Yang, J. Hu, Z. Chai, G. Luo, Y. Luo, W.-X. Zhang, Z. Xi, *J. Am. Chem. Soc.* **2019**, *141*, 6843–6847.

[211] B. Van Ijzendoorn, M. Mehta, *Dalton Trans.* **2020**, *49*, 14758–14765.

[212] D. Sarkar, C. Weetman, D. Munz, S. Inoue, *Angew. Chem. Int. Ed.* **2021**, *60*, 3519–3523.

[213] C. M. Hoidn, D. J. Scott, R. Wolf, *Chemistry* **2021**, *27*, 1886.

[214] M. Scheer, *Dalton Trans.* **2008**, 4372–4386.

[215] C. Schwarzmaier, A. Schindler, C. Heindl, S. Scheuermayer, E. V. Peresypkina, A. V. Virovets, M. Neumeier, R. Gschwind, M. Scheer, *Angew. Chem. Int. Ed.* **2013**, *52*, 10896–10899.

[216] T. Li, J. Wiecko, N. A. Pushkarevsky, M. T. Gamer, R. Köppe, S. N. Konchenko, M. Scheer, P. W. Roesky, *Angew. Chem. Int. Ed.* **2011**, *50*, 9491–9495.

[217] T. Li, M. T. Gamer, M. Scheer, S. N. Konchenko, P. W. Roesky, *Chem. Commun.* **2013**, *49*, 2183–2185.

[218] R. Yadav, B. Goswami, T. Simler, C. Schoo, S. Reichl, M. Scheer, P. W. Roesky, *Chem. Commun.* **2020**, *56*, 10207–10210.

[219] R. Yadav, T. Simler, B. Goswami, C. Schoo, R. Köppe, S. Dey, P. W. Roesky, *Angew. Chem. Int. Ed.* **2020**, *59*, 9443–9447.

[220] R. Yadav, T. Simler, S. Reichl, B. Goswami, C. Schoo, R. Ko?ppe, M. Scheer, P. W. Roesky, *J. Am. Chem. Soc.* **2019**, *142*, 1190–1195.

[221] R. S. Turbervill, J. M. Goicoechea, *Chem. Rev.* **2014**, *114*, 10807–10828.

[222] W. Dahlmann, H. G. v. Schnering, *Naturwissenschaften* **1972**, *59*, 420.

[223] N. Korber, J. Daniels, *Z. anorg. allg.*, *625*, 189–191.

[224] M. Arrowsmith, M. S. Hill, A. L. Johnson, G. Kociok-Köhn, M. F. Mahon, *Angew. Chem. Int. Ed.* **2015**, *54*, 7882–7885.

[225] C. Ganesamoorthy, C. Wölper, A. S. Nizovtsev, S. Schulz, *Angew. Chem. Int. Ed.* **2016**, *55*, 4204–4209.

[226] J. Krüger, C. Wölper, S. Schulz, *Inorg. Chem.* **2020**, *59*, 11142–11151.

[227] S. Krieck, H. Görls, L. Yu, M. Reiher, M. Westerhausen, *J. Am. Chem. Soc.* **2009**, *131*, 2977–2985.

[228] S. Harder, J. Brettar, *Angew. Chem. Int. Ed.* **2006**, *45*, 3474–3478.

[229] J. Spielmann, S. Harder, *Chem. Eur. J.* **2007**, *13*, 8928–8938.

[230] J. Spielmann, F. Buch, S. Harder, *Angew. Chem. Int. Ed.* **2008**, *47*, 9434–9438.

[231] J. Spielmann, S. Harder, *Eur. J. Inorg. Chem.* **2008**, *2008*, 1480–1486.

[232] J. Intemann, H. Bauer, J. Pahl, L. Maron, S. Harder, *Chem. Eur. J.* **2015**, *21*, 11452–11461.

[233] A. S. Wilson, M. S. Hill, M. F. Mahon, C. Dinoi, L. Maron, *Science* **2017**, *358*, 1168–1171.

[234] A. S. Wilson, M. S. Hill, M. F. Mahon, *Organometallics* **2018**, *38*, 351–360.

[235] M. S. Hill, M. F. Mahon, A. S. Wilson, C. Dinoi, L. Maron, E. Richards, *Chem. Commun.* **2019**, *55*, 5732–5735.

[236] A. S. S. Wilson, C. Dinoi, M. S. Hill, M. F. Mahon, L. Maron, E. Richards, *Angew. Chem. Int. Ed.* **2020**, *59*, 1232–1237.

[237] D. Mukherjee, D. Schuhknecht, J. Okuda, *Angew. Chem. Int. Ed.* **2018**, *57*, 9590–9602.

[238] W. Dahlmann, H. v. Schnering, *Naturwissenschaften* **1973**, *60*, 518–518.

[239] A. P. Dove, V. C. Gibson, P. Hormnirun, E. L. Marshall, J. A. Segal, A. J. P. White, D. J. Williams, *Dalton Trans.* **2003**, 3088–3097.

[240] A. Wiesner, S. Steinhauer, H. Beckers, C. Müller, S. Riedel, *Chem. Sci.* **2018**, *9*, 7169–7173.

[241] P. Pyykkö, S. Riedel, M. Patzschke, *Chem. Eur. J.* **2005**, *11*, 3511–3520.

[242] P. Kopecky, C. von Hänisch, F. Weigend, A. Kracke, *Eur. J. Inorg. Chem.* **2010**, *2010*, 258–265.

[243] S. Bestgen, C. Schoo, B. L. Neumeier, T. J. Feuerstein, C. Zovko, R. Köppe, C. Feldmann, P. W. Roesky, *Angew. Chem. Int. Ed.* **2018**, *57*, 14265–14269.

[244] S. J. Bonyhady, C. Jones, S. Nembenna, A. Stasch, A. J. Edwards, G. J. McIntyre, *Chem. Eur. J.* **2010**, *16*, 938–955.

[245] O. J. Scherer, T. Völmecke, G. Wolmershäuser, *Eur. J. Inorg. Chem.* **1999**, *1999*, 945–949.

[246] C. R. Groom, I. J. Bruno, M. P. Lightfoot, S. C. Ward, *Acta Crystallogr. Sect. B* **2016**, *72*, 171–179.

[247] P. Pyykkö, M. Atsumi, *Chem. Eur. J.* **2009**, *15*, 186–197.

[248] I. R. R. Peloso, A. Rodríguez, E. Carmona, K. Freitag, C. Jones, A. Stasch, A. J. Boutland, F. Lips, *Inorg. Synth. Vol. 37*, P.P. Power, John Wiley & Sons, Inc., **2018**, pp. 33–45.

[249] M. Westerhausen, M. H. Digeser, M. Krofta, N. Wiberg, H. Nöth, J. Knizek, W. Ponikwar, T. Seifert, *Eur. J. Inorg. Chem.* **1999**, *1999*, 743–750.

[250] K. X. Bhattacharyya, S. Dreyfuss, N. Saffon-Merceron, N. Mézailles, *Chem. Commun.* **2016**, *52*, 5179–5182.

[251] M. J. Frisch, G. W. Trucks, H. B. Schlegel, G. E. Scuseria, M. A. Robb, J. R. Cheeseman, G. Scalmani, V. Barone, G. A. Petersson, H. Nakatsuji, X. Li, M. Caricato, A. V. Marenich, J. Bloino, B. G. Janesko, R. Gomperts, B. Mennucci, H. P. Hratchian, J. V. Ortiz, A. F. Izmaylov, J. L. Sonnenberg, D. Williams-Young, F. Ding, F. Lipparini, F. Egidi, J. Goings, B. Peng, A. Petrone, T. Henderson, D. Ranasinghe, V. G. Zakrzewski, J. Gao, N. Rega, G. Zheng, W. Liang, M. Hada, M. Ehara, K. Toyota, R. Fukuda, J. Hasegawa, M. Ishida, T. Nakajima, Y. Honda, O. Kitao, H. Nakai, T. Vreven, K. Throssell, J. A. Montgomery, Jr., J. E. Peralta, F. Ogliaro, M. J. Bearpark, J. J. Heyd, E. N. Brothers, K. N. Kudin, V. N. Staroverov, T. A. Keith, R. Kobayashi, J. Normand, K. Raghavachari, A. P. Rendell, J. C. Burant, S. S. Iyengar, J. Tomasi, M. Cossi, J. M. Millam, M. Klene, C. Adamo, R. Cammi, J. W. Ochterski, R. L. Martin, K. Morokuma, O. Farkas, J. B. Foresman, D. J. Fox, Gaussian 16 Revision C.01, Gaussian Inc. Wallingford CT, **2016**.

[252] C. Lee, W. Yang, R. G. Parr, *Phys. Rev. B* **1988**, *37*, 785–789.

[253] A. D. Becke, *J. Chem. Phys.* **1993**, *98*, 5648–5652.

[254] P. J. Stephens, F. J. Devlin, C. F. Chabalowski, M. J. Frisch, *J. Phys. Chem.* **1994**, *98*, 11623–11627.

[255] R. Bader, *Atoms in Molecules: A Quantum Theory*, Clarendon: Oxford University Press, Oxford, **1990**.

[256] R. F. W. Bader, *Chem. Rev.* **1991**, *91*, 893–928.

[257] P. R. Varadwaj, I. Cukrowski, H. M. Marques, *J. Phys. Chem. A* **2008**, *112*, 10657–10666.

[258] P. R. Varadwaj, A. Varadwaj, H. M. Marques, *J. Phys. Chem. A* **2011**, *115*, 5592–5601.

[259] A. K. Singh, M. Usman, G. Sciortino, E. Garribba, S. P. Rath, *Chem. Eur. J.* **2019**, *25*, 10098–10110.

[260] E. Espinosa, E. Molins, C. Lecomte, *Chemical Physics Letters* **1998**, *285*, 170–173.

[261] M. V. Vener, A. N. Egorova, A. V. Churakov, V. G. Tsirelson, *J. Comput. Chem.* **2012**, *33*, 2303–2309.

[262] J. Hicks, M. Juckel, A. Paparo, D. Dange, C. Jones, *Organometallics* **2018**, *37*, 4810–4813.

[263] A. Jerschow, N. Müller, *J. Magn. Reson.* **1997**, *125*, 372–375.

[264] A. Macchioni, G. Ciancaleoni, C. Zuccaccia, D. Zuccaccia, *Chem. Soc. Rev.* **2008**, *37*, 479–489.

[265] H. C. Chen, S. H. Chen, *J. Phys. Chem.* **1984**, *88*, 5118–5121.

[266] D. Ben-Amotz, K. G. Willis, *J. Phys. Chem.* **1993**, *97*, 7736–7742.

[267] A. Bondi, *J. Phys. Chem.* **1964**, *68*, 441–451.

[268] S. Grimme, *J. Comput. Chem.* **2006**, *27*, 1787–1799.

[269] T. Lu, F. Chen, *J. Comput. Chem.* **2012**, *33*, 580–592.

[270] S. K. Chowdhury, V. S. Joshi, A. G. Samuel, V. G. Puranik, S. S. Tavale, A. Sarkar, *Organometallics* **1994**, *13*, 4092–4096.

[271] M. Nishio, *Cryst. Eng. Comm* **2004**, *6*, 130–158.

[272] S. Tsuzuki, A. Fujii, *Phys. Chem. Chem. Phys.* **2008**, *10*, 2584–2594.

[273] H. Brunner, T. Tsuno, M. Bodensteiner, *Organometallics* **2014**, *33*, 2257–2265.

[274] D. S. Glueck, *Synlett* **2007**, *2007*, 2627–2634.

[275] If the reaction products are precipitated, only a oily residue is formed, which cannot be analysed any further.

[276] H. Brake, E. Peresypkina, A. V. Virovets, M. Piesch, W. Kremer, L. Zimmermann, C. Klimas, M. Scheer, *Angew. Chem. Int. Ed.* **2020**, *59*, 16241–16246.

[277] H. Marco, *Phosphorus Sulfur Silicon Relat.* **1994**, *93*, 235–239.

[278] J. Ma, A. Hozaki, S. Inagaki, *Inorg. Chem.* **2002**, *41*, 1876–1882.

[279] M. Baudler, *Angew. Chem. Int. Ed.* **1982**, *21*, 492–512.

[280] M. Baudler, K. Glinka, *Chem. Rev.* **1993**, *93*, 1623–1667.

[281] M. Haeser, *J. Am. Chem. Soc.* **1994**, *116*, 6925–6926.

[282] J. T. Boronski, J. A. Seed, A. J. Wooles, S. T. Liddle, *Chem. Commun.* **2021**, *57*, 5090–5093.

[283] H.-P. Schrödel, A. Schmidpeter, *Magn. Reson. Chem.* **1996**, *34*, 227–232.

[284] M. Baudler, R. Riekehof-Böhmer, J. Hahn, *Z. Anorg. Allg. Chem.* **1987**, *544*, 81–86.

[285] F. Nief, L. Ricard, *J. Organomet. Chem.* **1994**, *464*, 149–154.

[286] D. W. Allen, B. F. Taylor, *J. Chem. Res. (S)* **1981**, 220.

[287] K. Jitsukawa, K. Iwai, H. Masuda, H. Ogoshi, H. Einaga, *Chem. Lett.* **1994**, *23*, 303–306.

[288] K. Issleib, W. Seidel, *Chem. Ber.* **1959**, *92*, 2681–2694.

[289] H. Hoffmann, P. Schellenbeck, *Chem. Ber.* **1966**, *99*, 1134–1142.

[290] H. T. Teunissen, C. B. Hansen, F. Bickelhaupt, *Phosphorus Sulfur Silicon Relat Elem .* **1996**, *118*, 309–312.

[291] P. Jutzi, H. Saleske, D. Nadler, *J. Organomet. Chem.* **1976**, *118*, C8–C10.

[292] P. Wucher, J. B. Schwaderer, S. Mecking, *ACS Catal.* **2014**, *4*, 2672–2679.

[293] Y. Tawada, T. Tsuneda, S. Yanagisawa, T. Yanai, K. Hirao, *J. Chem. Phys.* **2004**, *120*, 8425–8433.

[294] E. Caldeweyher, S. Ehlert, A. Hansen, H. Neugebauer, S. Spicher, C. Bannwarth, S. Grimme, *J. Chem. Phys.* **2019**, *150*.

[295] E. Caldeweyher, C. Bannwarth, S. Grimme, *J. Chem. Phys.* **2017**, *147*.

[296] J. Tomasi, B. Mennucci, R. Cammi, *Chem. Rev.* **2005**, *105*, 2999–3094.

[297] J.-D. Chai, M. Head-Gordon, *Phys. Chem. Chem. Phys.* **2008**, *10*, 6615–6620.

[298] D. Rappoport, F. Furche, *J. Chem. Phys.* **2010**, *133*.

[299] K. M. Fromm, *Coord. Chem. Rev.* **2020**, *408*, 213193.

[300] B. G. Gowenlock, W. E. Lindsell, B. Singh, *J. Chem. Soc. Dalton Trans.* **1978**, 657–664.

[301] D. Naglav, M. R. Buchner, G. Bendt, F. Kraus, S. Schulz, *Angew. Chem. Int. Ed.* **2016**, *55*, 10562–10576.

[302] K. Dehnicke, B. Neumüller, *Z. anorg. allg. Chem.* **2008**, *634*, 2703–2728.

[303] T. X. Gentner, B. Rösch, K. Thum, J. Langer, G. Ballmann, J. Pahl, W. A. Donaubauer, F. Hampel, S. Harder, *Organometallics* **2019**, *38*, 2485–2493.

[304] C. Ruspic, S. Harder, *Inorg. Chem.* **2007**, *46*, 10426–10433.

[305] S. Pillai Sarish, A. Jana, H. W. Roesky, T. Schulz, M. John, D. Stalke, *Inorg. Chem.* **2010**, *49*, 3816–3820.

[306] V. C. Gibson, J. A. Segal, A. J. P. White, D. J. Williams, *J. Am. Chem. Soc.* **2000**, *122*, 7120–7121.

[307] M. Westerhausen, *Dalton Trans.* **2006**, 4755–4768.

[308] M. Westerhausen, M. Gärtner, R. Fischer, J. Langer, L. Yu, M. Reiher, *Chem. Eur. J.* **2007**, *13*, 6292–6306.

[309] J. Langer, S. Krieck, H. Görls, G. Kreisel, W. Seidel, M. Westerhausen, *New J. Chem.* **2010**, *34*, 1667–1677.

[310] P. K. Freeman, L. L. Hutchinson, *J. Org. Chem.* **1983**, *48*, 879–881.

[311] B. Bogdanovic, N. Janke, H.-G. Kinzelmann, *Chem. Ber.* **1990**, *123*, 1507–1516.

[312] E. Bartmann, U. Bogdanovic, and Wilczok, S. Liao, *Chem. Ber.* **1990**, *123*, 1517–1528.

[313] B. Bogdanovic, *Acc. Chem. Res.* **1988**, *21*, 261–267.

[314] C. L. Raston, G. Salem, *J. Chem. Soc. Chem. Commun.* **1984**, 1702–1703.

[315] W. J. Transue, A. Velian, M. Nava, C. Garcia-Iriepa, M. Temprado, C. C. Cummins, *J. Am. Chem. Soc.* **2017**, *139*, 10822–10831.

[316] H. Bönnemann, B. Bogdanivic, R. Brinkmann, N. Egeler, R. Benn, I. Topalovic, K. Seevogel, *Main Group Met. Chem.* **1990**, *13*, 341–362.

[317] R. Fischer, M. Gärtner, H. Görls, M. Westerhausen, *Organometallics* **2006**, *25*, 3496–3500.

[318] M. Westerhausen, M. Gärtner, R. Fischer, J. Langer, L. Yu, M. Reiher, *Chem. Eur. J.* **2007**, *13*, 6292–6306.

[319] M. Fleischmann, S. Welsch, L. J. Gregoriades, C. Gröger, M. Scheer, *Z. Naturforsch. B* **2014**, *69*, 1348–1356.

[320] E. Peresypkina, M. Bielmeier, A. Virovets, M. Scheer, *Chem. Sci.* **2020**, *11*, 9067–9071.

[321] T. Chavez-Gil, J. Lugo, D. L. Cedeño, C. G. Hamaker, *J. Chem. Crystallogr.* **2015**, *45*, 189–192.

[322] X.-Z. Zhang, Y.-W. Song, F. HuiWu, Q.-F. Zhang, *Z. Naturforsch. B* **2007**, *62*, 778–782.

[323] C. D. Jeffries, H. Loeliger, H. H. Staub, *Phys. Rev.* **1952**, *85*, 478–479.

Acknowledgements

Finally I want to express my gratitude to:

- Prof. Dr. Manfred Scheer for the supervision of this work, proof reading of manuscripts and providing excellent working conditions even throughout a global pandemic as well as allowing a large degree of personal freedom in the exploration of the beautiful chemistry of polypnictogen complexes.

- Dr. Gábor Balázs for all the fruitful discussions, his endurance in reading my manuscripts and discussing the NMR spectra, the DFT calculations and for the pleasant working environment.

- Dr. Michael Seidl, Dr. Eugenia Peresypkina and Dr. Alexander Virovets for their crystallographic expertise and checking many of my structures and answering a lot of crystallographic questions.

- Prof. Dr. Peter Roesky and Dr. Ravi Yadav for their work during our cooperation in the exploration of the chemistry of N-donor-ligand stabilized group 2-15 element compounds.

- The staff of the central analytic department of the University of Regensburg: X-ray, EA, MS and NMR department. Special thanks to Georgine Stühler, Anette Schramm and Tuan Anh Nguyen for the measurement of countless, labour intensive NMR measurements.

- Prof. Rene Boeré from the University of Lethbridge, Canada, for his priceless advice for all our electro-analytical measurements and the help in defining standard operating procedures as well as establishing square-wave voltammetry measurements as a new analytical process in our working group.

- The staff of the glass blowing, mechanics and electronics department of the University as well as the facility management and waste disposal department for their valuable work.

- Dr. Julian Müller for his valuable advice and supervision during my master thesis, all the encouraging discussions and the everlasting endurance and calmness to tell me "you don't know what's really happening until you get a measurement" when discussing possible reaction mechanisms or side reactions.

- My other former lab mates and present colleagues in the lab on the other side of the hallway (the one with the sink) Dr. Maria Haimerl, Pavel Shelyganov, Dominik Venus, Robert Szlosek, Tatiana Prafeniuk and Lukas Adlbert for the great working atmosphere.

- Felix Lehnfeld for the long lasting friendship, all the fruitful discussions about chemistry and everything else, his endurance to repair the groups mass spectrometer (together with Dr. Haimerl) as well as the countless Leberkässemmeln he got for me from the cafeteria in the lunch break.

- My former fellow students Feli, Mutti, Simone, Beate, Manu, Andi, Dani and Miri for their company and the best moments during the chemistry studies.

- All the members of the AK Scheer online social club during the pandemic (imposters or otherwise): Maria, Helena, Feli, Luis, Claudia and Andrea as well as Boi, Tobi and Julian.

- All current and former members of the Scheer group for the good atmosphere, even through the tough years during the pandemic: Andrea, Jens, Mo, Felix R., Nase, Olli, Helena, Luis, Matthias Hautmann, Claudia, Tobi, Petra L. (thanks for all the Cp"'H), Martina A., Dani, Mehdi, Reini, Schotti, Andrea, Rudi, Lukas P., Lukas A. (a.k.a. Spezi), Martin P., Stephan, Lena, Jana, Anna, Pavel, Dominik, Tanja, Bin, Bijan, Tach, Christoph Riesinger (or was it Christian Reisinger ?), Lisa (thanks for the tomatoes), Robert, Julian, Max (for his everlasting bavarian wisdoms), Vroni, Kevin, Sarah (thanks for beer and ice cream), Boi (for the insights and discussions in the evenings), Billy, Sabrina, Sophie and Julian.

- Especially my family for their support during during my whole studies and the PhD.

- My loving wife Andrea for all the support even during the most difficult times.

"By convention sweet is sweet, bitter is bitter, hot is hot, cold is cold, color is color; but in truth there are only atoms and the void."

Democritus